



Università degli Studi di Ferrara

DOTTORATO DI RICERCA IN
SCIENZE DELLA TERRA

CICLO XXIV

COORDINATORE Prof. Beccaluva Luigi

The Greek Database of Seismogenic Sources: seismotectonic implications for North Greece

Settore Scientifico Disciplinare GEO/03

Dottorando

Dott. Sboras Sotirios

Tutore

Prof. Caputo Riccardo

Co-Tutore

Prof. Pavlides Spyros

Anni 2009/2011



Università degli Studi di Ferrara

DOTTORATO DI RICERCA IN
SCIENZE DELLA TERRA

CICLO XXIV

COORDINATORE Prof. Beccaluva Luigi

The Greek Database of Seismogenic Sources: seismotectonic implications for North Greece

Settore Scientifico Disciplinare GEO/03

Dottorando
Dott. Sboras Sotirios

Tutore
Prof. Caputo Riccardo

Co-Tutore
Prof. Pavlides Spyros

Anni 2009/2011

*Αφιερωμένο στον πατέρα μου και
στη μνήμη της μητέρας μου*

Preface

This dissertation has been a great opportunity to participate in a project that was almost lacking from the seismotectonic research field of Greece: the assembly of all proven and potential seismogenic sources in a database that will be applicable to any use. Following the examples of other similar and advanced national databases, the Greek Database of Seismogenic Sources (GreDaSS) project was set off in the pilot area of North Greece and was soon expanded in the rest Aegean Region. Based on the infrastructure of the Italian DISS database, GreDaSS will be available to any user and will provide the appropriate level of information according to his/her needs.

For the parameterization purposes of the database, two important parameters will be calculated: the maximum depth of the faults, which can be represented by the seismogenic layer thickness, and the slip rate. These two problems are based on two entirely different approaches. On one hand, the base of the seismogenic layer, which is reflected by the Brittle-Ductile Transition (BDT) zone, can be estimated by calculating the lithospheric strength through the rheological profiles. On the other hand, slip rate calculations rely on various geodetic strain rate field datasets, from which, by following the fundamental relationships of strain, it is feasible not only to calculate the short-term slip rate, but the rake as well.

During the parameterization process, a large amount of literature data becomes available, deriving from various types of investigations. Thus, a reliability issue for these data emerged. For this reason, two types of '*sources of information*' will be distinguished that involve the results that come from two different investigational approaches: the *single-event effects*-based and the *cumulative effects*-based investigations. The review of four case studies will provide a qualitative comparison of the two approaches in order to set the standards of confidence for the parametric information.

The completeness of GreDaSS in North Greece allows the usage of the database as a tool for various multi-disciplinary investigations, basically emphasising in the Seismic Hazard Assessment (SHA). The enhancement of SHA has a direct impact in society and economy by reducing the seismic risk. Towards this direction, two examples will be given in which GreDaSS has the leading role. These two examples include *i)* the proposal of a seismogenic zonation map for Greece, and *ii)* earthquake triggering scenarios based on the Coulomb stress change. Beyond SHA, GreDaSS contributes towards geodynamic modelling and seismotectonic interpretations. The homogeneity of the database can allow observations and comparisons between the seismogenic sources in every scale, from which it will be possible to comprehend or make suggestions about, for example, the pattern of the sources (*e.g.* clustering) or the tectonic structure of some areas (*e.g.* the existence of detachment faults).

Although the initial target is GreDaSS to cover the area of Northern Greece, the database will be able to expand in the broader region, supported by the SHARE project. SHARE (Seismic Hazard Harmonization in Europe; <http://www.share-eu.org>) is a European project which is running under the 7th Research program of the European Union. The project aims at delivering measurable progress in all steps, leading to a harmonized assessment of seismic hazard - in the definition of engineering requirements, in the collection and analysis of input data, in procedures for hazard assessment and in engineering applications. It has created a unified framework and computational infrastructure that will produce an integrated European probabilistic SHA (PSHA) model and specific scenario based modelling tools. Its results aim to deliver a long-lasting structural impact in areas of social and economic relevance; they will serve as a reference for the Eurocode 8 application, and will provide homogeneous input for the correct seismic safety assessment for critical industry, such as the energy infrastructures and the re-insurance sector. The structure of the SHARE project is divided into seven work packages, covering different steps and parts of studies of probabilistic seismic hazard assessment. The contribution of GreDaSS is involved in Work Package 3 (WP3), entitled “*Earthquake sources and activity rates*”, and especially in Tasks 3.2 and 3.4 that deal with the identification and parameterization of active faults and the compilation of seismic zones, respectively.

The structure of this dissertation includes seven chapters accompanied with an appendix. The first chapter is introductory, briefly describing the geological, geodynamic and seismotectonic setting of the study area, giving some general definitions and setting the primary targets of the thesis. The second chapter describes the structure and the management of the database and how the latter is navigated by the end-user. The following two chapters, the third and the fourth, deal with the calculation of the two seismotectonic parameters: the maximum fault depth and the slip rate, respectively. The contents of the database, *i.e.* the seismogenic sources of North Greece, are described and discussed in the fifth chapter, whereas the final discussion and the concluding remarks are included in the sixth chapter. The latter also encloses the discussion and conclusions of the reliability issue of the two ‘*sources of information*’ and two applications that use the database as a tool for the enhancement of SHA (seismogenic zonation and earthquake triggering scenarios). The seventh chapter summarises the results and briefly presents the general conclusions. The appendix contains the parametric information of all the seismogenic sources that are included in the fifth chapter.

Acknowledgements

During the three years of my thesis, many people contributed to this achievement, each one with his way. There is no doubt that my tutor, *Prof. Riccardo Caputo*, stood by me all along this research. Always available for any discussion, scientific or not, each of his advice was always illuminating. It is impossible to count the hours we worked together. For these reasons I would like to greatly thank him. Nevertheless, I was lucky enough to have *Prof. Spyros Pavlides* as a co-tutor. Our collaboration counts more than one decade, since the time when I was an undergraduate student in the Department of Geology at the Aristotle University of Thessaloniki. For all these years Prof. Pavlides has been a mentor and a friend and I am really grateful to him for his support.

Since the beginning of my PhD course, I had the pleasure to collaborate with *Dr. Gianluca Valensise* and *Dr. Roberto Basili*, who are both the leading members of the DISS Working Group in INGV and who greatly supported the development of the database for both the GreDaSS and the SHARE projects. At the same time, I would like to also thank the whole *DISS Working Group* for providing the DISS software, and especially *Mr. Gabriele Tarabusi* for his technical support. *Prof. Em. Hans-Gert Kahle* and *Ph.D.c. Michael Müller* from the ETH Zürich University are greatly acknowledged for kindly providing data that facilitated the slip rates calculation. My colleagues and friends, *Anastasia Michailidou*, *Dr. Alexandros Chatzipetros* and *Dr. Sotiris Valkaniotis*, are thanked for their contribution to the database, while *Prof. Ioannis Koukouvelas* and *Ass. Prof. Sotirios Kokkalas* are thanked for the fruitful discussions regarding the evolution and expansion of the database.

Nevertheless, none of these would have happened without the moral and psychological support of my father *Panagiotis S. Sboras*. Although she is no longer with us, I would also like to thank my mother *Maria Sboras-Kallinikidou*; I am sure that she would be very proud. Another close person I should thank is dear *Kyriaki Jordanidou* who showed great patience and gave priceless moral and psychological support during these three years. I would like to thank my old good friends from Greece *Demitris Agraftotis* and *Antonis Ioannides*, as well as my new good friends, who I had the pleasure to meet during this course in Italy, *Ahmed Rjoob* from Palestine, *Chiran Pokharel* from Nepal, *Thenesh Sathiyaseelan* from Sri-Lanka, *Haseeb Abdul Karak* from Pakistan, *Parviz Holakooei* from Iran and many others, for making these years pass easier.

Last but not least, the *Ministero dell'Istruzione, dell'Università e della Ricerca* (MIUR) of Italy is greatly acknowledged for providing me the economic support through the 3-year scholarship, which was essential for accomplishing this task, and of course the *Università degli Studi di Ferrara* is especially thanked for giving me the opportunity to carry out this thesis.

Acknowledgements

Contents

	Page
Preface.....	v
Acknowledgements.....	vii
Contents.....	ix
List of figures.....	xiii
1. Introduction.....	1
1.1. Geotectonic setting.....	1
1.2. Geodynamic setting.....	4
The Aegean Region.....	4
The Northern Greek mainland.....	7
The North Aegean Sea.....	8
Seismicity of North Greece.....	8
1.3. Seismogenic sources and active faults.....	10
Definitions.....	10
1.4. Fault inventories: an historical review.....	11
Worldwide national concepts.....	11
Other concepts in Greece.....	12
1.5. GreDaSS: the birth of.....	14
Needs and usage.....	14
General features.....	15
Philosophical approach.....	15
1.6. Aims and expected results.....	17
2. GreDaSS.....	19
2.1. Methodology.....	19
2.2. The seismogenic sources.....	19
2.3. Navigating GreDaSS.....	22
2.4. The parameters.....	27
Individual Seismogenic Sources (ISSs).....	27
Composite Seismogenic Sources (CSSs).....	31
General remarks.....	33
2.5. The GreDaSS development procedure.....	33
Fault Studio.....	34
The DISS software.....	34
3. Seismogenic layer thickness.....	37
3.1. Seismogenic layer thickness and BDT estimation.....	37
Introduction.....	37
Deformation mechanisms: an overview.....	39
Rheological models in theory.....	39
3.2. The deformational equations.....	41
The frictional sliding equation.....	41
The creep-law equation.....	42
The high-pressure brittle failure equation.....	42
3.3. Lithospheric stratification and composition.....	43

Lithosphere and rheological modelling: an introduction.....	43
Lithosphere and thickness.....	44
Crust and thickness.....	45
Sedimentary layer and thickness.....	47
Upper/lower crust and thickness.....	48
Lithospheric mantle and thickness.....	48
3.4. Geothermal gradients.....	48
Heat flow q	49
Heat production A	51
Thermal conductivity k and rock density ρ	53
Geothermal gradient equations.....	54
A temperature sensitivity test for the heat productive crust: the contribution of the thermophysical parameters k and A_0	55
3.5. The calibration of the strength envelopes.....	61
Parameters and conditions.....	61
The Kozani region case study.....	62
The South Thessaly case study.....	65
The central Mygdonia Basin case study.....	68
Discussion.....	71
4. Slip rate.....	73
4.1. Strain rate and slip rate	73
Slip rate definitions and theoretical approach.....	73
4.2. Strain.....	76
Strain rate definitions and formulae.....	76
Available datasets.....	77
4.3. Methodology.....	78
Case 1: principal axes and their orientation are known.....	78
Case 2: areal dilatation, maximum shear strain and principal axes orientations are known.....	79
4.4. Results and discussion.....	79
Results.....	79
Discussion.....	81
5. The seismogenic sources of North Greece.....	85
5.1. Introduction.....	85
5.2. The northern fault belt.....	87
Doxipara CSS.....	87
Maronia CSS.....	89
Thrace CSS (Komotini, Iasmos and Xanthi ISSs).....	89
Drama CSS (Drama and Prosotsani ISSs).....	90
Serres CSS.....	90
Belles CSS (Petritsi and Kastanoussa ISSs).....	91
5.3. The Chalkidiki fault system.....	91
Stratoni-Varvara CSS (Varvara, West Stratoni and East Stratoni ISSs).....	92
Gomati CSS.....	93
Singitikos Gulf CSS.....	94
Vourvourou ISS.....	94

Sochos CSS (Sochos and Mavrouda ISSs).....	94
Mygdonia CSS (Apollonia, Gerakarou and Langadhas ISSs).....	95
Asvestochori CSS.....	96
Pylaea CSS.....	96
Anthemountas CSS (Souroti and Angelochori ISSs).....	97
5.4. The ‘anti-Hellenides’ fault system.....	97
North Almopia CSS (Pozar, Promachi and Aetochori ISSs).....	98
Goumenissa ISS.....	99
South Almopia CSS.....	99
Amyndeio CSS (Nymfeio and Petron ISSs).....	100
Chimatidis ISS.....	101
Ptolemaida CSS (Vegora and Vegoritida ISSs).....	101
Perdika ISS.....	101
Komanos CSS (Mesovouni and Proastio ISSs).....	102
Peraea ISS.....	103
Aliakmonas CSS (Palaeochori, Rymnio, Servia and Chromio ISSs).....	103
Konitsa ISS/CSS.....	104
Petoussi CSS (Souli and Tomaros ISSs).....	105
Kerkyra CSS (Makrades and Spartylas ISSs).....	106
Palaeokastritsa ISS.....	106
5.5. The Thessalian fault system.....	106
Pagasitikos Gulf CSS (Volos and Nea Anchialos ISSs).....	107
Vasilika CSS (Righeo and Dasolofos ISSs).....	108
Domokos CSS (Ekkara ISS).....	108
South Tyrnavos Basin CSS (Larissa and Asmaki ISSs).....	109
Tyrnavos CSS (Tyrnavos ISS).....	109
North Tyrnavos Basin CSS (Rodia and Gyrtioni ISSs).....	110
Omolio CSS.....	110
South Kassandra offshore CSS.....	111
Mavrovouni offshore CSS.....	111
Pelion offshore CSS.....	111
5.6. The North Aegean Sea fault system.....	112
South Chalkidiki offshore CSS (Athos ISS).....	113
North Aegean Basin CSS (NAB segments A and B ISSs).....	113
South NAT CSS.....	114
North NAT CSS (Saros Gulf and Samothraki SE ISSs).....	115
North Samothraki ISS.....	115
Lemnos CSS.....	116
Aghios Efstratios ISS.....	116
6. Discussion and applications.....	117
6.1. General remarks.....	117
6.2. Reliability of <i>single-event effects</i> -based and <i>cumulative effects</i> -based investigation methods.....	120
East Heliki Fault (South Corinth Gulf Fault System).....	120
Domokos Fault System.....	123
Mygdonia Fault System.....	126

Contents

Aliakmonas Fault System.....	129
Comparison of approaches.....	133
Concluding remarks.....	135
6.3. Application examples of GreDaSS.....	136
Seismogenic zonation map of Greece.....	137
Stress transfer and earthquake triggering implications: an example from the Pagasitikos Gulf.....	141
6.4. Future expectations.....	148
7. Summary and conclusions.....	151
7.1. An Overview.....	151
7.2. Sommario.....	154
7.3. Σύνοψη.....	157
References.....	161
Appendix.....	197

List of figures

Fig.	Title	Page
1.1	The structural zones of the Hellenides (Mountrakis, 1986).	2
1.2	Lithospheric-scale cross-section of the Aegean region from the Balkan foreland to the African passive margin (Jolivet and Brun, 2010).	3
1.3	Schematic map of the principal tectonic settings in the Eastern Mediterranean (Taymaz <i>et al.</i> , 2007).	4
1.4	GPS velocities and geodetic strain rate map of the Aegean Region (Hollenstein <i>et al.</i> , 2008).	5
1.5	Geodetic and seismic strain rate maps of the Aegean Region (Jenny <i>et al.</i> , 2004).	6
1.6	Areal dilatation (a), maximum shear strain (b) and principal strain axes (c) of the Eastern Mediterranean and Middle East region, deriving from geodetic data (El-Fiky, 2000).	7
1.7	Seismicity map of the Aegean Region.	9
1.8	Map of the rupture (fault) zones in the Aegean Region (Papazachos <i>et al.</i> , 1999).	12
1.9	Map of capable faults in Greece (Pavlidis <i>et al.</i> , 2007).	13
1.10	The main active fault zones of North Greece (Mountrakis <i>et al.</i> , 2006).	14
2.1	Schematic representation of the ISSs and CSSs (Basili <i>et al.</i> , 2009).	21
2.2	The web interface of DISS for Italy (Basili <i>et al.</i> , 2008).	23
2.3	The Google TM earth interface of DISS for Italy (Basili <i>et al.</i> , 2008).	23
2.4	The standalone developers' interface of the DISS software for Greece	24
2.5	The main four informational pages of an ISS.	25
2.6	The FaultStudio interface (Basili <i>et al.</i> , 2008).	35
3.1	A simplified rheological profile model for the lithosphere (modified after Scholz, 1988).	37
3.2	Schematic diagram illustrating different theoretical rheological models for the long-term strength of continental lithosphere (Burov and Watts, 2006).	40
3.3	A standard profile of the continental crust (Wedepohl, 1995).	44
3.4	Moho depth maps for the Aegean Region (Tsokas and Hansen, 1997; Sodoudi <i>et al.</i> , 2006; Karagianni and Papazachos, 2007)	47
3.5	Typical geotherms for continental lithosphere (Chapman, 1986; Artemieva, 2006).	49
3.6	Surface heat flow maps of Europe (Cloetingh <i>et al.</i> , 2010; Hurter and Haenel, 2002).	50
3.7	A heat production model proposed for stable continental crust (Allis, 1979).	52
3.8	Geotherms of various UC compositions based on the on k and A_0 ranges.	57
3.9	Geotherms of various LC compositions based on the on k and A_0 ranges.	60
3.10	Geotherms and yield stress envelopes of the Kozani region and the comparison of the BDT with the 1995 aftershock distribution suggested by Hatzfeld <i>et al.</i> (1997).	64
3.11	Microseismic spatial distribution of South Thessaly (modified after Kementzetzidou, 1996; Hatzfeld <i>et al.</i> , 1999).	65
3.12	Geotherms and yield stress envelopes of South Thessaly.	68
3.13	Profiles of seismic vertical distribution in the Mygdonia Basin.	69
3.14	Geotherms and yield stress envelopes of the Mygdonia Basin.	71
4.1	Comparison of methods for calculating slip rates after McCaIpin (2009).	74

4.2	Schematic recurrence models (modified after Shimazaki and Nakata, 1980).	74
4.3	Schematic geodetic strain models	75
4.4	Examples of deformation and strain (modified from Leeder and Pérez-Arlucea, 2006; van der Pluijm and Marshak, 2004).	76
4.5	3D and 2D view sketches showing how the principal strain axes ε_1 and ε_3 are related with the slip vector.	78
4.6	Slip rate fluctuation maps for the broader Aegean Region, based on geodetically induced strain rate data.	82
5.1	Map of the seismogenic sources (CSSs and ISSs) completed for North Greece.	86
5.2	Map showing earthquakes that are associated, discussed or referenced in the description of the seismogenic sources.	87
5.3	The seismogenic sources of the ‘Northern fault belt’.	88
5.4	The seismogenic sources of the ‘Chalkidiki fault system’.	92
5.5	The seismogenic sources of the ‘anti-Hellenides fault system’.	98
5.6	The seismogenic sources of the ‘Thessalian fault system’.	107
5.7	The seismogenic sources of the ‘North Aegean Sea fault system’.	112
6.1	The seismogenic sources (CSSs in orange and ISSs in black colour) of the GreDaSS project for the broader Aegean Region.	117
6.2	Comparison of the single-event effects-based and cumulative effects-based models for the East Heliki ISS (1861 Valimitika earthquake).	121
6.3	Comparison of the single-event effects-based and cumulative effects-based models for the Domokos fault system (1954 Sophades earthquake).	124
6.4	Comparison of the single-event effects-based and cumulative effects-based models for the Mygdonia fault system (1978 Thessaloniki earthquake).	127
6.5	Comparison of the single-event effects-based and cumulative effects-based models for the Aliakmonas fault zone (1995 Kozani-Grevena earthquake).	130
6.6	The first seismic zonation map of the Aegean Region (Papazachos, 1990).	137
6.7	The most recently published seismic zonation map of the Aegean Region by Papaioannou and Papazachos (2000).	138
6.8	The most recently published seismic zonation map <i>versus</i> the CSSs of GreDaSS.	138
6.9	The preliminary modified seismic zonation map of the Aegean Region.	140
6.10	Coincidence of microseismic distribution within the area where the stress has been increased (Toda <i>et al.</i> , 2002).	141
6.11	The two models of uniform and tapered slip for the Volos and Nea Anchialos ISSs	143
6.12	3D and horizontal 2D views of the computed stress change, with the Nea Anchialos ISS set as a receiver fault.	144
6.13	Vertical and oblique profiles showing the computed stress change, with the Nea Anchialos ISS set as a receiver fault.	145
6.14	Deformation pattern after the reactivation of the Volos ISSs (tapered slip).	146
6.15	2D views of the computed stress change, considering both ISSs as source faults and faults of similar geometry and kinematics as receivers.	147
6.16	Deformation pattern in 2D and 3D views after the reactivation of both ISSs (tapered slip).	148
6.17	The various geographic informational levels of the Aliakmonas CSS shown as an example for GreDaSS.	149
A.1	Map of the CSSs as they appear in the appendix	201
A.2	Map of the ISSs as they appear in the appendix	202
A.3	Zoom in the Ptolemaida Basin for the CSSs and ISSs	203

CHAPTER 1

Introduction

1.1 Geotectonic setting

The geotectonic setting of the Aegean Region and its evolution mainly begins during the Mesozoic, when the discontinuous southwestward migration of the Alpidic orogenic process, characterized by intense collisional tectonics, caused successive subductions of the Tethyan oceanic basins producing a complete stack of several nappes (Brunn, 1956; Aubouin, 1959; Godfriaux, 1968; Mercier, 1968; Smith, 1971; Dewey *et al.*, 1973; Smith and Moores, 1974; Robertson and Dixon, 1984; Mountrakis, 1985; 1986). The plate tectonics theory changed the palaeogeographic and tectonic evolutionary models of the broader Aegean Region. Various models have been proposed arguing about the tectonic and palaeogeographic evolution of Tethys and the emplacement of the ophiolites, most of which are discussed by Robertson *et al.* (1996; see also Dercourt, 1972; Dewey *et al.*, 1973; Smith and Woodcock, 1976; Robertson and Dixon, 1984; Sengör *et al.*, 1984; Smith and Spray, 1984; Steininger and Rögl, 1984; Mountrakis, 1985; 1986; 2006; Dercourt *et al.*, 1986; 1993; Ricou *et al.*, 1986; 1998; Robertson *et al.*, 1991; Stampfli *et al.*, 1991; Jacobshagen, 1994; Garfunkel, 2004; Bortolotti and Principi, 2005; van Hinsbergen *et al.*, 2005a). Based on its palaeogeographic, environmental and structural evolution, the Aegean Region is divided into several *isopic* or else *structural zones* (fig. 1.1). The description of the zones following next is obtained from Mountrakis (1985; 2010), who supports the gradual rifting of various continental fragments from the Gondwana at the beginning of Mesozoic, their independent motion towards Eurasia that create a new oceanic crust to the rear, and their final collision with the Eurasia at the end of the Mesozoic. Additional information about the lithostratigraphy and structure of the Hellenides can be found in the IGRS-IFP (1966) monograph as well as in the paper of Smith and Moores (1974). The structural zones are (from east to west):

- i) The *Hellenic Hinterland*: the *Rhodope* and *Serbomacedonian Massifs* represent an old continental crust affected by Alpidic metamorphism. Both zones mainly consist of crystalline rocks bearing few neritic deposits and also document Late Eocene – Early Oligocene granitoid intrusions.
- ii) The *Internal Hellenides*: The *Circum-Rhodope* zone represents the continental slope of the Hellenic Hinterland towards the ocean that was ending up in a trough where the subduction of the Tethys was taking place. The general Alpidic lithostratigraphic succession includes volcanoclastic deposits, sea deposits ending up in deep-sea sediments westwards, and flysch. The *Vardar* zone corresponds to the ocean of Tethys characterized by the presence of deep-sea sediments and the obducted ophiolites. The *Pelagonian* zone is envisaged as a fragment of the Cimmerian

microcontinent and mainly consists of neritic sediments. The most characteristic lithological unit of the *Subpelagonian* zone are the obducted ophiolites. This zone is considered as the continental slope of the Cimmerian continent towards the ocean whose sedimentary remnants form the *Pindos* zone. Both zones consist of sea deposits showing a progressively deepening sea towards the west. The *Attico-Cycladic* zone, similar to the Pelagonian, is envisaged as a continental fragment having undergone neritic sedimentation.

iii) The *External Hellenides*: as part of the Apulian microplate, the External Hellenides correspond to a neritic continental sea depositional environment. They consist of the *Parnassos*, *Gavrovo-Tripolis*, *Ionian* and *Paxos* zones. A palaeogeographic difference of the Ionian zone is that, during the Middle-Upper Jurassic, it stood for an intracontinental basin with pelagic sediments. According to Doutsos *et al.* (2006), three major rift structures occurred during Mesozoic within the eastern margin of the Apulian continent, that were reactivated in the Tertiary by forming intracontinental thrusts.

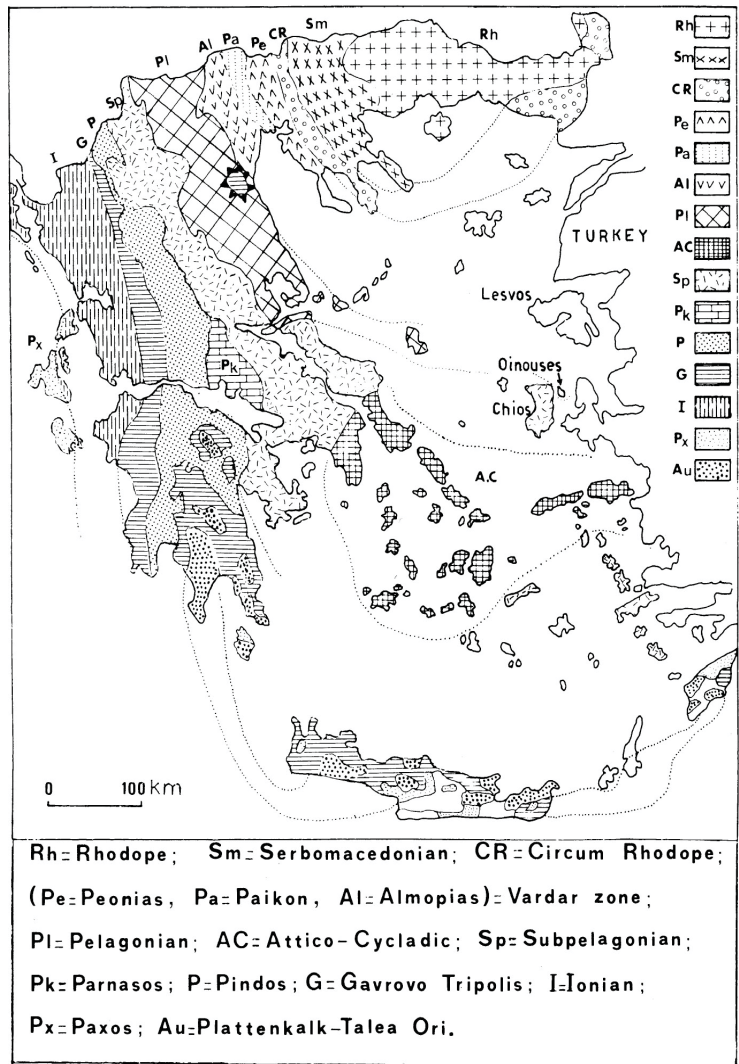


Fig. 1.1: Structural zones of the Hellenides after Mountrakis (1986). For further description see text.

All three groups of zones have undergone various tectonic phases that affected them diversely during geological time. The Alpidic orogenetic procedure documents two compressional stages (Mountrakis, 2006). The first one took place during the Late Jurassic and Cretaceous with the Meso-Tethys subduction, while the second one occurred during the Paleogene (Eocene-Oligocene-Miocene) with the final continental collision of the Apulia microplate with the Eurasia. According to the same author, the stacking of the nappes and the thickening of the crust, are attributed to the second Alpidic stage. Indeed, the broader Pindos Mountain chain documents a thick cover of successively repeated carbonate sedimentary layers.

The following late- to post-Alpidic tectonics and their effects are superimposed on the Alpidic structures. However, the limits of the Alpidic and post-Alpidic deformations are not discrete. While the orogenic front was reaching the westernmost part of Greece in the Middle Miocene, the Present day's regime started to develop behind it with the subduction zone of the modern Hellenic Arc migrating southwards. Thus, compression was progressively giving its place to extension possibly caused by gravitation collapse and crustal thinning (e.g. Caputo and Pavlides, 1993; Doutsos *et al.*, 1994; Mountrakis, 2006; Jolivet *et al.*, 2010), core complexes exhumation and detachment faults in the Rhodope, Cyclades, Menderes (West Turkey), Crete (e.g. Dinter and Royden, 1993; Gautier and Brun, 1994; Jolivet *et al.*, 1994; 2010; Kiliyas *et al.*, 1994; Forster and Lister, 1999; Bonev and Beccaletto, 2007; Brun and Sokoutis, 2007; Dilek *et al.*, 2009) and the formation of back-arc basins (e.g. Boccaletti *et al.*, 1974; Horvath *et al.*, 1981). One of the most significant structures of the late- to post-orogenic extensional tectonics is the Mesohellenic Trough, which is considered as a back-arc basin (Papanikolaou *et al.*, 1988) or a piggy-back basin (Doutsos *et al.*, 1994; Ferrière *et al.*, 1998; Vamvaka *et al.*, 2006), consisting of a flyschoid sequence at the bottom and a flyschoid to molassic sequence at the top (e.g. Brun, 1956; Papanikolaou *et al.*, 1988). The elongated trough, developed from the Late Eocene to the Late Miocene, is situated on the backbone of the Hellenides in northwestern Greece, running parallel to the Alpine isopic zones (Papanikolaou *et al.*, 1988; Doutsos *et al.*, 1994; Ferrière *et al.*, 1998; Vamvaka *et al.*, 2006).

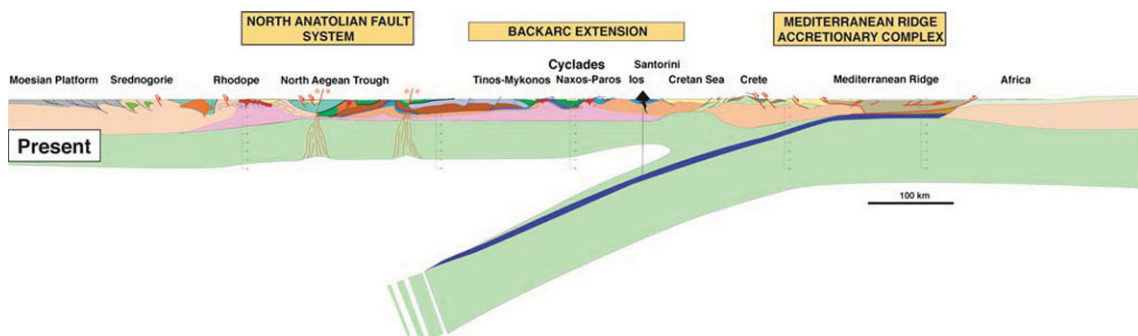


Fig. 1.2: Compiled lithospheric-scale cross-section of the Aegean region from the Balkan foreland to the African passive margin. This section is based upon surface geological observations as well as geophysical data from the literature (Jolivet and Brun, 2010).

The neotectonic evolution of the Aegean Region basically starts from the Late Pliocene-Early Pleistocene, when a roughly N-S crustal stretching regime develops. One of the most important key-features is the evolution of the Hellenic Arc (fig. 1.2). According to structural, seismological and paleomagnetic investigations (Le Pichon and Angelier, 1979; 1981; Laj *et al.*,

1982; Kissel *et al.*, 1985; Kissel and Laj, 1988; Taymaz *et al.*, 1991; Walcott and White, 1998), the present Aegean tectonic regime with the subduction of the African plate and Eurasia began 13 Ma ago and has undergone a clockwise rotation around a pole situated in the southern Adriatic Sea.

1.2 Geodynamic setting

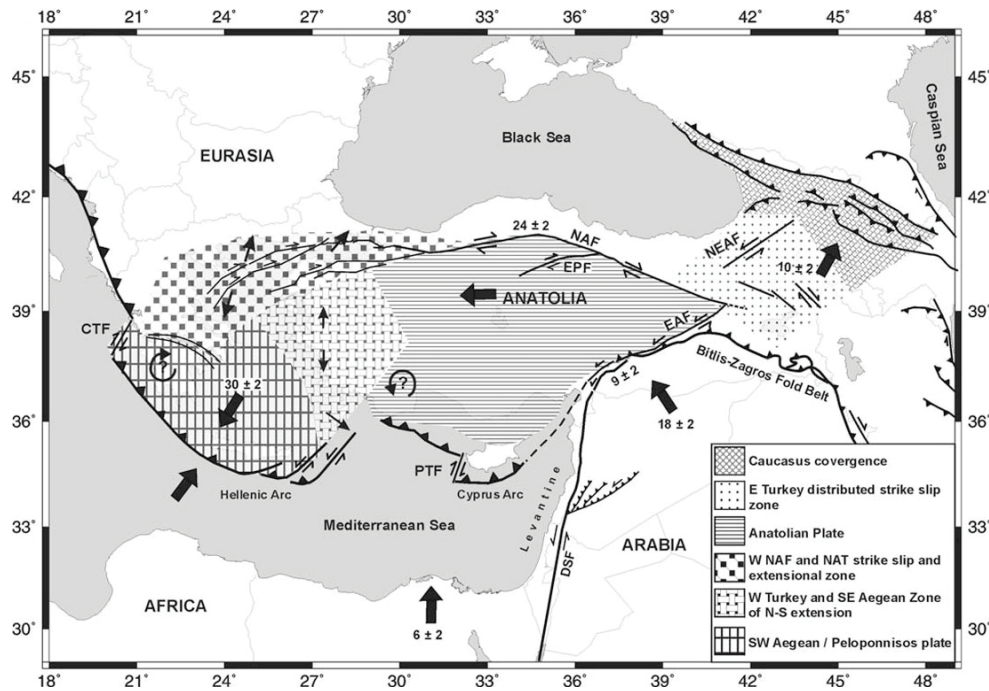


Fig. 1.3: Schematic map of the principal tectonic settings in the Eastern Mediterranean (Taymaz *et al.*, 2007). Hatching shows areas of coherent motion and zones of distributed deformation. Large arrows designate generalized regional motion (in mm/a) and errors (recompiled after McClusky *et al.*, 2000; 2003). NAF, North Anatolian Fault; EAF, East Anatolian Fault; DSF, Dead Sea Fault; NEAF, North East Anatolian Fault; EPF, Ezzinepazari Fault; CTF, Cephalonia Transform Fault; PTF, Paphos Transform Fault.

The Aegean Region

The broader Aegean Region is among the most tectonically active areas of the Mediterranean realm. The tectonic regime is rather complex producing earthquakes with many different orientations of P/T axes (Papazachos and Kiratzi, 1996; Hatzfeld, 1999; Kiratzi and Louvari, 2003) and a large variety of fault types both in terms of dimensions and kinematics (Kokkalas *et al.*, 2006; Mountrakis, 2006). The recent evolution of the broader Aegean is characterised by the westward motion of the Anatolian plate along the North Anatolian Fault (Jolivet, 2001; Armijo *et al.*, 2003; Flerit *et al.*, 2004) which in turn pushes the Aegean plate southwards (McKenzie, 1978; Taymaz *et al.*, 1991; Le Pichon *et al.*, 1995). This motion is related at the same time to the active lithospheric subduction of the retreating African plate beneath the Hellenic Trench (Caputo *et al.*, 1970; McKenzie, 1978; Jackson *et al.*, 1992) that formed the Aegean Sea since at

least Oligocene times (Le Pichon and Angelier, 1981; Gautier *et al.*, 1999; Jolivet and Faccenna, 2000; Jolivet and Brun, 2010). However, the tectonics of the Aegean cannot be described so simply, since the inner part undergoes internal deformation according to geological, geodetic, seismological and palaeomagnetic investigations (Angelier, 1979; Kissel and Laj, 1988; Hatzfeld, 1999; Papazachos, 1999; 2002; van Hinsbergen *et al.*, 2005b). The advance of the GPS technology and the enhancement of the seismographic networks have greatly contributed to the definition and quantification of the relative motions of the ‘microplates’ (fig. 1.3) as well as to the modelling of the strain rate accumulation in the Aegean Region (figs. 1.4, 1.5 and 1.6) (Meijer, 1995; Reilinger *et al.*, 1997; 2006; 2010; Kahle *et al.*, 1998; Cocard *et al.*, 1999; El-Fiky, 2000; McClusky *et al.*, 2000; 2003; Jenny *et al.*, 2004; Nyst and Thatcher, 2004; Hollenstein *et al.*, 2008; Caporali *et al.*, 2009; Floyd *et al.*, 2010).

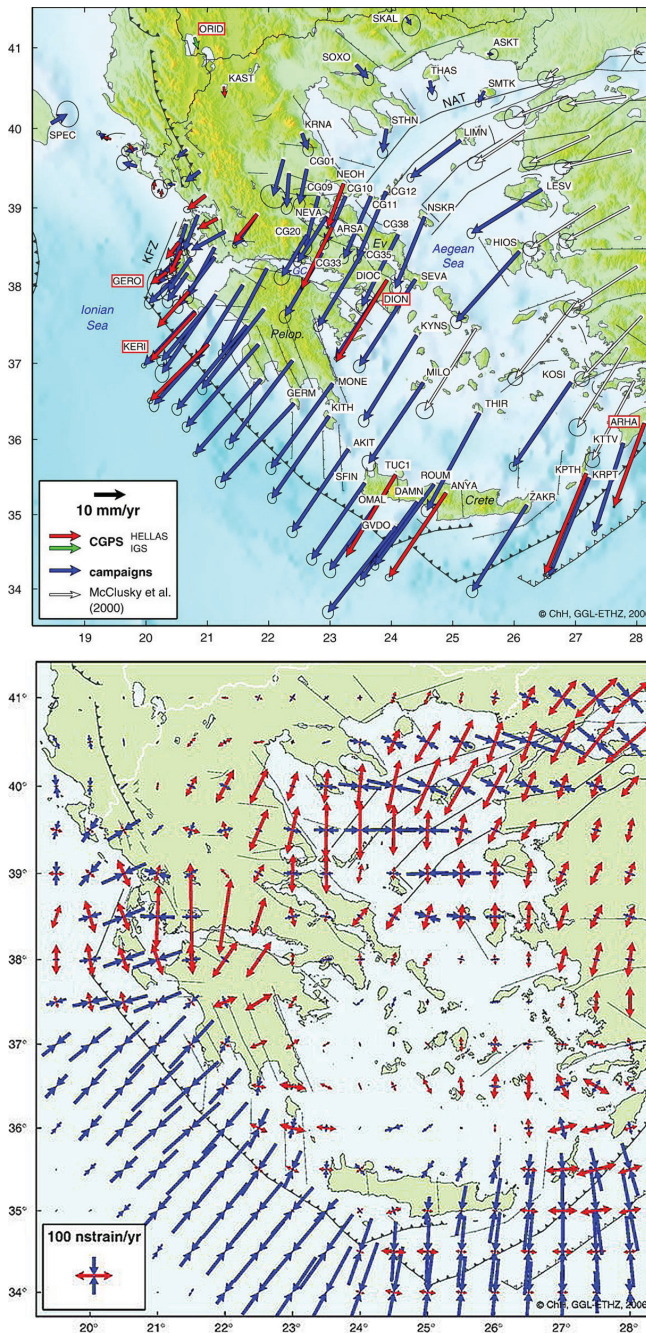


Fig. 1.4: (Top) GPS-velocities relative to Eurasia, for the period 1993–2003. The error ellipses represent the 1-sigma confidence region. (Bottom) Principle axes and eigen values of the strain rate tensor calculated from the velocity field shown above and some additional virtual rates representing the motion of the Nubian plate. Red arrows indicate extension, blue arrows compression. 100 nstrain corresponds to a relative motion of 1 mm over a distance of 10 km. After Hollenstein *et al.* (2008).

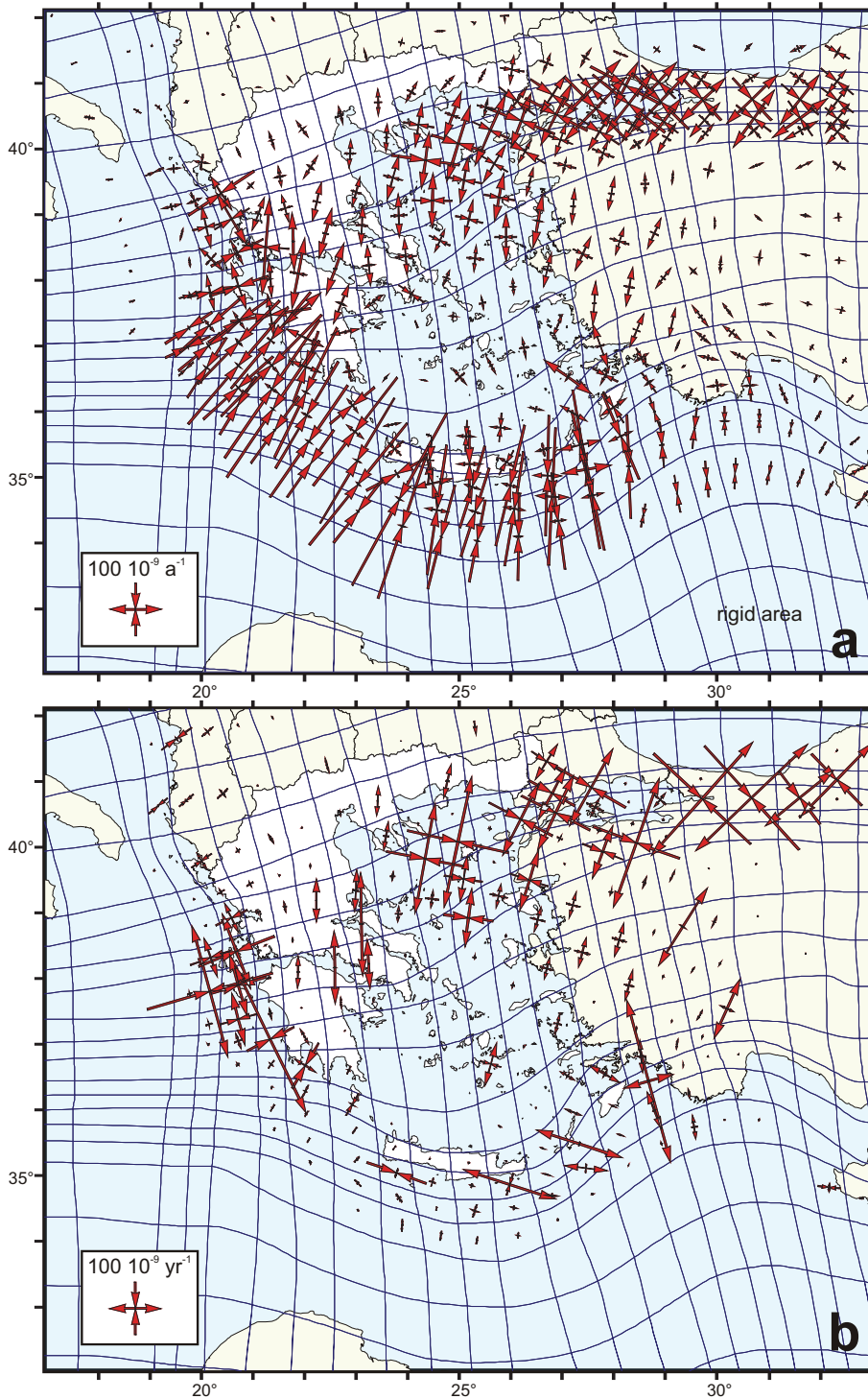


Fig. 1.5: Principal horizontal axes of the a) total geodetic strain rate field from fitting GPS velocities, and b) total seismic strain rate tensor obtained by combining the seismic moment rates of a combined 500-year catalogue. After Jenny *et al.* (2004).

Thus, the three large-scale tectonic structures that dominate the Aegean are: *i*) the Hellenic subduction zone, where the African plate is subducted underneath the Aegean; it is associated with a compressive stress field all along the arc (*e.g.* McKenzie, 1970); *ii*) the Inner Aegean region characterized by widespread, mainly N-S trending, crustal extension (*e.g.* Mercier,

1981); *iii*) the North Aegean Trough which represents a transtensional stress regime (*e.g.* Pavlides *et al.*, 1990) due to overlapping contribution of the western propagation of the purely strike-slip North Anatolian Fault and the Aegean extension (Pavlides and Caputo, 1994).

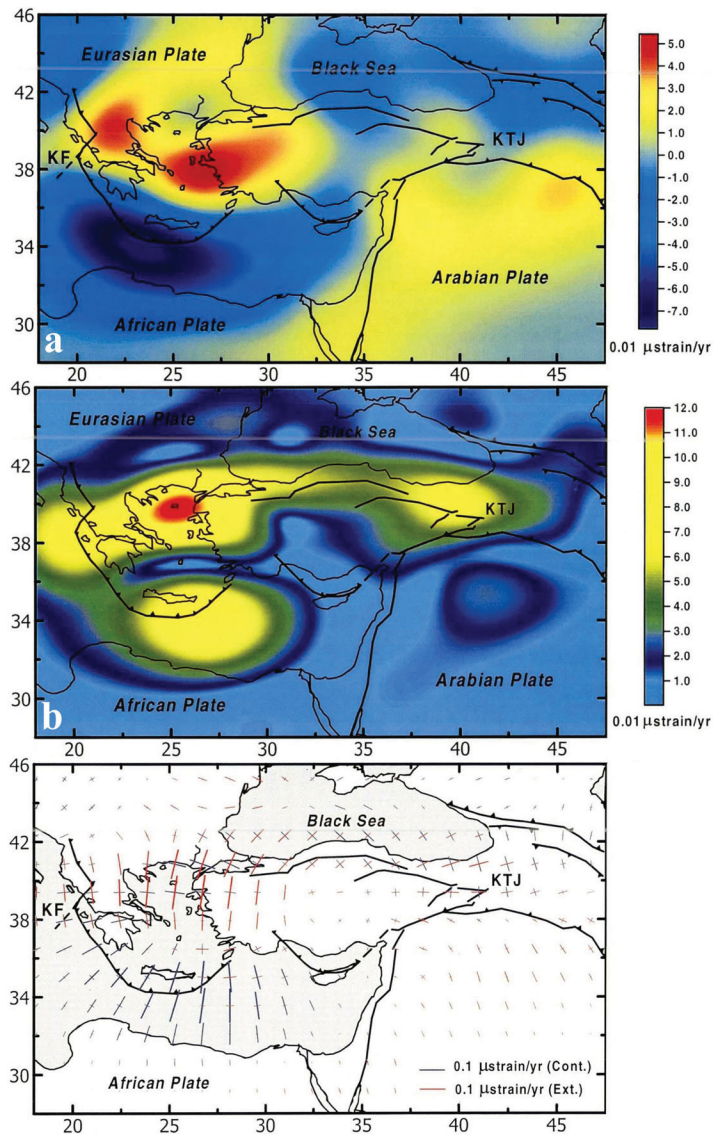


Fig. 1.6: Areal dilatation (a), maximum shear strain (b) and principal strain axes (c) of the Eastern Mediterranean and Middle East region, deriving from geodetic data (El-Fiky, 2000).

The Northern Greek mainland

Northern Greece lies in the inner part of the Hellenic orogen and consists of zones belonging to both Internal and External Hellenides. The Present-day tectonic regime is characterized by intra-continental brittle deformation (Mercier *et al.*, 1979). The roughly N-S extensional domain is superposed to the NW-SE-trending collapsed Early Cenozoic mountain belts of Rhodope and the Hellenides (Doutsos *et al.*, 1994; Jolivet and Brun, 2010).

The Present-day tectonic stress pattern in Macedonia and Rhodope (North Greece) is active since Pleistocene (Mercier *et al.*, 1979; Pavlides and Mountrakis, 1987; Caputo, 1990; Mountrakis, 2006), showing a slightly radial crustal extension varying from NNE-SSW in Rhodope (Lybérís, 1984; Mercier *et al.*, 1989), N-S to NNW-SSE in Central and East

Macedonia (Brooks and Williams, 1982; Mercier *et al.*, 1983; 1989; Lyb ris, 1984; Pavlides and Kili s, 1987; Mercier and Carey-Gailhardis, 1989; Voidomatis *et al.*, 1990; Papazachos *et al.*, 2001b; Vamvakaris *et al.*, 2006) and almost NW-SE in Western Macedonia (Pavlides and Mountrakis, 1987; Mercier *et al.*, 1989; Mountrakis *et al.*, 1998). The fault pattern is almost perpendicular to the stress field, cross-cutting the older NW-SE Alpine structures.

Thessaly and the broader Central Greece are also characterised by a stretching direction similar to Central Macedonia: an almost pure N-S extension with E-W-striking normal faults (Caputo and Pavlides, 1993; Papazachos *et al.*, 1993a; Caputo, 1996). However, like in Macedonia, it is not unusual to find old thrust faults reactivated as secondary inherited structures before the E-W-striking faults start dominating.

Epirus demonstrates a more complex pattern. In the mainland and along to the Pindos Mountain chain, the prevailing extension has a rough NW-SE direction being part of the same extensional regime of West Macedonia (Doutsos and Koukouvelas, 1998). Moving westwards to the Ionian Sea, the tectonic regime and the stress trajectories progressively change turning into ESE-WNW compression (Hatzfeld *et al.*, 1995; King *et al.*, 1983; Mu o, 1994; Tselentis *et al.*, 2006; Baker *et al.*, 1997), due to the increasingly affecting subduction zone. Moreover, the thick evaporitic layer at the base of the Mesozoic stratigraphic succession creates different mechanical behaviour between the upper and lower layers (Tselentis *et al.*, 2006).

The North Aegean Sea

The North Aegean Sea is dominated by two regional-scale tectonic structures that are directly connected: the *North Aegean Basin* (NAB) and the *North Aegean Trough* (NAT). The NAB is situated between the Chalkidiki peninsula, Thessalian coast and Sporades Islands, forming a triangular-shaped basin situated next to the western end of the NAT. The latter is represented by a crustal-scale negative flower structure affecting the sea bottom between the Callipoli peninsula (Gulf of Saros), the islands of Lemnos and Imbros to the south, and the island of Samothraki to the north ( agatay *et al.*, 1998; Yaltirak *et al.*, 1998; Kurt *et al.*, 2000; Koukouvelas and Aydin, 2002; Yaltirak and Alpar, 2002; McNeill *et al.*, 2004; Usta mer *et al.*, 2008). The fault zone also continues onshore cutting through the Callipoli peninsula and reaching the western part of the Marmara Sea (Ambraseys and Finkel, 1987; T ys z *et al.*, 1998; Armijo *et al.*, 1999; Altunel *et al.*, 2004; Kaya *et al.*, 2004; Aksoy *et al.*, 2010). This transtensional shear zone marks the mechanical-stress transition from the purely transcurrent tectonic regime of the North Anatolian Fault, to the east, and the prevailing extensional regime towards the west (NAB) (Pavlides *et al.*, 1990; Taymaz *et al.*, 1991; Pavlides and Caputo, 1994; Papanikolaou *et al.*, 2006). Due to this lateral variation, the basin of the NAB progressively widens and deepens westwards (Papanikolaou *et al.*, 2002). This transition is also documented by the faulting character of the NAB, which changes from almost pure right-lateral strike-slip eastwards, to almost pure extensional westwards. The combination of these complex tectonic processes produces an intense lithospheric fracturing and the formation of a large number of active faults.

Seismicity of North Greece

Seismicity in North Greece is not homogeneously distributed, either in frequency or density ([fig. 1.7](#)). Consequently, historical information is not uniform all over the region and even the

most complete and updated earthquake catalogues (Ambraseys and Jackson, 1990; 1998; Guidoboni *et al.*, 1994; Papazachos and Papazachou, 1997; 2003; Guidoboni and Comastri, 2005; Ambraseys, 2001; 2009) are in some cases contradicting or doubtful in describing past events, especially the older ones. In other words, the quantitative exploitation of the data and the correlation of the events with any recognized fault, sometimes become hard (Caputo *et al.*, 2008). For example, a quick view of the Aegean Region (fig. 1.7) and specifically the study area of Northern Greece, shows a sparse and infrequent seismicity in Eastern Macedonia and Thrace Region, where no significant seismicity is instrumentally recorded. On the contrary, Central Macedonia and Chalkidiki show intense activity including instrumentally recorded events (*e.g.* the 1932, Ierissos and the 1978, Thessaloniki earthquakes) and plenty records of historic events. West Macedonia was demonstrating extremely low seismicity (Voidomatis, 1989; Papazachos, 1990) until May 15, 1995, when a $M_w = 6.5$ earthquake occurred in the vicinity of Kozani. The pattern then changed back to sparse and infrequent seismicity with few instrumentally recorded moderate events in the area of Epirus and generally the broader northwestern Greece. A possible explanation for this difference is that the historical record is obviously richer in densely populated areas, while mountainous regions like Epirus and Western Macedonia were always sparsely populated. Nevertheless, instrumental seismicity seems to verify this difference, although the time window is too narrow. Finally, the North Aegean Sea shows the most intense and frequent seismicity. The highly active structures of the NAT and NAB have produced numerous strong to major events, many of which have been instrumentally recorded. However, historical events are hard to be associated with specific seismogenic sources, given that the sea prevents the intensity distribution documentation and any observation.

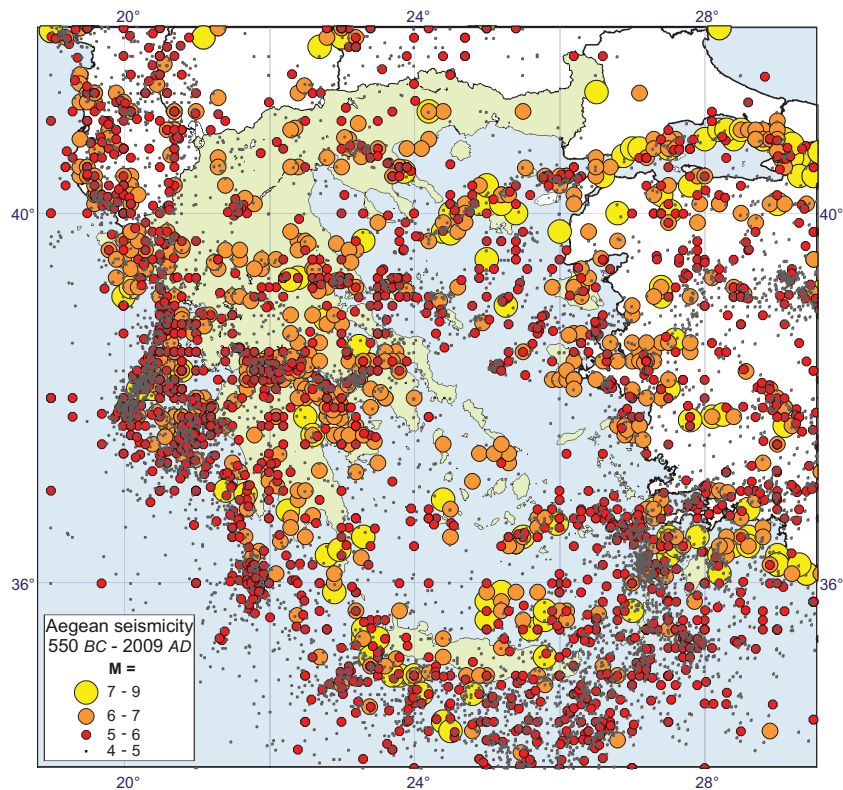


Fig. 1.7: Historical and instrumental seismicity of the Aegean Region, taken from the online catalogue of the Seismological Station of AUTH (<http://geophysics.geo.auth.gr/ss/>; Papazachos *et al.*, 2000; 2009).

1.3 Seismogenic Sources and Active faults

Definitions

The commonly used terminology for defining a fault is more or less similar and simple, *e.g.* “fault is any surface or zone in the Earth across which measurable slip (shear displacement) develops” (van der Pluijm and Marshak, 2004), or “[faults are] discrete surfaces or planes across which two bodies of rock have moved or slid past each other” (Kusky, 2005). However, faults have different derivatives according to their characteristics. For the purposes of this thesis, the fault zone definition of van der Pluijm and Marshak (2004) is used: “fault zone is either a band of finite width across which the displacement is partitioned among many smaller faults, or the zone of rock bordering the fault that has fractured during faulting”. However, a *shear zone* is defined as the zone of finite width along which displacement is attributed to major shear forces.

Generally, the common terminology for defining *active faults* and *capable faults* varies in the sense of the time window used. In the current thesis, the term of active fault is preferred instead of capable fault, since the former is considered also as capable of producing a future earthquake. Machette (2000), after revising various definitions given by various authors, organisations and committees, concludes that the time window used for characterizing faults should depend on the regional tectonic setting and the range of completeness of the regional seismic hazards. Thus, the term of *active fault* is applied when a fault shows evidence of *recent* reactivation and/or is capable of being reactivated in the future. The definition of *recent* is quite relative and can be very subjective, but it is always comparable to the seismotectonic regime of the Aegean Region. Moreover, activity can be implied by and constrained from the evidences. Therefore, according to the evidences, some criteria can be assigned to the active faults, all adapted suitably for the faulting character of the Aegean. The criteria described below, are based on the general guidelines of Pavlides *et al.* (2007) and they are hierarchically sorted, starting from the most irrefutable ones:

1. *Recorded Seismicity*: this is the most undeniable criterion of fault’s activity. Records can be either instrumental or historical. Concerning the former ones, not only large events are useful, but also microseismicity. However, this criterion is applicable only for a limited number of faults, given that historical seismicity in Greece starts from 550 BC and uncertainty is high.
2. *Geological and stratigraphic features*: the age and type of stratigraphic unit(s) affected by a fault scarp or a fault trace are crucial for estimating and constraining the last re-activation of a tectonic structure. The displacement of very recent sediments is a key indicator of recent activity. In this regard, the contribution of palaeoseismological investigations is essential.
3. *Geomorphological and morphotectonic features*: surface morphology can be strongly affected by active tectonics and hence many such features can be recognized and characterized based on field work and laboratory analyses. Among the most important and commonly used morphotectonic features are fault scarps, triangular facets and the

tilting of Quaternary sediments (e.g. Caputo, 1993b; Caputo and Helly, 2005b; Kokkalas and Koukouvelas, 2005). With the aid of remote sensing techniques and dedicated software, also many qualitative and quantitative morphometric parameters are generally considered, like the drainage pattern, stream orders, etc. (Zovoili *et al.*, 2004; Michailidou *et al.*, 2005; Sboras *et al.*, 2010). A less explicit indicator is the occurrence of a free-face developed in bedrock. In this case, it is not the age of the affected rocks, usually Palaeozoic or Mesozoic in the Greek territory, to be indicative of a recent activity, but the freshness of the morphological feature as well as the geometry and texture of the fault scarp (Caputo, 1993a; Stewart, 1996a). Steep, sleek and polished surfaces indicate a young fault. Even difference in colour can be a guideline for estimating successive co-seismic reactivations by linear morphogenic events. On the other hand, metamorphic rocks show poor evidence not only because of their greater erodibility, but also due to the internal fabric, like for example schistosity, which could generate differential erosional features morphologically convergent with the tectonic ones.

4. *Geodynamic setting*: the orientation of the fault plane with respect to the active stress field of the broader area is also an indication of possible activity (e.g. Pavlides *et al.*, 2007). However, this approach could be somehow misleading in specific areas, where the tectonic regime can be relatively complex showing lateral variations following contrasting reconstructions by different authors. Areas like the North Aegean Sea or the Ionian Sea belong to this complex regime.

Active faults in Greece show a large variety at all scales. However, small individual faults are insignificant for the aims of Seismic Hazard Assessment (SHA). For this reason, the structures studied in this thesis are the *seismogenic sources*. Based on the definition of Kastelic *et al.* (2008) for the DISS, *seismogenic sources* are active faults capable of generating $M_w > 5.5$ earthquakes. The latter definition is also suitable for the case of the study area, given that Pavlides and Caputo (2004) suggest that a magnitude larger than 5.5 is needed in order to have *linear morphogenic earthquakes* (*sensu* Caputo, 2005) in the Aegean Area.

1.4 Fault inventories: an historical review

Worldwide national concepts

Having foreseen the importance to hold and manage all collected data from active fault investigations, many research institutes worldwide have built databases at the national scale. For example, the Geological National Survey in New Zealand (GNS Science; <http://data.gns.cri.nz/af/>), the Institute of Advanced Industrial Science and Technology in Japan (AIST; http://riodb02.ibase.aist.go.jp/activefault/index_e.html), the Geological Survey in the United States (USGS; <http://pubs.usgs.gov/fs/2004/3033/fs-2004-3033.html>) and the Istituto Nazionale di Geofisica e Vulcanologia in Italy (INGV; <http://diss.rm.ingv.it/diss/>) have certainly the most developed databases of active faults. Basili *et al.* (2008) discuss that although some of the main philosophical features (national coverage, total completeness), methodological

approaches (use of all available literature data) and using purposes (SHA) are quite much in common, many qualitative differences can be observed in the main structure (representation style, variety of information) and the scientific content and approach (fault, characterization, parameterization).

Other concepts in Greece

During the late 1990s it was realized that documenting the active faults of Greece is of great importance for SHA analyses. The early efforts were focused on faults that were related with either historically or instrumentally recorded earthquakes. Ambraseys and Jackson (1998) associated historical and instrumental events with faulting for the East Mediterranean area, while Papazachos *et al.* (1999; 2001a) compiled a map of “rupture zones” representing faults responsible for recent events (fig. 1.8), also suggesting their geometric (strike, dip) and kinematic (rake) parameters. Nevertheless, their work was almost exclusively based on historical and instrumental seismological data. At the same time, in the frame of the European project “FAUST” (*Faults as a Seismologists’ Tool*; Mucciarelli and FAUST Working Group, 2000), the first, though preliminary, version of a database with fully parameterized active faults was compiled for the Aegean Region including *ca.* 50 sources. Although this was the first database complete of all principal seismotectonic parameters, most seismogenic sources were associated with recently reactivated faults, with few exceptions where geological information was also partially considered.

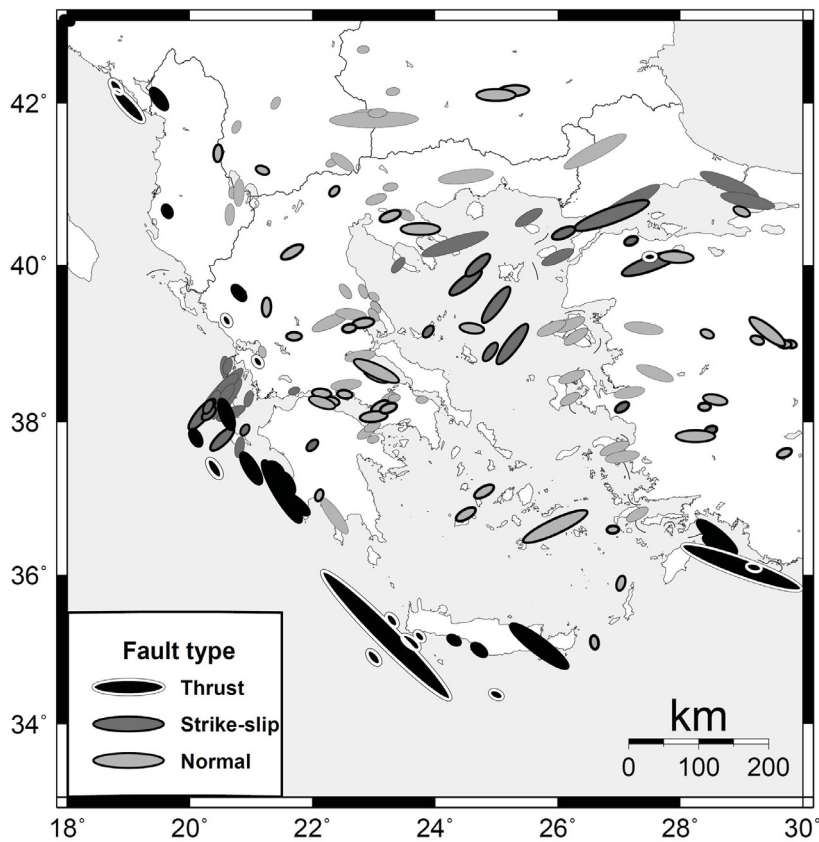


Fig. 1.8: The map of the rupture (fault) zones in the Aegean area as compiled by Papazachos *et al.* (1999).

From a geographic point of view, a more enriched and detailed study was the map of capable faults in Greece and the broader Aegean Region ([fig. 1.9](#)), compiled by Pavlides *et al.* (2007). A main difference to the previous compilations is represented by the fact that this map delineates in detail the scarps of all active faults with a clear morphological expression that meet one or more of the criteria concerning the identification of active faults, whether they are related with a known earthquake or not. The map, however, gives no other parametric information except the geographical one.

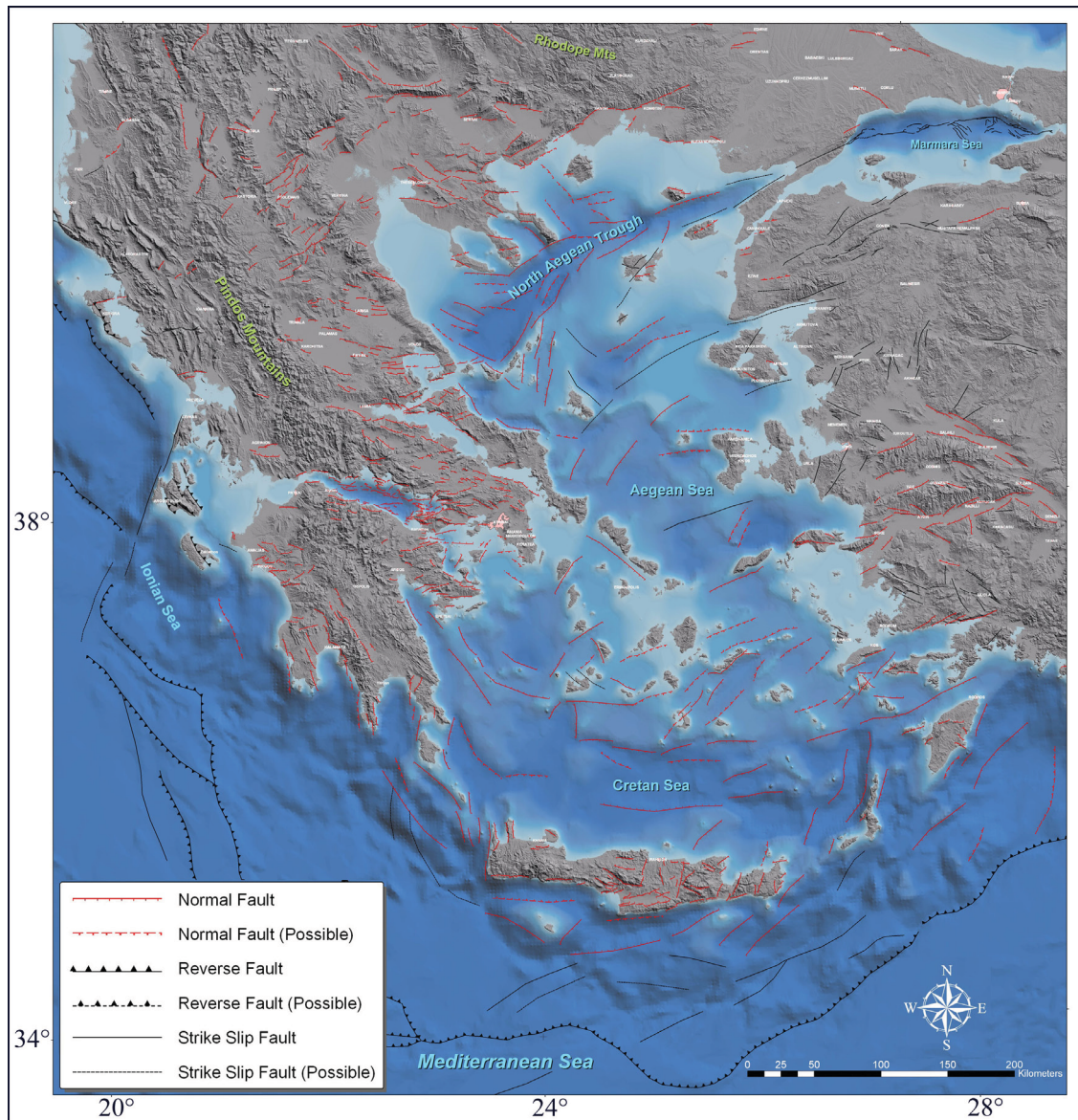


Fig. 1.9: The map of capable faults in Greece, as proposed by Pavlides *et al.* (2007).

More recently, Karakaisis *et al.* (2010) reassessed and enriched the previous seismologically-based compilations of Papazachos (1999; 2001a), while Mountrakis *et al.* (2006), using geological and seismological evidences, presented a review of the active faults of a limited sector of northern Greece (from Rhodope to West Macedonia; [fig. 1.10](#)). Like other

compilations, this is rather descriptive without containing any quantitative parametric information.

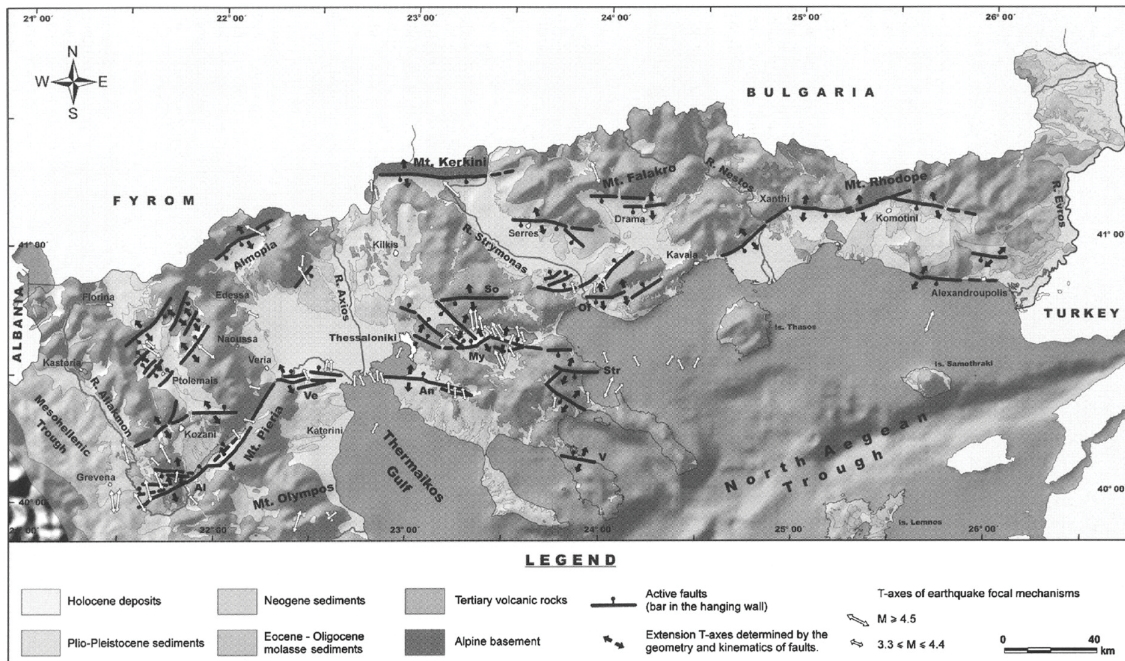


Fig. 1.10: The main active fault zones of North Greece (Mountrakis *et al.*, 2006). Al: Aliakmonas; An: Anthemountas; My: Mygdonia; Of: Ofirino; So: Sochos; Str: Stratoni; V: Vourvourou; Ve: Vergina.

It is obvious that in all previous works, crucial information was lacking, *e.g.* maps do not contain any other parametric data except of the geographic ones, while catalogues and compilations provide (and not always) only partial information, exclusively concerning some geometric and kinematic parameters.

1.5 GreDaSS: the birth of

Needs and Usage

Large earthquakes in Greece have attracted the interest of many researchers for two main reasons: *i)* for investigating the co-seismic rupture process and behaviour and the local secondary effects in order to contribute to the SHA of the region, and *ii)* for understanding the structure and the geodynamic process of the crust, usually for large-scale studies. Active faults are often studied individually or in a very regional scale. This causes two effects: firstly, data are scattered and sometimes “hidden” in various studies and secondly data are sometimes inconsistent when they derive from investigations carried out with different approaches and different authors. It is important thus, to have consistent and uniform information for all faults (location, geometry and kinematics) so as to be able to make a comparison between them at a regional scale.

The intensive and dense population of active faults has been a strong motivation for many scientists to perform different kinds of investigations, providing information that can be found in a large number of publications. After collecting all available information, the need came up for combining and organising these data in a unique environment that could contain both geographic and parametric information. The most modern and complete way to achieve this was to build a GIS-based database with a common set of formats, standards and methods that will be always updateable and could be placed in the public domain. Moreover, the database itself should be a useful tool for practical purposes, like SHA analyses and earthquake scenarios, and for scientific purposes, like building structural models or testing fault-based earthquake activity models against those based exclusively on smoothed seismicity. These goals are the primary targets of the recently set up Greek Database of Seismogenic Sources (GreDaSS).

General features

The GreDaSS is a continuously updatable open-file based on GIS software environment (MapInfo®). The overall database structure and informatics derive from the well tested, time-proven and worldwide acknowledged DISS proposed by the INGV, which represents the result of almost twenty years research experience of its Working Group (*e.g.* Valensise and Pantosti, 2001; Basili *et al.*, 2008). In the first stage, only shallow (crustal) tectonic structures have been considered, leaving the deeper structures of the Hellenic subduction for future investigations. Shallow structures are more important in terms of SHA since they are distributed all over the Aegean Region, close to and sometimes even directly affecting inhabited areas. Not only does GreDaSS contain and combine all kind of information that previous studies dealt with, but it also provides many basic and various levels of data that can be either independent or directly correlated.

Philosophical Approach

Initially, the GreDaSS was compiled with faults certainly or at least tentatively associated with historically and instrumentally recorded earthquakes ($M > 5.5$). For the historical period, all available catalogues for the broader Aegean Region were used (Ambraseys and Jackson, 1990; 1998; Guidoboni *et al.*, 1994; Papazachos and Papazachou, 1997; 2003; Guidoboni and Comastri, 2005; Ambraseys, 2001; 2009), while for the instrumental period, catalogues from the seismological networks of the Aristotle University of Thessaloniki (AUTH) (<http://geophysics.geo.auth.gr/ss/>; Papazachos *et al.*, 2000; 2009) and the Institute of Geodynamics (IG) of the National Observatory of Athens (NOA) (<http://www.gein.noa.gr/services/cat.html>) were also used. Scientific papers and internal reports focusing on single or few specific seismic events were also systematically analyzed.

The mostly investigated active faults are usually the ones related with large events that occurred during the past few decades, or in other words during the instrumental recording period. The quantity and quality of the recent seismological network and its instruments allow systematic analyses either of significant events or of microearthquake sequences. In particular, recent instrumental data commonly provide accurate constraints about the focal depth, magnitude, nodal planes and aftershock distributions and hence the geometry and kinematics of the source at depth. However, most of the seismological investigations provide information only for seismogenic sources that have been recently reactivated, leaving a huge gap to the

knowledge of fault activity for the pre-historical period. Furthermore, the incompleteness, ambiguity and lack of precision of historical events that are included in earthquake catalogues, especially for the very old ones (prior to the 19th century), make this gap even larger (Pavlidis and Caputo, 2004; Pavlidis *et al.*, 2007). Even for the instrumental period, which is not older than 100 years, accuracy started to be significant only after the 1970s when the Greek seismographic network was definitely improved. One typical example is the 1954, Sophades earthquake which was produced by a WNW-trending NNE-dipping fault according to geological investigations (Ambraseys and Jackson, 1990; Caputo, 1990; 1995; Pavlidis, 1993) and not by a N-S up to NW-SE-trending plane as suggested by the focal mechanism proposed by McKenzie (1972).

Following the discussion above, it is obvious that observations and data collection for the creation of a database of seismogenic sources cannot be limited to the analysis of instrumental or historical events. But probably the most important reason for searching alternative and complementary investigation approaches is due to the fact that a recently reactivated fault (*i.e.* a fault that has generated an instrumental or historical event) is unlikely to be reactivated again in the near future. In contrast, tectonic structures which can be geologically recognized as active (especially without instrumentally or even historically documented activity) might be mature enough to rupture in the next future as suggested, for example, for Northern Thessaly (Caputo, 1995). For the finalities of any serious SHA estimate, the degree of maturity of an active fault in the frame of its seismic cycle certainly represents the most crucial aspect. Two characteristic examples can be referred for Greece. The first is the 1995 Kozani earthquake that occurred in Western Macedonia, an area considered as a typical 'aseismic' or 'low seismicity' block (Voidomatis, 1989; Papazachos, 1990) exactly due to the lack of seismicity. The second is the 1999 Athens earthquake that occurred on the borders of the metropolitan city of Athens and caused many damages and human losses. This area was also considered as one of low seismic activity, given that important historical or instrumental seismic records were missing (Papadimitriou *et al.*, 2002; Pavlidis *et al.*, 2002). Both cases clearly show that seismicity, as a stand-alone tool for appreciating the seismic hazard, is certainly inadequate.

In order to examine this issue and show the importance of the geological data, the seismotectonic information is described and discussed, that can be obtained from the analysis of *single-event effects* with those obtained from *cumulative effects* of multiple co-seismic reactivations. The distinction between the two types of *sources of information* is not only a terminological issue but mainly a methodological one implying that the investigation tools used in the two cases are generally different (Caputo and Helly, 2008). Indeed, *single-event effects* are inherently associated with the re-activation of a fault mainly in historical and/or instrumental times, while all observations focus on, and are limited to, the specific co-seismic effects and associated features. Accordingly, commonly applied investigation methods are seismological studies, epicentral area surveys, palaeoseismological trenching, critical analysis of oral and/or written witnesses (historical seismology), investigations on 'disturbed' artefacts, like buildings and settlements (Archaeoseismology), geodetic surveys and DinSAR analyses (Caputo and Helly, 2008). It is obvious that all these methodological approaches have significant time constraints for their application because most of the investigations rely on technologically sophisticated instruments (seismographs, satellite products *etc.*) while surficial evidences (*e.g.*

co-seismic ground ruptures) are highly vulnerable to weathering and erosion and quickly fade away.

Conversely, *cumulative effects* represent all the evidences that derive from multiple and repeated fault reactivation(s) during the Quaternary. Investigating methods include several typical geological approaches (morphotectonic surveys, structural mapping, stratigraphic and pedological analyses, palaeoseismological trenching, *etc.*), remote sensing analyses of air photos and satellite imageries and several geophysical methods (electrical resistivity tomographies, ground penetrating radar, seismic profiles, microearthquake surveys, *etc.*).

From a practical point of view, the major difference between the two approaches is that a historically or instrumentally recorded earthquake generally makes evident the occurrence of a fault, therefore already addressing the scientists to investigate a specific structure making specific *single-event effects*-based observations. In contrast, most active faults not associated with recent strong events, need to be firstly recognised in the field and then investigated following a *cumulative effects*-based approach. A similar theoretical and practical distinction between *sources of information* and corresponding investigation approaches has been applied by Caputo *et al.* (2008), when analysing the magnitude distribution of 'linear morphogenic earthquakes' within the Mediterranean Region.

The reliability of both *single-event effects*-based and *cumulative effects*-based investigation methods is discussed in [chapter 6](#), after the presentation of the database's contents.

1.6 Aims and expected results

Completing the GreDaSS is a work that needs both dedication and multitasking. The time constrain of the Ph.D. programme is substantial for fully completing all recognized seismogenic sources of North Greece, but not sufficient for reaching the highest level of completeness for the whole Aegean Region. This can be expected if it is compared with other worldwide databases. In more particular, despite the time needed for the software development, the four databases mentioned before count at least one decade of dedicated work so as to reach a high level of completeness, a task usually performed by large groups of researchers and scientists, even though there was an already existing background in some cases. A second issue that should be considered is the high density of active faults in the Aegean which comes in contrast with the small number of the well investigated seismogenic sources. It is consequential that highly technologically advanced countries, like the US and Japan, can afford sophisticated equipment and large budgets for dedicated investigations, explicitly providing large amount and variety of data.

Taking into account the difficulties described above, the expected results concerning the GreDaSS development are *i)* to reach the highest level of completeness both in terms of seismogenic sources occurrence and included information for North Greece, and *ii)* to achieve the geographic representation of the majority of the existing faults for the rest of the Greek territory, including also at least a basic level of available information.

By accomplishing these two targets, data and information that were previously scattered and sometimes hidden among a large number of literature material will be homogenized and grouped. As a result, the direct comparison of the seismogenic sources will be available in local as well as in regional scale. Based on these outcomes, the database could reveal common similarities and/or differences that can be used for seismotectonically or geodynamically characterizing different areas or volumes. In any case, the database can be also a very useful tool for SHA analyses. The GreDaSS will be hopefully used for modifying and improving the current national seismic zonation map of Greece (Papaioannou and Papazachos, 2000), which strongly relies only on seismological data.

However, during the description of the database development, some issues will be assessed concerning the generally missing parametric data, such as the seismogenic layer thickness (related to the maximum fault depth; [chapter 3](#)) and slip rate ([chapter 4](#)). Moreover, by the end of the description of the seismogenic sources of GreDaSS for North Greece ([chapter 5](#)), the two *sources of information* (*single-event effects*-based and *cumulative effects*-based approaches) will be available for comparison ([chapter 6](#)), in order to define the confidence of the provided data and their calibration if needed.

2.1 Methodology

In order to develop a database of seismogenic sources, there are two basic steps that should be followed: first, all active faults affecting a specific region should be recognized, and second, each seismogenic structure should be seismotectonically parameterized. Both steps require systematic search and collection of all available literature data either published as papers or unpublished (*e.g.* reports, personal communications, *etc.*). Collected data are investigated through a critical revision before entering the multi-parametric fields of the database. For structures with ambiguous or lacking data, and for missing parameters, original investigations have been carried out as well, and further will be performed in the future.

A common practice for recognising seismogenic sources is to start analyzing the historical and instrumental seismicity affecting the specific area, especially in regions like the Aegean where earthquake catalogues cover a very long time period (*ca.* 2500 years) and are particularly rich and relatively complete for at least major events. In particular, major events are systematically taken into account and are tentatively associated with the likely causative faults. Following the discussion of the 'philosophical' approach in §1.5, active faults not related with any historically and instrumentally recorded earthquake must be recognised as well. This task requires a more detailed analysis of the available investigations in order to define whether faults qualify for being active based on the criteria described in the first chapter.

However, before entering into more details about the input and the parameterization procedure of the seismogenic sources, it would be better to have a summarized and condensed description of the GreDaSS structure and the environment in which the end-user will navigate the database.

2.2 The seismogenic sources

According to Basili *et al.* (2009), the seismogenic sources are divided into three main types: the *Individual Seismogenic Sources* (ISSs), the *Composite Seismogenic Sources* (CSSs) and the *Debated Seismogenic Sources* (DSSs). Their description below has been slightly modified to match better the philosophy of GreDaSS.

- The “*Individual Seismogenic Sources*” (ISSs) are obtained from geological and geophysical data and are characterized by a full set of geometric (strike, dip, length,

width and depth), kinematic (rake, average displacement per event) and seismological parameters (, magnitude, slip rate, return period). ISSs are assumed to exhibit “characteristic” behaviour with respect to rupture length/width and expected mean and maximum magnitude. They are tested against worldwide databases for internal consistence in terms of length, width, average displacement and magnitude. Moreover, ISSs can also be considered as fault segments of larger fault zones when there are evidences of individual rupture. This means that in case of earthquake-related seismogenic sources, more than one segment can be considered as the causative fault. However, to identify if a fault array is open, linked or fully breached (terms after Soliva and Benedicto, 2004) is a difficult and complicated task, based sometimes on expert judgement when data are either lacking or are poor. The ISSs favour accuracy of the information supplied over the completeness of the sources themselves. As such, they can be used for deterministic assessment of seismic hazard, for calculating earthquake and tsunami scenarios, and for tectonic and geodynamic investigations.

- The “*Composite Seismogenic Sources*” (CSSs) are also obtained from geological and geophysical data and characterized by geometric (strike, dip, width, min/max depth) and kinematic (rake) parameters, but their sliding surface geometry is more loosely defined and can contain an unspecified number of ISSs. They are not assumed to be capable of a characteristic earthquake but their potential can derive from existing earthquake catalogues or other geological considerations. A CSS is essentially inferred on the basis of regional surface and subsurface geological data that are exploited well beyond the simple identification of active faults or youthful tectonic features. Opposite to the previous case, this category of sources favours completeness of the record of potential earthquake sources over accuracy of source description. In conjunction with seismicity and modern strain data, CSSs can thus be used for regional probabilistic seismic hazard assessment and for investigating large-scale geodynamic processes. A CSS can represent a large fault zone which can consist of one or more well defined ISSs. However, it can also be ‘empty’ of ISSs if none can be recognized. The seismic behaviour of the CSSs can be completely independent for the ISSs, given that a potential event may rupture the total length of the source, whether it contains none, one or more ISSs. Like discussed in the ISSs description above, predicting the rupture behaviour is not straightforward and many times is based on expert judgement.
- The “*Debated Seismogenic Sources*” (DSSs) can be considered as potential seismogenic sources that contain large uncertainties and ambiguities. Ambiguities may concern the degree of activity of the source, or to put it differently, sources that barely follow the criteria of active faults. Additionally, uncertainties may involve the exact position and size of a source, the lack of literature support, the contradictions of literature information and the absence of most parametric data.

The styles (shape, colours, *etc.*) with which all three categories of seismogenic sources are graphically shown in the database are different in each case, but they are always based on the concept of a 3D perspective ([fig. 2.1](#)). A short description follows also based on the INGV’s technical report (Basili *et al.*, 2009).

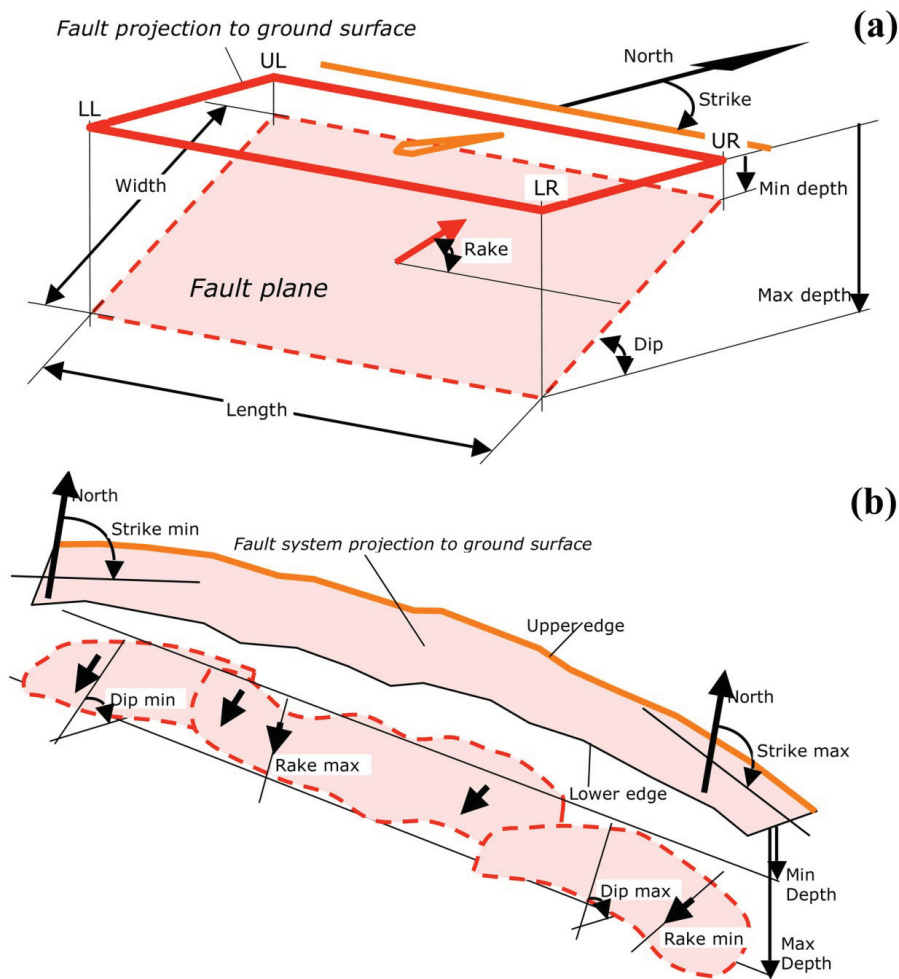


Fig. 2.1: Schematic representation of an ISS (a) and a CSS (b). For further explanations see the text. After Basili *et al.* (2009).

The ISSs are represented by a rectangular (polygon) with a vector located in its central part (fig. 2.1a). The rectangular is the vertical projection of the fault plane on the earth's surface. That means that one parallel pair of its sides represents the top and the bottom edge of the plane and therefore the fault length, while the other pair delimits the down-dip dimensions and equals to the width of the fault. The top edge coincides with the fault trace if the fault is emergent. On the contrary, if the fault is blind, a line parallel to the top edge appears as the section between the hypothetical continuation of the fault plane and the ground surface. The vector inside the rectangular represents the slip vector of the fault's motion.

The CSSs do not follow the strict rules of the ISSs, although their 3-D visual concept is similar (fig. 2.1b). Due to their capability of containing several ISSs (fault segments) and their data incompleteness, the shape of the CSSs is looser. The produced polygon has again two roughly parallel long sides corresponding to the top and bottom edges of the fault plane, and two short lines parallel to the width. The top edge is drawn with a thicker line which does not necessary reflects a surficial trace when it is about blind faults. Conversely, when the fault reaches the surface, the top edge smoothly follows the fault traces or scarps.

The DSSs are even looser in shape reflecting the lack of any data and information. The approximately rectangular shape of the DSSs is placed with the one roughly parallel side (top edge) along the ambiguous fault trace.

It is noteworthy to mention that the representation of the fault plane as an absolute geometric shape, especially in the case of the ISSs, does not accurately reflect nature's complexity. A rectangular shape is preferred because *i)* it is the simplest way to graphically plot the strictly constrained geometric parameters, and *ii)* it can easily be distinguished and understood, especially due to its 3-D perspective. However, two different scientific views exist about the shape that faults should have. Examples from 3-D seismic analysis and analogue modelling show that large-scale faults have a 'rough' rectangular shape (*e.g.* Childs *et al.*, 1995; Guglielmo *et al.*, 2000; Marchal *et al.*, 2003). On the contrary, an elliptical geometric shape is proposed by other authors for single isolated faults (*e.g.* Rippon, 1985a; 1985b; Watterson, 1986; Barnett *et al.*, 1987; Walsh and Watterson, 1987; 1991; Nicol *et al.*, 1996). Comparing the two different aspects about the fault plane shape, Benedicto *et al.* (2003) suggest that the architecture and physical properties of large crustal faults depend on the mechanical heterogeneity of the stratigraphic sequence, as well as on the seismogenic layer thickness.

Beyond the three main categories of seismogenic sources, there is also a supplementary layer of information (geographic and parametric) which can be directly connected with either ISSs, or CSSs, or both. The “*Active faults and folds*” (AFF) layer contains the morphological expression of the sources. Although it has not get equal attention in technical development like it has happened with the main categories, an effort has been made in GreDaSS to input fault scarps, which are the typical features of normal faults within the Aegean region (Caputo *et al.*, 2008).

2.3 Navigating GreDaSS

The end-user can navigate the database in a web browser ([fig. 2.2](#)) or in GoogleTM Earth ([fig. 2.3](#)). The standalone developers' interface, hosted by the MapInfo[®] software, has a similar navigating concept ([fig. 2.4](#)). The discussion that follows is a mixed description of both web- and developers'-based environments.

By opening the first webpage (homepage) of GreDaSS in a web browser ([fig. 2.2](#)), the user sees two frames. The main one (map frame) contains a pre-set map of the developer's choice (*e.g.* plain geographic map, shadow relief, *etc.*) and the features/objects (vector information) or images (raster information) that the user has selected to be visible in the other frame; all seismogenic sources are visible by default. The second frame, placed next to the map frame, consists of the main toolbox and the layers/objects list. The toolbox holds the necessary tools that allow the map navigation and the layers list that gives the ability of deciding which layers should be selectable and/or visible.

Except the default map-view, several sets of topographic, geological or any other available raster rectified thematic maps can be used. If any of the features is in vector format (*e.g.* rivers, cities, roads, *etc.*), then it can easily be set as visible and/or selectable from the main toolbox. Many useful additional vector data can be loaded, such as seismic catalogues. By choosing the

identifier tool and clicking on any object of our interest, a corresponding information window pops out.

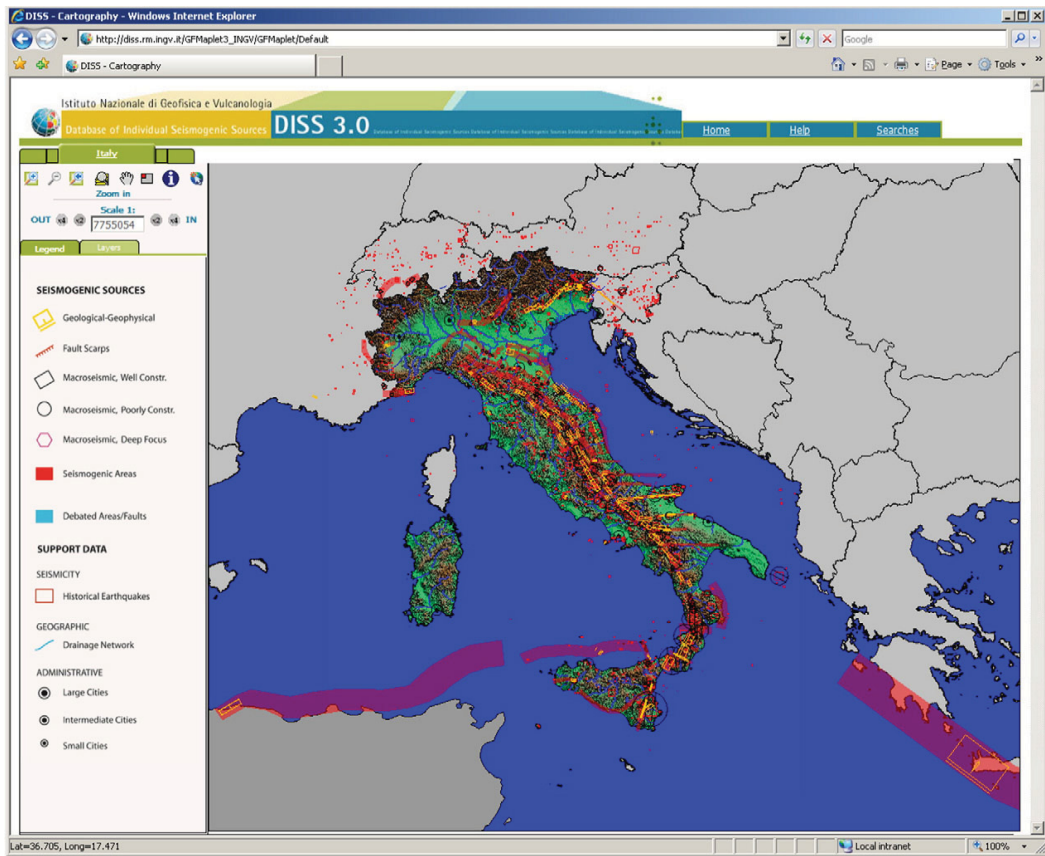


Fig. 2.2: Example from the web interface for Italy, based on ArcIMS GIS engine (Basili *et al.*, 2008). The main map frame is at the right side of the image. At the left side, the frame with the map navigation tools and the layer list is shown.

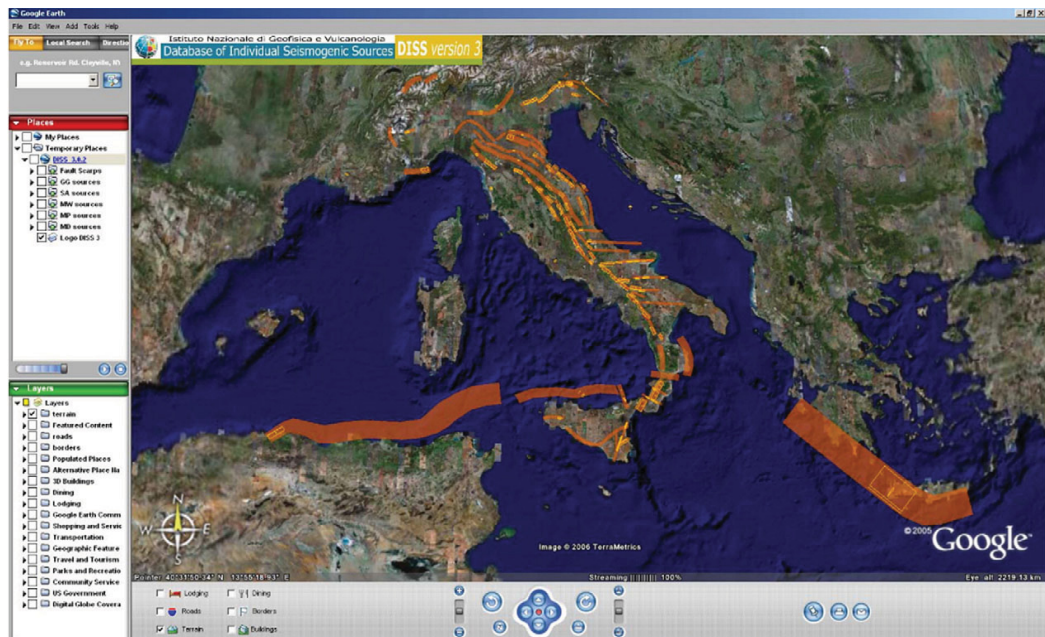


Fig. 2.3: Example from the GoogleTM earth interface for Italy (Basili *et al.*, 2008).

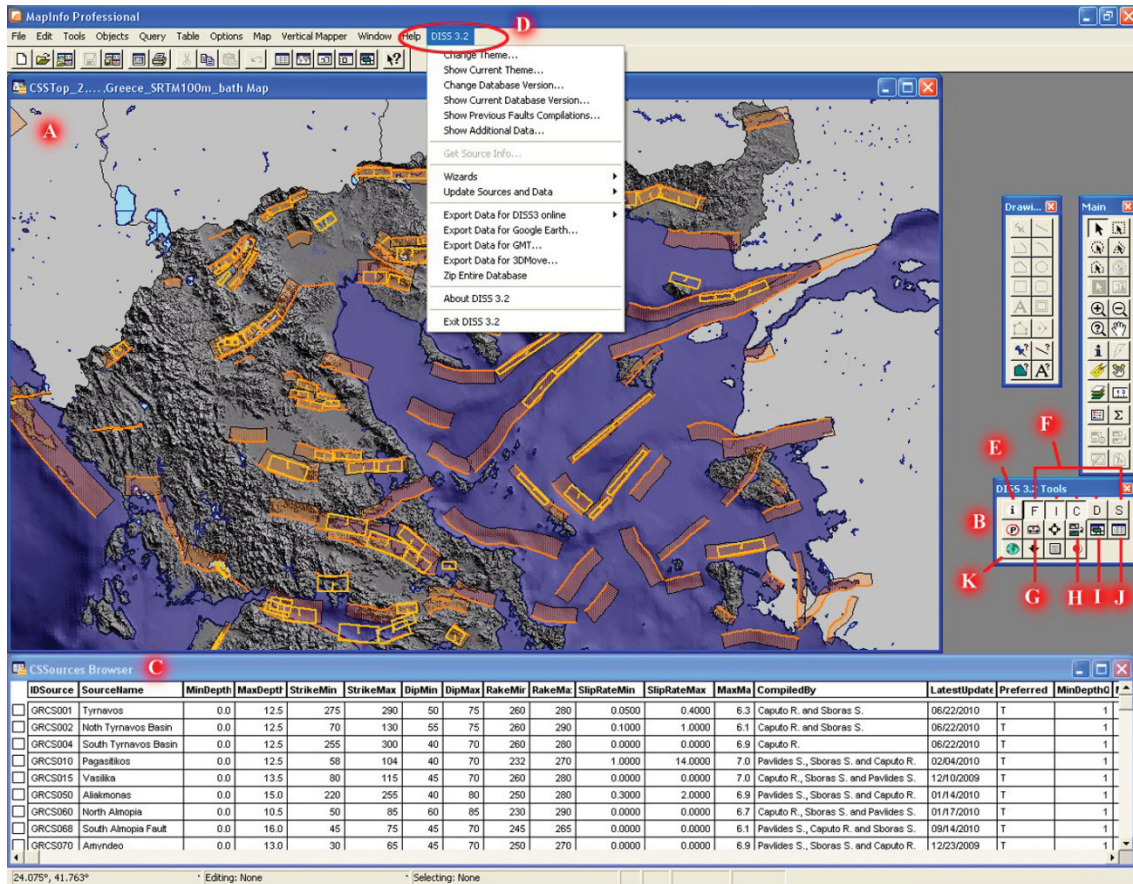



Fig. 2.4: The standalone developers' interface is hosted by the MapInfo® GIS software. The red ellipsis with the letter D shows the menu of the DISS 3.2 extension with the primary commands in the main toolbar of MapInfo®. The rest main features are the map window (A), the floating toolbox (B) and the browser window (C). The rest letters are explained in the text.

In both web browser and MapInfo®, the properties of a seismicogenic source (ISS, CSS or DSS) can be obtained by clicking on the object with the identifier tool (e.g. E in fig. 2.4). Then, a new web browser window pops out (information window) containing four different levels of metadata separated in to four html subpages. The informational window is similar for both ISSs and CSSs metadata. Only the DSSs window differs because of their lacking information. Starting from the main page of the informational window of both ISSs and CSSs, the four metadata pages are (fig. 2.5):

- i. **“Source Info Summary”**: this page contains the principal parameters (fig. 2.5a), which are the *“General information”* (Code, Name, Compilers, Contributors, Latest update date), the *“Parametric information”* (all geometric, kinematic and seismotectonic information) and the *“Associated earthquake”* (for ISSs only; latest and penultimate events that are associated with the specific source). Every parametric or seismic information is complemented by *qualification keys* that will be explained later and short comments (*“evidence”*) about the origin of the data (e.g. if data derive from morphotectonic mapping, focal mechanisms, etc.).
- ii. **“Commentary”**: this page contains three sections (fig. 2.5b): the *“Comments”*, *“Open Questions”* and *“Summaries”*. The first one contains comments that can help to

better describe the source, for instance, more details about the data acquisition, its interaction with adjacent faults, its seismotectonic behaviour, *etc.* Whichever parameter remains doubtful, or if there is a conflict between literature data, or if there are implications for the general seismotectonic behaviour, then these comments address to the *open questions*. The Summary includes all information relative to the source that can be extracted from the available literature. The strongest feature of the latter is that the user can get information from literature that was not preferred for the specific source, being able thus to make his own decision.

- iii. **“Pictures”**: the third page encloses in all pictures, images, figures and maps relative to the source and can be from both literature and original collections ([fig. 2.5c](#)).
- iv. **“References”**: in the last page the list with all the related literature used for the source is hosted ([fig. 2.5d](#)). If the literature (journal papers, reports, maps, *etc.*) exists in electronic version and more particular in portable document format (pdf), then a respective icon appears and the document can be available for viewing.



DISS 3.2.Complete: Seismogenic Source GRIS050 - Palaeochori Fault

a

[Source Info Summary](#)
[Commentary](#)
[Pictures](#)
[References](#)

General information

Code	GRIS050
Name	Palaeochori Fault
Compiled By	Sboras S.P.(1)
With contributions from	Pavlidis S.(2), Caputo R.(1)
Latest Update	10/01/2010

Parametric information

Parameter	Qual. Evidence
Location (Lat/Lon)	40.0857 / 21.6684 LD many geological and morphotectonic maps
Length (km)	21 LD many geological and morphotectonic maps
Width (km)	18 AR derived from other parameters (dip, minimum and maximum depth)
Min Depth (km)	0 LD direct field observations (several authors)
Max Depth (km)	14.7 EJ inferred from aftershock spatial distribution (Hatzfeld et al., 1997; 1998)
Strike (deg)	246 LD based on geological data (several authors)
Dip (deg)	55 EJ inferred from aftershock spatial distribution and geological data (several autho
Rake (deg)	255 LD based on kinematic indicators (several authors)
Slip Per Event (m)	0.57 ER estimated from multiple empirical relationships
Slip Rate (mm/y)	0.3 - 0.3 LD estimated from cumulative displacement (Doutsos and Koukouvelas, 1998)
Recurrence (y)	2000 - 30000 LD estimated from cumulative displacement and palaeoseismological data (several aut
Magnitude (Mw)	6.6 ER based on empirical and analytical relationships (various authors)

Q-keys: LD = Literature Data; OD = Original Data; ER = Empirical Relationship; AR = Analytical Relationship; EJ = Expert Judgement

Associated earthquake

Latest Eq	1995/05/13	Mw=6.5 event produced by two fault segments
Penultimate Eq	7000 BC	thermoluminescence dating of palaeoseismological data (Chatzipetros et al., 199
Elapsed Time	5	as of year 2000 (assigned datum)

Affiliations
 1) Università di Ferrara; Scienze della Terra; Via Saragat 1, 44100 Ferrara, Italy
 2) Aristotle University of Thessaloniki; Geology; 54124 Thessaloniki, Greece

Fig. 2.5: The main four pages containing information about the ISSs. **(a)** The Source Info Summary contains general information and important parameters. **(b)** The Commentary contains important comments, open questions and the summaries of relative literature. **(c)** The Pictures contains all relative figures, maps, photos *etc.* By clicking the desired photo a new window pops out with the picture and the caption. **(d)** The References contains all published data related to the specific source.

DISS 3.2.Complete: Seismogenic Source GRIS050 - Palaeochori Fault

Source Info Summary Commentary Pictures References

COMMENTS

The Palaeochori Fault is the westernmost segment of a larger fault zone, the Aliakmonas CS (GRCS050). The fault was reactivated along with the Rymnio Fault segment (GRGG051) during the May 13, 1995 Kozani earthquake. An old strike slip antithetic structure, the Chromio Fault (GRGG053), was also reactivated as a dip-slip fault according to spatial aftershock distribution (Hatzfeld et al., 1997; 1998; Resor et al., 2005) and field observations showing co-seismic surface ruptures (Pavlidis et al., 1995; Mountrakis et al., 1998; Doutsos and Koukouvelas, 1998). Although many studies refer to the co-seismic results of the event, very few things were known before. According to morphotectonic mapping and field observations from many authors before and after the event, the fault was not very clearly exposed on surface in contrast with the prominent easternmost Servia segment (GRGG052) which however was not reactivated at all. The co-seismic ground ruptures followed most of the fault scarps filling occasionally the gaps between the branches. Strike, length and rake are based on morphotectonic mapping and field observations from Pavlidis et al. (1995) and Mountrakis et al. (1998). Maximum depth is inferred from spatial aftershock distribution of the May 13, 1995 after Hatzfeld et al. (1997; 1998). It is largely accepted that the dip of the fault plane is relatively steep between surface and 9 km depth and progressively decreases in its deeper parts section (Mountrakis, et al., 1998; Meyer, et al., 1996; Drakatos, et al., 1998). The average dip is inferred from geological data (Pavlidis et al., 1995; Mountrakis et al., 1998) and the aftershock spatial distribution (Hatzfeld et al., 1997; 1998). Slip per event and Mw are based on analytical and empirical relationships (Kanamori and Anderson, 1975; Hanks and Kanamori, 1979, Wells and Coppersmith, 1994).

OPEN QUESTIONS

There is ambiguity about the fault's horizontal extension at both ends and the possible connection with other adjacent faults. Some authors (Meyer et al. 1996 and 1998; Hatzfeld et al., 1997, 1998; Chiarabba and Selvaggi, 1997; Goldsworthy and Jackson, 2001) suggest that the Palaeochori Fault is a parallel branch or a northward migration of the Deskati Fault, which is located 12 km southwards, and that the two structures join in depth. However, all authors agree on the lack of any evidence for the re-activation of the Deskati Fault during the 13 May, 1995 earthquake. There is also a suggestion by Doutsos and Koukouvelas (1998) that fault activity migrates westwards.

SUMMARIES

Mountrakis et al. (1995; 1996; 1998)

According to the authors, the total length of the fault segment is about 30 km and the dip is steeper at the surface than at depth. They suggest the occurrence of a geometrical segment boundary near the village of Goules associated with a right-stepping geometry with a small change in strike and separating the re-activated fault from the Servia Fault segment. Additionally, a series of sub-parallel antithetic surface fractures mainly striking E-W or ENE-WSW and south dipping were produced during the earthquake. These co-seismic ruptures follow older strike-slip faults but behave as normal ones antithetic to the principal seismogenic fault. The most important of these structures is the Chromio Fault which was partly. The authors divide the main activated fault into two segments: The Palaeochori and

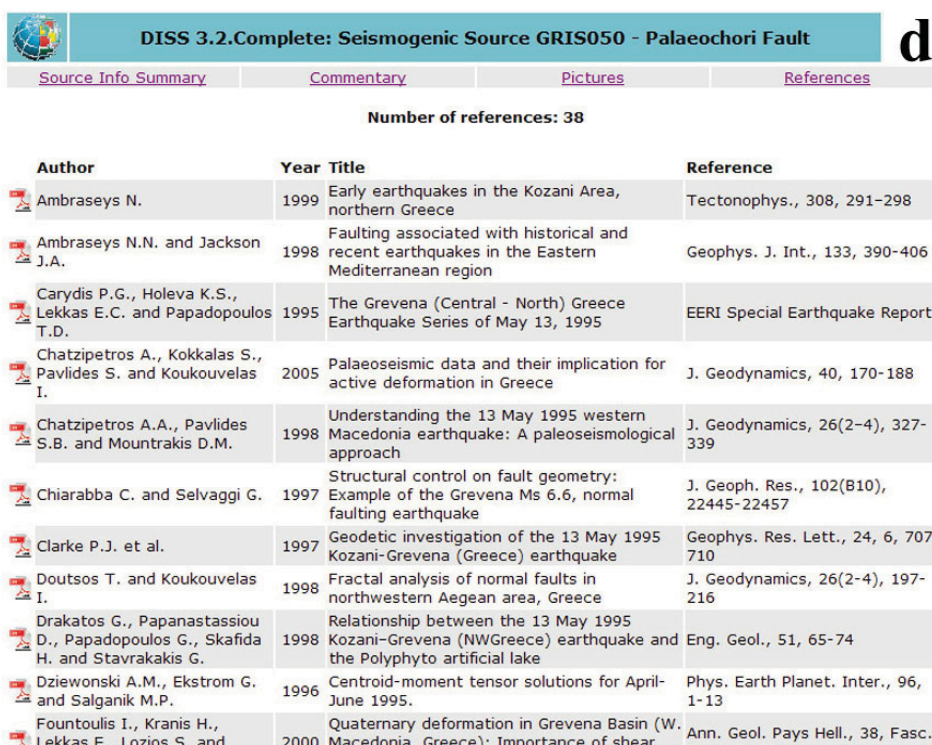
DISS 3.2.Complete: Seismogenic Source GRIS050 - Palaeochori Fault

Source Info Summary Commentary Pictures References

Number of pictures: 28

Picture	Title
Figure 01	- Tectonic sketch map of the Aliakmonas Fault Zone showing the epicentres of the 1995, Kozani event and the coseismic ruptures
Figure 02	- Structural map of the Aliakmonas Fault Zone showing also the coseismic ruptures of the 1995, Kozani event
Figure 03	- Geologic-tectonic map
Figure 04	- Focal mechanism of the main shock of the May 13, 1995 Kozani earthquake and structural analyses from slickensides
Figure 05	- Map of main shock and aftershock distribution of the 13 May 1995 event
Figure 06	- Vertical aftershock distribution of the 13 May 1995 event
Figure 07	- Fault model derived from earthquake tomographies and aftershock distribution
Figure 08	- Fault model and surface displacement using InSAR
Figure 09	- Fault model derived from tomography and InSAR
Figure 10	- Fault model derived from tomography and InSAR
Figure 11	- Fault model derived from tomography and InSAR
Figure 12	- Experimental model for the Palaeochori Fault
Figure 13	- Horizontal site displacement section of the model fault
Figure 14	- Palaeoseismological trench sketch on the Palaeochori fault segment
Figure 15	- Morphology and drainage
Figure 16	- Fault-drainage map and DEM
Figure 17	- Seismic moment distribution
Figure 18	- Displacement distribution
Figure 19	- Isoseismal map of 1995
Figure 20	- Accelerograms of the event
Figure 21	- Photograph of the fault
Figure 22	- Photographs of a ground rupture
Figure 23	- Photograph of the fault
Figure 24	- Fault and aftershock distribution
Figure 25	- DEM with aerial photographs
Figure 26	- Panoramic photograph
Figure 27	- Photographs on fault's cross section

Fig. 2.5: continued



Author	Year	Title	Reference
Ambraseys N.	1999	Early earthquakes in the Kozani Area, northern Greece	Tectonophys., 308, 291-298
Ambraseys N.N. and Jackson J.A.	1998	Faulting associated with historical and recent earthquakes in the Eastern Mediterranean region	Geophys. J. Int., 133, 390-406
Carydis P.G., Holeva K.S., Lekkas E.C. and Papadopoulos T.D.	1995	The Grevena (Central - North) Greece Earthquake Series of May 13, 1995	EERI Special Earthquake Report
Chatzipetros A., Kokkalas S., Pavlides S. and Koukouvelas I.	2005	Palaeoseismic data and their implication for active deformation in Greece	J. Geodynamics, 40, 170-188
Chatzipetros A.A., Pavlides S.B. and Mountrakis D.M.	1998	Understanding the 13 May 1995 western Macedonia earthquake: A paleoseismological approach	J. Geodynamics, 26(2-4), 327-339
Chiarabba C. and Selvaggi G.	1997	Structural control on fault geometry: Example of the Grevena Ms 6.6, normal faulting earthquake	J. Geoph. Res., 102(B10), 22445-22457
Clarke P.J. et al.	1997	Geodetic investigation of the 13 May 1995 Kozani-Grevena (Greece) earthquake	Geophys. Res. Lett., 24, 6, 707-710
Doutsos T. and Koukouvelas I.	1998	Fractal analysis of normal faults in northwestern Aegean area, Greece	J. Geodynamics, 26(2-4), 197-216
Drakatos G., Papanastassiou D., Papadopoulos G., Skafida H. and Stavrakakis G.	1998	Relationship between the 13 May 1995 Kozani-Grevena (NWGreece) earthquake and the Polyphyto artificial lake	Eng. Geol., 51, 65-74
Dziewonski A.M., Ekstrom G. and Salganik M.P.	1996	Centroid-moment tensor solutions for April-June 1995.	Phys. Earth Planet. Inter., 96, 1-13
Fountoulis I., Kranis H., Lekkas E., Lozios S. and	2000	Quaternary deformation in Grevena Basin (W. Macedonia, Greece): Importance of shear	Ann. Geol. Pays Hell., 38, Fasc.

Fig. 2.5: *continued*

Only small differences exist between the parametric information of ISS and CSS, because the former are more complete and well defined sources by definition. Thus, while the ISSs have a unique value of geometric and kinematic parameters, the CSSs use a range of values. Moreover, the CSSs cannot be directly associated to any well known earthquake because in this case an ISS would be the appropriate type of source.

2.4 The parameters

Before describing the database development, the parametric fields should be defined and qualitatively described. Due to the small differences between the ISSs and CSSs, the description will start with the former, taking into account the completeness and precision needed. The DSSs are excluded, since they lack data. Besides the definition and description of the parameters, the procedure and general criteria will also be discussed that are used for the best data acquisition and selection in the Aegean seismotectonic realm.

Individual Seismogenic Sources (ISSs)

- **Location [degrees]:** it corresponds to the coordinates of the centre of the object/source, or in simpler terms, the fault's location on the map. It is calculated automatically once it is drawn on the map.

Acquisition: when the fault is onshore, whether it is related or not with historical/instrumental seismicity, location is largely based on morphotectonic and geological mapping. Almost all crustal structures in the Aegean Region have a more or less clear fault trace allowing thus a detailed cartographic reconstruction. Pavlides and Caputo (2004) conclude that, for the broader Aegean Region, the minimum magnitude for an earthquake associated with crustal normal faulting and capable to produce a 'linear seismogenetic feature' (*sensu* Caputo, 2005) is around 5.5. For the offshore faults, detailed bathymetric maps and seismic profiles are generally used for recognizing a fault scarp and displacement at depth. Also the occurrence of seismicity, both micro- and major earthquakes, help constraining the location of active faults especially for multi-segmented CSSs.

- **Length [km]:** it corresponds to the length the fault plane. A unique value is required.

Acquisition: if a seismogenic source is well documented on Earth's surface, length is mainly measured on the basis of field mapping. Due to its simple geometry, length in ISSs coincides with the upper fault tip, while for the CSSs the value is measured along the smoothed fault trace. In case of earthquake-related faults, the length can be also estimated from various empirical relationships, like magnitude *versus* surface fault length (*e.g.* Wells and Coppersmith, 1994; Pavlides and Caputo, 2004). The latter procedure is usually followed for the offshore ISSs, where direct observations are not possible for capturing the entire rupture length. Nevertheless, the CSS length can be well inferred from the sea-floor morphology based on swath bathymetry or high-resolution seismic reflection profiles.

- **Minimum depth [km]:** it is the depth of the fault's top edge from the ground surface or the sea floor. It is important to mention that DISS uses a different reference level for this parameter (zero value corresponds to the mean sea level). A unique value is required.

Acquisition: like mentioned before, all continental faults affecting the Aegean Region and capable of generating moderate to strong ($M > 5.5$) events commonly reach the surface. Accordingly, this value is generally set to zero. However, for few exceptions minimum depth can only be obtained from geophysical (*e.g.* seismic reflection profiles) or seismological methods (*e.g.* microseismic spatial distribution).

- **Maximum depth [km]:** it is the depth of the bottom edge of the fault plane from the surface, generally reflecting the brittle-ductile transition (BDT) zone (Sibson, 1982; Meissner and Strehlau, 1982) and hence the seismogenic layer thickness. In most cases, it cannot be directly entered, but it can be automatically computed by the software using a trigonometric relationship involving width, dip-angle and minimum depth, and has a unique value.

Acquisition: defining maximum depth is not always straightforward. It can be estimated from microseismic or aftershock spatial distribution. Accuracy, however, is not very high and depends also on the density and general architecture of the seismographic network. Even in the best conditions, errors of 1-2 km in depth are the rule. For inferring this parameter, we focus on the deepest seismic clusters, though deeper isolated events are usually ignored. Nevertheless, these data are

generally rare and cover only few areas of interest. In order to apply a uniform estimation of the seismogenic layer thickness for the rest cases, and consequently of the BDT zone, strength profiles will be calculated and tested in this thesis. Both procedure and results will be discussed in the next chapter.

- **Width [km]:** it is the distance between the top and bottom edges of the fault plane. A unique value is required.
Acquisition: width is adjusted in such a way that the desired maximum depth is achieved, which is usually easier to be defined (see the corresponding parameter discussed before). Alternative methods for estimating width, based for example on empirical relationships, are less used because of their larger uncertainty.
- **Strike [degrees]:** it has no difference with the definition of fault's strike. Values belonging to the eastern semicircle (0-180°) have a dip direction (plunge) inside the southern semicircle (90-270°), while values belonging to the western semicircle (181-360°) have a dip-direction inside the northern semicircle (271-90°). Again, a unique value is required.
Acquisition: for onshore faulting, similar criteria to the location parameter are used. However, for offshore – and not only – sources, the nodal planes suggested by focal mechanisms, usually of a major event, play an important role in determining the strike of a seismogenic source. Sometimes they can even be the only evidence. Also in this case, the availability of very detailed bathymetric maps and/or serial high-resolution seismic profiles has been demonstrated useful for the purpose.
- **Dip [degrees]:** it is the dip-angle of the fault plane. The database requires a unique value representative of the whole plane and which directly affects the maximum depth parameter.
Acquisition: information for the dip-angle is usually hard to find; a puzzling restriction is the assumed planar geometry of the fault, which is in contrast with the listric shape of many normal faults. In this case, a compromise between surface structural measurements and the setting of the focal planes at depth is considered. For the offshore ISSs, the same method is followed, but instead of field measurements, seismic profiles can be used. The most reliable evidences come from microearthquake investigations (when available), from which the fault surface can be sometimes easily delineated. An alternative way for estimating dip would be the simple trigonometric relationship between the hypocentral location and the nearest point of the fault's surficial expression. Large errors of the hypocentral location though, produce large errors in dip; thus, this procedure is generally avoided. However, if none of the above information sources exists but there is a nearby fault showing similar characteristics, then the dip-angle of the latter is adopted.
- **Rake [degrees]:** it is the angle formed between the strike and the slip vector measured counter-clockwise. The range of rake is between 0° and 360°. Accordingly, rake would be 0° (or 360°) for the left-lateral strike-slip faults, 90° for the reverse dip-slip faults, 180° for the right-lateral strike-slip faults and 270° for the normal dip-slip faults. Only a unique value is required.

Acquisition: rake is obtained either from kinematic indicators from field measurements, or from focal mechanisms. If none is available, then rake is inferred from the local stress field pattern. In case of recent and cumulative displacements, morphological and/or stratigraphic information can be also used.

- **Slip-per-event [m]:** it represents the mean co-seismic displacement on the fault plane. It can be set directly or it can be suggested by the database software based on seismological scaling relationships. A unique value is required.

Acquisition: it can be obtained directly from seismological investigations or indirectly from palaeoseismological trenching. The latter captures the surface displacement of the fault. By comparing several cases, the maximum surface displacement of normal faults is certainly much smaller than maximum displacement at depth, but it is comparable with the mean value commonly used for the calculation of the seismic moment. Alternatively, the proposed co-seismic displacement of the software can be used. Obviously, slip-per-event values obtained with this procedure are affected by a larger uncertainty.

- **Slip rate [mm/a]:** by definition, slip-rate is the ratio between a displacement and the time necessary to produce it. Given that its estimation is many times based on rough calculations, a range of values is required.

Acquisition: Sometimes these data are obtained from palaeoseismological investigations, but in order to be meaningful, many earthquake cycles must be recorded and observed in the trench(es). Palaeoseismologically inferred slip rates are commonly referred to as 'short-term'. The cumulative displacement of morphotectonic markers, like post-last glacial maximum surfaces (*e.g. Caputo et al., 2010a*), could be also used for calculating a mean slip rate for the last *ca.* 15 ka. The displacement of stratigraphic horizons, like sedimentary or volcanic layers, is also largely used for obtaining information on the long-term slip rate of a fault. In general, the longer the considered period, the larger the number of seismic events and the more 'averaged' is the slip rate. Consequently the more uncertain is the real value associated with the very last seismic cycle, which would more probably apply to the next event. In the literature, it is rare to find slip rates explicitly stated. For this reason, an effort is made in the current thesis to uniformly calculate the slip rates based on geodetic strain rates. Both procedure and results will be discussed during the next chapters.

- **Recurrence [years]:** it is the recurrence interval time between two characteristic events. For the same reasons with slip rate, a value of ranges is required.

Acquisition: In order to define recurrence interval, several events are needed. Such kind of information can derive from historical catalogues (although old events can be hardly associated with the specific causative faults), dating of samples from palaeoseismological surveys and morphotectonic techniques. This information is usually rare. Recurrence could be tentatively estimated based on slip rate and assuming characteristic event behaviour by using empirical relationships between magnitude and co-seismic displacement (see *Caputo et al., 2006b* for discussion on the approach).

- **Magnitude [M_w]:** it can represent either the magnitude produced by a specific event, or the potential magnitude of the fault based on seismological scaling relationships. This parameter strongly depends on fault's dimensions and slip-per-event (see also the discussion that follows the parameters' description) as well as on few physical parameters (*e.g.* rigidity modulus). A unique value is required.
Acquisition: it is important to mention that in the case of earthquake related sources, magnitude sometimes appears greater than the literature magnitude. This means that the rest of the parameters affecting magnitude (length, width and slip-per-event) provide different magnitude estimation. An explanation of this is based on the fact that the source is capable of producing larger event. In any case, the instrumentally calculated (literature) magnitude is referred in the "Last earthquake" field.
- **Last earthquake [years]:** this field includes the date or the time elapsed (if it is an event based on dating methods) of the last characteristic earthquake. In the "Evidences" field next to it, the magnitude and the type of the record (historical/instrumental/palaeoseismological) are also discussed.
- **Penultimate earthquake [years]:** this information is rarely available, usually deriving from palaeoseismological investigations and rarely from historical references.
- **Elapsed time [years]:** it is the time interval between the last known earthquake and the year 2000 used as a reference.

It is obvious from the descriptions above that some of the parameters affect the others and *vice versa*. Indeed, this is a significant feature of the database, concerning only the ISSs and their require for completeness. In more detail (following the discussion of Basili *et al.*, 2008), length, width, single event displacement and magnitude are interconnected by seismological scaling relationships. Therefore, the internal consistency of these parameters can be verified by the compiler. When all these parameters are known from independent observations, the different estimations can be used alternately with the scaling relationships, and the consistency of a seismogenic source with some generalized model can be analyzed. However, the most common occasion is that only few, or even one, of these parameters are known and thus, they are the ones that should determine the others.

Composite Seismogenic Sources (CSSs)

- **Minimum depth [km]:** similar to the ISSs.
- **Maximum depth [km]:** similar to the ISSs.
- **Strike [degrees]:** same philosophy with the ISSs, with the only difference that in this case a range of values is required.
- **Dip [degrees]:** the definition is the same with the ISSs. A range of values is required.
Acquisition: the range of values usually reflects the variable dip-angle which is frequently steeper near to the ground surface and shallower at depth (listric

geometry). The range can become larger with very low values of dip-angle where low-angle normal shear zones occur. The range can also imply a gradual geometry change along the strike of the structure (*e.g.* the NAB). Nevertheless, general uncertainties also contribute to the range.

- **Rake [degrees]:** same definitions and considerations with the ISSs. However, a range of values is required.
- **Slip-rate [mm/a]:** same definitions and considerations with the ISSs.
- **Maximum magnitude [M_w]:** this parameter represents the potential magnitude, or else the maximum expected magnitude that the CSS can produce.
Acquisition: maximum magnitude can be only obtained from seismological scaling relationships, usually the ones that involve fault dimensions (*e.g.* Wells and Coppersmith, 1994) or sometimes surface fault rupture (*e.g.* Pavlides and Caputo, 2004; Wells and Coppersmith, 1994). It is important to mention that in most cases only a part of the CSSs length is used for estimating the maximum magnitude. This is due to the fact that the larger structure might contain segment barriers that likely prevent a total rupture (*e.g.* DePolo *et al.*, 1991). The occurrence of ISSs as fault segments and the consideration of their in-between linkage conditions, like, for instance, soft/hard linkage or open/linked/fully breached fault arrays (Soliva and Benedicto, 2004), can both give a different rupture model involving any of the included segments. In any case, such occasions and scenarios are always discussed in the “Comments” field of the “Commentary” html page.
- **Approximate location [degrees]:** similar to the ISSs, this is approximately the centre of the object/source. It is calculated automatically.
- **Total length [km]:** it is also calculated automatically and directly from the length of the top edge of the source.
- **Total width [km]:** it is calculated automatically based on the dip-angle information and the maximum depth.
- **Typical fault length [km]:** this parameter is calculated from seismological scaling relationships, based on the maximum magnitude field. It helps checking the consistency of the total length.
- **Typical fault width [km]:** this field derives from internal calculations between seismological scaling and analytical relationships, based on the maximum magnitude field, the dip angle range and the typical length.
- **Typical fault slip [m]:** Similar to the previous two parameters, typical fault slip is the average displacement per event and it is based on seismological scaling and analytical relationships, as well as the maximum magnitude field.

General remarks

Almost all of the parameters have *qualification keys*; these are: **LD** for *Literature Data*, **OD** for *Original Data*, **ER** for *Empirical Relationship*, **AR** for *Analytical Relationship* and **EJ** for *Expert Judgement*. A complementary field is also required to be filled in for many parameters. That is the *evidences*, a field shortly referring to the investigation method(s) from which the parameter is obtained.

It is obvious that there is a different level of confidence for each parameter. The most well defined are generally the geometric ones (location, length, width, minimum and maximum depth, strike and dip), as well as rake and magnitude. For these parameters a large variety of investigations are commonly available to support them. In contrast, it is often hard to estimate the other parameters. In order to fill in some debated or poorly constrained parameters, the use of 'expert judgement' approach is a common practice. In any case, this practice is always explicit so that the end-user of the database is able to decide the reliability of the information. If no estimations can be made then it is preferred to leave the parameter blank.

The two parameters with the most missing information were the maximum depth, which anyway could be roughly inferred from the seismogenic layer thickness of nearby known areas, and the slip rate. In order to avoid having these two fields poorly covered or missing throughout the database, original investigations have been carried out. For the first one, strength profiles are calculated, while for the second, the geodetic strain rate field is used. Respective information and descriptions about the procedures are discussed in [chapters 3 and 4](#).

A special attention should be also given to focal mechanisms, which can play an important role not only in defining the location of a source, but also for constraining strike, dip and rake. In case of several existing foci and almost completely missing field observations (*e.g.* in case of offshore sources), a selection of the appropriate nodal plane has to be made, especially when foci show great divergence. When they show small variations, then an average value is usually selected. In any case the quality of the fault plane solutions should be taken into account. Thus, focal mechanisms can be distinguished into two quality levels. The lower one generally corresponds to the first motion polarities method. The results sometimes can be totally wrong, especially for the old events that were recorded by a sparse seismological network. Moreover, it should be considered that the source parameters describe the initial rupture which can be different from the orientation of the whole rupture surface. The example of the 1954, Sophades earthquake, described in §1.5, can be recalled again. Higher quality results are provided by the body-wave inversions, a more recent method that can describe the whole rupture behaviour. Significant errors however, can also occur. The highest level of confidence occurs when both body-wave inversion focal mechanisms and well documented field observations are available.

2.5 The GreDaSS development procedure

The database software has been developed as a plug-in/extension (a MapBasic application) of the MapInfo® GIS software. It mainly consists of two independent, but interconnected,

extensions: the *FaultStudio v1.2* (Basili, 2006) and the core plug-in of *DISS v3.2* (DISS working group, 2011).

Since the database is built in a GIS environment, a collection of topographic and geologic material is used to geologically and geographically locate and plot the sources accurately. According to the desired detail, the following datasets are mainly used: various DEMs for both land elevation data, like the Shuttle Radar Topography Mission (SRTM; Bamler, 1999; Becker *et al.*, 2009) and the ASTER Global Digital Elevation Map (GDEM), and bathymetric data, like the Global Multi-Resolution Topography (GMRT); topographic maps of the Hellenic Military Geographical Service (HMGS) in various scales; maps of the geological and neotectonic series published by the Greek Institute of Geology and Mineral Exploration (IGME); various bathymetric maps (*e.g.* the International Bathymetric Chart of the Mediterranean; IOC, 1981); satellite images mainly obtained from GoogleTM Earth; airphotos obtained from HMGS. Many morphotectonic maps included in literature have also been used (*e.g.* the map for the NAB compiled Papanikolaou *et al.*, 2006). All maps had to be rectified to the appropriate coordinate projection system before they become ready for use.

Other complementary data used for GreDaSS are the seismicity catalogues of AUTH (<http://geophysics.geo.auth.gr/ss/>; Papazachos *et al.*, 2000; 2009) and IG-NOA (<http://www.gein.noa.gr/services/cat.html>). Moreover, catalogues of aftershock sequences for specific events found in various papers have been also used.

Fault Studio

Fault Studio is the main tool to create/modify a new/old ISS with all its geographic, geometric and kinematic information. The respective commands in the toolbox open a window with all the control fields ([fig. 2.6](#)). As mentioned in a previous session, length, width, single event displacement and magnitude are interconnected by seismological scaling relationships, while minimum/maximum depth, width and dip-angle are interconnected by geometric relationships. This means that if, for example, dip-angle or width is increased, maximum depth will be increased accordingly. With these constrains, we can be confident that our source is geometrically correct in terms of parameters and map projection as well.

After entering the desired parameters, the object/ISS is saved and then exported in a format that the DISS software can read. It is obvious that FaultStudio can only manage the ISSs because they use unique parameters on a strict geometric shape.

The DISS software

The DISS extension is the main workspace for creating, managing and viewing the seismogenic sources and their related information ([fig. 2.4](#)). A full description of all commands and abilities would be out of the scope of this paper; for this reason, only a brief description of the main tools and procedure will follow.

When DISS loads, the map window opens (*A* in [fig. 2.4](#)) containing a set of rectified maps and features (in raster and/or vector format) that we have previously selected as default and which can be changed any time by the “change theme” button (*K* in [fig. 2.4](#)) in the main DISS floating toolbox (*B* in [fig. 2.4](#)). Adding supplementary material (*e.g.* seismicity, morphotectonic

maps, etc.) is available at any time during this procedure, by opening the desired table from the File menu of MapInfo®. The DISS floating toolbox also contains buttons for managing the visibility of the seismogenic sources layers (ISSs, CSSs, DSSs and AFFs; *F* in fig. 2.4), the additional data (e.g. seismicity; *J* in fig. 2.4) and the additional map compilations (e.g. geological maps; *I* in fig. 2.4). The choice between various database versions (*H* in fig. 2.4) and the database maintenance (*G* in fig. 2.4) are also available.

The ISSs are always imported from the FaultStudio output files containing the principal geometric and kinematic parameters. In the DISS software only the descriptive information is entered (code, source name, compilers and contributors, slip-rate, recurrence, last and penultimate events and elapsed time), together with all the *qualification keys* and *evidences*.

The CSSs, DSSs and AFFs are created and managed in the DISS software exclusively. The making of new CSSs or DSSs is performed by manually drawing in free hand the polygon. All attributes are entered in the browser window of each layer/table (*C* in fig. 2.4). An important tool is available for controlling the consistency of the shape of the polygon against its geometric parameters. The “*CSSChecker*” as it is called, uses an algorithm to compare shape and data and accordingly suggests corrections and modifications.

AFFs are manually drawn as polylines and their attributes are entered in the respective browser. AFFs are connected with ISSs and/or CSSs.

The final step for publishing the data is to export the database in a format that can be read by web browsers (html), Google™ Earth, GMT and 3D Move. The export can be performed easily from the DISS 3.2 menu.

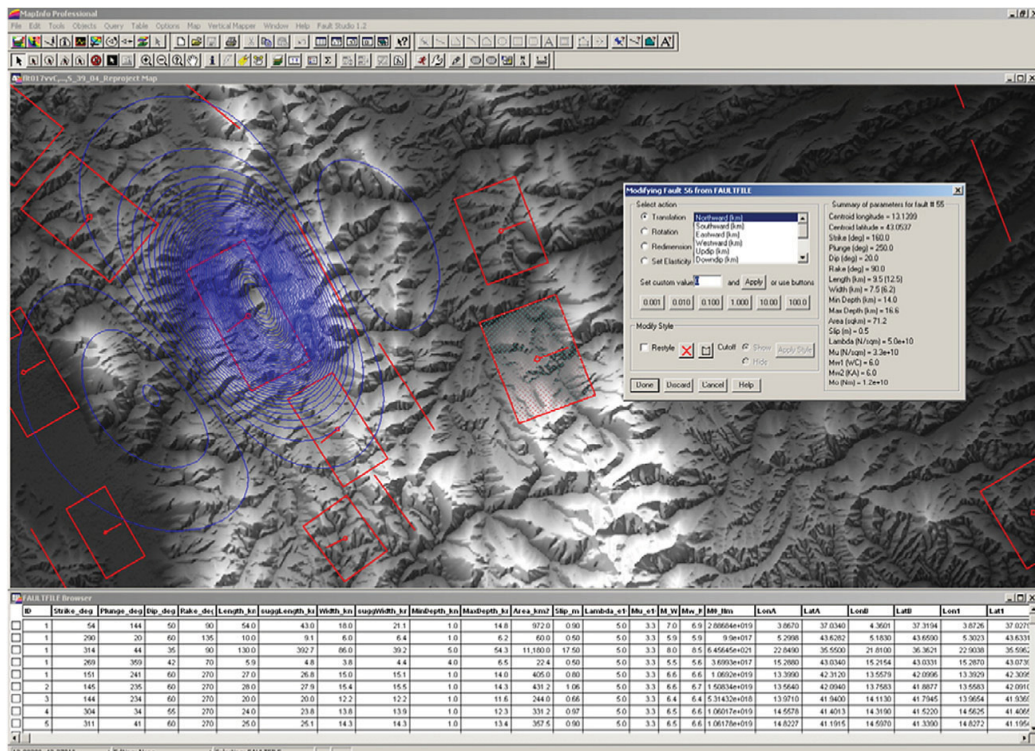


Fig. 2.6: FaultStudio is an additional extension hosted by the MapInfo® GIS software, available to the developers for manipulating the ISSs before they enter the DISS software (after Basili *et al.*, 2008).

3.1 Seismogenic layer thickness and BDT estimation

Introduction

In the effort of parameterizing the maximum depth of the seismogenic sources a problem often emerged: which is the thickness of the seismogenic layer and how can it be defined? This problem was common especially for all faults and/or fault zones that are lacking of microearthquake investigations from which the maximum seismogenic depth can be somehow constrained. Thus, a uniform criterion was needed to estimate the seismogenic layer thickness at least for the pilot area of North Greece.

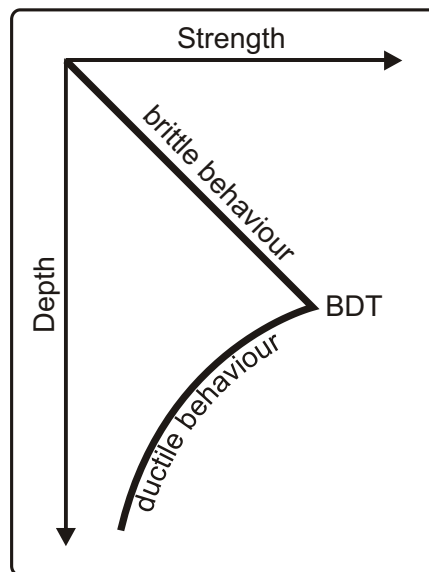


Fig. 3.1: A simplified rheological profile model for the lithosphere (modified after Scholz, 1988).

Near to the beginning of the 1980s, Goetze and Evans (1979), Brace and Kohlstedt (1980) and Kirby (1980) assembled laboratory data to produce a simple model of the rheology of the continental lithosphere. This model consists of two curves (fig. 3.1), the upper one corresponding to a friction law, whereas the lower part is the extrapolation of a high temperature steady-state flow law. The depth where the two curves intersect is taken to be the *brittle-ductile transition* (BDT) in the lithosphere, while this model is commonly referred to as *rheological profile* or *yield stress/strength envelope*. A little later on, Sibson (1982; 1983; 1984) observed the coincidence of the depth distribution of aftershocks, taken from many events in the western continental US, with the thickness of the brittle layer as suggested by the previous

model. He also observed that large ruptures were nucleated near to the BDT zone extending lateral and upwards. Similar observations were also made by Meissner and Strehlau (1982) for few regions worldwide, by Doser and Kanamori (1986) for the Imperial Valley (Western USA) and by many others later on, confirming that generally the location of the BDT zone (roughly) coincides with the bottom of the seismogenic layer and thus with the maximum depth of the faults. Many investigations followed trying to define the seismogenic layer thickness based on the depth of the BDT zone (e.g. Dragoni and Pondrelli, 1991; Lamontagne and Ranalli, 1996; Déverchère *et al.*, 2001; Tejero and Ruiz, 2002; Aldersons *et al.*, 2003; Boncio *et al.*, 2007; Boncio, 2008; Albaric *et al.*, 2009; *etc.*). However, two different concepts exist concerning the structure of the lithosphere and its effect to the strength profiles and the seismogenic layer thickness. Both theories will be discussed later in this chapter.

One-dimensional *rheological profiles* or *yield stress/strength envelopes* represent the plotting of the lesser value between the *brittle* and *ductile strength*. The strength of the lithosphere as a function of depth depends upon the deformation mechanism (e.g. Stein and Wysession, 2003). *Strength*, *failure strength* or *shear strength* are terms used to describe the critical value that *differential stress* must reach in order to cause rupture and sliding (e.g. Stüwe, 2007). At shallow depths, rocks fail either by *brittle fracture* or else *frictional sliding* usually on pre-existing faults. Both processes depend on the normal stress, with the rock strength increasing according to depth. Normal stress varies with overburden load (*i.e.* confining pressure) and pore fluid pressure (Sibson, 1974). At greater depths, where rocks show a prevailing plastic behaviour, the *ductile flow strength* is lower than the *brittle* (or *frictional*) *strength* and decreases with depth as temperature increases (Kirby, 1983; Ranalli, 1987; 1995). This means that the maximum strength is encountered in a zone where the BDT occurs (fig. 3.1). The BDT is better characterised as a zone because transition is gradual rather than sharp. However, behaviour depends on external parameters such as pressure, temperature and time (*i.e.* strain-rate), as well as on the rheological parameters of the material itself (Ranalli, 1987; 1995).

The commonly given definition of *rheology* is that it comprises the science of the deformation and flow characteristics of materials (Ranalli, 1987; 1995; Stüwe, 2007; van der Pluijm and Marshak, 2004). The rheological properties of the lithosphere have a strong effect on the resulting tectonic deformation (Kusznir and Park, 1987; Ranalli, 1997a; 1997b). The *strength envelopes*, used for estimating the strength of the lithosphere, depend strongly on these properties. Like mentioned before, strength as a function of depth changes differently in brittle and ductile regimes, with the depth of the highest strength being also the depth of the BDT zone. Moreover, it was also mentioned that strength of most rocks is lowered by increasing temperature. It is then obvious that strength strongly depends on temperature which, as a function of depth, can be expressed by the *geothermal gradient* (or *geotherm*) (Sibson, 1982; 1983; 1984; Kusznir and Park, 1987; Ranalli, 1987; 1995; 1997a; 1997b). But geotherms also depend on the rheological properties of the lithosphere. Although rheological properties and geotherms are the key parameters of strength calculations, it is noteworthy to mention that both of them are based on assumptions and approximations which limit their resolving power. However, strength profiles comprise a first order representation of the mechanical behaviour of the lithosphere (Lobkovsky and Kerchman, 1991; Ranalli, 1987; 1995; 1997a; 1997b).

Deformation mechanisms: an overview

But which are the deformation mechanisms and what is their meaning? According to Stüwe (2007), five mechanisms exist:

1. **Brittle deformation** is not really a deformation mechanism at all. It is the state when the stresses applied to rocks cannot be compensated elastically and thus permanent deformation will occur. The laws of brittle deformation only describe a stress state and not a relationship between stress and strain. The deformation law usually used to describe rocks in a brittle fashion is plastic deformation. Brittle failure is commonly described with the Mohr-Coulomb-criterion. The nucleation of an earthquake is most probable to initiate in the brittle part of the crust.
2. **Plastic deformation** law states that a constant stress is required to deform the rock. Irregardless how much or how fast we deform, the required force is all the same. Deforming sand is a good analogue model.
3. **Ductile deformation** is a term used when the deformation is not elastic and not brittle. It is therefore an extremely useful term for the field geologist who does not want to specify himself by using words like “viscous”, “plastic” or “dislocation creep” - all of which have very rigorously defined meanings.
4. **Elastic deformation** is the law that states that the strain of a rock is proportional to the applied total stress. As such, it is the only deformation mechanism which is not permanent: As soon as the stress is released, the strain is gone as well.
5. **Viscous deformation** is the law that is most commonly used to describe ductile deformation on the crustal scale. Viscous means that the strain rate of a rock is proportional to the applied deviatoric stress.

Rheological models in theory

Two basic theoretic models exist in order to define where strength is mainly accumulated (fig. 3.2). The earliest suggested model is widely known as “jelly sandwich” and describes the lithospheric structure as rheologically multi-layered with a strong upper crust overlying, a soft lower crust and a stronger (under most conditions) uppermost mantle (Chen and Molnar, 1983; Ranalli and Murphy, 1987; Burov and Diament, 1992; Ranalli, 1995; Watts and Burov, 2003; Handy and Brun, 2004; Burov and Watts, 2006; Burov, 2010). This model is based on the fact that even though the seismogenic layer potentially extends to the BDT, the level of stress may not be sufficiently large to cause failure at such depths. Therefore, in cases in which earthquakes might extend deeper into the brittle part of the mantle, two seismogenic layers should exist with an aseismic interposed layer. The second model, that usually meets the term “*crème brûlée*”, encloses all lithospheric strength in the upper (seismogenic) crust which overlies a softer upper mantle (Maggi *et al.*, 2000; Jackson, 2002; Priestley *et al.*, 2008). The suggestion of this model is based on the absence of seismicity that was observed in the (weak) lithospheric mantle of the studied areas (Iran, Tien-Shan and northern India), implying that seismic activity and strength are concentrated in the upper and lower crust. While discussing the dilemma between “jelly sandwich” and “*crème brûlée*”, Afonso and Ranalli (2004) suggest that this problem is far from being completely solved and that neither of the two models can have general applicability.

Thus, each lithosphere should be modelled according to its composition variation and tectono-thermal history which cause the lateral variability in rheological properties. While discussing the structural differences between continental and oceanic crust, Watts and Burov (2003) suggested that continental lithosphere, unlike its oceanic counterpart, is associated with a multi-layer rheology and small plate flexures, resulting in such stress levels that are unlikely to approach the very high brittle strength limits below the Moho.

The methodology used for defining the BDT zone in North Greece is independent from both main concepts and it is based on the discussion of Afonso and Ranalli (2004), that is focusing on the local lithospheric and thermophysical conditions.

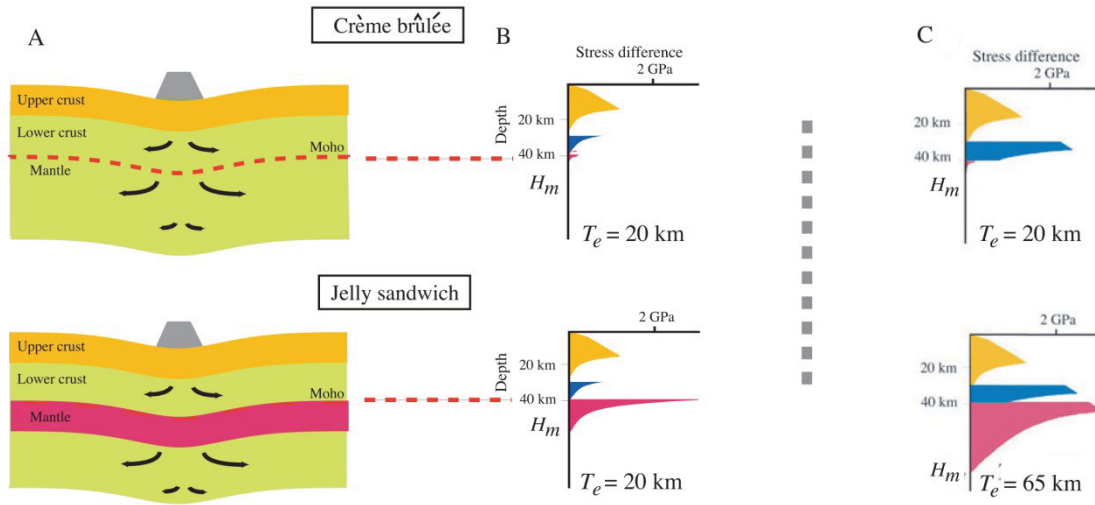


Fig. 3.2: Schematic diagram illustrating different models for the long-term strength of continental lithosphere. In the *crème-brûlée* model, the strength is confined to the uppermost brittle layer of the crust, and compensation is achieved mainly by flow in the weak upper mantle. In the *jelly sandwich* model, the mantle is strong and the compensation for surface loads occurs mainly in the underlying asthenosphere. **(A)** Models of deformation. Arrows schematically show the velocity field of the flow. **(B)** Strength envelopes for a thermo-tectonic age of 150 Ma, a weak, undried granulite lower crust, a uniform strain rate of 10^{-15} s^{-1} , and either a dry (*jelly sandwich*) or wet (*crème brûlée*) olivine mantle. H_m is the short-term mechanical thickness of the lithosphere; T_e is the long-term elastic thickness. The two envelopes yield a T_e of 20 km, which is similar to the thickness of the most competent layer. This is because the competent layers are mechanically decoupled by weak ductile layers and so the inclusion of a weak lower crust or strong mantle contributes little to T_e . **(C)** Strength envelopes for a thermo-tectonic age of 500 Ma. Other parameters are as in (B) except that a strong, dry, Maryland diabase has been assumed for the lower crust. The two envelopes show other possible rheological models: in one, the upper and lower crusts are strong and the mantle is weak (upper panel); in the other, the upper and lower crusts and the mantle are strong (lower panel). The assumption of a strong lower crust in the weak mantle model again contributes little to T_e because of decoupling, although T_e would increase from 20 to 40 km if the upper crust was strong at its interface with the lower crust. In contrast, a strong lower crust contributes significantly to the T_e of the strong mantle model. This is because the lower crust is strong at its interface with the mantle and so the crust and mantle are mechanically coupled. From Burov and Watts (2006).

3.2 The deformational equations

The frictional sliding equation

Sibson (1974) modified the *Anderson's theory* of faulting defining the effective overburden pressure as a function of depth classified for three different faulting regimes (thrust, normal and strike-slip faulting). The argument is applied for both occasions, sliding along pre-existing faults and formation of new faults, provided that internal friction is approximately the same as sliding friction and cohesive strength is negligible when compared with normal stress.

The equation describing the stress status, or else the *frictional sliding equation*, is (Sibson, 1974):

$$(\sigma_1 - \sigma_3)_f = \alpha \rho g z (1 - \lambda) \quad [3.1]$$

where, z is depth, ρ is the *rock density*, g the *gravity acceleration* and λ the *ratio of pore fluid pressure to lithostatic (overburden) pressure*. In this study, the suggested 'hydrostatic' value $\lambda \approx 0.4$ is adopted (Ranalli and Murphy, 1987; Fadaie and Ranalli, 1990; Albaric *et al.*, 2009). The symbol α represents the numerical parameter of fault type and equals to (Ranalli, 1995):

$$\begin{aligned} \alpha &= R - 1 \\ \alpha &= \frac{R - 1}{R} \\ \alpha &= \frac{(R - 1)}{1 + \beta(R - 1)} \end{aligned}$$

for thrust, normal and strike-slip faulting, respectively, where R is the σ_3/σ_1 ratio and, in the last equation, β is the stress ratio $(\sigma_2 - \sigma_3)/(\sigma_1 - \sigma_3)$ (Ranalli, 1997a). In terms of internal friction μ' , R can be expressed as:

$$R = \left(\sqrt{1 + \mu'^2} - \mu' \right)^{-2}$$

According to Ranalli (1997a), the friction coefficient range is $0.5 < \mu' < 0.8$, while the commonly used values of α for the three fault regimes are (Ranalli, 1995; Fadaie and Ranalli, 1990):

$\alpha = 3.0$ for thrust faulting,

$\alpha = 0.75$ for normal faulting, and

$\alpha = 1.2$ for strike-slip faulting,

assuming $\mu' = 0.65$ and $\beta = 0.5$.

The frictional slide is a linear function of pressure and is independent of temperature and strain rate.

The creep-law equation

The ductile regime is described by the *power-law creep* function, and in more detail, by the *Dorn empirical equation* (Ranalli, 1995):

$$(\sigma_1 - \sigma_3)_c = \left(\frac{\dot{\epsilon}}{A_D}\right)^{1/n} e^{\left(\frac{E}{nRT(z)}\right)} \quad [3.2]$$

where $\dot{\epsilon}$ is the *strain-rate*, R is the *gas constant* and T is *temperature* which depends on depth. A_D , n , and E are material parameters (*Dorn parameter*, *stress exponent* and *creep activation energy*, respectively).

It is obvious from the previous equation [3.2] that the only parameter that correlates strength with depth is temperature. This means that the geothermal gradient plays an important role which in turn depends from material parameters as well.

The high-pressure brittle failure equation

Models based only on the two previous equations usually ignore the *brittle fracture* deformation. Experiments show that the stress causing the brittle fracture of an intact rock will be less than that causing frictional sliding on fractures at some temperatures, pressures and strain rates (Shimada and Cho, 1990; Stesky *et al.*, 1974; Wei and Zang, 2006). Although frictional sliding depends linearly on pressure and is independent of temperature and strain rate, with increasing pressure, the critical stress difference in the brittle regime becomes nonlinearly dependent on all these factors (Ord and Hobbs, 1989; Shimada, 1993; Wei and Zang, 2006; Zang *et al.*, 2007). The *high-pressure brittle failure* (Pauselli *et al.*, 2010) is described by the following empirical equation (Wei and Zang, 2006; Zang *et al.*, 2007):

$$(\sigma_1 - \sigma_3)_b = B_0 \left[1 + K \left(\frac{P}{B_0}\right)^m \right] \left[1 + \alpha \left(\log \frac{T(z)}{T_0}\right)^\beta \right] \left[1 + \gamma \log \left(\frac{\dot{\epsilon}}{\dot{\epsilon}_0}\right) \right] \quad [3.3]$$

where B_0 , K , m , α , β and γ are empirical failure parameters listed in [table 3.1](#); P is the confining pressure (in MPa), $T(z)$ is the temperature as a function of depth in degree (Kelvin), $\dot{\epsilon}$ is the strain rate (in s^{-1}); $T_0 = 298 \text{ }^\circ\text{K}$ and $\dot{\epsilon}_0 = 10^{-5} \text{ } s^{-1}$ are the normalizing parameters. The effects of the size of the rock sample, confining pressure, temperature and strain rate on the fracture strength are all included (Wei and Zang, 2006).

Rocks	B_0 (MPa)	K	m	α	β	γ
Granite	34.1	4.57	0.52	-1.128	1.732	0.035
Gabbro	36.1	3.18	0.55	-2.536	2.340	0.035
Basalt	48.5	2.98	0.51	-2.536	2.340	0.035
Peridotite	28.3	3.35	0.68	-1.875	1.310	0.035

Table 3.1: Brittle fracture parameters of some rock types in the lithosphere (Zang *et al.*, 2007 and references therein). K , m , α , β and γ are dimensionless.

Pauselli *et al.* (2010) note the following remarks concerning the usage of the equation above: the *high-pressure brittle failure* equation results in a critical stress difference less than the

frictional strength as pressure increases. However, this equation is experimentally validated only for $P \leq 0.8$ GPa and $T \leq 900$ and $T \leq 1100$ °C, for crustal and upper mantle rocks, respectively. The temperature limitation is particularly severe for upper mantle rocks. As can be seen from the temperature term, the $(\sigma_1 - \sigma_3)$ for peridotite becomes negative for $T > 1240$ °K, which prevents the application of [equation \[3.3\]](#) to hot volumes of the lithospheric mantle. Moreover, Wei and Zang (2006) also mark the following possible limitations of the equation: *i)* the temperature effect is deduced from a small number of data, and *ii)* the fracture parameters of only few rocks are provided.

3.3 Lithospheric stratification and composition

Lithosphere and rheological modelling: an introduction

The knowledge of lithospheric structure is important for calculating geotherms and hence strength (*e.g.* Kuszniir and Park, 1987). Lithosphere, by definition, is divided into two major layers, the crust and the lithospheric mantle. Stratification used in various rheological models is usually conventional. The basic information that is needed concerns the number of layers, their thickness and their general composition. In ‘simple’ models, continental lithosphere is divided into three parts: the upper (UC) and lower (LC) crust and the lithospheric (or upper) mantle (LM). An additional subdivision within the UC is possible if a sedimentary layer (SL) exists. This layer is easier to be defined, even by surface observations, as it occupies a small topmost part of the crust. Obviously, more detailed and precise models need more detailed and precise data, considering also that composition inside lithosphere and its layers is neither uniform, nor is directly detectable, nor can it be abruptly separated from layer to layer since the change is gradual. For this reason, in most of rheological models found in the literature, either they deal with continental or local scale areas, it is preferred to use few layers with an average composition defined between principal (*i.e.* more diffuse) rock types (*e.g.* Steckler and ten Brink, 1986; Fadaie and Ranalli, 1990; Dragoni *et al.*, 1996; Fernández and Ranalli, 1997; Ranalli, 1997a; 1997b; 2000; Pasquale *et al.*, 1997; Moisisio *et al.*, 2000; Porth, 2000; Mouthereau and Petit, 2003; Watts and Burov, 2003; Afonso and Ranalli, 2004; Gueydan *et al.*, 2008). An example of a standard profile of the European continental crust is shown in [fig. 3.3](#) (Wedepohl, 1995).

An average composition of each layer can be inferred from the correlation of P - and S -wave velocities (V_P and V_S respectively) with the density and the type of rocks, as this has been suggested by Pakiser and Robinson (1966), Rybach and Buntebarth (1984), Christensen and Mooney (1995) and Christensen and Stanley (2003). For this reason, a synthesis of several studies is carried out, including 1-D, 2-D or even 3-D velocity models of local and/or large scale areas of the Aegean (Papazachos *et al.*, 1966; Makris, 1978; Drakatos and Drakopoulos, 1991; Ligdas and Lees, 1993; Papazachos and Nolet, 1997; Drakatos *et al.*, 1997; 1998b; 2005; Melis and Tselentis, 1998; Papazachos, 1998; Makris *et al.*, 2001; Bourova *et al.*, 2005; Karagianni *et al.*, 2005; Di Luccio and Pasyanos, 2007; Karagianni and Papazachos, 2007; Raykova and Nikolova, 2007; Endrun *et al.*, 2008; Peter *et al.*, 2008; Molinari and Morelli, 2011; Ormeni, 2011). For each case study, different combinations of available data are generally used.

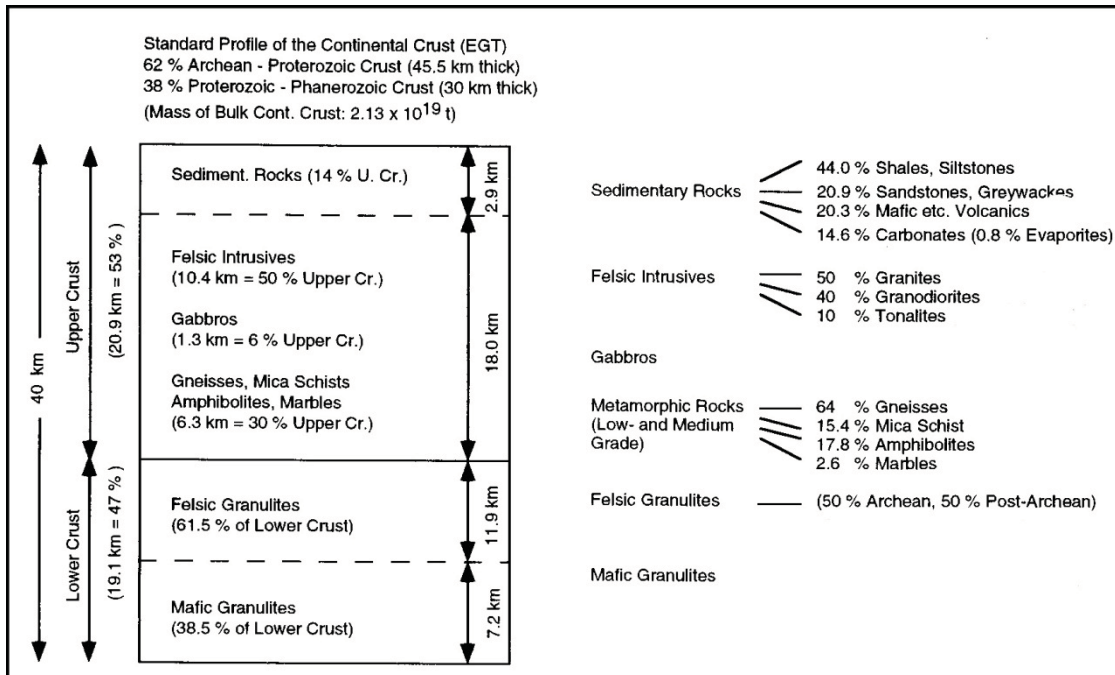


Fig. 3.3: Standard profile of the continental crust derived from the 3000 km-long European GeoTraverse (EGT) generalized on the basis of worldwide mapping, petrological studies and chemical balances. After Wedepohl (1995).

Lithosphere and thickness

Lithosphere is the uppermost rheological layer of the Earth and comprises the crust and the upper part of the mantle, also called *lithospheric mantle*. Although a unique definition does not exist, descriptions of its properties can be easily found in literature (*e.g.* Turcotte and Schubert, 1982; Hawkesworth *et al.*, 1999; White, 1999; van der Pluijm and Marshak, 2004; Stüwe, 2007; Zang and Stephansson, 2010). Lithosphere can be described by two different approaches: from a mechanical point of view, the strongest and rigidly behaving lithosphere floats up on the weak and plastically behaving asthenosphere, while from a thermal point of view, the base of the lithosphere is universally posed at the isotherm where the weakening (melting) temperature of the mineral olivine (mantle solidus) which dominates in the mantle peridotite occurs ($T_M \approx 1350^\circ \text{C}$). According to White (1999), the continental lithosphere, which is the case of this study, may be extremely old, reaching an age of several gigayears in the oldest known areas, and thus may accumulate a long and complex history. It is likely to have suffered multiple episodes of decompression melting as it responded to tectonic deformation, and to have been enriched by the accumulation of metasomatic melts throughout its long history. Buoyancy of continental lithosphere is a function of density, which is dependent on composition and, to a lesser extent, temperature (Hawkesworth *et al.*, 1999).

Few global-scale and local-scale maps of lithospheric thickness exist, all showing a variety in values. Calcagnile *et al.* (1982) and Calcagnile and Panza (1990) suggested a map of the lithosphere-asthenosphere isobaths for the Mediterranean area based mainly on the inversion of available surface-wave dispersion data. Conrad and Lithgow-Bertelloni (2006) produced a global lithosphere thickness map with a resolution of $1^\circ \times 1^\circ$, based on the method of Gung *et*

al. (2003). Sodoudi *et al.* (2006) computed the Aegean lithosphere-asthenosphere boundary from S receiver functions taken from seismograms of teleseismic events recorded at 65 temporary and permanent stations in the Aegean region. Cloetingh *et al.* (2010) produced an integrated model of lithospheric thickness in Europe with an error envelope of 25 km, based on a combined seismic, thermal, MT, electromagnetic and gravity interpretation. All proposed models for the broader area of North Greece generally show a lithospheric thickness ≥ 100 km. Differences in thickness between the various models for a specific location can reach 50 km. However, no greater values than *ca.* 180 km have been suggested for the study area. For the Central-Eastern Mediterranean, Viti *et al.* (1997) rheologically estimated the lithospheric thickness for the two different types of lithospheric nature: the mechanical and thermal lithosphere. In the former case an average thickness of 154 km and 46 km is suggested for NW Greece and Macedonia regions respectively, with corresponding intervals of 75-261 km and 12-70 km. In the latter case, the suggested thickness for NW Greece and Macedonia regions is 67 km and 12 km respectively, with corresponding intervals of 15-127 km and 7-18 km. The authors point out that only the thermal lithospheric thicknesses are comparable with the ones obtained from surface wave analyses studies.

Crust and thickness

The crustal – lithospheric mantle boundary is defined by the Mohorovičić discontinuity or else the *Moho*. Moho is a seismic transition boundary where *P*-wave velocities, as measured by seismic refraction data, increase from crustal to mantle values. The broadly tonalitic composition of the continental crust has been assessed in detail in a number of recent reviews (Taylor and McLennan, 1995; Rudnick and Fountain, 1995; Plank and Langmuir, 1998). Hawkesworth *et al.* (1999) indicate that the strength of the continental lithosphere is likely to be largely dictated by the mantle part of the lithosphere rather than the crust. According to them, the continental crust generally has a low density, and its rheology is usually approximated by quartz and/or plagioclase, which, like the authors note, is clearly an oversimplification. Nevertheless, they also suggest that even if the lower crust is quite mafic in composition (*e.g.* Rudnick and Fountain 1995), any compositional increases in strength will be mediated by thermal weakening due to increasing temperatures at depth.

Concerning the available data of the Moho depth in the study area and their acquisition methods, a brief discussion follows below.

A broad-scale averaged picture of the crustal structure in the Aegean region is given by Panagiotopoulos and Papazachos (1985) and later on by Papazachos (1993), based on travel-time inversions of local and regional earthquakes. In earlier papers, refraction profiles were used to map the shallow structure beneath specific areas in the Aegean (Makris, 1978; Makris and Stobbe, 1984; van der Meijde *et al.*, 2003), but data are few and of varying quality (Sodoudi *et al.*, 2006). Aegean-scale tomographic images based on large-scale teleseismic and regional studies (Spakman *et al.*, 1988; 1993; Spakman, 1990; Drakatos and Drakopoulos, 1991; Alessandrini *et al.*, 1997; Papazachos and Nolet, 1997), and local-scale images based on more detailed local tomographic studies using travel-time arrivals recorded by local networks (Christodoulou and Hatzfeld, 1988; Ligdas *et al.*, 1990; Ligdas and Main, 1991; Ligdas and Lees, 1993; Papazachos, 1998; Sachpazi *et al.*, 2007), show more homogeneity in results (Sodoudi *et al.*, 2006). According to Sodoudi *et al.* (2006), tomography as used by all the

studies above, is not the most appropriate tool to map the Moho depth over a large area. This is ascribed to the fact that tomographic investigations assume a layered starting velocity structure divided into blocks of various sizes in which the lateral variation in the velocity structure is computed; therefore, a travel-time delay for a specific block could be due to either a real low relative velocity zone in the block or a variation in the thickness of the block. The same authors combined *P* and *S* receiver functions from seismograms of teleseismic events, recorded at temporary and permanent stations in the Aegean region, to map the geometry of the subducted African and the overriding Aegean plates. Similar methodology was followed by Papazachos and Scordilis (1998) in order to produce tomographies of the crustal structure.

Other Moho depth maps derive from gravity investigations (Makris and Stobbe, 1984; Tsokas and Hansen, 1997; Tiberi *et al.*, 2001; Tirel *et al.*, 2004). However, Sodoudi *et al.* (2006) note that the maps produced by gravity data for the Aegean suffer severe limitations due to the corrections made for the subducted slab and the thickness of the shallow sediments, showing thus considerable differences.

The dispersion of the Rayleigh and Love waves are also used to either infer 3-D tomographic images of the shear wave velocity structure of the crust and upper mantle in the Aegean Region, or to produce Moho topography models (Kalogeras and Burton, 1996; Karagianni *et al.*, 2005; Karagianni and Papazachos, 2007; Bourova *et al.*, 2005; Di Luccio and Pasyanos, 2007; Raykova and Nikolova, 2007). These investigations are in agreement with the general characteristics estimated from the previous works in this area.

Based on seismological and other geophysical data, a gross stratification and thickness estimation is presented by Viti *et al.* (1997) for the two areas in NW Greece and Central Macedonia. The authors suggest a depth of 45 km of the base of the lower crust for both regions.

Small-scale and more integrated studies have been published for the Moho topography, including the European Region (Grad *et al.*, 2009; Molinari and Morelli, 2011) and Mediterranean Sea (Marone *et al.*, 2003; Özeren and Holt, 2010). Usually, these studies combine many already existing data taken from various types of investigations (*e.g.* *P* and *S* wave velocities, gravity data, *etc.*).

After summarising from all published papers and maps (few examples are shown in [fig 3.4](#)), it seems that the thickest crust is located along the Hellenides, with the Moho depth ranging between 33 and 53 km. An abrupt shallowness in depth occurs between Central-Western Macedonia and Thrace (Sodoudi *et al.*, 2006; Raykova and Nikolova, 2007; Grad *et al.*, 2009). A crustal thinning is also imaged in the vicinity of North Aegean Trough (Makris and Stobbe, 1984; Tsokas and Hansen, 1997; Tirel *et al.*, 2004; Raykova and Nikolova, 2007). A further analysis of the two crustal layers is discussed below.

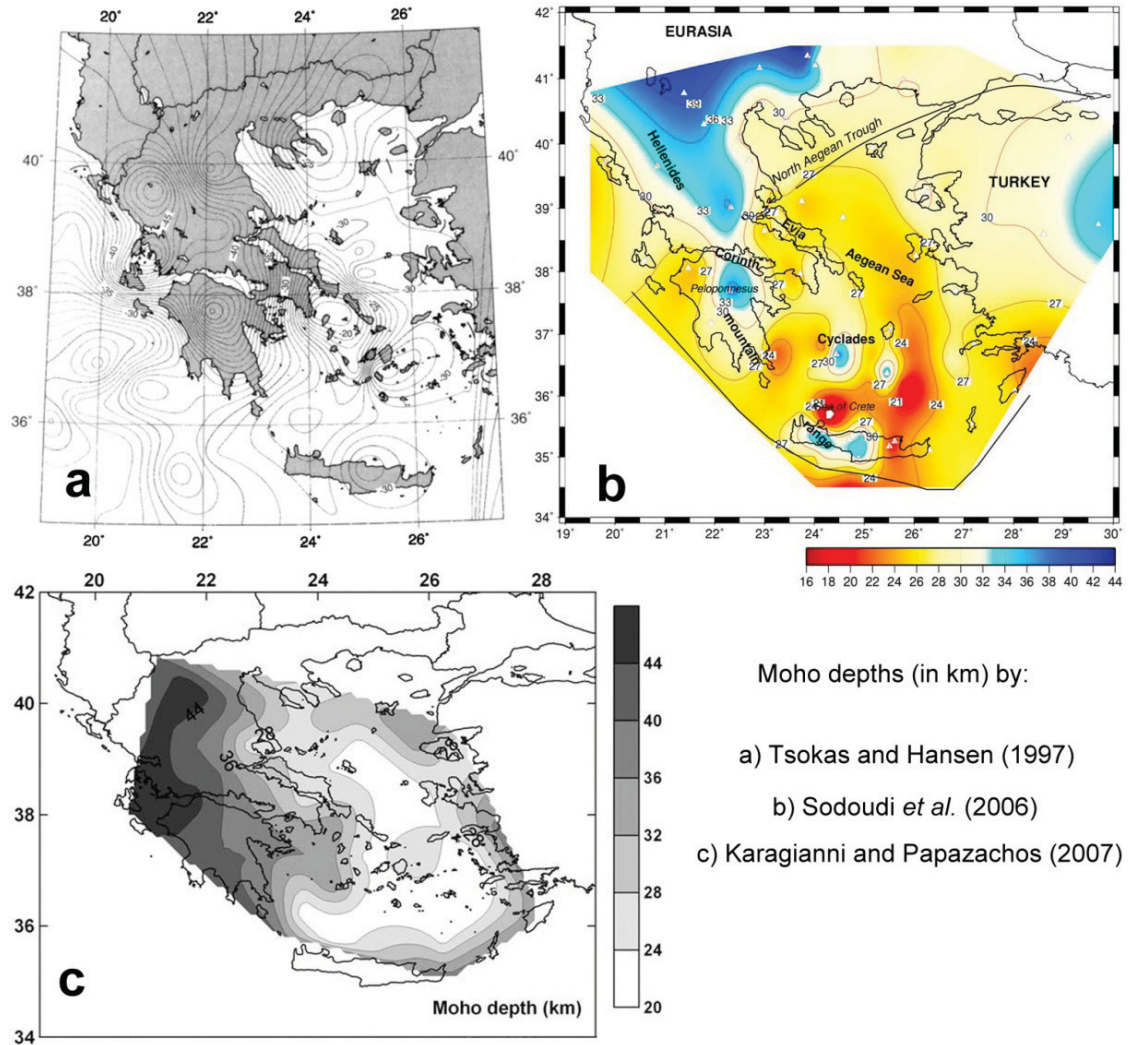


Fig. 3.4: Three samples of the available Moho depth maps for the Aegean Region. See text for more details.

Sedimentary layer and thickness

The sedimentary layer in North Greece varies along a rough E-W direction. The thickness of the sediments increases from few hundred metres of post-alpine deposits in the Thrace Basin, to several kilometres of Mesozoic carbonates and sea-ocean sediments in the Pindos Mountain chain. Depending on the location of the sites where the geotherms and strength profiles are applied, various suggestions and estimations are used for defining the general composition and thickness of the sediments (*e.g.* Smith and Moores, 1974; Ferrière *et al.*, 2004; Di Luccio and Pasyanos, 2007; Molinari and Morelli, 2011). Furthermore, the V_p and V_s of the upper parts of the crust are also taken under consideration.

Radiogenic heat production in the sedimentary layer is sometimes considered negligible and heat mainly transfers via conduction. In this case the temperature *versus* depth function is expressed linearly. However, for the calculations of the geotherms this small contribution of the

sediments is taken into account. Therefore, the temperature *versus* depth function is exponential (as it is shown in the following chapter), but close to linear.

Upper/lower crust and thickness

The upper-lower crust limit, also known as Conrad discontinuity, is the most hardly defined modelling parameter. In the broader Aegean Region, the synthesis of the crust is not clear, especially southwards, due to the presence of the subduction zone. Information is poor and contains large uncertainties in both results and interpretation. The gross stratification of Viti *et al.* (1997), based on seismic and other geophysical data, suggests a depth of the upper-lower crust limit down to 20 km for NW Greece (including 10 km of sediments thickness) and 30 km for Macedonia (without any presence of sediments). Moreover, based on crustal velocity structures (*e.g.* Makris, 1978; Novotný *et al.*, 2001; Drakatos *et al.*, 2005; Di Luccio and Pasyanos, 2007; Ormeni, 2011) the limit of the upper-lower crust can also be inferred. However, the recently published study of Molinari and Morelli (2011) provides a better view of the crustal structure of the study area.

Chapman (1986) notifies that the position of the upper-lower crust boundary is a relatively insensitive parameter for temperature calculations in the lower crust. In fact, the author suggests that, for a 20% increase of the Conrad depth, when the latter is assumed at 16 km, the temperature increases 1% for the continental shields and 3% for the continental rifts. This amount can be considered neglectful and consequently the temperature depending strength profiles are rather insensitive from the upper-lower crust boundary.

Given that both crustal layers produce radiogenic heat, the exponential function of temperature *versus* depth is applied for calculating the geothermal gradient (see in the following chapter).

Lithospheric mantle and thickness

Lithospheric mantle is the lowest part of the lithosphere where seismic wave velocities increase significantly. This layer consists of basic rocks of higher density. Its thickness is calculated by the subtraction of the lithospheric thickness minus the crustal one. The contribution of radiogenic heat production is negligible and heat mainly transfers by convection. Thus, temperature increases linearly along depth until it reaches the mantle solidus temperature of *ca.* 1350° C at the base of the layer.

3.4 Geothermal gradients

The connection between temperature and depth are expressed by the *geothermal gradient* (also simply called *geotherm*), or in other words the *vertical temperature profile*. Geotherms vary significantly between oceanic and continental lithospheres. Generalized global geotherm models of steady state continental lithospheres are shown in [fig. 3.5](#). However, steady-state continental geothermal gradients may vary significantly in local-scale regions because they strongly depend on the lithospheric composition.

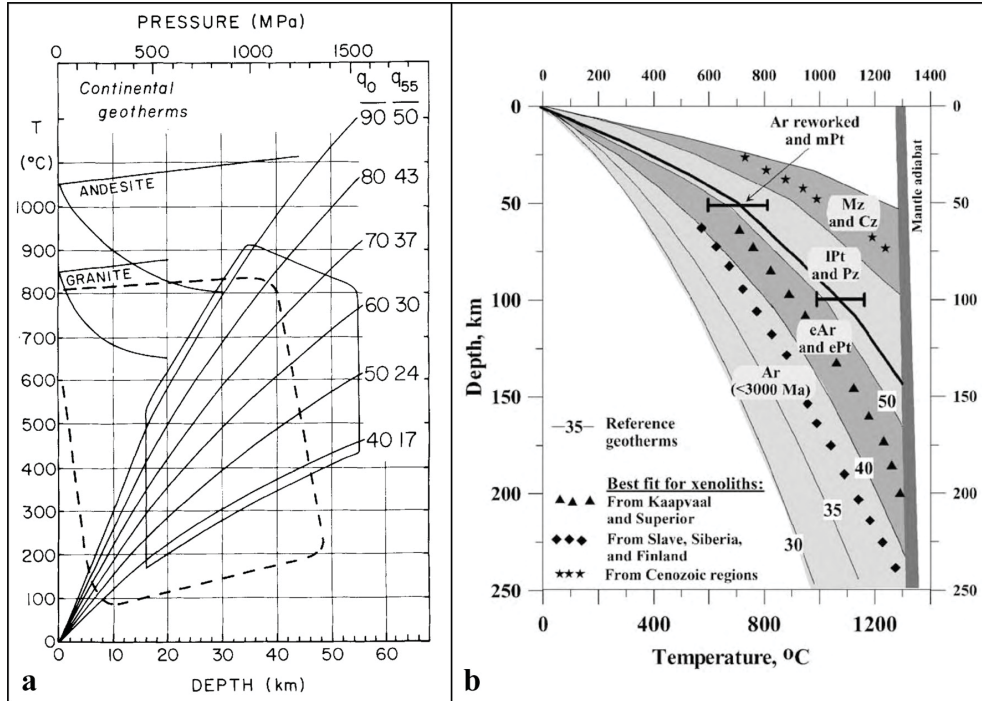


Fig. 3.5: (a) A set of steady state-static geotherms for continental lithosphere. Geotherm parameter is the characteristic surface heat flow q_0 in mW m^{-2} ; heat flow at a depth of 55 km (q_{55}) is also shown. Solid lines marked by labels ‘granite’ and ‘andesite’ show possible solidii brackets for wet (minimum) and dry (maximum) melting in the crust. Heavy dashed line encloses PT field appropriate for metamorphic rocks; solid line polygon encloses steady state PT field of lower crust in stable regions. Lack of complete overlap in temperature space can be explained by dynamic crustal forming processes. After Chapman (1986). (b) Typical continental geotherms constrained by heat flow data for stable regions and by xenolith data for active regions. Five groups of typical geotherms include (from the coldest to the warmest): 1) Archean terranes younger than 3.0 Ga; 2) older Archean cratons (which include mostly cratons of Gondwana-continents) and early Proterozoic terranes; 3) reworked Archean cratons that have mantle temperatures similar to middle Proterozoic terranes (shown by line with bars); 4) Paleozoic and late Proterozoic regions; 5) Meso-Cenozoic regions. Thin lines — conductive geotherms of Pollack and Chapman (1977), values are surface heat flow in mW m^{-2} . After Artemieva (2006).

Temperature depends on various factors and parameters, most of which are attributed to the rock properties. Before describing the basic concept of the geothermal gradients, a brief description of these factors would be useful.

Heat flow q

Heat flow q is the rate of heat energy transfer through a given surface; accordingly, its SI unit is W m^{-2} . It is usually confused with the *heat flux*, though the latter represents the time rate of the former ($\text{W m}^{-2} \text{s}^{-1}$).

The basic relationship of *conductive heat transfer* is given by *Fourier’s law*, which states that the *heat flux* or *heat flow* q at a point within a medium, is directly proportional to the temperature gradient at this point (Turcotte and Schubert, 1982). For one dimension it is expressed as:

$$q = -k \frac{dT}{dz}$$

or else:

$$T(z) = -\frac{q}{k}z \quad [3.4]$$

where k is the coefficient of *thermal conductivity*, T the *temperature* and z the spatial coordinate (*e.g.* depth in the crust). The significance of minus is to show that heat flows towards the decreasing temperature.

Surface heat flow q_0 is a considerable parameter for producing a 1-D steady-state geothermal gradient. Practically, it represents the vertical component of the heat being conducted through the outer few kilometres of the Earth's crust (Ranalli and Rybach, 2005). The mean measured heat flow for all continents is 56.5 mW m^{-2} (Turcotte and Schubert, 1982; Ranalli, 1987). Turcotte and Schubert (1982) suggest that regions of high surface heat flow in the continents are generally limited to active volcanic areas, which like the areas of active tectonics, they do not contribute significantly to the mean global heat flow. Viti *et al.* (1997), during their rheological calculations for the Central-Eastern Mediterranean, excluded areas of very high heat flow values ($> 200 \text{ mW m}^{-2}$) since the latter might be representative of volcanic regions or be associated to convective heat transfer.

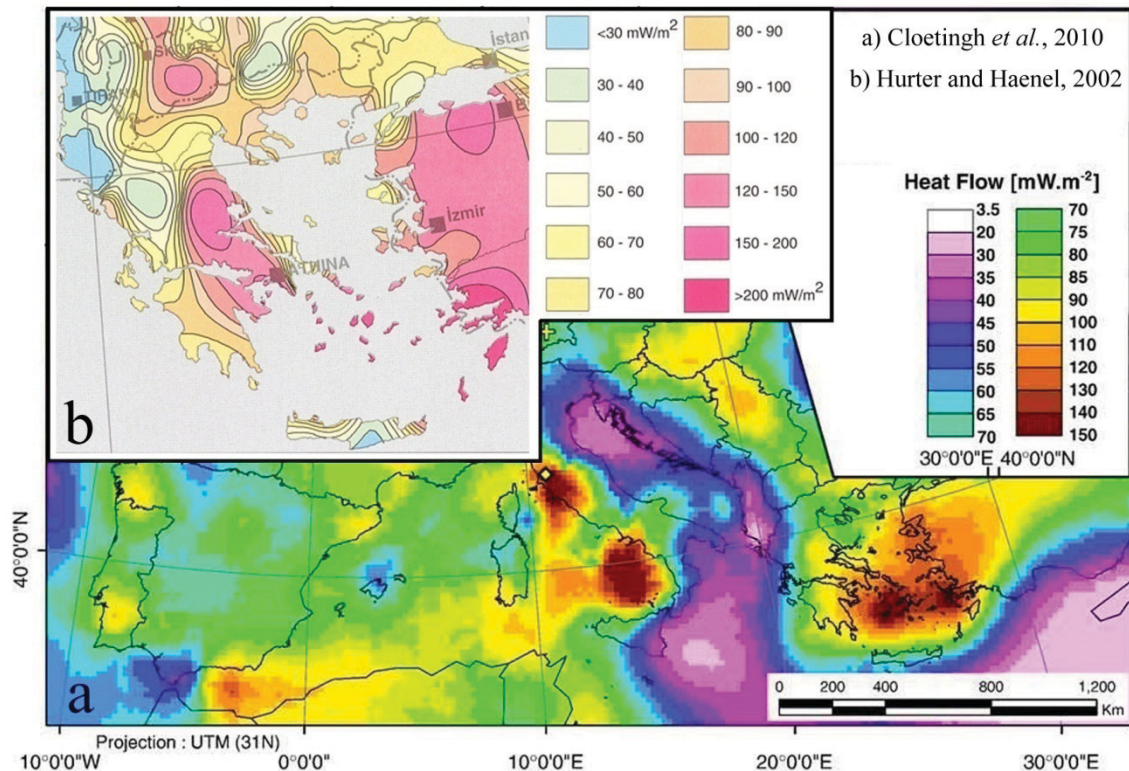


Fig. 3.6: Surface heat flow maps of Europe based on interpolated heat flow data. The inset (b) zooms in the Aegean Region. (a) after Cloetingh *et al.* (2010), (b) after Hurter and Haenel (2002).

Chapman (1986) quoted that the calculated temperatures in the geothermal gradient are overall most sensitive to surface heat flow. In fact, he specified that a 10% increase of the surface heat flow value in either a shield (40 mW m^{-2}) or a rift (80 mW m^{-2}) can cause 13% and 11% increase of temperature values at a depth of 50 km respectively.

Concerning the available heat flow data for the study area, only global or continental scale maps are usually found in literature (e.g. [fig. 3.6](#)). Several heat flow maps of such scale have been published (Haenel and Staroste, 1988; Pollack *et al.*, 1993; Artemieva and Mooney, 2001; Hurter and Haenel, 2002; Artemieva, 2006; Cloetingh *et al.*, 2010). However, a national-scale map has been proposed by Taktikos (2001) for the onshore area of Greece.

Heat production A

Heat is produced by three fundamentally different geological mechanisms, shortly described below: *radioactive heat* production, *mechanical heat* production and *chemical heat* production (e.g. Stüwe, 2007).

- **Radioactive** or **radiogenic heat** is produced in the Earth predominantly by the naturally occurring radioactive isotopes ^{238}U , ^{235}U , ^{232}Th and ^{40}K . Although the concentrations of these elements in rocks are quite low, the crustal heat production is significant. Radiogenic heat production in the continental crust is responsible for about half of the heat flow that can be measured on the earth's surface.
- **Mechanical heat** production derives from the forces that deform rocks. The mechanical energy that is added to the rock will be transformed into other form of energy like dislocation energy in crystal lattices, potential energy, noise and other forms of energy. However, it is widely accepted that the majority of this mechanically produced energy will be transformed into friction heat.
- **Chemical heat** production is represented by the internal heat of the rocks, defined by the strength of bonding of the atoms in the crystal lattices in the rock-forming minerals.

Specifying heat production of rocks, especially in the lower crust, is difficult and cannot be defined by a unique value. An indirect estimation method is represented by the experimental relationship between *P*-wave velocity (V_p) and heat production (Rybach and Buntebarth, 1984). This relationship was later filtered from the pressure and temperature effects on seismic velocities by Čermák *et al.* (1991).

Heat production can be also predicted from experimental models. For example, Lachenbruch (1968) proposed a geothermal model in which heat production exponentially decreases with depth ([fig. 3.7](#)). This model is expressed by the following equation:

$$A(z) = A_0 e^{-z/D} \quad [3.5]$$

where A_0 is the *surface heat production* and D is the *exponential decay constant*. A_0 belongs to the thermophysical properties of the rocks and is experimentally estimated ([table 3.2](#)); its units are [$\mu\text{W m}^{-3}$]. D has length dimensions and reflects the depth distribution of heat producing elements. Pollack and Chapman (1977) quote a restricted range for the D value for several heat

flow provinces. According to their estimations, a value of 8.5 ± 1.5 km encompasses most of their results.

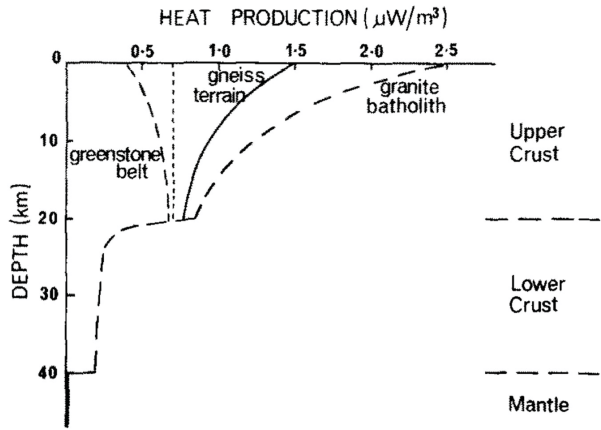


Fig. 3.7: A heat production model proposed for stable continental crust illustrated for three diverse types of surface geology found on exposed shields (Allis, 1979). The solid line is applicable to a shield with an “average” composition.

Rock (layer)	A_0 [$\mu\text{W m}^{-3}$]
various sediments	1.5 ⁽⁴⁾ , 1.45 ⁽¹⁴⁾
limestone	0.62 ⁽¹³⁾
metasediments	1.7 – 1.9 ⁽¹⁾ , 1.36 \pm 0.68 ⁽¹⁰⁾
metasediments (sandstone)	1.5 ⁽¹⁴⁾
marble	1.0 ⁽¹³⁾
granite (UC)	0.7 (Archaean) ⁽¹⁾ , 3.5 ⁽¹⁾ , 0.7 – 3.2 ⁽²⁾ , 3.0 \pm 0.7 ⁽⁵⁾ , 4.0 – 10.0 ⁽⁶⁾ , 3.6 \pm 1.6 ⁽⁷⁾ , 2.2 – 4.5 ⁽⁸⁾ , 1.4 – 3.3 ⁽⁹⁾ , 2.6 – 5.5 (23 Ma) ⁽¹²⁾ , 1.1 – 3.5 (< 20Ma) ⁽¹²⁾ , 2.3 ⁽¹⁴⁾ , 2.82 \pm 1.0 ⁽¹⁵⁾
granodiorite (UC)	0.8 ⁽¹⁾ , 1.7 \pm 0.4 ⁽⁷⁾ , 2.0 ⁽⁹⁾ , 2.45 \pm 1.3 ⁽¹⁵⁾
quartzite dry and wet (UC)	1.0 ⁽¹⁾ , 1.4 (wet) ⁽³⁾ , 2.5 ⁽⁴⁾
diorite (UC)	0.2 – 0.5 ⁽²⁾ , 0.5 (wet) ⁽⁴⁾ , 1.00 \pm 0.4 ⁽⁵⁾ , 0.8 – 1.6 ⁽⁹⁾ , 0.9 – 1.0 ⁽¹¹⁾ , 0.88 \pm 0.3 ⁽¹⁵⁾
gneiss (IC)	2.1 \pm 0.6 ⁽⁵⁾
diabase dry (LC)	0.2 – 0.5 ⁽²⁾ , 0.4 ⁽³⁾
diabase wet (LC)	0.4 ⁽³⁾
anorthosite (LC)	0.2 – 0.5 ⁽¹⁾ , 0.2 ⁽²⁾ , 0.1 ⁽¹⁰⁾ , 0.01 – 0.09 ⁽¹¹⁾
amphibolite (LC)	0.37 \pm 0.19 ⁽¹⁵⁾
granulite felsic (LC)	0.4 – 0.8 ⁽¹⁾ , 0.4 ⁽²⁾ , 0.4 – 0.5 ⁽³⁾
granulite mafic (LC)	0.2 ⁽¹⁾ , 0.25 – 0.4 ⁽³⁾ , 0.1 ⁽⁷⁾
peridotite (LM)	0.002 ⁽²⁾ , 0.006 ⁽³⁾ , 0.01 \pm 0.01 ⁽¹⁵⁾

Table 3.2: The surface heat production rate (A_0) for various rock types (UC for upper crust, IC for intermediate crust, LC for lower crust and LM for lithospheric mantle). Numbers in parentheses refer to: 1. Kukkonen and Jöeleht (1996) and references therein, 2. Moissio *et al.* (2000) and references therein, 3. Afonso and Ranalli (2004) and references therein, 4. Cloetingh *et al.* (2010) and references therein, 5. Lucazeau and Mailhé (1986), 6. Förster and Förster (2000), 7. Förster *et al.* (2010), 8. Verdoya *et al.* (1998), 9. Fernández *et al.* (1998), 10. Fountain (1986), 11. Ashwal *et al.* (1987), 12. Jaupart and Provost (1985), 13. Waples (2002), 14. Doser and Kanamori (1986). 15. Beardsmore and Cull (2001).

Regional and local differences in the chemical composition and age of similar rock types create a range of values, like in granites, which display variable, but usually high, radiogenic heat production (table 3.2 and fig. 3.7). For example, the low value of A_0 ($0.7 \mu\text{W m}^{-3}$) in granites, derives from an Archaean crust (Kukkonen and Jöeleht, 1996) which is expected to be colder. Going deeper towards the mantle from acid to basic chemical compositions, heat

generation decreases significantly, with values becoming nearly zero in the lithospheric mantle. According to [table 3.2](#), in the UC the typical heat production rate is greater than $1.0 \mu\text{W m}^{-3}$ and in the LC less than $1.0 \mu\text{W m}^{-3}$. Heat production in the SL is generally very low and in the LM can be considered practically negligible.

Thermal conductivity k and rock density ρ

The most important thermophysical parameters for vertical temperature calculations are the *thermal conductivity* k and *rock density* ρ . Their SI units are $[\text{W m}^{-1} \text{K}^{-1}]$ and $[\text{kg m}^{-3}]$ respectively. Although thermal conductivity of rocks in the lithosphere strongly depends on temperature and pressure (Birch and Clark, 1940; Seipold, 1992; 1998), it is a common practice in rheological investigations to assume it constant. In [table 3.3](#), the k and ρ values are shown for various types of rocks, as they have been collected from literature.

Rock	ρ [kg m^{-3}]	k [$\text{W m}^{-1} \text{K}^{-1}$]
Sedimentary		
Sandstone	2200-2700 ⁽¹⁾	1.5 – 4.2 ⁽¹⁾
Limestone	2200-2800 ⁽¹⁾ , 2605-2688 ⁽¹⁹⁾	2.0 – 3.4 ⁽¹⁾ , 2.0 ⁽¹⁸⁾ , 3.3 ⁽²⁰⁾ , 2.36 ⁽²¹⁾
Dolomite	2200-2800 ⁽¹⁾	3.2 – 5.0 ⁽¹⁾
Marble	2200-2800 ⁽¹⁾ , 2688 ⁽¹⁹⁾	2.5 – 3.0 ⁽¹⁾
Metamorphic		
Metasediments	2780 ⁽¹¹⁾	3.2 ⁽³⁾
Metasediments (sandstone)	2650 ⁽²²⁾	3.3 ⁽²²⁾
Gneiss	2700 ⁽¹⁾ , 2680-3080 ⁽¹¹⁾	2.1 – 4.2 ⁽¹⁾ , 3.0 ⁽³⁾ , 1.5 – 3.9 ⁽⁷⁾
Amphibolites	3000 ⁽¹⁾	2.5 – 3.8 ⁽¹⁾ , 2.5 – 3.0 ⁽³⁾
Quartzite	2650 ⁽²⁾	2.5 ⁽²⁾ , 6.0 ⁽³⁾ , 5.4 ⁽⁷⁾ , 5.3 – 8.0 ⁽¹⁰⁾ , 5.0 ± 2.4 ⁽¹³⁾ , 5.9 ± 0.8 ⁽¹⁴⁾ , 3.5 ± 0.4 ⁽¹⁵⁾ , 5.6 ± 1.9 ⁽¹⁶⁾ , 6.0 ⁽¹⁷⁾
Granulite felsic	2722 ⁽⁴⁾	3.0 – 3.5 ⁽⁵⁾ , 3.0 ^(3,8)
Granulite intermediate	2779 ⁽⁴⁾	3.0 – 3.5 ⁽⁵⁾ , 3.0 ⁽³⁾
Granulite mafic	2970 ⁽⁴⁾ , 2950-3150 ⁽⁹⁾	3.0 – 3.5 ⁽⁵⁾ , 2.5 ⁽³⁾
Igneous		
Basalt	2950 ⁽¹⁾	1.3 – 2.9 ⁽¹⁾
Granite	2650 ⁽¹⁾ , 2580-2610 ⁽⁹⁾	2.4 – 3.8 ^(1,2) , 2.5 – 3.5 ⁽⁸⁾ , 2.6 – 2.9 ⁽⁹⁾ , 3.3 – 3.8 ⁽¹²⁾ , 3.4 ± 1.2 ⁽¹³⁾ , 3.5 ± 0.4 ⁽¹⁵⁾ , 2.8 ± 0.6 ⁽¹⁶⁾ , 2.7 ⁽²²⁾
Diabase	2900 ⁽¹⁾	1.7 – 2.5 ⁽¹⁾
Diorite	2800 ⁽¹⁾	2.8 – 3.6 ⁽¹⁾ , 2.5 – 2.8 ⁽⁸⁾
Anorthosite	2750 ⁽¹⁾ , 2710 ⁽¹¹⁾	1.7 – 2.5 ⁽¹⁾ , 2.5 ^(3,8)
Granodiorite	2700-2740 ⁽⁶⁾ , 2690 ⁽⁹⁾	2.6 – 3.5 ⁽¹⁾ , 3.0 ⁽³⁾ , 2.6 – 2.9 ⁽⁶⁾ , 2.3 ⁽⁹⁾ , 2.2 – 2.7 ⁽¹⁰⁾
Mantle		
Peridotite	3250 ⁽¹⁾	2.3 – 3.0 ⁽¹⁾
Dunite	3250 ⁽¹⁾	3.7 – 4.6 ⁽¹⁾

Table 3.3: The thermophysical parameters of thermal conductivity k and density ρ for various rock types. More than one range of values is given according to the source of the literature data. The numbers in parentheses correspond to the following references: 1. Turcotte and Schubert (1982), 2. Cloetingh *et al.* (2010), 3. Kukkonen and Jöeleht (1996) and references therein, 4. Rao *et al.* (2006), 5. Jöeleht and Kukkonen (1998), 6. Arndt *et al.* (1997), 7. Ray *et al.* (2007), 8. Moisio *et al.* (2000) and references therein, 9. Förster *et al.* (2010), 10. Davis *et al.* (2007), 11. Fountain (1986), 12. Förster and Förster (2000), 13. Roy *et al.* (1981) after Beardsmore and Cull (2001), 14. Reiter and Tovar (1982) after Beardsmore and Cull (2001), 15. Drury (1986) after Beardsmore and Cull (2001), 16. Barker (1996) after Beardsmore and Cull (2001), 17. Raznjevic (1976) after Beardsmore and Cull (2001), 18. Dragoni *et al.* (1996), 19. Birch and Clark (1940). 20: Fernández *et al.* (1998), 21: Lucazeau and Mailhé (1986), 22: Doser and Kanamori (1986).

Geothermal gradient equations

According to Jaupart and Mareschal (2007) the *vertical temperature profile* must be divided into two main parts: an upper part where heat is transported by *conduction* and a lower part where heat is transported by *convection*. In a steady-state conductive upper part without any heat-producing (radiogenic) elements, *heat flow* is constant implying a constant temperature gradient for constant thermal conductivity, described by the *Fourier's law*. In contrast, if heat-producing elements are present, heat flow and temperature gradient are exponentially expressed. On the other hand, the temperature gradient in a convective layer is not constant and progressively tends to decrease in the underlying mantle. However, in a steady-state regime, the lithosphere is characterized by a nearly linear temperature-depth profile (e.g. Pollack and Chapman, 1977; Sleep, 2005).

Birch *et al.* (1968) proposed that, within a heat flow province, there is a linear relationship between the observed *heat flow* q and the local *heat production* A of rocks of the crystalline basement:

$$q = q_r + AD \quad [3.6]$$

In the equation above, D is the *exponential decay constant* and q_r represents the *reduced heat flow*, which characterizes the outflow of heat below a certain layer, in which the local variations of radioactivity produce the variations of *surface heat flow* q_0 (Rudnick *et al.*, 1998; Jaupart and Mareschal, 1999). Based on the meaning of the parameter D , two basic models have been proposed (after Čermák and Laštovičková, 1987):

- a) the exponential model of Lachenbruch (1968), that characterizes the Earth's crust as a product of magma solidification when the distribution of heat sources was governed by geochemical laws, and
- b) the step model of Roy *et al.* (1968) in which the crust is assumed to be composed of a series of blocks of vertically constant but horizontally varying radioactivity.

The preferred model is the first one because it is independent of the differential erosion of the surface rocks (Lachenbruch, 1970). From equation [3.4], if we replace heat production A with the exponential function of depth (equation [3.5]), the temperature profile of a variable layer will be (Lachenbruch, 1970):

$$T(z) = \frac{q_r z}{k} + \frac{A_0 D^2}{k} (1 - e^{-z/D})$$

If the same layer is beneath another one that produces heat, the boundary condition (at $z = 0$) is $T = T_0$. Therefore, the latter equation takes the form of (Čermák, 1982; Čermák and Laštovičková, 1987):

$$T(z) = T_0 + \frac{q_r z}{k} + \frac{A_0 D^2}{k} (1 - e^{-z/D})$$

Replacing the reduced heat flow q_r with the one of equation [3.6], and for $q_r = q_0$ and $A = A_0$, we obtain:

$$T(z) = T_0 + \frac{q_0 - DA_0}{k}z + \frac{A_0D^2}{k}(1 - e^{-z/D}) \quad [3.7]$$

The latter equation can be broadly used in geotherm calculations for heat transfer due to conduction. If a layer does not produce heat ($A_0 = 0$), then the above equation turns back to a linear function of depth (*Fourier's Law*).

Heat in the lithospheric mantle is transported mainly by convection. For this reason, temperature change *versus* depth is a linear function as suggested by *Dragoni et al. (1996)*:

$$T(z) = T_{0LM} + \frac{T_M - T_{0LM}}{thickness_{LM}} \cdot (z - thickness_{CL}) \quad [3.8]$$

where T_M is the mantle solidus, T_{0LM} is the Moho temperature and $thickness_{CL}$ is the thickness of the crust.

A temperature sensitivity test for the heat productive crust: the contribution of the thermophysical parameters k and A_0

Since the temperature distribution in the lithosphere is the key-element for computing strength envelopes, it is important to understand its behaviour along depth for different rock types. Although surface heat flow q_0 is known for being the strongest affecting parameter, there are also others that show variability and can also affect the geotherm significantly. Such parameters are the thermal conductivity k and surface heat production A_0 , two thermophysical attributes of rocks which are defined from laboratory experiments on samples and usually show not a unique, but a range of values that sometimes vary significantly ([tables 3.1](#) and [3.2](#)). Thus, before proceeding to any further calculations, it would be important to perform a sensitivity test and define the temperature limitations based on these factors.

Heat production is solely associated with crustal rocks, so temperature T as a function of depth is described by [equation \[3.7\]](#). The geothermal gradient in the crust strongly depends on the thermal conductivity coefficient k and the surface heat production rate A_0 . Since these two parameters belong to the rock properties and the two layers of upper and lower crust may consist of different lithologies, the sensitivity tests should be applied to both layers individually.

In order to test how variations in the two layers affect each other, on the top surface of the UC (which can be also directly exposed on the ground), temperature (T_0) is equal to the maximum temperature (max T_{sed}) at the bottom of the overlying sedimentary layer, or equal to the ground temperature T_G , if no sediments exist. At the Conrad interface, the maximum temperature of the UC (max T_{UC}) and the surface temperature of the LC (T_0) are equal. Practically, the temperature of the lower crust T_{LC} at every depth is equal to the maximum T_{UC} plus the temperature produced by the heat production of the LC itself (as if it was isolated). In other words, for every layer, the temperature at any specific depth is the sum of the maximum reached temperature of the overlying layer, which occurs at the bottom of the layer, and the temperature, as it is expressed by the heat production function (linear or exponential) of the layer itself. According to all above, the behaviour of the geotherms in the lower crust can be independently analysed from the other layers of the lithosphere.

Testing the UC

In order to test the geotherms behaviour, the modelling of the UC is carried out based on the most common rock types: granite, granodiorite, diorite and quartzite. The formula used is equation [3.7], for $T_0 = T_G = 286^\circ \text{K}$ and $D = 8.5 \text{ km}$. The UC thickness is assumed equal to 30 km (the maximum thickness that can be found in the Aegean). In order to understand the importance of q_0 , two relatively extreme values are taken, representative of the study area; these are 40 and 100 mW m^{-2} . The mean, minimum and maximum values of k and A_0 (table 3.4) are combined to define the maximum difference of temperature, $\max \Delta T$. There should be an appropriate combination that will produce the highest and lowest temperatures, or else the ‘warmest’ and ‘coolest’ UC curves (fig. 3.8).

Rock	$k \text{ [W m}^{-1} \text{ K}^{-1}]$			$A_0 \text{ [}\mu\text{W m}^{-3}]$		
	min	max	mean	min	max	mean
Granite	2.5	3.5	3.0	2.0	4.0	3.0
Granodiorite	2.2	3.2	2.7	1.0	2.0	1.5
Diorite	2.5	3.5	3.0	0.6	1.4	1.0
Quartzite	5.0	7.0	6.0	1.0	1.4	1.2

Table 3.4: The minimum, mean and maximum values of k and A_0 (taken from tables 3.2 and 3.3) used to define the temperature difference that they can produce in the UC.

The characterization of the crust as ‘warm’ or ‘cool’ is relative. The first refers to crusts where temperature generally increases fast with depth, while the second refers to crusts where temperature increases slower. This also means that the same temperature is met at shallower depths in a *warm* crust than in a *cool* one. Results show that in order to acquire a *warm* UC, the minimum values of k and A_0 are required and *vice versa*. This means that the $\max \Delta T$ can be obtained by using the minimum of k and A_0 (*warm* UC) and the maximum of k and A_0 (*cool* UC) (table 3.5). This sounds logical if we consider that inside a material with high conductivity and heat production (warm crust), a shorter distance (shallow depth) is needed in order for the temperature to be increased by 1° .

Rock type	$k \text{ [W/m K]}$ Perturbation (%)	$A_0 \text{ [}\mu\text{W/m}^3]$ Perturbation (%)	Depth (km)	$\max \Delta T \text{ (}^\circ \text{C)}$ $q_0 = 40 \text{ mW/m}^2$	$\max \Delta T \text{ (}^\circ \text{C)}$ $q_0 = 100 \text{ mW/m}^2$
Granite	3.0 ± 16.67	3.0 ± 33.33	10	57	124
			20	127	263
			30	200	405
Granodiorite	2.7 ± 18.52	1.5 ± 33.33	10	62	146
			20	131	300
			30	202	456
Diorite	3.0 ± 16.67	1.0 ± 40.00	10	51	119
			20	107	244
			30	166	371
Quartzite	6.0 ± 16.67	1.2 ± 16.67	10	23	56
			20	45	113
			30	68	171

Table 3.5: The maximum difference of temperature ($\max \Delta T$) as it is calculated at the main depths of 10, 20 and 30 km, in a 30 km-thick UC, after simultaneously perturbing the mean values (%) of k and A_0 to their extreme values (see also fig. 3.8). This method is applied for both minimum and maximum values of q_0 that can be met in the Aegean.

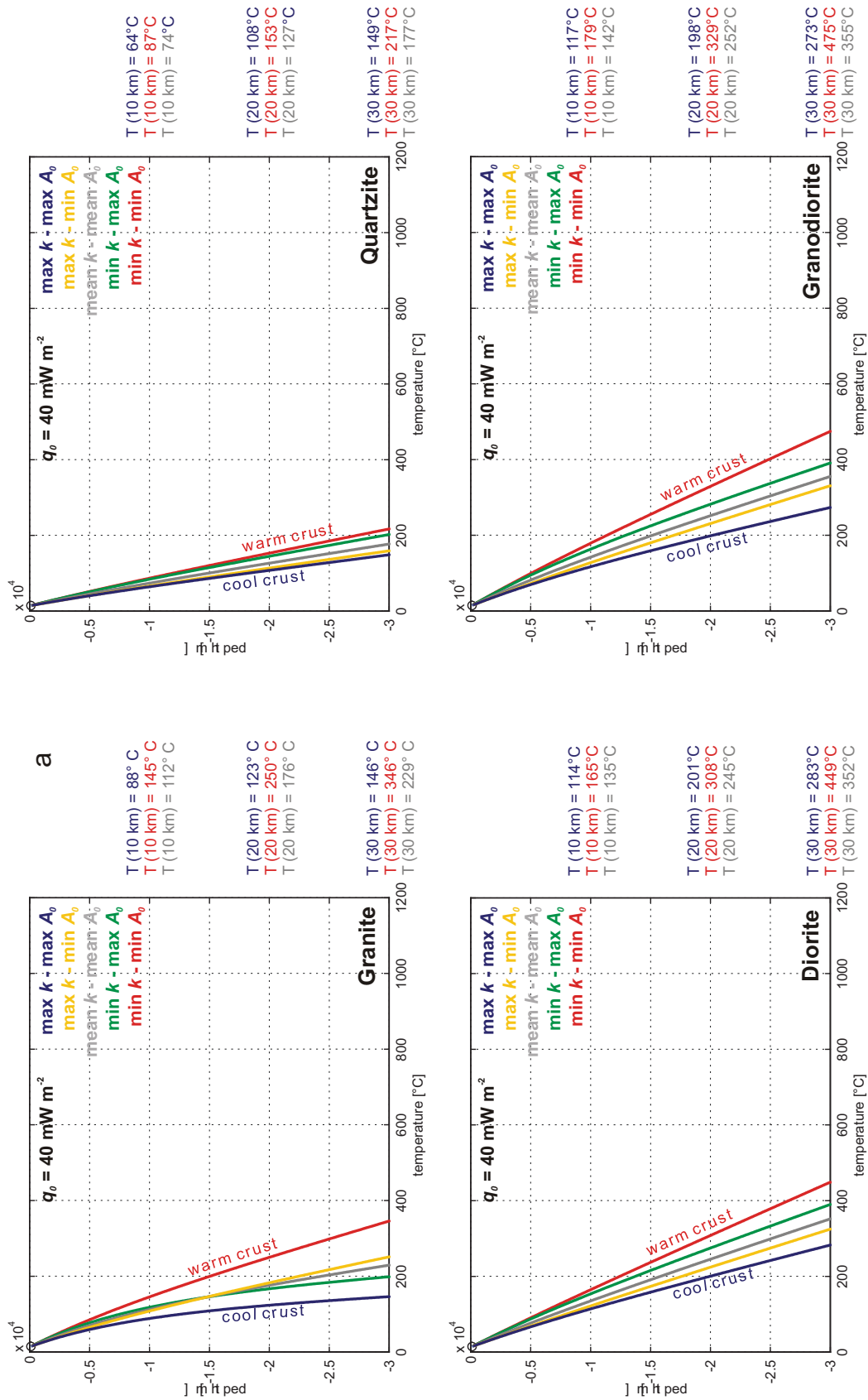


Fig. 3.8: Geotherms produced for various compositions of UC, showing their dependence on k and A_0 , for a) $q_0 = 40 \text{ mW m}^{-2}$, and b) $q_0 = 100 \text{ mW m}^{-2}$. See text for further discussion.

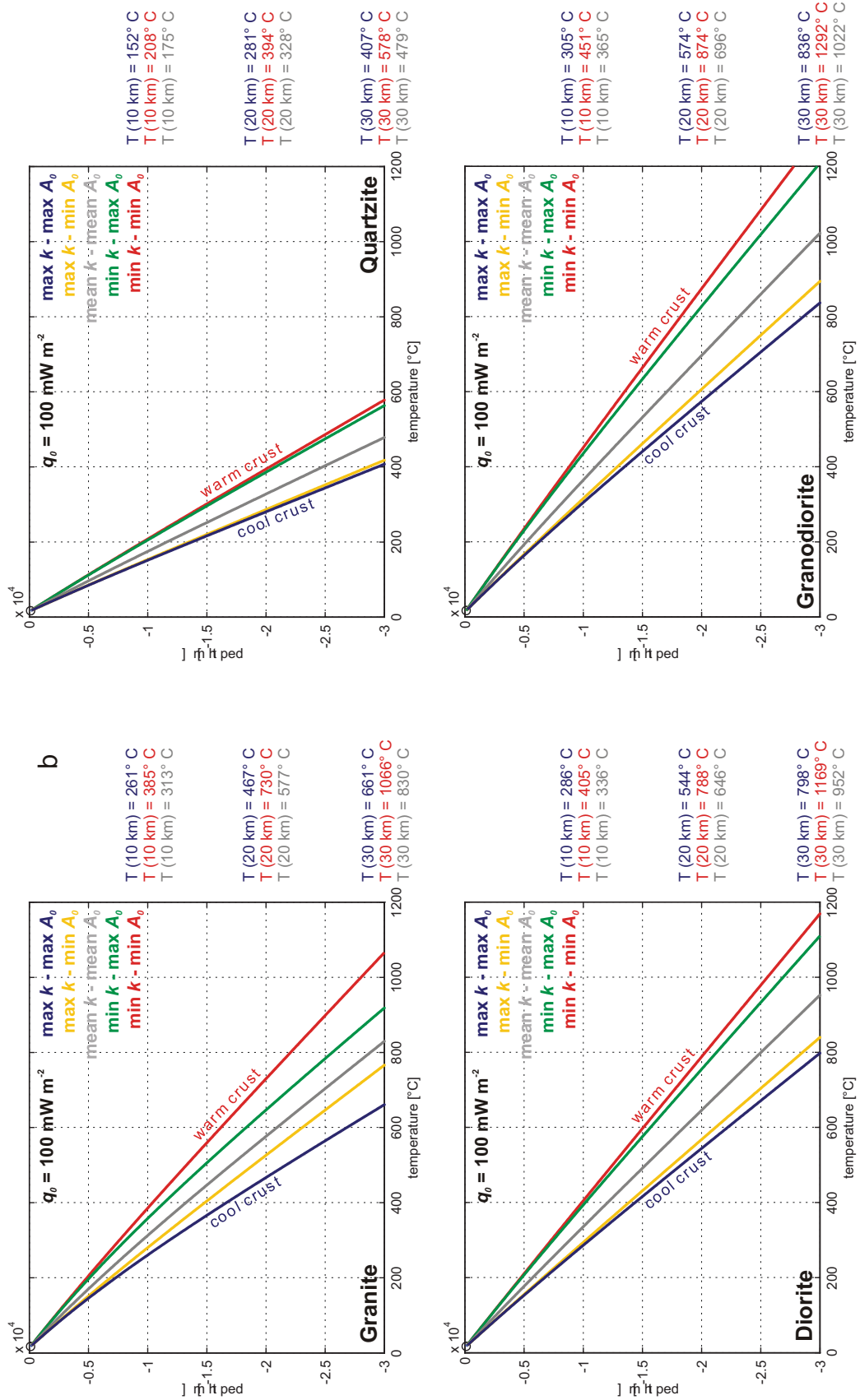


Fig. 3.8 .continued.

Both [fig. 3.8](#) and [table 3.5](#) indicate that when heat flow increases, the temperature spans between warm and cool UC increase, and consequently the sensitivity of k and A_0 increases. For the same heat flow regions, the shortest temperature difference is associated to quartzite, while the largest to granodiorite, which is almost similar to diorite.

Testing the LC

The LC test is carried out by applying the same approach and using the same model parameters ($T_0 = 286^\circ \text{ K}$, $D = 8.5 \text{ km}$, layer thickness = 30 km and $q_0 = 40$ and 100 mW m^{-2}). Again, two hypothetical surface heat flow values are selected, one with $q_0 = 40 \text{ mW m}^{-2}$ and the other with $q_0 = 100 \text{ mW m}^{-2}$. The basic change in the LC model concerns the composition of the layer. The rock types used for modelling LC are felsic and mafic granulite, diabase and anorthosite. Their k and A_0 values are given in [table 3.6](#).

Rock	$k \text{ [W m}^{-1} \text{ K}^{-1}]$			$A_0 \text{ [\mu W m}^{-3}]$		
	min	max	mean	min	max	mean
Felsic granulite	3.0	3.4	3.2	0.4	0.6	0.5
Mafic granulite	2.5	3.5	3.0	0.1	0.3	0.2
Diabase	1.7	2.5	2.1	0.3	0.5	0.4
Anorthosite	2.5	2.5	2.5	0.1	0.3	0.2

Table 3.6: The minimum, mean and maximum values of k and A_0 (taken from [tables 3.2](#) and [3.3](#)) used to define the temperature difference that they can produce in the LC.

Setting and approach are similar to the UC test. For this reason, only the warm, cool and average curves are shown in [fig. 3.9](#), as well as the $max \Delta T$ s at the depths of 10, 20 and 30 km (also in [table 3.7](#)).

Rock type	$k \text{ [W/m K]}$ Perturbation (%)	$A_0 \text{ [\mu W/m}^3]$ Perturbation (%)	Depth (km)	$max \Delta T \text{ (}^\circ \text{C)}$ $q_0 = 40 \text{ mW/m}^2$	$max \Delta T \text{ (}^\circ \text{C)}$ $q_0 = 100 \text{ mW/m}^2$
Granulite felsic	3.2 ± 6.25	0.5 ± 20.00	10	17	40
			20	36	83
			30	55	125
Granulite mafic	3.0 ± 16.67	0.2 ± 50.00	10	47	115
			20	96	232
			30	145	350
Diabase	2.1 ± 19.05	1.0 ± 33.33	10	76	187
			20	153	377
			30	230	-
Anorthosite	2.5 0	0.2 ± 50.00	10	1	3
			20	8	8
			30	15	15

Table 3.7: The maximum difference of temperature ($max \Delta T$) as it is calculated at the main depths of 10, 20 and 30 km, in a 30 km-thick LC, after simultaneously perturbing the mean values (%) of k and A_0 to their extreme values. The method is applied for both minimum and maximum values of q_0 that can be met in the Aegean.

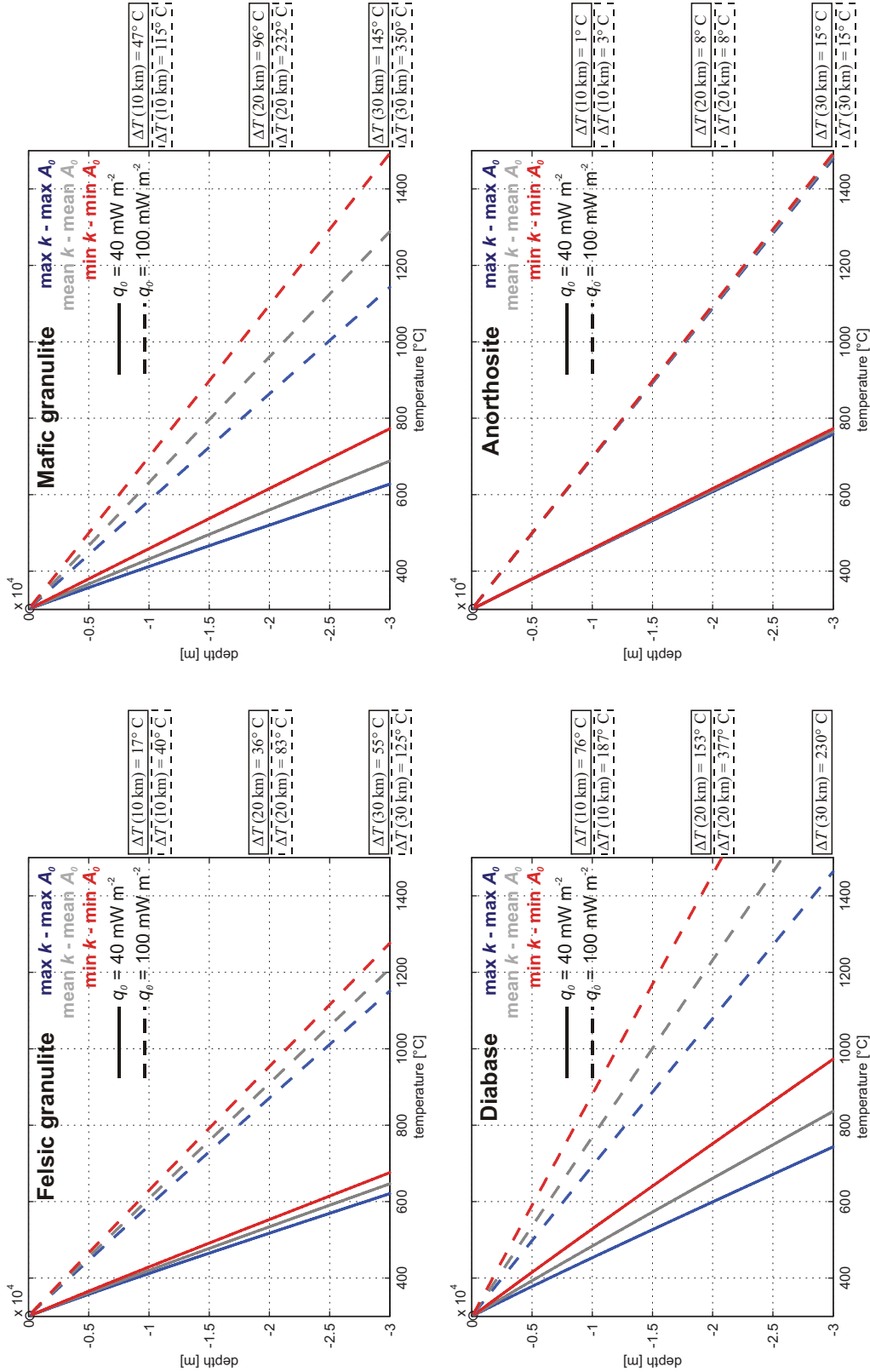


Fig. 3.9: Geotherms produced for various compositions of LC, showing their dependence on k and A_0 , for $q_0 = 40$ and 100 mW m^{-2} . Temperature on the abscissa starts from 300°C , which represents a logical temperature at the bottom of the UC. ΔT is the maximum temperature span at specific depths shown in parentheses. See also text for further discussion.

Comparing with the UC, the *max* ΔT s in LC are smaller. The smallest differences are observed in the anorthosite, whilst in contrast the diabase shows the largest temperature difference. Moreover, LC seems to be generally warmer than the UC.

3.5 The calibration of the strength envelopes

Parameters and conditions

Following the discussion above, geotherms strongly depend on the rock type of the crust, its thermal conductivity and its surface heat production. Consequently, the strength envelopes depend on all these factors, plus the creep parameters which are characteristic of each rock type (table 3.8). Thus, the choice of the appropriate rheological model for all lithospheric layers is essential for the correct calculation of the yield stress envelopes.

Rock type	A_D [MPa ⁻ⁿ s ⁻¹]	n	E [kJ mol ⁻¹]
Limestone (SL)	$4.00 \cdot 10^3$	2.1	210
Solnhofen limestone (SL)	$2.50 \cdot 10^3$	4.7	298
Yule marble (SL)	$2.50 \cdot 10^4$	7.7	256
Carrara marble (SL)	$1.30 \cdot 10^3$	7.6	418
Metasediments (sandstone)	$5.00 \cdot 10^{-6}$	3.0	190
Granite (UC)	$1.26 \cdot 10^{-9}$	2.9	106
Granite dry (UC)	$1.80 \cdot 10^{-9}$	3.2	123
Granite wet (UC)	$2.00 \cdot 10^{-4}$	1.9	137
Quartzite dry (UC)	$6.70 \cdot 10^{-6}$	2.4	156
Quartzite wet (UC)	$3.20 \cdot 10^{-4}$	2.3	154
Granodiorite to quartz diorite (UC)	$1.30 \cdot 10^{-3}$	2.4	219
Quartz diorite dry (UC)	$1.30 \cdot 10^{-3}$	2.4	219
Quartz diorite wet (UC)	$3.20 \cdot 10^{-2}$	2.4	212
Anorthosite (LC)	$3.20 \cdot 10^{-4}$	3.8	238
Granulite felsic (LC)	$8.00 \cdot 10^{-3}$	3.1	243
Granulite mafic (LC)	$1.40 \cdot 10^4$	4.2	445
Diabase dry (LC)	8.00	4.7	485
Diabase wet (LC)	$2.00 \cdot 10^{-4}$	3.4	260
Olivine (LM)	$4.00 \cdot 10^6$	3.0	510
Peridotite dry (LM)	$2.50 \cdot 10^4$	3.5	532
Peridotite wet (LM)	$2.00 \cdot 10^3$	4.0	471
Dunite dry (LM)	$9.55 \cdot 10^3$	3.35	444
Dunite wet (LM)	$2.00 \cdot 10^3$	4.0	471

Table 3.8: The creep parameters of various rock types commonly found in the lithosphere: A_D is the Dorn parameter, n is the power-law exponent and E is the activation energy (Schmid *et al.*, 1980; Chopra and Paterson, 1981; Kirby, 1983; Doser and Kanamori, 1986; Carter and Tsenn, 1987; Kirby and Kronenberg, 1987; Ranalli, 1987 and references therein; 1995 and references therein; Ranalli and Murphy, 1987; Wilks and Carter, 1990; Karato and Wu, 1993; Porth, 2000 and references therein).

Most of the modelling parameters can be either directly acquired (*e.g.* q_0 , creep parameters, *etc.*) or indirectly inferred (*e.g.* the composition of the lithospheric layers from the elastic waves velocities). In order to evaluate and calibrate the initial models, three study areas are selected

where seismic spatial distribution is well known. Aftershock and microseismic studies can provide estimation about the allocation of the events along depth, and therefore constrain the BDT zone. It is noteworthy to mention that the brittle part of the lithosphere can be equal or greater than the maximum depth of the observed hypocentres. The occurrence of an earthquake, especially if it is of small magnitude, does not necessary mean that the seismogenic layer has been totally ruptured. On the contrary, the opposite scenario is not valid: the brittle part cannot be shallower than seismic distribution.

At a certain temperature and pressure, one of the main rheological deformation mechanisms will become the dominant one. An unconventional division of the strength envelope models can be found in the literature. The first one, called “*conventional model*” (e.g. Pauselli *et al.*, 2010), involves the two older equations of frictional sliding and creep-law deformational behaviours (equations [3.1] and [3.2]). In this case the rock will be deformed by the dominant mechanism that satisfies the following condition:

$$\sigma_1 - \sigma_3 = \min\left[(\sigma_1 - \sigma_3)_f, (\sigma_1 - \sigma_3)_c\right]$$

The second one, which will be called as *three-deformational model* in this thesis, involves all three deformational behaviours described in §3.2 (equations [3.1], [3.2] and [3.3]). In this case the rock will be deformed by the dominant mechanism that satisfies the following condition:

$$\sigma_1 - \sigma_3 = \min\left[(\sigma_1 - \sigma_3)_f, (\sigma_1 - \sigma_3)_c, (\sigma_1 - \sigma_3)_b\right]$$

The selected study cases belong to the Kozani, South Thessaly and central Mygdonia Basin regions. These areas have been the investigational field of several seismological studies that have provided earthquake spatial distribution graphs and data. These data can be used to either calibrate and/or validate the rheological models based on the calculation of the strength envelopes. During this procedure, only the three main thermal types of crust discussed before (*cool, medium and warm crust*) will be used in the rheological models. In this way, it will be succeeded to calculate the lithospheric strength according to the extreme and average thermal conditions of the crust. In order to facilitate the calculations and the visualization of the results, a routine was programmed in the Matlab[®] software.

The Kozani region case study

The aftershock sequence of the May 13, 1995 ($M_w = 6.5$) Kozani earthquake was well studied (Hatzfeld *et al.*, 1997; 1998; Drakatos *et al.*, 1998a; Papanastassiou *et al.*, 1998; Papazachos *et al.*, 1998) by using temporary seismographic networks (Hatzfeld *et al.*, 1997; IG-NOA). The profiles indicate that the majority of the events occurred above the hypocentral depth of the mainshock (*ca.* 14.5 km), while fewer and sparse shocks occurred down to a maximum depth of *ca.* 17 km.

The rheological model for the Kozani area consists of four layers (SL, UC, LC and LM). The parameters of the rheological model used for the Kozani area are shown in [table 3.9](#). The selection of composition and thicknesses are based on the geophysical investigations discussed in the ‘*Lithospheric composition and models*’ section. However, the choice of wet peridotite instead of dry in the LM is preferred also for two other reasons: i) if we consider the study area as an old subduction zone (Tethys), then the water incorporated in the subducting slab of the

oceanic lithosphere, in hydrous minerals or as interstitial fluid, may be forced out of the slab by compaction or by breakdown of the hydrous minerals, migrating upwards into the warmer, overlying rocks of the LM (e.g. Wyllie, 1971; Boettcher, 1973; Davies and Bickle, 1991; Peacock, 1991; Katayama *et al.*, 2005), and ii) dry peridotite is more brittle causing a deepening of the BDT where seismicity is far from being present. Surface heat flow is obtained from the synthesis of all available literature data in the broader region (Haenel and Staroste, 1988; Pollack *et al.*, 1993; Taktikos, 2001; Hurter and Haenel, 2002; Cloetingh *et al.*, 2010). Local strain rate is estimated from various maps (e.g. Hollenstein *et al.*, 2008; Jenny *et al.*, 2004; El-Fiky, 2000; (figs. 1.4b, 1.5a and 1.6, respectively). The calculation of the geothermal gradients (fig. 3.10) is based on the same approach used in the geotherms tests.

Kozani Region		
q_0 :	50 mW m ⁻²	
Strain rate $\dot{\epsilon}$:	1 10 ⁻¹⁵ sec ⁻¹	
Fault-type α :	0.75 (extensional tectonic regime)	
pore fluid / lithostatic pressure ratio λ :	0.36	
Lithospheric thickness:	125 km	
SL:	thickness: 12 km rheology: limestone / Carrara marble / metasediments	low radiogenic heat production $k = 2.3 / 2.8 / 3.2 \text{ W m}^{-1} \text{ K}^{-1}$ $A_0 = 0.62 / 1.0 / 1.5 \text{ } \mu\text{W/m}^3$
UC	thickness: 13 km rheology: granodiorite warm / medium / cool	radiogenic heat production for k and A_0 see table 3.4 and text
LC	thickness: 15 km rheology: mafic granulite warm / medium / cool	radiogenic heat production for k and A_0 see table 3.6 and text
LM	thickness: 85 km rheology: peridotite wet	no heat production

Table 3.9: Rheological model and parameters used to calculate the strength envelopes in the Kozani region.

The results (fig. 3.10) show a variation in the depth of the BDT zone which is dependent on the temperature and the rheology of the layers, as well as on the strength envelope model that is used (conventional or three-deformational). It is important to notice that the strength values shown in the diagrams of fig. 3.10 and in the diagrams of the following case studies are the absolute ones. This selection was made simply for visualization reasons, given that for normal faulting the strength values should be negative.

In the conventional model, the limestone-granodiorite-granulite mafic-peridotite wet rheological model has the closest match with the observed aftershock spatial distribution of the 1995 event. The suggested BDT depths range between 17.1 and 19.7 km with the preferred model that corresponds to a medium geotherm showing 18.4 km of depth. A narrow area of possible ductile behaviour is observed between the depths of 9.2 and 12 km, but it is considered too narrow to halt rupture propagation. It is noteworthy that the soft layer can become even narrower if we use a limestone's k more than $2.3 \text{ W m}^{-1} \text{ K}^{-1}$ than the one used in the previous example (the geotherm becomes colder and the behaviour more brittle). The next closely matching results derive from the other two rock combinations, but with the warm crusts. The

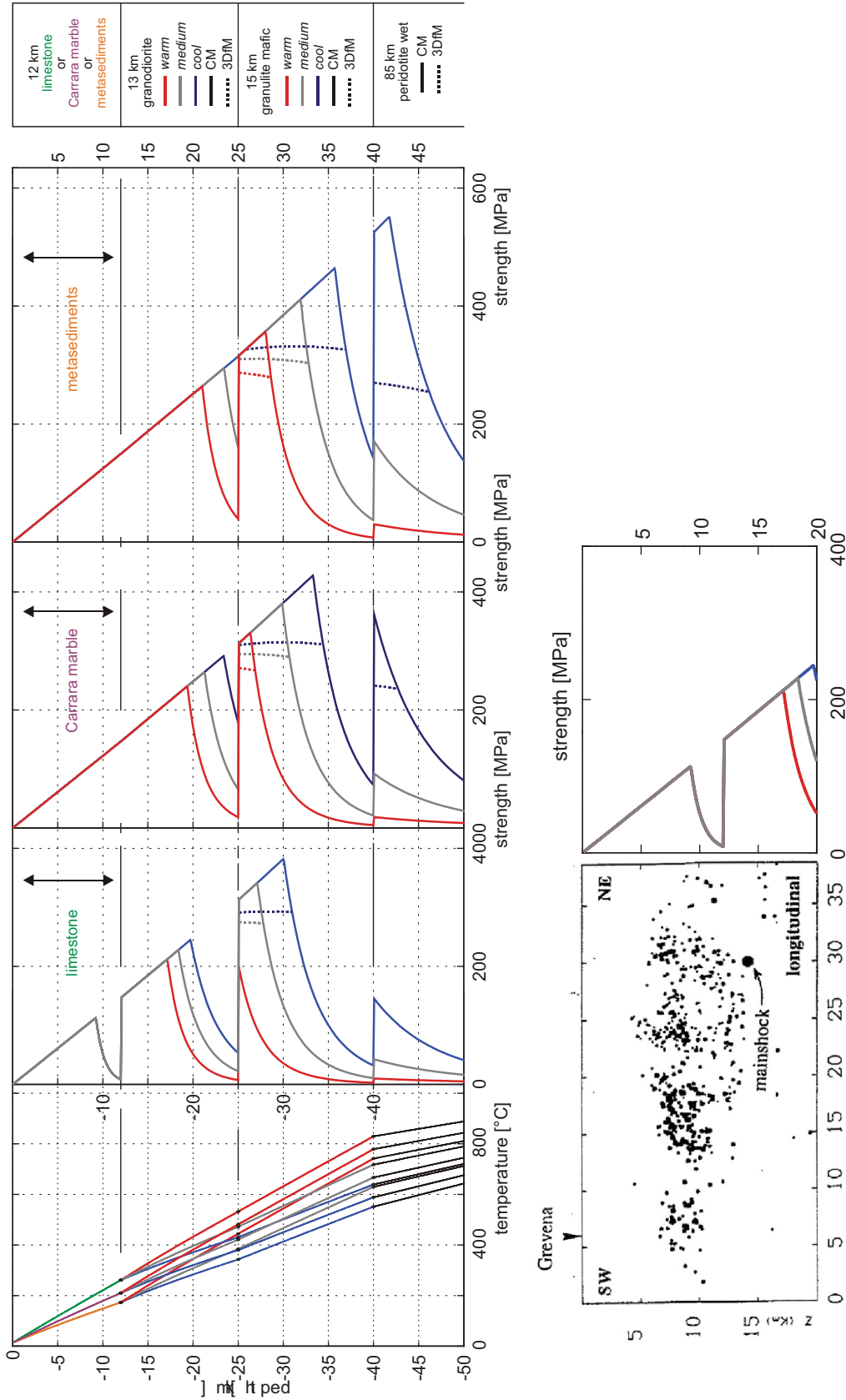


Fig. 3.10: Top: geotherms and yield stress envelopes of the Kozani region. Continuous lines belong to the conventional model (CM), while dotted lines belong to the *three-deformational* model (3DFM; see text for details). Red, grey and blue lines indicate warm, medium and cool crust respectively (see text for discussion). Bottom: comparison between the 1995 aftershock distribution as given by Hatzfeld *et al.* (1997) and the preferred model of limestone SL.

Carrara marble-warm granodiorite-warm granulite mafic-peridotite wet combination suggests a BDT depth of 19.3 km while, while the metasediments-warm granodiorite-warm granulite mafic-peridotite wet combination suggests a depth of 21 km. A significant characteristic of both combinations is that they do not show any gap of ductile behaviour until the BDT depths.

The three-deformational model shows some differences in the LC of all the rheological models. A brittle sector appears whose thickness increases from warm to cool crust and from limestones to Carrara marble and metasediments. In some cases this sector is thin and probably does not participate to the seismogenic layer thickness. However, the rheological model with the metasediment-consisting SL seems to be the most inappropriate model.

The South Thessaly case study

A similar procedure is followed for the definition of the BDT zone in the broader Pagasitikos Gulf area. In fact, based on the microseismic spatial distribution data of Kementzetzidou (1996) and Hatzfeld *et al.* (1999), the area can be divided into three sub-regions (fig. 3.11): the eastern, the central and the western sector. The profiles of the previous authors show a deepening of the seismogenic layer thickness from *ca.* 12 km to the east to *ca.* 18 km to the west.

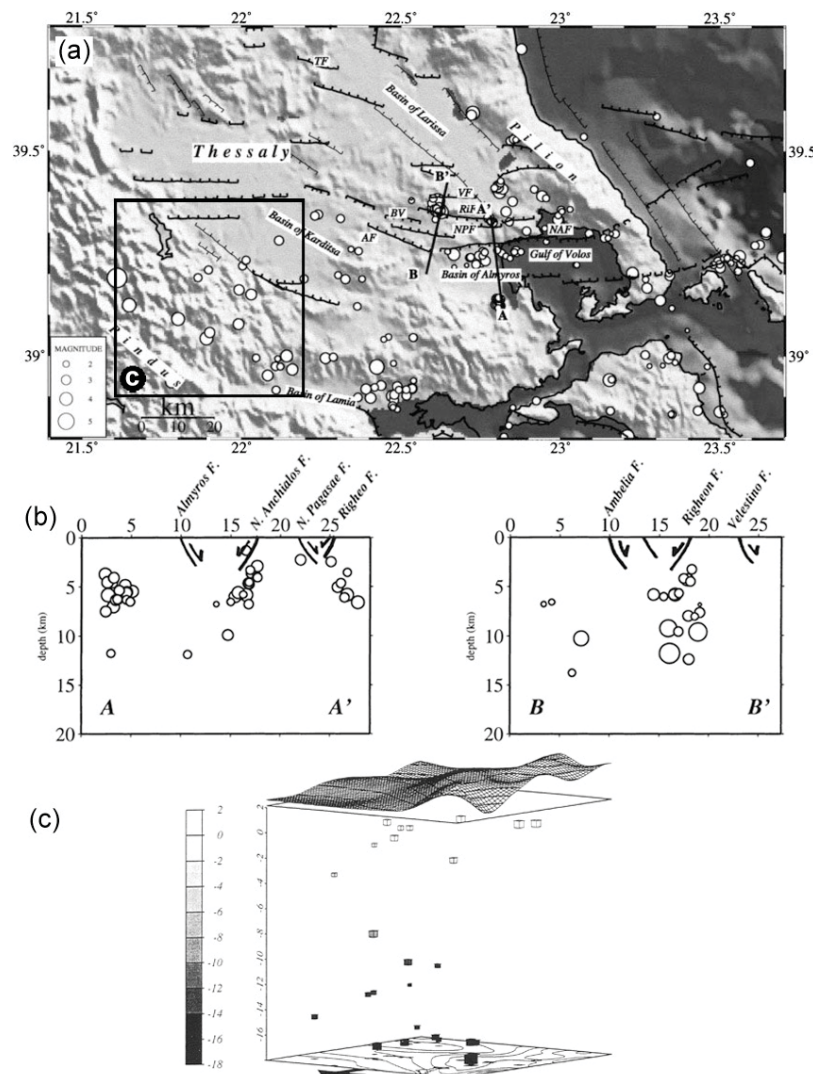


Fig. 3.11: Microseismic spatial distribution of South Thessaly (modified after Kementzetzidou, 1996; Hatzfeld *et al.*, 1999). (a) Map view of the epicentres, major faults, profile traces and the frame location of (c). (b) Profiles showing the vertical distribution in the eastern-central part of the study area. (c) 3D-view of microseismic distribution in the western part of the study area.

The rheological models (tables 3.10, 3.11 and 3.12) consist of four layers, like in the Kozani region. However, the Moho depth shows a gradual deepening from east to west (32 to 40 km respectively). Surface heat flow also changes accordingly, from 85 to 65 mW m⁻², with few localities of high heat flow (Haenel and Staroste, 1988; Pollack *et al.*, 1993; Taktikos, 2001; Hurter and Haenel, 2002; Cloetingh *et al.*, 2010). The rheological properties of the crust and LM have been assumed similar to the Kozani region, according to the V_p and V_s velocities. Meanwhile, the composition of the uppermost layer (SL) may be variable from metasediments towards the east to carbonate rocks towards the west. Southern Thessaly undergoes a faster deformation with an estimated strain rate of $5.0 \cdot 10^{-15} \text{ sec}^{-1}$ (e.g. Hollenstein *et al.*, 2008; Jenny *et al.*, 2004; El-Fiky, 2000; (figs. 1.4b, 1.5a and 1.6, respectively).

South Thessaly region – eastern section		
q_0 :	85 mW m ⁻²	
Strain rate:	$5 \cdot 10^{-15} \text{ sec}^{-1}$	
Fault-type α :	0.75 (extensional tectonic regime)	
pore fluid / lithostatic pressure ratio λ :	0.36	
Lithospheric thickness:	125 km	
SL:	thickness: 6 km rheology: limestone / metasediments	low radiogenic heat production $k = 2.5 / 3.2 \text{ W m}^{-1} \text{ K}^{-1}$ $A_0 = 0.62 / 1.5 \mu\text{W m}^{-3}$
UC	thickness: 13 km rheology: granodiorite warm / medium / cool	radiogenic heat production for k and A_0 see table 3.4
LC	thickness: 13 km rheology: mafic granulite warm / medium / cool	radiogenic heat production for k and A_0 see table 3.6
LM	thickness: 93 km rheology: Peridotite wet	no heat production

Table 3.10: Rheological model and parameters used to calculate the strength envelopes in the eastern sector of the South Thessaly.

South Thessaly region – central section		
q_0 :	70 mW m ⁻²	
Strain rate:	$5 \cdot 10^{-15} \text{ sec}^{-1}$	
Fault-type α :	0.75 (extensional tectonic regime)	
pore fluid / lithostatic pressure ratio λ :	0.36	
Lithospheric thickness:	125 km	
SL:	thickness: 8 km rheology: limestone	low radiogenic heat production $k = 2.5 \text{ W m}^{-1} \text{ K}^{-1}$ $A_0 = 0.62 \mu\text{W m}^{-3}$
UC	thickness: 14 km rheology: granodiorite warm / medium / cool	radiogenic heat production for k and A_0 see table 3.4
LC	thickness: 14 km rheology: mafic granulite warm / medium / cool	radiogenic heat production for k and A_0 see table 3.6
LM	thickness: 89 km rheology: peridotite wet	no heat production

Table 3.11: Rheological model and parameters used to calculate the strength envelopes in the central sector of the South Thessaly.

South Thessaly region – western section		
q_0 :	60 mW m ⁻²	
Strain rate:	5 10 ⁻¹⁵ sec ⁻¹	
Fault-type α :	0.75 (extensional tectonic regime)	
pore fluid / lithostatic pressure ratio λ :	0.36	
Lithospheric thickness:	125 km	
SL:	thickness: 10 km	low radiogenic heat production $k = 2.5 \text{ W m}^{-1} \text{ K}^{-1}$ $A_0 = 0.62 \text{ } \mu\text{W m}^{-3}$
	rheology: limestone	
UC	thickness: 15 km	radiogenic heat production for k and A_0 see table 3.4
	rheology: granodiorite warm/medium/cool	
LC	thickness: 15 km	radiogenic heat production for k and A_0 see table 3.6
	rheology: mafic granulite warm/medium/cool	
LM	thickness: 85 km	no heat production
	rheology: peridotite wet	

Table 3.12: Rheological model and parameters used to calculate the strength envelopes in the western sector of the South Thessaly.

The results of the geotherms and the strength envelopes are illustrated in [fig. 3.12](#). In the conventional model, the rheological model with the carbonate SL shows a gradual deepening of the BDT zone towards west, being in accordance with the suggested hypocentral depths of the microearthquake survey of Kementzetzidou (1996) and Hatzfeld *et al.* (1999). The BDT depth for the eastern sector ranges between 11.4 and 13.8 km, for warm and cool crusts respectively, having a 12.6 km BDT depth for a medium crust. At the central part of the study area, the same lithological combination suggests a respective BDT depth spanning between 13.7 and 16.5 km, for a warm and cool crust respectively, with a medium crust providing a depth of 15.1 km. At the western part, the BDT depth ranges between 16.0 and 19 km for warm and cool crusts respectively, while depth reaches 17.5 km for a medium crust. It is noteworthy that the metasediments-granodiorite-mafic granulite-wet peridotite stratific succession in the eastern sector provides BDT depths close to the observed hypocentral distribution. In particular, the suggested range is between 12.5 and 15.7 km for warm and cool crust respectively, and the depth of the medium crust is suggested to 14.1 km.

The three-deformational model of the cool crust thermal state rheological model shows a brittle sector in the LC. Its maximum thickness is around 6 km. In fact, in the case of limestone-consisting SL, this brittle sector can be considered negligible for the rheological model of the eastern sector. Due to its great distance from the upper brittle part of the lithosphere (4-8 km), any real seismogenic contribution is unlikely.

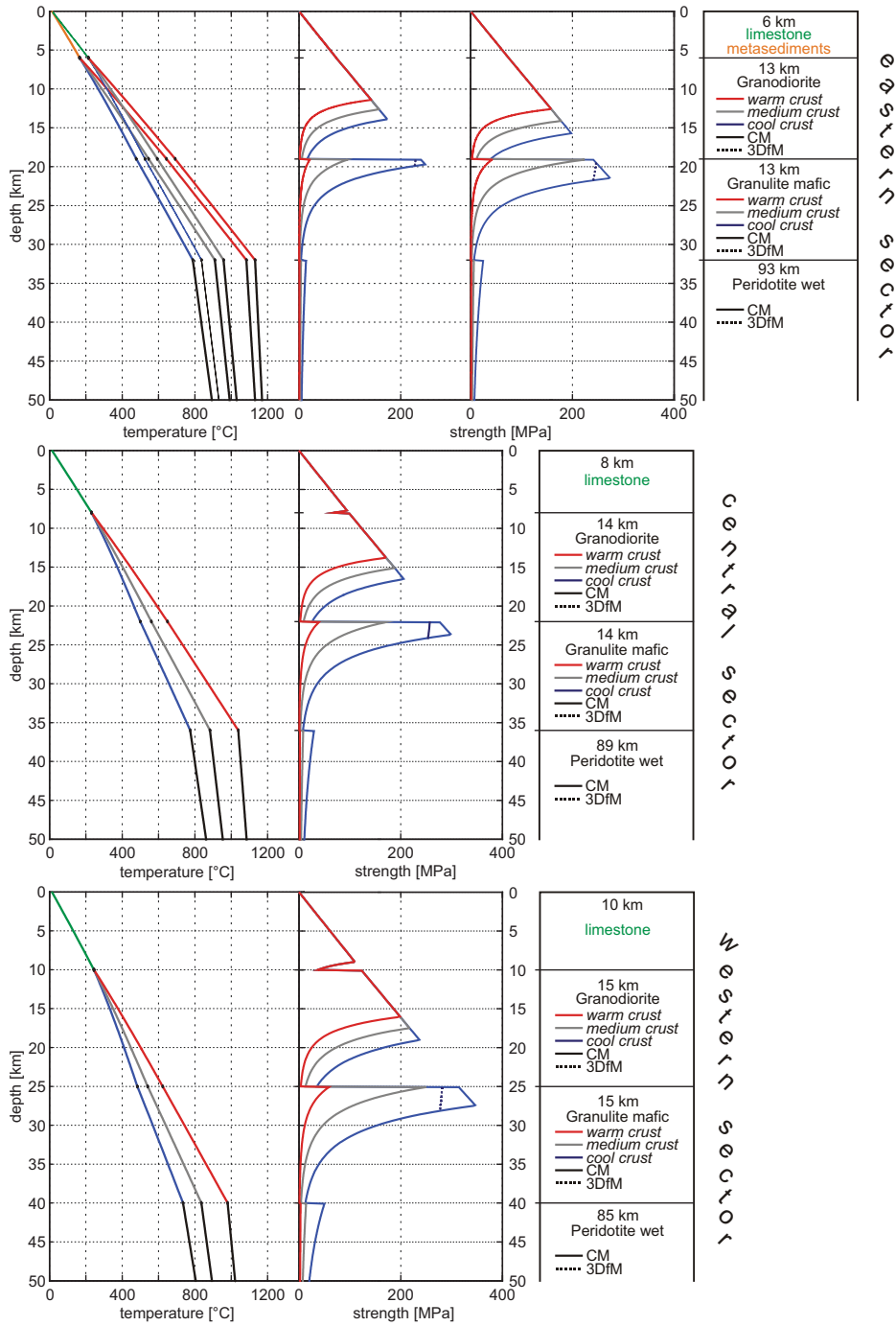


Fig. 3.12: Geotherms and yield stress envelopes of South Thessaly for the three sectors (eastern, central and western part). Symbols are similar to [fig. 3.10](#).

The central Mygdonia Basin case study

For the third experimental area both aftershock sequence and microseismic surveys are available. Indeed, the July 20, 1978 Thessaloniki event was followed by several aftershocks (Carver and Bolinger, 1981; Soufleris *et al.* 1982), while in the subsequent decades many microearthquake investigations were carried out in the broader area (Hatzfeld *et al.*, 1986/87;

Hatzidimitriou *et al.*, 1991; Galanis *et al.*, 2004; Paradisopoulou *et al.*, 2004; 2006). The hypocentral distributions obtained from all the studies above, are not deeper than *ca.* 17 km, with the only exception the one of Galanis *et al.* (2004) who suggest depths down to 20 km (fig. 3.13). The latter, however, seems to be rather overestimated.

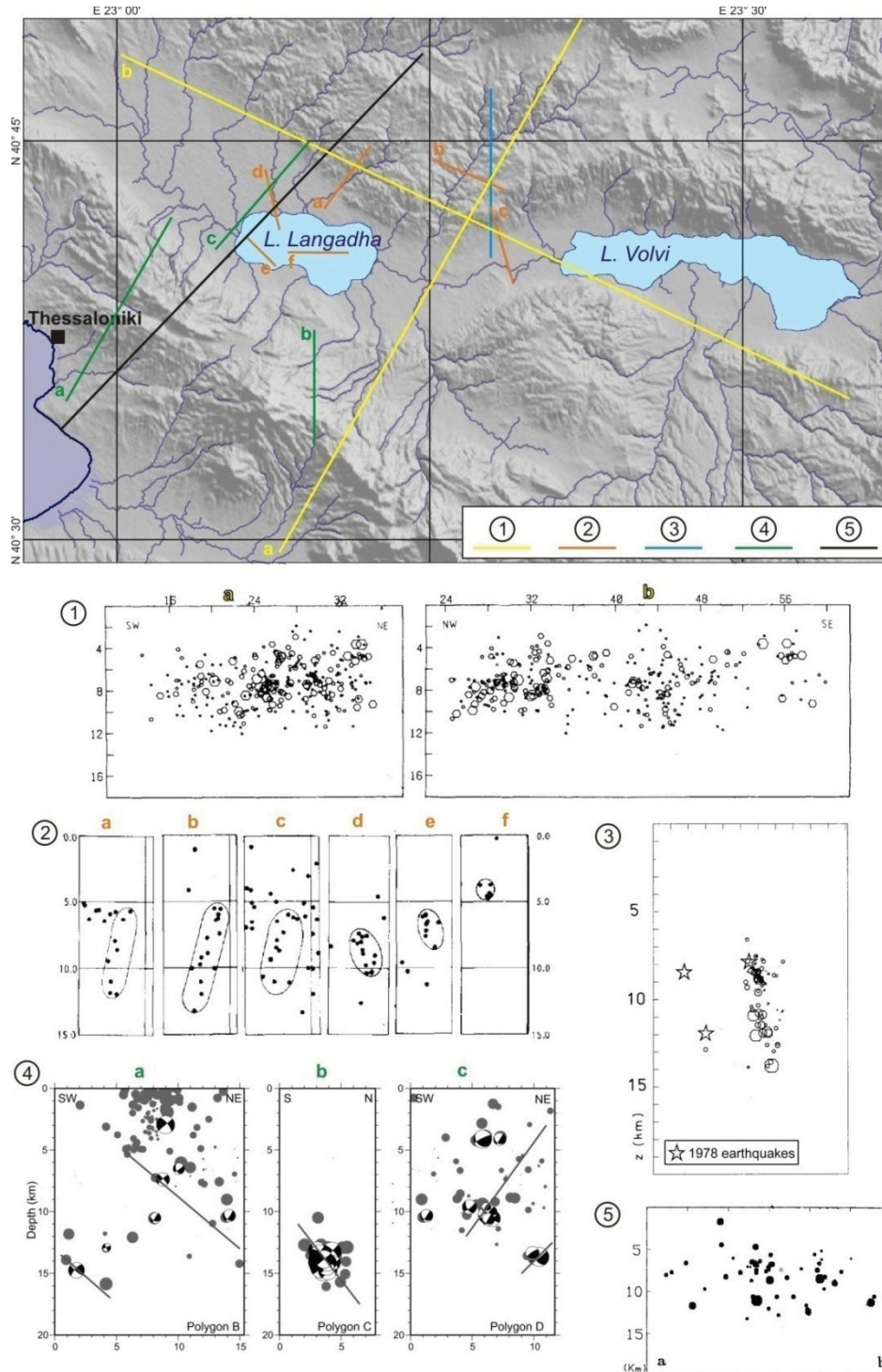


Fig. 3.13: Profiles of seismic vertical distribution in the Mygdonia Basin. *Top:* map of the profiles locations by (1) Soufleris *et al.* (1982), (2) Carver and Bollinger (1981), (3) Hatzfeld *et al.* (1986/87), (4) Paradisopoulou *et al.* (2006), and (5) Hatzidimitriou *et al.* (1991). *Bottom:* the profiles corresponding to the numbers in the map above.

The rheological model comprises four layers ([table 3.13](#)), which according to the V_P and V_S , consist of (from top to bottom): metasediments (also dominating as outcrops), granodiorite, felsic granulite and wet peridotite. The choice of felsic, instead of mafic, granulite in the LC is justified by the occurrence of a continental crust different from the Kozani area, as far as Central Macedonia was belonging to a different continental fragment. Surface heat flow varies inside the basin, with few localities showing high values due to the occurrence of geothermal fields. Nevertheless, an average value of 65 mW m^{-2} can be confidently estimated. The Mygdonia Basin undergoes an extensional deformation with an estimated strain rate of $5.0 \cdot 10^{-15} \text{ s}^{-1}$ (e.g. Hollenstein *et al.*, 2008; Jenny *et al.*, 2004; El-Fiky, 2000; ([figs. 1.4b](#), [1.5a](#) and [1.6](#), respectively).

Mygdonia Basin		
q_0 :	65 mW m^{-2}	
Strain rate:	$5 \cdot 10^{-15} \text{ sec}^{-1}$	
Fault-type α :	0.75 (extensional tectonic regime)	
pore fluid / lithostatic pressure ratio λ :	0.36	
Lithospheric thickness:	125 km	
SL:	thickness: 3 km rheology: metasediments	low radiogenic heat production $k = 3.2 \text{ W m}^{-1} \text{ K}^{-1}$ $A_0 = 1.5 \text{ } \mu\text{W m}^{-3}$
UC	thickness: 15 km rheology: granodiorite warm/medium/cool	radiogenic heat production for k and A_0 see table 3.4
LC	thickness: 15 km rheology: felsic granulite warm/medium/cool	radiogenic heat production for k and A_0 see table 3.6
LM	thickness: 92 km rheology: peridotite wet	no heat production

Table 3.13: Rheological model and parameters used to calculate the strength envelopes in the Mygdonia Basin.

Both diagrams of the geotherms and the strength envelopes are illustrated in [fig. 3.14](#). According to the conventional model, the BDT zone depth for a cool and warm crust is 20.0 and 14.9 km respectively. The corresponding BDT zone for a medium crust is 18 km. The hypocentral depth distribution is within and very close to the depth range of the suggested BDT. The model containing the high-pressure brittle failure equation shows a small differentiation only in the cool crust model, in which at the depth of around 30 km and for *ca.* 7.5 km the LM behaves again in a brittle way. However, even in this case, this brittle layer is too thin and too distant from the upper brittle section to allow a continuous rupture of the whole crust. Moreover, the lack of seismicity at such depths further supports this interpretation.

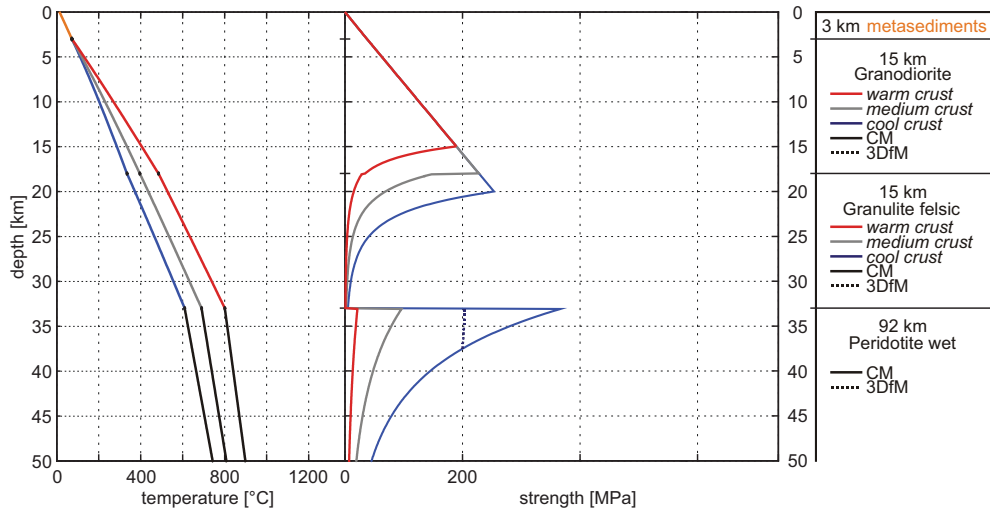


Fig. 3.14: Geotherms and yield stress envelopes of the Mygdonia Basin. Symbols are similar to [fig. 3.10](#).

Discussion

In the three test areas, the BDT zones obtained from the strength envelopes as described above are in good agreement with the suggested seismogenic layer thickness inferred from seismic distributions. The results of these tests are promising as far as the same methodology could be also applied to regions where microseismicity distribution is not available neither aftershock sequences. Following this approach and based on a careful selection of the most suited rheological model and its thermophysical parameters it could be thus possible to constrain the BDT depth and therefore the maximum depth and width of the seismogenic sources affecting these crustal volumes.

4.1 Strain rate and slip rate

Slip rate definitions and theoretical approach

Slip rate represents the amount of strain that accumulates and then is released across a fault in a given time period (McCalpin, 2009). Slip rates can be computed over spans of millions of years (many seismic cycles) to hundreds of years (a single seismic cycle, or a part of a cycle) (fig. 4.1). Most slip rates published to date have been calculated from the cumulative displacement of dated landforms or deposits, over multiple seismic cycles, and are termed mean slip rates, long-term slip rates, or geologic slip rates. Of more use to palaeoseismology are the slip rates of individual seismic cycles, called closed-cycle slip rates, short-term slip rates, or inter-event slip rates (McCalpin, 2009; Chang and Smith, 2002). According to Shimazaki and Nakata (1980), there are three recurrence models (fig. 4.2): *i*) a strictly periodic model, where slip on fault and time interval between large earthquakes are fixed, *ii*) a time-predictable model, where time between large earthquakes is proportional to the amount of slip preceding the earthquake, and *iii*) a slip-predictable model, where time interval between large earthquakes is proportional to the slip amount of earthquake about to occur. Nonetheless, it is not uncommon for earthquake events to be clustered in time and then be separated by relatively long periods of low activity (*e.g.* Coppersmith, 1988; Dieterich, 1994). This means that estimated short-term slip rates might be much different from the long-term ones. Another aspect of the geologically measured slip rate is the difficulty and uncertainty of assessing average slip rates from typically only a few data points along the fault. Along-strike variations in fault displacement patterns can be significant and often slip rate data are only available from a few selected sites, typically where the fault is best expressed in the youngest deposits. Thus, whether data from these sites are representative of average rates or are closer to maximum values is difficult to assess.

Slip rates are usually the result of palaeoseismic investigations and/or surficial studies (such as scarp morphology). The former provide the best determined results for well-defined, complete seismic cycles (*e.g.* Machette *et al.*, 1992; McCalpin, 2009), whereas the latter include unknown open-ended time periods that can bias results. These open-ended periods include *i*) the time since the most recent event and *ii*) the time between the age of the surface that the displacement is measured on and the time of the first event to offset the surface. Inclusion of large open-ended periods in long-term slip rate data from surficial studies may, in part, explain why observed short-term slip rates are much higher than long-term rates (Wong and Olig, 1998).

Methods of Calculating Slip Rate

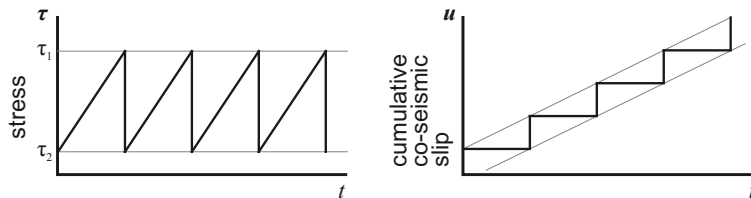
SLIP \ AGE	Total slip on Structure/ Basin (A)	Geomorphic Evidence		Stratigraphic Evidence; discrete Displacements (D)
		Faceted Spur Height (B)	Quaternary fault scarps on Surfaces (C)	
Time Since Initiation of Faulting (1)	A1 (Ex: 2000 m throw since 20 Ma = 0.1 m/ka = 0.1 mm/yr)			
Ages of Displaced Landforms (2)		B2 (dePolo, 1998)	C2 (scarp height D divided by landform age T; includes open cycles)	
Ages of Displacement Events (3)				D3 (D3a, open and closed cycles; D3b, closed cycles only)

MORE SEISMIC CYCLES ----- FEWER CYCLES
 (temporal variability assessed) (temporal variability unknown)

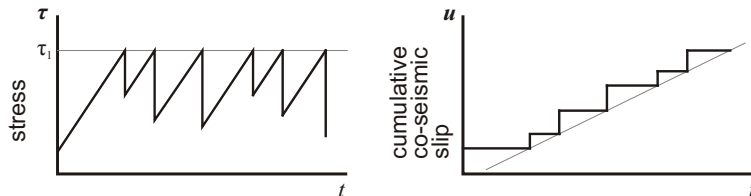
LESS PRECISION ----- MORE PRECISION
 On Slip and Age (Measurement Error, spatial variability) on Slip and Age (Measurement Error, spatial variability)

Fig. 4.1: Comparison of methods for calculating slip rates, based on the datum on which slip is measured (SLIP), and the time period over which it is measured (AGE). Methods A1 and B2 describe landscape elements that formed over hundreds of ka to a few Ma, and do not distinguish individual palaeoearthquakes or seismic cycles; thus they belong more to neotectonics than to palaeoseismology. Method C2 may be based on late Quaternary fault scarps produced by a small, known number of palaeoearthquakes. Method D3 is based on trenching investigations that date individual palaeoearthquake displacements directly. After McCalpin (2009).

a) strictly periodic model



b) time-predictable model



c) slip-predictable model

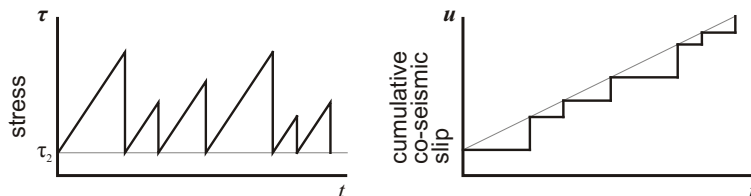


Fig. 4.2: Schematic recurrence models (modified after Shimazaki and Nakata, 1980): **a)** strictly periodic, **b)** time-predictable, and **c)** slip-predictable.

As slip rates are usually measured over longer time periods than recurrence intervals, they may not reflect the most recent palaeoseismic behaviour of a fault or its short-term variations. Because in performing probabilistic SHA, the intent is usually to assess the hazard in the near future for engineering applications, a characterization of the most recent behaviour of seismic sources is often desired. Unfortunately, detailed slip rate data to characterize possible short-term variations in activity is lacking for most faults. In the present research, it is attempted to estimate the short term slip rate from geodetic strain rates. The strain rate field, usually provided as maps, can be considered as the result of *i*) strain generated by faulting which is practically spread around in a buffer zone corresponding to the damage zone of the fault (fig. 4.3d), and *ii*) strain accumulated in the interposed volumes, which is produced by elastic or plastic deformation, part of which is taken up by diffuse micro-fracturing producing minor seismicity. Considering that the strain accumulated during the inter-seismic period is concentrated in a restricted volume surrounding the fault zone, a buffer zone can be defined across the fault trace (fig. 4.3d). During a seismic event, most of the so far accumulated elastic strain is suddenly released on the fault plane and transformed into relative slip, leaving a small, practically neglectful amount of plastic deformation (fig. 4.3e).

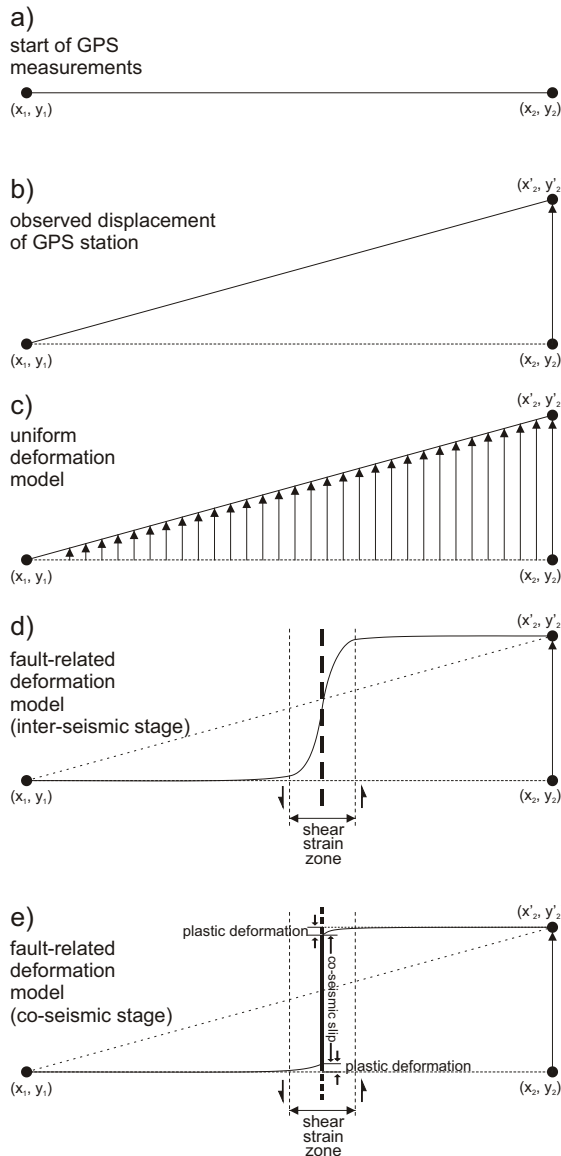


Fig 4.3: Schematic geodetic strain models from the initiation of the GPS measurements (a) until the final measurements (b) when the second GPS station (x_2, y_2) has been shifted to its new position (x'_2, y'_2) respective to the first one. The uniform deformation model (c) does not involve faulting. The fault-related deformation model (d and e), assumes that deformation is mostly elastic (with a minor plastic behaviour) which is translated to co-seismic slip on the fault due to the elastic rebounds of the two fault sides.

4.2 Strain

Strain rate definitions and formulae

In homogeneous deformation, the infinitesimal change in length normalised by the original length is expressed by the dimensionless *linear strain* ε :

$$\varepsilon = \frac{l - l_0}{l_0} = \frac{\Delta l}{l_0} \quad [4.1]$$

where l_0 , l and Δl are the initial length, the final length and their difference, respectively.

Angular strain ψ measures the change in angle between two lines that were initially perpendicular (fig. 4.4a). This deformation parameter is commonly expressed by the tangent of this angle and is called *shear strain* γ :

$$\gamma = \tan \psi \quad [4.2]$$

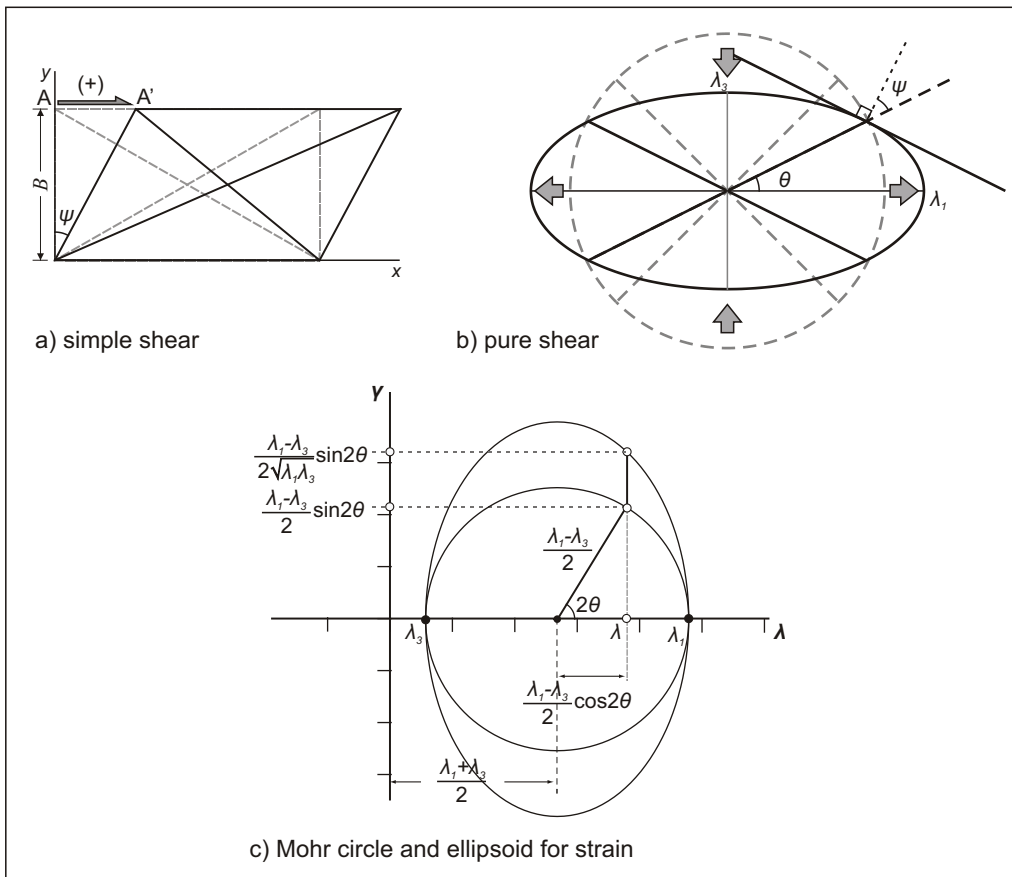


Fig. 4.4: Examples of deformation and strain: **a)** simple shear (B represents the buffer zone), **b)** pure shear, and **c)** Mohr circle and ellipsoid for strain (modified from Leeder and Pérez-Arlucea, 2006; van der Pluijm and Marshak, 2004). Displacement from A to A' in (a) is equal to the strike-slip displacement (s_{ss}).

For any strained body, shear strain can be calculated for any line forming an angle θ with respect to the maximum principal strain axis ε_1 if the orientation and values of ε_1 and ε_3 are known (fig. 4.4). In case of finite strain, a quantity called the *quadratic elongation* λ is preferred, which is defined as:

$$\lambda = \left(\frac{l}{l_0}\right)^2 = (1 + \varepsilon)^2 \quad [4.3]$$

From the representation of the finite deformation on the λ - γ Mohr plane (fig. 4.4c) and based on the maximum and minimum quadratic elongations λ_1 and λ_3 , it is possible to obtain both the *quadratic elongation* λ and the *shear strain* γ for any generic direction as a function of its relative angle θ with one principal strain axis:

$$\lambda = \frac{\lambda_1 + \lambda_3}{2} + \frac{\lambda_1 - \lambda_3}{2} \cos 2\theta \quad [4.4]$$

$$\gamma = \frac{\lambda_1 - \lambda_3}{2 \cdot \sqrt{\lambda_1 \lambda_3}} \sin 2\theta \quad [4.5]$$

Volume change Δ is expressed by the following equation:

$$\Delta = \frac{V - V_0}{V_0} = \sqrt{\lambda_1 \lambda_2 \lambda_3} - 1$$

where V_0 is the initial and V is the final deformed volume. In case of plane strain, the previous equation is reduced to:

$$\Delta = \sqrt{\lambda_1 \lambda_3} - 1 \quad [4.6]$$

As well known (fig. 4.4c), the *maximum shear strain* γ_{max} occurs when $\theta = 45^\circ$ and equation [4.5] becomes:

$$\gamma_{max} = \frac{(\lambda_1 - \lambda_3)}{2 \cdot \sqrt{\lambda_1 \lambda_3}} \quad [4.7]$$

Available datasets

Three strain rate datasets are available for the Aegean, all deriving from GPS velocities. Two of them, published by Hollenstein *et al.* (2008) and Jenny *et al.* (2004), consist of maps showing both principal strain axes ε_1 and ε_3 (figs. 1.4b and 1.5a, respectively). The third dataset, provided by El-Fiky (2000), consists of maps showing areal dilatation, maximum shear strain and principal strain axes orientation (fig. 1.6). Regarding the data shown in fig. 1.4b (Hollenstein *et al.*, 2008), these were kindly provided in ASCII format by Prof. Em. Hans-Gert Kahle and Ph.D.c. Michael Müller of the ETH Zürich University. In this way, accuracy and computation speed were facilitated.

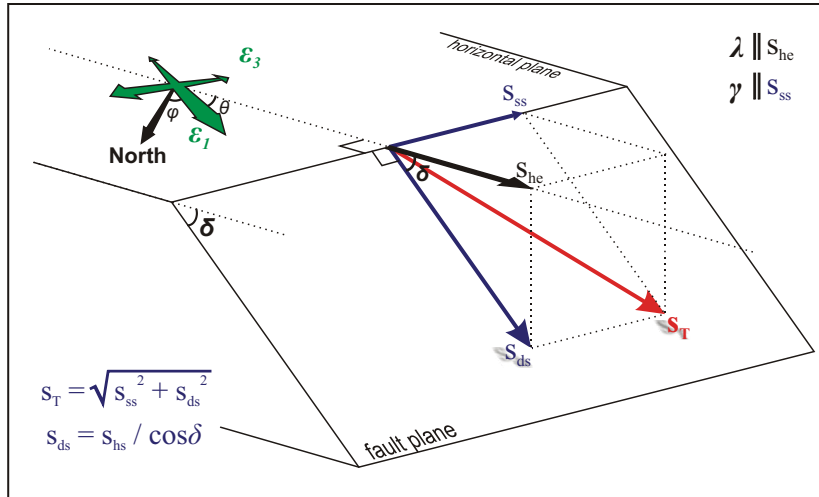


Fig. 4.5: 3D sketch showing how the principal strain axes ϵ_1 and ϵ_3 are related with the complete slip vector s_T . Angle φ is the azimuth of ϵ_1 that can provide angle θ (see text and [fig. 4.4](#)).

Both datasets of Jenny *et al.* (2004) and Hollenstein *et al.* (2008) needed further process in GIS environment: the principal strain axes ϵ_1 and ϵ_3 and the azimuth of ϵ_1 shown as angle φ in the example of [fig. 4.5](#), were interpolated into three distinct grids (by using the natural neighbour interpolation method) in order to be processed by the ‘zonal statistics’ tool of the ‘spatial analyst’ extension in ArcGIS software. With this procedure, the average values of all three parameters were computed within each fault’s buffer zone. After converting the φ angle to θ angle (based on the fault strike), the data were ready to be used for the further calculations. The dataset of El-Fiky (2000) needed no further processing, except from the measurement of the φ angle and its conversion to θ .

4.3 Methodology

Case 1: principal axes and their orientation are known

If the strain tensor (principal axes and their orientation) is known for a seismogenic area, it is possible to calculate either the quadratic elongation parallel to the dip-direction of the fault (eq. [4.4]) and the shear strain parallel to the strike of the fault (equation [4.5]; [fig. 4.5](#)). If both parameters are then multiplied by the width of the buffer zone (B) where strain concentrates, it is therefore possible to calculate the fault's heave (s_{he}) and the strike-slip component (s_{ss}) ([fig. 4.5](#)):

$$s_{ss} = \gamma \cdot B$$

$$s_{he} = \lambda \cdot B$$

Subsequently, from heave, strike-slip component and dip-angle (δ in [fig. 4.5](#)), the complete slip vector s_T can be easily computed using trivial trigonometric relationships (*viz.* rake; [fig.](#)

4.5). If the available starting values are strain-rates instead of strains and all the above parameters are divided by unit time the procedure will provide the slip rate of the seismogenic sources.

Case 2: areal dilatation, maximum shear strain and principal axes orientations are known

From areal dilatation and maximum shear strain we need to calculate the maximum and minimum quadratic elongations λ_1 and λ_3 . Solving equations [4.6] and [4.7] according to λ_1 and λ_3 , we get:

$$\lambda_1 = \gamma_{max} (1 + \Delta)^2 + (1 + \Delta) \cdot \sqrt{\gamma_{max}^2 (1 + \Delta)^2 + 1} \quad [4.8]$$

$$\lambda_3 = -\gamma_{max} (1 + \Delta)^2 + (1 + \Delta) \cdot \sqrt{\gamma_{max}^2 (1 + \Delta)^2 + 1} \quad [4.9]$$

Following this step, the procedure is similar to the one described in the previous case.

4.4 Results and discussion

Results

Both slip rate and rake for each CSS in North Greece are listed in [table 4.1](#), based on the three datasets of Jenny *et al.* (2004), El-Fiky (2000) and Hollenstein *et al.* (2008). In order to compare the results obtained from the three different strain datasets, the calculated slip rate values of all CSSs which are at present included in GreDaSS ([fig. 6.1](#)) have been interpolated by the natural neighbour method. Thus, based on this facilitation, we can observe that i) the three maps show the lateral variability of the slip rate in the different sectors of the broader Aegean Region emphasising the sectors characterised by more intense deformation ([fig. 4.6](#)), and ii) the major features and overall trends of the three maps do not differ significantly as expected being the very original GPS datasets largely overlapping. The slip rates found in the literature are also shown in [table 4.2](#) for direct comparison with the geodetically calculated ones.

Concerning the results deriving from the Hollenstein *et al.* (2008) dataset, these might show irregular values for the northernmost part of Greece. Indeed, the data coverage in this area is not complete and CSSs located near to the boundary might not have geologically meaningful results ([fig. 1.4b](#); [table 4.1](#)).

Fault code	Fault name	El-Fiky (2000)		Jenny <i>et al.</i> (2004)		Hollenstein <i>et al.</i> (2008)	
		Slip-rate (mm/a)	Rake (deg)	Slip-rate (mm/a)	Rake (deg)	Slip-rate (mm/a)	Rake (deg)
GRCS001	Tyrnavos*	0.62	290	0.44	262	1.02	268
GRCS002	North Tyrnavos Basin*	0.66	285	0.49	266	1.18	261
GRCS004	South Tyrnavos Basin*	0.52	286	0.42	256	0.91	257

Chapter 4: SLIP RATE

Fault code	Fault name	El-Fiky (2000)		Jenny <i>et al.</i> (2004)		Hollenstein <i>et al.</i> (2008)	
		Slip-rate (mm/a)	Rake (deg)	Slip-rate (mm/a)	Rake (deg)	Slip-rate (mm/a)	Rake (deg)
GRCS010	Pagazitikos Gulf*	0.50	257	0.52	238	0.97	238
GRCS015	Vasilika	0.55	284	0.56	260	0.90	260
GRCS020	Domokos*	0.47	302	0.54	282	0.39	304
GRCS025	Karditsa	0.54	276	0.43	273	0.36	305
GRCS040	Omolio	0.46	310	0.39	292	0.91	273
GRCS048	Deskati	0.43	271	0.28	276	0.56	249
GRCS050	Aliakmonas*	0.46	243	0.35	265	0.31	244
GRCS058	Vergina	0.47	271	0.31	287	0.12	222
GRCS060	North Almopia*	0.57	264	0.36	267	0.23	300
GRCS068	South Almopia Fault	0.34	247	0.25	259	0.24	266
GRCS070	Amyndeo	0.30	236	0.19	276	0.05	231
GRCS072	Ptolemaida	0.25	222	0.20	259	0.05	228
GRCS077	Komanos	0.33	233	0.28	264	0.11	260
GRCS080	Florina	0.31	247	0.16	285	0.03	172
GRCS090	Kastoria	0.37	282	0.12	306	0.13	231
GRCS100	Mygdonia*	0.45	295	0.37	292	0.16	39
GRCS110	Stratoni-Varvara	0.95	281	1.06	275	0.28	308
GRCS120	Sochos	0.78	266	0.68	270	0.15	12
GRCS130	Belles	0.34	272	0.24	270		
GRCS140	Drama	0.37	302	0.23	255		
GRCS145	Serres*	0.47	284	0.40	273	0.15	322
GRCS150	Thrace	0.44	228	0.24	209	0.32	224
GRCS155	Symvolon	0.41	192	0.28	161	0.33	170
GRCS160	Maronia	0.51	263	0.44	240	0.66	262
GRCS170	Doxipara	0.33	207	0.32	228		
GRCS240	Pylaea	0.42	283	0.32	291	0.13	42
GRCS245	Asvestochori	0.39	312	0.26	313	0.14	82
GRCS250	Anthemountas	0.46	285	0.37	292	0.15	4
GRCS260	Gomati	0.68	300	0.78	291	0.35	352
GRCS270	Singitikos Gulf	0.62	296	0.70	291	0.61	308
GRCS280	South Chalkidiki offshore	0.98	254	1.43	249	1.73	241
GRCS285	South Cassandra offshore	0.76	268	0.81	264	1.34	265
GRCS288	Samothraki	0.59	257	0.77	248	1.26	238
GRCS290	North NAT	1.96	261	2.51	252	3.15	252
GRCS300	Konitsa	0.37	227	0.20	257	0.10	191
GRCS310	Petoussi*	0.84	86	3.02	89	3.60	96
GRCS390	Kerkyra	0.59	263	0.39	283	0.45	28
GRCS800	South NAT	0.73	220	1.05	166	1.26	166
GRCS810	North Aegean Basin	0.54	159	0.92	150	1.23	152

Fault code	Fault name	El-Fiky (2000)		Jenny <i>et al.</i> (2004)		Hollenstein <i>et al.</i> (2008)	
		Slip-rate (mm/a)	Rake (deg)	Slip-rate (mm/a)	Rake (deg)	Slip-rate (mm/a)	Rake (deg)
GRCS815	Mavrovouni offshore	0.71	293	0.79	279	1.56	289
GRCS820	Pelion offshore	0.72	306	0.92	296	1.39	303
GRCS825	Lemnos	0.82	131	1.45	115	2.70	107
GRCS831	Aghios Efstratios*	0.78	131	1.20	122	1.56	126

Table 4.1: Slip-rate and rake values calculated for each seismogenic source in North Greece, deriving from the three geodetic strain rate datasets (El-Fiky, 2000; Jenny *et al.*, 2004; Hollenstein *et al.*, 2008). Sources with asterisks refer to faults with already existing slip-rates in literature (table 4.2). Some sources which are based on the strain rate of Hollenstein *et al.* (2008) have blank values because the provided grid does not cover the very northern parts of Greece. This issue might also cause problem to sources that are near to the edge of the covered area.

Fault code	Fault name	Slip rate (mm/a)	
		min	max
GRCS001	Tyrnavos	0.05	0.4
GRCS002	North Tyrnavos Basin	0.1	1.0
GRCS004	South Tyrnavos Basin	0.1	0.5
GRCS010	Pagazitikos Gulf	1.0	3.0
GRCS020	Domokos	0.3	0.5
GRCS050	Aliakmonas	0.3	2.0
GRCS060	North Almopia	1.0	1.0
GRCS100	Mygdonia	0.1	0.7
GRCS145	Serres	0.05	0.1
GRCS310	Petoussi	0.1	0.3
GRCS831	Aghios Efstratios	5.0	5.0

Table 4.2: Slip rates of the seismogenic sources for which literature data are available.

Discussion

Focusing on the study area (North Greece), the geodetically obtained slip-rates show reasonable values according to the regional tectonic regimes and the overall geodynamic setting. The reliability of the applied approach could be tested by comparing the results with the few geological slip rates defined or at least constrained for some of the seismogenic sources in Northern Greece (sources marked by an asterisk in table 4.1; see next chapter for each specific source). For the ten available sources (Tyrnavos, North and South Tyrnavos Basin, Pagazitikos Gulf, Domokos, Aliakmonas, North Almopia, Mygdonia, Serres and Aghios Efstratios) the geodetic slip rates are either similar to or at least they have the same order of magnitude of the geological ones. However, the calculated geodetic rates are usually less than the geological ones. This can be explained by the fact that GPS stations measure velocities during a very short period of a seismic cycle. Strain accumulation is not necessarily linear with time, so it cannot be inferred that its rate is steady during the seismic cycle. And since GPS stations are not dense enough to isolate measurements across specific faults, information is rather diffused. In other words, an ideal measurement would be at least two stations monitoring the footwall and

hanging-wall at the central part of a seismogenic source for at least one seismic cycle. Nonetheless, even if the first condition is satisfied, the second one is not realistic and would be pointless in terms of SHA. In summary, this preliminary approach is quite encouraging and the homogeneity of the results provides a uniform comparison of slip rates between various seismogenic sources.

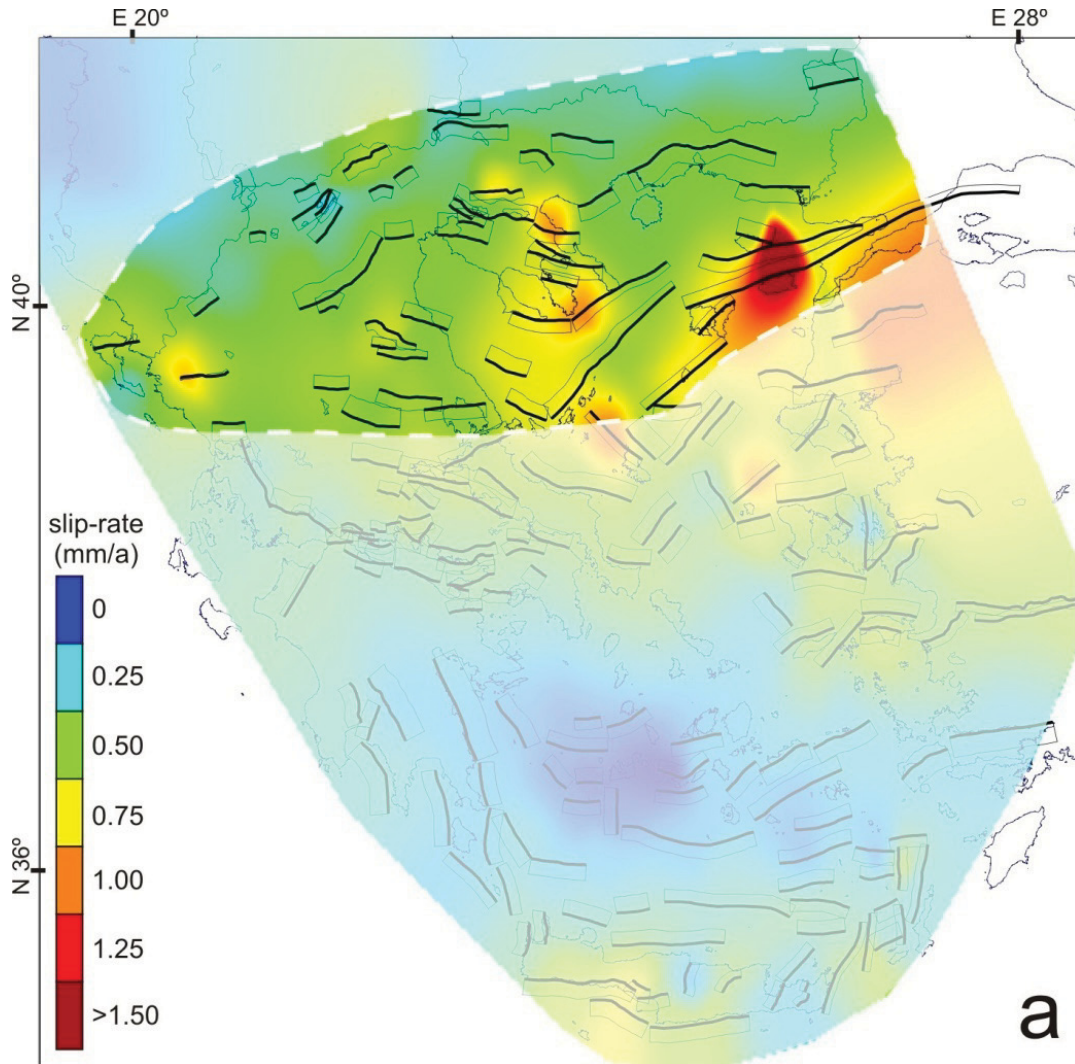


Fig. 4.6: Slip rate lateral variation maps of the study area (highlighted) and the broader Aegean Region, based on geodetically induced strain rate data taken from **a)** El-Fiky (2000), **b)** Jenny *et al.* (2004), and **c)** Hollenstein *et al.* (2008). The CSSs represent the state-of-the-art of GreDaSS (see also [fig. 6.1](#)).

The geodetically calculated rake in this study shows greater consistency with the ones geologically-seismologically determined for the CSSs of North Greece. The majority of the calculated values rarely fall outside the previously constrained range and when this happens the difference is lower than 10° . These latter cases are usually found in the transition areas between the transtensional region of NAT and NAB and the extensional surroundings. Larger discrepancies can be found in the westernmost part of Northern Greece (Kerkyra and Petoussi CSSs), where the calculated rake for the Petoussi CSS implies an almost purely reverse faulting,

while the geological information suggest a prevailing transcurrent kinematics. This discrepancy can be expected for this region if we consider its geodynamic and seismotectonic complexity due to the close presence of the Aegean-Apulian convergence zone.

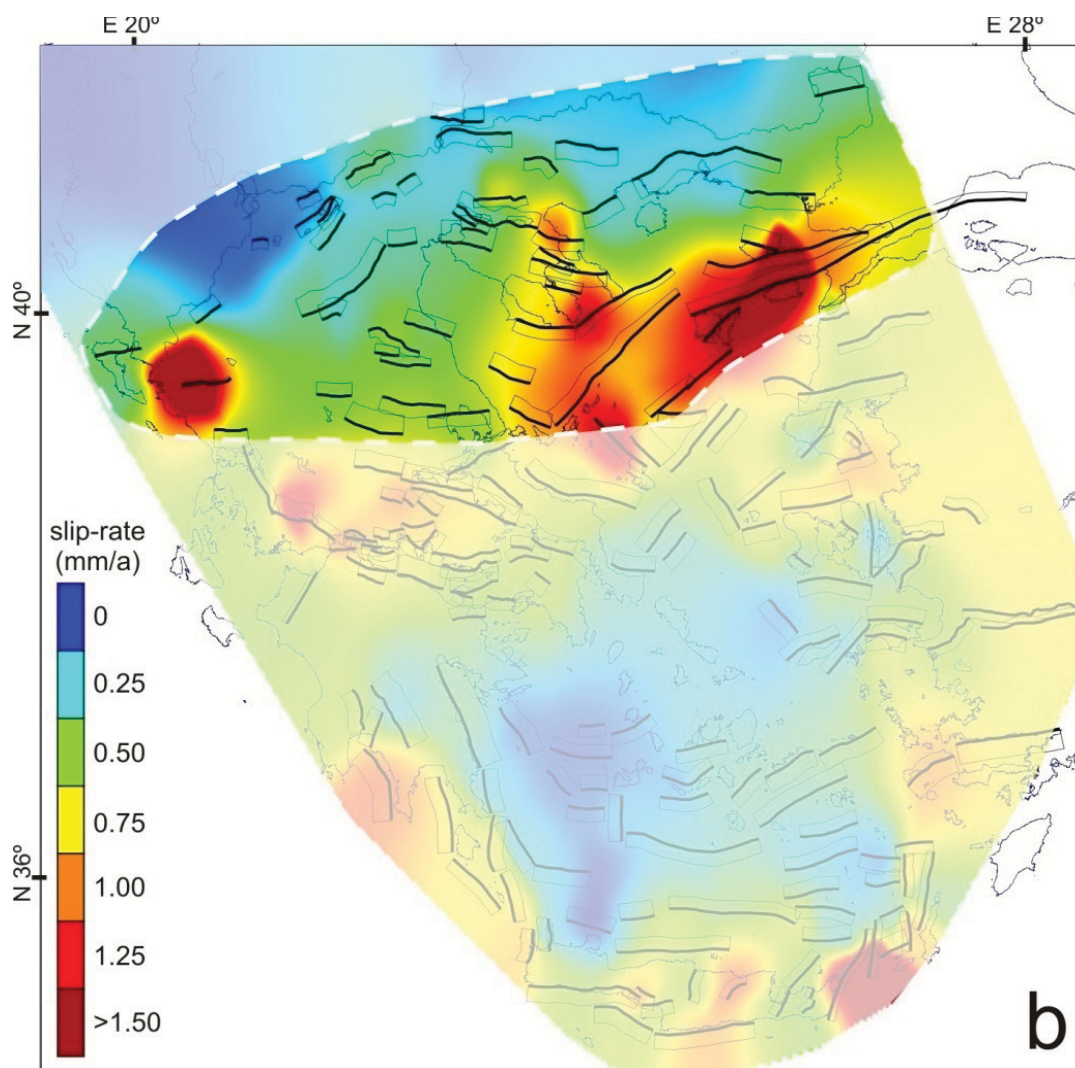


Fig. 4.6 continued.

Although the compilation of GreDaSS in central and southern Aegean is beyond the goals of this research, a preliminary version of the database was available during the final preparation stages of the Ph.D. thesis. By comparing the calculated rake values with the ones taken from GreDaSS outside the investigated area (North Greece), we may observe a similarity for northern Greece (from Gulf of Corinth and northwards), but an evident inconsistency in southern Greece and especially in the areas surrounding the subduction zone. For example in Crete, the calculated rakes suggest mostly reverse faulting, while geological-morphotectonic investigations (Angelier, 1979; Angelier *et al.*, 1982; ten Veen and Postma, 1999; Fassoulas, 2001; Ring *et al.*, 2001; Papanastassiou *et al.*, 2004; Peterek and Schwarze, 2004; Caputo *et al.*, 2006b; 2010a; 2010b) as well as focal mechanisms of shallow events (Delibasis *et al.*, 1999; Jost *et al.*, 2002; Kiratzi and Louvari, 2003), clearly show an extensional tectonic regime

affecting the upper crust. One possible answer about this inconsistency could be the fact that GPS stations in the South Aegean are sparse due to the sea. In all GPS campaigns, the closest stations north of Crete are positioned in the Cyclades, and more specifically on Melos and Thera Islands. Given that both islands belong to the volcanic arc of the Aegean and stand over magmatic chambers, it is not unlikely that these two stations could record 'local' movements not linked to the geodynamics and tectonics of the area. If both these stations are removed, the velocity difference between the Cyclades and Crete becomes significantly lower. Another possible explanation could be the fact that the contraction recorded by the GPS stations could reflect lithospheric-scale deformation that might not behave similarly to the shallower sector of the crust. The lack of a denser network cannot resolve this problem yet.

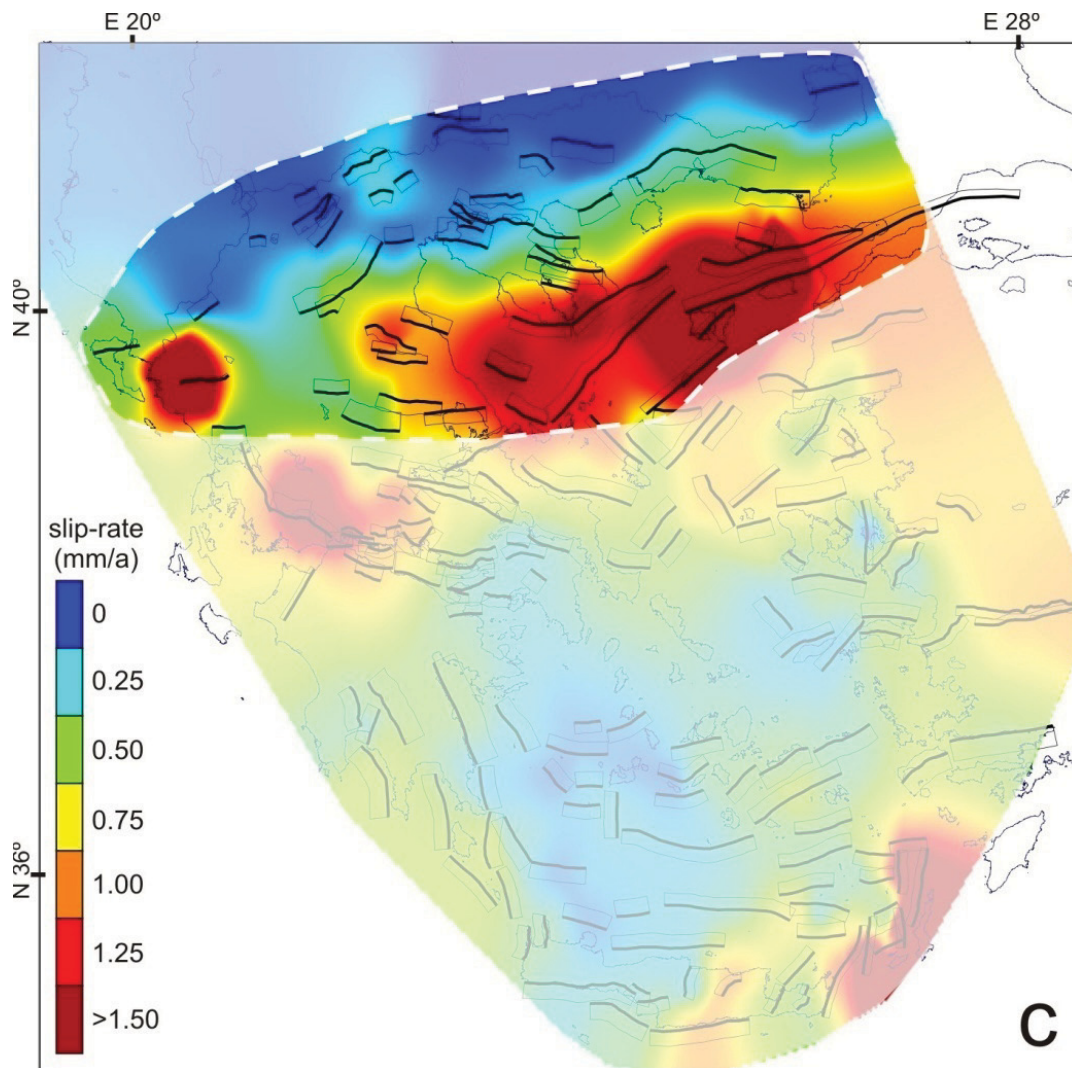


Fig. 4.6 continued.

*The seismogenic sources of North Greece***5.1 Introduction**

The most completed parameters and metadata of GreDaSS are included in the seismogenic sources of North Greece. After observing the geometry and kinematics of the sources in this area, a rough division in 5 sectors can be inferred ([fig. 5.1](#)): *i*) a northern E-W trending fault belt in Thrace and Eastern Macedonia (§5.2), *ii*) a complex E(SE)-W(NW) trending fault system affecting the Chalkidiki peninsula and possibly associated with low-angle detachments (§5.3), *iii*) the NE-SW trending ‘*anti-Hellenides*’ fault system in Western Macedonia and Epirus (§5.4), *iv*) the E(SE)-W(NW) trending Thessalian fault system (§5.5), and *v*) the (E)NE-(W)SW trending North Aegean Sea fault system, which is almost exclusively located offshore (§5.6). Based on this discrimination, in the following sections seismogenic sources will be synthetically described and discussed, in terms of seismotectonic parameters, relations with historical and instrumental earthquakes and seismotectonic behaviour wherever it differentiates. However, DSSs are excluded since they practically do not contain any useful information. It is important to mention that there are few CSSs that are either in progress or in debate. These sources, symbolized differently in the respective maps, are the *Symvolon* (GRCS155), *Vergina* (GRCS058), *Florina* (GRCS080), *Kastoria* (GRCS090), *Deskati* (GRCS048) and *Karditsa* (GRCS025). Moreover, seismogenic sources are also present near to, but out from, the borders of Greece. These sources can affect vital constructions or populated areas in the Greek territory and should be taken into account when estimating SHA. However, this exceeds the purposes of the thesis and it was decided not to be included.

In the following descriptions, each sector has an introductory text. Seismogenic sources are presented grouped when a CSS spans one or more ISSs. The discussion in such cases is cumulative and, like in individual cases, it includes reviews and critical analyses of data and non-parametric information that might concern fault’s behaviour, interaction, earthquake associations, *etc.* Furthermore, some minor fault segments might be discussed even if they do not qualify to be included in the database individually due to their small size and their low potential magnitude capability (below M 5.5). Their discussion, however, might contain useful information about their behaviour (interaction, linkage, *etc.*) inside the fault zone. Concerning earthquakes, [fig. 5.2](#) shows the events that are associated, discussed or referenced in the descriptions that follow. All geometric and seismotectonic numerical parametric information are included in [appendix I](#).

The geodetically calculated slip rates from the previous chapter have been taken into account for the CSSs. However, when literature (“geological”) information is also available (see §4.4), both data are revised and the best combination is selected for these specific sources.

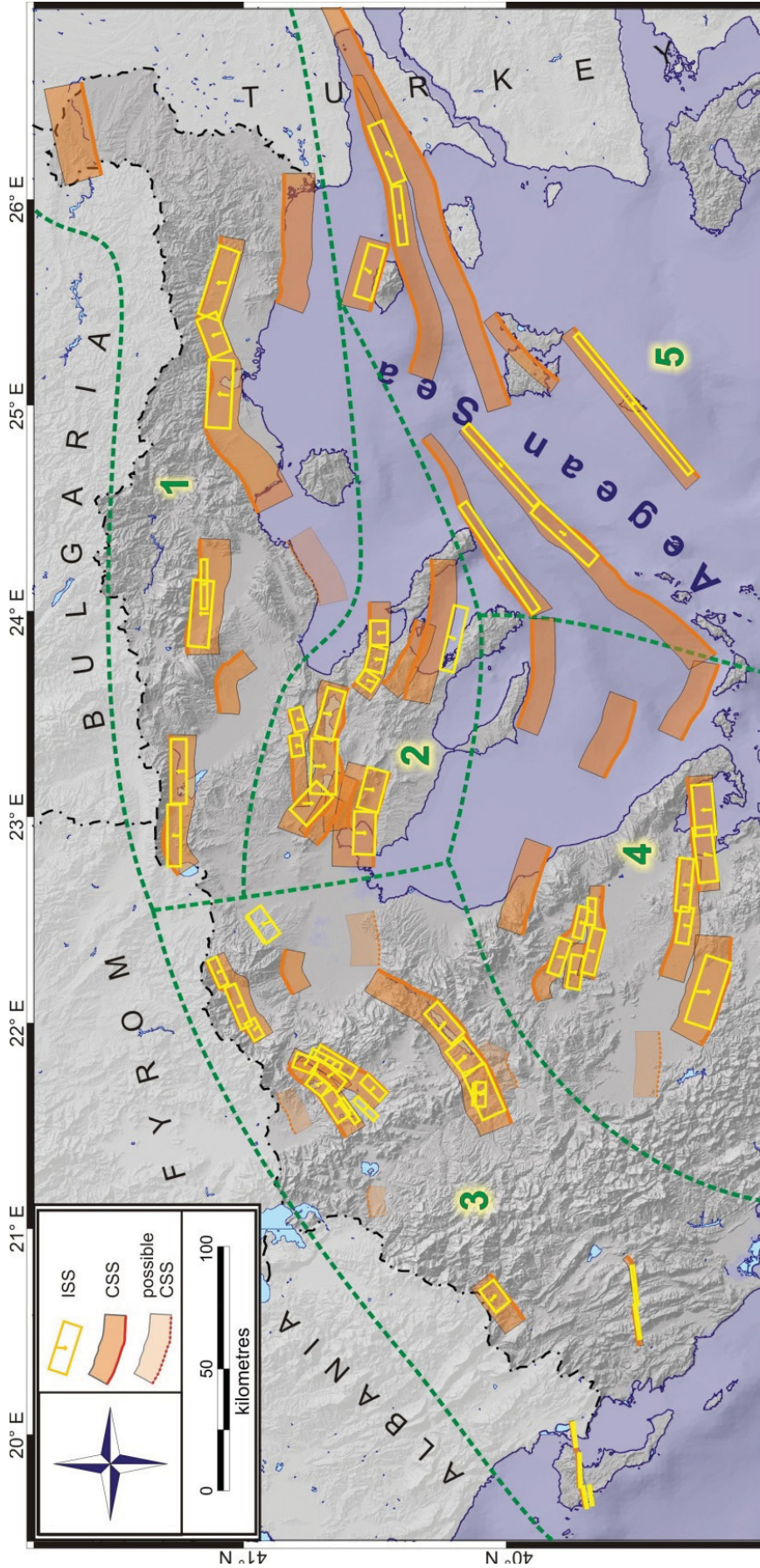


Fig. 5.1: Map of the seismogenic sources (CSSs and ISSs) completed for North Greece. Sources that are still in progress or out of the study area are not shown (see [fig. 6.1](#) for all the sources of the broader Aegean Region). The green dashed lines separate the area in five sectors (green numbers) as described in the text. Light coloured CSSs represent ambiguous sources. The names and codes of the sources can be found in the respective map in the Appendix.

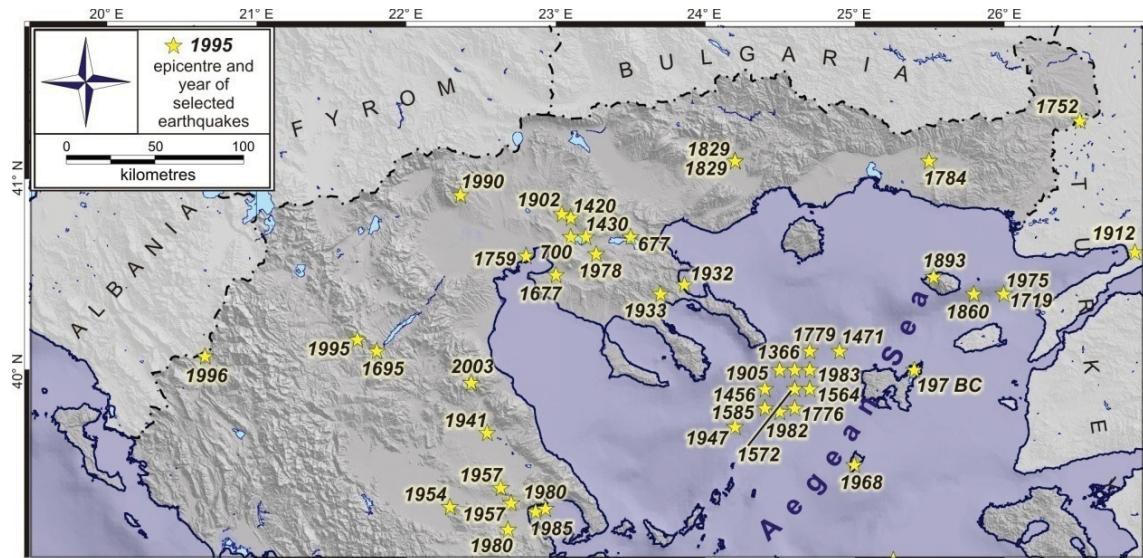


Fig. 5.2: Map showing earthquakes that are associated, discussed or referenced in the description of the seismogenic sources. The epicentres have been taken from the catalogue of Papazachos *et al.* (2000; 2009; <http://geophysics.geo.auth.gr/ss/>). Any doubts about epicentral locations (*e.g.* the 1978, Thessaloniki earthquake) are discussed in the text.

5.2 The northern fault belt

Northern continental Greece and particularly Thrace and Eastern Macedonia are affected by several roughly E-W trending normal faults forming an almost continuous regional-scale fault belt extending for more than 300 km starting from the border with Turkey to the Vardar Valley ([fig. 5.3](#)). In the database are included five CSSs some of which also contain well defined segments (ISSs).

Some historical seismic events, among which are the Komotini 1784, Drama 1829 and Xanthi 1829, occurred in this region and are discussed in the following together with the causative faults. However, no moderate-to-strong earthquakes have hit the area since then and certainly not during the instrumental period.

Doxipara CSS170

Relatively less explored, the *Doxipara CSS* probably exceeds the Greek borders from both sides inside the Bulgarian and Turkish territory (*e.g.* Görür and Okay, 1996). Having only few published data from Chatzipetros and Pavlides (2009) and more unpublished from Pavlides and his colleagues, the fault zone is characterized by normal dip-slip kinematics. It mainly dips towards NNW, but many antithetic faults also occur. The fault has uplifted Neogene sediments, forming a roughly oriented E-W set of hills on its footwall that have been smoothed due to erosion. Although morphology is not tectonically well formed, palaeoseismological evidences imply the connection of this structure with the 1752 Edirne earthquake. An older event that occurred between 960 BC and 2nd century AD might also be a possible candidate. Moreover, surface displacement is calculated to approximately 1 m, while recurrence interval should be quite long. Fault's historical activity is also evidenced by its effect on an archaeological site that consists of a tumulus of the 2nd century AD. In more detail, one of the two brick-built altars was found heavily deformed by a system of normal faults showing a total net displacement of *ca.* 0.9 m.

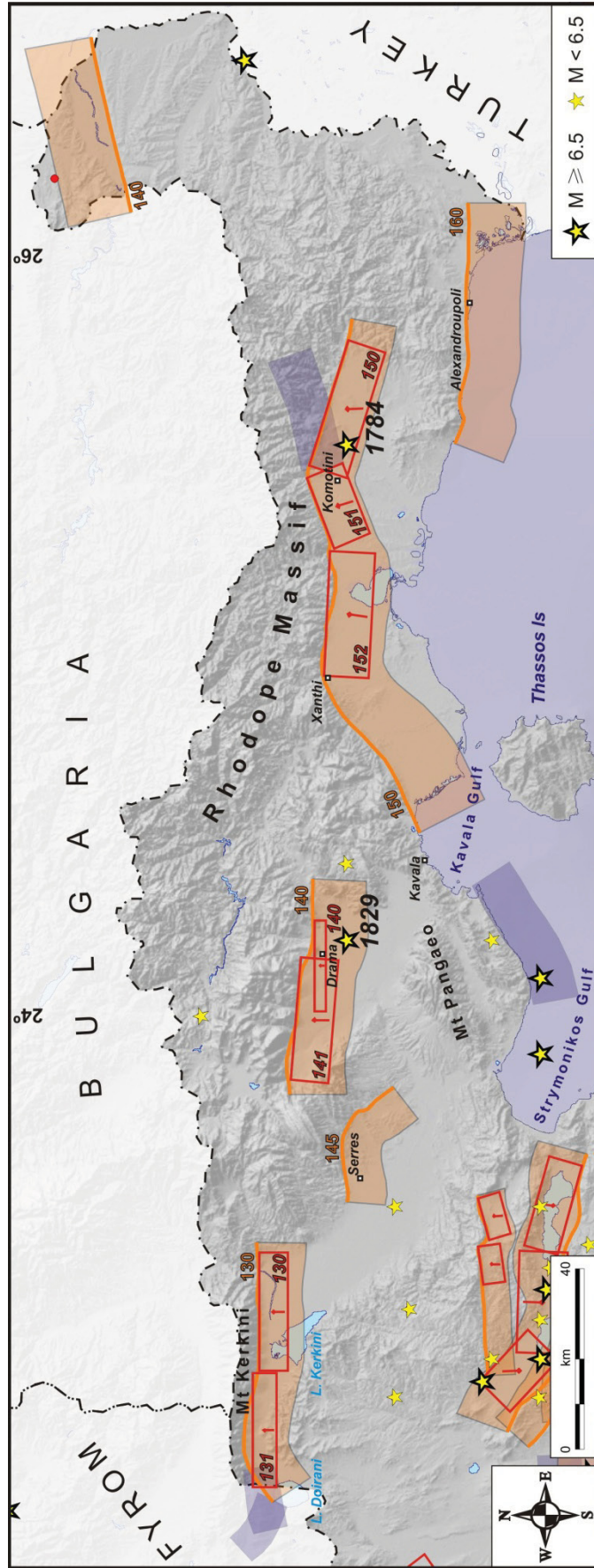


Fig. 5.3: The seismogenic sources of the ‘Northern fault belt’ (fig. 5.1). Orange sources and numbers: CSSs and their codes, read sources and numbers: ISSs and their numbers, blue sources: DSSs. The epicentres (stars) have been taken from the catalogue of Papazachos *et al.* (2000; 2009; <http://geophysics.geo.auth.gr/ss/>).

Maronia CSS160

The *Maronia CSS* has been studied by Chatzipetros and Pavlides (2004) and Mountrakis *et al.* (2006). It possibly continues offshore to the west, as suggested by bathymetric maps, while to the east, a microseismic sequence during June and July, 2004 (Kiratzi *et al.*, 2005) as well as some morphological evidences suggest that the fault probably extends eastwards to the Evros Valley. Chatzipetros and Pavlides (2004) recognize three segments. *i)* The Marmaritsa Fault, to the west strongly controls the shoreline by creating an impressive N110°-120° striking scarp associated with a southwards dipping (55°-60°) fault. This segment is characterised by an up to 5 m-thick brecciation zone, showing evidence of recent reactivations (corrugations, striations, *etc.*). *ii)* The central Messimvria Fault, striking E-W and dipping southwards (70°-75°) mainly extends offshore and is based on bathymetry. *iii)* The eastern Makri Fault, partially overlapping the Messimvria Fault, is associated with a group of minor south-dipping sliding planes affecting young (Late Quaternary?) sediments and elongated marine terraces. The latter is the most active segment among the three, but the dimensions are not sufficient to produce at least an intermediate event ($M > 5.5$), and therefore they have been not included in the database as ISSs. The investigation of the microseismic sequence in 2004 (Kiratzi *et al.*, 2005) suggests nodal planes of similar orientation (approximately E-W) and moderate dip-angles. It is also worth mentioning that the behaviour and interaction of the segments have not been sufficiently investigated.

The suggested maximum expected magnitude from the empirical relationships represents the worst case scenario which is a rupture of the entire fault length.

Thrace CSS150 (Komotini ISS150, Iasmos ISS151 and Xanthi ISS152)

This long S-dipping tectonic structure separates the Rhodope Mountain, to the north, from the Kavala-Xanthi-Komotini basin, to the south. The strike of the fault trace varies forming significant angular bends. Extensional faulting has been occurring since at least the Miocene and striations bear evidence of three tectonic phases (Lyb eris, 1984; Lyb eris and Sauvage, 1985). The trace has been well mapped by several researchers (Lyb eris, 1984; Mountrakis and Tranos, 2004; Rondoyanni *et al.*, 2004). Based on sea bottom seismic reflection profiles (Martin, 1987), the structure likely continues offshore westwards within the Gulf of Kavala.

This CSS is divided in four major segments (Mountrakis and Tranos, 2004; Mountrakis *et al.*, 2006), but only the three easternmost ones show clear morphological evidence of recent activity and they have been classified as distinct ISSs: *Komotini*, *Iasmos* and *Xanthi* (from east to the west, respectively). The fault barriers between segments are due to change in strike and dip generating overall zig-zag geometry. The dip seems to progressively decrease towards the west (Mountrakis and Tranos, 2004; Mountrakis *et al.*, 2006; Rondoyanni *et al.*, 2004). This probably implies that maximum depth of the fault zone also progressively decreases westwards. The slip vectors measured on fault outcrops indicate a generally dip-slip normal kinematics, though oblique-slip displacements locally prevail (Lyb eris, 1984; Mountrakis and Tranos, 2004; Mountrakis *et al.*, 2006; Rondoyanni *et al.*, 2004). Taking into account the characteristics of the geometrical barriers and assuming the possibility of a dynamic triggering model, the worst case scenario implies the contemporaneous rupture of more than one segment. The “softest” barrier is probably the one between the *Xanthi* and *Iasmos* segments which some authors already

describe as a unique structure (Lyb ris, 1984; Rondoyanni *et al.*, 2004). The maximum expected magnitude is obtained by assuming a 44 km-long potential rupture and using empirical relationships (Wells and Coppersmith, 1994; Pavlides and Caputo, 2004).

The *Komotini ISS* has been tentatively associated with the 1784, November 6 earthquake (Papazachos and Papazachou, 1997; 2003; Mountrakis *et al.*, 2006), though the estimated magnitude (6.7; Papazachos and Papazachou, 1997; 2003) could be much lower (*e.g.* Ambraseys, 2009). The more recent earthquake that occurred on April 11, 1829 in Xanthi is lively debated. Indeed, Papazachos and Papazachou (1997; 2003) consider it as a foreshock of the May 5, 1829 Drama earthquake (see the Drama CSS following), while the description in Ambraseys's (2009) catalogue mentions that the area near Xanthi town was mainly ruined, in contrast with the surrounding area of Drama that was mostly damaged by the second event. If this is the case, then the April 11 earthquake was not a foreshock of the same seismogenic source, but a distinct event that probably triggered the Drama earthquake *ca.* one month later, as also suggested by Pavlides and Caputo (2004). Accordingly, the April 11, 1829 earthquake has been associated with the *Xanthi ISS*.

Drama CSS140 (Drama ISS140 and Prosotsani ISS141)

The *Drama CSS*, bounding the Drama Basin to the north, is a S-dipping fault zone that consists of two major segments: the *Drama* and *Prosotsani ISSs*. Both segments are discerned based on detailed morphotectonic mapping (Mountrakis *et al.*, 2006) and show a right-stepping geometry with a significant overlap. Most geometric and kinematic parameters proposed by the same authors are in agreement with the focal mechanism of a moderate event ($M_w = 5.2$) that occurred on November 9, 1986 (Dziewonski *et al.*, 1986; Vannucci and Gasperini, 2003; 2004). In particular, where the overlap occurs both segments probably join at depth into a single shallow-angle fault plane.

Papazachos and Papazachou (1997; 2003) characterise the May 5, 1829, Drama earthquake as a catastrophic event with a magnitude of 7.3. Probably, this is an overestimated magnitude due to the occurrence of the strong nearby April 11 earthquake (see discussion in Thrace CSS). The May 5 event has been associated with the Drama CSS (Mountrakis *et al.*, 2006), but not to any of the two segments. The maximum expected magnitude of 7.0 is suggested after applying several empirical relationships (Wells and Coppersmith, 1994; Pavlides and Caputo, 2004) and confirms the overestimated earthquake of 1829 in Drama.

Serres CSS145

The *Serres fault zone* dips to the south and shows a slight curvature and consequent strike variation from WSW-ENE to NW-SE, from west to east, respectively (Tranos and Mountrakis, 2004; Mountrakis *et al.*, 2006). Four segments are suggested for the whole shear zone, but the length of each proposed segment is probably not sufficient to produce at least moderate events; additionally the geometric characteristics of the segment boundaries are not well defined. Accordingly, no specific ISSs have been included in the GreDaSS. The western E-W trending sector (*ca.* 20 km) shows the most prominent fault trace, while a subtle scarp in Pleistocene deposits continues SE-wards, possibly making the total length more than 30 km. Morphotectonic evidence of recent activity is not homogeneous along strike and it is mainly represented by a 7 m-high fault scarps affecting Late Pleistocene deposits in the central sector

(Tranos and Mountrakis, 2004). No historical nor instrumental earthquakes are associated with this fault zone, but this crustal scale tectonic structure is certainly capable of generating moderate (to strong) seismic events as far as it is optimally oriented with respect to the present-day stress field. Moreover, it fills a structural gap between the Drama CSS, to the east, and the Belles CSS, to the west, thus contributing to accommodate the regional N-S lithospheric stretching affecting the Southern Aegean.

Belles CSS130 (Petritsi ISS130 and Kastanoussa ISS131)

The *Belles CSS* is a long fault zone bordering an impressive linear mountain front and is characterized by thick multi-generation alluvial fans accumulated in the hanging-wall block (Psilovikos and Papaphilippou, 1990; Mariolakos *et al.*, 2004; Pavlides *et al.*, 2004a). The whole Mount Kerkini (commonly referred to as Belles), which represents the border between Greece and Bulgaria-FYROM, has been considered a recent tectonic horst by Psilovikos (1984). On the basis of morphotectonic mapping and morphometric analyses, the fault zone has been active during Quaternary and especially the Holocene, while the observed striations are mechanically compatible with the present-day extensional stress field (Pavlides *et al.*, 2004a).

Mountrakis *et al.* (2006) separated the fault zone into two major segments that were approximately adopted in the database: the *Petritsi* (to the east) and *Kastanoussa* (to the west) *ISSs*. Both segments have similar lengths and a slight right-stepping geometrical relationship. Lateral variations in the degree of activity are debated. For example, based on several geomorphic features (well-developed fault scarps with accelerated erosion, deposition of younger generations of alluvial fans upon older fan heads close to the fault zone, more extensive fan deposits, slightly entrenched torrents and much higher elevations of the fan heads), Psilovikos and Papaphilippou (1990) suggest a higher activity on the western segment, while based on the deflection of the Strymon River (Pavlides *et al.*, 2004a; Mariolakos *et al.*, 2004) and a low value of the mountain front sinuosity index, the eastern sector is suggested to be more active.

No major historical earthquakes are reported in the catalogues. It is noteworthy that immediately N-NW of Lake Doirani an instrumentally recorded seismic sequence (May-October 2009) with a $M_w = 5.2$ event as the strongest shock (Kiratzi, 2010) suggests the occurrence of an antithetic NNE-dipping normal fault. This implies that the Belles CSS comes to an end close to the Greece-FYROM border. The spatial distribution of this sequence provides a minimum suggested thickness of the seismogenic layer to *ca.* 12-13 km.

The worst case scenario of a possible reactivation involves a combined rupture of the two segments, given that their separation distance is not very long. Thus, a larger earthquake (*ca.* M 7.0) is a possible scenario.

5.3 The Chalkidiki fault system

The active faults affecting the Chalkidiki peninsula ([fig. 5.4](#)) are grouped separately from the northern E-W trending fault belt due to their slightly different mean orientation, which is ESE-

WNW, but especially because they form two fault sets consisting of shortly spaced subparallel synthetic highly-dipping normal faults possibly linked at depth by a low-angle shear zone (Sboras and Caputo, 2010). The eastern fault set is mainly SSW-dipping, while the western one is NNE-dipping. Both fault sets are delimited by an antithetic structure, south and north, respectively, also included in the database. The eastern set is formed by the Stratoniki-Varvara, Gomati and Singitikos Gulf CSSs and the Vourvourou ISS, while the western set of faults by the Sochos-Mavrouda, Mygdonia, Asvestochori, Pylaea and Anthemountas CSSs.

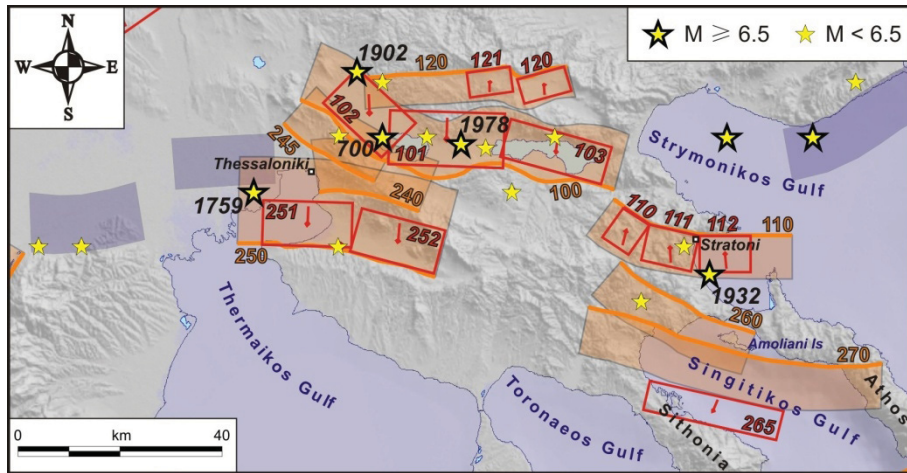


Fig. 5.4: The seismogenic sources of the ‘Chalkidiki fault system’ (fig. 5.1). Orange sources and numbers: CSSs and their codes, red sources and numbers: ISSs and their numbers, blue sources: DSSs. The epicentres (stars) have been taken from the catalogue of Papazachos *et al.* (2000; 2009; <http://geophysics.geo.auth.gr/ss/>).

In the area, three major earthquakes occurred during historical and recent times (fig. 5.2 and 5.4; 1932, Ierissos; 1978, Thessaloniki; 1933, May 11, Thessaloniki). For the former two events the causative fault is well established, while the latter has been tentatively associated with the Gomati CSS. All of them will be discussed in the following paragraphs. However, prior to the 20th century several moderate events are listed in the historical catalogues (Papazachos and Papazachou, 1997; 2003; Ambraseys, 2009). For example, in the western Mygdonia Basin are reported the following events (Papazachos and Papazachou, 1997; 2003): *i*) in 700 AD of $M_e = 6.5$, which is characterized as a ‘spurious’ event according to Ambraseys (2009), *ii*) in July, 1420 ($M_e = 6.0$), a quite destructive event for the city of Thessaloniki (Ambraseys, 2009), *iii*) on March 26, 1430 ($M_e = 6.0$), an event that caused some damage to the city walls (Ambraseys, 2009). At the eastern part of the basin only one event of magnitude 6.4 is reported in the catalogue of Papazachos and Papazachou (1997) in the year 677 AD, but is considered ‘spurious’ by Ambraseys (2009). The available historical information for all these events however is not sufficient to accurately locate the epicenter, to estimate the real magnitude and therefore to associate them to any specific causative fault.

Stratoniki-Varvara CSS110 (Varvara ISS110, West Stratoniki ISS111 and East Stratoniki ISS112)

The *Stratoniki-Varvara* CSS is a S-SW dipping fault zone affecting the eastern coast of Chalkidiki peninsula, bordering the south side of Mount Stratoniki and largely continuing

offshore. The CSS ruptured on September 26, 1932 by a strong linear morphogenic event with magnitude 7.0 (Papazachos and Papazachou, 1997; 2003) or 6.9 (Ambraseys and Jackson, 1998). Co-seismic effects were plentiful enough to confirm that the *Stratoni-Varvara* CSS was the causative tectonic structure. Ground ruptures (Floras, 1933), many of which coincided with the mapped geological fault, were preserved even decades afterwards (Pavlidis and Tranos, 1991). A coastal subsidence of 1.6 m was also reported by Floras (1933) and a downthrow of approximately 1.8 m across the fault scarp can be inferred from photographic archives (e.g. Georgalas and Galanopoulos, 1953).

Although the co-seismic ruptures and the large recorded magnitude suggest that the 1932 event ruptured the largest portion of the fault surface, morphotectonic investigations indicate that the *Stratoni-Varvara* CSS is segmented into three parts showing independent seismotectonic evolutions (Chatzipetros *et al.*, 2005b; Michailidou *et al.*, 2005; Pavlidis *et al.*, 2010). The *Varvara* ISS is the westernmost segment, 6.5 km-long and probably consisting of several parallel sliding planes with a general WNW-ESE strike. It forms an angular barrier with the adjacent *West Stratoni* ISS (10 km). The last segment (*East Stratoni* ISS) mainly runs offshore and clearly controls the E-W trending coastline up to the Eleftheronesos Island (10 km). Based on the observed maximum displacement documented near Stratoni and caused by the 1932, Ierissos earthquake (Floras, 1933; Georgalas and Galanopoulos, 1953; Pavlidis and Caputo, 2004), the CSS probably continues further eastwards, thus producing a total length of *ca.* 37 km. Field measurements along the fault trace (Pavlidis and Tranos, 1991) and the microseismicity distribution at depth (Galanis *et al.*, 2004) indicate a steeply dipping fault plane. On the basis of the available seismological information, the maximum depth of the structure is likely 16-18 km. The 1932 event ($M = 6.9-7.0$) likely corresponds to the worst case scenario and represents the maximum expected magnitude for this CSS.

Gomati CSS260

Roughly parallel to and synthetic with the *Stratoni-Varvara* CSS is the *Gomati* fault zone. Available information is generally scant and uncertainty for many parameters is consequently high. Mainly based on morphotectonic investigations and meso-structural analyses (Pavlidis and Kiliyas, 1987; Michailidou, 2005; Chatzipetros *et al.*, 2005b; Michailidou *et al.*, 2005), this tectonic structure is characterized by a major linear escarpment striking dipping towards the SSW. Field observations of slickenlines indicate a normal to oblique-slip motion with a left-lateral component (Pavlidis and Kiliyas, 1987). The 3-D relocation of a set of earthquakes in the Chalkidiki peninsula (Galanis *et al.*, 2004), indicate seismogenic depths up to 16-17 km for this zone, while a relocated seismic cluster by the same authors implies an eastward continuation of the fault zone offshore and north of the Island Amoliani.

In concomitance with the 1932 Ierissos seismic crisis, a large number of strong foreshocks and aftershocks were also recorded in the broader area (Papazachos and Papazachou, 1997; 2003). It is usually assumed that the magnitude $M = 6.3$ event which occurred on May 11, 1933 belongs to this seismic sequence and represents an aftershock of the Ierissos mainshock. However, based on a recent relocation of this event several kilometres southwards (Papazachos *et al.*, 2009) and taking into account the long time period elapsed since the mainshock, we tentatively associate the 1933 event with the *Gomati* CSS which was partly reactivated due to a

triggering effect. The maximum expected magnitude for the *Gomati* CSS is obtained from various empirical relationships (Wells and Coppersmith, 1994; Pavlides and Caputo, 2004).

Singitikos Gulf CSS270

The *Singitikos Gulf CSS* also belongs to the same system of SSW-dipping normal faults affecting the eastern sector of the Chalkidiki peninsula. However, its total length is double than the *Gomati* CSS and also greater than the *Stratoni-Varvara* CSS. The onshore part of this tectonic structure has been morphotectonically mapped (Pavlides and Kiliadis, 1987) showing oblique-slip kinematics with normal and left-lateral components. On the basis of detailed bathymetric maps, the CSS probably continues offshore running south of the Island Amoliani and generating the E-W trending coastal escarpment in the Athos Peninsula. It possibly continues eastwards across the Athos Peninsula, though specific field investigations have been not carried out. Information is also scant as concerns possible segmentation. Assuming the worst case scenario, a maximum expected magnitude of 7.1 is estimated from various empirical relationships (Wells and Coppersmith, 1994; Pavlides and Caputo, 2004).

Vourvourou ISS265

The southernmost structure of the east Chalkidiki peninsula fault set is represented by the *Vourvourou ISS* (Tranos, 1998; Mountrakis *et al.*, 2006); it is also referred to as *Sithonia Fault* by Goldsworthy *et al.* (2002). Although the strike of the fault is similar (ESE-WNW) to the nearby structures, this ISS is north-dipping, that makes antithetic with respect to the *Singitikos*, *Gomati* and *Stratoni-Varvara* CSSs. Morphotectonic investigation and meso-structural analyses across the *Sithonia* peninsula (Tranos, 1998) document a Quaternary activity for *ca.* 15 km and the occurrence of two minor segments, small enough to generate only moderate events. The assumed total length of 27 km for this seismogenic source also includes the offshore continuation as it has been documented by the sea-floor morphology and an earthquake cluster (Galanis *et al.*, 2004).

Sochos CSS120 (Mavrouda ISS120 and Sochos ISS121)

As mentioned above, another important fault set consisting of several subparallel and largely overlapping CSSs affects the central-western sector of the Chalkidiki peninsula. The northernmost structure, north of the *Mygdonia Basin*, is the *Sochos CSS*, which is antithetic with respect to the other ones, being the only one with a southward dip. This structure is responsible for the formation of small intra-mountain basins (Maravelakis, 1936). Its activity was constrained on the basis of morphotectonic analysis of the mountain front and of the thick Quaternary scree and fan sediments accumulated in the hanging-wall (Mountrakis *et al.*, 1996a; 2006). At least two fault segments have been recognized: the *Sochos* and *Mavrouda ISSs* (Goldsworthy *et al.*, 2002; Mountrakis *et al.*, 2006). The segment boundary is represented by a marked gap with a right-stepping underlapping geometry, therefore making a continuous rupture unlikely. Based on their length, each of the two segments are considered capable of producing a maximum earthquake of magnitude 6.3 (after the empirical relationships of Pavlides and Caputo, 2004). However, Zervopoulou (2004) suggest a maximum expected magnitude of 6.6 after taking into account a possible reactivation of more than one segments. The westernmost section of the fault zone is characterized by microseismic activity (Galanis *et*

et al., 2004; Paradisopoulou *et al.*, 2004). According to 3-D re-location of the local seismicity (Galanis *et al.*, 2004) the seismogenic layer thickness is approximately 13-15 km. The *Sochos* CSS is a possible candidate for the 1902, July 5, Assiros earthquake ($M = 6.5$; Papazachos and Papazachou, 1997), though the latter is tentatively attributed to the Langadhas ISS (see Mygdonia CSS) according to a critical revision of the available historical information.

Mygdonia CSS100 (Gerakarou ISS101, Langadhas ISS102 and Apollonia ISS103)

South of the *Sochos* CSS and bordering the southern margin of the Mygdonia Basin, the major *Mygdonia* CSS lies, with an antithetic north-dipping setting. The fault trace follows the mountain front and shows important strike variations due to segmentation. The fault zone was initially mapped by Kockel and Mollat (1977), but most of the structural and morphotectonic investigations were carried out after the 1978, June 20, Thessaloniki earthquake ($M_w = 6.5$), which reactivated the central segment of the *Mygdonia* CSS (Mercier *et al.*, 1979; 1983; Mountrakis *et al.*, 1996a; Tranos *et al.*, 2003). Three main segments can be recognised (from east to west): the *Apollonia*, *Gerakarou* and *Langadhas* ISSs.

The eastern *Apollonia* Fault segment, has sculptured a linear prominent morphology which is interrupted by the alluvial fan of the Megalo Rema seasonal river. A conservative value for the fault length is 20 km and the segment boundary with the Gerakarou Fault to the west is marked by a change in strike. Microearthquake surveys (Hatzfeld *et al.*, 1986/87) document dip-slip motion on the *Apollonia* ISS, while the 3-D relocation of the seismicity (Galanis *et al.*, 2004) shows activity down to a depth of 18 km and delineates a steeply dipping fault plane.

The central sector of the Mygdonia CSS is represented by the *Gerakarou* ISS which is the causative fault of the 1978 earthquake. This earthquake has been thoroughly studied due to its location very close to the city of Thessaloniki. Extended co-seismic ground ruptures were produced that splayed out in the Mygdonia Basin (Mercier *et al.*, 1979; 1983; Papazachos *et al.*, 1979; Soufleris and Stewart, 1981; Mountrakis *et al.*, 1996a). The most significant ones occurred along the southern margin of the basin, coinciding with the principal N-dipping fault escarpment. Two other groups of aligned ruptures were observed near to the centre of the basin, between lakes Koronia and Volvi. In particular, the northernmost one strikes NW-SE, shows a south-dipping normal displacement and it probably represents a secondary accommodation structure. Seismotectonic parameters are well constrained on the basis of focal mechanisms, source parameters of the mainshock and aftershock distribution (Kulhánek and Meyer, 1979; Papazachos *et al.*, 1979; Barker and Langston, 1981; Carver and Bollinger, 1981; Soufleris and Stewart, 1981; Soufleris *et al.*, 1982; Soufleris and King, 1983; Dziewonski *et al.*, 1987; Vannucci and Gasperini; 2003; 2004; Roumelioti *et al.*, 2007). Additionally, several morphotectonic investigations and meso-structural analyses have been carried out (Mercier *et al.*, 1979; 1983; Mountrakis *et al.*, 1996a; Tranos *et al.*, 2003). The ruptured fault plane strikes almost E-W, dips northwards with shallow to moderate angle and is characterized by an almost pure dip-slip normal motion associated with a N-S direction of crustal extension. Microearthquake surveys suggest listric fault geometry with a kink-point at 8 km depth and a seismogenic layer thickness ranging between 14 and 16 km (Hatzfeld *et al.*, 1986/87; Tranos *et al.*, 2003; Paradisopoulou *et al.*, 2006), which is shallower with respect to the eastern segment. Based on geodetic models, Stiros and Drakos (2000) suggest blind faulting during the 1978 event, considering the observed surface ruptures as only secondary effects. In contrast,

palaeoseismological trenches confirm the occurrence of repeated linear morphogenic events before the 1978 earthquake (Cheng *et al.*, 1994; Chatzipetros, 1998; Chatzipetros *et al.*, 2004) with a mean slip-per-event of 6.5-16 cm, a slip-rate of 0.06-0.7 mm/a and a recurrence interval ranging between 1000 and 1500 years. Slip-per-event at the fault-scale is probably underestimated considering the magnitude of the 1978 earthquake; based on seismic waveforms joint inversion and levelling data a value of 0.6 m is preferred (Roumelioti *et al.*, 2007).

The westernmost segment (*Langadhas ISS*) borders a sharp mountain front trending NW-SE. Although this structure has been clearly inherited from previous tectonic events (both alpine thrusting and Miocene-Pliocene NE-SW extension) and it is not ideally oriented with the present-day regional stress field, it shows evidences of recent reactivations with an oblique-slip kinematics (Mercier *et al.*, 1979; 1983) which are also supported by morphometric parameters (very low mountain-front sinuosity index). Quite the opposite is suggest by Tranos *et al.* (2003) who support that this portion of the Mygdonia CSS has been abandoned and that activity has migrated to the south towards the Asvestochori CSS (see next CSS). Microseismic activity (Galanis *et al.*, 2004; Paradisopoulou *et al.*, 2006) indicates a maximum depth of 14-16 km. As previously mentioned and according to the available historical information, the 1902, July 5, Assiros earthquake (M = 6.5; Papazachos and Papazachou, 1997; 2003), has been tentatively attributed to the *Langadhas ISS*.

Asvestochori CSS245

This fault zone lies very near to the urban area of Thessaloniki; it runs parallel to, and is synthetic with, the western segment (*Langadhas ISS*) of the Mygdonia CSS. The fault is reported in several morphotectonic and geological maps (Mountrakis *et al.*, 1996a; 1996b; Tranos *et al.* 2003; Zervopoulou, 2004). According to Mercier *et al.* (1983), the *Asvestochori Fault* was partially reactivated during the 1978 Thessaloniki earthquake. According to Tranos *et al.* (2003), the recent growth of this structure has progressively de-activated the *Langadhas ISS* and is going to produce a direct linkage with the central sector of the Mygdonia CSS. Information for the deeper parts of the fault is provided by microearthquake investigations (Paradisopoulou *et al.*, 2006) and geological considerations (Tranos *et al.*, 2003), both implying the existence of a listric geometry with a dip varying from 80° at the surface to 35° at depth. The maximum seismogenic depth, constrained to 15-16 km, is based on microseismic distribution (Galanis *et al.*, 2004; Paradisopoulou *et al.*, 2004).

Pylaea CSS240

This seismogenic structure is important because directly crosses the urban area of Thessaloniki and its gulf. The fault trace has been mapped by Tranos *et al.* (2003), Zervopoulou (2004) and Valkaniotis *et al.* (2005), providing constraints on its location, surface geometry and strike. Considering that this tectonic structure belongs to the broader normal fault set that affects the central-western Chalkidiki peninsula and that it possibly represents an upwards splay of a deeper low-angle normal detachment (Tranos *et al.*, 2003), the other principal seismotectonic parameters have been inferred accordingly.

Anthemountas CSS250 (Angelochori ISS251 and Souroti ISS252)

The *Anthemountas fault zone* is also an important structure for the Thessaloniki urban area because it bounds the southern side of the gulf (Mountrakis *et al.* 1996b; 2006; Tranos *et al.*, 2003; Zervopoulou, 2004; Zervopoulou and Pavlides, 2005; Zervopoulou *et al.*, 2007) and has been mapped for a total length of at least 40 km (Zervopoulou, 2004; Zervopoulou and Pavlides, 2005; Zervopoulou *et al.*, 2007). It possibly extends more to the west, offshore in the Thermaikos Gulf. According to Tranos *et al.* (2003) this structure represents the southernmost north-dipping steep splay fault joining at depth a regional-scale low-angle extensional shear zone kinematically linked to the Pylaea, Asvestochori and Mygdonia CSSs. The fault has been tentatively separated into two segments according to morphotectonic criteria (Zervopoulou, 2004; Zervopoulou and Pavlides, 2005; Zervopoulou *et al.*, 2007): the *Souroti* and *Angelochori ISSs*, east and west, respectively, both characterized by a length of *ca.* 17 km.

In 1759 an important seismic sequence affected the city of Thessaloniki (Papazachos and Papazachou, 1997; 2003; Ambraseys, 2009). The date of the major shock is debated. Papazachos and Papazachou (1997) suggest the 22nd of June, while Ambraseys (2009) states that during the same day, two 'violent' shocks indeed occurred, but the destructive event took place on the 3rd of July. The macroseismic magnitude was 6.5 and the aftershock sequence was intensive (Papazachos and Papazachou, 1997). According to the tentative location of the macroseismic epicenter the causative fault could be the *Angelochori ISS*. In 1677 another earthquake with estimated macroseismic magnitude 6.2 caused damages in several villages east of Thessaloniki (Papazachos and Papazachou, 1997; 2003; Ambraseys, 2009). Based on the suggested macroseismic epicenter and considering that approximately 80 years later the western segment was probably reactivated (1759 event), the 1677 earthquake is tentatively associated with the *Souroti ISS* (eastern segment). It is noteworthy that aseismic creep has been observed along the *Angelochori Fault* (Zervopoulou *et al.*, 2007). An entire fault rupture is a quite possible (worst) scenario for the *Anthemountas CSS*; in this case, the maximum expected magnitude, calculated from various empirical relationships (Wells and Coppersmith; Pavlides and Caputo, 2004), would be $M = 7.0$.

5.4 The 'anti-Hellenides' fault system

West of the Axios Valley, in Western Macedonia and Epirus, the orographic and morphological first-order texture of the region is characterized by the NW-SE trending Hellenic fold-and-thrust belt which has generated elongated mountain chains and interposed valleys ([fig. 5.5](#)). In this sector of northern Greece, all major active faults that have been recognized at present and included in the GreDaSS are oriented (E)NE-(W)SW, therefore showing a typical 'anti-Hellenides' setting. It is worth noting that stress trajectories reconstructed for this region show a NNW to NW orientation of the σ_3 stress axis (*e.g.* Mercier *et al.*, 1989; Jenny *et al.*, 2004).

Within this fault system GreDaSS includes several 'isolated' CSSs and ISSs, like the North Almopia, South Almopia, Goumenissa, Aliakmonas, Konitsa and Petoussi. In contrast, the

Ptolemaida Basin is affected by a group of sub-parallel, synthetic and antithetic, seismogenic structures which are possibly linked at depth by a low-angle shear zone, showing a seismotectonic setting similar to that described in the Chalkidiki peninsula (Sboras and Caputo, 2010).

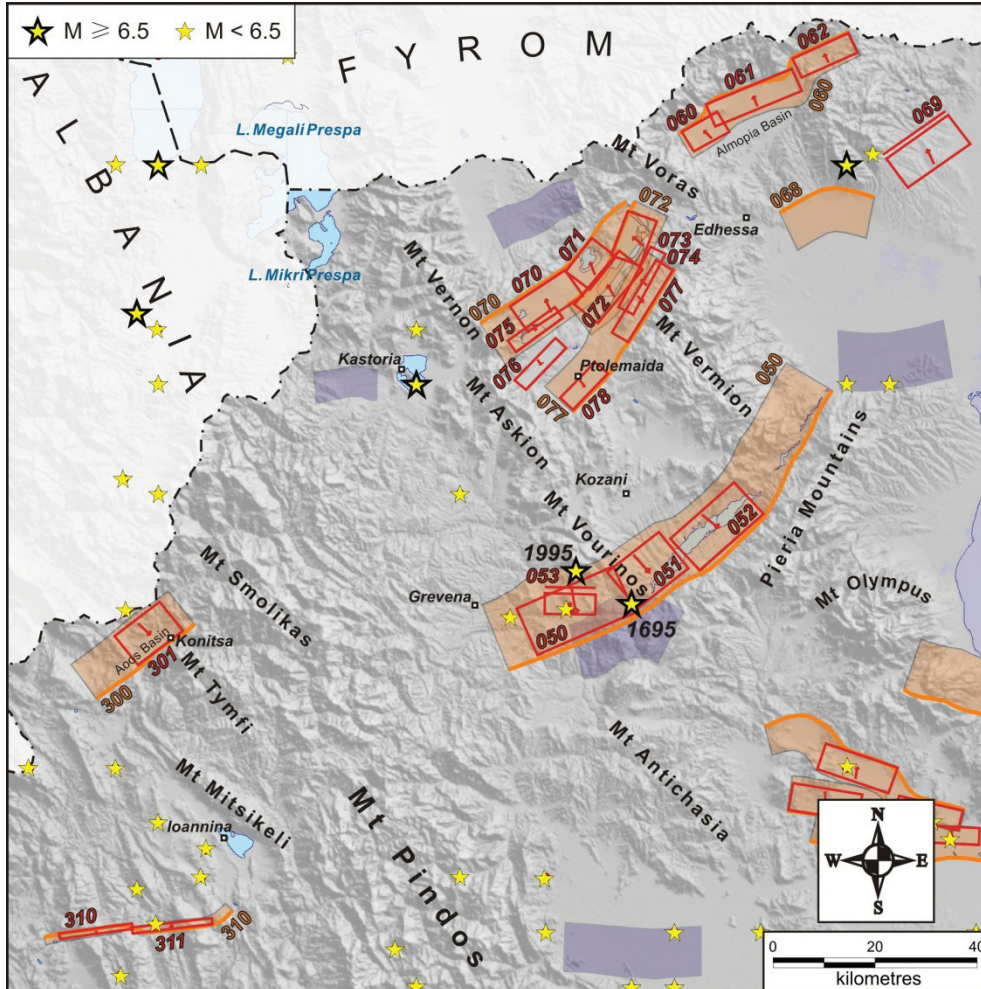


Fig. 5.5: The seismogenic sources of the ‘anti-Hellenides fault system’ (fig. 5.1). Orange sources and numbers: CSSs and their codes, read sources and numbers: ISSs and their numbers, blue sources: DSSs. The epicentres (stars) have been taken from the catalogue of Papazachos *et al.* (2000; 2009; <http://geophysics.geo.auth.gr/ss/>).

North Almopia CSS060 (Pozar ISS060, Promachi ISS061 and Aetochori ISS062)

The *North Almopia fault zone* bounds the northern margin of the Almopia Basin and a smaller adjacent basin to the northeast (Pavlidis *et al.*, 1990; Goldsworthy *et al.*, 2002; Vougioukalakis, 2002; Mountrakis *et al.*, 2006). The development of the Almopia Basin took place during Pliocene and was accompanied by significant volcanic activity (Mercier, 1981). Vougioukalakis (2002) however, suggests that the subsidence of the basin occurred only after the end of the volcanism (1.8 Ma).

The zone can be divided into three major segments (Goldsworthy *et al.*, 2002; Mountrakis *et al.*, 2006): the *Pozar*, *Promachi* and *Aetochori* ISSs (from east to west), forming an overall left-

stepping geometry. Meso-structural analyses provide important geometric and kinematic information (Mercier *et al.*, 1989; Pavlides *et al.*, 1990) indicating that two slightly different extensional tectonic phases took place from Middle Pleistocene to Present, with the most recent stress field characterized by a NNW-SSE direction of extension, similar to the azimuth of the slip-vector ($\sim 160^\circ$) that is measured on the Mesozoic limestones of the Promachi Fault free-face by Goldsworthy *et al.* (2002). Using electrical resistivity tomographies, borehole data and field observations, Vougioukalakis (2002) carried out a 3-D structural reconstruction of the basin and estimated for the central sector vertical and horizontal extension rates of 0.92 mm/a and 0.36 mm/a, respectively. Based on these rates, a slip-rate of *ca.* 1 mm/a can be estimated. The worst case rupture scenario of the fault zone involves the joint reactivation of the two western segments (*Pozar* and *Promachi ISSs*), given that the *Aetochori ISS* shows a great overstep and underlap, probably representing a strong barrier.

Goumenissa ISS069

Information for this seismogenic structure mainly derives from the December 21, 1990 ($M_s = 6.0$ according to Panagiotopoulos *et al.*, 1993; $M_w = 6.1$ according to Dziewonski *et al.*, 1991; Vannucci & Gasperini, 2003; 2004) Goumenissa earthquake (Panagiotopoulos *et al.*, 1993). The fault evidence at the surface is somehow questionable; the fault is possibly blind due to the fact that neither co-seismic ground rupture were observed, nor a prominent fault scarp is detectable. The estimated focal depth is *ca.* 16 km, whereas the macroseismic one is estimated to 12 km; similarly, the aftershock distribution is not deeper than 12 km (Panagiotopoulos *et al.*, 1993). This could imply that only a smaller patch was ruptured during the 1990 event. Focal mechanisms show a SE-dipping, NE-SW trending dip-slip normal fault (Dziewonski *et al.*, 1991; Panagiotopoulos *et al.*, 1993; Baker *et al.*, 1997; Vannucci and Gasperini, 2003; 2004).

In the vicinity of the *Goumenissa ISS*, the so-called Edessa earthquake (Ambraseys, 1999; 2009) occurred in October 1395, with a possible magnitude of 6.7 (Papazachos and Papazachou, 1997; 2003). However, the tentative location of the macroseismic epicenter is similarly close to the South Almopia CSS and not very far from the North Almopia CSS (see previous CSS). Accordingly, the state-of-knowledge does not allow associating this strong earthquake with any recognized structure.

South Almopia CSS068

The *South Almopia CSS* dips towards the south, showing a marked arcuate fault trace. Information about the fault derives from morphotectonic investigations (Pavlides, 1998), which document ENE-WSW-striking, dip-slip normal faults affecting the pyroclastic sediments deposited about 4.8 Ma ago. The mesostructural analysis of these deposits reveals a NNW-SSE direction of the σ_3 axis. The measured dip of the faults is high. The structure is considered active also due to its ideal orientation with respect to the regional stress field. Assuming a complete reactivation of the whole fault zone, a maximum magnitude of 6.7 can be expected, calculated by various empirical relationships (Wells and Coppersmith, 1994; Pavlides and Caputo, 2004). However, due to the geometry of the fault, a smaller rupture is more possible, decreasing the maximum expected magnitude.

Amyndeo CSS070 (Nymfaeo ISS070 and Petron ISS071)

As mentioned before, the Ptolemaida Basin is a tectonically controlled area characterized by alternating sub-parallel ridges and basins, all elongated in a NE-SW direction (Pavlides, 1985) and associated with subparallel fault zones possibly linked at depth by a low-angle SE-dipping shear zone. Several major fault zones, controlling large morphological structures, and smaller individual ones, but not less significant, have been recognised and studied (Pavlides, 1985; Pavlides and Mountrakis, 1987; Doutsos and Koukouvelas, 1998; Goldsworthy *et al.*, 2002). Field measurements of all the active tectonic structures in the Ptolemaida Basin indicate a (N)NW-(S)SE direction of the slip vector (Pavlides, 1985; Pavlides and Mountrakis, 1987; Doutsos and Koukouvelas, 1998). Although the morphotectonic features of the area indicate intensive and recent activity, neither historical nor instrumental significant seismic activity is recorded. The seismogenic layer thickness of *ca.* 14 km is inferred from seismotectonic considerations (*e.g.* thickness of nearby areas).

The northernmost structure is the *Amyndeo CSS* showing clear geological and morphological evidence of recent activity (Pavlides, 1985; Pavlides and Mountrakis, 1987; Doutsos and Koukouvelas, 1998; Goldsworthy *et al.*, 2002). The *Amyndeo fault zone* borders and tectonically controls the mountain front along a SW-trending ridge that separates the Ptolemaida Basin from the Florina Basin to the north and connects the two mountains of Voras, to the east, and Vernon, to the west. All along its almost 40 km of total length, it has produced a discrete morphological slope as a result of a major dip-slip normal motion with a slight right-lateral strike-slip component as documented by slickenlines (Pavlides, 1985). However, the fault zone is not entirely uniform. West of Petron village, the relief locally becomes subdued, while a slight change of the mountain front orientation is observed. Accordingly, the fault zone is divided into two segments: the *Petron* and *Nymfaeo ISSs*, to the NE and SW respectively.

The *Petron ISS* is a fault segment that controls the local depression where Lake Petron is located. The fault has shaped a linear and steep coastline on Mesozoic limestones, characterized by evident slickensides affecting scree deposits and cataclastic breccias (Pavlides, 1985). According to the same author, the fault trace continues northeastwards for 2-3 km along a small narrow valley. Towards the southwest the fault cuts through Neogene sediments (upper Miocene-lower Pliocene), while NNE-trending secondary structures affect also Pleistocene deposits (Pavlides, 1985). The southwestern fault-tip is covered by Pliocene-Pleistocene sediments suggesting that the Petron-Nymfaeo segment boundary likely corresponds to a permanent barrier.

The *Nymfaeo ISS* is a larger NE-SW trending structure showing angular segment boundary geometry. Near to its northeastern tip, the fault affects and downthrows Pliocene sediments (Pavlides, 1985). Towards the SW, a major escarpment possibly documents a cumulative displacement up to 700-800 m. The fault has been also detected by Vertical Electrical Soundings (VES) and boreholes (Atzemoglou *et al.*, 2003).

The two ISSs are capable of producing 6.0 and 6.2 earthquakes, respectively. However, both ISSs could possibly extend further NE and SW, respectively (worst case scenario); therefore the maximum expected magnitudes could be as high as 6.6-6.7.

Chimatidis ISS075

Parallel and antithetic to the Nymfaeo ISS, a nearly 12 km-long active tectonic structure lies along the southern shore of Lake Chimaditis (Pavlides, 1985; Pavlides and Mountrakis, 1987). The NW-dipping dip-slip normal *Chimaditis ISS* has generated a low elongated terrace on its footwall consisting of uplifted Neogene, Pleistocene and Holocene deposits (Pavlides, 1985). This structure probably joins the Nymfaeo ISS at depth constraining its maximum depth to *ca.* 7.5 km. Accordingly, the maximum expected magnitude is probably below 6.0.

Ptolemaida CSS072 (Vegora ISS072 and Vegoritida ISS073)

Parallel to and synthetic with the central-northern sector of the Amyndeo CSS, there is the 25 km-long *Ptolemaida CSS*. The fault zone shows clear morphotectonic evidences of recent activity and consists of two segments: the *Vegoritida* and *Vegora ISSs*, to the NE and SW respectively. Probably constrained by the Amyndeo CSS, the maximum depth of the fault zone should not exceed 11.5 km.

The *ca.* 10 km-long, (N)NE-trending *Vegoritida ISS* shows an impressive morphology with a high limestone cliff, bordering the homonymous lake. A minimum cumulative downthrow of 500 m is morphologically inferred (Pavlides, 1985), whereas high-resolution Boomer profiles carried out in the lake, suggest a vertical stratigraphic displacement of about 600-700 m (Sakellariou *et al.*, 2001). Mesostructural analyses document a recent NNW-SSE trending direction of stretching (Pavlides, 1985; Pavlides and Mountrakis, 1987; Doutsos and Koukouvelas, 1998; Mountrakis *et al.*, 2006).

The *Vegora ISS* continues for at least 12 km southwestwards forming an arcuate escarpment (Pavlides, 1985; Pavlides and Mountrakis, 1987; Doutsos and Koukouvelas, 1998). The absence of limestones in the footwall causes a more subtle morphology. Nevertheless, a few scattered limestone scarps bear striations that indicate a roughly dip-slip normal kinematics associated with a NW-SE direction of extension (Pavlides, 1985). Neogene and Quaternary sediments are also affected by the fault. The high-resolution Boomer profiles of the lake bottom suggest an offshore continuation of the fault (Sakellariou *et al.*, 2001). As a result, the fault seems to overlap the *Vegoritida ISS*, reaching probably a total length of more than 14 km.

The rupture of the entire fault zone is a possible (worst case) scenario, given that the segment boundary does not seem strong enough to prevent it. In this case, the maximum estimated magnitude, according to various empirical relationships (Wells and Coppersmith, 1994; Pavlides and Caputo, 2004), would be 6.6.

Perdika ISS076

Sub-parallel to and synthetic with the Chimatidis Fault (see §5.5), lies the *Perdika ISS* at a distance of about 6 km to the south (Pavlides, 1985; Pavlides and Mountrakis, 1987; Goldsworthy *et al.*, 2002; Mountrakis *et al.*, 2006). The *Perdika ISS* borders the northern hillside of the Bordeaux Heights, separating the Pliocene(?) sediments outcropping in the footwall from the Quaternary deposits of the plain. For similarity with the other structures of the broader Ptolemaida Basin and according to the regional stress field, the kinematics of the

Perdika Fault is basically dip-slip normal. Similar constraints to the other faults of the basin have been also applied for maximum depth.

Komanos CSS077 (Mesovouni ISS077 and Proastio ISS078)

The (N)NE-(S)SW trending and NW-dipping *Komanos CSS* bounds the southeasternmost margin of the Ptolemaida Basin (Pavlidis, 1985; Pavlidis and Mountrakis, 1987; Mountrakis *et al.*, 2006). Two major segments have been recognized: the *Mesovouni* and *Proastio ISSs*, to the NE and SW respectively (Mountrakis *et al.*, 2006). The fault zone has a total length of *ca.* 36 km, though morphological evidence in the central sector is poor and introduces some uncertainty in the location of the segment boundary. Both segments have a moderate to steep NW-dip.

The *Mesovouni ISS* runs along the northwestern front of the Mount Vermion (Pavlidis, 1985; Pavlidis and Mountrakis, 1987; Doutsos and Koukouvelas, 1998; Mountrakis *et al.*, 2006), showing a low value of the mountain front sinuosity index. Quaternary deposits have been mainly accumulated within a secondary accommodation structure (a 1.5 km-wide symmetric graben) thus suggesting the recent activity of this fault (Pavlidis, 1985; Pavlidis and Mountrakis, 1987; Mountrakis *et al.*, 2006). The measured cumulative displacements in Pliocene lignite deposits, deriving from borehole data, range from 20-40 m to up to 70 m (Pavlidis, 1985). On July 9, 1984 a moderate earthquake ($M_w = 5.2$) occurred between the *Mesovouni* and the *Peraea ISSs* (see next subchapter; Pavlidis and Simeakis, 1987/88; Dziewonski *et al.*, 1985; Anderson and Jackson, 1987). The obtained focal mechanisms are generally in agreement with the local tectonic setting and specifically with the seismotectonic features of the *Mesovouni Fault* (Dziewonski *et al.*, 1985; Anderson and Jackson, 1987). However, the low dipping angle suggested by the foci possibly corresponds to the deepest part of the fault where it probably merges with the antithetic normal dip-slip shear zone (Sboras and Caputo, 2010).

The *Proastio ISS* lies on the northern borders of the lignite mines (Pavlidis, 1985; Pavlidis and Mountrakis, 1987; Doutsos and Koukouvelas, 1998; Mountrakis *et al.*, 2006). It is expressed by a group of parallel minor fault scarps affecting Quaternary sediments (Pavlidis, 1985). Northwards in the hanging-wall it has been detected by boreholes showing a down-stepping throw of the Pliocene lignite deposits with a cumulative displacement of almost 300-400 m (Pavlidis, 1985). Secondary antithetic structures were also observed on the footwall forming a minor tectonic horst (Pavlidis, 1985; Diamantopoulos, 2006). Kinematic indicators document an almost pure dip-slip normal motion (Pavlidis, 1985; Pavlidis and Mountrakis, 1987) and a NW-SE direction of extension.

Since the boundary between the two segments is not clearly observed and especially its nature (*i.e.* strong or soft boundary), the possible rupture of the entire fault zone cannot be excluded a priori. In this case (worst case scenario), the maximum expected magnitude would be 6.8, according to various empirical relationships (Wells and Coppersmith, 1994; Pavlidis and Caputo, 2004).

Peraea ISS074

The *Peraea ISS* is an active structure close to but antithetic with the Komanos CSS (see previous CSS) and at the same time synthetic to the Ptolemaida CSS (see previous subchapters; Pavlides, 1985; Pavlides and Mountrakis, 1987; Goldsworthy and Jackson, 2000; 2001; Mountrakis *et al.*, 2006). The SE-dipping fault is marked by a discontinuous escarpment that extends for a total length of *ca.* 14 km. Well preserved slickensides and free faces put in contact the Mesozoic substratum with Holocene deposits (Pavlides, 1985; Goldsworthy and Jackson, 2000; 2001).

Aliakmonas CSS050 (Palaeochori ISS050, Rymnio ISS051, Servia ISS052 and Chromio ISS053)

The *Aliakmonas fault zone* is a NE-SW-trending, NW-dipping major tectonic structure controlling a large extent of the homonymous river. Geological and morphotectonic investigations suggest the occurrence of three major segments (Pavlides *et al.*, 1995; Doutsos and Koukouvelas, 1998; Mountrakis *et al.*, 1998; Meyer *et al.*, 1996; 1998): the *Palaeochori*, *Rymnio* and *Servia ISSs* (from SW to NE). The aftershock spatial distribution (Hatzfeld *et al.*, 1997; 1998) of an event that occurred during 1995 documents a maximum seismogenic depth of 17 km, which possibly becomes gradually shallower from the south-western to the north-eastern part of the fault zone. Moreover, based on morphological evidence, Doutsos and Koukouvelas (1998) suggest a recent westward migration of the tectonic activity.

The *Palaeochori ISSs* is marked by discontinuous escarpment that fades away towards the SW (Pavlides *et al.*, 1995; Doutsos and Koukouvelas, 1998; Mountrakis *et al.*, 1998). It ruptured during the May 13, 1995 Kozani earthquake ($M_w = 6.5$) producing aligned, but not continuous, co-seismic ground ruptures all along its length (Pavlides *et al.*, 1995; Mountrakis *et al.*, 1998). Based on nodal planes from focal mechanisms (Papazachos *et al.*, 1998; Dziewonski *et al.*, 1996; Kiratzi and Louvari, 2003; Vannucci and Gasperini, 2003; 2004), earthquake tomographies from the aftershocks (Chiarabba and Selvaggi, 1997), aftershock spatial distributions (Hatzfeld *et al.*, 1997; 1998; Drakatos *et al.*, 1998a; Papanastassiou *et al.*, 1998; Papazachos *et al.*, 1998), stress tensor inversions (Kiratzi, 1999), forward modelling of the source from strong motion waveforms (Suhadolc *et al.*, 2007) and InSAR images analyses (Meyer *et al.*, 1996; 1998; Rigo *et al.*, 2004; Resor *et al.*, 2005) it is possible to constrain several seismotectonic parameters. Based on palaeoseismological investigations a recurrence interval of 10-30 ka is tentatively suggested (Chatzipetros *et al.*, 1998). Taking into account the size of the *Palaeochori Fault*, its potential magnitude after the application of empirical relationships (Wells and Coppersmith, 1994) is higher than the magnitude of the 1995 mainshock. Moreover, given that co-seismic ruptures fade out towards the western tip but are also observed eastwards, along the adjacent Rymnio Fault, it can be then implied that during the 1995 event, parts from both faults were ruptured but not in all their extent. During the same seismic crisis, the aftershock spatio-temporal distribution also revealed the occurrence of a secondary antithetic structure, the *Chromio ISS* (Hatzfeld *et al.*, 1997; 1998), which also produced south-dipping co-seismic ground ruptures aligned in an E-W direction (Pavlides *et al.*, 1995; Mountrakis *et al.*, 1998). This fault is considered as an inherited S-dipping right-lateral strike-slip fault reactivated in the new tectonic regime as dip-slip normal fault antithetic to the *Palaeochori ISS* (Pavlides *et al.*, 1995; Mountrakis *et al.*, 1998; Hatzfeld *et al.*, 1997; 1998).

The *Rymnio ISS* falls northeast of the *Palaeochori ISS* and it is separated by an angular barrier. The fault is marked by a distinct escarpment especially in the northeastern sector (Pavlidis *et al.*, 1995; Doutsos and Koukouvelas, 1998; Mountrakis *et al.*, 1998). The northeastern boundary of the *Rymnio segment* corresponds to a strong geometric (right-stepping underlapping geometry) barrier as well (Pavlidis *et al.*, 1995; Doutsos and Koukouvelas, 1998; Mountrakis *et al.*, 1998; Meyer *et al.*, 1996; 1998). A partial rupture of this structure during the 1995 earthquake has been claimed based on some ground ruptures observed near to the Rymnio village. However, their occurrence along the lakeshore is likely caused by gravitational phenomena. Morphotectonic investigations (Pavlidis *et al.*, 1995; Doutsos and Koukouvelas, 1998; Mountrakis *et al.*, 1998; Meyer *et al.*, 1996; 1998) indicate similar geometry and kinematics with the nearby tectonic structures.

Next to Rymnio Fault is the *Servia ISS*, which represents the most prominent neotectonic structure of the *Aliakmonas CSS*. The fault is outcrops with a long, well polished sliding surface on limestones, which bears a set of fresh striations documenting a (N)NW-(S)SE direction of extension (Pavlidis *et al.*, 1995; Meyer *et al.*, 1996; 1998; Mountrakis *et al.*, 1998; Goldsworthy and Jackson, 2000). There was no sign of reactivation during the 1995 earthquake. The northeastern tip of the fault is not well defined. Based on the asymmetric shape of the along-strike displacement profile, Doutsos and Koukouvelas (1998) suggest a possible linkage between the *Servia* and *Rymnio ISSs*. Based on geomorphic markers a slip-rate of 1-2 mm/a and a mean recurrence interval of 1-2 ka are suggested (Meyer *et al.*, 1996). A maximum cumulative displacement of 2100 m has been proposed by Doutsos and Koukouvelas (1998) across the fault. On September 26, 1695 an earthquake ($M_e = 6.5$) struck the area with macroseismic epicentre tentatively located in the hanging-wall of the *Rymnio Fault* (Papazachos and Papazachou, 1997; 2003; Ambraseys, 1999; 2009). However, the lack of details prevents any straightforward correlation with any specific segments of the *Aliakmonas CSS*.

It is noteworthy that the *Aliakmonas CSS* continues northeastwards, following the valley that separates Mount Vermion from the Pieria Mountain chain. For this sector has been tentatively suggested a fourth distinct 25 km-long fault segment (referred to as *Polyphytos-Polydendri* by Mountrakis *et al.*, 2006), which however does not show definite evidence of recent seismogenic activity. Accordingly, this structure is included in the *CSS* without defining any specific *ISS* in *GreDaSS*.

Konitsa CSS300/ISS301

The *Konitsa ISS* is a NW-dipping structure bordering the mountain front of Mount Tymfi. Although the best evidence of recent activity is limited along the southern margin of the elongated *Aoos Basin*, there are some implications for a northeastern continuation (Goldsworthy *et al.*, 2002; Doutsos and Koukouvelas, 1998). In particular, Goldsworthy *et al.* (2002) suggest a possible connection with the fault system of the *Ptolemaida Basin* to the east, whereas Doutsos and Koukouvelas (1998) support that the fault is mechanically bounded by a roughly perpendicular Neogene thrust which causes displacement to decrease rapidly eastwards. Taking also into account a possible western prolongation, the *Konitsa ISS* gave birth to the homonymous *CSS*.

Based on several morphotectonic and structural investigations (Doutsos and Koukouvelas, 1998; Doutsos and Kokkalas, 2001; Goldsworthy *et al.*, 2002; Galanakis *et al.*, 2007) the *Konitsa ISS* is associated with a major escarpment delimited by a linear mountain front. Observations include many fresh slickensides, bearing also corrugations, on the Mesozoic limestone, usually delimiting the Miocene flysch, but sometimes also Quaternary deposits.

On July 26, 1996 a moderate earthquake of $M_s = 5.4$ (according to Papanastassiou, 2001) or $M_w = 5.1$ (according to EMMA catalogue: Vannucci and Gasperini, 2003; 2004) occurred near Konitsa town. A couple of weeks later, another moderate but stronger event of $M_s = 5.7$ (according to Papanastassiou, 2001) or $M_w = 5.3$ (according to Dziewonski *et al.*, 1997) occurred in the same seismogenic volume. Observed co-seismic ruptures (Galanakis *et al.*, 2007) and focal mechanisms (Dziewonski *et al.*, 1997; Papanastassiou, 2001; Vannucci and Gasperini, 2003; 2004) are in agreement with the mesostructural analyses (Doutsos and Koukouvelas, 1998; Doutsos and Kokkalas, 2001; Galanakis *et al.*, 2007) showing a normal dip-slip motion in a NW-extensional field. An average dip of 55° and a maximum depth of *ca.* 11 km are inferred from the aftershock spatial distribution, which also suggest a listric shape at depth (Papanastassiou, 2001). Although the largest instrumentally recorded magnitude during the 1996 sequence was the $M_w = 5.3$ shock, the maximum magnitude is expected to be greater for the *Konitsa ISS*, not only because of the estimations through the empirical relationships (Wells and Coppersmith, 1994), but also due to the size of the fault. If we also consider the longer and probably deeper (maximum depth of more than 12 km) structure of the *Konitsa CSS*, the maximum expected magnitude could be as high as 6.7 (calculated by the empirical relationships of Pavlides and Caputo, 2004).

Petoussi CSS310 (Souli ISS310 and Tomaros ISS311)

The *Petoussi CSS* is mainly inherited from the Mesozoic evolution and the Alpine tectonics (Caputo and Zouros, 1993; Boccaletti *et al.*, 1997). Although the fault zone has a different strike (~E-W) with respect to the other seismogenic sources included in the Western Macedonia-Epirus fault system, a regional-scale undulation of the orogene makes also this fault zone a typical anti-Hellenic structure. The *Petoussi CSS* is a sub-vertical fault zone with local changes in dip direction, bearing kinematic indicators that indicate a prominent left-lateral strike-slip motion (Caputo and Zouros, 1993). This geological setting has formed positive and negative flower structures as well as secondary splay faults (Boccaletti *et al.*, 1997). Based on these differences, we divided the fault zone into two major segments, the *Tomaros* and *Souli ISSs*, east and west respectively. The recent activity of the *Petoussi CSS* is based on morphotectonic investigations and palaeoseismological trenches which document along the *Souli Fault* at least 3 palaeo-events during the last *ca.* 30 ka BP (Boccaletti *et al.*, 1997), therefore suggesting a recurrence interval of several thousand years.

Microearthquake surveys (King *et al.*, 1983; Hatzfeld *et al.*, 1995; Tselentis *et al.*, 2006) document *i)* an eastward increase of the seismogenic depth from less than 12 km to more than 15 km, and *ii)* the occurrence of both strike-slip and normal dip-slip focal mechanisms. The worst case scenario would be an earthquake rupturing the whole length of the *Petoussi CSS*; in that case on the basis of scaling laws (Wells and Coppersmith, 1994) the maximum expected magnitude would be 6.9.

Kerkyra CSS390 (Makrades ISS390 and Spartylas ISS391)

The *Kerkyra CSS* is a large that crosses the homonymous island from west to east and continues inside the Albanian coast (Pavlidis *et al.*, 2001a), by crossing the Kerkyra strait. The on-island part of the fault zone had already been recognised during petroleum investigations (IGRS-IFP, 1966), while later on, geological and morphotectonic investigations (Caputo, 1984; 1986; 1987/88; unpublished data; Lekkas, 1995; Pavlidis *et al.*, 2001a) verified its recent activity, which is characterized by a normal (dip-slip)-oblique motion rather than the older right-lateral strike-slip one. Two fault segments can be recognised along this part: the *Makrades* and *Spartylas ISSs*. Both segments show left-stepping underlapping geometry that can prevent a possible continuous rapture along their cumulative length. In other words, the largest segment (*Spartylas ISS*) can produce the maximum magnitude.

Palaeokastritsa ISS392

Lying on the western side of the Corfu Island, near to the Palaeokastritsa village and antithetically to the previously described Makrades ISS, the *Palaeokastritsa ISS* shows similar geometric and kinematic characteristics with the Kerkyra CSS (Caputo, 1984; 1986; 1987/88; unpublished data; Lekkas, 1995).

5.5 The Thessalian fault system

The first-order topographic texture of Thessaly is characterized by a NW-SE-trending basin-and-range-like tectonic system of latest Miocene-Early Pleistocene age, affecting the region between the Pindos mountain chain, to the west, and the Aegean Sea, to the east (fig. 5.1). However, since the Middle Pleistocene the area has been in a N(NE)-S(SW) extensional regime that created mainly normal E-W-trending fault systems generally overprinting the older basins but locally exploiting inherited structures (Caputo and Pavlidis, 1991; 1993). As a consequence, the mean direction of the active faults is (E)SE-(W)NW. On land, structures are concentrated in the northern Larissa plain where they form the Tyrnavos Basin-Gonnoi Horst (South Tyrnavos Basin, Tyrnavos, North Tyrnavos Basin and Omolio CSSs) and in southern Thessaly (Pagasitikos Gulf, Vasilika and Domokos CSSs) generating an almost continuous belt from the Pagasitikos Gulf, to the east, to the Karditsa plain, to the west (Caputo, 1995). There is an important differentiation though, between the northern and southern sectors. Indeed, southern Thessaly has been struck by several strong earthquakes during historical as well as instrumental recording period (Papadopoulos, 1992), while in northern Thessaly no strong events have occurred during the last 2-3 centuries, with the only exception of the 1941 Larissa earthquake (Caputo and Helly, 2005a). Nevertheless, geological, paleoseismological, archaeoseismological and morphotectonic investigations clearly document the occurrence of strong linear morphogenic events also in the Tyrnavos Basin (Caputo *et al.*, 1994; 2003; 2004a). Based on this difference a seismic gap in northern Thessaly has been suggested (Caputo, 1995).

Three more CSSs belong to this geodynamic sector, which thus extends eastwards offshore the Thessalian coast (South Cassandra offshore, Mavrovouni offshore and Pelion offshore CSSs). These seismogenic sources are grouped here because of their parallelism with those

onland and especially due to the sharp angular relationship with the CSSs described in the Northern Aegean Sea fault system (see §5.6).

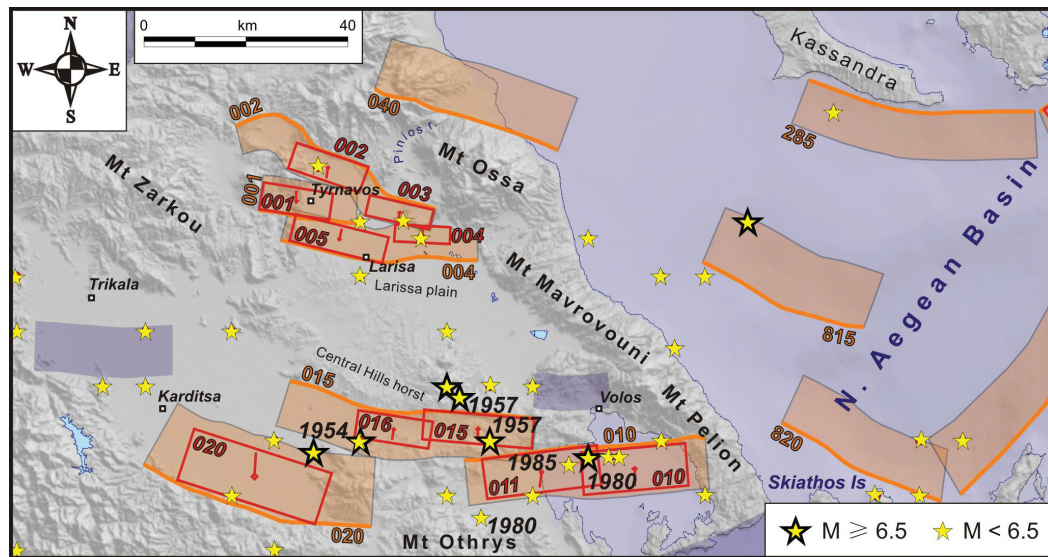


Fig. 5.6: The seismogenic sources of the ‘Thessalian fault system’ (fig. 5.1). Orange sources and numbers: CSSs and their codes, red sources and numbers: ISSs and their numbers, blue sources: DSSs. The epicentres (stars) have been taken from the catalogue of Papazachos *et al.* (2000; 2009; <http://geophysics.geo.auth.gr/ss/>).

Pagasitikos Gulf CSS010 (Volos ISS010 and Nea Anchialos ISS011)

As above mentioned, the southern Thessaly fault belt consists of three major CSSs. The easternmost is the ENE-WSW trending *Pagasitikos Gulf CSS*. It dips southwards, controlling the northern coastline of the homonymous gulf and the margin of the Almyros Basin. Its total length is estimated to be *ca.* 50 km, taking into account that the zone probably extends further to the east, across the southern Pelion peninsula. The morphological expression of the fault zone, its morphotectonic features and the two strongest events of the 1980 Magnesia earthquake sequence, document the existence of two distinct segments, the *Volos* and *Nea Anchialos ISSs*, which form a right-stepping partly overlapping geometry.

The *Volos ISS* is the eastern segment, almost totally lying offshore, controlling the northern coastline of the gulf, whilst morphological indications suggest onshore continuation across the Pelion peninsula. The roughly E-W-trending fault scarp is well-documented on the sea-floor from bathymetric surveys, seismic profiles and Holocene sediment distribution (Perissoratis *et al.*, 1991). The *Volos ISS* is responsible for the first strong shock ($M_w = 6.5$; July 9) of the 1980 seismic sequence. Calculated focal mechanisms of both the 1980 sequence and the April 30, 1985 ($M_s = 5.5$) event (Jackson *et al.*, 1982; Papazachos *et al.*, 1983; Dziewonski *et al.*, 1988; Ekström and England, 1989; Taymaz *et al.*, 1991; Vannucci and Gasperini, 2003; 2004) generally fit the geological observations, showing ENE-WSW-striking planes, shallow-dipping towards SSE with a normal dip-slip motion.

The western segment of the fault zone is the *Nea Anchialos ISS*, which borders the northern margin of Almyros Basin partly controlling the northern coastline of the Pagasitikos Gulf. It is

the causative fault of the second strong earthquake ($M_w = 6.1$) of the 1980 sequence which occurred 24 minutes after the first one, suggesting a triggering phenomenon. The mapped fault trace and co-seismic ruptures (Papazachos *et al.*, 1983; Ambraseys and Jackson, 1990; Caputo, 1996) indicate an ENE-WSW strike and a SSE dip (Papazachos *et al.*, 1983; Caputo and Pavlides, 1991; Mountrakis *et al.*, 1993a; Caputo, 1995; 1996; Galanakis *et al.*, 1998; Zovoili *et al.*, 2004). Microearthquake surveys (Kementzetzidou, 1996; Hatzfeld *et al.*, 1999) delineate a south-dipping fault plane at *ca.* 55° , which is the average of the suggested listric geometry (Papazachos *et al.*, 1983), and a seismogenic layer thickness of *ca.* 12 km. Both meso-structural analyses (Caputo and Pavlides, 1991; 1993; Caputo, 1996) and focal mechanisms (Jackson *et al.*, 1982; Papazachos *et al.*, 1983; Dziewonski *et al.*, 1988; Ekström and England, 1989; Taymaz *et al.*, 1991; Vannucci and Gasperini, 2003; 2004) indicate normal faulting associated with a N-S extension. Based on geomorphic markers, a slip-rate between 1 and 3 mm/a is estimated (Caputo, 1996) and based on historical seismicity, a recurrence interval of 1500 years is suggested (Zovoili *et al.*, 2004).

Vasilika CSS015 (Righeo ISS015 and Dasolofos ISS016)

Northwest of the Pagasitikos CSS (previous CSS) is the *Vasilika CSS* which obliquely crosses the Pliocene-Early Pleistocene Central Hills horst in an E-W to ESE-WNW direction, drawing a slightly curved fault trace (Caputo, 1996). The fault zone disappears under the Quaternary sediments of the Karditsa plain and its westward continuation is uncertain. In the central-eastern sector, two major fault segments have been defined (Caputo, 1995): the *Righeo* and *Dasolofos ISSs*, to the east and west respectively. The two segments have left-stepping partly overlapping geometry and show clear morphotectonic evidences of recent activity by affecting Late Pleistocene deposits (Caputo, 1995; Caputo and Pavlides, 1993). Meso-structural analyses indicate a SSW-dipping setting and a normal dip-slip kinematics compatible with a roughly N-S direction of extension. A microearthquake cluster has been instrumentally recorded within the seismogenic volume (Kementzetzidou, 1996; Hatzfeld *et al.*, 1999), thus documenting a seismogenic depth of at least 13-14 km and 60° - 70° of mean dip.

On March 8, 1957 two strong earthquakes ($M_s = 6.5$ and 6.6 respectively, according to Ambraseys and Jackson, 1990, or $M_w = 6.4$ according to Vannucci and Gasperini, 2003; 2004) occurred near Velestino and which can both be associated with this fault zone (Caputo, 1995). Although the poor seismological recordings and especially the time difference of 7 min between the two shocks hamper a separate reconstruction of the two macroseismic fields, a possible triggering effect could be tentatively suggested. Considering the magnitudes, it is likely that both segments (partly) ruptured. Ground ruptures are reported by local people only along the *Righeo ISS* (Ambraseys and Jackson, 1990).

Domokos CSS020 (Ekkara ISS020)

The westernmost seismogenic structure of the southern Thessaly fault belt is represented by the *Domokos CSS*, which is antithetic (*i.e.* NNE-dipping) with respect to the Pagasitikos and *Vasilika CSSs* (see previous *CSSs*). The fault trace is marked by a curvilinear scarp, varying in strike from E-W to (W)NW-(E)SE, moving westward. This is due to the interaction and linkage of an inherited WNW-ESE trending fault system with a more recent one trending E-W. Based on geological and morphotectonic investigations (Caputo and Pavlides, 1993; Pavlides, 1993),

the total length can be roughly estimated to be 48 km, while meso-structural analyses document dip-slip to oblique-slip motion compatible with a NNE-SSW direction of extension (Caputo, 1995). The central sector of the fault zone (*Ekkara ISS*) was reactivated during the April 30, 1954, Sophades earthquake, producing several km-long ground ruptures (Papastamatiou and Mouyiaris, 1986). The initially assessed surface magnitude was 7.0 (Papastamatiou and Mouyiaris, 1986), but it was likely overestimated ($M_s = 6.7$, Ambraseys and Jackson, 1990; $M_w = 6.6$, Vannucci and Gasperini, 2003; 2004). Recent palaeoseismological investigations clearly document that this structure ruptured in the past and suggest a minimum slip-rate of 0.3-0.5 mm/a and a recurrence interval greater than 3 ka (Palyvos *et al.*, 2010). The focal mechanism proposed by Vannucci and Gasperini (2003; 2004) suggests a WNW-trending NNE-dipping rupture plane, which is slightly different from that proposed by McKenzie (1972).

South Tyrnavos Basin CSS004 (Larissa ISS005 and Asmaki ISS004)

As mentioned before, northern Thessaly is characterized by very low historical and instrumental seismicity, but prominent neotectonic structures that show evidences of recent activity. The geological similarity and the contrasting seismological record suggest the occurrence of a seismic gap in the northern Larissa plain (Caputo, 1995). One of these neotectonic structures is the *South Tyrnavos Basin CSS* bordering to the south the homonymous graben and showing a NNE-dipping setting with a normal dip-slip kinematics (Caputo *et al.*, 1994). Two segments have been recognized: the *Larissa* and *Asmaki ISSs* (to the west and east respectively).

The *Larissa ISS* is associated with a prominent fault scarp separating the Pliocene-Early Pleistocene deposits of the Central Hills in the footwall from the recent alluvial sediments of the Pinios River filling the hanging-wall basin. Based on geological and morphotectonic investigations, as well as geophysical surveys (Caputo and Pavlides, 1993; Caputo *et al.*, 2003), a length of 19 km is suggested with a mean ESE-WNW orientation. The eastern tip corresponds to an angular barrier and a left-stepping underlapping geometry with the nearby structure.

In the eastern sector, morphological evidence is more subtle, probably due to an overall lower slip-rate. However, recent tectonic activity is well documented by the occurrence of few meters-high, but several km-long, E-W trending scarps affecting the Holocene sediments of the Larissa plain (Caputo *et al.*, 1994) and documenting three sub-parallel overlapping sub-emergent fault planes. One of these structures, the *Asmaki ISS*, has been probably ruptured in the March 1, 1941 Larissa earthquake based on the occurrence of co-seismic ground ruptures along one of these morphological alignments (Ambraseys and Jackson, 1990; Caputo, 1995). The focal mechanism indicates a NNE-dipping slightly oblique-slip nodal plane, while the magnitude of this event was $M_w = 6.1$ (Vannucci and Gasperini, 2003; 2004) or $M_e = 6.3$ according to Papazachos and Papazachou (1997; 2003). Although the eastern sector of the South Tyrnavos Basin CSS is longer than the Asmaki Fault, due to the above mentioned slip partitioning the 1941 possibly represents the maximum expected magnitude.

Tyrnavos CSS001 (Tyrnavos ISS001)

The *Tyrnavos CSS* is parallel to and synthetic with the South Tyrnavos Basin CSS (see previous CSS). With the latter structure it forms a largely overlapping right-stepping geometry that trends ESE-WNW with a total length of at least 20 km. The best defined section of the fault

is constrained to a length of 14 km and is conservatively represented by the *Tyrnavos ISS* which forms a prominent scarp affecting the Triassic rocks as well as Pliocene and Late Quaternary sediments (Caputo, 1993a; 1995). A continuous unweathered fresh scarp and 10-15 cm-high free-faces likely document recent co-seismic ruptures (Caputo, 1993a). The displacement of latest Pleistocene-Holocene alluvial deposits along a 8-10 m-high scarp as well as borehole data suggest a long-term slip-rate ranging between 0.1 and 0.4 mm/a (Caputo, 1993b; Caputo *et al.*, 2004a; 2006a). The fault surface has been also detected from geophysical surveys: GPR (Caputo and Helly, 2000), ERTs (Caputo *et al.*, 2003) and HSVR (Oliveto *et al.*, 2004). The results of several palaeoseismological trenches document the occurrence of at least 12-13 events during the last 25-30 ka and a mean recurrence interval of 1.5-2.5 ka (Caputo and Helly, 2007).

North Tyrnavos Basin CSS002 (Rodia ISS002 and Gyrtoni ISS003)

The Tyrnavos Basin is bounded to the north by another major CSS, the *North Tyrnavos Basin*, which is facing the previously described structures as an antithetic one. The fault zone is characterized by an articulated geometry due to the linkage of inherited NW-SE trending segments and newly formed E(SE)-W(NW) trending ones (Caputo, 1993b; Caputo and Helly, 2005b). Geological, structural, morphotectonic and geophysical investigations allowed detailed mapping of the CSS and documentation of its recent activity (Caputo, 1993b; 1995; Caputo and Pavlides, 1993; Caputo *et al.*, 1994; 2003), which is further confirmed by the results of palaeoseismological trenches (Caputo and Helly, 2000; 2005b; Caputo *et al.*, 2004b). Meso-structural analyses indicate a NNE-SSW direction of extension (Caputo, 1993b). Two major fault segments have been recognized (Caputo, 1993b; 1995; Caputo and Pavlides, 1993; Caputo *et al.*, 1994; Goldsworthy and Jackson, 2000): the *Rodia* and *Gyrtoni ISSs*, bearing the best evidence of recent activity.

The *Rodia ISS* separates the Palaeozoic metamorphic rocks of the Pelagonian Zone to the north, from the Pleistocene and Holocene sediments to the south. The latter consist of scree deposits coming from the mountain front interfingering with the alluvial deposits of the Pinios River. Palaeoseismological investigations document a Holocene linear morphogenic earthquake, dated at 2-3 ka BP, that bears a vertical displacement of 25-30 cm and a possible magnitude of 6.4 ± 0.2 (Caputo and Helly, 2005b). With the addition of morphotectonic and stratigraphic data, a slip-rate ranging between 0.1 and 1.0 mm/a has been suggested.

The *Gyrtoni ISS* is parallel to and synthetic with the *Rodia ISS* showing a right-stepping underlapping geometry. Along its 13 km of length, it is mainly marked by a morphological scarp separating Villafranchian lacustrine deposits (footwall) from Holocene alluvial sediments (Caputo *et al.*, 1994). Further evidence of its recent activity derives from high-resolution geophysical investigations (Caputo *et al.*, 2003).

The seismogenic layer thickness of the area is assumed to be 12.5 km by interpolation between the areas of the Aliakmonas and Pagasitikos CSSs. The complex geometry of the CSS suggests scenarios of total rupturing are unlikely.

Omolio CSS040

The *Omolio CSS* is the northernmost active structure of the Thessalian fault system. It separates the Palaeozoic-Mesozoic bedrock from the Holocene alluvial and deltaic deposits of

the Pinios River (eastern sector; Caputo, 1990). Together with the antithetic and diverging North Tyrnavos Basin CSS (see previous CSS) it delimits the Gonnoi Horst, which was strongly uplifted in recent times (Stiros *et al.*, 2004). The CSS is associated with a 38 km-long fault zone showing evidence for recent tectonic activity, such as a major linear escarpment and several suspended wine-glass valleys. On June 9, 2003 a moderate earthquake ($M_w = 5.3$) hit the area, showing a focal mechanism coherent with CSS geometry and kinematics (Pavlidis *et al.*, 2004b). The event was probably associated with this seismogenic volume, but was too deep and small to produce a clear surface expression. On the basis of the CSS dimensions the maximum expected magnitude is 6.5.

South Kassandra offshore CSS285

The *South Kassandra offshore CSS* is located on the western prolongation of the South Chalkidiki offshore CSS (see in the following seismogenic source description). Partially defined by several authors (Brooks and Ferentinos, 1980; Lyb eris, 1984; Papanikolaou *et al.*, 2002; 2006), the fault is characterized by a marked orientation change along strike, from E-W to ESE-WNW, while the motion is likely pure dip-slip normal (Papanikolaou *et al.*, 2002). It is associated with a major submarine escarpment following the coastline of the Kassandra peninsula, while its recent activity is inferred from high-resolution seismic reflection profiles (Papanikolaou *et al.*, 2006), which show a clear downthrown of the southern block and the deformation of the sea-floor sediments.

Mavrovouni offshore CSS815

Located at the western margin of the North Aegean Basin, the *Mavrovouni offshore CSS* shows similar characteristics with the southern, parallel and synthetic Pelion offshore CSS (see next source). Identified as a slightly oblique-slip with a prevailing normal dip-slip component structure (Papanikolaou and Papanikolaou, 2007), this CSS clearly affects the seafloor morphology (Papanikolaou *et al.*, 2002). Seismic reflection profiles carried out across this fault (Papanikolaou *et al.*, 2006), clearly document displacements and deformations of the sea floor sediments. The fault complexity towards the basin does not allow a good constrain of the fault's extension further to the east.

Pelion offshore CSS820

The *Pelion offshore CSS* follows the southwestern border of the NAB, offshore from the Pelion peninsula and north of Skiathos and Skopelos Islands and is represented by a (W)NW-(E)SE trending fault zone. This tectonic structure is *ca.* 36 km-long and NE-dipping as emphasized by a steep morphological submarine slope (Papanikolaou *et al.*, 2002). The location and geometry of the fault zone and its recent activity is also clear in the seismic reflection profiles showing clear displacements and deformations of the sea-bottom sediments (Laigle *et al.*, 2000; Papanikolaou *et al.*, 2006). Based on its orientation, geodynamic setting and sediments downthrow, the motion should be slightly oblique-slip, but with a prevailing normal dip-slip component.

5.6 The North Aegean Sea fault system

A strong limitation in investigating offshore faults is represented by the complete lack of direct observations; in terms of morphotectonic and geological approaches, only detailed bathymetric maps (e.g. Maley and Johnson, 1971; IOC, 1981; Papanikolaou *et al.*, 2002) and seismic reflection investigations (e.g. Brooks and Ferentinos, 1980; Mascle and Martin, 1990; Roussos and Lyssimachou, 1991; Papanikolaou *et al.*, 2006) are available. Accordingly, most of the information concerning offshore faults is provided by seismic data like focal mechanisms and microseismic distribution (e.g. Dziewonski *et al.*, 1983; 1984; Rocca *et al.*, 1985; Kiratzi, 1991; Taymaz *et al.*, 1991).

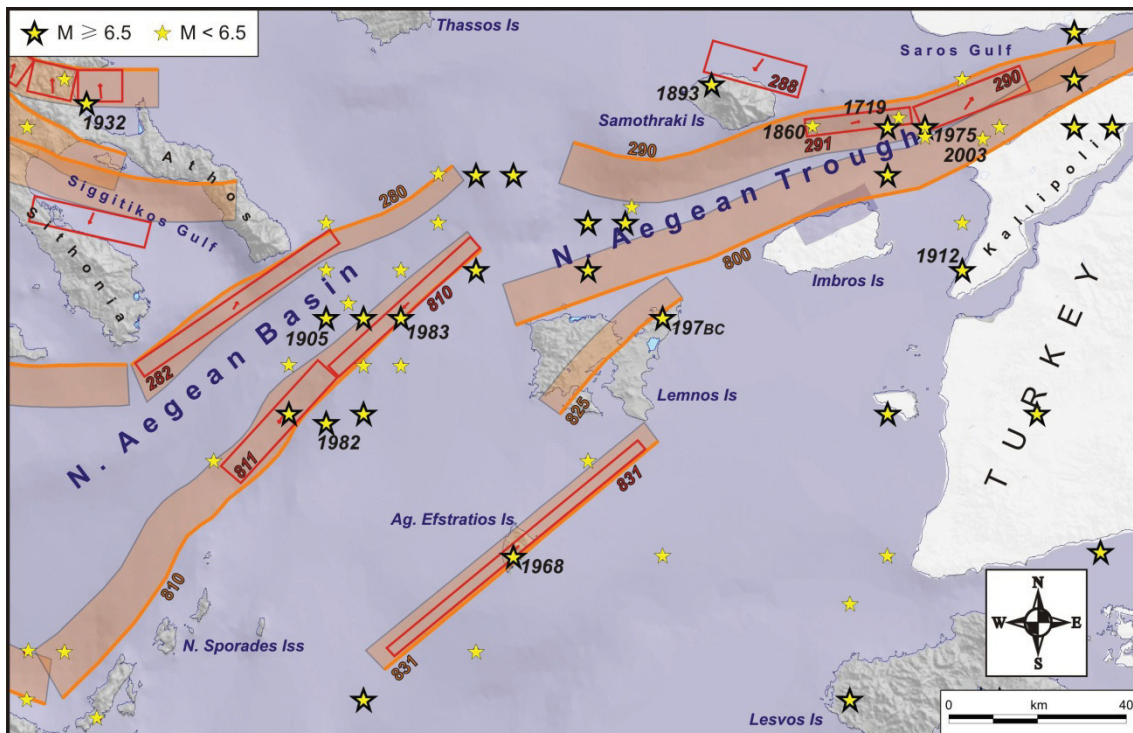


Fig. 5.7: The seismogenic sources of the ‘North Aegean Sea fault system’ (fig. 5.1). Orange sources and numbers: CSSs and their codes, read sources and numbers: ISSs and their numbers, blue sources: DSSs. The epicentres (stars) have been taken from the catalogue of Papazachos *et al.* (2000; 2009; <http://geophysics.geo.auth.gr/ss/>).

The North Aegean Sea is dominated by two regional-scale tectonic structures: the North Aegean Basin (NAB) and the North Aegean Trough (NAT) directly connected and representing the western continuation of the North Anatolian Fault (fig. 5.7). The NAB is situated between the Chalkidiki peninsula, Thessalian coast and Sporades Islands. Along strike, it is bordered by two major fault zones which are mainly characterized by a oblique-slip kinematics: the South Chalkidiki offshore and North Aegean Basin CSSs. Minor structures affect the interposed region, but the lack of sufficient data, their likely reduced dimensions (hence limited maximum expected magnitude) and their location far from the Greek coastlines, make at present their recognition more problematic and precise seismotectonic definition less urgent. For these reasons they have not yet been included in the database.

The other regional-scale tectonic structure, the NAT, is represented by a crustal-scale negative flower structure affecting the sea floor between Kallipoli (Gelibolu) peninsula, Lemnos and Imbros islands to the south, and Samothraki Island to the north. In this transtensional shear zone two CSSs have been recognized (*North NAT* and *South NAT*), marking the mechanical-stress transition between the purely transcurrent tectonic regime of the North Anatolian Fault to the east, and the prevailing extensional regime (NAB) towards the west (Pavlidis *et al.*, 1990; Taymaz *et al.*, 1991; Pavlidis and Caputo, 1994; Papanikolaou *et al.*, 2006). Due to this lateral variation, the NAT basin progressively widens and deepens westwards (Papanikolaou *et al.*, 2002). The description is constrained inside the Greek territory, skipping the part eastern from the Gulf of Saros.

Other active tectonic structures also occur in the North Aegean region, which are synthetic or kinematically associated with those of the NAB and NAT; these are the Aghios Efstratios and Samothraki ISSs and the Lemnos CSS.

South Chalkidiki offshore CSS280 (Athos ISS282)

The *South Chalkidiki offshore CSS* represents the northern boundary of the NAB. Its trace runs immediately south of the Sithonia and Athos peninsulas forming a NE-SW trending steep submarine slope for a total length of *ca.* 90 km as documented by bathymetric surveys (Maley and Johnson, 1971; Papanikolaou *et al.*, 2002) and seismic profiles (Ferentinos *et al.*, 1981; Roussos and Lyssimachou, 1991; Papanikolaou *et al.*, 2006). Based on slight strike variations and especially on the occurrence of a large earthquake likely associated with this fault zone, the *Athos ISS* is distinguished. The event occurred on November 8, 1905 and the macroseismic magnitude was 7.5 (Papazachos and Papazachou, 1997; 2003) or $M_s = 7.3$ (Ambraseys, 2001). This fault segment is *ca.* 54 km-long (Papanikolaou *et al.*, 2006). The maximum expected magnitude for the whole CSS is between 6.9 and possibly 7.2 as worst case scenario.

North Aegean Basin CSS810 (NAB segment A ISS810 and segment B ISS811)

The *North Aegean Basin CSS* is one of the longest structures of the region striking NE-SW and dipping to the NW. It represents the southern boundary of the NAB, running from north of Lemnos to the Sporades Islands. The fault zone is well expressed morphologically, as it has formed a deep and steep NW-dipping slope, clearly imaged in detailed bathymetric maps (Maley and Johnson, 1971; IOC, 1981; Papanikolaou *et al.*, 2002). The cumulative downthrown of the sea-bottom is *ca.* 1300 m. The fault zone is also clearly imaged in the seismic reflection profiles indicating significant cumulative displacements and especially the deformation of the sea-bottom sediments (Brooks and Ferentinos, 1980; Ferentinos *et al.*, 1981; Mascle and Martin, 1990; Roussos and Lyssimachou, 1991; Papanikolaou *et al.*, 2006). Along this zone, two strong earthquakes, likely produced by two adjacent fault segments, are well-documented. Accordingly, two ISSs are distinguished: the *NAB Segments A* and *B* (eastern and central, respectively).

The *NAB Segment A ISS* was responsible for the August 6, 1983 ($M_s = 6.8$ after Kiratzi *et al.*, 1991) earthquake that reactivated the northeastern portion of the NAB CSS. Based on the aftershock spatial distribution (Rocca *et al.*, 1985; Taymaz *et al.*, 1991) and the magnitude of the mainshock, a length of 44 km is inferred. The *NAB Segment B ISS* is associated with the January 18, 1982 ($M_w = 6.6$ after Dziewonski *et al.*, 1983) earthquake. Again, a length of 33 km

is inferred from the aftershock spatial distribution (Taymaz *et al.*, 1991) and the magnitude of the mainshock. There are many other focal mechanisms calculated for both the 1982 and 1983 seismic crises (Dziewonski *et al.*, 1984; Papazachos *et al.*, 1984; Rocca *et al.*, 1985; Ekström *et al.*, 1987; Ekström and England, 1989; Kiratzi *et al.*, 1991; Taymaz *et al.*, 1991; Jackson *et al.*, 1992; Vannucci and Gasperini, 2003; 2004) all suggesting a very steep (NW-dipping) to sub-vertical nodal planes and an almost pure right-lateral strike-slip kinematics. The proposed segmentation is in agreement with the seismogenic source segments proposed by Papanikolaou and Papanikolaou (2007).

The 1982 and 1983 events likely represent the maximum expected magnitudes for the two segments, while in case of a unique rupture event (worst case scenario) the expected magnitude is 7.6 (Papanikolaou and Papanikolaou, 2007). Nevertheless, many older strong events (June 1, 1366; November 12, 1456; 1471; August 12, 1564; April 12, 1572; June 28, 1585; December 5, 1776; February 3, 1779; June 4, 1947) are reported in the vicinity of the *NAB CSS*, especially to the central and northeastern part (Papazachos and Papazachou, 1997; 2003), but they are either ambiguous or loosely located in order to be connected with a specific ISS or CSS. In order to highlight this uncertainty, two examples of historical events are given, one occurred on June 1, 1366 ($M = 6.6$) and the other in 1471 ($M = 7.0$). Both events are absent from Ambraseys's (2009) catalogue, while only the second one is included in the catalogue of Guidoboni and Comastri (2005) as an event that occurred sometime between June 1470 and 1472, in the area north of Lemnos Island. However, a conflict might be also possible regarding the November 8, 1905 Athos earthquake. According to the descriptions though, it is preferred to be assigned to the Athos ISS (see the previous South Chalkidiki offshore CSS).

South NAT CSS800

The *South NAT CSS* is probably the longest active structure in the Aegean Sea. It is oriented ENE-WSW, running north of Lemnos and Imbros Islands, controlling the Saros Gulf and crossing the Kallipoli peninsula (Stanley and Perissoratis, 1977; Lybéris, 1984; Ambraseys and Finkel, 1987; Mercier *et al.*, 1989; Kiratzi, 1991; Tüysüz *et al.*, 1998; Yaltirak *et al.*, 1998; Armijo *et al.*, 1999; Saatçılar *et al.*, 1999; Papadimitriou and Sykes, 2001; Rockwell *et al.*, 2001; Ambraseys, 2002; Koukouvelas and Aydin, 2002; Yaltirak and Alpar, 2002; Altunel *et al.*, 2004; McNeill *et al.*, 2004; Kaya *et al.*, 2004; Janssen *et al.*, 2009; Koral *et al.*, 2009). This structure is hard to be separated from its mechanical continuity, the North Anatolian Fault. The fault segment that ruptured the Kallipoli peninsula (August 9, 1912; $M_w = 7.4$), from the Saros Gulf to the Marmara Sea (Ambraseys and Finkel, 1987; Tüysüz *et al.*, 1998; Yaltirak *et al.*, 1998; Rockwell *et al.*, 2001; Ambraseys, 2002; Yaltirak and Alpar, 2002; Altunel *et al.*, 2004; Kaya *et al.*, 2004; Janssen *et al.*, 2009), its prosecution will not be further discussed as it is getting far from the study area. The fault zone geometry is relatively well constrained based on bathymetric data, seismic reflection profiles, microseismic distributions and focal mechanisms of moderate and strong events (Maley and Johnson, 1971; Mascle and Martin, 1990; Kiratzi *et al.*, 1991; Papazachos *et al.*, 1991; Taymaz *et al.*, 1991; Çagatay *et al.*, 1998; Saatçılar *et al.*, 1999; Coskun, 2000; Kurt *et al.*, 2000; McNeill *et al.*, 2004; Karabulut *et al.*, 2006; Ustaömer *et al.*, 2008). Focal mechanisms document a prevailing strike-slip motion with some dip-slip component, while the distribution of microseismicity suggests a steep (to sub-vertical) fault plane. The total length of the fault zone probably exceeds 200 km. Based on the overall geometry, several segments certainly occur but the lack of specific data does not allow to

determine segment boundaries and especially their nature. Accordingly, the maximum expected magnitude could range between 6.5 and probably more than 7.5.

North NAT CSS290 (Saros Gulf ISS290 and Samothraki SE ISS291)

Mechanically associated with the South NAT CSS (see previous CSS) is the *North NAT CSS*, which runs sub-parallel and antithetic (SSE-dipping) to the former. The two fault zones progressively converge eastwards probably merging into a unique crustal-scale flower structure at the entrance in the Saros Gulf (Çagatay *et al.*, 1998; Yaltirak *et al.*, 1998; Coskun, 2000; Kurt *et al.*, 2000; Yaltirak and Alpar, 2002). The total length is probably more than 120 km demonstrating oblique-slip (to strike-slip) kinematics, according to available focal mechanisms of moderate to large earthquakes. Based on the slightly articulated geometry, at least two segments have been recognized and included in GreDaSS: the 26 km-long *Saros Gulf ISS* and the 24 km-long *Samothraki SE ISS*. These faults ruptured in $M_w = 6.6$ and $M_w = 5.7$ earthquakes, which occurred on March 27 1975 and July 6 2003 respectively, north of the Kallipoli peninsula and east of Samothraki Island (Kiratzi *et al.*, 1985; Taymaz *et al.*, 1991; Papazachos *et al.*, 1991; Jackson *et al.*, 1992; Papazachos and Papazachou, 1997; 2003; Vannucci and Gasperini, 2003; 2004; Karabulut *et al.*, 2006). Focal mechanisms suggest an oblique-slip motion (normal and dextral components) on a moderate SE-dipping fault plane for the *Saros Gulf ISS* (Kiratzi *et al.*, 1985; Taymaz *et al.*, 1991; Papazachos *et al.*, 1991; Jackson *et al.*, 1992) and an almost pure dextral strike-slip motion on a steeply SE-dipping fault plane for the *Samothraki SE ISS* (Karabulut *et al.*, 2006). The investigation of the 2003 sequence (Karabulut *et al.*, 2006) indicates a thick seismogenic layer of *ca.* 19 km and a structure of more than 20 km-long. However, according to the dimensions, the potential magnitude of the *Samothraki SE ISS* should be approximately 6.6, although the greatest shock of the 2003 sequence was only $M_w = 5.7$. Two historical large events are also reported in this area (Papazachos and Papazachou, 1997; 2003): the first on July 23, 1719 ($M_e = 6.7$) and the second on August 6, 1860 ($M_e = 6.2$). Although both events cannot be accurately located, at least one (1719) could be related with the Samothraki SE fault segment. A total reactivation of the *North NAT CSS* seems impossible. Nevertheless, based on the fault zone's geometry and the empirical relationships of Wells and Coppersmith (1994), a maximum magnitude of 7.1 could be the result of the worst case scenario.

North Samothraki ISS288

The fault crosses the northern coast of the Samothraki Island and continues on both sides offshore. From a mechanical point of view, this fault can be interpreted as a normal dip-slip secondary structure of the NAT. According to morphotectonic investigations (Pavlidis *et al.*, 2005), the fault is characterized by discrete scarps most of them aligned in an ESE-WNW direction and dipping northwards. The scarps form a steep morphology that controls the drainage pattern and cause deposition of massive colluvial and alluvial deposits. The *North Samothraki ISS* is probably the causative structure for the homonymous earthquake occurred on February 9, 1893 (Papazachos and Papazachos, 1997; 2003; Ambraseys, 2009). Based on the macroseismic magnitude of 6.8 (Papazachos and Papazachos, 1997; 2003), a conservative length of at least 22 km can be estimated.

Lemnos CSS825

Lemnos CSS is a NE-SW-striking, sub-vertical strike-slip right-lateral structure running across the homonymous island (Koukouvelas and Aydin, 2002; Pavlides *et al.*, 2009). It consists of several smaller segments, some of them controlling the coastline of the northeastern part of the island. The location, geometry and kinematics of this structure imply a possible connection with the South NAT CSS to the north. Even though regional instrumental seismicity is rather low, a strong ($M_e = 7.0$) historical (197 BC) earthquake is reported in the catalogue of Papazachos and Papazachou (1997; 2003) based on scripts of Pausanias, who refers to the sinking of Chrysi Island northeast from Lemnos. According to the empirical relationships (Wells and Coppersmith, 1994) the maximum expected magnitude of a total rupture of the fault zone is estimated to be M_w 6.8.

Aghios Efstratios CSS/ISS831

The *Aghios Efstratios ISS* is a NE-SW-striking, strike-slip tectonic structure, running south of the Lemnos Island and crossing the small Aghios Efstratios Island (Pavlides *et al.*, 1990; Pavlides and Tranos, 1991). Although it is parallel to the North Aegean Basin CSS (see previous CSSs of §5.6) its motion is mainly transcurrent based on the available focal mechanism of the 1968 event which ruptured most of the structure (McKenzie, 1972; Kiratzi *et al.*, 1991; Taymaz *et al.*, 1991; Vannucci and Gasperini, 2003; 2004). The field mapping indicates a NW-dipping steep to sub-vertical fault with significant right-lateral motion (Pavlides *et al.*, 1990; Pavlides and Tranos, 1991). Fault length is based on the aftershock distribution (Drakopoulos and Economides, 1972; North, 1977), while width and average displacement are based on North's (1977) estimations over the aftershock distribution and the $M_s = 7.1$ magnitude of the 1968 earthquake, respectively. However, more recent studies (Nalbant *et al.*, 1998; Papadimitriou and Sykes, 2001) suggest different dimensions and displacements (see discussion in Pavlides *et al.*, 2009). This uncertainty is represented by the homonymous CSS.

6.1 General remarks

At present, GreDaSS counts *ca.* 90 ISSs, 180 CSSs and 10 DSSs for the Aegean Region ([fig. 6.1](#)). These sources do not have the same level of analysis and hence, confidence. In the meantime, all sources contain a minimum level of information; that is the principal geometric

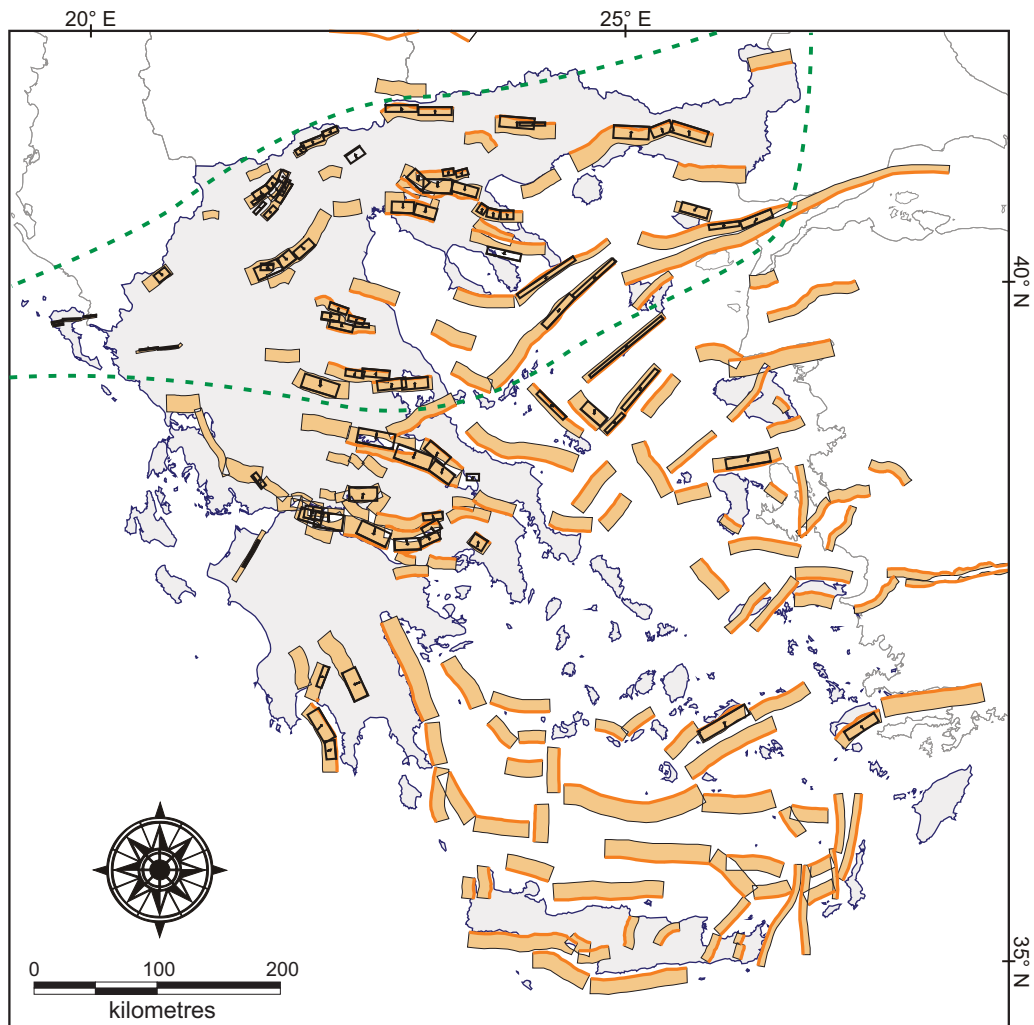


Fig. 6.1: The seismogenic sources (CSSs in orange and ISSs in black colour) of the broader Aegean Region as they have been developed (until today) for both GreDaSS and SHARE projects. The dashed line separates the thesis study area (northern Greece) and the area in which sources are still in progress (southern Greece).

and kinematic parameters which have been obtained after a preliminary, but thorough, revision of most available literature. These sources have been also included in the SHARE project (see *Preface* for more details). However, the sources discussed in the present thesis, limited to the northern part of Greece ([fig. 6.1](#)), have been revised thoroughly and have a high informational level in contrast with the other ones.

The homogenization of the seismogenic sources in North Greece provides a more comprehensive view of its geodynamic setting. Accordingly, sources can be grouped following common characteristics and similar seismotectonic behaviour as shown, for example, in [chapter 5 \(fig. 5.1\)](#).

In particular, the area of *Thrace* and *eastern Macedonia* shows normal faulting with a rough E-W trend, sparse seismicity and low slip rates ([fig. 4.6](#)). The northern part of *Central Macedonia* also shows a similar pattern. However, by moving southwards to the *Chalkidiki peninsula*, the density of both seismic occurrences and number of sources increase, with the latter showing locally higher slip rates. In *West Macedonia*, the orientation of the faults changes from E-W to NE-SW, partly following the change of the regional stress field. Kinematics maintains its character (dip-slip normal faulting), but slip rate is rather low with an increasing tendency towards the south. Besides the 1995 Kozani earthquake, strong instrumental events are lacking. In *Epirus*, seismogenic sources are quite sparse. Infrequent seismicity and local lithology are the main reasons that possible faults might not have been well recognized until now. Moreover, sparse population in mountainous areas might be an additional reason for the lack of historical reports. On the other hand, the erodibility of flysch is relatively high which means that this lithology does not preserve seismogenetic geomorphic features. Moving westwards and closer to the subduction zone out from the *Ionian coast*, the tectonic regime becomes more complex. The regional stress field changes gradually as we move away from a purely extensional (east) towards a compressional (west) regime. Although the prevailing E-W-striking faults (*e.g.* Petoussi and Kerkyra CSSs) show that they have been reactivated as strike-slip faults, superimposed striations document recent normal dip-slip motions. Slip rates locally show high values, which can be interpreted as the effect of the nearby subduction zone. The interference of the evaporitic layer in the area is not clear yet. *Thessaly*, on the other hand, more or less follows similar characteristics to the area of Central Macedonia. Faults appear in clusters with one located in the northern part and a second one located in the southern part. The northern fault system consists of subparallel CSSs that lie along a roughly N-S axis. The southern fault system lies along a major E-W trending zone. Seismicity appears to be different within the two sectors. In contrast with Southern Thessaly, the lack of significant historically and instrumentally recorded earthquakes in the northern part suggests the existence of a seismic gap (Caputo, 1995). Two offshore sources (Mesovouni and Pelion offshore CSSs) bordering the NAB to the west, likely belong to the same Thessalian fault system. In the *North Aegean Sea* the geodynamic setting changes significantly, a difference that is also reflected by the existence of large dominating tectonic structures, the NAB and the NAT. These structures belong to a transtensional regime (Pavlidis and Caputo, 1994) that is evidenced by the gradual changing of the kinematics from oblique (normal dip-slip and right-lateral components) to the west to almost pure dextral kinematics to the east.

Another observation that comes out from [fig. 5.1](#) is that many seismogenic sources are grouped in clusters (*e.g.* in Mygdonia Basin, East Chalkidiki, Ptolemaida Basin, North and

South Thessaly, NAB). What are the reasons for this phenomenon? A possible explanation could be that seismogenic sources in these regions affect areas that are characterised either by large tectonic basins. These areas have been recently shaped by extensional crustal activity, with the oldest one taking place since late Oligocene-Miocene (*e.g.* Psilovikos, 1984; Pavlides and Kiliias, 1987; Pavlides and Mountrakis, 1987; Pavlides *et al.*, 1990; Caputo and Pavlides, 1993; Papanikolaou *et al.*, 2002). During all this time, tectonic activity never ceased, although few changes have occurred as far as the extensional direction of the field concerns (*e.g.* Mercier *et al.*, 1979; 1989; Pavlides and Kiliias, 1987; Pavlides *et al.*, 1990; Caputo and Pavlides, 1993). Therefore, tectonic processes have mechanically weakened and thinned the upper crust providing a convenient place for regional deformation to concentrate. Interactions between seismogenic sources within the same crustal volume are quite possible. In this case, these sources can define a volume in which fault activity migrates from source to source. How interactions take place in these *seismogenic volumes*, for example if faults are randomly reactivated or not, is not clear and certainly needs further investigation. Moreover, the earthquake records are far too short, regarding the time span, in order to study successive reactivations. However, a preliminary study of few cases (Sboras and Caputo, 2010) implies the possible occurrence of low-angle normal faults at the base of these seismogenic volumes branching upwards into several steep fault planes. This structural model has some major consequences in terms of seismic hazard, because if the nucleation point is located on the low-angle segment, then the rupture, during the upwards propagation, could propagate along any of the steep faults that depart from the detachment fault. Therefore, the maximum expected magnitude could be greater compared to a distinct single fault plane crossing the seismogenic layer thickness with an approximately constant (steep) dip-angle. This is due to the fact that the rupture area is larger since it includes both the steep segment and part of the low-angle plane. Furthermore, it is not easily predictable which segment will be the next to rupture during a future seismic event. Accordingly, it could be not straightforward performing a probabilistic fault displacement hazard analysis (PFDHA). In terms of earthquake geology, the occurrence of such complex extensional fault systems could have strong implications because subsequent seismic reactivations could rupture different branches towards the surface. Accordingly, when performing palaeoseismological and morphotectonic investigations, researchers should clearly bear in mind the possibility of slip partitioning characterising such *seismogenic volumes*. For example, any estimation of the regional stretching and geological strain rate and especially of the earthquake recurrence interval should take into account the contribution provided by all the fault branches potentially connected with the low-angle fault plane at depth.

A final comment on the map of [fig. 5.1](#) concerns the completeness of the database. Indeed, *cumulative effects*-based investigations (see §1.5 and §6.2) are less applied offshore, whereas *single-event effects*-based investigations are not useful unless an earthquake occurs ('typical' examples are the 1995 Kozani and 1999 Athens earthquakes). At this regards, a major problem is that the offshore seismogenic sources are hard to be explored. Moreover, all types of investigations have been advanced quite recently giving insufficient time for extended surveys. This means that there are still unexplored regions, like it was for the Kozani (1995) and Athens (1999) earthquakes.

6.2 Reliability of *single-event effects*-based and *cumulative effects*-based investigation methods

In §1.5 two types of *sources of information* were defined according to the investigation methods from which data and information are acquired. It is time now to check the reliability of *single-event effects*-based and the *cumulative effects*-based investigating methods. For this purpose, four case studies are selected, all involving well expressed faults which have been recently reactivated by earthquakes, but in different epochs. In this way, the variable quality and degree of uncertainty may also be investigated regarding the seismotectonic information that can be obtained from the analysis of single-event effects caused by historical events or fully instrumental ones. Although the first case study (East Heliki Fault and the 1861 event) does not belong to the study area, it is the best example of early systematic field investigations in Greece and becomes a reference point for the further evolution of such kind of investigations. The other three cases, although they are described in the 5th chapter, information in this discussion is analyzed in a different way, in order to compare the two investigation methods. In [table 6.1](#) at the end of this session, the seismotectonic parameters for the considered case studies are listed allowing a concise view and brief analysis of the differences and similarities between the results obtained by applying the two methodological approaches. According to the reliability and accuracy of the results, a summarizing quality factor is also attributed. The quality scale varies from A, indicating fully reliable and accurate results, to E, representing poorly documented values generally tentatively inferred from empirical relationships and with large uncertainty.

East Heliki Fault (South Corinth Gulf Fault System)

The Gulf of Corinth is one of the most tectonically active regions worldwide, showing an intense seismicity both in terms of magnitude and frequency. The gulf is an asymmetric graben which is likely characterized underneath by a low-angle N-dipping master fault (detachment fault; Rigo *et al.*, 1996; Bernard *et al.*, 1997; Exadaktylos *et al.*, 2003; Sachpazi *et al.*, 2003; Flotté *et al.*, 2005; Gautier *et al.*, 2006; Skourtsos and Kranis, 2009). The southern side of the gulf near to the northern coast of Peloponnesus is affected by an important composite seismogenic source: the South Corinth Gulf Fault System. One of the major individual active structures of this complex shear zone is the East Heliki Fault (Rigo *et al.*, 1996; Le Meur *et al.*, 1997; Sorel, 2000; Chéry, 2001; Flotté and Sorel, 2001; Cianetti *et al.*, 2008), which was reactivated during the December 26, 1861 Valimitika earthquake ([fig. 6.2](#)). This case study has been selected because it represents the first example for Greece of penecontemporaneous systematic field investigations complete of a detailed ground ruptures map and scientific report of many seismically induced effects (Schmidt, 1867; 1879).

Single-event effects: The 1861 earthquake had a maximum intensity X (MCS) and a macroseismic field suggesting an E(SE)-W(NW) trending fault. The estimated M_c is 6.6 (Ambraseys and Jackson, 1997; Papadopoulos, 2000) or 6.7 according to Papazachos and Papazachou (1997; 2003). This magnitude could be considered the maximum expected event for this seismogenic source, given that it also matches the maximum recorded magnitudes from the broader Corinth Gulf (Papadopoulos, 2000). It should be noted, however, that on the basis of the inferred seismotectonic parameters (see [table 6.1](#)) the moment magnitude calculated via seismic moment would be smaller (~6.4).

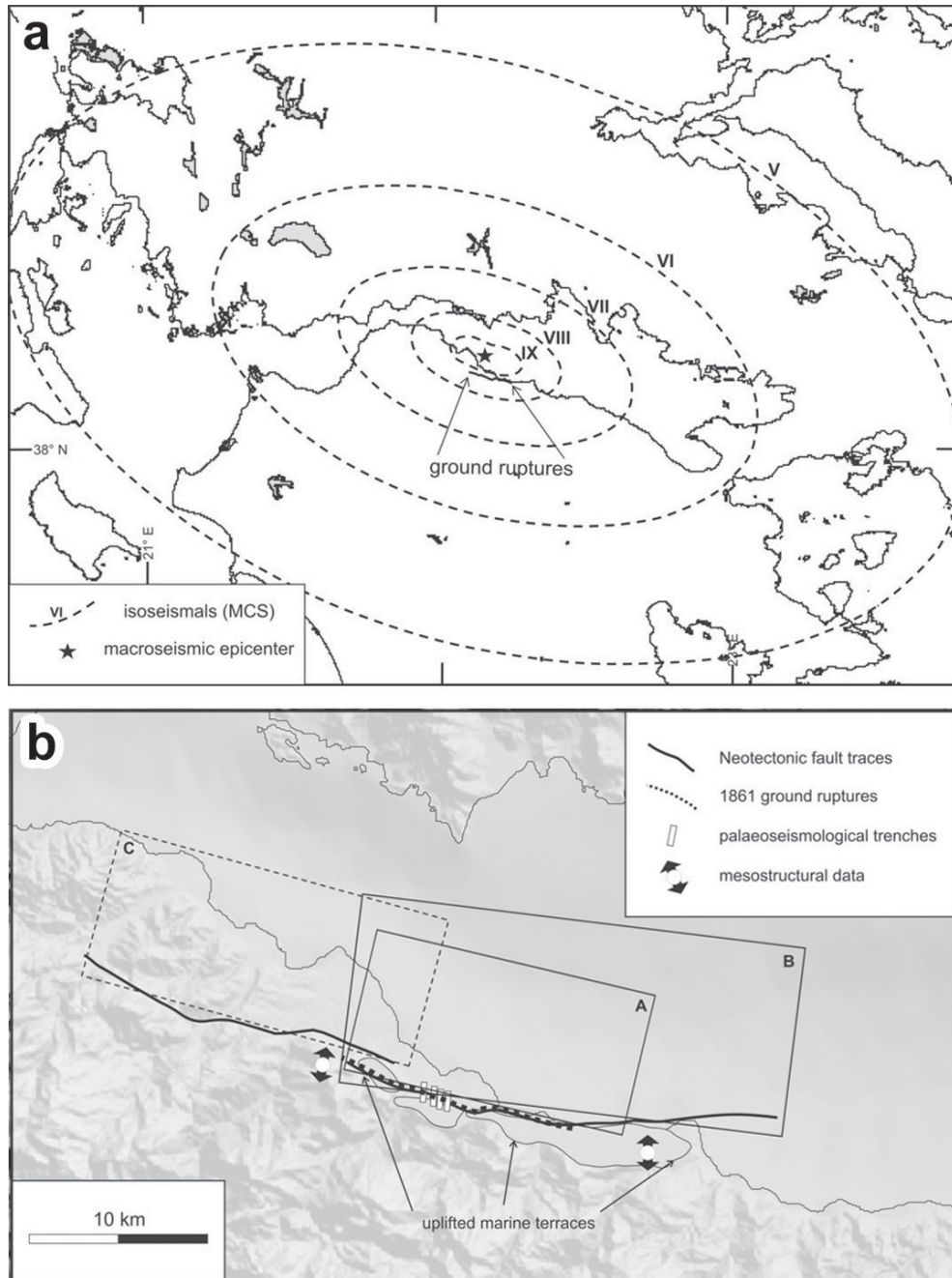


Fig. 6.2: a) Isoseismals and macroseismic epicentre of the 1861 Valimitika earthquake. b) Map of the South Corinth Gulf Fault System showing the East Heliki seismogenic source obtained from the analysis of *single-event effects* (box A) and *cumulative effects* (box B). The Neotectonic fault traces, the 1861 ground ruptures, the location of the palaeoseismological trenches, the results of meso-structural analyses and the area characterized by uplifted marine terraces and notches are also represented as well as the West Heliki Fault (box C) separated by an overstepping geometry, likely representing a 'strong' barrier. See text for discussion and full reference list. See [table 6.1](#) for the seismotectonic parameters.

As above mentioned, the 1861 earthquake represents the first case in Greece of systematic field investigations carried out within the epicentral area soon after the event thus providing many descriptions and observations about the co-seismic effects, like liquefaction, ground

ruptures and damages to buildings (Schmidt, 1867; 1879). The ground ruptures are aligned in an (E)SE-(W)NW direction being in agreement with the macroseismically inferred fault strike. The surface rupture length was 13-15 km. However, based on magnitude and empirical relationships, this value is certainly underestimated. Accordingly, the fault rupture likely continued offshore some more kilometres, but no specific information is available for this epoch. The surface displacement was normal (south up, north down) and the maximum observed value was about 1 m. No direct information is available for the maximum depth, dip-angle and hence width. The latter could be also tentatively inferred from empirical relationships ([table 6.1](#)).

The 1861 earthquake obviously represents the last event on the East Heliki Fault and therefore the elapsed time is 50 years. Box A in [fig. 6.2b](#) represents the seismogenic source as obtained from the above values.

Cumulative effects: The trace of the East Heliki Fault has been mapped in detail by several authors (Poulimenos and Doutsos, 1996; Roberts and Koukouvelas, 1996; Kokkalas and Koukouvelas, 2005; Koukouvelas *et al.*, 2001; 2005). Morphometric analyses document the recent activity of the fault (Koukouvelas *et al.*, 2001; Verrios *et al.*, 2004) which has also deflected the flow path of the Kerynitis, Vouraikos and Selinous rivers (Pavlidis *et al.*, 2004c; McNeill *et al.*, 2005).

The South Corinth Gulf Fault System consists of several segments, among which is the East Heliki Fault (box B in [fig. 6.2b](#)). This structure shows a right-stepping partially overlapping geometry with the West Heliki Fault (box C in [fig. 6.2b](#)). The stepping distance is about 3 km and, though this issue is debated, it could represent a stable segment boundary definitely halting the co-seismic rupture started from one segment. Considering only the East Heliki Fault, the geologically and morphotectonically mapped trace showing evidences of recent activity is at least 20 km (Roberts and Koukouvelas, 1996; Stewart, 1996b; Koukouvelas *et al.*, 2001; Micarelli *et al.*, 2003; Verrios *et al.*, 2004). However, the uplifted coast to the east documents the offshore continuation of the fault ([fig. 6.2b](#); Stewart, 1996b; Stewart and Vita-Finzi, 1996), which is further confirmed by seismic profiles (Bell *et al.*, 2008). Accordingly, the total length of the East Heliki Fault is estimated to *ca.* 25 km.

Structural analyses on fresh slickensides show clearly an almost pure dip-slip normal kinematics associated with a N-S-trending tensile stress field (Doutsos and Poulimenos, 1992; Stewart, 1996b; Cowie and Roberts, 2001; Micarelli *et al.*, 2003).

Microearthquake investigations in the broader area (Rietbrock *et al.*, 1996; Rigo *et al.*, 1996; Gautier *et al.*, 2006; Bourouis and Cornet, 2009), help constraining the seismogenic layer thickness (*ca.* 10 km), the geometry at depth and the possible interaction with the normal detachment underlying the Corinth Gulf. The merging between the steep East Heliki Fault and the low-angle fault plane occurs at 7-10 km-depth. Taking into account the overall geometry and assuming a joint rupture process with the detachment, a minimum width of 18 km and a mean dip-angle of 40° can be inferred (assuming a flat fault plane as required for GreDaSS).

Slip-per-event has been obtained from several palaeoseismological trenches (Koukouvelas *et al.*, 2001; Pavlidis *et al.*, 2001b; 2004c; Chatzipetros *et al.*, 2005a) and ranges from 0.5 to *ca.* 2.0 m.

The determination of the slip rate is based on different investigation methods that provide data for both short- and long-term values. Direct measurements, like palaeoseismological trenches or seismic reflection profiles (Koukouvelas *et al.*, 2005; Chatzipetros *et al.*, 2005a; McNeill *et al.*, 2005; Bell *et al.*, 2009) suggest values varying between 0.3 and *ca.* 5 mm/a. Indirect inferences, like using the coastal uplift or GPS extension rates (Pirazzoli *et al.*, 2004; McNeill and Collier, 2004; De Martini *et al.*, 2004) generally provide higher values (3-11 mm/a) that are commonly explained due to aseismic 'creep' and displacements on multiple subparallel faults. Palaeoseismological investigations suggest that during the Holocene, seismic reactivations were clustered in short time periods of higher slip-rate separated by long time periods of quiescence. Moreover, both trenches and raised marine notches document higher values during the Holocene with respect to the Late Quaternary, confirming a variable seismotectonic behaviour and a recently increased long-term slip rate (*e.g.* Stewart, 1996b; Koukouvelas *et al.*, 2005).

Hypothetically assuming to ignore the date of the 1861 event, palaeoseismological investigations could also contribute to constrain the timing of the last event (< 700 year BP) and therefore the elapsed time. A recurrence interval ranging between 200 and 1600 years can be inferred from geomorphological (Mouyiaris *et al.*, 1992; Stewart, 1996) and palaeoseismological analyses (Chatzipetros *et al.*, 2005a; McNeill *et al.*, 2005).

A maximum expected magnitude of 6.7 (M_w) can be estimated via seismic moment using the above values.

Domokos Fault System

The second case study is represented by a major fault zone, referred to in the literature as Domokos Fault System, which affects southwest Thessaly (Caputo, 1995). This structure runs along the boundary between the Karditsa plain, to the NE, and the Pindos mountain range, to the SW. The geological and tectonic complexity of the structure is certainly due to its poly-phased evolution and the present-day seismogenic source likely developed by exploiting several inherited sliding surfaces represented by NW-SE trending Oligocene-Miocene thrust planes, mainly inverted during the Pliocene (-Early Pleistocene) NE-SW extensional post-collisional collapse, which recently (Middle-Late Quaternary) started branching and linking with E-W trending, newly generated, fault segments. The Domokos Fault System was reactivated during the April 30, 1954 Sophades earthquake ([fig. 6.3](#)).

Single-event effects: Although the Sophades event occurred during the instrumental period, at that time the Greek and European seismographic network was not much developed and hence the available seismological information is relatively poor. According to the recordings of the National Observatory of Athens (after Papastamatiou and Mouyiaris, 1986), the originally proposed magnitude was $M_s = 7.0$, while a revised surface waves magnitude of 6.7 has been obtained by Ambraseys and Jackson (1990) and it is considered here as the maximum expected magnitude. Different epicentres have been proposed, all located north from the geological fault trace in the middle of the Karditsa plain ([fig. 6.3b](#)).

The focal mechanism of the main shock was proposed by McKenzie (1972), however based on first motion polarities from short period seismic recordings. It describes a N(W)-S(SE)-

trending nodal plane (box A in [fig. 6.3b](#)), in apparent agreement with the post-seismic field observations, with an oblique-slip kinematics (rake 300°).

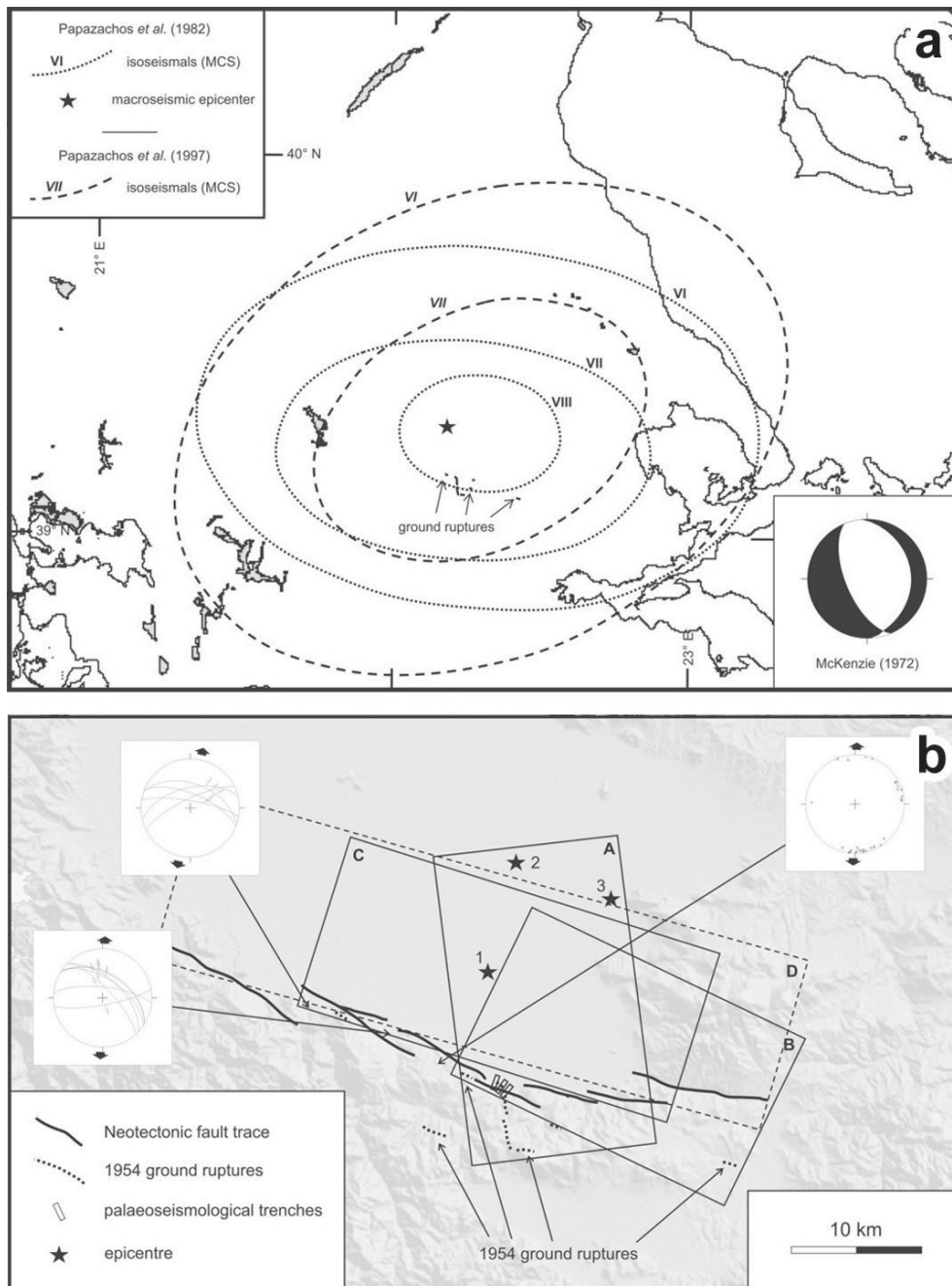


Fig. 6.3: **a)** Isoseismals and macroseismic epicentre of the 1954 Sophades earthquake. **b)** Map of the Domokos Fault System, Southern Thessaly, showing the seismicogenic sources obtained from the analysis of *single-event effects* (two alternative solutions: boxes A and B) and *cumulative effects* (box C). The Neotectonic fault traces, the 1954 ground ruptures, the location of the palaeoseismological trenches, the results of meso-structural analyses and the proposed epicentres (1: McKenzie, 1972); 2: National Observatory of Athens; 3: Papazachos *et al.*, 1982) are also represented together with a hypothetical, but discarded, alternative 'geological' solution (box D). See text for discussion and full reference list. See [table 6.1](#) for the seismotectonic parameters.

The macroseismic field has been investigated by Papazachos *et al.* (1982; 1997), which documented a maximum epicentral intensity MCS = IX-X and reconstructed the isoseismals of the event. Notwithstanding the large number of intensity points (152), in the two versions of the catalogue proposed by the authors (1982 and 1997), the intensity isolines are quite different both in orientation and shape (fig. 6.3a), possibly suggesting the large uncertainty intrinsic in the proposed maps and hence in the inferred fault strike.

Indeed, the first field observations of the co-seismic ground ruptures took place five days after the main shock (Papastamatiou and Mouyiaris, 1986), describing a major NNW-SSE-trending fracture only few kilometres-long (7-8 km; fig. 6.3b). This length is certainly not appropriate for an upper-crust normal fault strong event that should be associated with an emergent plane (*i.e.* linear morphogenic earthquake) more than 20 km-long (Pavlidis and Caputo, 2004). Speculating on some small ground fractures observed more than 10 km ESE, near the Domokos village (fig. 6.3b), and tentatively assuming the partly blind continuity of the co-seismic rupture, the total surface length would be *ca.* 23 km, but in a direction not consistent with the proposed focal mechanisms and the macroseismic field (box B in fig. 6.3b).

Maximum observed dislocation was 90 cm, characterized by a large heave and a left-lateral strike-slip component of relative motion, causing the subsidence of the eastern block. The authors hesitantly associate these surface fractures with the seismogenic fault (*i.e.* minimum depth >0 km).

In conclusion, information provided by *single-event effects* are somehow contradicting because the focal mechanism and some field observations suggest a NNW-SSE-trending almost blind oblique-slip (normal and left-lateral) fault, while the macroseismic field an E-W or even NE-SW trending plane. Geometric parameters, like width and maximum depth (see table 6.1) can be only tentatively inferred based on the dip-angle of the preferred nodal plane and using empirical relationships (Wells and Coppersmith, 1994; Pavlidis and Caputo, 2004). The reported magnitude, $M_s = 7.0$ (equivalent to $M_w = 7.0$) would be considered the maximum expected magnitude of this seismogenic source and the Sophades earthquake the last occurred event. By default, *single-event effects* do not provide information regarding the recurrence interval and the slip-rate.

Cumulative effects: Based on detailed geological and morphotectonic mapping (Caputo, 1990; 1995; Caputo and Pavlidis, 1993; Valkaniotis, 2005), a geometrically complex fault zone, certainly active during Quaternary, has been clearly documented. The structure is mechanically composite, probably still evolving and characterized by several minor segments interconnected due to the coalescence and reactivation of inherited sliding planes. The different segment boundaries are either angular or overstepping (fig. 6.3b). The fault strike is almost E-W, in the eastern sector, and NW-SE, in the western sector, therefore suggesting an overall mean WNW-ESE trend. The cumulative length of the fault zone bearing clear evidence of neotectonic activity (Caputo *et al.*, 2008) is *ca.* 50 km. However, considering only the segments showing a large overlapping geometry and distances of less than 1 km, therefore with 'soft' boundaries potentially not sufficient for arresting a co-seismic rupture, the total length of a potential seismogenic structure is *ca.* 30 km (box C in fig. 6.3b).

Maximum depth (~15 km) is constrained according to microseismicity distribution from nearby areas (Kementzetzidou, 1996; Hatzfeld *et al.*, 1999) and geological-geophysical considerations on the local crustal thickness. Assuming typical dip-angle for normal faults (*i.e.* 40°-60°), fault width parameters can be also estimated (*ca.* 19 km). The suggested value is in agreement with empirical relationships between geometric parameters.

Palaeoseismological investigations recently carried out by Palyvos *et al.* (2010) provide evidence that part of the ground ruptures observed after the 1954 Sophades earthquake near Ekkara village were likely connected with the seismogenic surface ([fig. 6.3b](#)). They also clearly document the occurrence of at least three linear morphogenic events, and possibly four, during the last 17-20 ka. The measured slip per event ranges between 1 and 2 m, but considering their hypothesis of additional events, the preferred value is about 1 m. The calculated slip-rate is 0.3-1.0 mm/a, while the suggested recurrence interval is >3.2 ka (Palyvos *et al.*, 2010).

Supposing to ignore the date of the last event (*e.g.* 1954), the same palaeoseismological investigations would have provided at least some chronological constraints for the elapsed time (< 1.5 ka BP), within the uncertainties of the applied archaeological dating technique.

Systematic meso-structural analyses (Caputo, 1990; Caputo and Pavlides, 1993) document a prevailing dip-slip kinematics with a slight left-lateral component associated with a N(NE)-S(SW) direction of extension ([fig. 6.3b](#)). This is also confirmed by observations within the palaeoseismological trenches.

Finally, the above parameters as obtained from the analysis of *cumulative effects* allow to estimate the maximum expected magnitude ($M_w = 6.8$), as a worst-case scenario assuming that several segments of the Domokos Fault, for a total length of 30 km, are reactivated (box C in [fig. 6.3b](#)).

Mygdonia Fault System

The southern border of the broad Mygdonia Basin is characterized by a large fault zone. This tectonic structure mainly strikes in an E-W direction, crossing obliquely the Alpide system and locally following NW-SE-trending inherited structures. A major segment of the fault system, the Gerakarou Fault, has been re-activated by the June 20, 1978 Stivos earthquake, which affected the city of Thessaloniki, the second largest metropolitan urban area of Greece.

Single-event effects: The epicentral area of the Stivos earthquake is located in the centre of the Mygdonia Basin, between the Lakes of Koronia and Volvi, about 35 km ENE of Thessaloniki ([fig. 6.4a](#)). The estimated seismic moment (M_0) ranges between $2.7 \cdot 10^{18}$ and $8.7 \cdot 10^{18}$ (corresponding to $M_w = 6.2-6.6$) and differences generally depend on the applied method, like *P*-wave spectrum analysis, trial-and-error waveform modelling, generalized inversion of teleseismic P and Sh waves or CMT (Kulhánek and Meyer, 1979; Soufleris and Stewart, 1981; Barker and Langston, 1981). A mean value of 6.5 could be considered the maximum expected magnitude ([table 6.1](#)).

Several focal mechanisms of the main shock have been proposed by different authors ([fig. 6.4a](#); Barker and Langston, 1981; Soufleris and Stewart, 1981; Dziewonski *et al.*, 1987; Vannucci and Gasperini; 2003; 2004). They substantially agree showing roughly E(SE)-

W(WN)-striking nodal planes (273° - 289°), dipping between 43° and 55° , with a prevailing dip-slip kinematics and some left-lateral component (rake 272° - 300°). The preferred plane is always the N-dipping one.

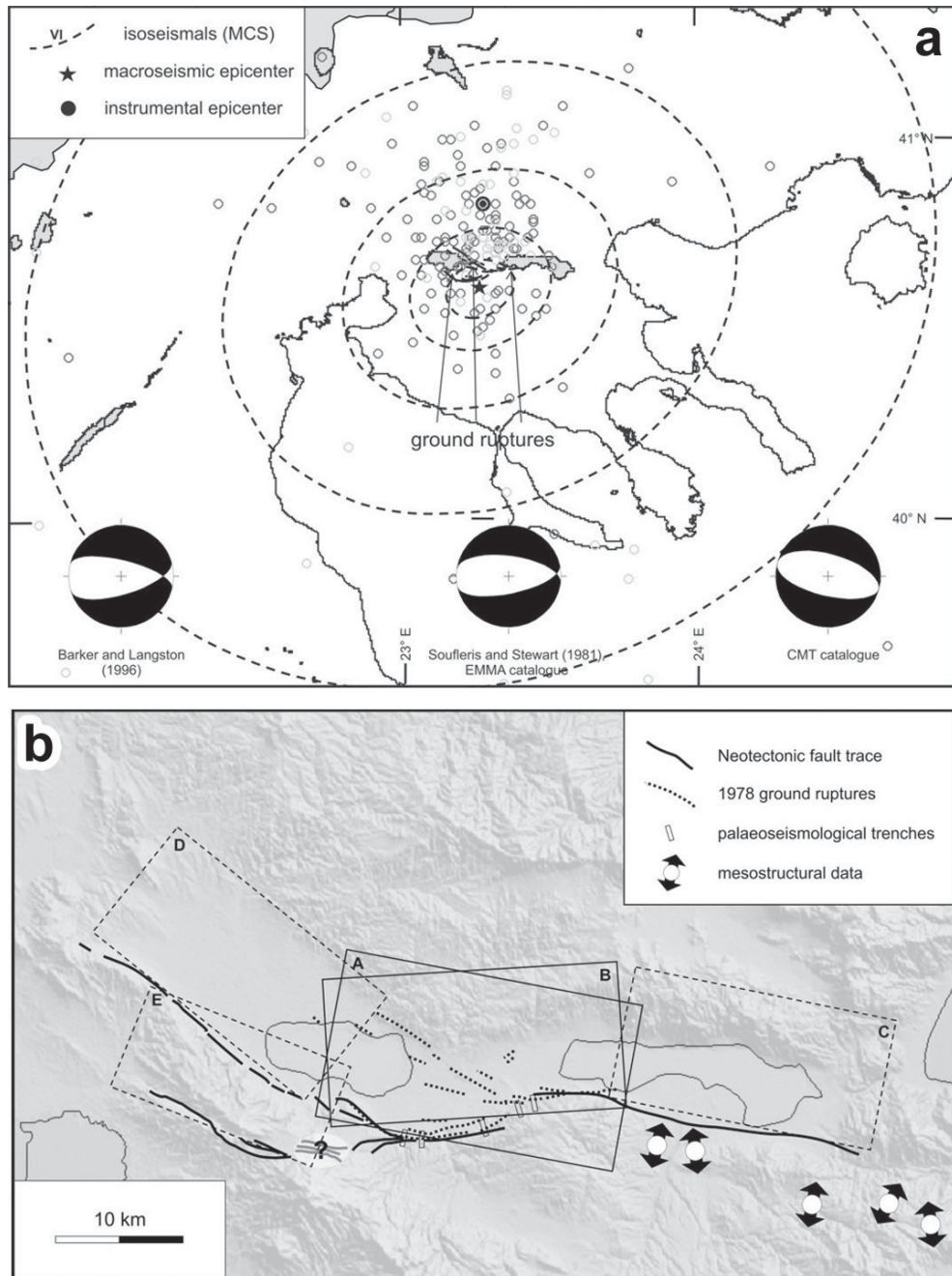


Fig. 6.4: **a)** Isoseismals, macroseismic and instrumental epicentres of the 1978 Stivos earthquake, showing the location of the ground ruptures and some focal mechanisms of the main shock. Foreshocks and aftershocks are also represented as light and dark gray circles, respectively. **b)** Map of the Mygdonia Fault System, Central Macedonia, showing the Gerakarou seismogenic source obtained from the analysis of *single-event effects* (box A) and *cumulative effects* (box B). The Neotectonic fault traces, the 1978 ground ruptures, the location of the palaeoseimological trenches and the results of meso-structural analyses are also represented. The other major segments of the fault system are: Lagadhas (box D), Apollonia (box C) and Asvestochori (box E). See text for discussion and full reference list. See [table 6.1](#) for the seismotectonic parameters.

Although seismic ruptures commonly start close to the brittle-ductile transition, focal depth information joined with the dip-angle of the fault plane does not provide the exact fault width but could help in constraining it. Proposed hypocentral depths are 8 km (Soufleris and Stewart, 1981), 10 km (Dziewonski *et al.*, 1987), 11 \pm 1 km (Barker and Langston, 1981), 12-15 km (according to NEIS and CSEM agencies, see Carver and Bollinger, 1981) and 16 \pm 5 km (Kulhánek and Meyer, 1979). Accordingly, 15 km is here considered the preferred value for the maximum depth of the seismogenic source. Also the aftershock distribution was monitored soon after the major event by a local, temporary network (Soufleris *et al.*, 1982). However, the results published in the literature are not sufficient for better defining shape and dimensions at depth of the fault surface. This was probably due to the odd geometry and density of the seismographic network, the technological limitations of the used instrumentation, or the velocity model applied for the inversion of the data. In conclusion, the fault width likely ranges between 18 and 22 km.

Fault length has been constrained on the basis of seismological data suggesting a 25 km-long rupture plane (Roumelioti *et al.*, 2007)

The co-seismic ground ruptures followed three major alignments characterized by different strike and kinematics (Papazachos *et al.*, 1979; Mercier *et al.*, 1983). The most important set of fractures, trending ENE-WSW, runs parallel to the southern margin of the basin for *ca.* 23 km and likely corresponds to the surface expression of the causative fault, though Stiros and Drakos (2000) propose a blind faulting model and consider the observed ground ruptures only secondary co-seismic effects.

The average and maximum displacements observed in the field are 8-10 cm and 25 cm, respectively (Pavlidis and Caputo, 2004).

The inversion of *P* and *Sh* waveforms (Roumelioti *et al.*, 2007) provides the slip distribution on the fault plane. The mean seismologically estimated co-seismic displacement varies from 0.25 to 0.95 m (Kulhánek and Meyer, 1979; Soufleris and Stewart, 1981; Soufleris *et al.*, 1982; Soufleris and King, 1983; Roumelioti *et al.*, 2007), while the geodetic models suggest a mean co-seismic displacement of 0.45 or 0.57 m (Stiros and Drakos, 2000). A mean value of 0.5 m has been considered (see box A in [fig. 6.4b](#) and [table 6.1](#)).

Cumulative effects: Geological and morphotectonic mapping of the Mygdonia Fault System clearly documents the occurrence of recent fault scarps and associated faults running along the southern margin of the plain ([fig. 6.4b](#); Kockel and Mollat, 1977; Mercier *et al.*, 1979; Mountrakis *et al.*, 1996a; Tranos *et al.*, 2003). The structure is composed by few major segments trending between E(NE)-W(SW) and (W)NW-(E)SE. In the central sector of the fault system the Gerakarou Fault is located (box B in [fig. 6.4b](#)) which is delimited to the east by an angular boundary with the Apollonia Fault (box C in [fig. 6.4b](#)), while towards the west it shows an angular boundary with the (W)NW-(E)SE trending Langadha Fault (box D in [fig. 6.4b](#)) and a geometric gap with the Asvestochori Fault (box E in [fig. 6.4b](#)). The total Neotectonic fault length of the Gerakarou Fault is *ca.* 22 km.

Mesostructural analyses along the mountain front show sliding planes in a general E-W direction, bearing striations representative of the recent N-S-trending extensional field (Mercier *et al.*, 1979; Pavlidis and Kiliadis, 1987).

Aftershock distribution (Carver and Bollinger, 1981; Soufleris *et al.*, 1982) and microearthquake investigations in general (Hatzfeld *et al.*, 1986/87; Tranos *et al.*, 2003; Galanis *et al.*, 2004; Paradisopoulou *et al.*, 2006), constrain the seismogenic layer thickness down to a maximum depth of 16 km, suggesting a listric fault surface characterized by a dip-angle varying between 70° (upper 8 km) and 46° (deeper than 8 km; Hatzfeld *et al.*, 1986/87). According to maximum depth, dip-angle and overall geometry, the estimated width is ~19 km.

Palaeoseismological investigations (Cheng *et al.*, 1994; Chatzipetros, 1998; Chatzipetros *et al.*, 2005a) confirm that the 1978 co-seismic rupture reached the surface with a dip-angle of 65°-74°. They also document the occurrence of at least other four linear morphogenic earthquakes, characterized by slip-per-event ranging between 10 and 25 cm and a mean recurrence interval of 1.0-1.5 ka. Supposing to ignore the date of the last earthquake (*e.g.* 1978), palaeoseismological trenches document the occurrence of two events after 910 AD. The older is tentatively associated with the 1430 AD earthquake and therefore chronologically constrains the last event occurred on this seismogenic source within the past 570 years, and similarly the elapsed time.

Based on the observed co-seismic slips and the constrained ages of the palaeoevents, the slip-rate varies between 0.26 and 0.7 mm/a (Chatzipetros, 1998; Chatzipetros *et al.*, 2005a), thus emphasizing the lateral variability of the fault behaviour and the possible occurrence of some amount of post-seismic creep causing an over-estimation of this parameter (see discussion in Caputo *et al.*, 2008).

The maximum expected magnitude calculated on the basis of the above parameters is 6.5 (M_w).

Aliakmonas Fault System

Western Macedonia region is affected by an important fault system, which cuts across the orographic and morphological first-order texture of the NW-SE trending Hellenic fold-and-thrust belt. Although the broader region was considered a rigid 'aseismic' block (Voidomatis, 1989; Papazachos, 1990) the Aliakmonas Fault System ([fig. 6.5](#)) was partly reactivated by the May 13, 1995 Kozani-Grevena earthquake, one of the strongest events affecting northern Greece during the last decades.

Single-event effects: The causative fault of the 1995 ($M_w = 6.4-6.5$) earthquake has been well located from the focal parameters and the co-seismic ground ruptures. Estimated seismic moments derived from seismological data vary from $4.9 \cdot 10^{18}$ to $7.6 \cdot 10^{18}$ N·m (Dziewonski *et al.*, 1996; Hatzfeld *et al.*, 1997; Ambraseys, 1999; Vannucci and Gasperini, 2003; 2004) corresponding to $M_w = 6.4-6.5$. Also InSAR modelling (Rigo *et al.*, 2004) suggests $M_0 = 7.8 \cdot 10^{18}$ N·m ($M_w \sim 6.5$), while according to geodetic modelling the seismic moment was $16.3 \cdot 10^{18}$ N·m ($M_w \sim 6.7$; Clarke *et al.*, 1997). Assuming the 1995 earthquake was a characteristic event, a preferred value of 6.5 is considered as the maximum magnitude of this seismogenic source.

The seismogenic fault plane is well described by the proposed focal mechanisms (Dziewonski *et al.*, 1996; Papazachos *et al.*, 1998; Hatzfeld *et al.*, 1997; Kiratzi and Louvari, 2003; Vannucci and Gasperini, 2003; 2004; Suhadolc *et al.*, 2007) documenting a (E)NE-

(W)SW-striking (240° - 243°), NW-dipping (38° - 47°), almost purely dip-slip normal fault plane (rake 259° - 269°).

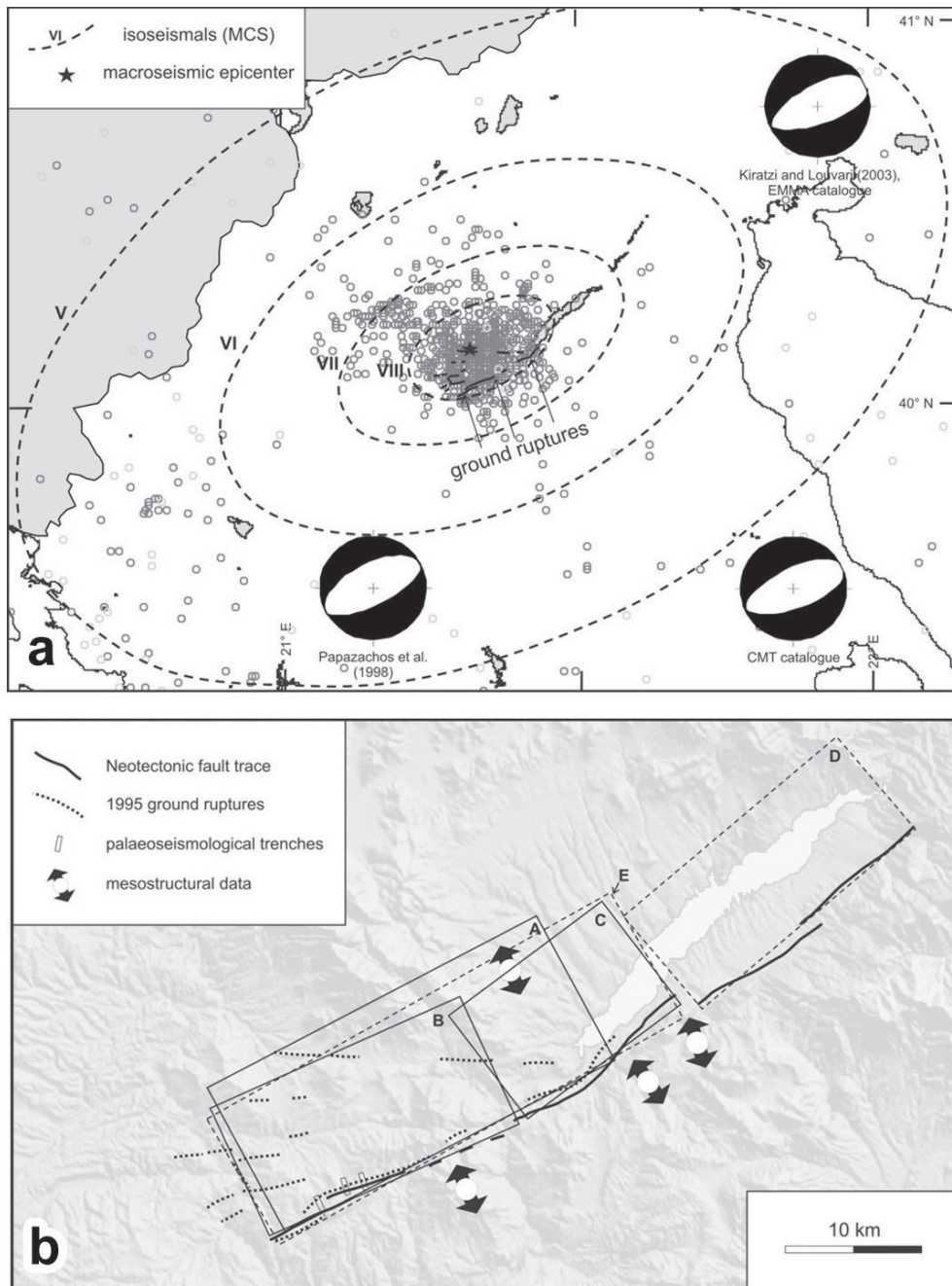


Fig. 6.5: **a)** Isoseismals and macroseismic epicentre of the 1995 Kozani-Grevena earthquake. Some focal mechanism of the main shock as well as the foreshocks and aftershocks are also represented as light and dark gray circles, respectively. **b)** Map of the Aliakmonas Fault System, Western Macedonia, showing the seismogenic source obtained from the analysis of *single-event effects* (box A). *Cumulative effects* suggest the occurrence of three segments (box B: Palaeochori Fault; box C: Rymnio Fault; box D: Servia Fault) of which the former two could represent a unique 'earthquake segment' (*sensu dePolo et al.*, 1991; box E). The Neotectonic fault traces, the 1995 ground ruptures, the location of the palaeoseimological trenches and the results of mesostructural analyses are also represented. See text for discussion and full reference list. See [table 6.1](#) for the seismotectonic parameters.

As a consequence of the seismic event, several ground ruptures were formed between the Rymnio and Sarakina villages, oriented ENE-WSW with a total length of 27 km, showing the northern block subsided (Pavlidis *et al.*, 1995; Mountrakis *et al.*, 1998), though according to Meyer *et al.* (1996; 1998) the surface breaks were only 8-12 km-long. The surface ground deformation was also captured by DInSAR imageries (Meyer *et al.*, 1996; Rigo *et al.*, 2004; Resor *et al.*, 2005) suggesting a comparable fault length.

The maximum slip observed at the surface was less than 20 cm (Pavlidis *et al.*, 1995; Meyer *et al.*, 1996; Mountrakis *et al.*, 1998), while from geodetic modelling the maximum slip on the fault plane was 1.2 m (Clarke *et al.*, 1997).

It should be noted that based on seismological data and geodetic modelling, it has been suggested that the seismic process did not reach the surface (Papazachos *et al.*, 1998; Hatzfeld *et al.*, 1997; Clarke *et al.*, 1997) and the rupture tip (*i.e.* minimum depth) was at *ca.* 5 km. This hypothesis is however in contrast with field observations (Pavlidis *et al.*, 1995; Mountrakis *et al.*, 1998) and InSAR models (Meyer *et al.*, 1996; Rigo *et al.*, 2004; Resor *et al.*, 2005). The latter also suggest a complex 3D rupture surface consisting of several variably oriented segments. If strike, dip and rake are averaged out for resembling a planar fault model as required in GreDaSS, the values obtained are in good agreement. Similarly, considering the aftershocks distribution, the focal mechanisms and the location of both hypocentral location and surface ruptures (Hatzfeld *et al.*, 1997; Drakatos *et al.*, 1998a; Rigo *et al.*, 2004; Resor *et al.*, 2005), as well as stress tensor inversion (Kiratzi, 1999). The fault plane is shallow dipping at depth and becomes steeper towards the surface.

Spatio-temporal aftershock distribution (Hatzfeld *et al.*, 1997) and stress tensor inversion (Kiratzi, 1999) suggest also the occurrence of an antithetic fault plane, the Chromio Fault, that was probably reactivated as a secondary inherited structure. The antithetic fault also produced ground ruptures (Pavlidis *et al.*, 1995; Mountrakis *et al.*, 1998) showing its normal character.

A maximum depth of 15 km is inferred from hypocentral depths either of the mainshock and the aftershock sequence (Hatzfeld *et al.*, 1997; Papazachos *et al.*, 1998).

Different fault's dimensions have been suggested by combining the nodal plane's geometry and the aftershock spatial distribution (25 x 25 km, or 17 x 25 km if the rupture did not reach the surface; Hatzfeld *et al.*, 1997), by forward modelling of the strong motion waveforms (18 x 9 km or 25 x 17 km considering an antithetic fault; Suhadolc *et al.*, 2007) and geodetic modelling (27 x 16 km; Clarke *et al.*, 1997).

Cumulative effects: Geological and morphotectonic investigations indicate the Aliakmonas Fault System as one of the major tectonic structures affecting Western Macedonia ([fig. 6.5b](#)). The whole structure cuts perpendicularly across the mean orogenic trend of the Hellenides, showing clear evidences of recent activity for more than 50 km along strike. Detailed mapping emphasizes the occurrence of three major segments (Palaeochori, Rymnio and Servia faults, from SW to NE, respectively; boxes B, C, and D in [fig. 6.5b](#)). The Servia Fault shows the most prominent features of recent activity being associated with a major escarpment developed in carbonate rocks and bordering the Polyphytos Lake (Pavlidis *et al.*, 1995; Doutsos and Koukouvelas, 1998; Mountrakis *et al.*, 1998; Goldsworthy and Jackson, 2000), while the two southwestern segments (Palaeochori and Rymnio ISSs) show discontinuous and subdued scarps,

as a consequence of the affected lithologies mainly belonging to the ophiolitic suite. The three segments have been distinguished and separated in correspondence with a right-stepping underlapping geometry (Rymnioi-Servia ISSs) and a slight angular boundary and possible geometric gap (Palaeochori-Rymnio ISSs). As far as the 1995 Kozani-Grevena earthquake ruptured the southwestern portion of the fault system, this chapter is focused on these two geologically defined segments (boxes B and C in [fig. 6.5b](#)). The ENE-WSW-striking scarps composing the Palaeochori Fault extend for a length of *ca.* 21 km and progressively disappears towards the SW, while the Rymnio Fault extends for a total length of 13 km.

Seismic tomographies obtained from the aftershocks of the 1995 event (Chiarabba and Selvaggi, 1997), which could be considered equivalent to a typical microearthquake investigation used in the *cumulative effects* approach, allow to delineate the deeper geometry of the fault characterized by a shallow-dipping setting at depth becoming progressively steeper upwards, therefore suggesting a mean dip-angle of 40°. The same dataset also helps constraining a seismogenic layer thickness of *ca.* 15 km (Drakatos *et al.*, 1998a; Hatzfeld *et al.*, 1997). Accordingly, based on minimum and maximum depth and the overall geometry, it is possible to estimate a fault's width of 23 km.

Mesostructural analyses along the Aliakmonas Fault System (Meyer *et al.*, 1996; 1998; Mountrakis *et al.*, 1998), show a (N)NW-trending direction of extension similar to the one measured in nearby structures (Ptolemaida Basin; Pavlides and Mountrakis, 1987) and compatible with the observed ground fractures.

Palaeoseismological investigations carried out across the Palaeochori segment (Chatzipetros *et al.*, 1998) reveal the occurrence of at least three older linear morphogenic events before the 1995 earthquake. The measured amount of slip largely varies for different events and from trench to trench (10-80 cm) and suggests that previous co-seismic ruptures were not always located on the same fracture line along the fault, but they can be distributed over subparallel fault strands. A mean value of 0.5 m is assumed.

The poorly constrained TL-datings could suggest a very low slip-rate and a mean recurrence interval longer than 10 ka (and less than 30 ka). However, based on geological and morphological considerations Doutsos and Koukouvelas (1998) estimate a faster long-term slip-rate (0.3 mm/a) also suggesting a much shorter recurrence interval (2 ka).

Based on the obtained values (see [table 6.1](#)), the moment magnitude calculated via seismic moment would be 6.6 and 6.4, respectively. These values agree also with those derived by empirical relationships (6.6-6.7 and 6.3-6.5; Wells and Coppersmith, 1994; Pavlides and Caputo, 2004).

In this case study, the occurrence of the last event, and hence the elapsed time, supposing we ignore the 1995 earthquake, is very poorly constrained due to the paucity of available and reliable datings from the palaeoseismological investigations. The last rupture observed in the trenches clearly affects layers containing several pottery fragments, which are Neolithic at the oldest (*i.e.* 5-6 ka BP), but unfortunately are not dated.

Comparison of approaches

In this session, the numerical results obtained by separately exploiting the two *sources of information* are analysed, and both similarities and differences among the principal seismotectonic parameters are discussed. In this way, the advantages and limitations of the two approaches will be emphasized. All values are synthetically reported in [table 6.1](#).

parameters	East Heliki Fault		Domokos Fault System		Mygdonia Fault System		Aliakmonas Fault System	
	single-event effects	cumul. effects	single-event effects	cumul. effects	single event effects	cumul. effects	single event effects	cumul. effects
location	(B)	(A)	(C)	(B)	(A)	(A)	(B)	(B)
length [km]	17 (C)	25 (B)	20 (C)	30 (B)	23 (B)	22 (B)	27 (B)	34 (B)
width [km]	8 (E)	15 (C)	20 (E)	19 (C)	20 (C)	19 (C)	23 (C)	23 (C)
min depth [km]	0 (A)	0 (A)	1 (C)	0 (A)	0 (A)	0 (A)	1 (E)	0 (A)
max depth [km]	10 (E)	10 (C)	14 (E)	15 (C)	15 (B)	16 (B)	15 (B)	15 (B)
strike [deg]	280 (B)	277 (A)	353 (D)	285 (A)	280 (B)	265 (B)	240 (A)	242 (A)
dip [deg]	45 (D)	40 (B)	45 (D)	50 (C)	49 (B)	55 (B)	42 (B)	40 (B)
rake [deg]	270 (D)	280 (B)	300 (D)	285 (C)	286 (B)	260 (C)	264 (B)	270 (C)
slip per event [m]	1 (C)	0.80 (B)	0.9 (B)	1.0 (C)	0.5 (C)	0.25 (B)	0.2 (B)	0.5 (C)
slip-rate [mm/a]	n.a.	0.5-2.0 (C)	n.a.	0.3-1.0 (B)	n.a.	0.3-0.7 (C)	n.a.	0.01-0.3 (D)
recurrence [ka]	n.a.	0.2-1.6 (C)	n.a.	3.2 (B)	n.a.	1.0-1.5 (B)	n.a.	2-10 (C)
maximum expected magnitude	6.6 (D)	6.7 (B)	6.7 (C)	6.8 (B)	6.5 (B)	6.5 (B)	6.5 (B)	6.7 (B)
last ethq [AD]	1861 (A)	>1300 (C)	1954 (A)	>500 (D)	1978 (A)	>1500 (D)	1995 (A)	>5000 BP (E)
elapsed time [years]	50 (A)	<600 (D)	56 (A)	<1500 (D)	33 (A)	<570 (D)	15 (A)	<5000 (E)

Table 6.1: Synthetic table showing the numerical values obtained from the analysis of *single-event effects* and *cumulative effects* for the four case studies. For the definition of each parameter see §1.5. Numerical values for 'location' are not reported here but graphically shown in the corresponding figures. A qualitative index, from A (best accuracy) to E (lowest reliability and largest uncertainty), is attributed to each numerical value and indicated in brackets.

In the first case study (the Heliki Fault), both approaches give comparable results for location, strike and minimum depth. Also kinematics can be grossly obtained by the *single-event effects*, but it is certainly more accurate based on structural analyses (*cumulative effects*). Similarly, the real fault length is poorly determined with the first methodological approach, but better constrained with the second one. Palaeoseismological data match, within uncertainties,

the measured surface displacement of the co-seismic ground ruptures. In this example, other parameters like width, maximum depth, dip and recurrence interval could be directly derived from *cumulative effects*-based investigations, but they could be only tentatively and very roughly inferred from the *single-event effects*, using *e.g.* empirical relationships. The major difference is probably represented by the maximum expected magnitude based on the calculated seismic moment: 6.4 and 6.7 according to the two different *sources of information*. On the contrary the difference is reduced if we consider the historic information and the inferred equivalent magnitude ($M_e = 6.6$). Finally, slip rate and recurrence interval cannot be obtained by the first approach and this is so also for the other case studies. Conversely, the timing of the last event and hence the elapsed time are not precisely determined, but only chronologically constrained using 'geological' data.

In the second case study, the Domokos Fault System, the difference in location, geometry and kinematics, as obtained from the analysis of *single-event effects* with respect to the *cumulative effects*, is evident. For the purpose of supplementing seismotectonic parameters in GreDaSS, the former *source of information* is generally considered less reliable principally because it provides contradicting seismogenic sources (compare boxes A and B in [fig. 6.3b](#)). Taking into account the seismological solution (box A in [fig. 6.3b](#)) the problems are *i*) the left-lateral NNW-SSE-trending ground ruptures were probably secondary conjugate structures, *ii*) the similarly oriented nodal plane proposed by McKenzie (1972) is based on a poor seismological network and especially on short-period recordings, and *iii*) the suggested rake is not in agreement with the Present-day stress-field. By taking into account the other solution (box B in [fig. 6.3b](#)), *i*) most ground ruptures should be not considered of co-seismic origin, which would be strange for a crustal strong earthquake, and *ii*) the epicentres would be outside the plane. On the other hand the slip rate, slip-per event and recurrence interval inferred from *cumulative effects* observations (Caputo, 1995; Palyvos *et al.*, 2010) are in good agreement with the regional strain rate calculated from GPS measurements and other similar Aegean-type active faults in the broader area (Clarke *et al.*, 1998; Hollenstein *et al.*, 2008). As concerns the maximum expected magnitude, we should consider *i*) the likely immature stage of development of the Domokos Fault System due to its young age (Middle Pleistocene-Present), *ii*) the relatively low crustal deformation rate, and *iii*) its oblique setting with respect to the first-order tectonic texture of the Hellenides. As a consequence, linkage processes and lateral propagation of minor sliding surfaces originally independent is still in progress and the assumption of a partial co-seismic rupture only across the soft segment boundaries is probably most likely (*i.e.* seismogenic length = 30 km; box C in [fig. 6.3b](#)), while considering the whole Neotectonic fault length (~50 km) the calculated maximum magnitude ($M_w \sim 7.0$) would be overestimated (box D in [fig. 6.3b](#)).

In the third case study represented by the Gerakarou Fault which belongs to the Mygdonia Fault System, both *sources of information* are able to provide most of the seismotectonic parameters, with some slight differences in the degree of confidence and uncertainty though (see [table 6.1](#)), possibly suggesting the reliability of the results from the two datasets and associated investigation techniques.

The last case study is the Aliakmonas Fault System. A major difference in seismotectonic information obtained from the two approaches seems to be represented by the fact that the Palaeochori and the Rymnio faults (boxes B and C in [fig. 6.5b](#)) have been described as two

distinct segments on the basis of *cumulative effects* observations, while the analysis of *single-event effects* clearly show that the 1995 Kozani-Grevena earthquake ruptured most of the Palaeochori fault and part of the Rymnio structure (box A in [fig. 6.5b](#)). Nevertheless, fault's dimensions and seismic moment based on seismological or geodetic models (*single-event effects*) and proposed by various authors show a large variability and hence uncertainty. Considering this variability by analysing *single-event effects* and taking into account that the Palaeochori-Rymnio segment boundary is likely 'soft' due to the relatively small variation in strike and limited geometric gap (*cumulative effects* observations), a geologically-based worst-case scenario would also imply the likelihood of a unique rupture for the two segments (box E in [fig. 6.5b](#)), therefore suggesting a larger fault and a stronger expected earthquake ($M_w \sim 6.7$).

Concluding remarks

The four case studies have been selected diachronically starting from the 1861 Valimitika earthquake, which represents the first complete example for Greece of penecontemporaneous systematic field investigations including a detailed ground ruptures map and a scientific report of all seismically induced effects (Schmidt, 1867; 1879). The subsequent three case studies not only are more recent, but they all represent instrumentally recorded events occurred in different stages of the technological evolution (1954 Sophades, 1978 Stivos and 1995 Kozani-Grevena earthquakes). After that, it is possible to emphasize the differences, in both quality and quantity, of the raw data provided by *single-event effects*-based investigations. For example, the Sophades event occurred at the dawn of the Greek seismographic network development when the international network was still in an embryonic phase. Conversely, during the 1995 Kozani-Grevena event the national and regional networks were highly improved in terms of used technology and architecture, whilst other *single-event effects*-based investigation techniques, like GPS surveys and InSAR images, started to be available to researchers.

In practice, the key limitations of the two approaches are the following. On one side, *single-event effects* cannot provide either the slip rate or the recurrence interval, unless the specific seismogenic source is characterized by very short recurrence intervals, historically well documented, which is commonly not the case for the Aegean Region. On the other hand, the methodological approaches generally applied to analyse *cumulative effects* are usually not able to sufficiently constrain the timing of the last linear morphogenic earthquake and consequently of the elapsed time.

According to the above discussion and comparing the results shown in [table 6.1](#), two major conclusions follow. Firstly, the decreasing reliability and increasing degree of uncertainty with increasing age of the historical and instrumental events is evident, relative to the seismotectonic parameters obtained from *single-event effects*. Secondly, although the information inferred from *cumulative effects* has in general a slightly larger uncertainty, if compared with the most recent events, especially when these are recorded by multiple high-technology apparatuses. Thus, this 'geological' approach always gives a sufficient quality level, provided that specific investigations have been carried out. The latter issue is obviously a matter of research funding, but sometimes it is also a matter of bias which affects the researchers. Indeed, many capable faults in the Aegean Region are to be recognized yet, while for researchers it is certainly more attractive to investigate 'famous' seismogenic sources than poorly known ones.

Another significant difference between the two *sources of information* is due to the fact that the various *cumulative effects*-based investigations could be generally repeated as many times as desired and, in principle, they can be carried out by any researcher for their possible scientific falsification. Furthermore, the progressively improving technology and the increasing geological and seismotectonic knowledge may further potentially reduce their degree of uncertainty. In contrast, *single-event effects*-based data are unique, that is to say if a seismometer or a satellite has some temporary failure (alternatively, the seismographic network or the InSAR imageries are not sufficiently dense at the time of the earthquake) there is no second chance to obtain again the specific information by the same method. In other words, even if in the analysis of a specific seismic event the 'resolution' provided by *cumulative effects* is somehow lower (but only if compared with recent earthquakes), its statistical representativeness is potentially much larger. For these reasons, the analysis of *cumulative effects* certainly represents a much more powerful tool for seismotectonic investigations and for the compilation of a database like GreDaSS.

A major goal of this comparison is the calibration of the 'geological' approaches used in seismotectonic investigation. This is because, most of the active faults or potentially active faults (capable faults) affecting the broader Aegean Region have been not reactivated by a recent earthquake included in historical and/or instrumental catalogues. Taking into account the typical recurrence interval of the Aegean-type faults, such tectonic structures are likely associated with a higher level of seismic hazard and hence are certainly much more dangerous than recently reactivated ones. Accordingly, this research is an attempt to calibrate the different methodological approaches based on the analysis of *cumulative effects* and particularly to understand the degree of uncertainty of the several principal seismotectonic parameters. This exercise is important for showing the importance of geological information for the compilation of a database of seismogenic sources.

6.3 Application examples of GreDaSS

The purpose of GreDaSS is not supposed to be just an “encyclopaedia” of active faults, but to be a useful multi-purposed tool, like *e.g.* for SHA, earthquake scenarios and geodynamic modelling. Concerning the former, an improvement of the currently existing seismic zonation map of the broader Aegean (Papaioannou and Papazachos, 2000) is suggested in this dissertation. Stress transfer models related to earthquake triggering effects are just a sample of earthquake scenarios that can be again used in SHA. Especially for the earthquake triggering effects, the interpretation of the location, density, geometry and kinematics of the seismogenic sources is facilitated with GreDaSS, given that data are eventually homogeneous and their completeness is rather high. Even though interpretation can be rather subjective, the data provided by GreDaSS maintain an objective nature. Nevertheless, since the database is always updatable, all outcomes can be respectively updated.

Seismogenic zonation map of Greece

Seismic zonation maps are crucial tools for SHA. The first seismic zonation map of the broader Aegean was introduced by Papazachos (1990) based only on historically and instrumentally recorded seismicity (fig. 6.6). The ignorance of significant seismogenic regions is obvious, with the two areas where the most recently destructive earthquakes occurred not being included in this map; these are the Kozani (May 13, 1995) and the Athens (September 9, 1999) events. This resulted in the revision of the map 10 years later (fig. 6.7) by Papaioannou and Papazachos (2000). This latest edition was more enriched with the most updated – until then – seismological data. However, as it can be seen in fig. 6.8, even this more recent seismic zonation map brings major active tectonic structures into conflict.

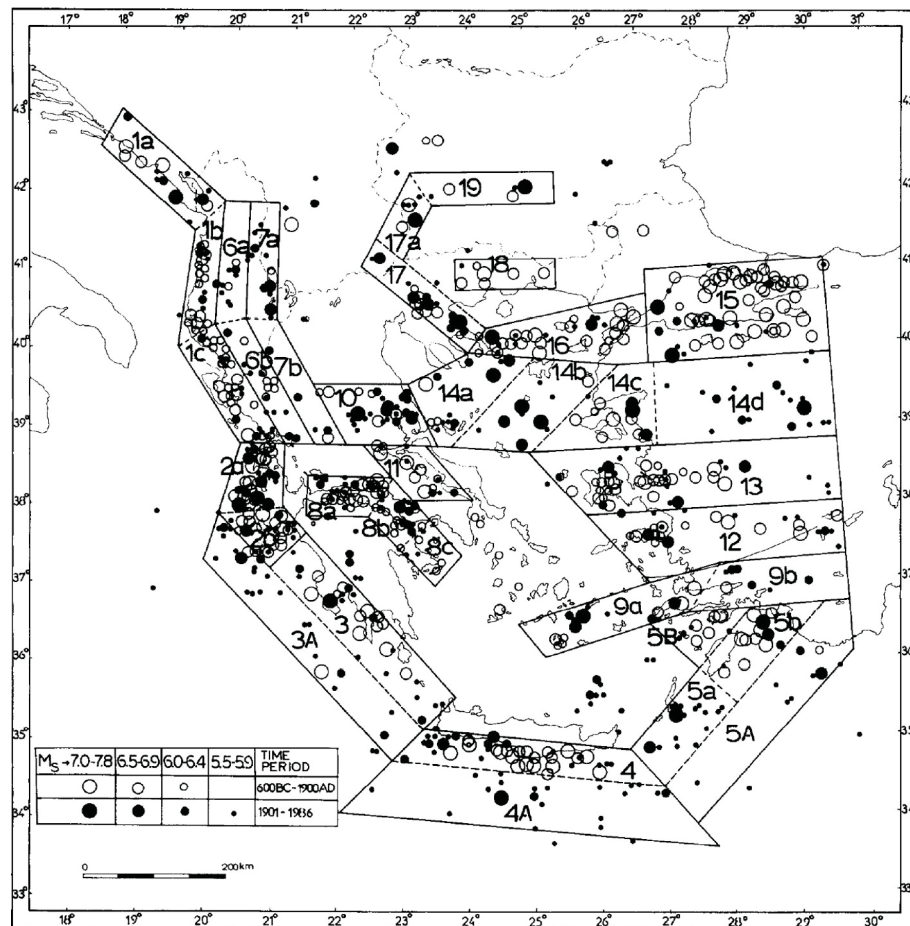


Fig. 6.6: The seismic zones (1, 2,..., 19) and seismic sources (1a, 1b,..., 19) of shallow earthquakes in Greece and the surrounding area, according to Papazachos (1990). Take a notice of the two gaps in West Macedonia and Attica.

It then became clear that such maps are insufficient to describe seismogenic zones with similar attributes. That is why the term of *seismogenic zonation* maps is preferred in this thesis. In this occasion, a list of variously weighted factors is suggested that should be considered, besides seismicity. These factors hierarchically are (from more to less important):

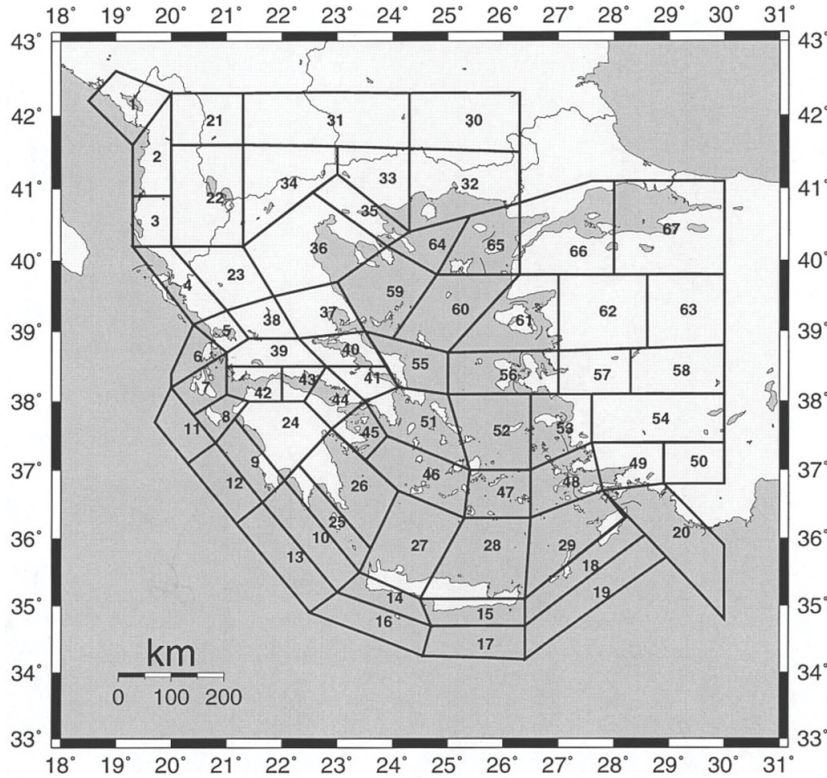


Fig. 6.7: Seismic zonation map of the shallow earthquakes in Greece and surrounding area by Papaioannou and Papazachos (2000). The two regions that were out of the previous zonation map (fig. 6.6) are now included after the two earthquakes of Kozani (1995) and Athens (2000).

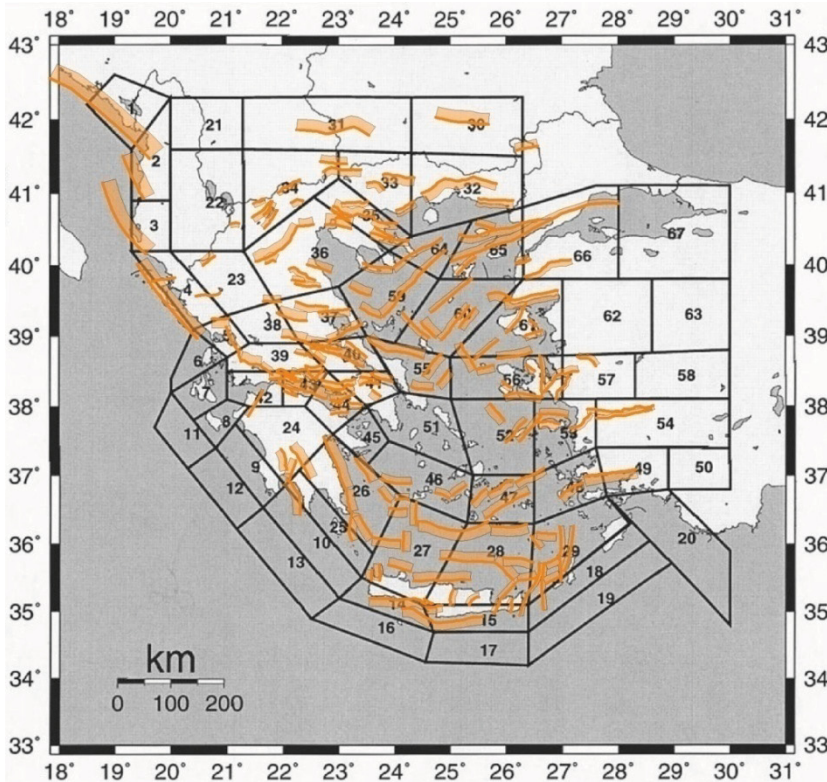


Fig. 6.8: The latest version of seismic zonation map of Greece (Papaioannou and Papazachos, 2000) versus the CSSs of GreDaSS. In many cases (e.g. NAB, NAT, Gulf of Corinth), cells cut seismogenic sources unexpectedly (e.g. cells 59-64, 65-66 and 42-43-44, respectively).

1. The seismogenic sources. The location and distribution of faults with similar seismotectonic behaviour can define the shape of the zones. Large fault zones, like for example the NAT and NAB, should not be split (see [fig. 6.8](#)). Therefore, GreDaSS should have the highest priority.
2. The active stress field pattern. The stress field characterises the seismotectonic behaviour of any possible fault. Even if there are no recognized faults, changes in the stress trajectories should imply a change of zone.
3. The focal mechanisms. They represent the main source parameters and usually reflect both previous factors. This kind of data, however, is not always available and sometimes needs reconsideration.
4. Geomorphology. Almost all of the seismogenic sources in the Aegean that produce shallow events have a strong impact on the relief. Large scale structures, like recently formed basins, elongated valleys, and linear steep slopes are few indicators that reveal the presence of similar tectonic structures (see also §6.2). For example, the separation of an elongated basin or graben, especially when it is preferably oriented to the local stress field pattern, is generally avoided, unless changes in shape and/or orientation occur. Recent and detailed DEMs for onshore structures and bathymetric charts for offshore structures are strong tools in order to distinguish tectonically active landscapes that can help in defining zone boundaries.
5. Alpidic structure. The geotectonic division of the alpidic orogenesis is important, given that it provides information about the origin, composition and thickness of the crust. Such kind of variation causes changes in the mechanical behaviour of the seismogenic layer and therefore affects the geometry and kinematics of the seismogenic sources.
6. Neogene-Quaternary sedimentation. Recent sediments usually fill in tectonically formed basins and valleys. Their presence is a useful supplementary clue especially when they are combined with the geomorphological structures.
7. Geothermal fields. The presence of geothermal fields is usually related with high tectonic activity.

The first three factors can be stand-alone evidences in defining seismogenic zones. The others are secondary ones and need a more thorough consideration before using them.

Based also on the latest edition of seismic zonation map (Papaioannou and Papazachos, 2000), a new (though still preliminary) seismogenic zonation map is proposed in this thesis ([fig. 6.9b](#)). The compilation of the map was carried out based on all criteria described above (*e.g.* see [fig. 6.9a](#) to observe how zones are calibrated according to seismogenic sources), as well as the earthquake density ([fig. 6.9a](#)) produced from the catalogue (1900-2007) submitted to the SHARE project by Prof. Kostas Makropoulos. It is important to mention that the crucial contribution of seismicity is missing, highlighting the need for further collaboration between geologists and seismologists in the future.

In any case, the purpose of this preliminary modified seismogenic zonation map does not intend to replace the old one; it only suggests an alternative approach that involves more features/criteria than the seismological aspect. GreDaSS puts new standards for such maps compilations.



Fig. 6.9: **a)** Map of the broader Aegean Region showing CSSs and earthquake density. The red dashed lines delimit the seismic zones as they were taken out from the previous data. **b)** The preliminary seismic zonation map (black outlined polygons) of the Aegean Area.

Stress transfer and earthquake triggering implications: an example from the Pagasitikos Gulf

When an earthquake occurs, the average value of stress on the fault that slipped is reduced, while stress is increased at the tips of its plane and at sites around it (*e.g.* Reasenbeg and Simpson, 1992; Harris *et al.*, 1995). An immediate result of this stress transfer is the generation of aftershocks (*e.g.* Toda *et al.*, 2002).

The accumulation and release of stress on a fault are controlled not only by the regional stress field and rock property, but also by its surrounding faults. That is to say, the interaction among different faults offers their communications. Earthquake will cause stress to increase or decrease at other faults, and thereby trigger or delay earthquake on them; this is called the effect of earthquake triggering and delaying (King *et al.*, 1994; Hodgkinson *et al.*, 1996; King and Cocco, 2001; Zhang *et al.*, 2003).

The theoretical background of fault interaction by elastic stress changes can be found in the article of King and Cocco (2001). In the present thesis, only the application of this methodology on a specific example will be described, in order to show the importance of the GreDaSS and its contribution to SHA.

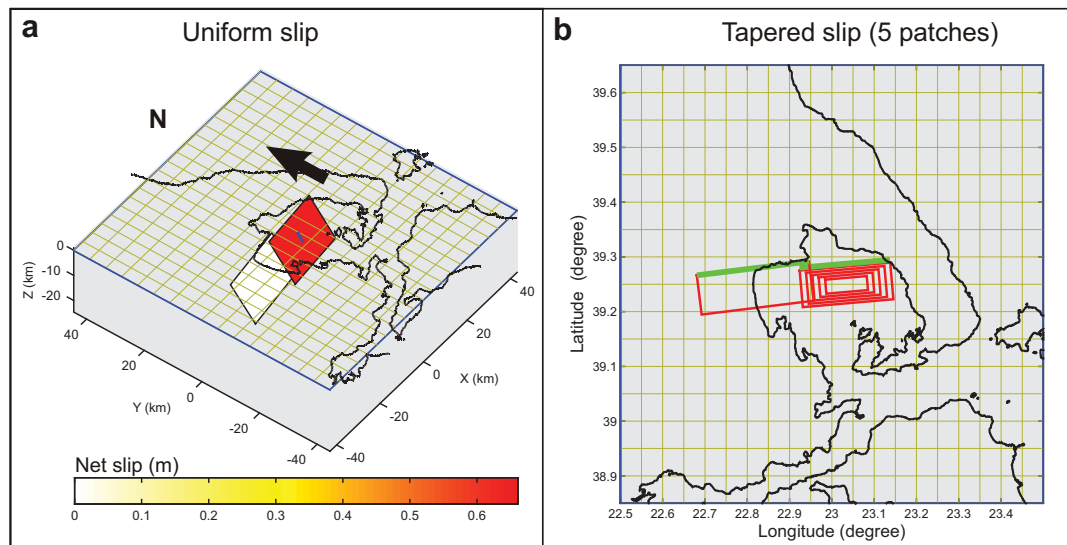


Fig. 6.10: The two ISSs (Volos to the east and Nea Anchialos to the west) responsible for the two largest shocks of the 1980 earthquake sequence (see text for more details). **a)** 3D view (towards NW) of the two sources bearing uniform slip. In this example, the Nea Anchialos ISS has no slip because it represents the receiver fault. **b)** Map view of the two sources which is similar to their representation in GreDaSS. In order to make the slip on Volos ISS more realistic, it has been tapered into 5 patches (decreasing slip from centre towards the tips).

The software used for the Coulomb stress transfer is the Coulomb 3.2, a Matlab-based application developed by the Coulomb Team of USGS (Toda S., Lin J., Stein R.S. and Sevilgen V.). The software can compute both stress change and deformation produced by a ruptured fault. Stress change is based on the Coulomb failure criterion, while the deformation pattern is based on the Okada model (elastic half-space with uniform isotropic elastic properties; Okada, 1992). Software's requirements for the faults input are identical with the parametric information

that GreDaSS provides, and more specifically of the ISSs. Indeed, the visualisation of the fault plane and the slip vector ([fig. 6.10](#)) and the included parameters are similar, making the application of the Coulomb software fast and easy. More details about the usage and potentials of the software can be found in the user's guide (Toda *et al.*, 2011). As an example of possible triggering effect, the Volos and Nea Anchialos ISSs (GRIS010 and GRIS011, respectively) are selected, both participating in the 1980, Volos seismic sequence.

Modelling

During July 9, 1980, two strong events occurred with a difference of 24 minutes. The first event, which was also the strongest one ($M_w = 6.5$), was probably produced by the Volos ISS, while the second one ($M_w = 6.1$) was probably produced by the Nea Anchialos ISS. Two models will be described below dealing with the effects of the two rupture events.

The *first model* involves the Volos ISS as the 'source fault' and the Nea Anchialos ISS as the 'receiver fault'. This means that slip on the receiver fault is (set to) zero ([fig. 6.10a](#)). The Volos ISS was the first to rupture and therefore its effects are modelled on the Nea Anchialos ISS. The software allows to input slip on the source fault in two ways: *i*) a uniform slip, or in other words, an average displacement ([fig. 6.10a](#)), and *ii*) a tapered slip ([fig. 6.10b](#)), which helps to remove unrealistic stress considerations at the edges of the fault. Tapering slip is simulated by dividing the fault plane into a number of homocentric patches in which slip is reduced from edges towards the centre. Concerning the model, a linear tapering is selected with the following settings: distance from edges along strike = 5 km, down dip = 4 km and number of nested patches = 5. Stress change can be visualised into two dimensions, either on horizontal, or vertical, or even oblique sections. Regarding this example, several horizontal sections at various depths (12, 6 and 2 km) have been carried out for both cases of uniform and tapered slip ([fig. 6.11](#)). Moreover, various vertical cross sections perpendicular and parallel to both faults' strike have been performed, as well as inclined profiles parallel to the fault plane of both ISSs ([fig. 6.12](#)). Stress change can be also computed on the receiver's fault surface. In order to get more detail of the stress change distribution, the latter has been tiled into 10x6 cells ([fig. 6.11 top](#)). Taking also advantage of the deformation calculations that the software offers, a set of 2D and 3D images of the displacement distribution, caused by the reactivation of Volos ISS, are also produced ([fig. 6.13](#)). Relying on the fact that tapered slip produces more realistic displacement fields.

The *second model* assumes both Volos and Nea Anchialos ISSs as source faults. This model is useful to suggest if stress was accumulated on other existing nearby faults. As discussed above, tapered slip is a more realistic approach and will be thus used for both ISSs keeping the same tapering settings of the previous model. It is important to know the orientation/geometry and kinematics of the faults in the surrounding because stress changes depend on them. The broader area of South Thessaly is characterised by E-W-striking, normal faults similar to Volos and Nea Anchialos ISSs. Based on this assumption, the stress changes are calculated for faults striking 84° , dipping 55° and with a rake of 264° ([fig. 6.14](#)). As for the previous model, the cumulative deformation pattern is also computed and represented in both 2D and 3D views ([fig. 6.15a and b](#) respectively).

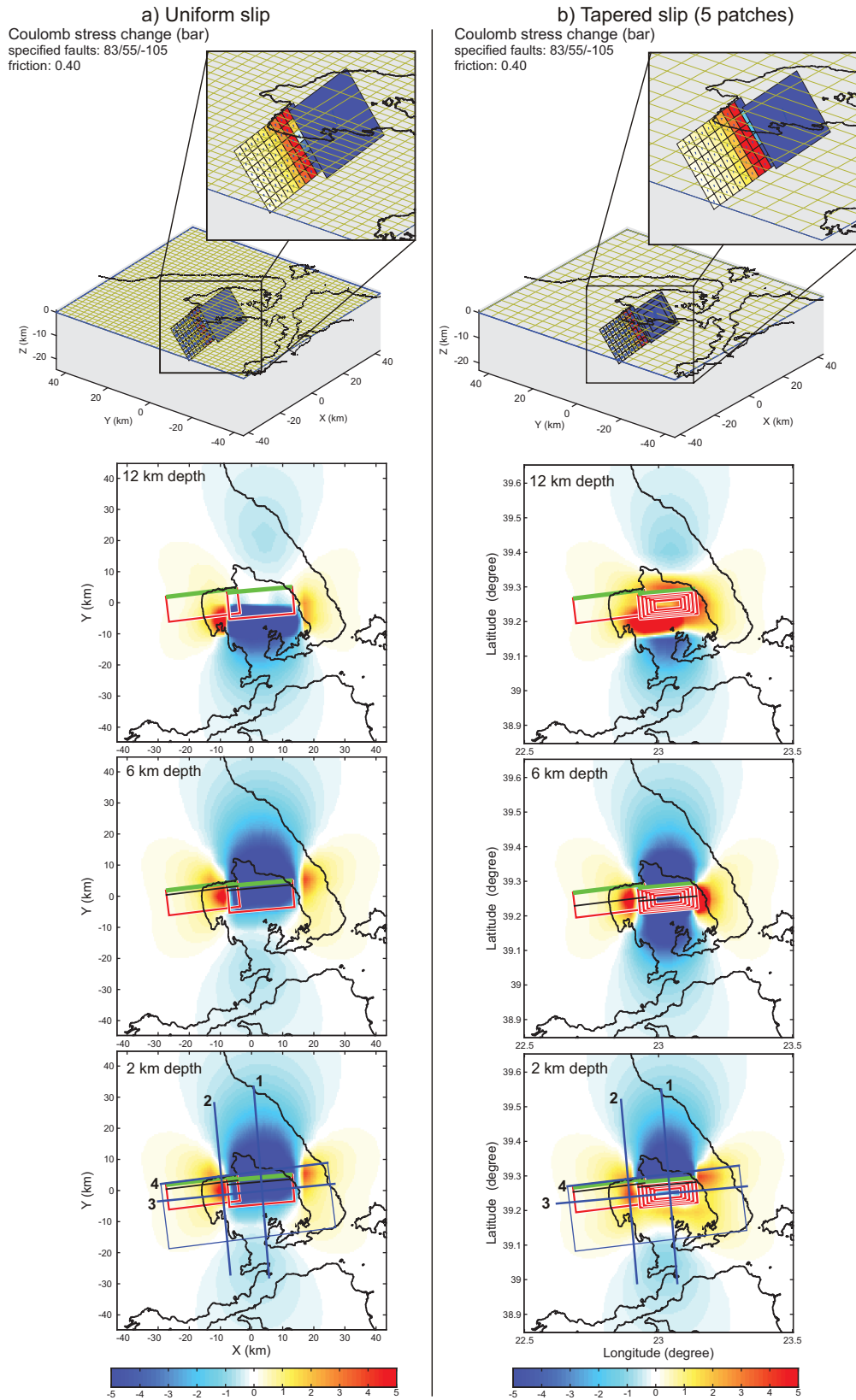


Fig. 6.11: (top) Stress change computed directly on the receiver's (Nea Anchialos) fault plane for both **a)** uniform slip, and **b)** tapered slip. The grid on the receiver's plane is 10x6 cells. (bottom) Horizontal distribution of stress change at various depths (12, 6 and 2 km) for the respective slip variations. Lines numbered from 1 to 3 and rectangular No 4 in the lowest sections, correspond to the paths of the cross sections and the oblique one, respectively, in [fig. 6.12](#).

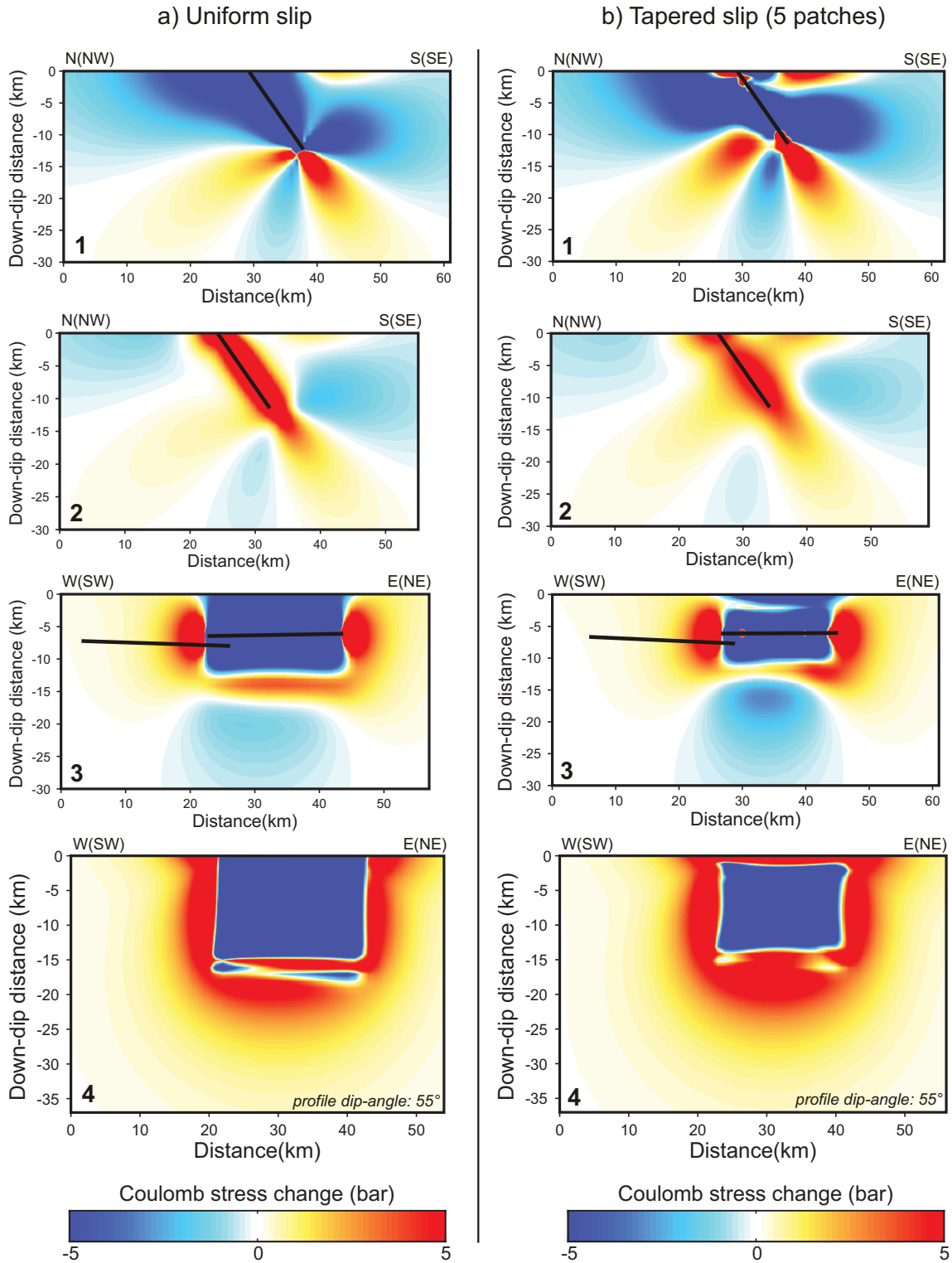


Fig. 6.12: Profiles across (top two), along (third) and oblique-parallel (bottom) to both ISSs, respective to the paths shown in [fig. 6.11](#), showing how stress changes according to depth and around the fault tips of the source fault, for a) uniform slip, and b) tapered slip. The black lines represent the intersections with the fault planes.

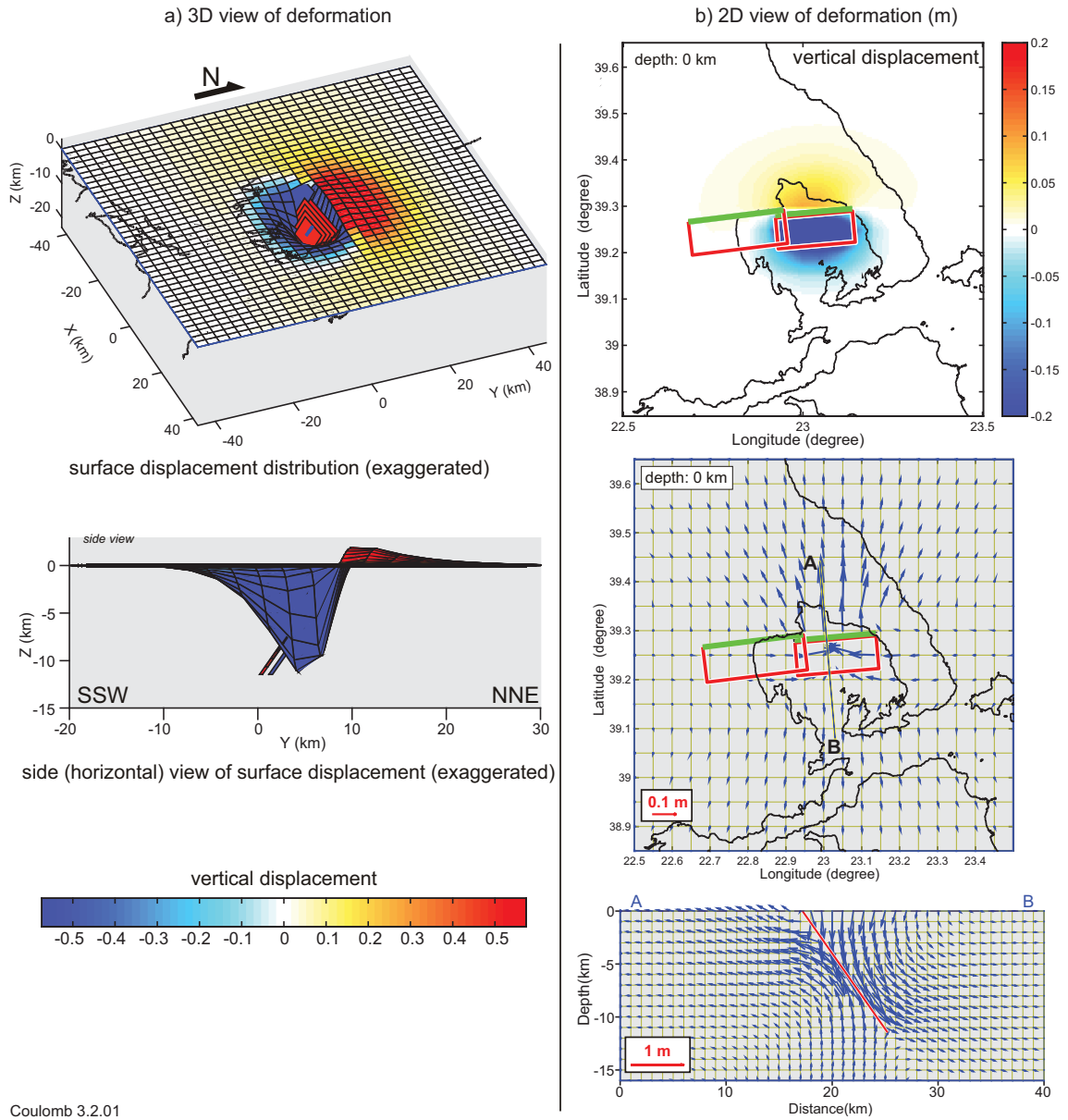


Fig. 6.13: Computed deformation pattern after the reactivation of the Volos ISSs (tapered slip), based on the Okada model. The left side **(a)** shows the surface displacement distribution (exaggerated) in 3-D models, and the right side **(b)** shows surface vertical displacement (top), surface horizontal displacement (middle), and vertical displacement (bottom) distributions. The trace of the cross section (AB) is shown in the middle figure, whilst the fault plane is represented by a red line.

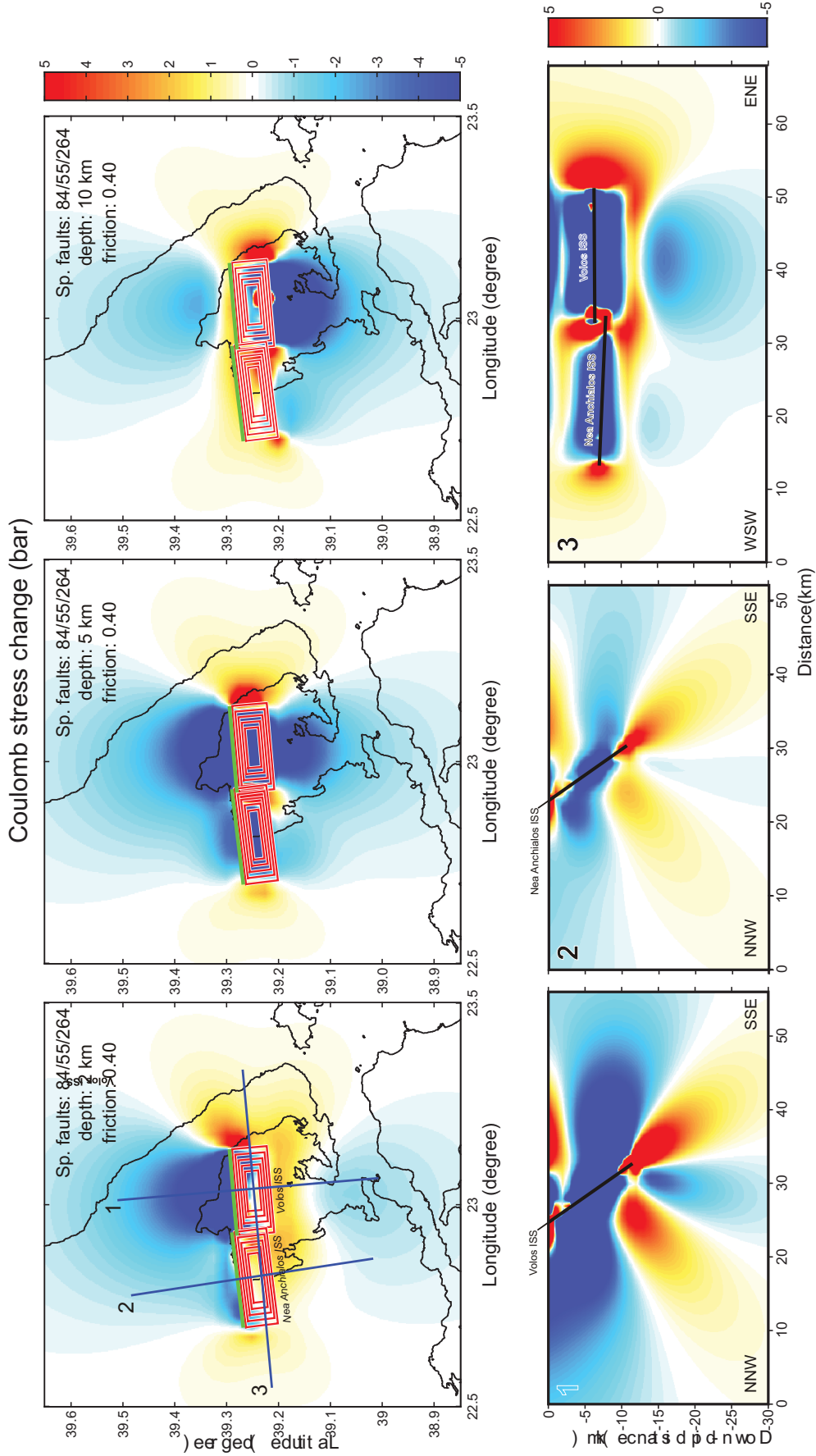


Fig. 6.14: The stress change pattern computed by having both Volos and Nea Anchialos ISSs as source faults and as possible receivers, faults that have similar characteristics (strike 84° , dip 55° and rake 206°). Both source faults have been tapered into five patches each.

a) 2D views of deformation

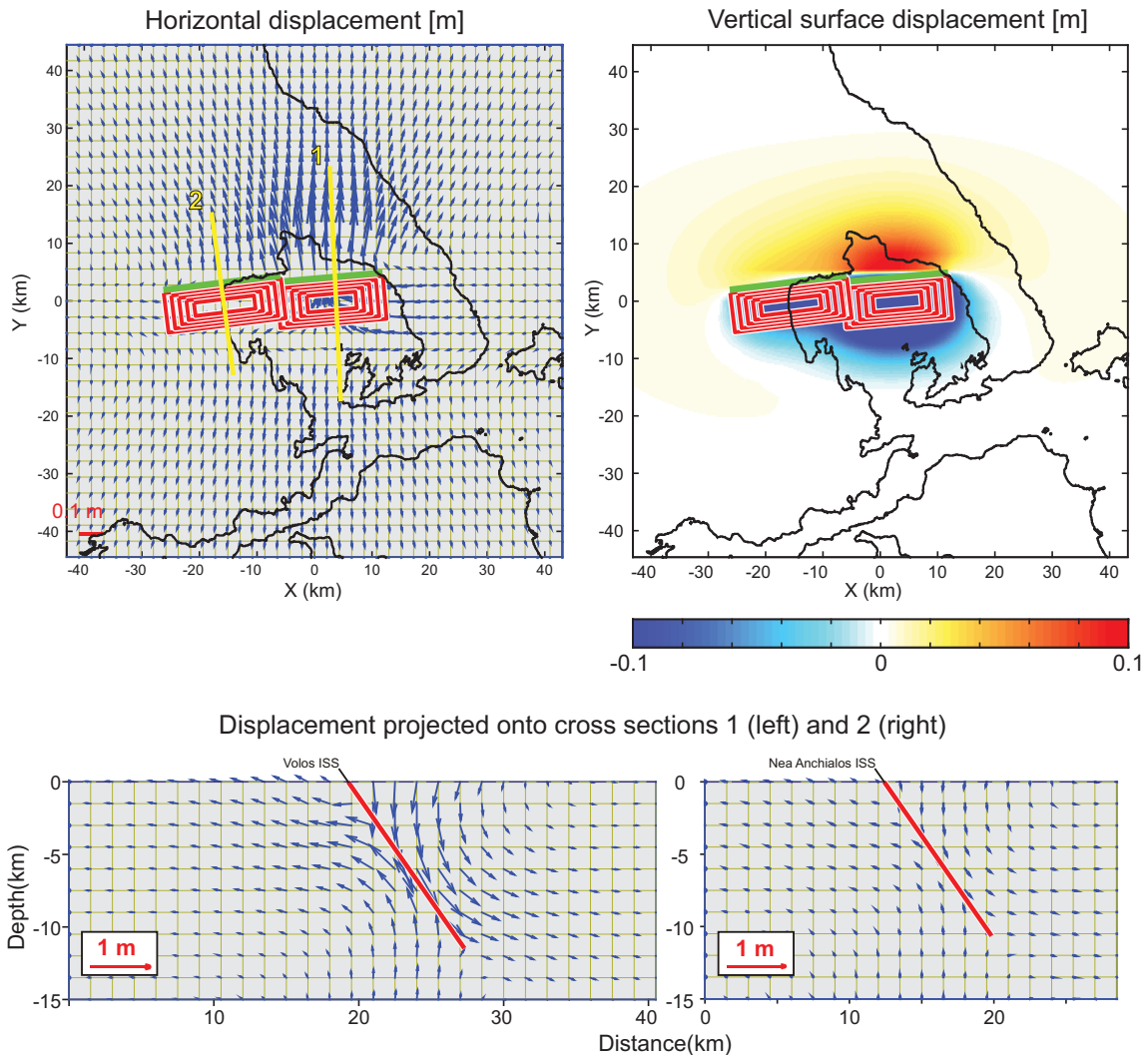


Fig. 6.15: a) 2-D views of horizontal and vertical displacement pattern after the reactivation of both Volos and Nea Anchialos ISSs, and perpendicular cross sections to the faults. b) 3-D model view of the vertical surface deformation in various zoom levels, after the reactivation of both Volos and Nea Anchialos ISSs. Depth is exaggerated.

Concluding remarks

The results of the first model show that after the reactivation of the Volos ISS, stress was mainly accumulated at both lateral tips (figs. 6.11 bottom and 6.12). Seeing also the stress change computed on the fault plane of the Nea Anchialos ISS (fig. 6.11 top), it seems logical to expect that the nucleation of the second shock would be located towards this area. The detail and the accuracy of the hypocentral location, however, are low enough to suggest this. Unfortunately, neither there are accurately recorded aftershocks in order to see whether the latter are accumulated in areas where stress has been accumulated.

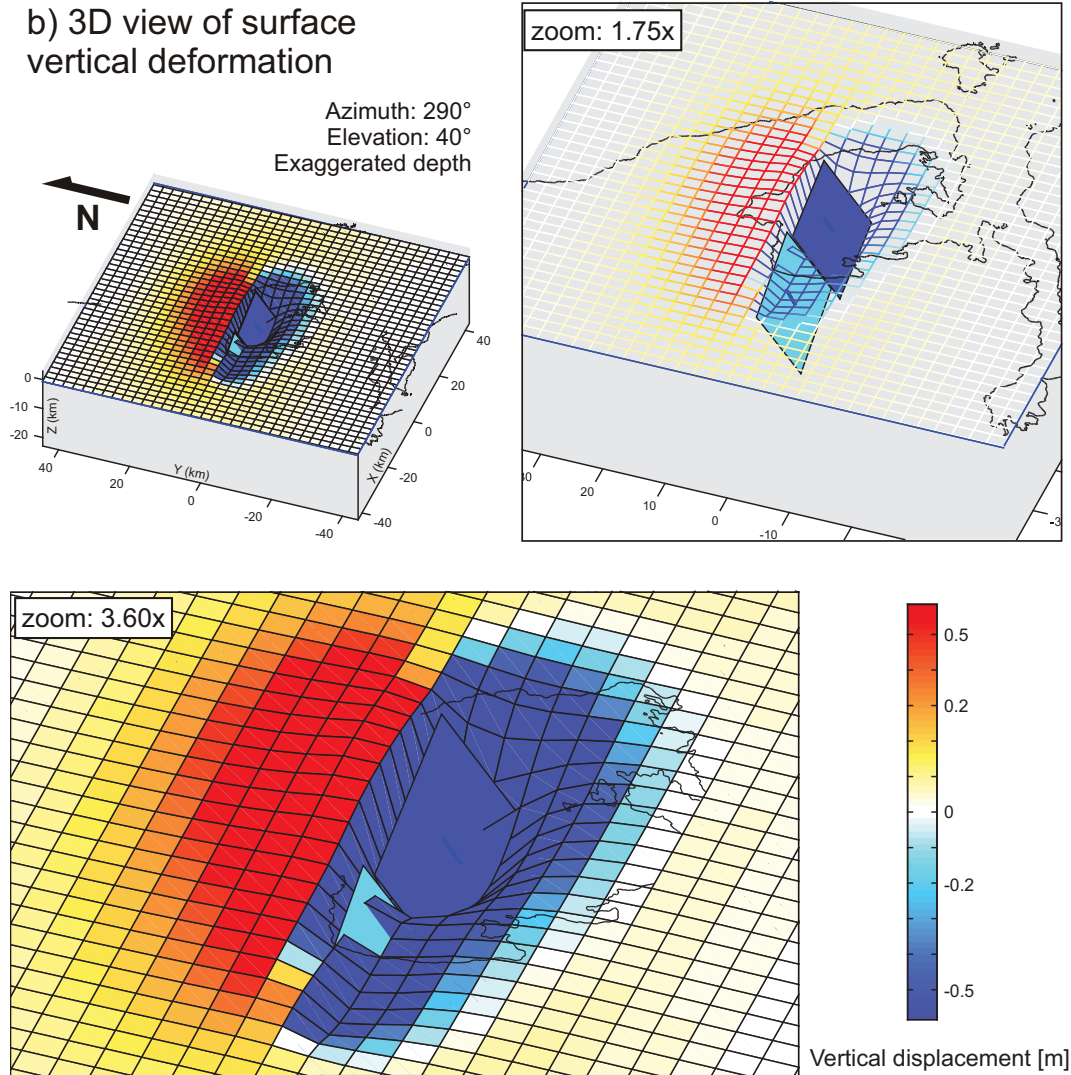


Fig. 6.15 *Continued.*

Stress change of the second model is also accumulated bilaterally from both ends of both faults, but mainly towards the east. The extension of the stress increase is constrained into few tens of kilometres. Thus, only faults very close to the two ones can be directly affected. However, in order to see the cumulative effect of all adjacent faults that were reactivated in the area (*e.g.* Rigehe ISS), a more detailed study is needed.

6.4 Future expectations

In this chapter it is shown some possible ways GreDaSS can be exploited. As an open and always updatable database, GreDaSS will never stop being enhanced. Nevertheless, at this point the database is still in progress and needs to be enriched in terms of seismogenic sources, some or many of which are yet undiscovered, as well as in terms of information in many of the

existing ones. A large part of the existing literature remains to be reviewed and new investigations should and will follow. In fact, GreDaSS provides the opportunity to check which sources have lack of data and proceed to further investigations. But another advantage of GreDaSS is its multi-layering provided information that can contribute differently in the improvement of SHA. The three kinds of seismogenic sources representation (CSSs, ISSs and fault traces/scarps) allows the user to chose the appropriate dataset for his/her needs (fig. 6.16). However, the success of GreDaSS also depends on team work. Collaboration between researchers of different disciplines is wanted and needed. Especially at the national level, GreDaSS should be recognised among the scientific community and become the base of any future SHA.

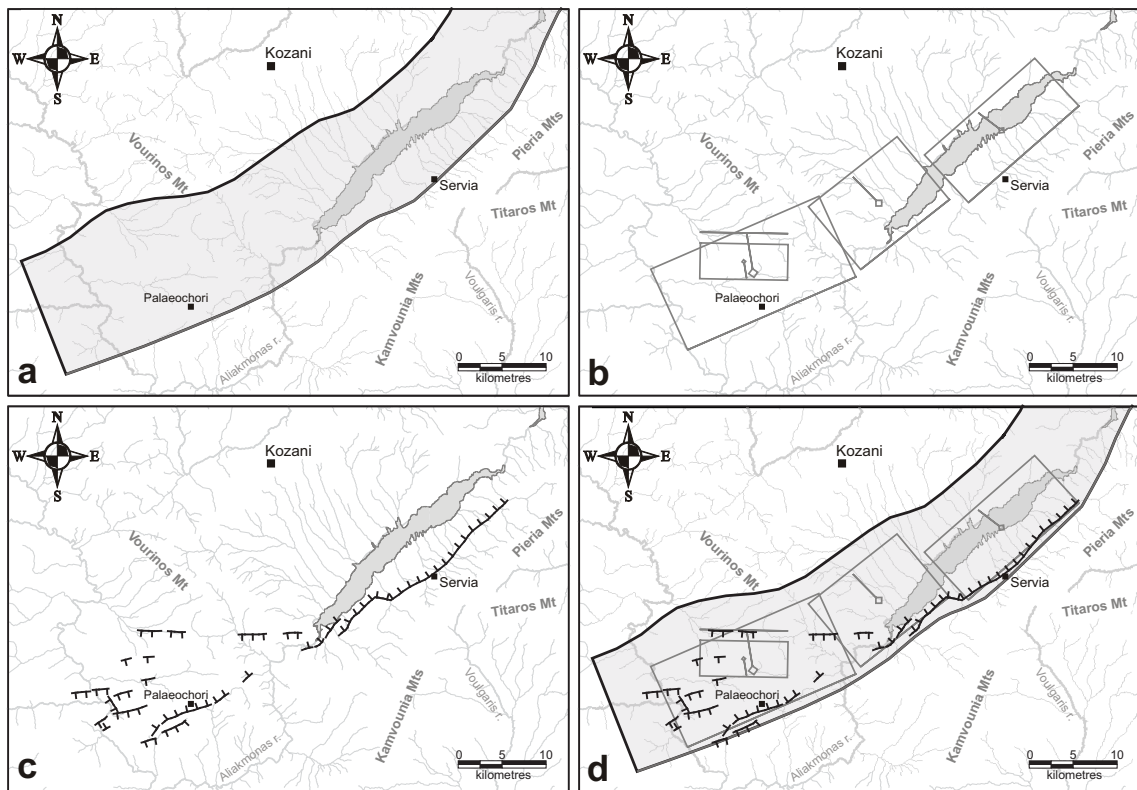


Fig. 6.16: The various geographic information levels of GreDaSS as seen in the example of the Kozani area: **a)** the general extension of the Aliakmonas CSS, **b)** the comprising segments of the Aliakmonas CSS corresponding to ISSs (from east to west: Servia, Rymnio, Palaeochori and its antithetic Chromio), **c)** the detailed mapping of the fault traces/scarps and/or co-seismic ground ruptures, and **d)** all layers above combined together.

The constraint of maximum fault depth through the estimation of the BDT zone for the selected study areas that was carried out in this thesis can be also expanded to the rest of the Aegean Region. Rheological profiles have been broadly used in other regions worldwide, where structural regimes are much simpler and data are richer. The variety of the enrolled parameters requires data of various disciplines. In other words, regional integrated investigations are needed so as to be confident of the produced results. These investigations can focus on lithospheric seismic velocities (for defining the lithospheric structure), thermophysical rock

properties and surface heat flow. If these parameters are well defined, then the method can be applied to local areas and produce a map of interpolated data for at least the northern Aegean.

But beyond its own improvement, GreDaSS can be a powerful tool for other studies. Concerning the examples that have been briefly shown in this chapter, GreDaSS has a lot to offer. In more detail, improved or new geodynamic models can be introduced. For example, following the discussion in §6.1 a cluster of seismogenic sources can define a *seismogenic volume* in which faults might interact, making the prediction of the next candidate fault impossible. A further study could require geophysical surveys to investigate the deeper parts of the faults and seek for the existence of low-angle shear zones.

Seismic or seismogenic hazard zonation maps are important for both DSHA and PSHA and the ones existing so far for the Aegean Region rely only on seismological analyses. However, the modified map introduced in §6.3 is mostly based on geological criteria. This means that in order to have an integrated and more realistic seismogenic hazard zonation map, both disciplines need to cooperate.

The calculation of stress changes after fault reactivations is the basis for making earthquake triggering scenarios. The example given in §6.3 is a simple one, based on the possible interaction of two nearby faults. A more comprehensive study though, should take under consideration previous reactivations of faults in the vicinity as well as the remote stress field. Moreover, similar models and scenarios can be produced for further areas of the Aegean Region. As more GreDaSS gets completed the more accurate the results will be.

7.1 An overview

Although Greece and the broader Aegean Region belong to the most tectonically and seismically active places in the world, a GIS-based database of seismogenic sources was lacking. Data and information concerning the occurrence and behaviour of numerous active faults are usually scattered or hidden in the rich literature, making their acquirement a hard and time-consuming task. On the other hand, such data and information are useful for several purposes: SHA (and especially probabilistic SHA), geodynamic models and seismotectonic interpretations are some of the disciplines for which such a database can be an irreplaceable tool.

The core of this research is the development of GreDaSS which was started from North Greece as a pilot area (Sboras *et al.*, 2009a; 2009b; Pavlides *et al.*, 2010). The compilation procedure includes several stages. The first stage is the recognition of a seismogenic source and the collection of its respective available data and information. The synthesis, critical analysis and homogenization of the collected material follows, in order to define the principal seismotectonic parameters, to plot the source in a geographic coordinate system according to its geometric attributes and to fill in all the corresponding informational fields (comments, open questions, summaries, pictures and references). The final stage includes a processing of all informational levels in order to be linked and interactive. This procedure was followed for 38 CSSs and 58 ISSs that belong to the study area (North Greece). However, some of those steps were also followed for the rest sources of the broader Aegean Region in the frame of the SHARE project (Basili *et al.*, 2010; Sboras *et al.*, 2011).

During the parameterization process, an important issue came up: given that the majority of the seismogenic sources in Greece is not connected with recently (historically or instrumentally) recorded earthquakes – which is the more hazardous case, the only data to rely on are the ones based on *cumulative effects*-based investigations (or generally characterized as geological investigations). On the other hand, investigations based on *single-event effects* (having the seismological investigations as the most prevailing method) sometimes provide wrong information especially when it is about old events. The comparison of these two different approaches is important to define the reliability of the provided data and information. Based on four characteristic case studies which all involve a major earthquake covering a wide period of the historical and instrumental era, it is shown that *i)* the *single-event effects*-based investigations provide improved results as technology advances, and *ii)* the *cumulative effects*-based investigations steadily provide reliable results regardless if the seismogenic source is associated with recent earthquakes or not.

Another important matter that emerged during parameterization is the determination of two important SHA parameters: the maximum fault depth and the slip rate. Defining the maximum fault depth is important because the faults dimensions can be constrained and hence its maximum expected magnitude. For crustal faults, maximum depth is limited within the seismogenic layer, which can be defined by the brittle-ductile transition zone (BDT). Although it is not necessary that a fault will rupture the entire thickness of the seismogenic layer, by estimating the depth of the BDT we can set the maximum depth which a possible rupture can reach. The estimation of the BDT depth relies on the calculation of the strength profiles that reflect the mechanical behaviour of the upper lithosphere. In the current dissertation, the rheological models of three different areas are compared and calibrated based on the local seismic distribution. Since temperature is the key-factor of lithospheric strength, the geothermal gradients are also calculated. However, in the radiogenic heat productive crust, the geotherm equations depend on some thermophysical parameters. For this reason several sensitivity tests were run for various compositions of the upper and lower crust which allowed distinguishing two relative thermal conditions of the crust: the *cool* and *warm crust*. Based on these tests and on rheological modelling, the BDT depth of the three case studies is calculated and it is compared with the available seismic distributions. The results are in good match and verify the rheological models of each case study, giving confidence for further application in the surrounding areas.

The calculation of the slip rate is based on the geodetic strain rate field that derives from GPS measurements. Given that GPS measurements span only few decades, short-term slip rate is actually calculated by this method. The theoretical approach relies on the fact that the deformation between two GPS stations that move relatively to each other is not uniform, but it is concentrated within a zone around the fault plane. During a seismic event, most of the so far accumulated elastic strain is suddenly released on the fault plane and transformed into relative slip, leaving a small, practically neglectful, amount of plastic deformation. The calculation process is based on a series of strain fundamental formulas that can provide the two slip rate components: the strike-slip component and heave which provides the dip-slip component. The obtained results derive from three different datasets that provide either the principal strain axes, or dilatation and maximum shear strain. The patterns coming from the three results are quite similar, although some differences exist in their absolute values. The geodetically calculated slip rates are also compared with the ones found in the literature (wherever these are available), which are basically obtained by geological methods. The comparison suggests that the former not only show reasonable values, but they are of the same order of magnitude. The usually lower values of the geodetic slip rates can be explained by the fact that GPS stations measure velocities during a very short period of a seismic cycle, and that strain accumulation is not necessarily linear with time, so it could be wrong to infer that its rate is steady. It is important to mention that during the calculation process rake is also calculated as a collateral result.

The completeness of GreDaSS for North Greece, including all seismogenic sources that are known so far, allowed the separation of the area into five sectors, each documenting an internal uniform behaviour. Moreover, the pattern, geometry and the geodynamic setting of some regions imply the presence of low-angle normal (detachment) faults defining a *seismogenic volume* in which faults' behaviour can change significantly (fault interaction,

random rupture path, *etc.*). Nevertheless, beyond these qualitative observations, the database can offer several other applications especially for the enhancement of SHA. Two examples are given in this thesis. The first one concerns the improvement of the seismic zonation map of Greece by introducing a new *seismogenic zonation* map. Until now, seismic zonation of Greece was based only on seismological data. This method produces several inconsistencies with major seismotectonic features in the Aegean. The proposed seismogenic zonation map of this thesis relies on other geological criteria and especially the seismogenic sources of GreDaSS. However, the best solution would be a map that would take into account both geological and seismological criteria. The second application example involves earthquake triggering scenarios that are based on Coulomb stress transfer. The Volos and Nea Anchialos ISSs, both lying in the Pagasitikos Gulf, are selected as a case study. Each fault is responsible for one of the two strongest shocks of the 1980 Volos earthquake sequence. Coulomb stress change models based on the seismogenic sources of GreDaSS suggest that earthquake triggering between these two ISSs is a possible scenario.

Concluding, the development and the state-of-the-art of GreDaSS for North Greece are presented in this dissertation, along with the calculation of two basic parameters, the observation of some seismotectonic features and the usage of the database as a SHA tool. It is important to mention though, that the database is always updatable, which means that whenever new data and information are available these will be included in GreDaSS.

7.2 Sommario

La Grecia e tutta la regione Egea sono fra le aree tettonicamente e sismicamente più attive al mondo. Ciononostante, un database GIS basato sulle sorgenti sismogeniche e le faglie capaci di generare terremoti moderati-forti è tuttora praticamente inesistente. Dati e informazioni per riconoscere la presenza ed il comportamento di numerose faglie attive sono generalmente dispersi o nascosti nella ricchissima letteratura scientifica, rendendo la loro acquisizione un compito lungo e difficile. E' da notare che gli stessi dati possono trovare diverse applicazioni; ad esempio, l'analisi di pericolosità sismica (SHA), la creazione od il miglioramento di modelli geodinamici e le interpretazioni sismotettoniche sono alcune delle discipline per le quali un simile database può essere uno strumento insostituibile.

Il principale scopo di questa ricerca è lo sviluppo di una banca dati delle faglie sismogeniche della Grecia (**Greek Database of Seismogenic Sources - GreDaSS**) ed è iniziato dalla Grecia settentrionale come area pilota. La procedura di compilazione comprende diverse fasi. La prima fase è il riconoscimento del maggior numero possibile di sorgenti sismogeniche e la raccolta di tutti i dati disponibili. Segue una fase di sintesi, di analisi critica e di omogeneizzazione del materiale raccolto, al fine di *i*) definire e quantificare i principali parametri sismotettonici, *ii*) tracciare le sorgenti sismogeniche in un sistema di coordinate geografiche sulla base delle loro caratteristiche geometriche e *iii*) compilare tutte le schede contenenti tutte le principali informazioni associate (commenti, domande aperte, riassunti, immagini e riferimenti). La fase finale comprende un trattamento di tutti i livelli informativi (metadati) per collegarli e renderli interattivi. Questa procedura è stata seguita per 38 *sorgenti sismogeniche composite* (composite seismogenic sources - CSSs) e 58 *sorgenti sismogeniche individuali* (individual seismogenic sources - ISSs) presenti nell'area di indagine (Grecia Settentrionale). Inoltre, nell'ambito del progetto europeo *Seismic Hazard Harmonisation in Europe* (SHARE), sono state analizzate e preliminarmente incluse nella banca dati anche numerose altre sorgenti presenti in tutta la regione Egea.

Un aspetto importante affrontato durante il presente lavoro di tesi è il seguente. Considerando che la maggior parte delle sorgenti sismogeniche in Grecia non è associata a terremoti recenti (storici o strumentali), gli unici dati su cui è in generale possibile contare sono quelli provenienti dall'analisi degli *effetti cumulativi* e prevalentemente ricavati da indagini di carattere geologico. In alternativa, le analisi sugli *effetti di un singolo evento* (primariamente effettuate con approcci di tipo sismologico), possono fornire informazioni non precise e/o di scarsa qualità soprattutto per gli eventi più antichi. Il confronto tra questi due diversi approcci ha permesso di stabilire il grado di affidabilità delle informazioni fornite. Sulla base di quattro casi di studio, tutti associati ad un forte terremoto e che coprono un ampio periodo sia storico sia strumentale, è possibile concludere che *i*) gli effetti associati ad un singolo evento forniscono ottimi risultati soprattutto per i terremoti più recenti e, in generale, l'informazione ricavata migliora con il progredire della tecnologia, e *ii*) indagini basate sugli effetti cumulativi offrono risultati più che affidabili anche indipendentemente dal fatto che la sorgente sismogenica sia associata a terremoti recenti o meno. Ciò permette di concludere l'importanza delle informazioni geologiche nella compilazione di una simile banca dati.

Un'altro aspetto che è stato affrontato in dettaglio durante la parametrizzazione delle sorgenti è la determinazione di due parametri particolarmente importanti per la SHA: la *profondità massima di rottura* e il *tasso di scorrimento*. Definire la profondità massima di rottura risulta cruciale perché è possibile vincolare le dimensioni massime delle faglie e quindi la magnitudo massima attesa. Per rotture crostali, la profondità massima è normalmente delimitata dalla transizione fragile-duttile (BDT). Anche se non è necessario che un evento sismico rompa l'intero spessore a comportamento fragile, stimando la profondità della BDT è possibile vincolare la profondità massima di rottura. La stima della profondità della BDT si basa sul calcolo dei cosiddetti profili di resistenza che descrivono il comportamento meccanico della litosfera superiore. Nel presente lavoro di tesi, i modelli reologici di tre diverse aree sono stati confrontati e calibrati sulla base della distribuzione sismica locale. Poiché la temperatura è il fattore chiave per la resistenza litosferica, i gradienti geotermici sono stati calcolati prestando particolare attenzione e tenendo conto del calore radiogenico, delle equazioni geotermiche e dei diversi parametri termofisici. Per questo motivo, sono stati eseguiti diversi test di sensibilità per varie composizioni della crosta inferiore e superiore suddividendo il comportamento termico in freddo e caldo. Sulla base di tali test e sulla modellazione reologica, la profondità della BDT nei tre casi di studio è stata calcolata e confrontata con la distribuzione della sismicità in profondità. I risultati mostrano un buon accordo permettendo così di avvalorare i modelli reologici proposti per i diversi casi di studio e ciò da fiducia per ulteriori applicazioni alle regioni circostanti.

Il calcolo del tasso di scorrimento a breve termine delle strutture sismogeniche si basa sul campo di velocità di deformazione geodetica come comunemente ricavata dalle misurazioni GPS. L'approccio teorico si basa sul fatto che la deformazione tra due stazioni GPS che si muovono una rispetto all'altra non è uniformemente distribuita, ma è concentrata in un volume nell'intorno del piano di faglia. Durante un evento sismico, la maggior parte della deformazione elastica accumulata fino a quel momento viene improvvisamente rilasciata sul piano di faglia e trasformata in uno slittamento relativo, lasciando soltanto una componente trascurabile come deformazione plastica. Il processo di calcolo si basa su alcune equazioni fondamentali della deformazione che permettono di ricavare le due componenti del vettore scorrimento (trascorrente e dip-slip) per ogni singola struttura sismogenica. I risultati ottenuti derivano da tre differenti set di dati che forniscono gli assi principali della deformazione, o la dilatazione e la deformazione massima di taglio. I risultati ottenuti dai tre diversi dataset mostrano soluzioni abbastanza simili fra loro, anche se esistono alcune differenze nei valori assoluti. I tassi di scorrimento calcolati geodeticamente sono stati anche confrontati con quelli presenti in letteratura (ove disponibili) e generalmente ottenuti con metodi geologici (paleosismologia e morfotettonica). Il confronto mostra che i valori sono ragionevoli e hanno lo stesso ordine di grandezza. Valori dei tassi di scorrimento geodetico talvolta inferiori di quelli 'geologici' possono essere spiegati con il fatto che le stazioni GPS campionano un periodo molto breve del ciclo sismico, mentre l'accumulo della deformazione non è necessariamente lineare con il tempo. Pertanto, potrebbe essere sbagliato dedurre che il suo tasso è costante. E' importante infine ricordare che l'approccio utilizzato permette di calcolare anche la direzione di movimento sul piano di faglia (rake).

La completezza di GreDaSS per la Grecia Settentrionale, tra cui tutte le sorgenti sismogeniche finora note, ha permesso di suddividere l'area di indagine in cinque settori

caratterizzati da un comportamento interno relativamente uniforme. La distribuzione, la geometria e l'assetto geodinamico di alcune regioni implicano la presenza di faglie normali e basso angolo (scollamenti) che definiscono volumi sismogenici dove il comportamento delle faglie può cambiare in modo significativo (interazione fra faglie, percorso di rottura casuale, ecc.). Tuttavia, al di là di queste osservazioni qualitative, il database è in grado di offrire numerose altre applicazioni, specialmente per il miglioramento della SHA. Due esempi sono stati brevemente investigati nell'ambito di questa tesi. Il primo riguarda il miglioramento della zonazione sismica della Grecia con l'introduzione di una nuova mappa. Fino ad ora, infatti, la zonazione sismica della Grecia era basata solo su dati sismologici. Tale metodo, però, produce una serie di incongruenze con le principali caratteristiche sismotettoniche della regione Egea. La mappa di zonazione sismogenica proposta in questa tesi, seppur preliminare, si basa invece su criteri geologici e soprattutto sulle sorgenti sismogeniche incluse nel GreDaSS. La soluzione ideale sarebbe una mappa che tenga conto sia dei criteri geologici che sismologici. L'esempio per una possibile seconda applicazione riguarda gli scenari di riattivazione di faglie a causa di terremoti vicini e si basa sul *trasferimento di sforzo di Coulomb* (*Coulomb failure function* - CFF). Le due sorgenti sismogeniche individuali di Volos e di Nea Anchialos nel Golfo Pagasitikos, entrambe incluse in GreDaSS, sono state selezionate come caso di studio. Ogni faglia è responsabile di una delle due scosse maggiori avvenute durante la sequenza sismica di Volos del 1980. Il cambiamento del campo di sforzi ricavato dalla CFF e considerando le suddette sorgenti sismogeniche supporta l'ipotesi che il secondo evento sismico sia stato scatenato dal primo.

In sintesi, lo sviluppo e lo stato dell'arte di GreDaSS per la Grecia Settentrionale sono presentati in questo lavoro di tesi di dottorato, insieme al calcolo di due parametri sismotettonici di base, l'osservazione di alcune caratteristiche sismotettoniche e l'utilizzo del database come strumento di SHA. E' importante ricordare, però, che il database è continuamente aggiornabile, il che significa che ogni volta che nuovi dati e informazioni saranno disponibili potranno essere inclusi in GreDaSS.

7.3 Σύνοψη

Ο Ελλαδικός και ο ευρύτερος Αιγιακός χώρος ανήκουν στις πιο τεκτονικά και σεισμικά ενεργές περιοχές παγκοσμίως, με αποτέλεσμα να συναντάται μια πληθώρα ενεργών τεκτονικών δομών από τις οποίες κάποιες έχουν μελετηθεί ενδελεχώς, κάποιες λιγότερο, ενώ κάποιες άλλες παραμένουν ακόμα ανεξερεύνητες. Αυτό έχει ως αποτέλεσμα την ύπαρξη μιας μεγάλης ποικιλίας δεδομένων από διάφορες έρευνες, τόσο σε ποσότητα όσο και σε ποιότητα, τα οποία είναι είτε διάχυτα ή κρυμμένα μέσα στην πολυάριθμη βιβλιογραφία. Η ανομοιογένεια αυτή κάνει την ανεύρεση πληροφοριών, μια δύσκολη και χρονοβόρο διαδικασία, με αποτέλεσμα η δημιουργία μιας βάσης δεδομένων να φαίνεται αναγκαία. Μία τέτοιου είδους βάση δεν είναι χρήσιμη μόνο για επιστημονικούς σκοπούς, όπως π.χ. για τη δημιουργία γεωδυναμικών μοντέλων ή την ερμηνεία της σεισμοτεκτονικής συμπεριφοράς διαφόρων περιοχών. Η εκτίμηση της σεισμικής επικινδυνότητας, η οποία και έχει άμεσο κοινωνικοοικονομικό αντίκτυπο, είναι μία ακόμη σημαντική έρευνα για την οποία μια βάση δεδομένων μπορεί να αποτελέσει αναπόσπαστο εργαλείο.

Κεντρικό θέμα της παρούσας έρευνας αποτελεί η δημιουργία της κύριας δομής και η συμπλήρωση της Ελληνικής Βάσης Δεδομένων Σεισμογενετικών Πηγών (GreDaSS) η οποία ξεκίνησε πιλοτικά πριν από λίγα χρόνια έχοντας τη Βόρεια Ελλάδα ως πρώτη περιοχή εφαρμογής (Sboras *et al.*, 2009a, 2009b, Pavlides *et al.*, 2010 και Sboras *et al.*, 2011). Η διαδικασία συμπλήρωσης της βάσης περιλαμβάνει αρκετά στάδια. Το πρώτο στάδιο αφορά την αναγνώριση της σεισμογενούς πηγής-ρήγματος και τη συλλογή των αντίστοιχων δεδομένων και πληροφοριών που σε πρώτη φάση περιορίζεται στη βιβλιογραφία. Έπειτα ακολουθεί η διαδικασία της παραμετροποίησης που περιλαμβάνει τη σύνθεση, κριτική ανάλυση και ομογενοποίηση του συλλεχθέντος υλικού ώστε να ορισθούν οι βασικές σεισμοτεκτονικές παράμετροι, να χαρτογραφηθεί και να σχεδιασθεί κάθε ρήγμα που χαρακτηρίζεται ως ενεργό σύμφωνα με τα τρισδιάστατα γεωμετρικά χαρακτηριστικά του και να συμπληρωθούν τα απαιτούμενα πεδία πληροφοριών (σχόλια, ανοιχτά ερωτήματα, περιλήψεις, εικόνες και βιβλιογραφικές αναφορές). Το τελικό στάδιο περιλαμβάνει την κατάλληλη επεξεργασία όλων των παραπάνω πληροφοριακών επιπέδων ώστε αυτά να συνδεθούν μεταξύ τους και να γίνουν διαδραστικά. Η παραπάνω διαδικασία ακολουθήθηκε για κάθε μία από τις 38 σύνθετες σεισμογενείς πηγές (CSSs) και τις 58 διακριτές σεισμογενείς πηγές (ISSs) που βρίσκονται στη περιοχή μελέτης. Ωστόσο, κάποια από τα παραπάνω στάδια καθώς και η συμπλήρωση κάποιων επιμέρους πληροφοριακών πεδίων που ανήκουν στις υπόλοιπες πηγές του ευρύτερου Αιγιακού χώρου (και κατά συνέπεια στο ευρωπαϊκό πρόγραμμα SHARE), παραλείφθηκαν.

Κατά τη διαδικασία της παραμετροποίησης τέθηκε το θέμα της αξιοπιστίας των εισαγόμενων δεδομένων (§1.5). Για το λόγο αυτό διακρίθηκαν δύο βασικές κατηγορίες δεδομένων προερχόμενα από αντίστοιχου είδους έρευνες. Η πρώτη κατηγορία (*single-event effects*) αφορά έρευνες που ασχολούνται αποκλειστικά με τις επιπτώσεις που προκαλούνται από συγκεκριμένες σεισμικές δραστηριοποιήσεις. Τέτοιες έρευνες αποτελούν κυρίως οι σεισμολογικές, καθώς επίσης και πιο πρόσφατες, τεχνολογικά ανεπτυγμένες, μέθοδοι, όπως π.χ. η τηλεπισκόπηση. Είναι προφανές ότι το χρονικό εύρος αυτών των ερευνών περιορίζεται στην πρόσφατα καταγεγραμμένη (ιστορική ή ενόργανη) σεισμική δραστηριότητα. Πολλές όμως σεισμογενείς πηγές στην Ελλάδα δε συνδέονται με πρόσφατη

δραστηριότητα, περίπτωση που ενέχει μεγαλύτερη επικινδυνότητα αν λάβουμε υπόψη ότι ο σεισμικός κύκλος μπορεί να εκτείνεται από μερικές εκατοντάδες έως μερικές χιλιάδες χρόνια και επομένως ένα προσφάτως ενεργοποιημένο ρήγμα θα επαναδραστηριοποιηθεί πολύ αργότερα. Τα δεδομένα, λοιπόν, που προέρχονται από έρευνες που μελετούν άμεσα ή έμμεσα τις τεκτονικές δομές οι οποίες παρουσιάζουν όλα τα χαρακτηριστικά ενός ενεργού ρήγματος αλλά δεν συνδέονται με συγκεκριμένη σεισμική δραστηριότητα, ανήκουν στη δεύτερη κατηγορία (*cumulative effects*). Όπως προαναφέρθηκε, τα δεδομένα αυτά μπορεί να συνδέονται άμεσα με ένα ενεργό ρήγμα και μπορεί να προέρχονται π.χ. από υπαίθριες μετρήσεις, ποσοτικές τεκτονικές και μορφοτεκτονικές αναλύσεις, γεωφυσικές διασκοπήσεις κ.α., ή έμμεσα, όπως π.χ. από την τοπική μικροσεισμικότητα. Η σύγκριση των δύο κατηγοριών βασίζεται στη μελέτη τεσσάρων χαρακτηριστικών περιπτώσεων οι οποίες όλες περιλαμβάνουν από έναν ισχυρό σεισμό, καλύπτοντας μια ευρεία περίοδο της ιστορικής και ενόργανης καταγραφής (§6.2). Τα συμπεράσματα δείχνουν ότι α) οι έρευνες που ανήκουν στην πρώτη κατηγορία προσφέρουν δεδομένα που γίνονται όλο και πιο αξιόπιστα με την πάροδο του χρόνου και την εξέλιξη της τεχνολογίας, και β) οι έρευνες που ανήκουν στη δεύτερη κατηγορία δίνουν διαχρονικά σταθερά αξιόπιστα δεδομένα, ανεξαρτήτως αν το ρήγμα συνδέεται ή όχι με καταγεγραμμένο σεισμό. Άρα, η χρήση των δεδομένων της δεύτερης κατηγορίας μπορούν να χρησιμοποιηθούν με μεγάλο βαθμό εμπιστοσύνης στο GreDaSS.

Κατά τη διαδικασία της παραμετροποίησης διαπιστώθηκε ότι δύο βασικοί παράμετροι απουσιάζουν συστηματικά ή συναντώνται σπάνια στη σχετική βιβλιογραφία. Ο προσδιορισμός των δύο αυτών παραμέτρων, του μέγιστου βάθους των ρηγμάτων (κεφ. 3) και του ρυθμού ολίσθησης (κεφ. 4), είναι σημαντικός για την εκτίμηση της σεισμικής επικινδυνότητας, γιατί π.χ. μπορούν να καθοριστούν οι διαστάσεις ενός ρήγματος και κατά συνέπεια το μέγιστο αναμενόμενο μέγεθος ενός μελλοντικού σεισμού. Για τα ρήγματα του φλοιού, το μέγιστο βάθος ενός ρήγματος περιορίζεται εντός του σεισμογενούς στρώματος του οποίου η βάση αντιπροσωπεύεται από το όριο θραυσιγενούς-πλαστικής συμπεριφοράς. Αν και δεν είναι απαραίτητο ένα ρήγμα να διαρρηγνύει όλο το πάχος του σεισμογενούς στρώματος, η εκτίμηση του ορίου θραυσιγενούς-πλαστικής συμπεριφοράς θέτει το μέγιστο βάθος στο οποίο το ρήγμα μπορεί να διαρρηχθεί. Η εκτίμηση του ορίου βασίζεται στον υπολογισμό της μηχανικής αντοχής της ανώτερης λιθόσφαιρας που επιτυγχάνεται με τον υπολογισμό των ρεολογικών προφίλ. Στην παρούσα διατριβή συγκρίθηκαν τα ρεολογικά μοντέλα τριών διαφορετικών περιοχών βάσει της τοπικής χωρικής σεισμικής κατανομής της κάθε περιοχής. Από τη στιγμή που η θερμοκρασία επηρεάζει άμεσα την αντοχή της λιθόσφαιρας, ο υπολογισμός της γεωθερμικής βαθμίδας υπήρξε απαραίτητος. Ωστόσο, στον θερμικά ραδιογενή φλοιό, η γεωθερμική βαθμίδα εξαρτάται από διάφορες θερμοφυσικές παραμέτρους. Γι' αυτό το λόγο πραγματοποιήθηκε μια σειρά από ελέγχους ευαισθησίας της θερμοκρασίας ως προς την θερμική αγωγιμότητα και παραγωγικότητα των πετρωμάτων που συνθέτουν τον ανώτερο και κατώτερο φλοιό, για δύο ακραίες τιμές της επιφανειακής θερμικής ροής που συναντώνται στον αιγιακό χώρο. Με αυτό τον τρόπο επιτεύχθηκε ο διαχωρισμός του φλοιού, σύμφωνα με τις θερμικές του συνθήκες, σε ψυχρό και θερμό. Από τα αποτελέσματα των ρεολογικών προφίλ που υπολογίστηκαν σε τρεις πειραματικές περιοχές, την περιοχή της Κοζάνης-Γρεβενών, την κεντρική περιοχή της Μυγδονίας λεκάνης και της Νότιας Θεσσαλίας, συγκρίθηκαν με την χωροκατανομή της τοπικής σεισμικότητας. Από τη σύγκριση προκύπτει ότι τα ρεολογικά προφίλ και η σεισμική χωροκατανομή είναι

απολύτως συμβατά, επιβεβαιώνοντας την ορθότητα των ρεολογικών μοντέλων και δίνοντας την απαραίτητη ασφάλεια για τη μελλοντική χρήση της μεθόδου σε γειτονικές περιοχές όπου τοπικές σεισμικές μελέτες απουσιάζουν.

Ο υπολογισμός του ρυθμού ολίσθησης βασίζεται στο γεωδαιτικό πεδίο κατανομής του ρυθμού παραμόρφωσης που προέρχεται από πολυετείς μετρήσεις σταθμών GPS. Είναι εμφανές ότι αφού οι μετρήσεις GPS καλύπτουν χρονικά μερικές μόνο δεκαετίες, η μέθοδος που εφαρμόστηκε στην παρούσα διατριβή αφορά τον υπολογισμό του βραχυπρόθεσμου ρυθμού ολίσθησης. Η θεωρητική προσέγγιση της μεθόδου βασίζεται στο γεγονός ότι η παραμόρφωση που συντελείται μεταξύ δύο σταθμών, οι οποίοι μετατοπίζονται σχετικά ο ένας ως προς τον άλλο, δεν κατανέμεται ομοιόμορφα, αλλά συγκεντρώνεται σε μια ζώνη που περικλείει την επιφάνεια του ρήγματος. Κατά τη διάρκεια ενός σεισμού, το μεγαλύτερο ποσοστό της έως τότε συσσωρευμένης ελαστικής παραμόρφωσης, απελευθερώνεται απότομα επί του ρήγματος ως ολίσθηση, αφήνοντας ένα σχεδόν αμελητέο ποσοστό να παραμείνει ως πλαστική παραμόρφωση. Η διαδικασία υπολογισμού βασίζεται στις θεμελιώδεις εξισώσεις της παραμόρφωσης από τις οποίες προκύπτουν η παράλληλη προς την παράταξη του ρήγματος συνιστώσα ολίσθησης και η οριζόντια, κατά τη διεύθυνση του ρήγματος, συνιστώσα ολίσθησης, από την οποία προκύπτει η παράλληλη προς την βύθιση του ρήγματος συνιστώσα (σχ. 4.5). Τα αρχικά δεδομένα προέρχονται από τρεις ομάδες που περιέχουν είτε τους βασικούς άξονες παραμόρφωσης ή την εφελκυστική (εκτατική) και μέγιστη διατμητική παραμόρφωση. Οι χαρτογραφικές απεικονίσεις των τριών αποτελεσμάτων (σχ. 4.6) δείχνουν ότι και τα τρία έχουν παρόμοια διάταξη και κατανομή, διαφέροντας ωστόσο ως προς τις απόλυτες τιμές τους. Επίσης, τα αποτελέσματα των γεωδαιτικά υπολογισμένων ρυθμών ολίσθησης συγκρίθηκαν με τους προτεινόμενους, από την υπάρχουσα βιβλιογραφία, ρυθμούς ολίσθησης οι οποίοι προέρχονται κυρίως από γεωλογικές μεθόδους (πιν. 4.1 και 4.2). Η σύγκριση δείχνει πως οι πρώτοι δεν έχουν απλά και μόνο λογικές τιμές, αλλά βρίσκονται και στην ίδια τάξη μεγέθους με τους δεύτερους. Οι συνήθως χαμηλότερες τιμές των υπολογισθέντων ρυθμών ολίσθησης μπορούν να εξηγηθούν από το γεγονός ότι οι σταθμοί GPS μετρούν τις ταχύτητες μιας μικρής χρονικής περιόδου του σεισμικού κύκλου, καθώς και ότι η συσσώρευση της παραμόρφωσης δεν σημαίνει πως είναι γραμμική σε συνάρτηση με τον χρόνο οπότε και θα ήταν λάθος να υποθέσουμε ότι ο ρυθμός της είναι σταθερός. Είναι σημαντικό να αναφερθεί ότι από την διαδικασία υπολογισμού του ρυθμού ολίσθησης προέκυψε επίσης και ο υπολογισμός της γωνίας ολίσθησης.

Η ολοκλήρωση του GreDaSS για τη Βόρεια Ελλάδα, που περιλαμβάνει όλες τις γνωστές μέχρι σήμερα σεισμικές πηγές, επέτρεψε το διαχωρισμό της περιοχής σε πέντε τομείς (σχ. 5.1), το εσωτερικό των οποίων χαρακτηρίζεται από μία ομοιόμορφη σεισμοτεκτονική συμπεριφορά (§6.1). Επιπλέον, η μορφή, η γεωμετρία και το γεωδυναμικό καθεστώς κάποιων περιοχών, υποδηλώνουν την πιθανή ύπαρξη ρηγμάτων αποχωρισμού που οριοθετούν σεισμογενείς όγκους, εντός των οποίων η ρηξιγενής συμπεριφορά μπορεί να αλλάζει σημαντικά (αλληλεπίδραση ρηγμάτων, τυχαία διαδρομή διάρρηξης, κλπ., §6.1). Πέρα όμως από τις ποιοτικές παρατηρήσεις, η βάση δεδομένων μπορεί να προσφερθεί και ως εργαλείο για ποικίλες εφαρμογές, όπως η συμβολή στον προσδιορισμό της σεισμικής επικινδυνότητας. Δύο επιμέρους εφαρμογές δίνονται ως παραδείγματα στα πλαίσια της παρούσας διατριβής (§6.3). Η πρώτη εφαρμογή αφορά τη βελτίωση του χάρτη σεισμικών

ζωνών της Ελλάδος συστήνοντας έναν νέο χάρτη σεισμογενών ζωνών. Μέχρι σήμερα η σεισμική ζώνωση της Ελλάδος βασιζόταν αποκλειστικά και μόνο σε σεισμολογικά δεδομένα. Η μέθοδος όμως αυτή προκαλεί ανακολουθίες και ασυμβατότητες με σημαντικές ενεργά τεκτονικές δομές. Ο προτεινόμενος χάρτης σεισμογενών ζωνών της διατριβής αυτής βασίζεται κυρίως σε γεωλογικά κριτήρια και ειδικότερα στις σεισμογενείς πηγές του GreDaSS. Παρά ταύτα, τη καλύτερη λύση για τη δημιουργία τέτοιων χαρτών αποτελεί ο συνδυασμός τόσο των γεωλογικών όσο και των σεισμικών κριτηρίων. Η δεύτερη εφαρμογή αφορά τα σενάρια ρηξιγενούς διαδραστικότητας (ή αλλιώς αλληλεπίδρασης) όπως αυτά μελετούνται από τη μεταβολή τάσης του Coulomb. Τα ρήγματα του Βόλου και της Νέας Αγχιάλου που βρίσκονται στον Παγασητικό Κόλπο επιλέχθηκαν ως τυπικό παράδειγμα. Τα δύο αυτά ρήγματα ευθύνονται για τις δυο ισχυρότερες σεισμικές δονήσεις της σεισμικής ακολουθίας του Βόλου που συνέβη το 1980. Οι παράμετροι των μοντέλων που μελετούν την αλλαγή της τάσης κατά Coulomb μπορούν εύκολα να εισαχθούν βασιζόμενοι στις σεισμικές πηγές του GreDaSS. Κατά την μοντελοποίηση προκύπτει ότι η αλληλεπίδραση μεταξύ των δύο ρηγμάτων του παραδείγματος είναι ένα πιθανό σενάριο.

Εν κατακλείδι, η εκπόνηση της παρούσας διατριβής περιλαμβάνει το ξεκίνημα, την εξέλιξη και τη παρουσίαση της πιο πρόσφατης εκδοχής της βάσης δεδομένων GreDaSS για την Βόρεια Ελλάδα. Κατά τη διάρκεια της παραμετροποίησης υπολογίστηκαν επίσης οι δύο βασικές σεισμοτεκτονικές παράμετροι του μεγίστου βάθους και του ρυθμού ολίσθησης των ρηγμάτων. Μετά την ολοκλήρωση της βάσης έγιναν εφικτές ποιοτικές παρατηρήσεις επί των σεισμοτεκτονικών χαρακτηριστικών των ρηγμάτων και της κατανομής τους στο χώρο. Επίσης, η βάση χρησιμοποιήθηκε πειραματικά σε εφαρμογές που εξυπηρετούν την εκτίμηση της σεισμικής επικινδυνότητας, όπως η δημιουργία των σεισμογενών ζωνών και η υπόθεση της αλληλεπίδρασης ρηξιγενών τμημάτων στην περιοχή του Παγασητικού Κόλπου. Είναι σημαντικό όμως να αναφερθεί πως η βάση είναι πάντα ανοιχτή και αναβαθμίσιμη, που σημαίνει πως η εκάστοτε εμφάνιση νέων στοιχείων θα λαμβάνεται πάντα υπόψη και τα νέα δεδομένα θα είναι πάντα στη διάθεση του GreDaSS για τη συνεχή βελτίωση του.

References

A

- Afonso J.C. and Ranalli G. (2004): Crustal and mantle strengths in continental lithosphere: is the jelly sandwich obsolete? *Tectonophysics*, **394**, 221-232.
- Aki K. (1966): Generation and propagation of G-waves from the Niigata earthquake of June 16, 1964. 2. Estimation of earthquake movement, released energy and stress-strain drop from G spectrum. *Bull. Earthq. Res. Inst.*, **44**, 23-88.
- Aksoy M.E., Meghraoui M., Vallée M. and Çakır Z. (2010): Rupture characteristics of the A.D. 1912 Mürefte (Ganos) earthquake segment of the North Anatolian fault (western Turkey). *Geology*, **38**(11), 991-994.
- Albaric J., Déverchère J, Petit C., Perrot J. and Le Gall B. (2009): Crustal rheology and depth distribution of earthquakes: Insights from the central and southern East African Rift System. *Tectonophysics*, **468**, 28-41.
- Aldersons F., Ben-Avraham Z., Hofstetter A., Kissling E. and Al-Yazjeen T. (2003): Lower-crustal strength under the Dead Sea basin from local earthquake data and rheological modeling. *Earth Planet. Sci. Lett.*, **214**(1-2), 129-142.
- Alessandrini B., Beranzoli L., Drakatos G., Falcone C., Karantonis G., Mele F.M. and Stavrakakis G.N. (1997): Tomographic image of the crust and uppermost mantle of the Ionian and Aegean regions. *Ann. Geofisica*, **40**(1), 151-160.
- Allis R.G. (1979): A heat production model for stable continental crust. *Tectonophysics*, **57**, 151-165.
- Altunel E., Meghraoui M., Akyüz H.S. and Dikbas A. (2004): Characteristics of the 1912 co-seismic rupture along the North Anatolian Fault Zone (Turkey): implications for the expected Marmara earthquake. *Terra Nova*, **16**, 198-204.
- Ambraseys N.N. (1999): Early earthquakes in the Kozani area, northern Greece. *Tectonophysics*, **308**, 291-298.
- Ambraseys N.N. (2001): Reassessment of earthquakes, 1900-1999, in the Eastern Mediterranean and the Middle East. *Geophys. J. Int.*, **145**, 471-485.
- Ambraseys N. (2002): The Seismic Activity of the Marmara Sea Region over the Last 2000 Years. *Bull. Seism. Soc. Am.*, **92**, 1-18.
- Ambraseys N. (2009): *Earthquakes in the Mediterranean and Middle East: A Multidisciplinary Study of Seismicity up to 1900*. Cambridge University Press, Cambridge, 968 pp.
- Ambraseys N.N. and Finkel C.F. (1987): The Saros-Marmara earthquake of 9 August 1912. *Earthq. Eng. Struct. Dyn.*, **15**, 189-211.
- Ambraseys N.N. and Jackson J.A. (1990): Seismicity and associated strain of central Greece between 1890 and 1988. *Geophys. J. Int.*, **101**, 663-708.

- Ambraseys N.N. and Jackson J.A. (1997): Seismicity and strain in the Gulf of Corinth (Greece) since 1694. *J. Earthq. Eng.*, **1**(3), 433-474.
- Ambraseys N.N. and Jackson J.A. (1998): Faulting associated with historical and recent earthquakes in the Eastern Mediterranean region. *Geophys. J. Int.*, **133**, 390-406.
- Anderson H. and Jackson J. (1987): Active tectonics of the Adriatic Region. *Geophys. J. R. astr. Soc.*, **91**, 937-983.
- Angelier J. (1979): Recent Quaternary tectonics in the Hellenic arc: examples of geological observations on land. *Tectonophysics*, **52**, 267-275.
- Angelier J., Lyberis N., Le Pichon X., Barrier E. and Huchon P. (1982): The tectonic development of the Hellenic arc and the Sea of Crete: a synthesis. *Tectonophysics*, **86**, 159-196.
- Armijo R., Meyer B., Hubert A. and Barka A. (1999): Westward propagation of the North Anatolian fault into the northern Aegean: Timing and kinematics. *Geology*, **27**, 267-270.
- Armijo R., Flerit F., King G. and Meyer B. (2003): Linear elastic fracture mechanics explains the past and present evolution of the Aegean. *Earth Planet. Sci. Lett.*, **217**, 85-95.
- Arndt J., Bartel T., Scheuber E. and Schilling F. (1997): Thermal and rheological properties of granodioritic rocks from the Central Andes, North Chile. *Tectonophysics*, **271**, 75-88.
- Artemieva I.M. (2006): Global $1^{\circ} \times 1^{\circ}$ thermal model TC1 for the continental lithosphere: Implications for lithosphere secular evolution. *Tectonophysics*, **416**, 245-277.
- Artemieva I.M. and Mooney W.D. (2001): Thermal thickness and evolution of Precambrian lithosphere: A global study. *J. Geophys. Res.*, **106**(B8), 16387-16414.
- Ashwal L.D., Morgan P., Kelley S.A. and Percival J.A. (1987): Heat production in an Archean crustal profile and implications for heat flow and mobilization of heat-producing elements. *Earth Planet. Sci. Lett.*, **85**, 439-450.
- Atzemoglou A., Tsourlos P. and Pavlides S. (2003): Investigation of the Tectonic Structure of the NW Part of the Amynteon Basin (NW Greece) by means of a Vertical Electrical Sounding (VES) survey. *J. Balkan Geophys. Soc.*, **6**(4), 188-201.
- Aubouin J. (1959): Contribution à l'étude de la Grèce septentrionale; les confins de l'Épire et de la Thessalie. *Ann. Géol. Pays Helléniques*, **10**, 1-483.
- B**
- Baker C., Hatzfeld D., Lyon-Caen H., Papadimitriou E. and Rigo A. (1997): Earthquake mechanisms of the Adriatic Sea and western Greece. *Geophys. J. Int.*, **131**, 559-594.
- Bamler R. (1999): The SRTM Mission: A World-Wide 30 m Resolution DEM from SAR Interferometry in 11 days. In: Fritsch D. and Spiller R. (Eds.), *Photogrammetric Week '99*, Wichmann Verlag, Heidelberg, 1999.
- Barker C. (1996): *Thermal Modeling of Petroleum Generation: Theory and Applications*. Elsevier, Amsterdam.
- Barker J. S. and Langston C.A. (1981): Inversion of teleseismic body waves for the moment tensor of the 1978 Thessaloniki, Greece, earthquake. *Bull. Seism. Soc. Am.*, **71**, 1423-1444.
- Barnett J.A.M., Mortimer J., Rippon J.H., Walsh J.J. and Watterson J. (1987): Displacement geometry in the volume containing a single normal fault. *Am. Assoc. Petr. Geol. Bull.*, **71**, 925-937.
- Basili R. (2006): Fault Studio 1.2: A MapBasic application.

- Basili R., Valensise G., Vannoli P., Burrato P., Fracassi U., Mariano S., Tiberti M.M., Boschi E. (2008): The database of individual seismogenic sources (DISS), version 3: summarizing 20 years of research on Italy's Earthquake Geology. *Tectonophysics*, **453**(1-4), 20-43.
- Basili R., Kastelic V., Valensise G. and DISS Working Group 2009 (2009): DISS3 tutorial series: Guidelines for compiling records of the database of individual seismogenic sources, version 3. INGV, *Rapporti Tecnici*, **108**, 16 pp.
- Basili R., Garcia Moreno D., Kastelic V., Nemser E., Petricca P., Sboras S. and Valensise G. (2010): Developing seismogenic source models based on geologic fault data in the Euro-Mediterranean area: SHARE mission accomplished? 32nd Assembly of the European Seismological Commission, September 6-10, 2010, Montpellier, France, *Abstracts*, 86 pp.
- Beardmore G.R. and Cull J.P. (2001): *Crustal Heat Flow: A Guide to Measurement and Modelling*. Cambridge University Press, New York, 324 pp.
- Becker J.J., Sandwell D.T., Smith W.H.F., Braud J., Binder B., Depner J., Fabre D., Factor J., Ingalls S., Kim S-H., Ladner R., Marks K., Nelson S., Pharaoh A., Trimmer R., Von Rosenberg J., Wallace G. and Weatherall P. (2009): Global Bathymetry and Elevation Data at 30 Arc Seconds Resolution: SRTM30_PLUS, *Mar. Geod.*, **32**(4), 355-371.
- Bell R.E., McNeill L.C, Bull J.M. and Henstock T.J. (2008): Evolution of the offshore western Gulf of Corinth. *Bull. Geol. Soc. Am.*, **120**, 156-178.
- Benedicto A., Schultz R.A. and Soliva R. (2003): Layer thickness and the shape of faults. *Geophys. Res. Lett.*, **30**(20), 2076.
- Bernard P., Briole P., Meyer B., Lyon-Caen H., Gomez J.-M., Tiberi C., Berge C., Cattin R., Hatzfeld D., Lachet C., Lebrun B., Deschamps A., Courboux F., Larroque C., Rigo A., Massonnet D., Papadimitriou P., Kassaras J., Diagourtas D., Makropoulos K., Veis G., Papazisi E., Mitsakaki C., Karakostas V., Papadimitriou E., Papanastassiou D., Chouliaras G. and Stavrakakis G. (1997): The $M_s = 6.2$, June 15, 1995, Aigion earthquake (Greece): evidence for low angle normal faulting in the Corinth rift. *J. Seismol.*, **1**, 131-150.
- Birch F. and Clark H. (1940): The thermal conductivity of rocks and its dependence upon temperature and composition. *Am. J. Sci.*, **238** (8), 529-558.
- Birch F., Roy R.F. and Decker E.R. (1968): Heat flow and thermal history in New England and New York. In: Zen E., White W.S., Hadley J.B. and Thompson J.B. Jr. (Eds.), *Studies of Appalachian Geology: Northern and Maritime*. Interscience Publishers, New York, 437-451.
- Boccaletti M., Manetti P. and Peccerillo A. (1974): The Balkanids as an Instance of Back-Arc Thrust Belt: Possible Relation with the Hellenids. *Bull. Geol. Soc. Am.*, **85**, 1077-1084.
- Boccaletti M., Caputo R., Mountrakis D., Pavlides S. and Zouros N. (1997): Paleoseismicity of the Souli Fault, Epirus, Western Greece, *J. Geodyn.*, **24**(1-4), pp. 117-127.
- Boettcher A.L. (1973): Volcanism and orogenic belts - the origin of andesites. *Tectonophysics*, **17**(3), 223-240.
- Boncio P. (2008): Deep-crust strike-slip earthquake faulting in southern Italy aided by high fluid pressure: insights from rheological analysis. In: Wibberley C.A.J., Kurz W., Imber J., Holdsworth R.E. and Collettini C. (Eds.), *The Internal Structure of Fault Zones: Implications for Mechanical and Fluid-Flow Properties*. *Geol. Soc. London, Spec. Publ.*, **299**, 195-210.
- Boncio P., Mancini T., Lavecchia G. and Selvaggi G. (2007): Seismotectonics of strike-slip earthquakes within the deep crust of southern Italy: Geometry, kinematics, stress field and

- crustal rheology of the Potenza 1990-1991 seismic sequences (M_{\max} 5.7). *Tectonophysics*, **445**, 281-300.
- Bonev N. and Beccaletto L. (2007): From syn- to post-orogenic Tertiary extension in the north Aegean region: constraints on the kinematics in the eastern Rhodope-Thrace, Bulgaria-Greece and the Biga Peninsula, NW Turkey. *In*: Taymaz, T., Yilmaz, Y. and Dilek, Y. (Eds.), *The Geodynamics of the Aegean and Anatolia. Geol. Soc. London Spec. Publ.*, **291**, 113-142.
- Bortolotti V. and Principi G. (2005): Tethyan ophiolites and Pangea break-up. *The Island Arc*, **14**, 442-470.
- Bourouis S. and Cornet F.H. (2009): Microseismic activity and fluid fault interactions: some results from the Corinth Rift Laboratory (CRL), Greece. *Geophys. J. Int.*, **178**(1), 561-580.
- Bourova E., Kassaras I., Pedersen H.A., Yanovskaya T., Hatzfeld D. and Kirtazi A. (2005): Constraints on absolute S velocities beneath the Aegean Sea from surface wave analysis. *Geophys. J. Int.*, **160**, 1006-1019.
- Brace W.E. and Kohlstedt D. (1980): Limits on lithospheric stress imposed by laboratory experiments. *J. Geophys. Res.*, **85**, 6248-6252.
- Brooks M. and Ferentinos G. (1980): Structure and evolution of the Sporadhes basin of the North Aegean trough. *Tectonophysics*, **68**, 15-30.
- Brooks M. and Williams G.D. (1982): Extensional tectonics in Neogene and Quaternary sequences at the western margin of the Axios basin, northern Greece. *J. Geol. Soc. London*, **139**, 293-297.
- Brun J.-P. and Sokoutis D. (2007): Kinematics of the Southern Rhodope Core Complex (North Greece). *Int. J. Earth Sci. (Geol. Rundsch.)*, **96**, 1079-1099.
- Brunn J.H. (1956): Contribution à l'étude géologique du Pinde septentrional et d'une partie de la Macédonie occidentale. *Ann. Géol. Pays Helléniques*, **7**, 1-358.
- Burov E.B. (2010): The equivalent elastic thickness (T_e), seismicity and the long-term rheology of continental lithosphere: Time to burn-out "crème brûlée"? Insights from large-scale geodynamic modeling. *Tectonophysics*, **484**, 4-26.
- Burov E.B. and Diament M. (1992): Flexure of the continental lithosphere with multilayer rheology. *Geophys. J. Int.*, **109**, 449-468.
- Burov E.B. and Watts A.B. (2006): The long-term strength of continental lithosphere: "jelly sandwich" or "crème brûlée"? *GSA Today*, **16**(1), 4-10.
- C**
- Çagatay M.N., Görür N., Alpar B., Saatçılar R., Akkök R., Sakiñç M., Yüce H., Yaltirak C. and Kuscu I. (1998): Geological evolution of the Gulf of Saros, NE Aegean Sea. *Geo-Mar. Lett.*, **18**, 1-9.
- Calcagnile G. and Panza G.F. (1990): Crustal and upper mantle structure of the Mediterranean area derived from surface-wave data. *Phys. Earth Planet. Inter.*, **60**, 163-168.
- Calcagnile G., D'Ingeo F., Farrugia P. and Panza G.F. (1982): The lithosphere in the Central-eastern Mediterranean area. *Pure Appl. Geophys.*, **120**, 389-406.
- Caporali A., Aichhorn C., Barlik M., Becker M., Fejes I., Gerhatova L., Ghitau D., Grenerczy G., Hefty J., Krauss S., Medak D., Milev G., Mojzes M., Mulic M., Nardo A., Pesec P., Rus T., Simek J., Sledzinski J., Solaric M., Stangl G., Stopar B., Vespe F. and Virag G. (2009): Surface kinematics in the Alpine-Carpathian-Dinaric and Balkan region inferred from a new multi-network GPS combination solution. *Tectonophysics*, **474**, 295-321.

- Caputo M., Panza G.F. and Postpischil D. (1970): Deep structure of the Mediterranean Basin. *J. Geophys. Res.*, **75**, 4919-4923.
- Caputo R. (1984): *Geologia della zona trascorrente di Corfu (Grecia)*. Thesis, Univ. Ferrara, pp.130, unpublished.
- Caputo R. (1986): Analisi mesostrutturale lungo un settore della Linea di Corfu. *Boll. Soc. Geol. It.*, **105**(3/4), 297-305.
- Caputo R. (1987/88): The Neogenic dextral trascurrent system of Corfu (Central Mediterranean). *Ann. Geol. Pays Helleniques*, **33**, 327-335.
- Caputo R. (1990): Geological and structural study of the recent and active brittle deformation of the Neogene-Quaternary basins of Thessaly (Greece). *Scientific Annals*, **12**, Aristotle University of Thessaloniki, 2 vol., 5 encl., 252 pp.
- Caputo R. (1993a): Morphotectonics and kinematics of the Tyrnavos Fault, northern Larissa plain, Greece. *Z. Geomorph. N. E.*, **94**, 167-185.
- Caputo R. (1993b): The Rodia fault system: an active complex shear zone (Larissa plain, Central Greece). *Bull. Geol. Soc. Greece*, **28**(1), 447-456.
- Caputo R. (1995): Inference of a seismic gap from geological data: Thessaly (Central Greece) as a case study. *Ann. Geofisica*, **38**, 1-19.
- Caputo R. (1996): The active Nea Anchialos Fault System (Central Greece): comparison of geological, morphotectonic, archaeological and seismological data. *Ann. Geofisica*, **39**(3), 557-574.
- Caputo R. (2005): Ground effects of large morphogenic earthquakes. *J. Geodyn.*, **40**, 2-3, 113-118.
- Caputo R. and Helly B. (2000): Archéosismicité de l'Égée: étude des failles actives de la Thessalie. *Bull. Corresp. Hell.*, **124**(2), 560-588.
- Caputo R. and Helly B. (2005a): Archaeological evidences of past earthquakes: a contribution to the SHA of Thessaly, Central Greece. *J. Earthq. Eng.*, **9**(2), 199-222.
- Caputo R. and Helly B. (2005b): The Holocene activity of the Rodia Fault, Central Greece. *J. Geodyn.*, **40**(2-3), 153-169.
- Caputo R. and Helly B. (2007): The European Palaeoseismological Museum of Tyrnavos, Central Greece. EGU General Assembly, Vienna, April 16-20, 2007, *Geophysical Research Abstracts*, **9**, 00283.
- Caputo R. and Helly B. (2008): The use of distinct disciplines to investigate past earthquakes. *Tectonophysics*, **453**(1-4), 7-19.
- Caputo R. and Pavlides S. (1991): Neotectonics and structural evolution of Thessaly (Central Greece). *Bull. Geol. Soc. Greece*, **25**(3), 119-133.
- Caputo R. and Pavlides S. (1993): Late Cainozoic geodynamic evolution of Thessaly and surroundings (central-northern Greece). *Tectonophysics*, **223**, 339-362.
- Caputo R. and Zouros N. (1993): Examples of Alpidic deformation from Epirus: local anomalies or need to re-evaluate the amount of shortening in the Western Hellenides?, *Bull. Geol. Soc. Greece*, **28**(1), 315-326.
- Caputo R., Bravard J.-P. and Helly B. (1994): The Pliocene-Quaternary tecto-sedimentary evolution of the Larissa Plain (Eastern Thessaly, Greece). *Geodinamica Acta*, **7**(4), 219-231.

- Caputo R., Piscitelli S., Oliveto A., Rizzo E. and Lapenna V. (2003): The use of electrical resistivity tomography in Active Tectonic. Examples from the Tyrnavos Basin, Greece. *J. Geodyn.*, **36**(1-2), 19-35.
- Caputo R., Helly B., Pavlides S. and Papadopoulos G. (2004a): Palaeoseismological investigation of the Tyrnavos Fault (Thessaly, Central Greece). *Tectonophysics*, **394**, 1-20.
- Caputo R., Oliveto A. and Helly B. (2004b): Palaeoseismological researches along the Rodia Fault, Central Greece. 5th International Symposium on Eastern Mediterranean Geology, 14-20 April 2004, Thessaloniki, Greece, *Proceedings*, Ref: S2-6.
- Caputo R., Helly B. Pavlides S. and Papadopoulos G. (2006a): Archaeo- and palaeoseismological investigations in Northern Thessaly (Greece): Insights for the seismic potential of the region. *Nat. Hazards*, **39**, 195-212.
- Caputo R., Monaco C. and Tortorici L. (2006b): Multiseismic cycle deformation rates from Holocene normal fault scarps on Crete (Greece). *Terra Nova*, **18**, 181-190.
- Caputo R., Mucciarelli M. and Pavlides S. (2008): Magnitude distribution of linear morphogenic earthquakes in the Mediterranean region: insights from palaeoseismological and historical data. *Geophys. J. Int.*, **174**, 930-940.
- Caputo R., Catalano S., Monaco C., Romagnoli G., Tortorici G. and Tortorici L. (2010a): Active faulting on the island of Crete (Greece). *Geophys. J. Int.*, **183**, 111-126.
- Caputo R., Catalano S., Monaco C., Romagnoli G., Tortorici G. and Tortorici L. (2010b): Middle-Late Quaternary geodynamics of Crete, southern Aegean, and seismotectonic implications. *Bull. Geol. Soc. Greece*, **43**(1), 400-408.
- Carter N.L. and Tsenn M.C. (1987): Flow properties of continental lithosphere. *Tectonophysics*, **136**, 27-63.
- Carver D. and Bollinger G.A. (1981): Aftershocks of the June 20, 1978 Greece earthquake: a multimode faulting sequence. *Tectonophysics*, **73**, 343-363.
- Čermák V. (1982): Crustal temperature and mantle heat flow in Europe. *Tectonophysics*, **83**, 123-142.
- Čermák V. and Laštovičková M. (1987): Temperature Profiles in the Earth of Importance to Deep Electrical Conductivity Models. *Pure Appl. Geophys.*, **125**(2/3), 255-284.
- Čermák V., Bodri L. and Rybach L. (1991): Radioactive heat production in the Continental Crust and its depth dependence. In: Čermák V. and Rybach L. (Eds.), *Heat flow and lithospheric structure*. Springer, 23-69.
- Chang W.L. and Smith R.B. (2002): Integrated seismic-hazard analysis of the Wasatch Front, Utah. *Bull. Seism. Soc. Am.*, **92**(5), 1904-1922.
- Chapman D.S. (1986): Thermal gradients in the continental crust. In: Dawson J.B., Carswell D.A., Hall J. and Wedepohl K.H. (Eds.), *The Nature of the Lower Continental Crust*. *Geol. Soc. London Spec. Publ.*, **24**, 63-70.
- Chatzipetros A. (1998). *Paleoseismological and morphotectonic study of the active fault systems at Mygdonia basin, eastern Chalkidiki and Kozani-Grevena* [in Greek]. PhD Thesis, Aristotle University of Thessaloniki, Greece, 354 pp.
- Chatzipetros A. and Pavlides S. (2004): Geometry and kinematics of the Maronia-Makri active fault (Thrace, northeastern Greece). 4th National Geophysical Conference of the Bulgarian Geophysical Society, October 4-5, 2004, Sofia, Bulgaria, Session 1, 61-63.
- Chatzipetros A. and Pavlides S. (2009): A rare case of preserved earthquake ruptures in an archaeological site: Mikri Doxipara - Zoni, NE Greece. 1st INQUA-IGCP-567 International

- Workshop on Earthquake Archaeology and Palaeoseismology, September 7-13 2009, Baelo Claudia, Spain, *Abstract Volume*, 20-22.
- Chatzipetros A.A., Pavlides S.B. and Mountrakis D.M. (1998): Understanding the 13 May 1995 Western Macedonia earthquake: A paleoseismological approach. *J. Geodyn.*, **26**(2-4), 327-339.
- Chatzipetros A., Pavlides S. and Mourouzidou O. (2004): Re-evaluation of Holocene earthquake activity in Mygdonia basin, Greece, based on new paleoseismological results. 5th International Symposium on Eastern Mediterranean Geology, 14-20 April 2004, Thessaloniki, Greece, *Proceedings*, Ref: S2-15.
- Chatzipetros A., Kokkalas S., Pavlides S. and Koukouvelas I. (2005a): Palaeoseismic data and their implications for active deformation in Greece: *J. Geodyn.*, **40**(2-3), 170-188.
- Chatzipetros A., Michailidou A., Tsapanos Th. and Pavlides S. (2005b): Morphotectonics and seismotectonics of the Stratonii-Barbara and Gomati-Megali Panagia active fault (eastern Chalkidiki, Northern Greece). *Bull. Geol. Soc. Greece*, **37**, 127-142.
- Chen W.-P. and Molnar P. (1983): Focal depths of intracontinental and intraplate earthquakes and their implications for the thermal and mechanical properties of the lithosphere. *J. Geophys. Res.*, **88**, 4183-4214.
- Cheng S., Fang Z., Pavlides S. and Chatzipetros A. (1994): Preliminary study of paleoseismicity of the southern Langada-Volvi basin margin fault zone, Thessaloniki, Greece. *Bull. Geol. Soc. Greece*, **30**(1), 401-407.
- Chéry J. (2001): Core complex mechanics: From the Gulf of Corinth to the Snake Range, *Geology*, **29**, 439-442.
- Chiarabba C. and Selvaggi G. (1997): Structural control on fault geometry: example of the Grevena Ms 6.6, normal faulting earthquake. *J. Geophys. Res.*, **102**, 22445-22457.
- Childs C., Watterson J. and Walsh J.J. (1995): Fault overlap zones within developing normal fault systems. *J. Geol. Soc. London*, **152**, 535-549.
- Chopra P.N. and Paterson M.S. (1981): The experimental deformation of dunite. *Tectonophysics*, **78**, 453-473.
- Christensen N.I. and Mooney W.D. (1995): Seismic velocity structure and composition of the continental crust: A global view. *J. Geophys. Res.*, **100**(B7), 9761-9788.
- Christensen N.I. and Stanley D. (2003): Seismic Velocities and Densities of Rocks. In: Lee W.H.K., Kanamori H., Jennings P.C. and Kisslinger C. (Eds.), *International Handbook of Earthquake and Engineering Seismology. International Geophysics Series*, **81**(B), 1587-1594.
- Christodoulou A. and Hatzfeld D. (1988): Three-dimensional crustal and upper mantle structure beneath Chalkidiki (northern Greece). *Earth Planet. Sci. Lett.*, **88**, 153-168.
- Cianetti S., Tinti E., Giunchi C. and Cocco M. (2008): Modelling deformation rates in the western Gulf of Corinth: rheological constraints. *Geophys. J. Int.*, **174**, 749-757.
- Clarke P., Paradisis D., Briole P., England P., Parson B., Billiris H., Veis G. and Ruegg J.-C. (1997): Geodetic investigation of the 13 May 1995 Kozani-Grevena (Greece) earthquake. *Geophys. J. Int.*, **135**, 195-214.
- Clarke P.J., Davies R.R., England P.C., Parsons B., Billiris H., Paradisis D., Veis G., Cross P.A., Denys P.H., Ashkenazi V., Bingley R., Kahle H.-G., Müller M.V. and Briole P. (1998): Crustal strain in central Greece from repeated GPS measurements in the interval 1989-1997. *Geophys. J. Int.*, **135**(1), 195-214.

- Cloetingh S., van Wees J.D., Ziegler P.A., Lenkey L., Beekman F., Tesauro M., Förster A., Norden B., Kaban M., Hardebol N., Bonté D., Genter A., Guillou-Frottier L., Ter Voorde M., Sokoutis D., Willingshofer E., Cornu T. and Worum G. (2010): Lithosphere tectonics and thermo-mechanical properties: An integrated modelling approach for Enhanced Geothermal Systems exploration in Europe. *Earth-Sci. Reviews*, **102**, 159-206.
- Cocard M., Kahle H.-G., Peter Y., Geiger A., Veis G., Felekis S., Billiris H. and Paradissis D. (1999): New constraints on the rapid crustal motion of the Aegean region: recent results inferred from GPS measurements (1993–1998) across the West Hellenic Arc, Greece. *Earth Planet. Sci. Lett.*, **172**, 39-47.
- Conrad C.P. and Lithgow-Bertelloni C. (2006): Influence of continental roots and asthenosphere on plate-mantle coupling, *Geophys. Res. Lett.*, **33**, L05312.
- Coppersmith K.J. (1988): Temporal and spatial clustering of earthquake activity in the central and eastern United States. *Seism. Res. Lett.*, **59**(4), 299-304.
- Coskun B. (2000): North Anatolian Fault-Saros Gulf relationships and their relevance to hydrocarbon exploration, northern Aegean Sea, Turkey. *Mar. Petrol. Geol.*, **17**, 751-772.
- Cowie P.A. and Roberts G.P. (2001): Constraining slip rates and spacings for active normal faults. *J. Struct. Geol.*, **23**, 1901-1915.
- D**
- Davies J.H. and Bickle M.J. (1991): A physical model for the volume and composition of melt produced by hydrous fluxing above subduction zones. *Phil. Trans. R. Soc. Lond. A*, **335**, 355-364.
- Davis M.G., Chapman D.S., Van Wagoner T.M. and Armstrong P.A. (2007): Thermal conductivity anisotropy of metasedimentary and igneous rocks. *J. Geophys. Res.*, **112**, B05216.
- De Martini P.M., Pantosti D., Palyvos N., Lemeille F., McNeill L. and Collier R. (2004): Slip rates of the Aigion and Eliki faults from uplifted marine terraces, Corinth Gulf, Greece. *C. R. Geoscience*, **336**, 325-334.
- Delibasis N., Ziazia M., Voulgaris N., Papadopoulos T., Stavrakakis G., Papanastassiou D. and Drakatos G. (1999): Microseismic activity and seismotectonics of Heraklion Area (central Crete Island, Greece). *Tectonophysics*, **308**, 237-248.
- DePolo C.M., Clark D.G., Slemmons D.B. and Ramelli A.R. (1991): Historical surface faulting in the Basin and Range province, western North America: implications for fault segmentation. *J. Struct. Geol.*, **13**(2), 123-136.
- Dercourt J. (1972): The Canadian cordillera, the Hellenides and the sea floor spreading theory. *Can. J. Earth Sci.*, **9**, 709-743.
- Dercourt J., Zonenshain L.P., Ricou L.-E., Kazmin V.G., Le Pichon X., Knipper A.L., Grandjacquet C., Sbertshikov I.M., Geyssant J., Lepvrier C., Pechersky D.H., Bouhn J., Sibuet J.-C., Savostin L.A., Sorokhtin O., Westphal M., Bazhenov M.L., Lauer J.P. and Biju-Duval B. (1986): Geological evolution of the Tethys belt from the Atlantic to the Pamirs since the Lias. *Tectonophysics*, **123**, 241-315.
- Dercourt J., Ricou L.E. and Vrielynck B. (1993): *Atlas Tethys Paleoenvironmental maps*. Paris, Gauthier-Villars.
- Déverchère J., Petit C., Gileva N., Radziminovitch N., Melnikova V. and San'kov V. (2001): Depth distribution of earthquakes in the Baikal rift system and its implications for the rheology of the lithosphere. *Geophys. J. Int.*, **146**, 714-730.

- Dewey J.F., Pitman W.C., Ryan W.B.F. and Bonnin J. (1973): Plate Tectonics and the Evolution of the Alpine System. *Bull. Geol. Soc. Am.*, **84**, 3137-3180.
- Di Luccio F. and Pasyanos M.E. (2007): Crustal and upper-mantle structure in the Eastern Mediterranean from the analysis of surface wave dispersion curves. *Geophys. J. Int.*, **169**, 1139-1152.
- Diamantopoulos A. (2006): Plio–Quaternary Geometry and Kinematics of Ptolemais Basin (Northern Greece): Implications for the Intra-Plate Tectonics in Western Macedonia. *Geologia Croatica*, **59**(1), 85-96.
- Dieterich J. (1994): A constitutive law for rate of earthquake production and its application to earthquake clustering. *J. Geophys. Res.*, **99**(B2), 2601-2618.
- Dilek Y, Altunkaynak S. and Öner Z. (2009): Syn-extensional granitoids in the Menderes core complex and the late Cenozoic extensional tectonics of the Aegean province. *In: Ring U. and Wernicke B. (Eds.), Extending a Continent: Architecture, Rheology and Heat Budget. Geol. Soc. London Spec. Publ.*, **321**, 197-223.
- Dinter D.A. and Royden L. (1993): Late Cenozoic extension in northeastern Greece: Strymon valley detachment system and Rhodope metamorphic core complex. *Geology*, **21**, 45-48.
- DISS Working Group (2011): Database of Individual Seismogenic Sources (version 3.2): A compilation of potential sources for earthquakes larger than M 5.5 in Italy and surrounding areas. <http://diss.rm.ingv.it/diss/>
- Doser D.I. and Kanamori H. (1986): Depth of seismicity in the Imperial Valley Region (1977-1983) and its relationship to heat flow, crustal structure, and the October 15, 1979, earthquake. *J. Geophys. Res.*, **91**(B1), 675-688.
- Doutsos T. and Kokkalas S. (2001): Stress and deformation patterns in the Aegean region. *J. Struct. Geol.*, **23**, 455-472.
- Doutsos T. and Koukouvelas I. (1998): Fractal analysis of normal faults in northwestern Aegean area, Greece. *J. Geodyn.*, **26**(2-4), 197-216.
- Doutsos T. and Poulimenos G. (1992): Geometry and kinematics of active faults and their seismotectonic significance in the western Corinth-Patras rift (Greece). *J. Struct. Geol.*, **14**(6), 689-699.
- Doutsos T., Koukouvelas I., Zelilidis A. and Kontopoulos N. (1994): Intracontinental wedging and post-orogenic collapse in the Mesohellenic Trough. *Geol. Rundsch.*, **83**, 257-275.
- Doutsos T., Koukouvelas I.K. and Xypolias P. (2006): A new orogenic model for the External Hellenides. *In: Robertson A.H.F. and Mountrakis D. (Eds.), Tectonic Development of the Eastern Mediterranean Region. Geol. Soc. London Spec. Publ.*, **260**, 507-520.
- Dragoni M. and Pondrelli S. (1991): Depth of the Brittle-ductile Transition in a Transcurrent Boundary Zone. *Pure Appl. Geophys.*, **135**, 447-461.
- Dragoni M., Doglioni C., Mongelli F. and Zito G. (1996): Evaluation of stress in two geodynamically different areas; stable foreland and extensional backarc. *Pure Appl. Geophys.*, **146**, 319-341.
- Drakatos G. and Drakopoulos J. (1991): 3-D velocity structure beneath the crust and upper mantle of the Aegean Sea region. *Pure Appl. Geophys.*, **135**(3), 401-420.
- Drakatos G., Karantonis G. and Stavrakakis G.N. (1997): P-wave crustal tomography of Greece with use of an accurate two-point ray tracer. *Ann. Geofisica*, **40**(1), 25-36.
- Drakatos G., Papanastassiou D., Papadopoulos G., Skafida H. and Stavrakakis G. (1998a): Relationship between the 13 May 1995 Kozani-Grevena (NW Greece) earthquake and the Polyphyto artificial lake. *Eng. Geol.*, **51**, 65-74.

- Drakatos G., Papanastassiou D., Voulgaris N. and Stavrakakis G. (1998b): Observations on the 3-D crustal velocity structure in the Kozani-Grevena (NW Greece) area. *J. Geodyn.*, **26**(2-4), 341-351.
- Drakatos G., Voulgaris N., Pirlis M., Melis N. and Karakostas B. (2005): 3-D Crustal Velocity Structure in Northwestern Greece. *Pure Appl. Geophys.*, **162**, 37-51.
- Drakopoulos J.C. and Economides A.C. (1972): Aftershocks of February 19, 1968 earthquake in Northern Aegean Sea and related problems. *Pure Appl. Geophys.*, **95**, 100-115.
- Drury M.J. (1986): Thermal Conductivity, Thermal Diffusivity, Density and Porosity of Crystalline Rocks. Earth Physics Branch open file report no. 86-5. Ottawa: Earth Physics Branch.
- Dziewonski A.M., Friedman A., Giardini D. and Woodhouse J.H. (1983): Global seismicity of 1982: centroid-moment tensor solutions for 308 earthquakes. *Phys. Earth Planet. Inter.*, **33**, 76-90.
- Dziewonski A.M., Franzen J.E. and Woodhouse J.H. (1984): Centroid-moment tensor solutions for July-September, 1983. *Phys. Earth Planet. Inter.*, **34**, 1-8.
- Dziewonski A.M., Franzen J.E. and Woodhouse J.H. (1985): Centroid-moment tensor solutions for July-September, 1984. *Phys. Earth Planet. Inter.*, **38**, 203-213.
- Dziewonski A.M., Franzen J.E. and Woodhouse J.H. (1986): Centroid-moment tensor solutions for October-December 1985. *Phys. Earth Planet. Inter.*, **43**, 185-195.
- Dziewonski A.M., Ekström G., Franzen J.E. and Woodhouse, J.H. (1987): Global seismicity of 1978: centroid-moment tensor solutions for 512 earthquakes. *Phys. Earth Planet. Inter.*, **46**, 316-342.
- Dziewonski A. M., Ekström G., Franzen J. E. and Woodhouse J. H. (1988): Global seismicity of 1980: centroid-moment tensor solutions for 515 earthquakes. *Phys. Earth Planet. Inter.*, **50**, 127-154.
- Dziewonski A.M., Ekström G., Woodhouse J.H. and Zwart G. (1991): Centroid-moment tensor solutions for October–December 1990. *Phys. Earth Planet. Inter.*, **68**, 201-214.
- Dziewonski A.M., Ekström G. and Salganik M.P. (1996): Centroid-moment tensor solutions for April-June 1995. *Phys. Earth Planet. Inter.*, **96**, 1-13.
- Dziewonski A.M., Ekström G., Maternovskaya N.N. and Salganik M.P. (1997): Centroid-moment tensor solutions for July-September, 1996. *Phys. Earth Planet. Inter.*, **102**, 133-143.
- E**
- Ekström G. and England P. (1989): Seismic Strain Rates in Regions of Distributed Continental Deformation. *J. Geophys. Res.*, **94**(B8), 10231-10257.
- Ekström G., Dziewonski A.M. and Woodhouse J.H. (1987): Centroid-moment tensor solutions for the 51 IASPEI selected earthquakes, 1980-1984. *Phys. Earth Planet. Inter.*, **47**, 62-66.
- El-Fiky G.S. (2000): Crustal Strains in the Eastern Mediterranean and Middle East as Derived from GPS Observations. *Bull. Earthq. Res. Inst. Univ. Tokyo*, **75**, 105-125.
- Endrun B., Meier T., Lebedev S., Bohnhoff M., Stavrakakis G. and Harjes H.-P. (2008): S velocity structure and radial anisotropy in the Aegean region from surface wave dispersion. *Geophys. J. Int.*, **174**, 593-616.
- Exadaktylos G.E., Vardoulakis I., Stavropoulou M.C. and Tsombos P. (2003): Analogue and numerical modeling of normal fault patterns produced due to slip along a detachment zone. *Tectonophysics*, **376**, 117-134.

F

- Fadaie K. and Ranalli G. (1990): Rheology of the lithosphere in the East African Rift System. *Geophys. J. Int.*, **102**, 445-453.
- Fassoulas C. (2001): The tectonic development of a Neogene basin at the leading edge of the active European margin: the Heraklion basin, Crete, Greece. *J. Geodyn.*, **31**, 49-70.
- Ferentinos G., Brooks M. And Collins M. (1981): Gravity-induced deformation on the north flank and floor of the Sporadhes Basin of the North Aegean Sea Trough. *Mar. Geol.*, **44**, 289-302.
- Fernàndez M. and Ranalli G. (1997): The role of rheology in extensional basin formation modelling. *Tectonophysics*, **282**, 129-145.
- Fernàndez M., Marzán I., Correia A. and Ramalho E. (1998): Heat flow, heat production, and lithospheric thermal regime in the Iberian Peninsula. *Tectonophysics*, **291**, 29-53.
- Ferrière J., Reynaud J.Y., Migiros G., Proust J.N., Bonneau M., Pavlopoulos A. and Houze A. (1998): Initiation of a piggy-back basin: the example of the mesohellenic trough, Tertiary, Greece. *C.R. Acad. Sci. IIA*, **326**(8), 567-574.
- Ferrière J., Reynaud J.-Y., Pavlopoulos A., Bonneau M., Migiros G., Chanier F., Proust J.-N. and Gardin S. (2004): Geologic evolution and geodynamic controls of the Tertiary intramontane piggyback Meso-Hellenic Basin, Greece. *Bull. Soc. Géol. Fr.*, **175**, 361-381.
- Flerit F., Armijo R., King G. and Meyer B. (2004): The mechanical interaction between the propagating North Anatolian Fault and the back-arc extension in the Aegean. *Earth Planet. Sci. Lett.*, **224**, 347-362.
- Floras D. (1933): The destructions of the Chalkidiki earthquakes. *Tech. Chron.*, **25**, 21-28 (in Greek).
- Flotté N. and Sorel D. (2001): Structural cross sections through the Corinth-Patras detachment fault-system in northern Peloponnesus (Aegean arc, Greece). *Bull. Geol. Soc. Greece*, **34**(1), 235-241.
- Flotté N., Sorel D., Muller C. and Tensi J. (2005): Along strike changes in the structural evolution over a brittle detachment fault: Example of the Pleistocene Corinth-Patras rift (Greece). *Tectonophysics*, **403**, 77-94.
- Floyd M.A., Billiris H., Paradissis D., Veis G., Avallone A., Briole P., McClusky S., Nocquet J.-M., Palamartchouk K., Parsons B. and England P.C. (2010): A new velocity field for Greece: Implications for the kinematics and dynamics of the Aegean. *J. Geophys. Res.*, **115**, B10403.
- Forster M.A. and Lister G.S. (1999): Detachment faults in the Aegean core complex of Ios, Cyclades, Greece. *In: Ring U., Brandon M.Y., Lister, G.S. and Willett S.D. (Eds.), Exhumation Processes: Normal Faulting, Ductile Flow and Erosion. Geol. Soc. London Spec. Publ.*, **154**, 305-323.
- Förster A. and Förster H.-J. (2000): Crustal composition and mantle heat flow: Implications from surface heat flow and radiogenic heat production in the Variscan Erzgebirge (Germany). *J. Geophys. Res.*, **105**(B12), 27917-27938.
- Förster H.-J., Förster A., Oberhänsli R. and Stromeyer D. (2010): Lithospheric composition and thermal structure of the Arabian Shield in Jordan. *Tectonophysics*, **481**, 29-37.
- Fountain D.M. (1986): Is there a relationship between seismic velocity and heat production for crustal rocks? *Earth Planet. Sci. Lett.*, **79**, 145-150.

G

- Galanakis D., Pavlides S. and Mountrakis D. (1998): Recent brittle tectonic in Almyros-Pagasetikos, Maliakos, N. Euboea and Pilio. *Bull. Geol. Soc. Greece*, **42**(1), 263-273.
- Galanakis D., Paschos P., Rondoyanni T. and Georgiou C. (2007): Neotectonic Activity of Konitsa Area and the 1996 Earthquakes. *Hell. J. Geosciences*, **42**, 57-64.
- Galanis O.C., Papazachos C.B., Hatzidimitriou P.M. and Scordilis E.M. (2004): Application of 3-D velocity models and ray tracing in double difference earthquake location algorithms: application to the Mygdonia basin (northern Greece). *Bull. Geol. Soc. Greece*, **36**(3), 1396-1405.
- Garfunkel Z. (2004): Origin of the Eastern Mediterranean basin: a reevaluation. *Tectonophysics*, **391**, 11-34.
- Gautier P. and Brun J.P. (1994): Crustal-scale geometry and kinematics of late-orogenic extension in the central Aegean (Cyclades and Evvia Island). *Tectonophysics*, **238**, 399-424.
- Gautier P., Brun J.-P., Moriceau R., Sokoutis D., Martinod J. and Jolivet L. (1999): Timing, kinematics and cause of Aegean extension: a scenario based on a comparison with simple analogue experiments. *Tectonophysics*, **315**, 31-72.
- Gautier S., Latorre D., Virieux J., Deschamps A., Skarpelos C., Sotiriou A., Serpetsidaki A. and Tselentis A. (2006): A New Passive Tomography of the Aigion Area (Gulf of Corinth, Greece) from the 2002 Data Set. *Pure Appl. Geophys.*, **163**, 431-453.
- Georgalas G. and Galanopoulos A. (1953): Das grosse Erdbeben der Chalkidike vom 26 September 1932. *Bull. Geol. Soc. Greece*, **1**, 11-63.
- Godfriaux I. (1968): Etude géologique de l'Olympe (Grèce). *Ann. Géol. Pays Helléniques*, **19**, 1-280.
- Goetze C. and Evans B. (1979): Stress and temperature in the bending lithosphere as constrained by experimental rock mechanics. *Geophys. J. R. astr. SOC.*, **59**, 463-478.
- Goldsworthy M. and Jackson J. (2000): Active normal fault evolution in Greece revealed by geomorphology and drainage patterns. *J. Geol. Soc. London*, **157**, 967-981.
- Goldsworthy M. and Jackson J. (2001): Migration of activity within normal fault systems: examples from the Quaternary of mainland Greece. *J. Struct. Geol.*, **23**, 489-506.
- Goldsworthy M., Jackson J. and Haines J. (2002): The continuity of active fault systems in Greece. *Geophys. J. Int.*, **148**, 596-618.
- Görür N. and Okay A.I. (1996): A fore-arc origin for the Thrace Basin, NW Turkey. *Geol. Rundsch.*, **85**, 662-668.
- Grad M., Tiira T. and ESC Working Group (2009): The Moho depth map of the European Plate. *Geophys. J. Int.*, **176**, 279-292.
- Gueydan F., Morency C. and Brun J.-P. (2008): Continental rifting as a function of lithosphere mantle strength. *Tectonophysics*, **460**, 83-93.
- Guglielmo J.G., Vendeville B.C. and Jackson M.P.A. (2000): 3-D visualization and isochore analysis of extensional diapirs overprinted by compression, *Am. Assoc. Petr. Geol. Bull.*, **84**, 1095– 1108.
- Guidoboni E. and Comastri A. (2005): *Catalogue of earthquakes and tsunamis in the Mediterranean area from the 11th to the 15th century*. INGV-SGA, Bologna, 1037 pp.
- Guidoboni E., Comastri A. and Traina G. (1994): *Catalogue of ancient earthquakes in the Medi-terranean area up to 10th century*. INGV-SGA, Bologna, 504 pp.

Gung Y., Panning M. and Romanowicz B. (2003): Global anisotropy and the thickness of continents. *Nature*, **422**, 707-711.

H

Haenel R. and Staroste E. (1988): *Atlas of Geothermal Resources in the European Community Austria and Switzerland*. Commission of the European Communities, ESC, EEC, EAEC, Brussels, Publication No. EUR 11026.

Handy M.R. and Brun, J.-P. (2004): Seismicity, structure and strength of the continental lithosphere. *Earth Planet. Sci. Lett.*, **223**, 427-441.

Hanks T.C. and Kanamori H. (1979): A Moment Magnitude Scale. *J. Geophys. Res.*, **84**(B5), 2348-2350.

Harris A.R., Simpson R.W. and Reasenber P.A. (1995): Influence of static stress changes on earthquake locations in Southern California. *Nature*, **375**, 221-224.

Hatzfeld D. (1999): The present-day tectonics of the Aegean as deduced from seismicity. In: Durand B., Jolivet L., Horvath E and Séranne M. (Eds.): *The Mediterranean Basins: Tertiary Extension within the Alpine Orogen*. *Geol. Soc. London Spec. Publ.*, **156**, 415-426.

Hatzfeld D., Christodoulou A.A., Scordilis E.M., Panagiotopoulos D. and Hatzidimitriou P.M. (1986/87): A microearthquake study of the Mygdonian graben (northern Greece). *Earth Planet. Sci. Lett.*, **81**, 379-396.

Hatzfeld D., Kassaras I., Panagiotopoulos D., Amorese D., Makropoulos K., Karakaisis G. and Coutant O. (1995): Microseismicity and strain pattern in northwestern Greece, *Tectonics*, **14**(4), 773-785.

Hatzfeld D., Karakostas V., Ziazia M., Selvaggi G., Lebogne S., Berge C., Guiguet R., Paul A., Voidomatis, P., Diagourtas D., Kassaras I., Koutsikos I., Makropoulos K., Azzara R., Di Bona M., Baccheschi S., Bernard P. and Papaioannou C. (1997): The Kozani-Grevena (Greece) earthquake of 13 May 1995 revisited from a detailed seismological study. *Bull. Seism. Soc. Am.*, **87**(2), 463-473.

Hatzfeld D., Karakostas V., Ziazia M., Selvaggi G., Lebogne S., Berge C. and Makropoulos K. (1998): The Kozani-Grevena (Greece) earthquake of May 13, 1995, a seismological study. *J. Geodyn.*, **26**(2-4), 245-254.

Hatzfeld D., Ziazia M., Kementzetzidou D., Hatzidimitriou P., Panagiotopoulos D., Makropoulos K., Papadimitriou P. and Deschamps A. (1999): Microseismicity and focal mechanisms at the western termination of the North Anatolian Fault and their implications for continental tectonics. *Geophys. J. Int.*, **137**, 891-908.

Hatzidimitriou P.M., Hatzfeld D., Scordilis E.M., Papadimitriou E.E. and Christodoulou A.A. (1991): Seismotectonic evidence of an active normal fault beneath Thessaloniki (Greece). *Terra Nova*, **3**, 648-654.

Hawkesworth C.J., Pearson D.G. and Turner S.P. (1999): Chemical and temporal variations in the Earth's lithosphere. *Phil. Trans. R. Soc. Lond. A*, **357**, 647-669.

Hodgkinson K.M., Stein R.S. and King G.C.P. (1996): The 1954 Rainbow Mountain - Fairview Peak - Dixie Valley earthquake: A triggered normal faulting sequence. *J. Geophys. Res.*, **101**, 25459-25471.

Hollenstein C., Müller M.D., Geiger A. and Kahle H.-G. (2008): Crustal motion and deformation in Greece from a decade of GPS measurements, 1993-2003. *Tectonophysics*, **449**, 17-40.

Horvath F., Berckhemer H., Stegena L. and Coulon C. (1981): Models of Mediterranean Back-Arc Basin Formation. *Phil. Trans. R. Soc. Lond. A*, **300**, 383-402.

Hurter S. and Haenel R. (2002): *Atlas of Geothermal Resources in Europe*. Commission of the European Communities, Publication Nr. 1781 1.

I

IGRS-IFP (1966): *Étude géologique de l'Épire (Grèce Nord-Occidentale)*. Ed. Technip, Paris, 306 pp.

IOC – Intergovernmental Oceanographic Commission (1981): *International bathymetric chart of the Mediterranean*. 1st ed., 1:1,000,000, Head Department of Navigation and Oceanography, Ministry of Defence, Leningrad, USSR.

J

Jackson J.A. (2002): Strength of the continental lithosphere: time to abandon the jelly sandwich? *GSA Today*, **12**, 4-10.

Jackson J.A., King G. and Vita-Finzi C. (1982): The neotectonics of the Aegean: an alternative view. *Earth Planet. Sci. Lett.*, **61**, 303-318.

Jackson A., Haines J. and Holt W. (1992): The Horizontal Velocity Field in the Deforming Aegean Sea Region Determined from the Moment Tensors of Earthquakes. *J. Geophys. Res.*, **97**(B12), 17657-17684.

Jacobshagen V. (1994): Orogenic evolution of the Hellenides: new aspects. *Geol. Rundsch.*, **83**, 249-256.

Janssen C., Bohnhoff M., Vapnik Y., Görgün E., Bulut F., Plessen B., Pohl D., Aktar M., Okay A.I. and Dresen G. (2009): Tectonic evolution of the Ganos segment of the North Anatolian Fault (NW Turkey). *J. Struct. Geol.*, **31**, 11-28.

Jaupart C. and Mareschal J.C. (1999): The thermal structure and thickness of continental roots. *Lithos*, **48**, 93-114.

Jaupart C. and Mareschal J.-C. (2007): Heat Flow and Thermal Structure of the Lithosphere. *Treatise on Geophysics*, **6.05**, 217-251.

Jaupart C. and Provost A. (1985): Heat focussing, granite genesis and inverted metamorphic gradients in continental collision zones. *Earth Planet. Sci. Lett.*, **73**, 385-397.

Jenny S., Goes S., Giardini D. and Kahle H.G. (2004): Earthquake recurrence parameters from seismic and geodetic strain rates in the eastern Mediterranean. *Geophys. J. Int.*, **157**, 1331-1347.

Jöeleht A. and Kukkonen I.T. (1998): Thermal properties of granulite facies rocks in the Precambrian basement of Finland and Estonia. *Tectonophysics*, **291**, 195-203.

Jolivet L. (2001): A comparison of geodetic and finite strain in the Aegean, geodynamic implications. *Earth Planet. Sci. Lett.*, **187**, 95-104.

Jolivet L. and Brun J.-B. (2010): Cenozoic geodynamic evolution of the Aegean. *Int. J. Earth Sci.*, **99**(1), 109-138.

Jolivet L. and Faccenna C. (2000): Mediterranean extension and the Africa-Eurasia collision. *Tectonics*, **19**, 1095-1106.

Jolivet L., Daniel J.M., Truffert C. and Goffé B. (1994): Exhumation of deep crustal metamorphic rocks and crustal extension in arc and back-arc regions. *Lithos*, **33**, 3-30.

Jolivet L., Lecomte E., Huet B., Denèle Y., Lacombe O., Labrousse L., Le Pourhiet L. and Mehl C. (2010): The North Cycladic Detachment System. *Earth Planet. Sci. Lett.*, **289**, 87-104.

Jost M.L., Knabenbauer O., Cheng J. and Harjes H.-P. (2002): Fault plane solutions of microearthquakes and small events in the Hellenic arc. *Tectonophysics*, **356**, 87-114.

K

- Kahle H.-G., Straub C., Reilinger R., McClusky S., King R.W., Hurst K., Veis G., Kastens K. and Cross P. (1998): The strain rate field in the eastern Mediterranean region, estimated by repeated GPS measurements. *Tectonophysics*, **294**, 237-252.
- Kalogeras I.S. and Burton P.W. (1996): Shear-wave velocity models from Rayleigh-wave dispersion in the broader Aegean area. *Geophys. J. Int.*, **125**, 679-695.
- Karabulut H., Roulmelioti Z., Benetatos C., Mutlu A.K., Özalaybey S., Aktar M. and Kiratzi A. (2006): A source study of the 6 July 2003 (Mw 5.7) earthquake sequence in the Gulf of Saros (Northern Aegean Sea): Seismological evidence for the western continuation of the Ganos fault. *Tectonophysics*, **412**, 195-216.
- Karagianni E.E. and Papazachos C.B. (2007): Shear velocity structure in the Aegean region obtained by joint inversion of Rayleigh and Love waves. In: Taymaz T., Yilmaz Y. and Dilek Y. (Eds.), *The Geodynamics of the Aegean and Anatolia*, *Geol. Soc. Lond. Spec. Publ.*, **291**, 159-181.
- Karagianni E.E., Papazachos C.B., Panagiotopoulos D.G., Suhadolc P., Vuan A. and Panza G.F. (2005): Shear velocity structure in the Aegean area obtained by inversion of Rayleigh waves. *Geophys. J. Int.*, **160**, 127-143.
- Karakaisis G.F., Papazachos C.B. and Scordilis E.M. (2010): Seismic sources and main seismic faults in the Aegean and surrounding area. *Bull. Geol. Soc. Greece*, **43**(4), 2026-2042.
- Karato S.-i. and Wu P. (1993): Rheology of the upper mantle: a synthesis. *Science*, **260**, 771-778.
- Kastelic V., Vannoli P., Burrato P., Barba S., Basili R., Fracassi U., Tiberti M.M. and Valensise G. (2008): Seismogenic sources of the Adriatic domain: an overview from the Database of Individual Seismogenic Sources (DISS 3.1.0). *Rendiconti online Soc. Geol. It.*, **2**, 1-3.
- Katayama I., Karato S.-i. and Mark Brandon M. (2005): Evidence of high water content in the deep upper mantle inferred from deformation microstructures. *Geology*, **33**, 613-616.
- Kaya Ş., Müftüoğlu O. and Tüysüz O. (2004): Tracing the geometry of an active fault using remote sensing and digital elevation model: Ganos segment, North Anatolian Fault zone, Turkey. *Int. J. Remote Sens.*, **25**(19), 3843-3855.
- Kementzetzidou D. (1996): *Étude sismotectonique du système Thessalie-iles Sporades (Grèce centrale)*. PhD Thesis, Observatoire de Grenoble, 151 pp.
- Kilias A., Fassoulas C. and Mountrakis D. (1994): Tertiary extension of continental crust and uplift of Psiloritis metamorphic core complex in the central part of the Hellenic Arc (Crete, Greece). *Geol. Rundsch.*, **83**, 417-430.
- King G.C.P. and Cocco M. (2001): Fault interaction by elastic stress changes: New clues from earthquake sequences. *Adv. Geophys.*, **44**, 1-38.
- King G.C.P., Tselentis A., Gombert J., Molnar P., Roecker S.W., Sinval H., Soufleris C. and Stock J.M. (1983): Microearthquake seismicity and active tectonics of northwestern Greece. *Earth Plan. Sci. Lett.*, **66**, 279-288.
- King G.C.P., Stein R.S. and Lin J. (1994): Static Stress Changes and the Triggering of Earthquakes. *Bull. Seism. Soc. Am.*, **84**(3), 935-953.
- Kiratzi A.A. (1991): Rates of Crustal Deformation in the North Aegean Trough-North Anatolian Fault Deduced from Seismicity. *Pure Appl. Geophys.*, **136**(4), 421-432.

- Kiratzi A.A. (1999): Stress tensor inversion in Western Greece using earthquake focal mechanisms from the Kozani-Grevena 1995 seismic sequence. *Ann. Geofis.*, **42**(4), 725-734.
- Kiratzi A. (2010): The 24 May 2009 Mw5.2 earthquake sequence near Lake Doirani (FYROM-Greek borders): Focal mechanisms and slip model using empirical source time functions inversion. *Tectonophysics*, **490**, 115-122.
- Kiratzi A. and Louvari E. (2003): Focal mechanisms of shallow earthquakes in the Aegean Sea and the surrounding lands determined by waveform modelling: a new database. *J. Geodyn.*, **36**, 251-274.
- Kiratzi A.A., Karakaisis G.F., Papadimitriou E.F. and Papazachos B.C. (1985): Seismic Source-Parameter Relations for Earthquakes in Greece. *Pure Appl. Geophys.*, **123**, 27-41.
- Kiratzi A., Wagner G. and Langston C. (1991): Source parameters of some large earthquakes in Northern Aegean determined by body waveform modelling. *Pure Appl. Geophys.*, **135**, 515-527.
- Kiratzi A., Benetatos C. and Roumelioti Z. (2005): Seismicity and seismotectonic characteristics of NE Aegean Sea and its surrounding lands. *Bull. Geol. Soc. Greece*, **37**, 9-18.
- Kirby S. (1980): Tectonic stress in the lithosphere: constraints provided by the experimental deformation of rocks. *J. Geophys. Res.*, **85**, 6353-6363.
- Kirby S.H. (1983): Rheology of the Lithosphere. *Rev. Geophys. Space Phys.*, **21**(6), 1458-1487.
- Kirby S.H. and Kronenberg A.K. (1987): Rheology of the lithosphere: Selected topics. *Rev. Geophys.*, **25**(6), 1219-1244.
- Kissel C. and Laj C. (1988): The tertiary geodynamical evolution of the Aegean arc; a paleomagnetic reconstruction. *Tectonophysics*, **146**, 183-201.
- Kissel C., Laj C. and Mialler C. (1985): Tertiary geodynamical evolution of northwestern Greece: paleomagnetic results. *Earth Planet. Sci. Lett.*, **72**, 190-204.
- Kockel F. and Mollat H. (1977): *Erläuterungen zur Geologischen Karte der Chalkidiki und angrenzender Gebiete 1:100.000 (Nord Griechenland)*. Bundesanstalt für Geowissenschaften und Rohstoffe, Hannover.
- Kokkalis S. and Koukouvelas I.K. (2005): Fault-scarp degradation modeling in central Greece: The Kaparelli and Eliki faults (Gulf of Corinth) as a case study. *J. Geodyn.*, **40**, 200-215.
- Kokkalis S., Xypolias P., Koukouvelas I. and Doutsos T. (2006): Postcollisional contractional and extensional deformation in the Aegean region. In: Dilek Y. and Pavlides S. (Eds.), *Postcollisional tectonics and magmatism in the Mediterranean region and Asia*. Geol. Soc. Am., Spec. Paper, **409**, 97-123.
- Koral H., Öztürk H. and Haniçi N. (2009): Tectonically induced coastal uplift mechanism of Gökçeada Island, Northern Aegean Sea, Turkey. *Quatern. Int.*, **197**, 43-54.
- Koukouvelas I.K. and Aydin A. (2002): Fault structure and related basins of the North Aegean Sea and its surroundings. *Tectonics*, **21**(5), 1046, 17 pp.
- Koukouvelas I., Stamatopoulos L., Katsonopoulou D. and Pavlides S. (2001): A palaeoseismological and geoarchaeological investigation of the Eliki fault, Gulf of Corinth, Greece. *J. Struct. Geol.*, **23**, 531-543.
- Koukouvelas I.K., Katsonopoulou D., Soter S. and Xypolias P. (2005): Slip rates on the Helike Fault, Gulf of Corinth, Greece: new evidence from geoarchaeology. *Terra Nova*, **17**, 158-164.

- Kukkonen I.T. and Jöeleht A. (1996): Geothermal modelling of the lithosphere in the central Baltic Shield and its southern slope. *Tectonophysics*, **255**, 25-45.
- Kulhánek O. and Meyer K. (1979): Source Parameters of the Volvi-Langadhas Earthquake of June 20, 1978 deduced from Body-Wave Spectra at Stations Uppsala and Kiruna. *Bull. Geol. Soc. Am.*, **69**(4), 1289-1294.
- Kurt H., Demirbag E. and Kusçu I. (2000): Active submarine tectonism and formation of the Gulf of Saros, Northeast Aegean Sea, inferred from multi-channel seismic reflection data. *Mar. Geol.*, **165**, 13-26.
- Kusky T. (2005): *Encyclopedia of earth science*. Facts on File, Inc., New York, 510 pp.
- Kusznr N.J. and Park R.G. (1987): The extensional strength of the continental lithosphere: its dependence on geothermal gradient, and crustal composition and thickness. In: Coward M.P., Dewey J.F. and Hancock P.L. (Eds.), *Continental Extensional Tectonics*, *Geol. Soc. Lond. Spec. Publ.*, **28**, 35-52.
- L**
- Lachenbruch A.H. (1968): Preliminary Geothermal Model of the Sierra Nevada. *J. Geophys. Res.*, **73**(22), 6977-6989.
- Lachenbruch A.H. (1970): Crustal Temperature and Heat Production: Implications of the Linear Heat-Flow Relation. *J. Geophys. Res.*, **75**(17), 3291-3300.
- Laigle M., Hirn A., Sachpazi M. and Roussos N. (2000): North Aegean crustal deformation: An active fault imaged to 10 km depth by reflection seismic data. *Geology*, **28**, 71-74.
- Laj C., Jamet M., Sorel D. and Valente J.P. (1982): First paleomagnetic results from Mio-Pliocene series of the Hellenic sedimentary arc. *Tectonophysics*, **86**, 45-67.
- Lamontagne M. and Ranalli G. (1996): Thermal and rheological constraints on the earthquake depth distribution in the Charlevoix, Canada, intraplate seismic zone. *Tectonophysics*, **257**, 53-69.
- Le Meur H., Virieux J. and Podvin P. (1997): Seismic tomography of the Gulf of Corinth: a comparison of methods. *Ann. Geophys.*, **40**(1), 1-24.
- Le Pichon X. and Angelier J. (1979): The Hellenic Arc and Trench System: a key to the neotectonic evolution of the Eastern Mediterranean Area. *Tectonophysics*, **60**, 1-42.
- Le Pichon X. and Angelier J. (1981): The Aegean Sea. *Philos. Trans. R. Soc. Lond.*, **300**, 357-372.
- Le Pichon X., Chamot-Rooke N., Lallemand S., Noomen R. and Veis G. (1995): Geodetic determination of the kinematics of central Greece with respect to Europe: Implications for eastern Mediterranean tectonics. *J. Geophys. Res.*, **100**(B7), 12675-12690.
- Leeder M. and Pérez-Arlucea M. (2006): *Physical Processes in Earth and Environmental Sciences*. Blackwell Publ., 321 pp.
- Lekkas E.L. (1995): *Neotectonic Map of Greece*. 1:100000, Corfu Island sheet (in Greek). University of Athens-Prefecture of Corfu.
- Ligdas C.N. and Lees J.M. (1993): Seismic velocity constrains in the Thessaloniki and Chalkidiki areas (northern Greece) from a 3-D tomographic study. *Tectonophysics*, **228**, 97-121.
- Ligdas C.N. and Main I.G. (1991): On the resolving power of tomographic images in the Aegean area. *Geophys. J. Int.*, **107**, 197-203.
- Ligdas C.N., Main I.G. and Adams R.D. (1990): 3-D structure of the lithosphere in the Aegean Sea region, *Geophys. J. Int.*, **102**, 219-229.

- Lobkovsky L.I. and Kerchman V.I. (1991): A two-level concept of plate tectonics: application to geodynamics. *Tectonophysics*, **199**, 343-374.
- Lucazeau F. and Mailhé D. (1986): Heat flow, heat production and fission track data from the Hercynian basement around the Provençal Basin (Western Mediterranean). *Tectonophysics*, **128**, 335-356.
- Lybérís N. (1984): Tectonic evolution of the North Aegean trough. *Geol. Soc. London Spec. Publ.*, **17**, 709-725.
- Lybérís N. and Sauvage J. (1985): Evolution tectonique de la région nord égéenne (Grèce) du Pliocène au Pléistocène. *Bull. Soc. Geol. France*, **8**, I, 4, 581-595.
- M**
- Machette M.N. (2000): Active, capable, and potentially active faults - a paleoseismic perspective. *J. Geodyn.*, **29**, 387-392.
- Machette M.N., Personius S.F. and Nelson A.R. (1992): Paleoseismology of the Wasatch fault zone: A summary of recent investigations, conclusions and interpretations, Chapter A. In: Gori P.L. and Hays W.W., (Eds.), Assessment of regional earthquake hazards and risk along the Wasatch Front area, Utah. *U.S. Geological Survey, Professional Paper*, **1500**, A1-A71.
- Maggi A., Jackson J.A., McKenzie D. and Priestley K. (2000): Earthquake focal depths, effective elastic thickness, and the strength of the continental lithosphere. *Geology*, **28**, 495-498.
- Makris J. (1978): The crust and upper mantle of the Aegean Region from deep soundings. *Tectonophysics*, **46**, 269-284.
- Makris J. and Stobbe C. (1984): Physical properties and state of the crust and upper mantle of the eastern Mediterranean Sea deduced from geophysical data. *Mar. Geol.*, **55**, 347-363.
- Makris J., Papouliá J., Papanikolaou D. and Stavrakakis G. (2001): Thinned continental crust below northern Evoikos Gulf, central Greece, detected from deep seismic soundings. *Tectonophysics*, **341**, 225-236.
- Maley T.S. and Johnson G.L. (1971): Morphology and structure of the Aegean Sea. *Deep-Sea Res.*, **18**, 109-122.
- Maravelakis M. (1936): *Study on the earthquakes of Chalkidiki* (in Greek). Publ. C. Theodoridou, Thessaloniki, 7, 43 pp.
- Marchal D., Guiraud M. and Rives Thierry (2003): Geometric and morphologic evolution of normal fault planes and traces from 2D to 4D data. *J. Struct. Geol.*, **25**(1), 135-158.
- Mariolakos I., Zagorchev I., Fountoulis I. and Ivanov M. (2004): Neotectonic Transect Moesia Apulia. Field Trip Guide Book-B26, 32nd Int. Geol. Congr., Pre-Congress Field Trip B26, 72 pp.
- Marone F., van der Meijde M., van der Lee S. and Giardini D. (2003): Joint inversion of local, regional and teleseismic data for crustal thickness in the Eurasia-Africa plate boundary region. *Geophys. J. Int.*, **154**, 499-514.
- Martin L. (1987): *Structure et évolution récente de la mer Egée: Apports d'une étude par sismique réflexion*. Laboratoire de Géodynamique Sous-marine, Villefranche-Sur-Mer, 305 pp.
- Masclé J. and Martin L. (1990): Shallow structure and recent evolution of the Aegean Sea: A synthesis based on continuous reflection profiles. *Mar. Geol.*, **94**, 271-299.
- McCalpin J.P. (2009): *Paleoseismology*. Academic Press, 2nd edition, 613 pp.

- McClusky S., Balassanian S., Barka A., Demir C., Ergintav S., Georgiev I., Gurkan O., Hamburger M., Hurst K., Kahle H.-G., Kastens K., Kekelidze G., King R.W., Kotzev V., Lenk O., Mahmoud S., Mishin A., Nadariya M., Ouzounis A., Paradissis D., Peter Y., Prilepin M., Reilinger R., Sanli I., Seeger H., Tealeb A., Toköz M. and Veis G. (2000): Global Positioning System constraints on plate kinematics and dynamics in the eastern Mediterranean and Caucasus. *J. Geophys. Res.*, **105**(B3), 5695-5719.
- McClusky S., Reilinger R., Mahmoud S., Ben Sari D. and Tealeb A. (2003): GPS constraints on Africa (Nubia) and Arabia plate motions. *Geophys. J. Int.*, **155**, 126-138.
- McKenzie D.P. (1970): Plate Tectonics of the Mediterranean Region. *Nature*, **226**, 239-243.
- McKenzie D. (1972): Active Tectonics of the Mediterranean Region. *Geophys. J. R. Astr. Soc.*, **30**, 109-185.
- McKenzie D. (1978): Active tectonics of the Alpine-Himalayan belt: the Aegean Sea and surrounding regions. *Geophys. J. R. Astr. Soc.*, **55**, 217-254.
- McNeill L.C. and Collier R.E.LI. (2004): Uplift and slip rates of the eastern Eliki fault segment, Gulf of Corinth, Greece, inferred from Holocene and Pleistocene terraces. *J. Geol. Soc.*, **161**, 81-92.
- McNeill L.C., Mille A., Minshull T.A., Bull J.M., Kenyon N.H. and Ivanov M. (2004): Extension of the North Anatolian Fault into the North Aegean Trough: Evidence for transtension, strain partitioning, and analogues for Sea of Marmara basin models, *Tectonics*, **23**, TC2016.
- McNeill L.C., Cotterill C.J., Henstock T.J., Bull J.M., Stefatos A., Collier R.E.LI., Papatheoderou G., Ferentinos G. and Hicks S.E. (2005): Active faulting within the offshore western Gulf of Corinth, Greece: Implications for models of continental rift deformation. *Geology*, **33**, 241-244.
- Meijer P. (1995): Dynamics of active continental margins: the Andes and the Aegean Region (Ph.D. Thesis). *Geol. Ultraiectina*, **130**, 220 pp.
- Meissner R. and Strehlau J. (1982): Limits of stress in continental crust and their relation to the depth-frequency relation of shallow earthquakes. *Tectonics*, **1**, 73-89.
- Melis N.S. and Tselentis G.-A. (1998): 3-D P-wave Velocity Structure in Western Greece Determined from Tomography Using Earthquake Data Recorded at the University of Patras Seismic Network (PATNET). *Pure Appl. Geophys.*, **152**, 329-348.
- Mercier J.-L. (1968): Etude géologique des zones internes des Hellenides en Macédoine central (Grèce). *Ann. Géol. Pays Helléniques*, **20**, 1-792.
- Mercier J.-L. (1981): Extensional-Compressional Tectonics Associated with the Aegean Arc: Comparison with the Andean Cordillera of South Peru - North Bolivia. *Phil. Trans. R. Soc. Lond. A*, **300**, 337-355.
- Mercier J.-L. and Carey-Gailhardis E. (1989): Regional state of stress and characteristic fault kinematics instabilities shown by aftershock sequences: the aftershock sequences of the 1978 Thessaloniki (Greece) and 1980 Campania-Lucania (Italia) earthquakes as examples. *Earth Planet. Sci. Lett.*, **92**, 247-264.
- Mercier J.L., Mouyaris N., Simeakis C., Roundoyannis T. and Angelidis C. (1979): Intra-plate deformation: a quantitative study of the faults activated by the 1978 Thessaloniki earthquakes. *Nature*, **278**, 45-48.
- Mercier J.-L., Carey E., Mouyaris N., Simeakis K., Roundoyannis T. and Anghelidhis C. (1983): Structural analysis of recent and active faults and regional state of stress in the

- epicentral area of the 1978 Thessaloniki earthquakes (Northern Greece). *Tectonics*, **2**(6), 577-600.
- Mercier J.-L., Simeakis K., Sorel D. and Vergely P. (1989): Extensional tectonic regimes in the Aegean basins during the Cenozoic. *Basin Research*, **2**, 49-71.
- Meyer B., Armijo R., Massonet D., De Chabaliere J.-B., Delacourt C., Ruegg J.-C., Achache C., Briole P. and Papanastassiou D. (1996): The 1995 Grevena (Northern Greece) earthquake: fault model constrained with tectonic observations and SAR interferometry. *Geophys. Res. Lett.*, **23**, 2677-2680.
- Meyer B., Armijo R., Massonet D., de Chabaliere J.B., Delacourt C., Ruegg J.C., Achache J. and Papanastassiou D. (1998): Comment on “Geodetic investigation of the 13 May Kozani-Grevena (Greece) earthquake” by Clarke *et al.*, *Geophys. Res. Lett.*, **25**, 129-130.
- Micarelli L., I. Moretti, J.M. Daniel (2003): Structural properties of rift-related normal faults: the case study of the Gulf of Corinth, Greece. *J. Geodyn.*, **36**, 275-303.
- Michailidou A. (2005): GIS-based morphotectonic and microtectonic analysis of Stratonivara and Gomati (eastern Chalkidiki) fault systems [in Greek]. MSc Thesis, Aristotle University of Thessaloniki, *unpublished*.
- Michailidou A., Chatzipetros A. and Pavlides S. (2005): Quantitative analysis–tectonic geomorphology indicators of the faults at the region of Stratonivara Gomati-M. Panagia in the Eastern Chalkidiki. *Bull. Geol. Soc. Greece*, **38**, 14-29.
- Moisio K., Kaikkonen P. and Beekman F. (2000): Rheological structure and dynamical response of the DSS profile BALTIC in the SE Fennoscandian Shield. *Tectonophysics*, **320**, 175-194.
- Molinari I. and Morelli A. (2011): EPcrust: a reference crustal model for the European Plate. *Geophys. J. Int.*, **185**, 352-364.
- Mountrakis D. M. (1985): *Geologia tis Elladas*. University Studio Press, Thessaloniki, 207 pp., in Greek.
- Mountrakis D. (1986): The Pelagonian Zone in Greece: A Polyphase-Deformed Fragment of the Cimmerian Continent and Its Role in the Geotectonic Evolution of the Eastern Mediterranean. *J. Geol.*, **94**, 335-347.
- Mountrakis D. (2006): Tertiary and Quaternary tectonics of Greece. In: Dilek Y. and Pavlides S. (Eds.): *Postcollisional tectonics and magmatism in the Mediterranean region and Asia*, *Geol. Soc. Am. Spec. Paper*, **409**, 125-136.
- Mountrakis D.M. (2010): *Geologia kai geotektoniki exeliki tis Elladhas*. University Studio Press, Thessaloniki, 374 pp.
- Mountrakis D.M. and Tranos M.D. (2004): The Kavala-Xanthi-Komotini fault (KXKF): a complicated active fault zone in Eastern Macedonia-Thrace (Northern Greece). 5th International Symposium on Eastern Mediterranean Geology, Thessaloniki, Greece, 14-20 April 2004, Thessaloniki, Greece, *Proceedings*, Ref.: S1-19.
- Mountrakis D., Kiliadis A., Pavlides S., Zouros N., Spyropoulos N., Tranos M. and Soulakelis N. (1993): Field study of the Southern Thessaly highly active Fault Zone. 2nd Congress of the Hellenic Geophysical Union, 5-7 May 1993, Florina, Greece, *Proceedings*, 603-614.
- Mountrakis D., Kiliadis A., Pavlides S., Sotiriadis L., Psilovikos A., Astaras Th., Vavliakis E., Koufos G., Dimopoulos G., Soulios G., Christaras V., Skordilis M., Tranos M., Spyropoulos N., Patras D., Syrides G., Lambrinos N. and Laggalis T. (1996a): *Neotectonic map of Greece, Langadhas sheet*. 1:100,000, Earthquake Planning and Protection Organisation and European Centre on Prevention and Forecasting of Earthquakes.

- Mountrakis D., Kiliadis A., Pavlides S., Sotiriadis L., Psilovikos A., Astaras Th., Vavliakis E., Koufos G., Christaras V., Skordilis M., Tranos M., Spyropoulos N., Patras D., Syrides G., Lambrinos N. and Laggalis T. (1996b): *Neotectonic map of Greece, Thessaloniki sheet*. 1:100,000, Earthquake Planning and Protection Organisation and European Centre on Prevention and Forecasting of Earthquakes.
- Mountrakis D., Pavlides S., Zouros N., Astaras T. and Chatzipetros A. (1998): Seismic fault geometry and kinematics of the 13 May 1995 western Macedonia (Greece) earthquake. *J. Geodyn.*, **26**(2-4), 175-196.
- Mountrakis D., Tranos M., Papazachos C., Thomaidou E., Karagianni E. and Vamvakaris D. (2006): Neotectonic and seismological data concerning major active faults, and the stress regimes of Northern Greece. *In: Robertson A.H.F. and Mountrakis D. (Eds.), Tectonic Development of the Eastern Mediterranean Region. Geol. Soc. London Spec. Publ.*, **260**, 649-670.
- Mouthereau F. and Petit C. (2003): Rheology and strength of the Eurasian continental lithosphere in the foreland of the Taiwan collision belt: Constraints from seismicity, flexure, and structural styles. *J. Geophys. Res.*, **108**(B11), 2512.
- Mouyaris N., Papastamatiou D. and Vita-Finzi C. (1992): The Helice Fault? *Terra Nova*, **4**, 124-129.
- Mucciarelli M. and FAUST Working Group (2000): Faults as a seismologists' tool: current advancement of the EC project "FAU.S.T". XXVII General Assembly of the European Seismological Commission (ESC), 10-15 September 2000, Lisbon University, Lisbon, Portugal, *Proceedings*, 319-324.
- Muço B. (1994): Focal mechanism solutions for Albanian earthquakes for the years 1964-1988. *Tectonophysics*, **231**, 311-323.
- N**
- Nalbant S.S., Hubert A. and King G.C.P. (1998): Stress coupling between earthquakes in northwest Turkey and the north Aegean Sea. *J. Geophys. Res.*, **103**, 24469-24486.
- Nicol A., Watterson J., Walsh J.J. and Childs C. (1996): The shapes, major axis orientations and displacement patterns of fault surfaces. *J. Struct. Geol.*, **18**(2/3), 235-248.
- North R.G. (1977): Seismic moment, source dimensions, and stress associated with earthquakes in the Mediterranean and Middle East. *Geophys. J. R. astr. Soc.*, **48**, 137-161.
- Novotný O., Zahradník J. and Tselentis G-A. (2001): Northwestern Turkey Earthquakes and the Crustal Structure Inferred from Surface Waves Observed in Western Greece. *Bull. Seism. Soc. Am.*, **91**(4), 875-879.
- Nyst M. and Thatcher W. (2004): New constraints on the active tectonic deformation of the Aegean. *J. Geophys. Res.*, **109**, B11406.
- O**
- Okada Y. (1992): Internal deformation due to shear and tensile faults in a half-space. *Bull. Seism. Soc. Am.*, **82**(2), 1018-1040.
- Oliveto A., Mucciarelli M. and Caputo R. (2004): HVSR prospecting in multi-layered environments: An example from the Tyrnavos Basin (Greece). *J. Seismology*, **8**, 395-406.
- Ord A. and Hobbs B.E. (1989): The strength of the continental crust, detachment zones and the development of plastic instabilities. *Tectonophysics*, **158**, 269-289.

- Ormeni R. (2011): P, S wave velocity model of the crust and upper most mantle of Albania region. *Tectonophysics*, **497**, 114-121.
- Özeren M.S. and Holt W.E. (2010): The dynamics of the easternMediterranean and eastern Turkey. *Geophys. J. Int.*, **183**, 1165-1184.
- P**
- Pakisier L.C. and Robinson R. (1966): Composition and evolution of the continental crust as suggested by seismic observation. *Tectonophysics*, **3**(6), 547-557.
- Palyvos N., Pavlopoulos K., Froussou E., Kranis H., Pustovoytov K., Forman S.L. and Minopoulos D. (2010): Paleoseismological investigation of the oblique-normal Ekkara ground rupture zone accompanying the M 6.7–7.0 earthquake on 30 April 1954 in Thessaly, Greece: Archaeological and geochronological constraints on ground rupture recurrence. *J. Geophys. Res.*, **115**, B06301.
- Panagiotopoulos D.G. and Papazachos B.C. (1985): Travel times of Pn waves in the Aegean and surrounding area. *Geophys. J.R. Astron. Soc.*, **80**, 165-176.
- Panagiotopoulos D.G., Papadimitriou E.E., Papaioannou Ch.A., Scordilis E.M. and Papazachos B.C. (1993): Source Properties of the 21 December 1990 Goumenissa Earthquake in Northern Greece. 2nd Congress of the Hellenic Geophysical Union, 5-7 May 1993, Florina, Greece, *Proceedings*, 286-296.
- Papadimitriou E.E and Sykes L.R. (2001): Evolution of the stress field in the northern Aegean Sea (Greece). *Geophys. J. Int.*, **146**, 747-759.
- Papadimitriou P., Voulgaris N., Kassaras I., Kaviris G., Delibasis N. and Makropoulos K. (2002): The Mw = 6.0, 7 September 1999 Athens Earthquake. *Nat. Hazards*, **27**, 15-33.
- Papadopoulos G.A. (1992): Rupture zones of strong earthquakes in the Thessalia region, Central Greece. XXIII General Assembly ESC, Prague, September 2, 1992, *Proceedings*, **2**, 337-340.
- Papadopoulos G.A. (2000): *Historical earthquakes and tsunamis in the Corinth Rift, Central Greece*. National Observatory of Athens, Institute of Geodynamics, Publ. n. 12, Athens, 128 pp.
- Papaioannou C.A. and Papazachos B.C. (2000): Time-Independent and Time-Dependent Seismic Hazard in Greece Based on Seismogenic Sources. *Bull. Seism. Soc. Am.*, **90**(1), 22-33.
- Papanastassiou D. (2001): The Konitsa, Epirus-NW Greece, July 26 (Ms = 5.4) and August 5, 1996, (Ms = 5.7) earthquakes sequence. *Bull. Geol. Soc. Greece*, **34**(4), 1555-1562.
- Papanastassiou D., Drakatos G., Voulgaris N. and Stavrakakis G. (1998): The May 13, 1995, Kozani-Grevena (NW Greece) earthquake: source study and its tectonic implications. *J. Geodyn.*, **26**(2-4), 233-244.
- Papanastassiou D., Gaki-Papanastassiou K., Maroukian H. and Karymbalis E. (2004): Late Quaternary activity of the Ierapetra normal fault (East Crete – Greece). 5th International Symposium on Eastern Mediterranean Geology, 14-20 April 2004, Thessaloniki, Greece, *Proceedings*, Ref.: S1-22.
- Papanikolaou I.D. and Papanikolaou D.I. (2007): Seismic hazard scenarios from the longest geologically constrained active fault of the Aegean. *Quatern. Int.*, **171-172**, 31-44.
- Papanikolaou D.J., Lekkas E.L., Mariolakos I.D. and Mirkou R.M. (1988): Contribution to the geodynamic evolution of the Mesohellenic basin. *Bull. Geol. Soc. Greece*, **20**, 17-36.

- Papanikolaou D., Alexandri M., Nomikou P. and Ballas D. (2002): Morphotectonic structure of the western part of the North Aegean Basin based on swath bathymetry. *Mar. Geol.*, **190**, 465-492.
- Papanikolaou D., Alexandri M. and Nomikou P. (2006): Active faulting in the North Aegean basin. *In: Dilek Y. and Pavlides S. (Eds.), Postcollisional Tectonics and Magmatism in the Mediterranean Region and Asia. Geol. Soc. Am., Special Paper*, **409**, 189-209.
- Papastamatiou D. and Mouyiaris N. (1986): The Sophadhes earthquake occurred on April 30th 1954 - field observations by Yannis Papastamatiou. *Geol. & Geoph. Res., Sp. Issue*, 341-362.
- Papazachos B.C. (1990): Seismicity of the Aegean and surrounding area. *Tectonophysics*, **178**, 287-308.
- Papazachos B. and Papazachou C. (1997): *The earthquakes of Greece*. Second edition, Editions ZITI, Thessaloniki, 304 pp.
- Papazachos B. and Papazachou C. (2003): *Oi seismoi tis Elladhas* (in Greek). Third edition, Editions ZITI, Thessaloniki, 286 pp.
- Papazachos B.C., Comninakis P.E. and Drakopoulos J.C. (1966): Preliminary results of an investigation of crustal structure in southeastern Europe. *Bull. Seism. Soc. Am.*, **56**(6), 1241-1168.
- Papazachos B., Mountrakis D., Psilovikos A. and Leventakis G. (1979): Surface fault traces and fault plane solutions of the May-June 1978 major shocks in the Thessaloniki area, Greece. *Tectonophysics*, **53**, 171-183.
- Papazachos B.C., Comninakis P.E., Hatzidimitriou P.M., Kiriakidis E.C., Kiratzi A.A., Panagiotopoulos D.G., Papadimitriou E.E., Papaioannou C.A. and Pavlides S. (1982): *Atlas of isoseismal maps for earthquakes in Greece 1902-1981*. Publ. Geophys. Lab. Univ. Thessaloniki, **4**, 126 pp.
- Papazachos B.C., Panagiotopoulos D.G., Tsapanos T.M., Mountrakis D.M. and Dimopoulos G.Ch. (1983): A study of the 1980 summer seismic sequence in the Magnesia region of Central Greece. *Geophys. J. R. astr. Soc.*, **75**, 155-168.
- Papazachos B.C., Kiratzi A.A., Voidomatis P. and Papaioannou C.A. (1984): A study of the December 1981 - January 1982 seismic activity in Northern Aegean Sea. *Boll. Geofis. Teor. Appl.*, **26**(101-102), 101-113.
- Papazachos B., Kiratzi A. and Papadimitriou E. (1991): Regional Focal Mechanisms for Earthquakes in the Aegean Area. *Pure Appl. Geophys.*, **136**(4), 405-420.
- Papazachos B.C., Hatzidimitriou P.M., Karakaisis G.F., Papazachos C.B. and Tsokas G.N. (1993a): Rupture zones and active crustal deformation in southern Thessalia, Central Greece. *Boll. Geofis. Teor. Appl.*, **35**(139), 363-374.
- Papazachos B.C., Papaioannou Ch.A., Papazachos B.C. and Savvaidis A.S. (1997): *Atlas of isoseismal maps for strong shallow earthquakes in Greece and surrounding area (426 BC-1995)*. Publ. Geophys. Lab. Univ. Thessaloniki, **4**, 176 pp.
- Papazachos B.C., Karakostas B.G., Kiratzi A.A., Papadimitriou E.E. and Papazachos C.B. (1998): A model for the 1995 Kozani-Grevena seismic sequence. *J. Geodyn.*, **26**, 217-231.
- Papazachos B.C., Papaioannou C.A., Papazachos C.B. and Savvaidis A.S. (1999): Rupture zones in the Aegean region. *Tectonophysics*, **308**, 205-221.
- Papazachos B.C., Comninakis P.E., Karakaisis G.F., Karakostas B.G., Papaioannou C.A., Papazachos C.B. and Scordilis E.M. (2000): *A catalogue of earthquakes in Greece and*

- surrounding area for the period 550BC-1999. Publ. Geophys. Laboratory, University of Thessaloniki, **1**, 333pp.
- Papazachos B.C., Mountrakis D.M., Papazachos C.B., Tranos M.D., Karakaisis G.F. and Savvaidis A.S. (2001a): The faults which have caused the known major earthquakes in Greece and surrounding region between the 5th century BC and today. 2nd Greek Conference on Earthquake Engineering and Engineering Seismology, Thessaloniki, 28-30 September 2001, *Proceedings*, **1**, 17-26.
- Papazachos B.C., Comninakis P.E., Scordilis E.M., Karakaisis G.F. and Papazachos C.B. (2009): *A catalogue of earthquakes in the Mediterranean and surrounding area for the period 1901 - Sep2009*. Publ. Geophys. Laboratory, University of Thessaloniki.
- Papazachos C. (1993): Determination of crustal thickness by inversion of travel times: An application in the Aegean area. 2nd Congress of the Hellenic Geophysical Union, 5-7 May 1993, Florina, Greece, *Proceedings*, **2**, 483-491.
- Papazachos C.B. (1998): Crustal *P*- and *S*-velocity structure of the Serbomacedonian Massif (Northern Greece) obtained by non-linear inversion of traveltimes. *Geophys. J. Int.*, **134**, 25-39.
- Papazachos C.B. (1999): Seismological and GPS evidence for the Aegean-Anatolia interaction. *Geophys. Res. Lett.*, **26**(17), 2653-2656.
- Papazachos C.B. (2002): The active crustal deformation field of the Aegean Area inferred from seismicity and GPS data. 11th General Assembly of the Wegener Project, 12-14 June, Athens, Greece, *Proceedings*.
- Papazachos C. and Kiratzi A. (1996): A detailed study of the active crustal deformation in the Aegean and surrounding area: *Tectonophysics*, **253**, 129-153.
- Papazachos C.B. and Nolet G. (1997): *P* and *S* deep velocity structure of the Hellenic area obtained by robust nonlinear inversion of travel times. *J. Geophys. Res.*, **102**(B4), 8349-8367.
- Papazachos C.B. and Skordilis E.M. (1998): Crustal structure of the Rhodope and surrounding area obtained by non-linear inversion of *P* and *S* travel times and its tectonic implications. *Acta Vulcanologica*, **10**(2), 339-345.
- Papazachos C.B., Kiratzi A.A. and Papazachos B.C. (1993b): Rates of active crustal deformation in the Aegean and the surrounding area. *Bull. Geol. Soc. Greece*, **28**(1), 21-32.
- Papazachos C.B., Vamvakaris D.A., Vargemezis G.A. and Aidona E.V. (2001b): A study of the active tectonics and deformation in the Mygdonia Basin (N. Greece) using seismological and neotectonic data. *Bull. Geol. Soc. Greece*, **34**(1), 303-309.
- Paradisopoulou P.M., Karakostas V.G., Papadimitriou E.E., Tranos M.D., Papazachos C.B. and Karakaisis G.F. (2004): Microearthquake study of the broader Thessaloniki area. 5th International Symposium on Eastern Mediterranean Geology, 14-20 April 2004, Thessaloniki, Greece, *Proceedings*, **2**, 623-626.
- Paradisopoulou P.M., Karakostas V.G., Papadimitriou E.E., Tranos M.D., Papazachos C.B. and Karakaisis G.F. (2006): Microearthquake study of the broader Thessaloniki area (Northern Greece). *Ann. Geophys.*, **49**(4/5), 1081-1093.
- Pasquale V., Verdoya M., Chiozzi P. and Ranalli G. (1997): Rheology and seismotectonic regime in the northern central Mediterranean. *Tectonophysics*, **270**, 239-257.
- Pauselli C., Ranalli G. and Federico C. (2010): Rheology of the Northern Apennines: Lateral variations of lithospheric strength. *Tectonophysics*, **484**, 27-35.

- Pavlidis S. (1985): *Neotectonic evolution of the Florina-Vegoritiss-Ptolemais basin (W. Macedonia, Greece)*. Ph.D. Thesis, University of Thessaloniki, Greece, 265 pp.
- Pavlidis S. (1993): Active faulting in multi-fractured seismogenic areas; examples from Greece. *Z. Geomorph. N.F.*, **94**, 57-72.
- Pavlidis S.B. (1998): Dating the neotectonisms in south Almopias (Central Macedonia, N. Greece). *Bull. Geol. Soc. Greece*, **32**(1), 189-197.
- Pavlidis S. and Caputo R. (1994): The North Aegean region: a tectonic paradox? *Terra Nova*, **6**, 37-44.
- Pavlidis S. and Caputo R. (2004): Magnitude *versus* faults' surface parameters: quantitative relationships from the Aegean *Tectonophysics*, **380**, 159-188.
- Pavlidis S.B. and Kiliass A.A. (1987): Neotectonic and active faults along the Serbomacedonian zone (SE Chalkidiki, northern Greece). *Ann. Tectonicae*, **1**(2), 97-104.
- Pavlidis S.B. and Mountrakis D.M. (1987): Extensional tectonics of northwestern Macedonia, Greece, since the late Miocene. *J. Struct. Geol.*, **9**(4), 385-392.
- Pavlidis S. and Simeakis K. (1987/88): Neotectonics and active tectonics in low seismicity areas of Greece: Vegoritiss (NW Macedonia) and Melos isl complex (Cyclades) - comparison. *Ann. Géol. Pays Helléniques*, **33**(2), 161-176.
- Pavlidis S.B. and Tranos M.D. (1991): Structural characteristics of two strong earthquakes in the North Aegean: Ierissos (1932) and Agios Efstratios (1968). *J. Struct. Geol.*, **13**, 205-214.
- Pavlidis S., Mountrakis D., Kiliass A. and Tranos M. (1990): The role of strike-slip movements in the extensional area of Northern Aegean (Greece). A case of transtensional tectonics. *Ann. Tectonicae*, **4**(2), 196-211.
- Pavlidis S.B., Zouros N.C., Chatzipetros A.A., Kostopoulos D.S. and Mountrakis D.M. (1995): The 13 May 1995 western Macedonia, Greece (Kozani Grevena) earthquake; preliminary results. *Terra Nova*, **7**, 544-549.
- Pavlidis S., Kociu S., Mukelli, P., Hyseni A. and Zouros N. (2001a): Neotectonics of southwestern Albania and archaeological evidence for seismic activity in Butrint. 4th International Symposium on Eastern Mediterranean Geology, 21-25 May, 2001, Isparta, Turkey, *Proceedings*, 1-20.
- Pavlidis S., Koukouvelas I., Stamatopoulos L., Agrafiotis D., Alexandris G.-A., Zygouri B. and Sboras S. (2001b): Palaeoseismological investigation of the Eastern 'segment' of the Heliki Fault, Gulf of Corinth, Greece. *Bull. Geol. Soc. Greece*, **34**(1), 199-205.
- Pavlidis S.B., Papadopoulos G. and Ganas A. (2002): The Fault that Caused the Athens September 1999 Ms = 5.9 Earthquake: Field Observations. *Nat. Hazards*, **27**, 61-84.
- Pavlidis S., Chatzipetros A. and Tsapanos Th. (2004a): The Kerkini-Sidirokastro (northern Strymon valley, Greece) active fault and its seismic potential. 4th National Geoph. Conf., 4-5 October 2004, Sofia, *Abstracts*.
- Pavlidis S., Kouskouna V. Ganas A., Caputo R., Karastathis V. and Sokos E. (2004b): The Gonnoi (NE Thessaly - Greece) earthquake (June 2003, Ms=5.5) and the neotectonic regime of Lower Olympus. 5th International Symposium on Eastern Mediterranean Geology, 14-20 April 2004, Thessaloniki, Greece, *Proceedings*, **2**, 627-630.
- Pavlidis S.B., Koukouvelas I.K., Kokkalas S., Stamatopoulos L., Keramydas D. and Tsodoulos I. (2004c): Late Holocene evolution of the East Eliki fault, Gulf of Corinth (Central Greece). *Quat. Int.*, **115-116**, 139-154.

- Pavlidis S., Valkaniotis S., Kurcel A., Papathanassiou G. and Chatzipetros A. (2005): Neotectonics of Samothraki Island (NE Aegean, Greece) in relation to the North Anatolian Fault. *Bull. Geol. Soc. Greece*, **37**, 19-28.
- Pavlidis S.B., Valkaniotis S. and Chatzipetros A. (2007): Seismically capable faults in Greece and their use in seismic hazard assessment. 4th Int. Conf. Earthq. Geotech. Eng., June 25-28, 2007, Thessaloniki, *Proceedings*, paper n. 1609.
- Pavlidis S., Tsapanos T., Zouros N., Sboras S., Koravos G. and Chatzipetros A. (2009): Using Active Fault Data for Assessing Seismic Hazard: A Case Study from NE Aegean Sea, Greece. *17th Int. Conf. Soil Mech. & Geotechn. Eng.*, 2-3 October 2009, Alexandria, Egypt.
- Pavlidis S., Caputo R., Sboras S., Chatzipetros A., Papathanassiou G. and Valkaniotis S. (2010): The Greek Catalogue of Active Faults and Database of Seismogenic Sources. *Bull. Geol. Soc. Greece*, **43**(1), 486-494.
- Peacock S.M. (1991): Numerical simulation of subduction zone pressure-temperature-time paths: constraints on fluid production and arc magmatism. *Phil. Trans. R. Soc. Lond. A*, **335**, 341-353.
- Perissoratis C., Angelopoulos I. and Mitropoulos D. (1991): *Surficial Sediment Map of the Aegean Sea Floor: Pagasitikos Sheet*. 1:200,000, IGME editions, Athens, Greece.
- Peter D., Boschi L., Deschamps F., Fry B., Ekström G., and Giardini D. (2008): A new finite-frequency shear-velocity model of the European-Mediterranean region. *Geophys. Res. Lett.*, **35**, L16315.
- Peterek A. and Schwarze J. (2004): Architecture and Late Pliocene to recent evolution of outer-arc basins of the Hellenic subduction zone (south-central Crete, Greece). *J. Geodyn.*, **38**, 19-55.
- Pirazzoli P.A., Stiros S.C., Fontugne M. and M. Arnold (2004): Holocene and Quaternary uplift in the central part of the southern coast of the Corinth Gulf (Greece). *Marine Geology*, **212**, 35-44.
- Plank T. and Langmuir C.H. (1998): The geochemical composition of subducting sediment and its consequences for the crust and mantle. *Chem. Geol.*, **145**, 325-394.
- Pollack H.N. and Chapman D.S. (1977): On the regional variation of heat flow, geotherms, and lithospheric thickness. *Tectonophysics*, **38**, 279-296.
- Pollack H.N., Hurter S.J. and Johnson J.R. (1993): Heat flow from the Earth's interior: analysis of the global data set. *Rev. Geophys.*, **31**, 267-280.
- Porth R. (2000): A strain-rate-dependent force model of lithospheric strength. *Geophys. J. Int.*, **141**, 647-660.
- Poulimenos G. and Doutsos T. (1996): Barriers on seismogenic faults in Central Greece. *J. Geodyn.*, **22**, 119-135.
- Priestley K., Jackson J. and McKenzie D. (2008): Lithospheric structure and deep earthquakes beneath India, the Himalaya and southern Tibet. *Geophys. J. Int.*, **172**, 345-362.
- Psilovikos A. (1984): Geomorphological and structural modification of the Serbomacedonian massif during the neotectonic stage. *Tectonophysics*, **110**, 27-45.
- Psilovikos A. and Papaphilippou E. (1990): Pediments, alluvial fans and neotectonic movements of the Mt Kerkini/Belassitsa. *Geologica Rhodopica*, **2**, Aristotle University Press, Thessaloniki, 95-103.

R

- Ranalli G. (1987): *Rheology of the Earth*. 1st ed., Allen & Unwin, Boston, 366 pp.

- Ranalli G. (1995): *Rheology of the Earth*. 2nd ed., Chapman & Hall, London, 413 pp.
- Ranalli G. (1997a): Rheology and deep tectonics. *Ann. Geofisica*, **40**(3), 671-680.
- Ranalli G. (1997b): Rheology of the lithosphere in space and time. In: Burg J.-P. and Ford M. (Eds.), *Orogeny Through Time*, *Geol. Soc. Lond. Spec. Publ.*, **121**, 19-37.
- Ranalli G. (2000): Rheology of the crust and its role in tectonic reactivation. *J. Geodyn.*, **30**, 3-15.
- Ranalli G. and Murphy D.C. (1987): Rheological stratification of the lithosphere. *Tectonophysics*, **132**, 281-295.
- Ranalli G. and Rybach L. (2005): Heat flow, heat transfer and lithosphere rheology in geothermal areas: Features and examples. *J. Volcanol. Geoth. Res.*, **148**, 3-19.
- Rao M.V.M.S., Prasanna Lakshmi K.J., Sarma L.P. and Chary K.B. (2006): Elastic properties of granulite facies rocks of Mahabalipuram, Tamil Nadu, India. *J. Earth Syst. Sci.*, **115**(6), 673-683.
- Ray L., Bhattacharya A. and Roy S. (2007): Thermal conductivity of Higher Himalayan Crystallines from Garhwal Himalaya, India. *Tectonophysics*, **434**, 71-79.
- Raykova R. and Nikolova S. (2007): Tomography and velocity structure of the crust and uppermost mantle in southeastern Europe obtained from surface wave analysis. *Stud. Geophys. Geod.*, **51**, 165-184.
- Raznjevic K. (1976). *Handbook of Thermodynamic Tables and Charts*. Hemisphere Publishing Corp., Washington DC, 392 pp.
- Reasenbeg P.A. and Simpson R.W. (1992): Response of regional seismicity to the static stress change produced by the Loma Prieta earthquake. *Science*, **255**, 1687-1690.
- Reilinger R.E., McClusky S.C., Oral M.B., King R.W., Toksoz M.N., Barka A.A., Kinik I., Lenk O. and Sanli I. (1997): Global Positioning System measurements of present-day crustal movements in the Arabia-Africa-Eurasia plate collision zone. *J. Geophys. Res.*, **102**(B5), 9983-9999.
- Reilinger R., McClusky S., Vernant P., Lawrence S., Ergintav S., Cakmak R., Ozener H., Kadirov F., Guliev I., Stepanyan R., Nadariya M., Hahubia G., Mahmoud S., Sakr K., ArRajehi A., Paradissis D., Al-Aydrus A., Prilepin M., Guseva T., Evren E., Dmitrotsa A., Filikov S.V., Gomez F., Al-Ghazzi R. and Karam G. (2006): GPS constraints on continental deformation in the Africa–Arabia–Eurasia continental collision zone and implications for the dynamics of plate interactions. *J. Geophys. Res.*, **111**(B5), B05411.
- Reilinger R, McClusky S., Paradissis D., Ergintav S. and Vernant P. (2010): Geodetic constraints on the tectonic evolution of the Aegean region and strain accumulation along the Hellenic subduction zone. *Tectonophysics*, **488**, 22-30.
- Reiter M.A. and Tovar R.J.C. (1982): Estimates of terrestrial heat flow in Northern Chihuahua, Mexico. *Can. J. Earth Sci.*, **22**, 1503-17.
- Resor P.G., Pollard D.D., Wright T.J. and Beroza G.C. (2005): Integrating high-precision aftershock locations and geodetic observations to model coseismic deformation associated with the 1995 Kozani-Grevena earthquake, Greece. *J. Geophys. Res.*, **110**, B09402.
- Ricou L.E., Dercourt J., Geysant J., Grandjacquet C., Lepvrier C. and Biju-Duval B. (1986): Geological constraints on the Alpine evolution of the Mediterranean Tethys. *Tectonophysics*, **123**, 83-122.
- Ricou L.-E., Burg J.-P., Godfriaux I. and Ivanov Z. (1998): Rhodope and Vardar: the metamorphic and the olistostromic paired belts related to the Cretaceous subduction under Europe. *Geodin. Acta*, **11**(6), 285-309.

- Rietbrock A., Tiberi C., Scherbaum F and Lyon-Caen H. (1996): Seismic slip on a low angle normal fault in the Gulf of Corinth: Evidence from high-resolution cluster analysis of microearthquakes. *Geophys. Res. Lett.*, **23**(14), 1817-1820.
- Rigo A., Lyon-Caen H., Armijo R., Deschamps A., Hatzfeld D., Makropoulos K., Papadimitriou P. and Kassaras (1996): A microseismic study in the western part of the Gulf of Corinth (Greece): implications for large-scale normal faulting mechanisms. *Geophys. J. Int.*, **126**, 663-688.
- Rigo A., de Chabaliér J.-B., Meyer B. and Armijo R. (2004): The 1995 Kozani-Grevena (northern Greece) earthquake revisited: An improved faulting model from synthetic aperture radar interferometry. *Geophys. J. Int.*, **157**, 727-736.
- Ring U., Brachert T. and Fassoulas C. (2001): Middle Miocene graben development in Crete and its possible relation to large-scale detachment faults in the southern Aegean. *Terra Nova*, **13**, 297-304.
- Rippon J. (1985a): Contoured patterns of the throw and hade of normal faults in the Coal Measures (Westphalian) of north-east Derbyshire. *Proc. Yorks. geol. Soc.*, **45**, 147-161.
- Rippon J. (1985b): New methods of forecasting the throw and hade of faults in some North Derbyshire Collieries. *Trans. Inst. Min. Engrs*, **145**, 198-204.
- Roberts G.P. and Koukouvelas I. (1996): Structural and seismological segmentation of the Gulf of Corinth fault system: implications for models of fault growth. *Ann. Geophys.*, **39**(3), 619-646.
- Robertson A.H.F. and Dixon J.F. (1984): Introduction: aspects of the geological evolution of the Eastern Mediterranean. In: Dixon J.E. and Robertson A.H.F. (Eds.): The Geological Evolution of the Eastern Mediterranean. *Geol. Soc. London Spec. Publ.*, **17**, 1-74.
- Robertson A.H.F., Clift P.D., Degnan P.J. and Jones G. (1991): Palaeogeographic and palaeotectonic evolution of the Eastern Mediterranean Neotethys. *Palaeogeogr., Palaeoclimatol., Palaeoecol.*, **87**, 289-343.
- Robertson A.H.F., Dixon J.E., Brown S., Collins A., Morris A., Pickett E., Sharp I. and Ustaömer T. (1996): Alternative tectonic models for the Late Palaeozoic-Early Tertiary development of Tethys in the Eastern Mediterranean region. In: Morris A. and Tarling D.H. (Eds.), Palaeomagnetism and Tectonics of the Mediterranean Region. *Geol. Soc. London Spec. Publ.*, **105**, 239-263.
- Rocca A.C., Karakaisis G.F., Karacostas B.G., Kiratzi A.A., Scordilis E.M. and Papazachos B.C. (1985): Further evidence on the strike-slip faulting of the Northern Aegean Trough based on properties of the August-November 1983 seismic sequence. *Boll. Geofis. Teor. Appl.*, **27**(106), 101-109.
- Rockwell T., Barka A., Dawson T., Akyuz S. and Thorup K. (2001): Paleoseismology of the Gazikoy-Saros segment of the North Anatolia fault, northwestern Turkey: Comparison of the historical and paleoseismic records, implications of regional seismic hazard, and models of earthquake recurrence. *J. Seismol.*, **5**, 433-448.
- Rondoyanni Th., Georgiou Ch., Galanakis D. and Kourouzis M. (2004): Evidences of active faulting in Thrace region (Northeastern Greece). *Bull. Geol. Soc. Greece*, **36**, 1671-1678.
- Roumelioti Z., Theodulidis N. and Kiratzi A. (2007): The 20 June 1978 Thessaloniki (Northern Greece) earthquake revisited: Slip distribution and forward modeling of geodetic and seismological observations. 4th Int. Conf. Earthq. Geotech. Eng., June 25-28, *Proceedings*, Paper No. 1594.

- Roussos N and Lyssimachou T. (1991): Structure of the Central North Aegean Trough: an active strike-slip deformation zone. *Basin Research*, **3**, 39-48.
- Roy R.F., Blackwell D.D. and Birch F. (1968): Heat generation of plutonic rocks and continental heat flow provinces. *Earth Planet. Sci. Lett.*, **5**, 1-12.
- Roy R.F., Beck A.E. and Touloukian Y.S. (1981): Thermophysical properties of rocks. In: Touloukian Y.S., Judd W.R. and Roy R.F. (Eds.), *Physical Properties of Rocks and Minerals*, McGraw-Hill, New York, 409-502.
- Rudnick R.L. and Fountain D.M. (1995): Nature and composition of the continental crust; a lower crustal perspective. *Rev. Geophys.*, **33**, 267-309.
- Rudnick R.L., McDonough W.F. and O'Connell R.J. (1998): Thermal structure, thickness and composition of continental lithosphere. *Chem. Geol.*, **145**, 395-411.
- Rybach L. and Buntebarth G. (1984): The variation of heat generation, density and seismic velocity with rock type in the continental lithosphere. *Tectonophysics*, **103**, 335-344.

S

- Saatçılar R., Ergintav S., Demirbag E. and Inan S. (1999): Character of active faulting in the North Aegean Sea. *Mar. Geol.*, **160**, 339-353.
- Sachpazi M., Clément C. Laigle M., Hirn A. and Roussos N. (2003): Rift structure, evolution, and earthquakes in the Gulf of Corinth, from reflection seismic images. *Earth Planet. Sci. Lett.*, **216**, 243-257.
- Sachpazi M., Galvé A., Laigle M., Hirn A., Sokos E., Serpetsidaki A., Marthelot J.-M., Pi Alperin J.M., Zelt B. and Taylor B. (2007): Moho topography under central Greece and its compensation by Pn time-terms for the accurate location of hypocenters: The example of the Gulf of Corinth 1995 Aigion earthquake. *Tectonophysics*, **440**, 53-65.
- Sakellariou D., Roussakis G., Kranis C., Kamperi E., Georgiou P. and Skoulikidis N. (2001): Neotectonic Movements, Sedimentation and Water-Level Fluctuation of the Lake Vegoritis in Upper Quaternary. *Bull. Geol. Soc. Greece*, **34**(1), 207-216.
- Sboras S. and Caputo R. (2010): Possible occurrence of low-angle normal faults in Central and Northern Greece. 29° Convegno Nazionale di GNGTS, 26-28 October 2009, Prato, Italy, *Extended Abstracts*, 195-198.
- Sboras S., Caputo R., Pavlides S., Chatzipetros A., Papathanasiou G. and Valkaniotis S. (2009a): The Greek Database of Seismogenic sources (GreDaSS): state-of-the-art. 28° Convegno Nazionale GNGTS, 16-19 November, 2009, Trieste, *Extended Abstracts*, 126-128.
- Sboras S., Caputo R., Pavlides S., Chatzipetros A., Papathanasiou G., Valkaniotis S., Basili R., and Valensise G. (2009b): The Greek Database of Seismogenic Sources: state-of-the-art on the northern Greece pilot area. *Geophysical Research Abstracts*, **11**, EGU2009-485-3.
- Sboras S., Ganas A. and Pavlides S. (2010): Morphotectonic analysis of the neotectonic and active faults of Beotia (Central Greece), using G.I.S. techniques. *Bull. Geol. Soc. Greece*, **43**(3), 1607-1618.
- Sboras S., Pavlides S., Caputo R., Chatzipetros A., Michailidou A., Valkaniotis S. and Papathanasiou G. (2011): Improving the resolution of seismic hazard estimates for critical facilities: the Database of Greek crustal seismogenic sources in the frame of the SHARE project. 30° Convegno Nazionale GNGTS, 14-17 November, 2011, Trieste, *Extended Abstracts*, 232-235.

- Schmid S.M., Paterson M.S. and Boland J.N. (1980): High temperature flow and dynamic recrystallization in Carrara marble. *Tectonophysics*, **65**, 245-280.
- Schmidt J.F. (1867): *Pragmatia peri tou genomenou to 1861 Dec. 26 seismou tou Aigiou*. Ethniko Typografio, Athens, 52 pp. [in Greek].
- Schmidt J. (1879): *Studien über Erdbeben*. Leipzig, Carl Schottze, Leipzig, 68-83.
- Scholz C.H. (1988): The brittle-plastic transition and the depth of seismic faulting. *Geol. Rund.*, **77**(1), 319-328.
- Seipold U. (1992): Depth dependence of thermal transport properties for typical crustal rocks. *Phys. Earth Planet. Inter.*, **69**, 299-303.
- Seipold U. (1998): Temperature dependence of thermal transport properties of crystalline rocks - a general law. *Tectonophysics*, **291**, 161-171.
- Sengör A.M.C., Yılmaz Y. and Sungurly O. (1984): Tectonics of the Mediterranean Cimmerides: Nature and evolution of the western termination of Paleo-Tethys. In: Dixon J.E. and Robertson A.H.F. (Eds.), *The Geological Evolution of the Eastern Mediterranean*. *Geol. Soc. London Spec. Publ.*, **17**, 77-112.
- Shimada M. (1993): Lithosphere strength inferred from fracture strength of rocks at high confining pressures and temperatures. *Tectonophysics*, **217**, 55-64.
- Shimada M. and Cho A. (1990): Two types of brittle fracture of silicate rocks under confining pressure and their implications in the earth's crust. *Tectonophysics*, **175**, 221-235.
- Shimazaki K. and Nakata T. (1980): Time-predictable recurrence model for large earthquakes. *Geophys. Res. Lett.*, **7**(4), 279-282.
- Sibson R.H. (1974): Frictional constraints on thrust, wrench and normal faults. *Nature*, **249**, 542-544.
- Sibson R.H. (1982): Fault zone models, heat flow, and the depth distribution of earthquakes in the continental crust of the United States. *Bull. Seism. Soc. Am.*, **72**(1), 151-163.
- Sibson R.H. (1983): Continental fault structure and the shallow earthquake source. *J. Geol. Soc. London*, **140**, 741-767.
- Sibson R.H. (1984): Roughness at the Base of the Seismogenic Zone: Contributing Factors. *J. Geophys. Res.*, **89**(B7), 5791-5799.
- Skourtsos E. and Kranis H. (2009): Structure and evolution of the western Corinth Rift, through new field data from the Northern Peloponnesus. *Geol. Soc. London Spec. Publ.*, **321**, 119-138.
- Sleep, N.H., 2005. Evolution of the continental lithosphere. *Annu. Rev. Earth Pl. Sc.*, **33**, 369-393.
- Smith A.G. (1971): Alpine Deformation and the Oceanic Areas of the Tethys, Mediterranean, and Atlantic. *Bull. Geol. Soc. Am.*, **82**, 2039-2070.
- Smith A.G. and Moores E.M. (1974): Hellenides. *Geol. Soc. London Spec. Publ.*, **4**, 159-185.
- Smith A.G. and Spray J.G. (1984): A half-ridge transform model for the Hellenic-Dinaric ophiolites. In: Dixon J.E. and Robertson A.H.F. (Eds.): *The Geological Evolution of the Eastern Mediterranean*, *Geol. Soc. London Spec. Publ.*, **17**, 629-644.
- Smith A.G. and Woodcock N.H. (1976): Emplacement model for some "Tethyan" ophiolites. *Geology*, **4**, 653-656.
- Soudoufi F., Kind R., Hatzfeld D., Priestley K., Hanka W., Wylegalla K., Stavrakakis G., Vafidis A., Harjes H.-P. and Bohnhoff M. (2006): Lithospheric structure of the Aegean obtained from P and S receiver functions. *J. Geophys. Res.*, **111**, B12307.

- Soliva R. and Benedicto A. (2004): A linkage criterion for segmented normal faults. *J. Struct. Geol.*, **26**, 2251-2267.
- Sorel D. (2000): A Pleistocene and still-active detachment fault and the origin of the Corinth-Patras rift, Greece. *Geology*, **28**, 83-86.
- Soufleris Ch. and King G. (1983): A source study of the largest foreshock (on May 23) and the mainshock (on June 20) of the Thessaloniki 1978 earthquake sequence. In: Papazachos B.C. and Carydis P.G. (Eds.), *The Thessaloniki, Northern Greece, earthquake of June 20, 1978 and its seismic sequence*, Technical Chamber of Greece, 201-222.
- Soufleris C. and Stewart G. (1981): A source study of the Thessaloniki (northern Greece) 1978 earthquake sequence. *Geophys. J. R. Astr. Soc.*, **67**, 343-358.
- Soufleris C., Jackson J.A., King G.C.P., Spencer C.P. and Scholz C.H. (1982): The 1978 earthquake sequence near Thessaloniki (northern Greece). *Geophys. J. R. astr. Soc.*, **68**, 429-458.
- Spakman W. (1990): Tomographic images of the upper mantle below central Europe and the Mediterranean. *Terra Nova*, **2**, 542-553.
- Spakman W., Wortel M.J.R. and Vlaar N.J. (1988): The Hellenic subduction zone: A tomographic image and its geodynamical implications. *Geophys. Res. Lett.*, **15**(1), 60-63.
- Spakman W., Van der Lee S. and Van der Hilst R.D. (1993): Travel time tomography of the European-Mediterranean mantle down to 1400 km. *Phys. Earth Planet. Int.*, **79**, 3-74.
- Stampfli G., Marcoux J. and Baud A. (1991): Tethyan margins in space and time. *Palaeogeogr., Palaeoclimatol., Palaeoecol.*, **87**, 373-409.
- Stanley D.J. and Perissoratis C. (1977): Aegean Sea ridge barrier-and-basin sedimentation patterns. *Mar. Geol.*, **24**, 97-107.
- Steckler M.S. and ten Brink U.S. (1986): Lithospheric strength variations as a control on new plate boundaries: examples from the northern Red Sea region. *Earth Planet. Sci. Lett.*, **79**, 120-132.
- Stein S. and Wysession M. (2003): *An introduction to seismology, earthquakes and Earth structure*. Blackwell Publishing Ltd., 512 pp.
- Steininger F.F. and Rögl F. (1984): Paleogeography and palinspastic reconstruction of the Neogene of the Mediterranean and Paratethys. In: Dixon J.E. and Robertson A.H.F. (Eds.), *The Geological Evolution of the Eastern Mediterranean*. *Geol. Soc. London Spec. Publ.*, **17**, 659-668.
- Stesky R.M., Brace W.F., Riley D.K. and Robin P.-Y.F. (1974): Friction in faulted rock at high temperature and pressure. *Tectonophysics*, **23**, 177-203.
- Stewart I. (1996a): A rough guide to limestone fault scarps. *J. Struct. Geol.*, **18**(10), 1259-1264.
- Stewart I. (1996b): Holocene uplift and palaeoseismicity on the Eliki Fault, Western Gulf of Corinth, Greece. *Ann. Geophys.*, **39**(3), 575-588.
- Stewart I. and Vita-Finzi C. (1996): Coastal uplift on active normal faults: The Eliki Fault, Greece. *Geophys. Res. Lett.*, **23**(14), 1853-1856.
- Stiros S.C. and Drakos A. (2000): Geodetic constrains on the fault pattern of the 1978 Thessaloniki (Northern Greece) earthquake (Ms=6.4). *Geophys. J. Int.*, **143**, 679-688.
- Stiros S., Triantafillides P. and Chasapis A. (2004): Geodetic evidence for active uplift of the Olympus Mt., Greece. *Bull. Geol. Soc. Greece*, **36**(4), 1697-1705.
- Stüwe K. (2007): *Geodynamics of the Lithosphere: An introduction*. 2nd ed., Springer-Verlag, Berlin, Heidelberg, 493 pp.

Suhadolc P., Moratto L., Costa G. and Triantafyllidis P. (2007): Source Modeling of the Kozani and Arnea 1995 Events with Strong Motion Estimates for the City of Thessaloniki. *J. Earthq. Eng.*, **11**(4), 560-581.

T

Taktikos S. (2001): *Heat flow – Underground temperatures of Greece* (in Greek). 2 volumes and 12 maps set, Institute of Geology and Mineral Exploration, Athens, 72 pp.

Taylor S.R. and McLennan S.M. (1995): The geochemical evolution of the continental crust. *Rev. Geophys.*, **33**, 241-265.

Taymaz T., Jackson J. and McKenzie D. (1991): Active tectonics of the north and central Aegean Sea. *Geophys. J. Int.*, **106**, 433-490.

Taymaz T., Yilmaz Y. and Dilek Y. (2007): The geodynamics of the Aegean and Anatolia: introduction. In: Taymaz T. Yilmaz Y. and Dilek Y. (Eds.), *The Geodynamics of the Aegean and Anatolia. Geol. Soc. London Spec. Publ.*, **291**, 1-16.

Tejero R. and Ruiz J. (2002): Thermal and mechanical structure of the central Iberian Peninsula lithosphere. *Tectonophysics*, **350**, 49-62.

ten Veen J.H. and Postma G. (1999): Neogene tectonics and basin fill patterns in the Hellenic outer-arc (Crete, Greece). *Basin Res.*, **11**, 223-241.

Tiberi C., Diament M., Lyon-Caen H. and King T. (2001): Moho topography beneath the Corinth Rift area (Greece) from inversion of gravity data. *Geophys. J. Int.*, **145**, 797-808.

Tirel C., Gueydan F., Tiberi C. and Brun J.-P. (2004): Aegean crustal thickness inferred from gravity inversion Geodynamical implications. *Earth Planet. Sci. Lett.*, **228**, 267-280.

Toda S., Stein R.S. and Sagiya T. (2002): Evidence from the AD 2000 Izu islands earthquake swarm that stressing rate governs seismicity. *Nature*, **419**, 58-62.

Toda S., Stein R.S., Sevilgen V. and Lin J. (2011): *Coulomb 3.3 graphic-rich deformation and stress-change software-user guide*. U.S. Geological Survey Open-File Report 2011-1060, 63 pp.

Tranos M.D. (1998): *Contribution to the study of the neotectonic deformation in the region of Central Macedonia and North Aegean*. PhD thesis, Aristotle University of Thessaloniki, 349 pp.

Tranos M.D. and Mountrakis D.M. (2004): The Serres fault zone (SZF): an active fault zone in Eastern Macedonia (Northern Greece). 5th International Symposium on Eastern Mediterranean Geology, 14-20 April 2004, Thessaloniki, Greece, *Proceedings*, Ref.: S1-18.

Tranos M., Papadimitriou E. and Kiliyas A. (2003): Thessaloniki-Gerakarou Fault Zone (TGFZ): the western extension of the 1978 Thessaloniki earthquake fault (Northern Greece) and seismic hazard assessment. *J. Struct. Geol.*, **25**, 2109-2123.

Tselentis G.-A., Sokos E., Martakis N. and Serpetsidaki A. (2006): Seismicity and Seismotectonics in Epirus, Western Greece: Results from a Microearthquake Survey, *Bull. Seism. Soc. Am.*, **96**(5), 1706-1717.

Tsokas G.N. and Hansen R.O. (1997): Study of the crustal thickness and subducting lithosphere in Greece from gravity data. *J. Geophys. Res.*, **102**, 20585-20597.

Tüysüz O., Barka A., Yigitbas E. (1998): Geology of the Saros graben and its implications for the evolution of the North Anatolian fault in the Ganos-Saros region, northwestern Turkey. *Tectonophysics*, **293**, 105-126.

Turcotte D.L. and Schubert G. (1982): *Geodynamics: Applications of continuum physics to Geological Problems*. John Wiley & Sons, New York, 450 pp.

U

Ustaömer T., Gökaşan E., Tur H., Görüm T., Batuk F.G., Kalafat D., Alp H., Ecevitoglu B. and Birkan H. (2008): Faulting, mass-wasting and deposition in an active dextral shear zone, the Gulf of Saros and the NE Aegean Sea, NW Turkey. *Geo-Mar. Lett.*, **28**, 171-193.

V

Valensise G. and Pantosti D. (Eds.) (2001): Database of potential sources for earthquakes larger than M 5.5 in Italy. *Ann. Geofisica*, **44**(4), 797-807.

Valkaniotis S. (2005): *Research of active faults in Western Thessaly*. M.Sc. thesis, Aristotle University of Thessaloniki, 122 pp. (unpublished, in Greek).

Valkaniotis S., Zervopoulou A., Ganas A. and Pavlides S. (2005): Urban Expansion and Seismic Hazard Increase: Athens and Thessaloniki Examples. In Conference: "Metropolitan Geography: Phenomenon Aspects in Greek Territory", 21-23 October 2005, Thessaloniki, Greece. (in Greek)

Vamvaka A., Kiliyas A., Mountrakis D. and Papaoikonomou J. (2006): Geometry and structural evolution of the Mesohellenic Trough (Greece): a new approach. In: Robertson A.H.F. and Mountrakis D. (Eds.), *Tectonic Development of the Eastern Mediterranean Region*. *Geol. Soc. London Spec. Publ.*, **260**, 521-538.

Vamvakaris D.A., Papazachos C.B., Karagianni E.E., Scordilis E.M. and Hatzidimitriou P.M. (2006): Small-scale spatial variation of the stress field in the back-arc Aegean area: Results from the seismotectonic study of the broader area of Mygdonia basin (N. Greece). *Tectonophysics*, **417**, 249-267.

van der Meijde M., van der Lee S. and Giardini D. (2003): Crustal structure beneath broad-band seismic stations in the Mediterranean region. *Geophys. J. Int.*, **152**, 729-739.

van der Pluijm B.E. and Marshak S. (2004): *Earth Structure: an introduction to structural geology and tectonics*. 2nd ed., W.W. Norton & Company, New York, 656 pp.

van Hinsbergen D.J.J., Hafkenscheid E., Spakman W., Meulenkaamp J.E. and Wortel M. J.R. (2005a): Nappe stacking resulting from subduction of oceanic and continental lithosphere below Greece. *Geology*, **33**, 325-328.

van Hinsbergen D.J.J., Langereis C.G. and Meulenkaamp J.E. (2005b): Revision of the timing, magnitude and distribution of Neogene rotations in the western Aegean region. *Tectonophysics*, **396**, 1-34.

Vannucci G. and Gasperini P. (2003): A database of revised fault plane solutions for Italy and surrounding regions. *Computers & Geosciences*, **29**, 903-909.

Vannucci G. and Gasperini P. (2004): The new release of the database of Earthquake Mechanisms of the Mediterranean Area (EMMA Version 2). *Ann. Geofis.*, supplement to Vol. **47**, 307-334.

Verdoya M., Pasquale W., Chiozzi P. and Kukkonen I.T. (1998): Radiogenic heat production in the Variscan crust: new determinations and distribution models in Corsica (northwestern Mediterranean). *Tectonophysics*, **291**, 63-75.

Verrios S., Zygouri V. and Kokkalas S. (2004): Morphotectonic analysis in the Eliki Fault zone (Gulf of Corinth, Greece). *Bull. Geol. Soc. Greece*, **36**, 1706-1715.

- Viti M., Albarello D. and Mantovani E. (1997): Rheological profiles in the Central-Eastern Mediterranean. *Ann. Geofisica*, **40**(4), 849-864.
- Voidomatis P. (1989): Some aspects of a seismotectonic synthesis in the North Aegean Sea and surrounding area. *Boll. Geofis. Teor. Appl.*, **31**, 49-61.
- Voidomatis Ph.S., Pavlides S.B. and Papadopoulos G.A. (1990): Active deformation and seismic potential in the Serbomacedonian zone, northern Greece. *Tectonophysics*, **179**, 1-9.
- Vougioukalakis G. (2002): *Petrological, Geochemical and Volcanological study of the Almopias Pliocene volcanic formations and their correlation with the geothermal manifestations in the area*. PhD Thesis, Aristotle University of Thessaloniki, 303 pp.

W

- Walcott C.R. and White S.H. (1998): Constraints on the kinematics of post-orogenic extension imposed by stretching lineations in the Aegean region. *Tectonophysics*, **298**, 155-175.
- Walsh J.J. and Watterson J. (1987): Distributions of cumulative displacement and seismic slip on a single normal fault surface. *J. Struct. Geol.*, **9**(8), 1039-1046.
- Walsh J.J. and Watterson J. (1991): Geometric and kinematic coherence and scale effects in normal fault systems. In: Roberts A.M., Yielding G. and Freeman B. (Eds.), *The Geometry of Normal Faults*. *Geol. Soc. London Spec. Publ.*, **56**, 193-203.
- Waples D.W. (2002): A New Model for Heat Flow in Extensional Basins: Estimating Radiogenic Heat Production. *Nat. Resour. Res.*, **11**(2), 125-133.
- Watterson J. (1986): Fault Dimensions, Displacements and Growth. *Pure Appl. Geophys.*, **124**(1/2), 365-373.
- Watts A.B. and Burov E.B. (2003): Lithospheric strength and its relationship to the elastic and seismogenic layer thickness. *Earth Planet. Sci. Lett.*, **213**, 113-131.
- Wedepohl K. H. (1995): The composition of the continental crust. *Geochim. Cosmochim. Ac.*, **59**(7), 1217-1232.
- Wei R.-Q. and Zang S.-X. (2006): Effects of temperature and strain rate on fracture strength of rocks and their influence on rheological structure of the lithosphere. *Chinese J. Geophys.*, **49**(6), 1576-1584.
- Wells D.L. and Coppersmith J.K. (1994): New Empirical Relationships among Magnitude, Rupture Length, Rupture Width, Rupture Area, and Surface Displacement. *Bull. Seism. Soc. Am.*, **84**, 974-1002.
- White R.S. (1999): The lithosphere under stress. *Phil. Trans. R. Soc. Lond. A*, **357**, 901-915.
- Wilks K.R. and Carter N.L. (1990): Rheology of some continental lower crustal rocks. *Tectonophysics*, **182**, 57-77.
- Wong I.G. and Olig S.S. (1998): Seismic hazards in the Basin and Range Province: perspectives from probabilistic analyses. In: Lund W.R. (Ed.), *Proceedings volume: Basin and Range Province Seismic-Hazards summit*. Utah Geological Survey, Miscellaneous Publication, **98-2**, 110-127.
- Wyllie P.J. (1971): The role of water in magma generation and initiation of diapiric uprise in the mantle. *J. Geophys. Res.*, **76**, 1328-1338.

Y

- Yaltirak C. and Alpar B. (2002): Kinematics and evolution of the northern branch of the North Anatolian Fault (Ganos Fault) between the Sea of Marmara and the Gulf of Saros. *Mar. Geol.*, **190**, 351-366.

Yaltirak C., Alpar B. and Yüce H. (1998): Tectonic elements controlling the evolution of the Gulf of Saros (northeastern Aegean Sea, Turkey). *Tectonophysics*, **300**, 227-248.

Z

Zang A. and Stephansson O. (2010): *Stress Field of the Earth's Crust*. Springer, 322 pp.

Zang S.X., Wei, R.Q. and Ning J.Y. (2007): Effect of the brittle fracture on the rheological structure of the lithosphere and its applications in the Ordos. *Tectonophysics*, **429**, 267-285.

Zervopoulou A. (2004): *Preliminary Report of the active and possible active faults of the broader area of the city of Thessaloniki which will affect the urban area during a probable reactivation* (in Greek). Report Department of Geology, Aristotle University of Thessaloniki, Greece, 35 pp.

Zervopoulou A. and Pavlides S. (2005): Morphotectonic study of the broader area of Thessaloniki for the cartography of neotectonic faults. *Bull. Geol. Soc. Greece*, **38**, 30-41.

Zervopoulou A., Chatzipetros A., Tsiokos L., Syrides G. and Pavlides S. (2007): Non-seismic surface faulting: the Peraia Fault case study (Thessaloniki, N. Greece). 4th Int. Conf. Earthq. Geotech. Eng., June 25-28, *Proceedings*, Paper No. 1610.

Zhang Q., Zhang P., Wang C., Wang Y. and Ellis M.A. (2003): Earthquake triggering and delaying caused by fault interaction on Xianshuihe fault belt, southwestern China. *Acta Seismologica Sinica*, **16**, 156-165.

Zovoili E., Konstantinidi E. and Koukouvelas I.K. (2004): Tectonic geomorphology of escarpments: the cases of Kompotades and Nea Anchialos Faults, *Bull. Geol. Soc. Greece*, **36**(4), 1716-1725.

APPENDIX

The parametric information of the seismogenic sources in North Greece

This appendix contains the parametric information of the seismogenic sources in table form, as they are discussed in [chapter 4](#). The way the tables appear is similar to the one when navigating the database (Source Info tab, [§2.3](#), [fig. 2.5a](#)). The order of the tables is the same with the order that sources are discussed in [chapter 5](#), having CSSs first.

The abbreviations used in the following tables concern the qualification keys. These are: *LD* = Literature Data, *OD* = Original Data, *EJ* = Expert Judgement, *AR* = Analytical Relationship, *ER* = Empirical Relationships.

The parametric information is preceded by a list of contents, while the respective maps of CSSs and ISSs can be found before the tables ([figs. A.1, A.2](#) respectively and [A.3](#) for the Ptolemaida Basin).

A.1 List of sources

Name (code)	page
• The northern fault belt	205-211
○ Doxipara (GRCS170)	205
○ Maronia (GRCS160)	205
○ Thrace (GRCS150)	206
▪ Komotini F. (GRIS150)	206
▪ Iasmos F. (GRIS151)	207
▪ Xanthi F. (GRIS152)	207
○ Drama (GRCS140)	208
▪ Drama F. (GRIS140)	208
▪ Prosotsani F. (GRIS141)	209
○ Serres (GRCS145)	209
○ Belles (GRCS130)	210
▪ Petritsi F. (GRIS130)	210
▪ Kastanoussa F. (GRIS131)	211
• The Chalkidiki fault system	211-220
○ Stratoni-Varvara (GRCS110)	211
▪ Varvara (GRIS110)	212
▪ West Stratoni (GRIS111)	212
▪ East Stratoni (GRIS112)	213
○ Gomati (GRCS260)	213
○ Singitikos (GRCS270)	214
○ Vourvourou F. (GRIS265)	214
○ Sochos-Mavrouda (GRCS120)	215
▪ Mavrouda F. (GRIS120)	215
▪ Sochos F. (GRIS121)	216
○ Mygdonia (GRCS100)	216
▪ Gerakarou F. (GRIS101)	217
▪ Langadhas F. (GRIS102)	217
▪ Apollonia F. (GRIS103)	218
○ Asvestochori (GRCS245)	218
○ Pylaea (GRCS240)	219
○ Anthemountas (GRCS250)	219
▪ Angelochori F. (GRIS251)	220
▪ Souroti F. (GRIS252)	220
• The ‘anti-Hellenides’ fault system	221-236
○ North Almopia (GRCS060)	221
▪ Pozar F. (GRIS060)	221
▪ Promachi F. (GRIS061)	222
▪ Aetochori F. (GRIS062)	222
○ Goumenissa F. (GRIS069)	223
○ South Almopia (GRCS068)	223
○ Amyndeo (GRCS070)	224
▪ Nymfaeo F. (GRIS070)	224
▪ Petron F. (GRIS071)	225
○ Chimaditis F. (GRIS075)	225
○ Ptolemaida (GRCS072)	226
▪ Vegora F. (GRIS072)	226
▪ Vegoritida F. (GRIS073)	227
○ Perdika F. (GRIS076)	227

○ Komanos (GRCS077)	228
▪ Mesovouni F. (GRIS077)	228
▪ Proastio F. (GRIS078)	229
○ Peraea F. (GRIS074)	229
○ Aliakmonas (GRCS050)	230
▪ Palaeochori F. (GRIS050)	230
▪ Rymnio F. (GRIS051)	231
▪ Servia F. (GRIS052)	231
▪ Chromio F. (GRIS053)	232
○ Konitsa (GRCS300)	232
▪ Konitsa F. (GRIS301)	233
○ Petoussi (GRCS310)	233
▪ Souli F. (GRIS310)	234
▪ Tomaros F. (GRIS311)	234
○ Kerkyra (GRCS390)	235
▪ Makrades F. (GRIS390)	235
▪ Spartylas F. (GRIS391)	236
○ Palaeokastritsa F. (GRIS392)	236
● The Thessalian fault system	237-246
○ Pagasitikos Gulf (GRCS010)	237
▪ Volos F. (GRIS010)	237
▪ Nea Anchialos F. (GRIS011)	238
○ Vasilika (GRCS015)	238
▪ Righeo F. (GRIS015)	239
▪ Dasolofos F. (GRIS016)	239
○ Domokos (GRCS020)	240
▪ Ekkara F. (GRIS020)	240
○ South Tyrnavos Basin (GRCS004)	241
▪ Larissa F. (GRIS005)	241
▪ Asmaki F. (GRIS004)	242
○ Tyrnavos (GRCS001)	242
▪ Tyrnavos F. (GRIS001)	243
○ North Tyrnavos Basin (GRCS002)	243
▪ Rodia F. (GRIS002)	244
▪ Gyrtioni F. (GRIS003)	244
○ Omolio (GRCS040)	245
○ South Kassandra offshore (GRCS285)	245
○ Mavrovouni offshore (GRCS815)	246
○ Pelion offshore (GRCS820)	246
● The North Aegean Sea fault system	A247-252
○ South Chalkidiki offshore (GRCS280)	247
▪ Athos F. (GRIS282)	247
○ North Aegean Basin (NAB) (GRCS810)	248
▪ NAB segment A (GRIS810)	248
▪ NAB segment B (GRIS811)	249
○ South NAT (GRCS800)	249
○ North NAT (GRCS290)	250
▪ Saros Gulf F. (GRIS290)	250
▪ Samothraki SE F. (GRIS291)	251
○ North Samothraki F. (GRIS288)	251
○ Lemnos (GRCS825)	252
○ Aghios Efstratios F. (GRIS831)	252

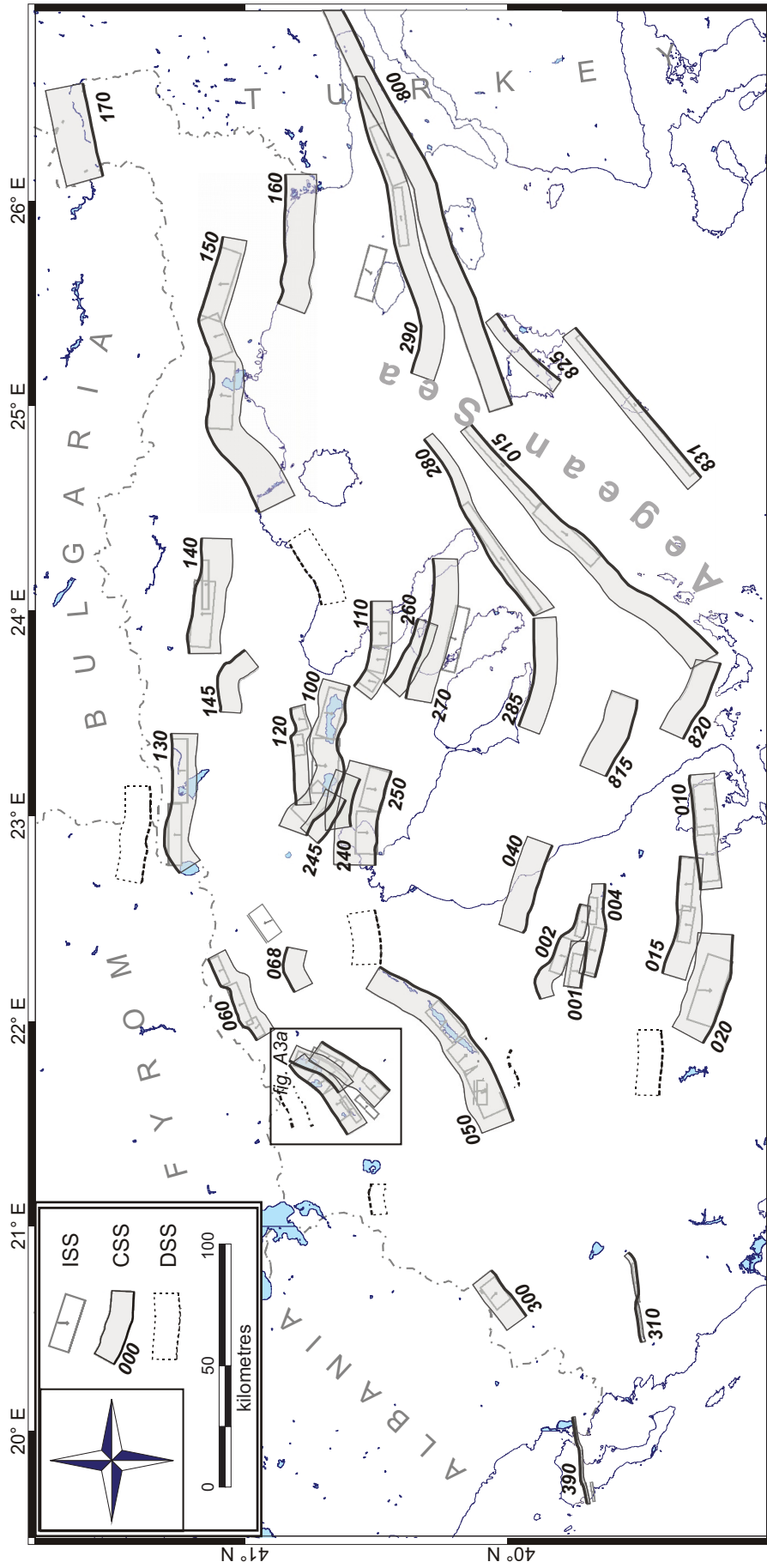


Fig. A.1: Map of the seismogenic sources that are included in the study area only. The CSSs are highlighted. The numbers refer to the respective CSSs of the appendix. The frame refers to [fig. A.3a](#).

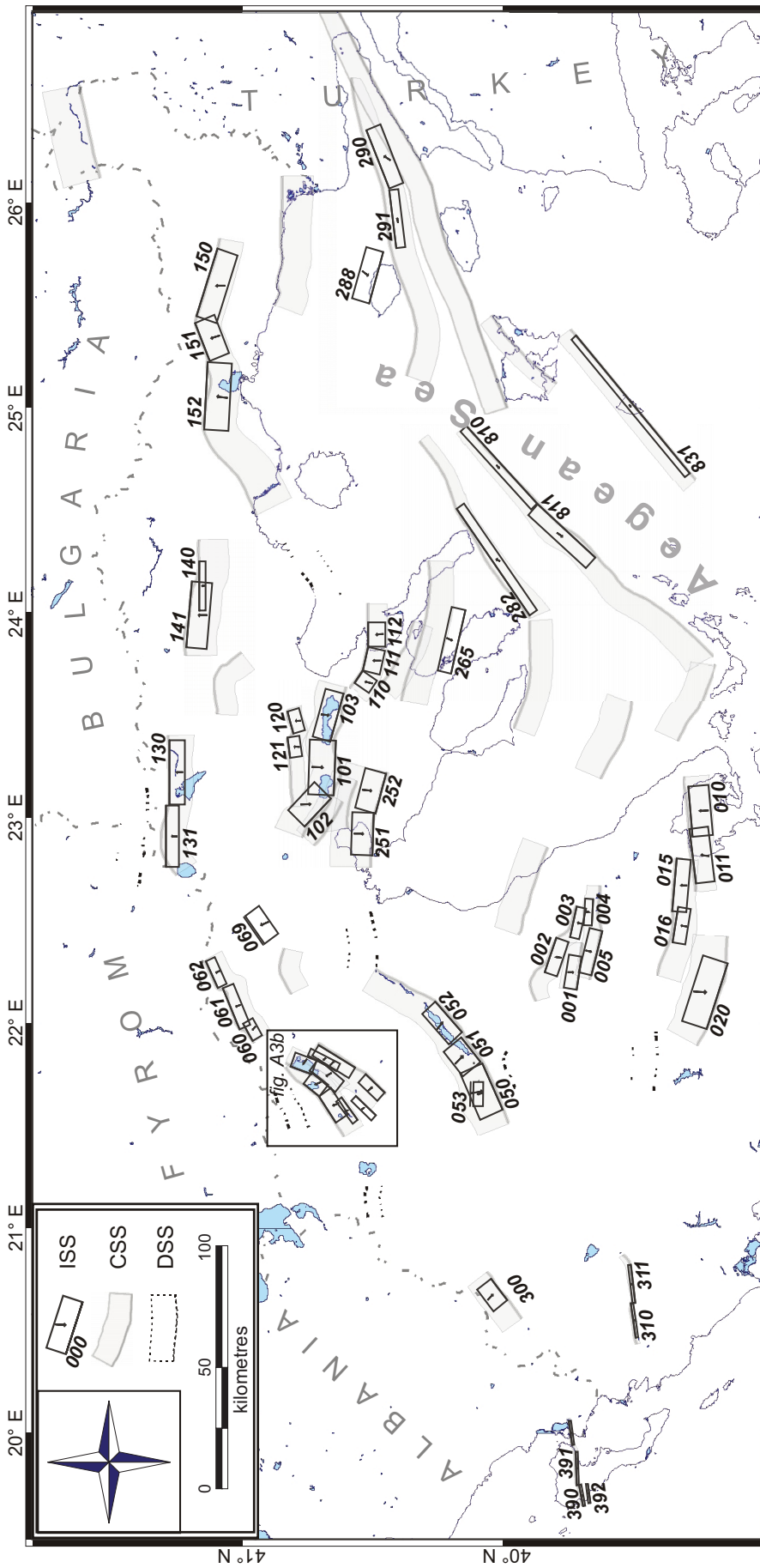


Fig. A.2: Map of the seismic sources that are included in the study area only. The ISSs are highlighted. The numbers refer to the respective ISSs of the appendix. The frame refers to [fig. A.3b](#)

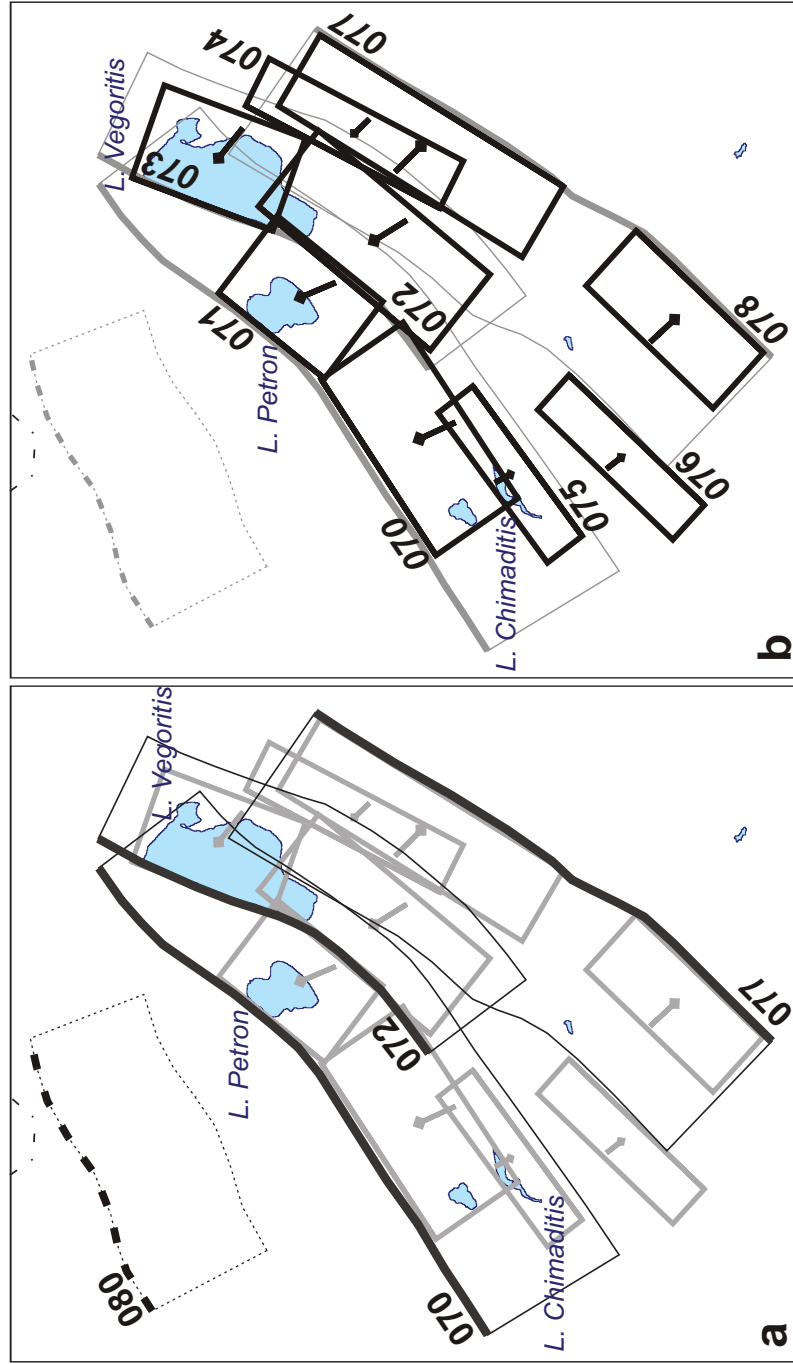


Fig A.3: Zoom of the complex system of the CSSs (a) and the ISSs (b) in the Ptolemaida Basin (frames shown in [fig. A.1](#) and [ans A.2](#), respectively). The CSS080 ("Florina") in (a) is not included in the descriptions of the 5th chapter because it is still debated.

Appendix

General information			
Code:	GRCS170		
Name:	Doxipara		
Associated ISSs:	None		
Parametric information			
	Parameter	Qual.	Evidence
Min depth (km)	0	LD	palaeoseismological investigation (Chatzipetros and Pavlides, 2009)
Max depth (km)	14	EJ	inferred from seismogenic layer thickness of nearby areas
Strike (deg)	245 - 260	LD	morphotectonic map (Chatzipetros and Pavlides, 2009)
Dip (deg)	45 - 80	EJ	inferred from palaeoseismological trenches (Chatzipetros and Pavlides, 2009)
Rake (deg)	240 - 270	LD	palaeoseismological trenches (Chatzipetros and Pavlides, 2009)
Slip rate (mm/a)	0.3 – 0.3	AR	calculated from geodetic strain rate field
Max magnitude (Mw)	6.9	ER	calculated from the empirical relationships of Wells and Coppersmith (1994)
Approximate location (Lat/Lon)	41.599 / 26.446	AR	map derived
Total length (km)	38.6	AR	map derived
Total width (km)	17.0	AR	derived from depth and dip
Typical fault length (km)	37.2	ER	derived from maximum Magnitude
Typical fault width (km)	18.8	ER	derived from maximum Magnitude
Typical fault slip (m)	1.34	AR	derived from Moment and Fault Size

General information			
Code:	GRCS160		
Name:	Maronia		
Associated ISSs:	None		
Parametric information			
	Parameter	Qual.	Evidence
Min depth (km)	0	LD	geomorphic records (several authors)
Max depth (km)	14	EJ	inferred from seismogenic layer thickness of nearby areas
Strike (deg)	80 - 120	LD	various geological/morphotectonic maps and field measurements
Dip (deg)	45 - 75	LD	field measurements and focal mechanisms (various authors)
Rake (deg)	230 - 280	LD	field measurements and focal mechanisms (various authors)
Slip rate (mm/a)	0.4 – 0.7	AR	calculated from geodetic strain rate field
Max magnitude (Mw)	7.0	ER	calculated from the empirical relationships of Wells and Coppersmith (1994)
Approximate location (Lat/Lon)	40.847 / 26.000	AR	map derived
Total length (km)	53.9	AR	map derived
Total width (km)	17.1	AR	derived from depth and dip
Typical fault length (km)	41.7	ER	derived from maximum Magnitude
Typical fault width (km)	20.4	ER	derived from maximum Magnitude
Typical fault slip (m)	1.56	AR	derived from Moment and Fault Size

Appendix

General information			
Code:	GRCS150		
Name:	Thrace		
Associated ISSs:	Komotini (GRIS150), Iasmos (GRIS151) and Xanthi (GRIS152)		
Parametric information			
	Parameter	Qual.	Evidence
Min depth (km)	0	LD	geomorphic records (several authors)
Max depth (km)	14	EJ	inferred from seismogenic layer thickness of nearby areas
Strike (deg)	40 - 115	LD	various geological/morphotectonic maps
Dip (deg)	35 - 80	LD	field measurements (several authors)
Rake (deg)	200 - 290	LD	kinematic indicators (several authors)
Slip rate (mm/a)	0.2 – 0.5	AR	calculated from geodetic strain rate field
Max magnitude (Mw)	7.0	EJ	fault geometry considerations and application of empirical relationships (Wells and Coppersmith, 1994)
Approximate location (Lat/Lon)	41.052 / 24.944	AR	map derived
Total length (km)	123.1	AR	map derived
Total width (km)	19.5	AR	derived from depth and dip
Typical fault length (km)	41.7	ER	derived from maximum magnitude
Typical fault width (km)	20.4	ER	derived from maximum magnitude
Typical fault slip (m)	1.56	AR	derived from moment and fault size

General information			
Code:	GRIS150		
Name:	Komotini Fault		
Associated CSS:	Thrace (GRCS150)		
Parametric information			
	Parameter	Qual.	Evidence
Location (Lat/Lon)	41.094 / 25.589	LD	geological/morphotectonic maps (Mountrakis and Tranos, 2004)
Length (km)	29	LD	geological/morphotectonic maps (Mountrakis and Tranos, 2004)
Width (km)	15.5	AR	derives from other parameters (dip, minimum and maximum depth)
Min depth (km)	0	LD	geomorphic records (various authors)
Max depth (km)	12.7	EJ	inferred from seismogenic layer thickness of nearby areas
Strike (deg)	108	LD	various geological/morphotectonic maps
Dip (deg)	55	LD	field measurements (several authors)
Rake (deg)	290	LD	inferred from kinematic indicators (Mountrakis <i>et al.</i> , 2006)
Slip per event (m)	0.9	AR	calculated from Mo (Aki, 1966)
Slip rate (mm/a)	0 - 0	UN	unknown
Recurrence (y)	0 - 0	UN	unknown
Max Magnitude (Mw)	6.7	ER	after the relationships of Wells and Coppersmith (1994) and Hanks and Kanamori (1979)
Associated earthquake			
Latest Eq	1784/11/06		historical event of M=6.7 (Papazachos & Papazachou, 2003)
Penultimate Eq	N/A		unknown
Elapsed Time	216		as of year 2000 (assigned datum)

Appendix

General information			
Code:	GRIS151		
Name:	Iasmos Fault		
Associated CSS:	Thrace (GRCS150)		
Parametric information			
	Parameter	Qual.	Evidence
Location (Lat/Lon)	41.114 / 25.336	LD	various geological/morphotectonic maps
Length (km)	16.7	LD	various geological/morphotectonic maps
Width (km)	15.5	AR	derives from other parameters (dip, minimum and maximum depth)
Min depth (km)	0	LD	geomorphic records (various authors)
Max depth (km)	12.7	EJ	inferred from seismogenic layer thickness of nearby areas
Strike (deg)	68	LD	various geological/morphotectonic maps
Dip (deg)	55	LD	field measurements (several authors)
Rake (deg)	265	LD	inferred from kinematic indicators (various authors)
Slip per event (m)	0.55	AR	calculated from Mo (Aki, 1966)
Slip rate (mm/a)	0 - 0	UN	unknown
Recurrence (y)	0 - 0	UN	unknown
Max Magnitude (Mw)	6.4	ER	after the relationships of Wells and Coppersmith (1994) and Hanks and Kanamori (1979)
Associated earthquake			
Latest Eq	N/A	unknown	
Penultimate Eq	N/A	unknown	
Elapsed Time	N/A	unknown	

General information			
Code:	GRIS152		
Name:	Xanthi Fault		
Associated CSS:	Thrace (GRCS150)		
Parametric information			
	Parameter	Qual.	Evidence
Location (Lat/Lon)	41.091 / 25.050	LD	geological/morphotectonic maps (Mountrakis and Tranos, 2004)
Length (km)	27.5	LD	geological/morphotectonic maps (Mountrakis and Tranos, 2004)
Width (km)	16	AR	derives from other parameters (dip, minimum and maximum depth)
Min depth (km)	0	LD	field observations (several authors)
Max depth (km)	12.3	EJ	inferred from seismogenic layer thickness of nearby areas
Strike (deg)	93	LD	various geological/morphotectonic maps
Dip (deg)	50	LD	based on geological considerations (Mountrakis <i>et al.</i> , 2006)
Rake (deg)	265	LD	based on geological considerations (Mountrakis and Tranos, 2004)
Slip per event (m)	0.7	AR	calculated from Mo (Aki, 1966)
Slip rate (mm/a)	0 - 0	UN	unknown
Recurrence (y)	0 - 0	UN	unknown
Max Magnitude (Mw)	6.6	ER	after the relationships of Wells and Coppersmith (1994) and Hanks and Kanamori (1979)
Associated earthquake			
Latest Eq	1829/04/11	Mw=7.3 (see text for discussion)	
Penultimate Eq	N/A	unknown	
Elapsed Time	171	as of year 2000 (assigned datum)	

Appendix

General information			
Code:	GRCS140		
Name:	Drama		
Associated ISSS:	Drama (GRIS140) and Prosotsani (GRIS141)		
Parametric information			
	Parameter	Qual.	Evidence
Min depth (km)	0	LD	geomorphic records (Mountrakis <i>et al.</i> , 2006)
Max depth (km)	15	EJ	inferred from seismogenic layer thickness of nearby areas
Strike (deg)	80 - 135	LD	geological/morphotectonic maps (Mountrakis <i>et al.</i> , 2006)
Dip (deg)	40 - 65	LD	inferred from field descriptions (Mountrakis <i>et al.</i> , 2006)
Rake (deg)	265 - 280	LD	inferred from field descriptions (Mountrakis <i>et al.</i> , 2006)
Slip rate (mm/a)	0.2 – 0.4	AR	calculated from geodetic strain rate field
Max magnitude (Mw)	7.0	ER	calculated from the empirical relationships of Wells and Coppersmith (1994)
Approximate location (Lat/Lon)	41.169 / 24.187	AR	map derived
Total length (km)	48.1	AR	map derived
Total width (km)	19.9	AR	derived from depth and dip
Typical fault length (km)	41.7	ER	derived from maximum magnitude
Typical fault width (km)	20.4	ER	derived from maximum magnitude
Typical fault slip (m)	1.56	AR	derived from moment and fault size

General information			
Code:	GRIS140		
Name:	Drama Fault		
Associated CSS:	Drama (GRCS140)		
Parametric information			
	Parameter	Qual.	Evidence
Location (Lat/Lon)	41.150 / 24.129	LD	geological/morphotectonic maps (Mountrakis <i>et al.</i> , 2006)
Length (km)	20	LD	geological/morphotectonic maps (Mountrakis <i>et al.</i> , 2006)
Width (km)	10	AR	derives from other parameters (dip, minimum and maximum depth)
Min depth (km)	0	LD	geomorphic records (Mountrakis <i>et al.</i> , 2006)
Max depth (km)	9.7	EJ	inferred from seismogenic layer thickness of nearby areas
Strike (deg)	90	LD	geological/morphotectonic maps (Mountrakis <i>et al.</i> , 2006)
Dip (deg)	75	LD	inferred from field descriptions (Mountrakis <i>et al.</i> , 2006)
Rake (deg)	275	LD	inferred from field descriptions (Mountrakis <i>et al.</i> , 2006)
Slip per event (m)	0.5	AR	calculated from Mo (Aki, 1966)
Slip rate (mm/a)	0 - 0	UN	unknown
Recurrence (y)	0 - 0	UN	unknown
Max Magnitude (Mw)	6.3	ER	after the relationships of Wells and Coppersmith (1994) and Hanks and Kanamori (1979)
Associated earthquake			
Latest Eq	1829/05/05	Mw=7.3 (see text for discussion)	
Penultimate Eq	N/A	unknown	
Elapsed time	171	as of year 2000 (assigned datum)	

Appendix

General information			
Code:	GRIS141		
Name:	Prosotsani Fault		
Associated CSS:	Drama (GRCS140)		
Parametric information			
	Parameter	Qual.	Evidence
Location (Lat/Lon)	41.162 / 23.986	LD	geological/morphotectonic maps (Mountrakis <i>et al.</i> , 2006)
Length (km)	27	LD	geological/morphotectonic maps (Mountrakis <i>et al.</i> , 2006)
Width (km)	15	AR	derives from other parameters (dip, minimum and maximum depth)
Min depth (km)	0	LD	geomorphic records (Mountrakis <i>et al.</i> , 2006)
Max depth (km)	12.3	EJ	inferred from seismogenic layer thickness of nearby areas
Strike (deg)	95	LD	geological/morphotectonic maps (Mountrakis <i>et al.</i> , 2006)
Dip (deg)	55	LD	inferred from field descriptions (Mountrakis <i>et al.</i> , 2006)
Rake (deg)	275	LD	inferred from field descriptions (Mountrakis <i>et al.</i> , 2006)
Slip per event (m)	0.7	AR	calculated from Mo (Aki, 1966)
Slip rate (mm/a)	0 - 0	UN	unknown
Recurrence (y)	0 - 0	UN	unknown
Max Magnitude (Mw)	6.6	ER	after the relationships of Wells and Coppersmith (1994) and Hanks and Kanamori (1979)
Associated earthquake			
Latest Eq	1829/05/05	Mw=7.3 (see text for discussion)	
Penultimate Eq	N/A	unknown	
Elapsed Time	171	as of year 2000 (assigned datum)	

General information			
Code:	GRCS145		
Name:	Serres		
Associated ISSs:	none		
Parametric information			
	Parameter	Qual.	Evidence
Min depth (km)	0	LD	geomorphic records (Tranos and Mountrakis, 2004)
Max depth (km)	16	EJ	inferred from seismogenic layer thickness of nearby areas
Strike (deg)	80 - 140	LD	geological/morphotectonic maps (Tranos and Mountrakis, 2004)
Dip (deg)	50 - 80	EJ	inferred from field measurements and geological considerations
Rake (deg)	260 - 280	LD	inferred from field descriptions (Mountrakis <i>et al.</i> , 2006)
Slip rate (mm/a)	0.05 – 0.1	LD	displacement of dated Quaternary sediments (Tranos and Mountrakis, 2004)
Max magnitude (Mw)	6.8	ER	calculated from the empirical relationships of Wells and Coppersmith (1994)
Approximate location (Lat/Lon)	41.026 / 23.650	AR	map derived
Total length (km)	31.1	AR	map derived
Total width (km)	18.6	AR	derived from depth and dip
Typical fault length (km)	33.1	ER	derived from maximum magnitude
Typical fault width (km)	17.4	ER	derived from maximum magnitude
Typical fault slip (m)	1.16	AR	derived from moment and fault size

Appendix

General information			
Code:	GRCS130		
Name:	Belles		
Associated ISSs:	none		
Parametric information			
	Parameter	Qual.	Evidence
Min depth (km)	0	LD	geomorphic records (various authors)
Max depth (km)	15	EJ	inferred from hypocentral distribution (Kiratzi, 2009)
Strike (deg)	50 - 115	LD	various geological/morphotectonic maps
Dip (deg)	45 - 70	EJ	inferred from field measurements and geological considerations
Rake (deg)	250 - 280	OD	kinematic and geomorphic indicators
Slip rate (mm/a)	0.2 – 0.4	AR	calculated from geodetic strain rate field
Max magnitude (Mw)	7.0	ER	calculated from the empirical relationships of Wells and Coppersmith (1994)
Approximate location (Lat/Lon)	41.281 / 23.261	AR	map derived
Total length (km)	59.3	AR	map derived
Total width (km)	18.6	AR	derived from depth and dip
Typical fault length (km)	41.7	ER	derived from maximum magnitude
Typical fault width (km)	20.4	ER	derived from maximum magnitude
Typical fault slip (m)	1.56	AR	derived from moment and fault size

General information			
Code:	GRIS130		
Name:	Petritsi Fault		
Associated CSS:	Belles (GRCS130)		
Parametric information			
	Parameter	Qual.	Evidence
Location (Lat/Lon)	41.247 / 23.221	LD	various geological/morphotectonic maps
Length (km)	26	LD	various geological/morphotectonic maps
Width (km)	13	AR	derives from other parameters (dip, minimum and maximum depth)
Min depth (km)	0	LD	geomorphic records (various authors)
Max depth (km)	11.3	EJ	inferred from seismogenic layer thickness of nearby areas
Strike (deg)	90	LD	various geological/morphotectonic maps
Dip (deg)	60	EJ	inferred from field observations (various authors) and geological considerations
Rake (deg)	270	LD	kinematic indicators (various authors)
Slip per event (m)	0.61	AR	calculated from Mo (Aki, 1966)
Slip rate (mm/a)	0 - 0	UN	unknown
Recurrence (y)	0 - 0	UN	unknown
Max Magnitude (Mw)	6.5	ER	after the relationships of Wells and Coppersmith (1994) and Hanks and Kanamori (1979)
Associated earthquake			
Latest Eq	N/A	unknown	
Penultimate Eq	N/A	unknown	
Elapsed Time	N/A	unknown	

Appendix

General information			
Code:	GRIS131		
Name:	Kastanoussa Fault		
Associated CSS:	Belles (GRCS130)		
Parametric information			
	Parameter	Qual.	Evidence
Location (Lat/Lon)	41.265 / 22.910	LD	various geological/morphotectonic maps
Length (km)	25	EJ	various geological/morphotectonic maps and geological considerations
Width (km)	13	AR	derives from other parameters (dip, minimum and maximum depth)
Min depth (km)	0	LD	geomorphic records (various authors)
Max depth (km)	11.8	EJ	inferred from seismogenic layer thickness of nearby areas
Strike (deg)	90	LD	various geological/morphotectonic maps
Dip (deg)	65	EJ	inferred from field observations (various authors) and geological considerations
Rake (deg)	270	LD	kinematic indicators (various authors)
Slip per event (m)	0.60	AR	calculated from Mo (Aki, 1966)
Slip rate (mm/a)	0 - 0	UN	unknown
Recurrence (y)	0 - 0	UN	unknown
Max Magnitude (Mw)	6.5	ER	after the relationships of Wells and Coppersmith (1994) and Hanks and Kanamori (1979)
Associated earthquake			
Latest Eq	N/A	unknown	
Penultimate Eq	N/A	unknown	
Elapsed Time	N/A	unknown	

General information			
Code:	GRCS110		
Name:	Stratoni-Varvara		
Associated ISSS:	Varvara (GRIS110), West Stratoni (GRIS111) and East Stratoni (GRIS112)		
Parametric information			
	Parameter	Qual.	Evidence
Min depth (km)	0	LD	geomorphic records (various authors)
Max depth (km)	17	EJ	inferred from hypocentral distribution (Galanis <i>et al.</i> , 2004)
Strike (deg)	85 - 130	LD	various geological/morphotectonic maps
Dip (deg)	65 - 85	EJ	inferred from hypocentral distribution and field observations (various authors)
Rake (deg)	270 - 290	LD	kinematic indicators (Pavlidis and Kiliadis, 1987)
Slip rate (mm/a)	0.3 – 1.1	AR	calculated from geodetic strain rate field
Max magnitude (Mw)	7.0	ER	calculated from the empirical relationships of Wells and Coppersmith (1994)
Approximate location (Lat/Lon)	40.522 / 23.836	AR	map derived
Total length (km)	36.9	AR	map derived
Total width (km)	17.9	AR	derived from depth and dip
Typical fault length (km)	41.7	ER	derived from maximum magnitude
Typical fault width (km)	20.4	ER	derived from maximum magnitude
Typical fault slip (m)	1.56	AR	derived from moment and fault size

Appendix

General information			
Code:	GRIS110		
Name:	Varvara Fault		
Associated CSS:	Stratoni-Varvara (GRCS110)		
Parametric information			
	Parameter	Qual.	Evidence
Location (Lat/Lon)	40.526 / 23.662	LD	various geological/morphotectonic maps
Length (km)	6.2	LD	morphotectonic analysis and field observations (various authors)
Width (km)	17	AR	derives from other parameters (dip, minimum and maximum depth)
Min depth (km)	0	LD	geomorphic records (various authors)
Max depth (km)	15.9	EJ	inferred from hypocentral distribution (Galanis <i>et al.</i> , 2004)
Strike (deg)	124	LD	various geological/morphotectonic maps
Dip (deg)	65	EJ	inferred from hypocentral distribution and field measurements (various authors)
Rake (deg)	290	LD	kinematic indicators (Pavlidis and Kiliias, 1987)
Slip per event (m)	0.33	AR	calculated from Mo (Aki, 1966)
Slip rate (mm/a)	0 - 0	UN	unknown
Recurrence (y)	0 - 0	UN	unknown
Max Magnitude (Mw)	6.0	ER	after the relationships of Wells and Coppersmith (1994) and Hanks and Kanamori (1979)
Associated earthquake			
Latest Eq	1932/09/26	Mw = 7.0 from instrumental recordings (see text for discussion)	
Penultimate Eq	N/A	unknown	
Elapsed Time	68	as of year 2000 (assigned datum)	

General information			
Code:	GRIS111		
Name:	West Stratoni Fault		
Associated CSS:	Stratoni-Varvara (GRCS110)		
Parametric information			
	Parameter	Qual.	Evidence
Location (Lat/Lon)	40.495 / 23.765	LD	various geological/morphotectonic maps
Length (km)	10.0	LD	morphotectonic analysis and field observations (various authors)
Width (km)	17.5	AR	derives from other parameters (dip, minimum and maximum depth)
Min depth (km)	0	LD	geomorphic records (various authors)
Max depth (km)	15.9	EJ	inferred from hypocentral distribution (Galanis <i>et al.</i> , 2004)
Strike (deg)	103	LD	various geological/morphotectonic maps
Dip (deg)	65	EJ	inferred from hypocentral distribution and field measurements (various authors)
Rake (deg)	285	LD	kinematic indicators (Pavlidis and Kiliias, 1987)
Slip per event (m)	0.43	AR	calculated from Mo (Aki, 1966)
Slip rate (mm/a)	0 - 0	UN	unknown
Recurrence (y)	0 - 0	UN	unknown
Max Magnitude (Mw)	6.2	ER	after the relationships of Wells and Coppersmith (1994) and Hanks and Kanamori (1979)
Associated earthquake			
Latest Eq	1932/09/26	Mw = 7.0 from instrumental recordings (see text for discussion)	
Penultimate Eq	N/A	unknown	
Elapsed Time	68	as of year 2000 (assigned datum)	

Appendix

General information			
Code:	GRIS112		
Name:	East Stratoni Fault		
Associated CSS:	Stratoni-Varvara (GRCS110)		
Parametric information			
	Parameter	Qual.	Evidence
Location (Lat/Lon)	40.485 / 23.892	LD	various geological/morphotectonic maps
Length (km)	10.0	LD	morphotectonic analysis and field observations (various authors)
Width (km)	17.5	AR	derives from other parameters (dip, minimum and maximum depth)
Min depth (km)	0	LD	geomorphic records (various authors)
Max depth (km)	15.9	EJ	inferred from hypocentral distribution (Galanis <i>et al.</i> , 2004)
Strike (deg)	90	LD	various geological/morphotectonic maps
Dip (deg)	65	EJ	inferred from hypocentral distribution and field measurements (various authors)
Rake (deg)	275	LD	kinematic indicators (Pavlidis and Kiliyas, 1987)
Slip per event (m)	0.43	AR	calculated from Mo (Aki, 1966)
Slip rate (mm/a)	0 - 0	UN	unknown
Recurrence (y)	0 - 0	UN	unknown
Max Magnitude (Mw)	6.2	ER	after the relationships of Wells and Coppersmith (1994) and Hanks and Kanamori (1979)
Associated earthquake			
Latest Eq	1932/09/26	Mw = 7.0 from instrumental recordings (see text for discussion)	
Penultimate Eq	N/A	unknown	
Elapsed Time	68	as of year 2000 (assigned datum)	

General information			
Code:	GRCS260		
Name:	Gomati		
Associated ISSs:	none		
Parametric information			
	Parameter	Qual.	Evidence
Min depth (km)	0	LD	geomorphic records (various authors)
Max depth (km)	16	EJ	inferred from hypocentral distribution (Galanis <i>et al.</i> , 2004)
Strike (deg)	110 - 135	LD	various geological/morphotectonic maps and field measurements
Dip (deg)	60 - 85	LD	inferred from field measurements and hypocentral distribution (various authors)
Rake (deg)	300 - 325	LD	kinematic indicators (various authors)
Slip rate (mm/a)	0.3 – 0.8	AR	calculated from geodetic strain rate field
Max magnitude (Mw)	6.7	ER	calculated from the empirical relationships of Wells and Coppersmith (1994)
Approximate location (Lat/Lon)	40.389 / 23.81	AR	map derived
Total length (km)	30.6	AR	map derived
Total width (km)	17.3	AR	derived from depth and dip
Typical fault length (km)	29.5	ER	derived from maximum magnitude
Typical fault width (km)	16	ER	derived from maximum magnitude
Typical fault slip (m)	1.00	AR	derived from moment and fault size

Appendix

General information			
Code:	GRCS270		
Name:	Singitikos Gulf		
Associated ISSs:	none		
Parametric information			
	Parameter	Qual.	Evidence
Min depth (km)	0	LD	geomorphic records (Pavlidis and Kiliias, 1987)
Max depth (km)	16	EJ	inferred from seismogenic layer thickness of nearby areas
Strike (deg)	90 - 130	LD	geological/morphotectonic maps (Pavlidis and Kiliias, 1987)
Dip (deg)	45 - 75	EJ	inferred from local geotectonic setting
Rake (deg)	280 - 320	EJ	inferred from regional stress field pattern
Slip rate (mm/a)	0.6 – 0.7	AR	calculated from geodetic strain rate field
Max magnitude (Mw)	7.0	ER	calculated from the empirical relationships of Wells and Coppersmith (1994)
Approximate location (Lat/Lon)	40.300 / 23.946	AR	map derived
Total length (km)	59.7	AR	map derived
Total width (km)	19.6	AR	derived from depth and dip
Typical fault length (km)	41.7	ER	derived from maximum magnitude
Typical fault width (km)	20.4	ER	derived from maximum magnitude
Typical fault slip (m)	1.56	AR	derived from moment and fault size

General information			
Code:	GRIS265		
Name:	Vourvourou Fault		
Associated CSS:	none		
Parametric information			
	Parameter	Qual.	Evidence
Location (Lat/Lon)	40.200 / 23.865	LD	various geological/morphotectonic maps
Length (km)	27	LD	various geological/morphotectonic maps, seismicity and bathymetry
Width (km)	14	AR	derives from other parameters (dip, minimum and maximum depth)
Min depth (km)	0	LD	geomorphic records (various authors)
Max depth (km)	12.7	EJ	inferred from seismogenic layer thickness of nearby areas
Strike (deg)	283	LD	various geological/morphotectonic maps
Dip (deg)	65	EJ	field descriptions (Tranos, 1998) and geological considerations
Rake (deg)	260	LD	kinematic indicators (Tranos, 1998)
Slip per event (m)	0.63	AR	calculated from Mo (Aki, 1966)
Slip rate (mm/a)	0 - 0	UN	unknown
Recurrence (y)	0 - 0	UN	unknown
Max Magnitude (Mw)	6.6	ER	after the relationships of Wells and Coppersmith (1994) and Hanks and Kanamori (1979)
Associated earthquake			
Latest Eq	N/A	unknown	
Penultimate Eq	N/A	unknown	
Elapsed Time	N/A	unknown	

Appendix

General information			
Code:	GRCS120		
Name:	Sochos		
Associated ISSs:	Mavrouda (GRIS120) and Sochos (GRIS121)		
Parametric information			
	Parameter	Qual.	Evidence
Min depth (km)	0	LD	geomorphic records (various authors)
Max depth (km)	15	EJ	inferred from hypocentral distribution (various authors)
Strike (deg)	70 - 100	LD	various geological/morphotectonic maps
Dip (deg)	60 - 85	EJ	inferred from hypocentral distribution (various authors)
Rake (deg)	260 - 280	LD	kinematic indicators (Mountrakis <i>et al.</i> , 2006)
Slip rate (mm/a)	0.1 – 0.8	AR	calculated from geodetic strain rate field
Max magnitude (Mw)	6.6	LD	geological considerations and application of empirical relationships (Zervopoulou, 2004)
Approximate location (Lat/Lon)	40.813 / 23.147	AR	map derived
Total length (km)	41.1	AR	map derived
Total width (km)	16.2	AR	derived from depth and dip
Typical fault length (km)	26.3	ER	derived from maximum magnitude
Typical fault width (km)	14.8	ER	derived from maximum magnitude
Typical fault slip (m)	0.86	AR	derived from moment and fault size

General information			
Code:	GRIS120		
Name:	Mavrouda Fault		
Associated CSS:	Sochos (GRCS120)		
Parametric information			
	Parameter	Qual.	Evidence
Location (Lat/Lon)	40.793 / 23.472	LD	various geological/morphotectonic maps
Length (km)	9.5	LD	various geological/morphotectonic maps
Width (km)	15	AR	derives from other parameters (dip, minimum and maximum depth)
Min depth (km)	0	LD	geomorphic records (various authors)
Max depth (km)	14.1	EJ	inferred from microseismic spatial distribution (various authors)
Strike (deg)	74	LD	various geological/morphotectonic maps
Dip (deg)	70	EJ	inferred from microseismic spatial distribution (various authors)
Rake (deg)	255	EJ	inferred from various focal mechanisms and regional stress field pattern
Slip per event (m)	0.39	AR	calculated from Mo (Aki, 1966)
Slip rate (mm/a)	0 - 0	UN	unknown
Recurrence (y)	0 - 0	UN	unknown
Max Magnitude (Mw)	6.1	ER	after the relationships of Wells and Coppersmith (1994) and Hanks and Kanamori (1979)
Associated earthquake			
Latest Eq	N/A	unknown	
Penultimate Eq	N/A	unknown	
Elapsed Time	N/A	unknown	

Appendix

General information			
Code:	GRIS121		
Name:	Sochos Fault		
Associated CSS:	Sochos (GRCS120)		
Parametric information			
	Parameter	Qual.	Evidence
Location (Lat/Lon)	40.798 / 23.346	LD	various geological/morphotectonic maps
Length (km)	8.5	LD	various geological/morphotectonic maps
Width (km)	15	AR	derives from other parameters (dip, minimum and maximum depth)
Min depth (km)	0	LD	geomorphic records (various authors)
Max depth (km)	14.1	EJ	inferred from microseismic spatial distribution (various authors)
Strike (deg)	82	LD	various geological/morphotectonic maps
Dip (deg)	70	EJ	inferred from microseismic spatial distribution (various authors)
Rake (deg)	260	EJ	inferred from various focal mechanisms and regional stress field pattern
Slip per event (m)	0.36	AR	calculated from Mo (Aki, 1966)
Slip rate (mm/a)	0 - 0	UN	unknown
Recurrence (y)	0 - 0	UN	unknown
Max Magnitude (Mw)	6.1	ER	after the relationships of Wells and Coppersmith (1994) and Hanks and Kanamori (1979)
Associated earthquake			
Latest Eq	N/A	unknown	
Penultimate Eq	N/A	unknown	
Elapsed Time	N/A	unknown	

General information			
Code:	GRCS100		
Name:	Mygdonia		
Associated ISSs:	Gerakarou (GRIS101), Langadhas (GRIS102) and Apollonia (GRIS103)		
Parametric information			
	Parameter	Qual.	Evidence
Min depth (km)	0	LD	geomorphic records and co-seismic ruptures (various authors)
Max depth (km)	17	EJ	inferred from hypocentral distribution (various authors)
Strike (deg)	250 - 320	LD	various geological/morphotectonic maps and focal mechanisms
Dip (deg)	30 - 80	EJ	inferred from hypocentral distribution and field observations (various authors)
Rake (deg)	250 - 315	LD	kinematic indicators and focal mechanisms (various authors)
Slip rate (mm/a)	0.1 - 0.7	LD	morphotectonic considerations (Tranos <i>et al.</i> , 2003)
Max magnitude (Mw)	6.6	EJ	geological considerations and application of empirical relationships (Wells and Coppersmith, 1994)
Approximate location (Lat/Lon)	40.754 / 23.337	AR	map derived
Total length (km)	68.6	AR	map derived
Total width (km)	25.6	AR	derived from depth and dip
Typical fault length (km)	26.3	ER	derived from maximum magnitude
Typical fault width (km)	14.8	ER	derived from maximum magnitude
Typical fault slip (m)	0.86	AR	derived from moment and fault size

Appendix

General information			
Code:	GRIS101		
Name:	Gerakarou Fault		
Associated CSS:	Mygdonia (GRCS100)		
Parametric information			
	Parameter	Qual.	Evidence
Location (Lat/Lon)	40.694 / 23.246	LD	various geological/morphotectonic maps and co-seismic ruptures
Length (km)	22.5	LD	co-seismic ruptures and seismological data (various authors)
Width (km)	17	AR	derives from other parameters (dip, minimum and maximum depth)
Min depth (km)	0	LD	co-seismic ruptures and geomorphic records (various authors)
Max depth (km)	13	EJ	inferred from seismic spatial distribution (various authors)
Strike (deg)	272	LD	geological/morphotectonic maps, foci and co-seismic ruptures (various authors)
Dip (deg)	50	LD	focal mechanisms (various authors)
Rake (deg)	270	LD	kinematic indicators and focal mechanisms (various authors)
Slip per event (m)	0.60	LD	seismic waveforms joint inversion and levelling data (Roumelioti <i>et al.</i> , 2007)
Slip rate (mm/a)	0.1 - 0.7	LD	palaeoseismological data (Chatzipetros, 1998)
Recurrence (y)	1000 - 1500	LD	palaeoseismological data for magnitudes ~6.5 (Chatzipetros <i>et al.</i> , 2004)
Max Magnitude (Mw)	6.5	ER	after the relationships of Wells and Coppersmith (1994) and Hanks and Kanamori (1979)
Associated earthquake			
Latest Eq	1978/06/20	Mw=6.5 (instrumental recordings)	
Penultimate Eq	1430	Ms=6.5 from palaeoseismological data (Chatzipetros <i>et al.</i> , 2004)	
Elapsed Time	22	as of year 2000 (assigned datum)	

General information			
Code:	GRIS102		
Name:	Langadhas Fault		
Associated CSS:	Mygdonia (GRCS100)		
Parametric information			
	Parameter	Qual.	Evidence
Location (Lat/Lon)	40.742 / 23.066	LD	various geological/morphotectonic maps
Length (km)	16	LD	various geological/morphotectonic maps
Width (km)	15	AR	derives from other parameters (dip, minimum and maximum depth)
Min depth (km)	0	LD	geomorphic records (various authors)
Max depth (km)	11.5	EJ	inferred from microseismic spatial distribution (various authors)
Strike (deg)	314	LD	various geological/morphotectonic maps
Dip (deg)	50	EJ	microseismic spatial distribution and field observations (various authors)
Rake (deg)	315	LD	kinematic indicators (Mercier <i>et al.</i> , 1983)
Slip per event (m)	0.51	AR	calculated from Mo (Aki, 1966)
Slip rate (mm/a)	0.0 - 0.0	UN	unknown
Recurrence (y)	0.0 - 0.0	UN	unknown
Max Magnitude (Mw)	6.4	ER	after the relationships of Wells and Coppersmith (1994) and Hanks and Kanamori (1979)
Associated earthquake			
Latest Eq	1902/07/05	M=6.5 historical record (Papazachos & Papazachou, 1997; 2003)	
Penultimate Eq	N/A	unknown	
Elapsed Time	98	as of year 2000 (assigned datum)	

Appendix

General information			
Code:	GRIS103		
Name:	Apollonia Fault		
Associated CSS:	Mygdonia (GRCS100)		
Parametric information			
	Parameter	Qual.	Evidence
Location (Lat/Lon)	40.671 / 23.500	LD	various geological/morphotectonic maps
Length (km)	20.5	LD	various geological/morphotectonic maps
Width (km)	18.5	AR	derives from other parameters (dip, minimum and maximum depth)
Min depth (km)	0	LD	geomorphic records (various authors)
Max depth (km)	16.8	EJ	inferred from microseismic spatial distribution (various authors)
Strike (deg)	286	LD	various geological/morphotectonic maps
Dip (deg)	65	EJ	microseismic spatial distribution (various authors) and geological considerations
Rake (deg)	280	LD	focal mechanisms (Hatzfeld <i>et al.</i> , 1986/87) and regional stress field pattern
Slip per event (m)	0.65	AR	calculated from Mo (Aki, 1966)
Slip rate (mm/a)	0.0 - 0.0	UN	unknown
Recurrence (y)	0.0 - 0.0	UN	unknown
Max Magnitude (Mw)	6.6	ER	after the relationships of Wells and Coppersmith (1994) and Hanks and Kanamori (1979)
Associated earthquake			
Latest Eq	N/A	unknown	
Penultimate Eq	N/A	unknown	
Elapsed Time	N/A	unknown	

General information			
Code:	GRCS245		
Name:	Asvestochori		
Associated ISSs:	none		
Parametric information			
	Parameter	Qual.	Evidence
Min depth (km)	0	LD	geomorphic records (various authors)
Max depth (km)	16	EJ	inferred from microseismic spatial distribution (various authors)
Strike (deg)	280 - 320	LD	various geological/morphotectonic maps
Dip (deg)	35 - 80	LD	inferred from seismotectonic considerations (several authors)
Rake (deg)	270 - 300	LD	kinematic indicators and focal mechanisms (various authors)
Slip rate (mm/a)	0.1 – 0.4	AR	calculated from geodetic strain rate field
Max magnitude (Mw)	6.3	LD	geological considerations and application of empirical relationships (Zervopoulou, 2004)
Approximate location (Lat/Lon)	40.732 / 23.042	AR	map derived
Total length (km)	21.5	AR	map derived
Total width (km)	22.1	AR	derived from depth and dip
Typical fault length (km)	18.6	ER	derived from maximum magnitude
Typical fault width (km)	11.6	ER	derived from maximum magnitude
Typical fault slip (m)	0.55	AR	derived from moment and fault size

Appendix

General information			
Code:	GRCS240		
Name:	Pylaea		
Associated ISSs:	none		
Parametric information			
	Parameter	Qual.	Evidence
Min depth (km)	0	LD	geomorphic records (various authors)
Max depth (km)	16	EJ	inferred from microseismic spatial distribution (various authors)
Strike (deg)	260 - 295	LD	various geological/morphotectonic maps
Dip (deg)	35 - 70	LD	inferred from seismotectonic considerations (Tranos <i>et al.</i> , 2003)
Rake (deg)	260 - 280	LD	kinematic indicators, focal mechanisms and regional stress field (various authors)
Slip rate (mm/a)	0.1 – 0.4	AR	calculated from geodetic strain rate field
Max magnitude (Mw)	6.0	LD	geological considerations and application of empirical relationships (Zervopoulou, 2004)
Approximate location (Lat/Lon)	40.600 / 23.013	AR	map derived
Total length (km)	20.3	AR	map derived
Total width (km)	22.5	AR	derived from depth and dip
Typical fault length (km)	13.2	ER	derived from maximum magnitude
Typical fault width (km)	9.1	ER	derived from maximum magnitude
Typical fault slip (m)	0.35	AR	derived from moment and fault size

General information			
Code:	GRCS250		
Name:	Anthemountas		
Associated ISSs:	Angelochori (GRIS251) and Souroti (GRIS252)		
Parametric information			
	Parameter	Qual.	Evidence
Min depth (km)	0	LD	geomorphic records (various authors)
Max depth (km)	20	EJ	inferred from microseismic spatial distribution (Paradisopoulou <i>et al.</i> , 2004; 2006)
Strike (deg)	265 - 295	LD	various geological/morphotectonic maps
Dip (deg)	30 - 87	EJ	inferred from microseismic spatial distribution and field measurements (various authors)
Rake (deg)	260 - 290	LD	kinematic indicators, focal mechanisms and regional stress field (various authors)
Slip rate (mm/a)	0.1 – 0.5	AR	calculated from geodetic strain rate field
Max magnitude (Mw)	7.0	ER	calculated from the empirical relationships of Wells and Coppersmith (1994)
Approximate location (Lat/Lon)	40.499 / 22.889	AR	map derived
Total length (km)	40	AR	map derived
Total width (km)	30	AR	derived from depth and dip
Typical fault length (km)	41.7	ER	derived from maximum magnitude
Typical fault width (km)	20.4	ER	derived from maximum magnitude
Typical fault slip (m)	1.56	AR	derived from moment and fault size

Appendix

General information			
Code:	GRIS251		
Name:	Angelochori Fault		
Associated CSS:	Anthemountas (GRCS250)		
Parametric information			
	Parameter	Qual.	Evidence
Location (Lat/Lon)	40.540 / 22.923	LD	various geological/morphotectonic maps
Length (km)	17.5	LD	morphotectonic maps (Zervopoulou, 2004)
Width (km)	18	AR	derives from other parameters (dip, minimum and maximum depth)
Min depth (km)	0	LD	geomorphic records (various authors)
Max depth (km)	15.6	LD	inferred from geological considerations (Tranos <i>et al.</i> , 2003)
Strike (deg)	272	LD	various geological/morphotectonic maps
Dip (deg)	60	EJ	inferred from geological considerations (Tranos <i>et al.</i> , 2003)
Rake (deg)	270	LD	kinematic indicators (Mountrakis <i>et al.</i> , 2006) and regional stress field pattern
Slip per event (m)	0.59	AR	calculated from Mo (Aki, 1966)
Slip rate (mm/a)	0.0 - 0.0	UN	unknown
Recurrence (y)	0.0 - 0.0	UN	unknown
Max Magnitude (Mw)	6.5	ER	after the relationships of Wells and Coppersmith (1994) and Hanks and Kanamori (1979)
Associated earthquake			
Latest Eq	1759/07/3	M=6.5 historical event (see text for further discussion)	
Penultimate Eq	N/A	unknown	
Elapsed Time	241	as of year 2000 (assigned datum)	

General information			
Code:	GRIS252		
Name:	Souroti Fault		
Associated CSS:	Anthemountas (GRCS250)		
Parametric information			
	Parameter	Qual.	Evidence
Location (Lat/Lon)	40.509 / 23.132	LD	various geological/morphotectonic maps
Length (km)	17	LD	morphotectonic maps (Zervopoulou, 2004)
Width (km)	18	AR	derives from other parameters (dip, minimum and maximum depth)
Min depth (km)	0	LD	geomorphic records (various authors)
Max depth (km)	15.6	LD	inferred from geological considerations (Tranos <i>et al.</i> , 2003)
Strike (deg)	285	LD	various geological/morphotectonic maps
Dip (deg)	60	EJ	inferred from geological considerations (Tranos <i>et al.</i> , 2003)
Rake (deg)	280	LD	kinematic indicators (Mountrakis <i>et al.</i> , 2006) and regional stress field pattern
Slip per event (m)	0.58	AR	calculated from Mo (Aki, 1966)
Slip rate (mm/a)	0.0 - 0.0	UN	unknown
Recurrence (y)	0.0 - 0.0	UN	unknown
Max Magnitude (Mw)	6.5	ER	after the relationships of Wells and Coppersmith (1994) and Hanks and Kanamori (1979)
Associated earthquake			
Latest Eq	1677	M=6.2 historical event (see text for further discussion)	
Penultimate Eq	N/A	Unknown	
Elapsed Time	323	as of year 2000 (assigned datum)	

Appendix

General information			
Code:	GRCS060		
Name:	North Almopia		
Associated ISSs:	Pozar (GRIS060), Promachi (GRIS061) and Aetochori (GRIS062)		
Parametric information			
	Parameter	Qual.	Evidence
Min depth (km)	0	LD	geomorphic records (various authors)
Max depth (km)	12.0	EJ	inferred from seismogenic layer thickness of nearby areas
Strike (deg)	50 - 85	LD	various geological/morphotectonic maps
Dip (deg)	60 - 85	EJ	inferred from field measurements and geological profiles (various authors)
Rake (deg)	230 - 290	LD	kinematic indicators (various authors)
Slip rate (mm/a)	1.0 – 1.0	LD	after the extension/subsidence rates of Vougioukalakis (2002)
Max magnitude (Mw)	6.6	EJ	fault geometry considerations and application of empirical relationships (Wells and Coppersmith, 1994)
Approximate location (Lat/Lon)	41.044 / 22.078	AR	map derived
Total length (km)	41.2	AR	map derived
Total width (km)	13.0	AR	derived from depth and dip
Typical fault length (km)	26.3	ER	derived from maximum magnitude
Typical fault width (km)	14.8	ER	derived from maximum magnitude
Typical fault slip (m)	0.86	AR	derived from moment and fault size

General information			
Code:	GRIS060		
Name:	Pozar Fault		
Associated CSS:	North Almopia (GRIS060)		
Parametric information			
	Parameter	Qual.	Evidence
Location (Lat/Lon)	40.958 / 21.970	LD	various geological/morphotectonic maps
Length (km)	8	LD	various geological/morphotectonic maps
Width (km)	11	AR	derives from other parameters (dip, minimum and maximum depth)
Min depth (km)	0	LD	geomorphic records (various authors)
Max depth (km)	10	EJ	inferred from seismogenic layer thickness of nearby areas
Strike (deg)	60	LD	various geological/morphotectonic maps
Dip (deg)	65	LD	3-D structural model of the basin (Vougioukalakis, 2002)
Rake (deg)	285	LD	kinematic indicators (Mercier <i>et al.</i> , 1989; Pavlides <i>et al.</i> , 1990)
Slip per event (m)	0.3	AR	calculated from Mo (Aki, 1966)
Slip rate (mm/a)	1.0 - 1.0	LD	after the extension/subsidence rates of Vougioukalakis (2002)
Recurrence (y)	0.0 - 0.0	UN	unknown
Max Magnitude (Mw)	5.9	ER	after the relationships of Wells and Coppersmith (1994) and Hanks and Kanamori (1979)
Associated earthquake			
Latest Eq	N/A	unknown	
Penultimate Eq	N/A	unknown	
Elapsed Time	N/A	unknown	

Appendix

General information			
Code:	GRIS061		
Name:	Promachi Fault		
Associated CSS:	North Almopia (GRIS060)		
Parametric information			
	Parameter	Qual.	Evidence
Location (Lat/Lon)	41.021 / 22.082	LD	various geological/morphotectonic maps
Length (km)	18.2	LD	various geological/morphotectonic maps
Width (km)	11.5	AR	derives from other parameters (dip, minimum and maximum depth)
Min depth (km)	0	LD	geomorphic records (various authors)
Max depth (km)	10.4	EJ	inferred from seismogenic layer thickness of nearby areas
Strike (deg)	67	LD	various geological/morphotectonic maps
Dip (deg)	65	LD	3-D structural model of the basin (Vougioukalakis, 2002)
Rake (deg)	270	LD	kinematic indicators (various authors)
Slip per event (m)	0.47	AR	calculated from Mo (Aki, 1966)
Slip rate (mm/a)	1.0 - 1.0	LD	after the extension/subsidence rates of Vougioukalakis (2002)
Recurrence (y)	0.0 - 0.0	UN	unknown
Max Magnitude (Mw)	6.3	ER	after the relationships of Wells and Coppersmith (1994) and Hanks and Kanamori (1979)
Associated earthquake			
Latest Eq	N/A	unknown	
Penultimate Eq	N/A	unknown	
Elapsed Time	N/A	unknown	

General information			
Code:	GRIS062		
Name:	Aetochori Fault		
Associated CSS:	North Almopia (GRIS060)		
Parametric information			
	Parameter	Qual.	Evidence
Location (Lat/Lon)	41.097 / 22.248	LD	various geological/morphotectonic maps
Length (km)	12	LD	various geological/morphotectonic maps
Width (km)	10	AR	derives from other parameters (dip, minimum and maximum depth)
Min depth (km)	0	LD	geomorphic records (various authors)
Max depth (km)	9.1	EJ	inferred from seismogenic layer thickness of nearby areas
Strike (deg)	65	LD	geological/morphotectonic maps (Goldsworthy <i>et al.</i> , 2002)
Dip (deg)	65	EJ	inferred from adjacent faults
Rake (deg)	270	EJ	inferred from regional stress field
Slip per event (m)	0.36	AR	calculated from Mo (Aki, 1966)
Slip rate (mm/a)	0.0 - 0.0	UN	unknown
Recurrence (y)	0.0 - 0.0	UN	unknown
Max Magnitude (Mw)	6.1	ER	after the relationships of Wells and Coppersmith (1994) and Hanks and Kanamori (1979)
Associated earthquake			
Latest Eq	N/A	unknown	
Penultimate Eq	N/A	unknown	
Elapsed Time	N/A	unknown	

Appendix

General information			
Code:	GRIS069		
Name:	Goumenissa Fault		
Associated CSS:	none		
Parametric information			
	Parameter	Qual.	Evidence
Location (Lat/Lon)	40.923 / 22.487	EJ	inferred from focal properties (various authors) and remote sensing
Length (km)	14	EJ	inferred from aftershock spatial distribution (Panagiotopoulos <i>et al.</i> , 1993)
Width (km)	12.5	AR	derives from other parameters (dip, minimum and maximum depth)
Min depth (km)	1.0	EJ	absence of scarps and co-seismic ruptures
Max depth (km)	11.2	EJ	inferred from aftershock spatial distribution (Panagiotopoulos <i>et al.</i> , 1993)
Strike (deg)	54	LD	focal mechanisms (Panagiotopoulos <i>et al.</i> , 1993; Baker <i>et al.</i> , 1997)
Dip (deg)	55	EJ	inferred from foci (various authors) and geological considerations
Rake (deg)	257	LD	focal mechanisms (Panagiotopoulos <i>et al.</i> , 1993; Baker <i>et al.</i> , 1997)
Slip per event (m)	0.34	AR	calculated from Mo (Aki, 1966)
Slip rate (mm/a)	0.0 - 0.0	UN	unknown
Recurrence (y)	0.0 - 0.0	UN	unknown
Max Magnitude (Mw)	6.1	ER	after the relationships of Wells and Coppersmith (1994) and Hanks and Kanamori (1979)
Associated earthquake			
Latest Eq	1990/12/21	Mw=6.1 (Vannucci & Gasperini, 2003; 2004; Dziewonski <i>et al.</i> , 1991)	
Penultimate Eq	N/A	unknown	
Elapsed Time	10	as of year 2000 (assigned datum)	

General information			
Code:	GRCS068		
Name:	South Almopia		
Associated ISSs:	none		
Parametric information			
	Parameter	Qual.	Evidence
Min depth (km)	0	LD	geomorphic records (Pavlides, 1998)
Max depth (km)	16	EJ	inferred from seismogenic layer thickness of nearby areas
Strike (deg)	45 - 75	LD	geological/morphotectonic maps (Pavlides, 1998)
Dip (deg)	45 - 70	EJ	field measurements (Pavlides, 1998) and geological considerations
Rake (deg)	245 - 265	LD	kinematic indicators (Pavlides, 1998)
Slip rate (mm/a)	0.2 – 0.4	AR	calculated from geodetic strain rate field
Max magnitude (Mw)	6.3	EJ	fault geometry considerations and application of empirical relationships (Wells and Coppersmith, 1994)
Approximate location (Lat/Lon)	40.774 / 22.305	AR	map derived
Total length (km)	20.1	AR	map derived
Total width (km)	19.8	AR	derived from depth and dip
Typical fault length (km)	18.6	ER	derived from maximum magnitude
Typical fault width (km)	11.6	ER	derived from maximum magnitude
Typical fault slip (m)	0.55	AR	derived from moment and fault size

Appendix

General information			
Code:	GRCS070		
Name:	Amyndeo		
Associated ISSs:	Nymfaeo (GRIS070) and Petron (GRIS071)		
Parametric information			
	Parameter	Qual.	Evidence
Min depth (km)	0	LD	geomorphic records (various authors)
Max depth (km)	13	LD	schematic profile (Pavlidis and Simeakis, 1987/88)
Strike (deg)	30 - 65	LD	various geological/morphotectonic maps
Dip (deg)	45 - 70	LD	schematic profile (Pavlidis and Simeakis, 1987/88)
Rake (deg)	250 - 270	LD	kinematic indicators (various authors)
Slip rate (mm/a)	0.1 – 0.3	AR	calculated from geodetic strain rate field
Max magnitude (Mw)	6.6	EJ	fault geometry considerations and application of empirical relationships (Wells and Coppersmith, 1994)
Approximate location (Lat/Lon)	40.700 / 21.623	AR	map derived
Total length (km)	38.2	AR	map derived
Total width (km)	16.1	AR	derived from depth and dip
Typical fault length (km)	26.3	ER	derived from maximum magnitude
Typical fault width (km)	14.8	ER	derived from maximum magnitude
Typical fault slip (m)	0.86	AR	derived from moment and fault size

General information			
Code:	GRIS070		
Name:	Nymfaeo Fault		
Associated CSS:	Amyndeo (GRCS070)		
Parametric information			
	Parameter	Qual.	Evidence
Location (Lat/Lon)	40.650 / 21.601	LD	various geological/morphotectonic maps
Length (km)	13	LD	various geological/morphotectonic maps
Width (km)	12.5	AR	derives from other parameters (dip, minimum and maximum depth)
Min depth (km)	0	LD	geomorphic records (various authors)
Max depth (km)	10.8	LD	schematic profile (Pavlidis and Simeakis, 1987/88)
Strike (deg)	56	LD	various geological/morphotectonic maps
Dip (deg)	60	EJ	field measurements (various authors) and geological considerations
Rake (deg)	260	LD	kinematic indicators (various authors)
Slip per event (m)	0.48	AR	calculated from Mo (Aki, 1966)
Slip rate (mm/a)	0.0 - 0.0	UN	unknown
Recurrence (y)	0.0 - 0.0	UN	unknown
Max Magnitude (Mw)	6.2	ER	after the relationships of Wells and Coppersmith (1994) and Hanks and Kanamori (1979)
Associated earthquake			
Latest Eq	N/A	unknown	
Penultimate Eq	N/A	unknown	
Elapsed Time	N/A	unknown	

Appendix

General information			
Code:	GRIS071		
Name:	Petron Fault		
Associated CSS:	Amyndeo (GRCS070)		
Parametric information			
	Parameter	Qual.	Evidence
Location (Lat/Lon)	40.718 / 21.704	LD	various geological/morphotectonic maps
Length (km)	8.5	LD	various geological/morphotectonic maps
Width (km)	12	AR	derives from other parameters (dip, minimum and maximum depth)
Min depth (km)	0	LD	geomorphic records (various authors)
Max depth (km)	10.4	LD	schematic profile (Pavlidis and Simeakis, 1987/88)
Strike (deg)	38	LD	various geological/morphotectonic maps
Dip (deg)	60	EJ	field measurements and schematic profile (various authors)
Rake (deg)	240	LD	kinematic indicators (various authors)
Slip per event (m)	0.38	AR	calculated from Mo (Aki, 1966)
Slip rate (mm/a)	0.0 - 0.0	UN	unknown
Recurrence (y)	0.0 - 0.0	UN	unknown
Max Magnitude (Mw)	6.0	ER	after the relationships of Wells and Coppersmith (1994) and Hanks and Kanamori (1979)
Associated earthquake			
Latest Eq	N/A	unknown	
Penultimate Eq	N/A	unknown	
Elapsed Time	N/A	unknown	

General information			
Code:	GRIS075		
Name:	Chimaditis Fault		
Associated CSS:	none		
Parametric information			
	Parameter	Qual.	Evidence
Location (Lat/Lon)	40.598 / 21.575	LD	various geological/morphotectonic maps
Length (km)	11.5	LD	various geological/morphotectonic maps
Width (km)	8	AR	derives from other parameters (dip, minimum and maximum depth)
Min depth (km)	0	LD	geomorphic records (various authors)
Max depth (km)	7.5	EJ	inferred from seismotectonic considerations
Strike (deg)	233	LD	various geological/morphotectonic maps
Dip (deg)	70	EJ	inferred from field measurements (Pavlidis, 1985; Pavlidis & Mountrakis, 1987)
Rake (deg)	260	LD	kinematic indicators (various authors)
Slip per event (m)	0.36	AR	calculated from Mo (Aki, 1966)
Slip rate (mm/a)	0.0 - 0.0	UN	unknown
Recurrence (y)	0.0 - 0.0	UN	unknown
Max Magnitude (Mw)	5.9	ER	after the relationships of Wells and Coppersmith (1994) and Hanks and Kanamori (1979)
Associated earthquake			
Latest Eq	N/A	unknown	
Penultimate Eq	N/A	unknown	
Elapsed Time	N/A	unknown	

Appendix

General information			
Code:	GRCS072		
Name:	Ptolemaida		
Associated ISSs:	Vegora (GRIS072) and Vegoritida (GRIS073)		
Parametric information			
	Parameter	Qual.	Evidence
Min depth (km)	0	LD	geomorphic records (various authors)
Max depth (km)	11.5	EJ	inferred from seismotectonic considerations
Strike (deg)	15 - 50	LD	various geological/morphotectonic maps
Dip (deg)	50 - 65	LD	schematic profile (Pavlidis and Simeakis, 1987/88)
Rake (deg)	250 - 270	LD	kinematic indicators (various authors)
Slip rate (mm/a)	0.1 – 0.3	AR	calculated from geodetic strain rate field
Max magnitude (Mw)	6.6	ER	calculated from the empirical relationships of Wells and Coppersmith (1994)
Approximate location (Lat/Lon)	40.728 / 21.750	AR	map derived
Total length (km)	25.3	AR	map derived
Total width (km)	13.9	AR	derived from depth and dip
Typical fault length (km)	26.3	ER	derived from maximum magnitude
Typical fault width (km)	14.8	ER	derived from maximum magnitude
Typical fault slip (m)	0.86	AR	derived from moment and fault size

General information			
Code:	GRIS072		
Name:	Vegora Fault		
Associated CSS:	Ptolemaida (GRCS072)		
Parametric information			
	Parameter	Qual.	Evidence
Location (Lat/Lon)	40.676 / 21.745	LD	various geological/morphotectonic maps
Length (km)	14	LD	various geological/morphotectonic maps
Width (km)	12	AR	derives from other parameters (dip, minimum and maximum depth)
Min depth (km)	0	LD	geomorphic records (various authors)
Max depth (km)	10.4	EJ	inferred from seismotectonic considerations
Strike (deg)	39	LD	various geological/morphotectonic maps
Dip (deg)	60	LD	schematic profile (Pavlidis and Simeakis, 1987/88)
Rake (deg)	250	LD	kinematic indicators (various authors)
Slip per event (m)	0.49	AR	calculated from Mo (Aki, 1966)
Slip rate (mm/a)	0.0 - 0.0	UN	unknown
Recurrence (y)	0.0 - 0.0	UN	unknown
Max Magnitude (Mw)	6.2	ER	after the relationships of Wells and Coppersmith (1994) and Hanks and Kanamori (1979)
Associated earthquake			
Latest Eq	N/A	unknown	
Penultimate Eq	N/A	unknown	
Elapsed Time	N/A	unknown	

Appendix

General information			
Code:	GRIS073		
Name:	Vegoritida Fault		
Associated CSS:	Ptolemaida (GRCS072)		
Parametric information			
	Parameter	Qual.	Evidence
Location (Lat/Lon)	40.764 / 21.805	LD	various geological/morphotectonic maps
Length (km)	9.5	LD	various geological/morphotectonic maps
Width (km)	12	AR	derives from other parameters (dip, minimum and maximum depth)
Min depth (km)	0	LD	geomorphic records (various authors)
Max depth (km)	10.4	EJ	inferred from seismotectonic considerations
Strike (deg)	20	LD	various geological/morphotectonic maps
Dip (deg)	60	LD	schematic profile (Pavlides and Simeakis, 1987/88)
Rake (deg)	250	LD	kinematic indicators (various authors)
Slip per event (m)	0.40	AR	calculated from Mo (Aki, 1966)
Slip rate (mm/a)	0.0 - 0.0	UN	unknown
Recurrence (y)	0.0 - 0.0	UN	unknown
Max Magnitude (Mw)	6.0	ER	after the relationships of Wells and Coppersmith (1994) and Hanks and Kanamori (1979)
Associated earthquake			
Latest Eq	N/A	unknown	
Penultimate Eq	N/A	unknown	
Elapsed Time	N/A	unknown	

General information			
Code:	GRIS076		
Name:	Perdika Fault		
Associated CSS:	none		
Parametric information			
	Parameter	Qual.	Evidence
Location (Lat/Lon)	40.535 / 21.588	LD	various geological/morphotectonic maps
Length (km)	11.7	LD	various geological/morphotectonic maps
Width (km)	8.5	AR	derives from other parameters (dip, minimum and maximum depth)
Min depth (km)	0	LD	geomorphic records (various authors)
Max depth (km)	8	EJ	inferred from seismotectonic considerations
Strike (deg)	223	LD	various geological/morphotectonic maps
Dip (deg)	70	EJ	field measurements (various authors) and geological considerations
Rake (deg)	260	LD	kinematic indicators (various authors)
Slip per event (m)	0.37	AR	calculated from Mo (Aki, 1966)
Slip rate (mm/a)	0.0 - 0.0	UN	unknown
Recurrence (y)	0.0 - 0.0	UN	unknown
Max Magnitude (Mw)	6.0	ER	after the relationships of Wells and Coppersmith (1994) and Hanks and Kanamori (1979)
Associated earthquake			
Latest Eq	N/A	unknown	
Penultimate Eq	N/A	unknown	
Elapsed Time	N/A	unknown	

Appendix

General information			
Code:	GRCS077		
Name:	Komanos		
Associated ISSs:	Mesovouni (GRIS077) and Proastio (GRIS078)		
Parametric information			
	Parameter	Qual.	Evidence
Min depth (km)	0	LD	geomorphic records (various authors)
Max depth (km)	14.0	EJ	inferred from seismotectonic considerations
Strike (deg)	205 - 235	LD	various geological/morphotectonic maps
Dip (deg)	45 - 80	LD	schematic profile (Pavlidis and Simeakis, 1987/88)
Rake (deg)	250 - 270	LD	kinematic indicators (various authors)
Slip rate (mm/a)	0.1 – 0.3	AR	calculated from geodetic strain rate field
Max magnitude (Mw)	6.8	ER	calculated from the empirical relationships of Wells and Coppersmith (1994)
Approximate location (Lat/Lon)	40.635 / 21.708	AR	map derived
Total length (km)	35.5	AR	map derived
Total width (km)	17.0	AR	derived from depth and dip
Typical fault length (km)	33.1	ER	derived from maximum magnitude
Typical fault width (km)	17.4	ER	derived from maximum magnitude
Typical fault slip (m)	1.16	AR	derived from moment and fault size

General information			
Code:	GRIS077		
Name:	Mesovouni Fault		
Associated CSS:	Komanos (GRCS077)		
Parametric information			
	Parameter	Qual.	Evidence
Location (Lat/Lon)	40.649 / 21.814	LD	various geological/morphotectonic maps
Length (km)	18	LD	various geological/morphotectonic maps
Width (km)	12	AR	derives from other parameters (dip, minimum and maximum depth)
Min depth (km)	0	LD	geomorphic records (various authors)
Max depth (km)	10.9	EJ	inferred from seismotectonic considerations
Strike (deg)	211	LD	geological/morphotectonic maps and foci (various authors)
Dip (deg)	65	EJ	inferred from field measurements and foci (various authors)
Rake (deg)	255	LD	kinematic indicators and foci (various authors)
Slip per event (m)	0.48	AR	calculated from Mo (Aki, 1966)
Slip rate (mm/a)	0.0 - 0.0	UN	unknown
Recurrence (y)	0.0 - 0.0	UN	unknown
Max Magnitude (Mw)	6.3	ER	after the relationships of Wells and Coppersmith (1994) and Hanks and Kanamori (1979)
Associated earthquake			
Latest Eq	N/A	unknown	
Penultimate Eq	N/A	unknown	
Elapsed Time	N/A	unknown	

Appendix

General information			
Code:	GRIS078		
Name:	Proastio Fault		
Associated CSS:	Komanos (GRCS077)		
Parametric information			
	Parameter	Qual.	Evidence
Location (Lat/Lon)	40.505 / 21.688	LD	various geological/morphotectonic maps
Length (km)	11	LD	various geological/morphotectonic maps
Width (km)	11	AR	derives from other parameters (dip, minimum and maximum depth)
Min depth (km)	0	LD	geomorphic records (various authors)
Max depth (km)	10	EJ	inferred from seismotectonic considerations
Strike (deg)	223	LD	various geological/morphotectonic maps
Dip (deg)	65	EJ	inferred from field measurements (various authors) and geological considerations
Rake (deg)	265	LD	kinematic indicators (various authors)
Slip per event (m)	0.35	AR	calculated from Mo (Aki, 1966)
Slip rate (mm/a)	0.0 - 0.0	UN	unknown
Recurrence (y)	0.0 - 0.0	UN	unknown
Max Magnitude (Mw)	6.1	ER	after the relationships of Wells and Coppersmith (1994) and Hanks and Kanamori (1979)
Associated earthquake			
Latest Eq	N/A	unknown	
Penultimate Eq	N/A	unknown	
Elapsed Time	N/A	unknown	

General information			
Code:	GRIS074		
Name:	Peraea Fault		
Associated CSS:	none		
Parametric information			
	Parameter	Qual.	Evidence
Location (Lat/Lon)	40.687 / 21.823	LD	various geological/morphotectonic maps
Length (km)	13.8	LD	various geological/morphotectonic maps
Width (km)	9.5	AR	derives from other parameters (dip, minimum and maximum depth)
Min depth (km)	0	LD	geomorphic records (various authors)
Max depth (km)	8.9	EJ	inferred from seismotectonic considerations
Strike (deg)	27	LD	various geological/morphotectonic maps
Dip (deg)	70	LD	schematic profile (Pavlidis and Simeakis, 1987/88)
Rake (deg)	250	LD	kinematic indicators (various authors)
Slip per event (m)	0.43	AR	calculated from Mo (Aki, 1966)
Slip rate (mm/a)	0.0 - 0.0	UN	unknown
Recurrence (y)	0.0 - 0.0	UN	unknown
Max Magnitude (Mw)	6.1	ER	after the relationships of Wells and Coppersmith (1994) and Hanks and Kanamori (1979)
Associated earthquake			
Latest Eq	N/A	unknown	
Penultimate Eq	N/A	unknown	
Elapsed Time	N/A	unknown	

Appendix

General information			
Code:	GRCS050		
Name:	Aliakmonas		
Associated ISSs:	Palaeochori (GRIS050), Rymnio (GRIS051), Servia (GRIS052) and Chromio (GRIS053)		
Parametric information			
	Parameter	Qual.	Evidence
Min depth (km)	0	LD	geomorphic records, remote sensing (various authors)
Max depth (km)	17	EJ	inferred from aftershock spatial distribution (various authors)
Strike (deg)	210 - 255	LD	geological/morphotectonic maps and focal mechanisms (various authors)
Dip (deg)	40 - 80	EJ	inferred from field measurements and focal mechanisms (various authors)
Rake (deg)	250 - 280	LD	kinematic indicators and focal mechanisms (various authors)
Slip rate (mm/a)	0.3 – 2.0	LD	morphotectonic investigations (Doutsos and Koukouvelas, 1998; Meyer <i>et al.</i> , 1996)
Max magnitude (Mw)	6.9	EJ	fault geometry considerations and application of empirical relationships (Wells and Coppersmith, 1994)
Approximate location (Lat/Lon)	40.21 / 21.930	AR	map derived
Total length (km)	89.1	AR	map derived
Total width (km)	21.9	AR	derived from depth and dip
Typical fault length (km)	37.2	ER	derived from maximum magnitude
Typical fault width (km)	18.8	ER	derived from maximum magnitude
Typical fault slip (m)	1.34	AR	derived from moment and fault size

General information			
Code:	GRIS050		
Name:	Palaeochori Fault		
Associated CSS:	Aliakmonas (GRCS050)		
Parametric information			
	Parameter	Qual.	Evidence
Location (Lat/Lon)	40.086 / 21.668	LD	geological/morphotectonic maps, co-seismic ruptures and remote sensing
Length (km)	21	LD	various geological/morphotectonic maps
Width (km)	18	AR	derives from other parameters (dip, minimum and maximum depth)
Min depth (km)	0	LD	geomorphic records, remote sensing (various authors)
Max depth (km)	14.7	EJ	inferred from aftershock spatial distribution (various authors)
Strike (deg)	246	LD	geological/morphotectonic maps and focal mechanisms (various authors)
Dip (deg)	55	EJ	from various aftershock spatial distributions, foci and field measurements
Rake (deg)	255	LD	focal mechanisms and kinematic indicators (various authors)
Slip per event (m)	0.65	AR	calculated from Mo (Aki, 1966)
Slip rate (mm/a)	0.3 - 0.3	LD	morphotectonics (Doutsos and Koukouvelas, 1998)
Recurrence (y)	2000 - 30000	LD	morphotectonics and palaeoseismology (various authors)
Max Magnitude (Mw)	6.6	ER	after the relationships of Wells and Coppersmith (1994) and Hanks and Kanamori (1979)
Associated earthquake			
Latest Eq	1995/05/13	Mw=6.5 produced by partial reactivation of two segments	
Penultimate Eq	7000 BC	palaeoseismology (Chatzipetros <i>et al.</i> , 1998)	
Elapsed Time	5	as of year 2000 (assigned datum)	

Appendix

General information			
Code:	GRIS051		
Name:	Rymnio Fault		
Associated CSS:	Aliakmonas (GRCS050)		
Parametric information			
	Parameter	Qual.	Evidence
Location (Lat/Lon)	40.159 / 21.837	LD	geological/morphotectonic maps, co-seismic ruptures and remote sensing
Length (km)	13	LD	various geological/morphotectonic maps
Width (km)	16.5	AR	derives from other parameters (dip, minimum and maximum depth)
Min depth (km)	0	LD	geomorphic records, remote sensing (various authors)
Max depth (km)	13.5	EJ	inferred from aftershock spatial distribution (various authors)
Strike (deg)	231	LD	geological/morphotectonic maps and focal mechanisms (various authors)
Dip (deg)	55	EJ	from various aftershock spatial distributions, foci and field measurements
Rake (deg)	275	LD	focal mechanisms and kinematic indicators (various authors)
Slip per event (m)	0.48	AR	calculated from Mo (Aki, 1966)
Slip rate (mm/a)	0.3 - 0.3	LD	morphotectonics (Doutsos and Koukouvelas, 1998)
Recurrence (y)	2000 - 2000	LD	morphotectonics (Doutsos and Koukouvelas, 1998)
Max Magnitude (Mw)	6.3	ER	after the relationships of Wells and Coppersmith (1994) and Hanks and Kanamori (1979)
Associated earthquake			
Latest Eq	1995/05/13	Mw=6.5 produced by partial reactivation of two segments	
Penultimate Eq	N/A	unknown	
Elapsed Time	5	as of year 2000 (assigned datum)	

General information			
Code:	GRIS052		
Name:	Servia Fault		
Associated CSS:	Aliakmonas (GRCS050)		
Parametric information			
	Parameter	Qual.	Evidence
Location (Lat/Lon)	40.236 / 22.001	LD	various geological/morphotectonic maps
Length (km)	16.9	LD	various geological/morphotectonic maps
Width (km)	15	AR	derives from other parameters (dip, minimum and maximum depth)
Min depth (km)	0	LD	geomorphic records (various authors)
Max depth (km)	13	EJ	inferred from regional seismogenic layer thickness
Strike (deg)	228	LD	various geological/morphotectonic maps
Dip (deg)	60	EJ	from regional seismotectonic setting and field measurements (various authors)
Rake (deg)	280	LD	kinematic indicators (various authors)
Slip per event (m)	0.52	AR	calculated from Mo (Aki, 1966)
Slip rate (mm/a)	1.0 – 2.0	LD	morphotectonics (Meyer <i>et al.</i> , 1996)
Recurrence (y)	1000 - 2000	LD	morphotectonics (Meyer <i>et al.</i> , 1996)
Max Magnitude (Mw)	6.4	ER	after the relationships of Wells and Coppersmith (1994) and Hanks and Kanamori (1979)
Associated earthquake			
Latest Eq	N/A	unknown	
Penultimate Eq	N/A	unknown	
Elapsed Time	N/A	unknown	

Appendix

General information			
Code:	GRIS053		
Name:	Chromio Fault		
Associated CSS:	Aliakmonas (GRCS050)		
Parametric information			
	Parameter	Qual.	Evidence
Location (Lat/Lon)	40.098 / 21.656	LD	co-seismic ground ruptures and aftershock spatial distribution (various authors)
Length (km)	10	LD	co-seismic ground ruptures and geological/morphotectonic maps (various authors)
Width (km)	6.5	AR	constrained from the Palaeochori ISS (GRIS050)
Min depth (km)	1.5	LD	co-seismic ground ruptures and geomorphic records (various authors)
Max depth (km)	6.5	AR	derives from other parameters (dip, width and minimum depth)
Strike (deg)	91	LD	co-seismic ground ruptures, focal mechanisms and aftershock spatial distribution
Dip (deg)	50	LD	aftershock spatial distribution (various authors)
Rake (deg)	280	LD	focal mechanisms and co-seismic ground ruptures
Slip per event (m)	0.22	AR	calculated from Mo (Aki, 1966)
Slip rate (mm/a)	0 - 0	UN	unknown
Recurrence (y)	0 - 0	UN	unknown
Max Magnitude (Mw)	5.8	ER	after the relationships of Wells and Coppersmith (1994) and Hanks and Kanamori (1979)
Associated earthquake			
Latest Eq	1995/05/13		reactivated as a secondary structure (see Palaeochori GRIS050)
Penultimate Eq	N/A		unknown
Elapsed Time	N/A		unknown

General information			
Code:	GRCS300		
Name:	Konitsa		
Associated ISSs:	Konitsa (GRIS301)		
Parametric information			
	Parameter	Qual.	Evidence
Min depth (km)	0	LD	geomorphic records (various authors)
Max depth (km)	14	EJ	inferred from aftershock spatial distribution (Papanastassiou, 2001)
Strike (deg)	220 - 240	LD	various geological/morphotectonic maps
Dip (deg)	45 - 75	LD	aftershock spatial distribution (Papanastassiou, 2001)
Rake (deg)	250 - 280	LD	kinematic indicators and focal mechanisms (various authors)
Slip rate (mm/a)	0.1 – 0.4	AR	calculated from geodetic strain rate field
Max magnitude (Mw)	6.6	ER	calculated from the empirical relationships of Wells and Coppersmith (1994)
Approximate location (Lat/Lon)	40.002 / 20.681	AR	map derived
Total length (km)	24.2	AR	map derived
Total width (km)	17.1	AR	derived from depth and dip
Typical fault length (km)	26.3	ER	derived from maximum magnitude
Typical fault width (km)	14.8	ER	derived from maximum magnitude
Typical fault slip (m)	0.86	AR	derived from moment and fault size

Appendix

General information			
Code:	GRIS301		
Name:	Konitsa Fault		
Associated CSS:	Konitsa (GRCS300)		
Parametric information			
	Parameter	Qual.	Evidence
Location (Lat/Lon)	40.044 / 20.678	LD	various geological/morphotectonic maps
Length (km)	11.3	LD	various geological/morphotectonic maps
Width (km)	13	AR	derives from other parameters (dip, minimum and maximum depth)
Min depth (km)	0	LD	geomorphic records (various authors)
Max depth (km)	10.6	EJ	inferred from spatial aftershock distribution (Papanastassiou, 2001)
Strike (deg)	232	LD	geological/morphotectonic maps and focal mechanisms (various authors)
Dip (deg)	55	LD	inferred from spatial aftershock distribution and foci (various authors)
Rake (deg)	280	LD	kinematic indicators and focal mechanisms (various authors)
Slip per event (m)	0.39	AR	calculated from Mo (Aki, 1966)
Slip rate (mm/a)	0 - 0	UN	unknown
Recurrence (y)	0 - 0	UN	unknown
Max Magnitude (Mw)	6.1	ER	after the relationships of Wells and Coppersmith (1994) and Hanks and Kanamori (1979)
Associated earthquake			
Latest Eq	1996/08/05	Ms=5.7 mainshock preceded by a foreshock (Ms=5.4) on July 26	
Penultimate Eq	N/A	unknown	
Elapsed Time	4	as of year 2000 (assigned datum)	

General information			
Code:	GRCS310		
Name:	Petoussi		
Associated ISSs:	Souli (GRIS310) and Tomaros (GRIS311)		
Parametric information			
	Parameter	Qual.	Evidence
Min depth (km)	0	LD	geomorphic records (various authors)
Max depth (km)	16	EJ	inferred from various microseismic surveys
Strike (deg)	80 - 260	LD	various geological/morphotectonic maps
Dip (deg)	80 - 90	EJ	field observations (various authors) and geological considerations
Rake (deg)	315 - 355	LD	kinematic indicators (various authors)
Slip rate (mm/a)	0.1 – 0.3	LD	palaeoseismological data (Boccaletti <i>et al.</i> , 1997)
Max magnitude (Mw)	6.7	EJ	calculated from the empirical relationships of Wells and Coppersmith (1994)
Approximate location (Lat/Lon)	39.508 / 20.692	AR	map derived
Total length (km)	39.1	AR	map derived
Total width (km)	16.1	AR	derived from depth and dip
Typical fault length (km)	38.4	ER	derived from maximum magnitude
Typical fault width (km)	11.2	ER	derived from maximum magnitude
Typical fault slip (m)	1.10	AR	derived from moment and fault size

Appendix

General information			
Code:	GRIS310		
Name:	Souli Fault		
Associated CSS:	Petoussi (GRCS310)		
Parametric information			
	Parameter	Qual.	Evidence
Location (Lat/Lon)	39.502 / 20.555	LD	various geological/morphotectonic maps
Length (km)	14.6	LD	various geological/morphotectonic maps
Width (km)	12	AR	derives from other parameters (dip, minimum and maximum depth)
Min depth (km)	0	LD	geomorphic records (various authors)
Max depth (km)	12	EJ	inferred from various microseismic surveys
Strike (deg)	82	LD	various geological/morphotectonic maps
Dip (deg)	85	EJ	field observations (various authors) and geological considerations
Rake (deg)	330	LD	kinematic indicators (various authors)
Slip per event (m)	0.51	AR	calculated from Mo (Aki, 1966)
Slip rate (mm/a)	0 - 0	UN	unknown
Recurrence (y)	0 - 0	UN	unknown
Max Magnitude (Mw)	6.3	ER	after the relationships of Wells and Coppersmith (1994) and Hanks and Kanamori (1979)
Associated earthquake			
Latest Eq	24000 BC		palaeoseismological data from Boccaletti <i>et al.</i> (1997)
Penultimate Eq	N/A		unknown
Elapsed Time	26000		as of year 2000 (assigned datum)

General information			
Code:	GRIS311		
Name:	Tomaros Fault		
Associated CSS:	Petoussi (GRCS310)		
Parametric information			
	Parameter	Qual.	Evidence
Location (Lat/Lon)	39.512 / 20.732	LD	various geological/morphotectonic maps
Length (km)	16.1	LD	various geological/morphotectonic maps
Width (km)	14	AR	derives from other parameters (dip, minimum and maximum depth)
Min depth (km)	0	LD	geomorphic records (various authors)
Max depth (km)	13.9	EJ	inferred from various microseismic surveys
Strike (deg)	263	LD	various geological/morphotectonic maps
Dip (deg)	85	EJ	field observations (various authors) and geological considerations
Rake (deg)	30	LD	kinematic indicators (various authors)
Slip per event (m)	0.59	AR	calculated from Mo (Aki, 1966)
Slip rate (mm/a)	0 - 0	UN	unknown
Recurrence (y)	0 - 0	UN	unknown
Max Magnitude (Mw)	6.4	ER	after the relationships of Wells and Coppersmith (1994) and Hanks and Kanamori (1979)
Associated earthquake			
Latest Eq	N/A		unknown
Penultimate Eq	N/A		unknown
Elapsed Time	N/A		unknown

Appendix

General information			
Code:	GRCS390		
Name:	Kerkyra		
Associated ISSs:	Makrades (GRIS390) and Spartylas (GRIS391)		
Parametric information			
	Parameter	Qual.	Evidence
Min depth (km)	0	LD	geomorphic records (various authors)
Max depth (km)	12	EJ	inferred from seismogenic layer thickness of nearby areas
Strike (deg)	65 - 90	LD	various geological/morphotectonic maps
Dip (deg)	65 - 85	EJ	field observations (various authors) and geological considerations
Rake (deg)	190-260	LD	kinematic indicators (various authors)
Slip rate (mm/a)	0.4 – 0.6	AR	calculated from geodetic strain rate field
Max magnitude (Mw)	6.3	EJ	fault geometry considerations and application of empirical relationships (Wells and Coppersmith, 1994)
Approximate location (Lat/Lon)	39.725 / 19.826	AR	map derived
Total length (km)	36.9	AR	map derived
Total width (km)	12.6	AR	derived from depth and dip
Typical fault length (km)	21.7	ER	derived from maximum magnitude
Typical fault width (km)	8.7	ER	derived from maximum magnitude
Typical fault slip (m)	0.62	AR	derived from moment and fault size

General information			
Code:	GRIS390		
Name:	Makrades Fault		
Associated CSS:	Kerkyra (GRCS390)		
Parametric information			
	Parameter	Qual.	Evidence
Location (Lat/Lon)	39.701 / 19.703	LD	various geological/morphotectonic maps
Length (km)	9.0	LD	geological/morphotectonic maps (Caputo, 1984; 1986; 1987/88)
Width (km)	10.0	AR	derives from other parameters (dip, minimum and maximum depth)
Min depth (km)	0	LD	geomorphic records (various authors)
Max depth (km)	10.5	EJ	inferred from seismogenic layer thickness of nearby areas
Strike (deg)	79	LD	various geological/morphotectonic maps
Dip (deg)	85	LD	field observations (Caputo, 1984; 1986; 1987/88)
Rake (deg)	20	LD	kinematic indicators (Caputo, 1984; 1986; 1987/88)
Slip per event (m)	0.30	AR	calculated from Mo (Aki, 1966)
Slip rate (mm/a)	0 - 0	UN	unknown
Recurrence (y)	0 - 0	UN	unknown
Max Magnitude (Mw)	5.9	ER	after the relationships of Wells and Coppersmith (1994) and Hanks and Kanamori (1979)
Associated earthquake			
Latest Eq	N/A	unknown	
Penultimate Eq	N/A	unknown	
Elapsed Time	N/A	unknown	

Appendix

General information			
Code:	GRIS391		
Name:	Spartylas Fault		
Associated CSS:	Kerkyra (GRCS390)		
Parametric information			
	Parameter	Qual.	Evidence
Location (Lat/Lon)	39.720 / 19.834	LD	various geological/morphotectonic maps
Length (km)	14.0	LD	geological/morphotectonic maps (Caputo, 1984; 1986; 1987/88)
Width (km)	10.0	AR	derives from other parameters (dip, minimum and maximum depth)
Min depth (km)	0	LD	geomorphic records (various authors)
Max depth (km)	10.5	EJ	inferred from seismogenic layer thickness of nearby areas
Strike (deg)	88	LD	various geological/morphotectonic maps
Dip (deg)	85	EJ	field observations (Caputo, 1984; 1986; 1987/88) and geological considerations
Rake (deg)	30	LD	kinematic indicators (Caputo, 1984; 1986; 1987/88)
Slip per event (m)	0.30	AR	calculated from Mo (Aki, 1966)
Slip rate (mm/a)	0 - 0	UN	unknown
Recurrence (y)	0 - 0	UN	unknown
Max Magnitude (Mw)	6.0	ER	after the relationships of Wells and Coppersmith (1994) and Hanks and Kanamori (1979)
Associated earthquake			
Latest Eq	N/A	unknown	
Penultimate Eq	N/A	unknown	
Elapsed Time	N/A	unknown	

General information			
Code:	GRIS392		
Name:	Palaeokastritsa Fault		
Associated CSS:	none		
Parametric information			
	Parameter	Qual.	Evidence
Location (Lat/Lon)	39.678 / 19.712	LD	various geological/morphotectonic maps
Length (km)	8.0	LD	various geological/morphotectonic maps
Width (km)	10.0	AR	derives from other parameters (dip, minimum and maximum depth)
Min depth (km)	0	LD	geomorphic records (various authors)
Max depth (km)	10.5	EJ	inferred from seismogenic layer thickness of nearby areas
Strike (deg)	262	LD	various geological/morphotectonic maps
Dip (deg)	85	EJ	field observations (Caputo, 1984; 1986; 1987/88) and geological considerations
Rake (deg)	25	LD	kinematic indicators (Caputo, 1984; 1986; 1987/88)
Slip per event (m)	0.20	AR	calculated from Mo (Aki, 1966)
Slip rate (mm/a)	0 - 0	UN	unknown
Recurrence (y)	0 - 0	UN	unknown
Max Magnitude (Mw)	5.7	ER	after the relationships of Wells and Coppersmith (1994) and Hanks and Kanamori (1979)
Associated earthquake			
Latest Eq	N/A	unknown	
Penultimate Eq	N/A	unknown	
Elapsed Time	N/A	unknown	

Appendix

General information			
Code:	GRCS010		
Name:	Pagasitikos Gulf		
Associated ISSs:	Volos (GRIS010) and Nea Anchialos (GRIS011)		
Parametric information			
	Parameter	Qual.	Evidence
Min depth (km)	0	LD	geomorphic records (various authors)
Max depth (km)	12.5	EJ	microseismic spatial distribution (Kementzetzidou, 1996; Hatzfeld <i>et al.</i> , 1999)
Strike (deg)	58 - 104	LD	various geological/morphotectonic maps and focal mechanisms
Dip (deg)	40 - 70	EJ	field measurements, foci and microseismic surveys (various authors)
Rake (deg)	232 - 270	LD	kinematic indicators and focal mechanisms (various authors)
Slip rate (mm/a)	1.0 - 3.0	LD	geomorphic markers (Caputo, 1996)
Max magnitude (Mw)	7.0	ER	calculated from the empirical relationships of Wells and Coppersmith (1994)
Approximate location (Lat/Lon)	39.278 / 22.779	AR	map derived
Total length (km)	48.5	AR	map derived
Total width (km)	16.4	AR	derived from depth and dip
Typical fault length (km)	41.7	ER	derived from maximum magnitude
Typical fault width (km)	20.4	ER	derived from maximum magnitude
Typical fault slip (m)	1.56	AR	derived from moment and fault size

General information			
Code:	GRIS010		
Name:	Volos Fault		
Associated CSS:	Pagasitikos Gulf (GRCS010)		
Parametric information			
	Parameter	Qual.	Evidence
Location (Lat/Lon)	39.249 / 23.035	LD	seismic reflection survey (Perissoratis <i>et al.</i> , 1991) and earthquake epicentre
Length (km)	21	EJ	inferred from seismic reflection survey of Perissoratis <i>et al.</i> (1991)
Width (km)	15	AR	derives from other parameters (dip, minimum and maximum depth)
Min depth (km)	0	LD	seismic reflection survey of Perissoratis <i>et al.</i> (1991)
Max depth (km)	12.3	EJ	inferred from microseismic survey (Kementzetzidou, 1996; Hatzfeld <i>et al.</i> , 1999)
Strike (deg)	85	LD	seismic reflection survey (Perissoratis <i>et al.</i> , 1991) and various foci
Dip (deg)	55	EJ	seismic reflection survey, foci and microseismic survey (various authors)
Rake (deg)	266	LD	various foci and seismic reflection survey (Perissoratis <i>et al.</i> , 1991)
Slip per event (m)	0.63	AR	calculated from Mo (Aki, 1966)
Slip rate (mm/a)	1.0 – 3.0	EJ	assumed from the adjacent Nea Anchialos GRIS011 fault
Recurrence (y)	0 - 0	UN	unknown
Max Magnitude (Mw)	6.5	ER	after the relationships of Wells and Coppersmith (1994) and Hanks and Kanamori (1979)
Associated earthquake			
Latest Eq	1980/07/09	Mw=6.5 (1 st shock)	
Penultimate Eq	N/A	unknown	
Elapsed Time	20	as of year 2000 (assigned datum)	

Appendix

General information			
Code:	GRIS011		
Name:	Nea Anchialos Fault		
Associated CSS:	Pagasitikos Gulf (GRCS010)		
Parametric information			
	Parameter	Qual.	Evidence
Location (Lat/Lon)	39.243 / 22.819	LD	various geological/morphotectonic maps
Length (km)	23	LD	various geological/morphotectonic maps
Width (km)	14	AR	derives from other parameters (dip, minimum and maximum depth)
Min depth (km)	0	LD	geomorphic records (various authors)
Max depth (km)	11.5	EJ	inferred from microseismic survey (Kementzetzidou, 1996; Hatzfeld <i>et al.</i> , 1999)
Strike (deg)	83	LD	various geological/morphotectonic maps and focal mechanisms
Dip (deg)	55	EJ	geological/morphotectonic maps, foci and microseismic survey (various authors)
Rake (deg)	255	LD	kinematic indicators and focal mechanisms (various authors)
Slip per event (m)	0.18	AR	calculated from Mo (Aki, 1966)
Slip rate (mm/a)	1.0 – 3.0	LD	geomorphic markers (Caputo, 1996)
Recurrence (y)	1500 - 1500	LD	inferred from historical seismicity (Zovoili <i>et al.</i> , 2004)
Max Magnitude (Mw)	6.1	ER	after the relationships of Wells and Coppersmith (1994) and Hanks and Kanamori (1979)
Associated earthquake			
Latest Eq	1980/07/09	Mw=6.1 (2 nd shock)	
Penultimate Eq	N/A	unknown	
Elapsed Time	20	as of year 2000 (assigned datum)	

General information			
Code:	GRCS015		
Name:	Vasilika		
Associated ISSs:	Righeo (GRIS015) and Dasolofos (GRIS016)		
Parametric information			
	Parameter	Qual.	Evidence
Min depth (km)	0	LD	geomorphic records (Caputo, 1990; 1995)
Max depth (km)	14.5	EJ	inferred from microseismic survey (Kementzetzidou, 1996; Hatzfeld <i>et al.</i> , 1999)
Strike (deg)	80 - 115	LD	geological/morphotectonic maps (Caputo, 1990; 1995)
Dip (deg)	45 - 70	EJ	field measurements/microseismic surveys (various authors) and geological considerations
Rake (deg)	260 - 280	LD	kinematic indicators and regional stress field pattern (various authors)
Slip rate (mm/a)	0.6 – 0.9	AR	calculated from geodetic strain rate field
Max magnitude (Mw)	7.0	EJ	fault geometry considerations and application of empirical relationships (Wells and Coppersmith, 1994)
Approximate location (Lat/Lon)	39.356 / 22.582	AR	map derived
Total length (km)	50.3	AR	map derived
Total width (km)	18	AR	derived from depth and dip
Typical fault length (km)	41.7	ER	derived from maximum magnitude
Typical fault width (km)	20.4	ER	derived from maximum magnitude
Typical fault slip (m)	1.56	AR	derived from moment and fault size

Appendix

General information			
Code:	GRIS015		
Name:	Righeo Fault		
Associated CSS:	Vasilika (GRCS015)		
Parametric information			
	Parameter	Qual.	Evidence
Location (Lat/Lon)	39.322 / 22.671	LD	geological/morphotectonic maps (Caputo, 1990; 1995)
Length (km)	22	LD	geological/morphotectonic maps (Caputo, 1990; 1995)
Width (km)	14	AR	derives from other parameters (dip, minimum and maximum depth)
Min depth (km)	0	LD	geomorphic records (Caputo, 1990; 1995)
Max depth (km)	12.7	EJ	microseismic spatial distribution (Kementzetzidou, 1996; Hatzfeld <i>et al.</i> , 1999)
Strike (deg)	95	LD	geological/morphotectonic maps (Caputo, 1990; 1995)
Dip (deg)	65	EJ	microseismic spatial distribution (Kementzetzidou, 1996; Hatzfeld <i>et al.</i> , 1999)
Rake (deg)	275	LD	regional stress field pattern (various authors)
Slip per event (m)	0.8	AR	calculated from Mo (Aki, 1966)
Slip rate (mm/a)	0 – 0	UN	unknown
Recurrence (y)	0 - 0	UN	unknown
Max Magnitude (Mw)	6.5	ER	after the relationships of Wells and Coppersmith (1994) and Hanks and Kanamori (1979)
Associated earthquake			
Latest Eq	1957/03/08		large foreshock, mainshock and aftershock in the same day (M>6.0)
Penultimate Eq	1773/03/16		poor macroseismic data (in various catalogues)
Elapsed Time	43		as of year 2000 (assigned datum)

General information			
Code:	GRIS016		
Name:	Dasolofos Fault		
Associated CSS:	Vasilika (GRCS015)		
Parametric information			
	Parameter	Qual.	Evidence
Location (Lat/Lon)	39.321 / 22.475	LD	geological/morphotectonic maps (Caputo, 1990; 1995)
Length (km)	15	LD	geological/morphotectonic maps (Caputo, 1990; 1995)
Width (km)	13	AR	derives from other parameters (dip, minimum and maximum depth)
Min depth (km)	0	LD	geomorphic records (Caputo, 1990; 1995)
Max depth (km)	11.8	EJ	microseismic spatial distribution (Kementzetzidou, 1996; Hatzfeld <i>et al.</i> , 1999)
Strike (deg)	99	LD	geological/morphotectonic maps (Caputo, 1990; 1995)
Dip (deg)	65	EJ	microseismic spatial distribution (Kementzetzidou, 1996; Hatzfeld <i>et al.</i> , 1999)
Rake (deg)	270	LD	regional stress field pattern (various authors)
Slip per event (m)	0.6	AR	calculated from Mo (Aki, 1966)
Slip rate (mm/a)	0 – 0	UN	unknown
Recurrence (y)	0 – 0	UN	unknown
Max Magnitude (Mw)	6.3	ER	after the relationships of Wells and Coppersmith (1994) and Hanks and Kanamori (1979)
Associated earthquake			
Latest Eq	1942/06/01		Mw=5.6 (Papazachos <i>et al.</i> , 2009)
Penultimate Eq	N/A		unknown
Elapsed Time	58		as of year 2000 (assigned datum)

Appendix

General information			
Code:	GRCS020		
Name:	Domokos		
Associated ISSs:	Ekkara (GRIS020)		
Parametric information			
	Parameter	Qual.	Evidence
Min depth (km)	0	LD	geomorphic records and palaeoseismology (various authors)
Max depth (km)	17.5	EJ	inferred from microseismic survey (Kementzetzidou, 1996)
Strike (deg)	270 - 300	LD	various geological/morphotectonic maps
Dip (deg)	40 - 60	EJ	palaeoseismology (Palyvos <i>et al.</i> , 2010) and geological considerations
Rake (deg)	270 - 280	LD	kinematic indicators and regional stress field pattern (various authors)
Slip rate (mm/a)	0.3 – 0.5	LD	palaeoseismological data (Palyvos <i>et al.</i> , 2010)
Max magnitude (Mw)	7.0	ER	calculated from the empirical relationships of Wells and Coppersmith (1994)
Approximate location (Lat/Lon)	39.294 / 22.245	AR	map derived
Total length (km)	48.1	AR	map derived
Total width (km)	23.7	AR	derived from depth and dip
Typical fault length (km)	41.7	ER	derived from maximum magnitude
Typical fault width (km)	20.4	ER	derived from maximum magnitude
Typical fault slip (m)	1.56	AR	derived from moment and fault size

General information			
Code:	GRIS020		
Name:	Ekkara Fault		
Associated CSS:	Domokos (GRCS020)		
Parametric information			
	Parameter	Qual.	Evidence
Location (Lat/Lon)	39.232 / 22.152	LD	geological/morphotectonic maps, co-seismic ruptures, palaeoseismology (various authors)
Length (km)	29	EJ	inferred from co-seismic ruptures (Papastamatiou and Mouyiaris, 1986)
Width (km)	17	EJ	inferred from epicentral location
Min depth (km)	0	LD	geomorphic records, co-seismic ruptures, palaeoseismology (various authors)
Max depth (km)	13	AR	derives from other parameters (dip, width and minimum depth)
Strike (deg)	288	LD	geological/morphotectonic maps and co-seismic ruptures (various authors)
Dip (deg)	50	EJ	epicentral location, foci and palaeoseismology (various authors)
Rake (deg)	285	LD	regional stress field pattern, palaeoseismology and foci (various authors)
Slip per event (m)	0.75	AR	calculated from Mo (Aki, 1966)
Slip rate (mm/a)	0.3 – 0.5	LD	palaeoseismological data (Palyvos <i>et al.</i> , 2010)
Recurrence (y)	3195 - 3195	LD	palaeoseismological data (Palyvos <i>et al.</i> , 2010)
Max Magnitude (Mw)	6.7	ER	after the relationships of Wells and Coppersmith (1994) and Hanks and Kanamori (1979)
Associated earthquake			
Latest Eq	1954/04/30	Mw=6.6 (EMMA catalogue)	
Penultimate Eq	N/A	unknown	
Elapsed Time	46	as of year 2000 (assigned datum)	

Appendix

General information			
Code:	GRCS004		
Name:	South Tyrnavos Basin		
Associated ISSs:	Larissa (GRIS005) and Asmaki (GRIS004)		
Parametric information			
	Parameter	Qual.	Evidence
Min depth (km)	0	LD	geomorphic records and ERTs (various authors)
Max depth (km)	13	EJ	inferred from seismogenic layer thickness of nearby areas
Strike (deg)	255 - 300	LD	geological/morphotectonic maps (Caputo, 1990; Caputo <i>et al.</i> , 1994)
Dip (deg)	40 - 70	EJ	field measurements (Caputo, 1990; Caputo <i>et al.</i> , 1994) and geological considerations
Rake (deg)	260 - 280	LD	regional stress field pattern (Caputo, 1990; Caputo <i>et al.</i> , 1994)
Slip rate (mm/a)	0.1 – 0.5	LD	morphotectonic estimations (Caputo, 1995)
Max magnitude (Mw)	6.8	EJ	fault geometry considerations and application of empirical relationships (Wells and Coppersmith, 1994)
Approximate location (Lat/Lon)	39.695 / 22.533	AR	map derived
Total length (km)	39.9	AR	map derived
Total width (km)	17	AR	derived from depth and dip
Typical fault length (km)	33.1	ER	derived from maximum magnitude
Typical fault width (km)	17.4	ER	derived from maximum magnitude
Typical fault slip (m)	1.16	AR	derived from moment and fault size

General information			
Code:	GRIS005		
Name:	Larissa Fault		
Associated CSS:	South Tyrnavos Basin (GRCS004)		
Parametric information			
	Parameter	Qual.	Evidence
Location (Lat/Lon)	39.669 / 22.349	LD	geological/morphotectonic maps (Caputo, 1990; Caputo <i>et al.</i> , 1994)
Length (km)	19	LD	geological/morphotectonic maps (Caputo, 1990; Caputo <i>et al.</i> , 1994)
Width (km)	13	AR	derives from other parameters (dip, minimum and maximum depth)
Min depth (km)	0	LD	geomorphic records and ERTs (various authors)
Max depth (km)	11.8	EJ	inferred from seismogenic layer thickness of nearby areas
Strike (deg)	284	LD	geological/morphotectonic maps (Caputo, 1990; Caputo <i>et al.</i> , 1994)
Dip (deg)	65	EJ	field measurements (Caputo, 1990; Caputo <i>et al.</i> , 1994) and geological considerations
Rake (deg)	270	EJ	regional stress field pattern (Caputo, 1990; Caputo <i>et al.</i> , 1994)
Slip per event (m)	0.4	AR	calculated from Mo (Aki, 1966)
Slip rate (mm/a)	0.1 – 0.5	LD	morphotectonic estimations (Caputo, 1995)
Recurrence (y)	500 - 1500	LD	archaeoseismological evidences (Caputo & Helly, 2005a)
Max Magnitude (Mw)	6.3	ER	after the relationships of Wells and Coppersmith (1994) and Hanks and Kanamori (1979)
Associated earthquake			
Latest Eq	N/A	unknown	
Penultimate Eq	N/A	unknown	
Elapsed Time	N/A	unknown	

Appendix

General information			
Code:	GRIS004		
Name:	Asmaki Fault		
Associated CSS:	South Tyrnavos Basin (GRCS004)		
Parametric information			
	Parameter	Qual.	Evidence
Location (Lat/Lon)	39.677 / 22.542	LD	geological/morphotectonic maps (Caputo <i>et al.</i> , 1994)
Length (km)	11	LD	geological/morphotectonic maps (Caputo <i>et al.</i> , 1994)
Width (km)	10	AR	derives from other parameters (dip, minimum and maximum depth)
Min depth (km)	0	LD	geomorphic records (Caputo <i>et al.</i> , 1994)
Max depth (km)	9.4	EJ	inferred from seismogenic layer thickness of nearby areas
Strike (deg)	273	LD	geological/morphotectonic maps (Caputo <i>et al.</i> , 1994)
Dip (deg)	70	EJ	field observations (Caputo <i>et al.</i> , 1994) and geological considerations
Rake (deg)	270	EJ	regional stress field pattern (various authors)
Slip per event (m)	0.25	AR	calculated from Mo (Aki, 1966)
Slip rate (mm/a)	0.1 – 0.1	LD	morphotectonic estimations (Caputo, 1995)
Recurrence (y)	0 - 0	UN	unknown
Max Magnitude (Mw)	5.9	ER	after the relationships of Wells and Coppersmith (1994) and Hanks and Kanamori (1979)
Associated earthquake			
Latest Eq	1941/03/01	M _w =6.1 (Vanucci and Gasperini, 2003; 2004)	
Penultimate Eq	N/A	unknown	
Elapsed Time	59	as of year 2000 (assigned datum)	

General information			
Code:	GRCS001		
Name:	Tyrnavos		
Associated ISSs:	Tyrnavos (GRIS001)		
Parametric information			
	Parameter	Qual.	Evidence
Min depth (km)	0	LD	geomorphic records (Caputo, 1990; 1993a)
Max depth (km)	14	EJ	inferred from seismogenic layer thickness of nearby areas
Strike (deg)	275 - 290	LD	geological/morphotectonic maps (Caputo, 1990; 1993a)
Dip (deg)	50 - 75	EJ	field observations (Caputo, 1990; 1993a) and geological considerations
Rake (deg)	260 - 280	LD	kinematic indicators (Caputo, 1990; 1993a)
Slip rate (mm/a)	0.05 – 0.4	LD	palaeoseismology and morphotectonics (Caputo, 1993; Caputo <i>et al.</i> , 2004a)
Max magnitude (Mw)	6.3	LD	palaeoseismological investigations (Caputo <i>et al.</i> , 2004a; 2006)
Approximate location (Lat/Lon)	39.766 / 22.335	AR	map derived
Total length (km)	19.7	AR	map derived
Total width (km)	16.4	AR	derived from depth and dip
Typical fault length (km)	18.6	ER	derived from maximum magnitude
Typical fault width (km)	11.6	ER	derived from maximum magnitude
Typical fault slip (m)	0.55	AR	derived from moment and fault size

Appendix

General information			
Code:	GRIS001		
Name:	Tyrnavos Fault		
Associated CSS:	Tyrnavos (GRCS001)		
Parametric information			
	Parameter	Qual.	Evidence
Location (Lat/Lon)	39.737 / 22.249	LD	geological/morphotectonic maps (Caputo, 1990; 1993a)
Length (km)	14	LD	geological/morphotectonic maps (Caputo, 1990; 1993a)
Width (km)	13	AR	derives from other parameters (dip, minimum and maximum depth)
Min depth (km)	0	LD	geomorphic records (Caputo, 1990; 1993a)
Max depth (km)	11.8	EJ	inferred from seismogenic layer thickness of nearby areas
Strike (deg)	279	LD	geological/morphotectonic maps (Caputo, 1990; 1993a)
Dip (deg)	65	EJ	field observations (Caputo, 1990; 1993a) and geological considerations
Rake (deg)	280	LD	kinematic indicators (Caputo, 1990; 1993a)
Slip per event (m)	0.3	LD	palaeoseismological investigations (Caputo <i>et al.</i> , 2004a; 2006)
Slip rate (mm/a)	0.05 – 0.4	LD	palaeoseismology and morphotectonics (Caputo, 1993; Caputo <i>et al.</i> , 2004a)
Recurrence (y)	1500 - 2500	LD	inferred from palaeoseismological investigations (Caputo <i>et al.</i> , 2006)
Max Magnitude (Mw)	6.1	ER	after the relationships of Wells and Coppersmith (1994) and Hanks and Kanamori (1979)
Associated earthquake			
Latest Eq	since 5.3 ka BP	M=6.3-6.7	from palaeoseismological investigations (Caputo <i>et al.</i> , 2004;2006)
Penultimate Eq	since 5.3 ka BP	M=6.3-6.7	from palaeoseismological investigations (Caputo <i>et al.</i> , 2004;2006)
Elapsed Time	N/A	unknown	

General information			
Code:	GRCS002		
Name:	North Tyrnavos Basin		
Associated ISSs:	Rodia (GRIS002) and Gyrtoni (GRIS003)		
Parametric information			
	Parameter	Qual.	Evidence
Min depth (km)	0	LD	geomorphic records (Caputo, 1990; 1993b)
Max depth (km)	12.5	EJ	inferred from seismogenic layer thickness of nearby areas
Strike (deg)	70 - 130	LD	geological/morphotectonic maps (Caputo, 1990; 1993b)
Dip (deg)	55 - 75	EJ	field measurements (Caputo, 1990; 1993b) and geological considerations
Rake (deg)	260 - 290	LD	kinematic indicators (Caputo, 1990; 1993b)
Slip rate (mm/a)	0.1 – 1.0	LD	palaeoseismology and morphotectonics (Caputo, 1993b; Caputo and Helly, 2005a; 2005b)
Max magnitude (Mw)	6.2	EJ	fault geometry considerations and application of empirical relationships (Wells and Coppersmith, 1994)
Approximate location (Lat/Lon)	39.773 / 22.300	AR	map derived
Total length (km)	46.9	AR	map derived
Total width (km)	14.1	AR	derived from depth and dip
Typical fault length (km)	16.6	ER	derived from maximum magnitude
Typical fault width (km)	10.7	ER	derived from maximum magnitude
Typical fault slip (m)	0.47	AR	derived from moment and fault size

Appendix

General information			
Code:	GRIS002		
Name:	Rodia Fault		
Associated CSS:	North Tyrnavos Basin (GRCS002)		
Parametric information			
	Parameter	Qual.	Evidence
Location (Lat/Lon)	39.798 / 22.323	LD	geological/morphotectonic maps (Caputo, 1990; 1993b)
Length (km)	15	LD	geological/morphotectonic maps (Caputo, 1990; 1993b)
Width (km)	13	AR	derives from other parameters (dip, minimum and maximum depth)
Min depth (km)	0	LD	geomorphic records (Caputo, 1990; 1993b)
Max depth (km)	11.8	EJ	inferred from seismogenic layer thickness of nearby areas
Strike (deg)	109	LD	geological/morphotectonic maps (Caputo, 1990; 1993b)
Dip (deg)	65	EJ	field observations (Caputo, 1990; 1993b) and geological considerations
Rake (deg)	280	LD	kinematic indicators (Caputo, 1990; 1993b)
Slip per event (m)	0.3	LD	palaeoseismological investigations (Caputo and Helly, 2005b)
Slip rate (mm/a)	0.1 – 1.0	LD	palaeoseismology and morphotectonics (Caputo, 1993; Caputo <i>et al.</i> , 2004b)
Recurrence (y)	0 - 0	UN	unknown
Max Magnitude (Mw)	6.1	ER	after the relationships of Wells and Coppersmith (1994) and Hanks and Kanamori (1979)
Associated earthquake			
Latest Eq	N/A	unknown	
Penultimate Eq	N/A	unknown	
Elapsed Time	N/A	unknown	

General information			
Code:	GRIS003		
Name:	Gyrtoni Fault		
Associated CSS:	North Tyrnavos Basin (GRCS002)		
Parametric information			
	Parameter	Qual.	Evidence
Location (Lat/Lon)	39.717 / 22.489	LD	geological/morphotectonic maps (Caputo, 1990; 1995)
Length (km)	13	LD	geological/morphotectonic maps (Caputo, 1990; 1995)
Width (km)	12	AR	derives from other parameters (dip, minimum and maximum depth)
Min depth (km)	0	LD	geomorphic records (Caputo, 1990) and ERTs (Caputo <i>et al.</i> , 2003)
Max depth (km)	11.3	EJ	inferred from seismogenic layer thickness of nearby areas
Strike (deg)	103	LD	geological/morphotectonic maps (Caputo, 1990; 1995)
Dip (deg)	70	EJ	inferred from geological considerations
Rake (deg)	270	EJ	regional stress field pattern (various authors)
Slip per event (m)	0.3	AR	calculated from Mo (Aki, 1966)
Slip rate (mm/a)	0.01 – 0.1	LD	geological considerations (Caputo, 1995)
Recurrence (y)	0 - 0	UN	unknown
Max Magnitude (Mw)	6.1	ER	after the relationships of Wells and Coppersmith (1994) and Hanks and Kanamori (1979)
Associated earthquake			
Latest Eq	N/A	unknown	
Penultimate Eq	N/A	unknown	
Elapsed Time	N/A	unknown	

Appendix

General information			
Code:	GRCS040		
Name:	Omolio		
Associated ISSs:	none		
Parametric information			
	Parameter	Qual.	Evidence
Min depth (km)	0	LD	geological/morphotectonic maps (Caputo, 1990)
Max depth (km)	14	EJ	inferred from seismogenic layer thickness of nearby areas
Strike (deg)	280 - 310	LD	geological/morphotectonic maps (Caputo, 1990)
Dip (deg)	40 - 70	EJ	inferred from geological considerations
Rake (deg)	260 - 280	EJ	inferred from regional stress field pattern
Slip rate (mm/a)	0.4 – 0.9	AR	calculated from geodetic strain rate field
Max magnitude (Mw)	6.5	EJ	fault geometry considerations and application of empirical relationships (Wells and Coppersmith, 1994)
Approximate location (Lat/Lon)	39.901 / 22.592	AR	map derived
Total length (km)	38.7	AR	map derived
Total width (km)	18.3	AR	derived from depth and dip
Typical fault length (km)	23.4	ER	derived from maximum magnitude
Typical fault width (km)	13.6	ER	derived from maximum magnitude
Typical fault slip (m)	0.74	AR	derived from moment and fault size

General information			
Code:	GRCS285		
Name:	South Kassandra offshore		
Associated ISSs:	none		
Parametric information			
	Parameter	Qual.	Evidence
Min depth (km)	0	LD	various airgun seismic profiles and detailed bathymetry
Max depth (km)	14.5	EJ	inferred from seismogenic layer thickness of nearby areas
Strike (deg)	70 - 115	LD	various airgun seismic profiles and detailed bathymetry
Dip (deg)	50 - 80	EJ	inferred from seismic profiles and geological considerations
Rake (deg)	210 - 245	EJ	inferred from seismic profiles and regional stress field pattern
Slip rate (mm/a)	0.8 – 1.4	AR	calculated from geodetic strain rate field
Max magnitude (Mw)	6.9	ER	calculated from the empirical relationships of Wells and Coppersmith (1994)
Approximate location (Lat/Lon)	39.898 / 23.735	AR	map derived
Total length (km)	46.0	AR	map derived
Total width (km)	16.8	AR	derived from depth and dip
Typical fault length (km)	37.2	ER	derived from maximum magnitude
Typical fault width (km)	18.8	ER	derived from maximum magnitude
Typical fault slip (m)	1.34	AR	derived from moment and fault size

Appendix

General information			
Code:	GRCS815		
Name:	Mavrovouni offshore		
Associated ISSs:	none		
Parametric information			
	Parameter	Qual.	Evidence
Min depth (km)	0	LD	swath bathymetric and seismic profiles (Papanikolaou <i>et al.</i> , 2002; 2006)
Max depth (km)	14	EJ	inferred from seismogenic layer thickness of nearby areas
Strike (deg)	280 - 300	LD	swath bathymetric and seismic profiles (Papanikolaou <i>et al.</i> , 2002; 2006)
Dip (deg)	50 - 80	EJ	seismic profiles (Papanikolaou <i>et al.</i> , 2006) and geological considerations
Rake (deg)	270 - 310	EJ	seismic profiles (Papanikolaou <i>et al.</i> , 2006) and regional stress field pattern
Slip rate (mm/a)	0.7 – 1.6	AR	calculated from geodetic strain rate field
Max magnitude (Mw)	6.8	ER	calculated from the empirical relationships of Wells and Coppersmith (1994)
Approximate location (Lat/Lon)	39.642 / 23.453	AR	map derived
Total length (km)	35.2	AR	map derived
Total width (km)	16.2	AR	derived from depth and dip
Typical fault length (km)	33.1	ER	derived from maximum magnitude
Typical fault width (km)	17.4	ER	derived from maximum magnitude
Typical fault slip (m)	1.16	AR	derived from moment and fault size

General information			
Code:	GRCS820		
Name:	Pelion offshore		
Associated ISSs:	none		
Parametric information			
	Parameter	Qual.	Evidence
Min depth (km)	0	LD	swath bathymetric charts and various seismic profiles
Max depth (km)	12.5	EJ	inferred from seismogenic layer thickness of nearby areas
Strike (deg)	290 - 315	LD	swath bathymetric charts and various seismic profiles
Dip (deg)	60 - 80	EJ	various seismic profiles and geological considerations
Rake (deg)	270 - 300	EJ	various seismic profiles and regional stress field pattern
Slip rate (mm/a)	0.7 – 1.4	AR	calculated from geodetic strain rate field
Max magnitude (Mw)	6.7	ER	calculated from the empirical relationships of Wells and Coppersmith (1994)
Approximate location (Lat/Lon)	39.329 / 23.611	AR	map derived
Total length (km)	35.9	AR	map derived
Total width (km)	13.0	AR	derived from depth and dip
Typical fault length (km)	29.5	ER	derived from maximum magnitude
Typical fault width (km)	16.0	ER	derived from maximum magnitude
Typical fault slip (m)	1.0	AR	derived from moment and fault size

Appendix

General information			
Code:	GRCS280		
Name:	South Chalkidiki offshore		
Associated ISSs:	Athos Fault (GRIS282)		
Parametric information			
	Parameter	Qual.	Evidence
Min depth (km)	0	LD	swath bathymetric charts and various seismic profiles
Max depth (km)	17	EJ	inferred from seismogenic layer thickness of nearby areas
Strike (deg)	50 - 115	LD	swath bathymetric charts and various seismic profiles
Dip (deg)	65 - 85	EJ	various seismic profiles and geological considerations
Rake (deg)	210 - 245	EJ	various seismic profiles and regional stress field pattern
Slip rate (mm/a)	1.0 – 1.7	AR	calculated from geodetic strain rate field
Max magnitude (Mw)	7.2	EJ	fault geometry considerations and application of empirical relationships (Wells and Coppersmith, 1994)
Approximate location (Lat/Lon)	40.092 / 24.383	AR	map derived
Total length (km)	87.4	AR	map derived
Total width (km)	17.9	AR	derived from depth and dip
Typical fault length (km)	52.5	ER	derived from maximum magnitude
Typical fault width (km)	24	ER	derived from maximum magnitude
Typical fault slip (m)	2.1	AR	derived from moment and fault size

General information			
Code:	GRIS282		
Name:	Athos Fault		
Associated CSS:	South Chalkidiki offshore (GRCS280)		
Parametric information			
	Parameter	Qual.	Evidence
Location (Lat/Lon)	40.027 / 24.258	EJ	bathymetry, seismic profiles, epicentral location
Length (km)	54	EJ	bathymetry and various seismic profiles
Width (km)	17	AR	derives from other parameters (dip, minimum and maximum depth)
Min depth (km)	0	LD	swath bathymetric charts and various seismic profiles
Max depth (km)	16.6	EJ	inferred from seismogenic layer thickness of nearby areas
Strike (deg)	55	LD	detailed bathymetric maps (Papanikolaou <i>et al.</i> , 2002)
Dip (deg)	77	EJ	inferred from various seismic profiles
Rake (deg)	205	EJ	inferred from regional stress field pattern (various authors)
Slip per event (m)	1.23	AR	calculated from Mo (Aki, 1966)
Slip rate (mm/a)	0 - 0	UN	unknown
Recurrence (y)	0 - 0	UN	unknown
Max Magnitude (Mw)	7.0	ER	after the relationships of Wells and Coppersmith (1994) and Hanks and Kanamori (1979)
Associated earthquake			
Latest Eq	1905/11/08	M=7.5, Papazachos and Papazachou (2003) - overestimated?	
Penultimate Eq	N/A	unknown	
Elapsed Time	95	as of year 2000 (assigned datum)	

Appendix

General information			
Code:	GRCS810		
Name:	North Aegean Basin		
Associated ISSs:	NAB segment A (GRIS810) and segment B (GRIS811)		
Parametric information			
	Parameter	Qual.	Evidence
Min depth (km)	0	LD	swath bathymetric charts and various seismic profiles
Max depth (km)	17	EJ	inferred from seismogenic layer thickness of nearby areas
Strike (deg)	200 - 240	LD	swath bathymetric charts and various seismic profiles
Dip (deg)	60 - 85	LD	various focal mechanisms and seismic profiles
Rake (deg)	170 - 190	LD	various focal mechanisms and seismic profiles
Slip rate (mm/a)	1.0 – 2.5	AR	calculated from geodetic strain rate field
Max magnitude (Mw)	7.6	LD	worst case scenario estimated by Papanikolaou and Papanikolaou (2007)
Approximate location (Lat/Lon)	39.680 / 24.329	AR	map derived
Total length (km)	143.1	AR	map derived
Total width (km)	18.3	AR	derived from depth and dip
Typical fault length (km)	138.7	ER	derived from maximum magnitude
Typical fault width (km)	19.6	ER	derived from maximum magnitude
Typical fault slip (m)	3.88	AR	derived from moment and fault size

General information			
Code:	GRIS810		
Name:	NAB segment A		
Associated CSS:	NAB (GRCS810)		
Parametric information			
	Parameter	Qual.	Evidence
Location (Lat/Lon)	40.019 / 24.704	LD	bathymetry, seismic profiles, epicentral location and aftershock distribution
Length (km)	44	EJ	detailed bathymetric maps and epicentral location
Width (km)	18	AR	derives from other parameters (dip, minimum and maximum depth)
Min depth (km)	0	LD	swath bathymetric charts and various seismic profiles
Max depth (km)	17.7	EJ	inferred from seismogenic layer thickness of nearby areas
Strike (deg)	227	LD	seismic profiles, detailed bathymetry and foci (various authors)
Dip (deg)	79	LD	various focal mechanisms and seismic profiles
Rake (deg)	180	LD	various focal mechanisms
Slip per event (m)	0.88	AR	calculated from Mo (Aki, 1966)
Slip rate (mm/a)	0 - 0	UN	unknown
Recurrence (y)	0 - 0	UN	unknown
Max Magnitude (Mw)	6.9	ER	after the relationships of Wells and Coppersmith (1994) and Hanks and Kanamori (1979)
Associated earthquake			
Latest Eq	1983/08/06	Ms = 6.8 (Kiratzi <i>et al.</i> , 1991)	
Penultimate Eq	N/A	see text for discussion	
Elapsed Time	17	as of year 2000 (assigned datum)	

Appendix

General information			
Code:	GRIS811		
Name:	NAB segment B		
Associated CSS:	NAB (GRCS810)		
Parametric information			
	Parameter	Qual.	Evidence
Location (Lat/Lon)	39.779 / 24.371	EJ	epicentral location, aftershock distribution, seismic profiles and bathymetry
Length (km)	33	EJ	detailed bathymetric maps and epicentral location
Width (km)	17.5	AR	derives from other parameters (dip, minimum and maximum depth)
Min depth (km)	0	LD	swath bathymetric charts and various seismic profiles
Max depth (km)	16.4	EJ	inferred from seismogenic layer thickness of nearby areas
Strike (deg)	222	LD	foci, seismic profiles, detailed bathymetry and aftershock spatial distribution
Dip (deg)	70	LD	various focal mechanisms and seismic profiles
Rake (deg)	188	LD	various focal mechanisms
Slip per event (m)	0.97	AR	calculated from Mo (Aki, 1966)
Slip rate (mm/a)	0 - 0	UN	unknown
Recurrence (y)	0 - 0	UN	unknown
Max Magnitude (Mw)	6.8	ER	after the relationships of Wells and Coppersmith (1994) and Hanks and Kanamori (1979)
Associated earthquake			
Latest Eq	1982/01/18	Mw = 6.6 (Dziewonski <i>et al.</i> , 1983) or 6.5 (Taymaz <i>et al.</i> , 1991)	
Penultimate Eq	N/A	see text for discussion	
Elapsed Time	18	as of year 2000 (assigned datum)	

General information			
Code:	GRCS800		
Name:	South NAT		
Associated ISSs:	none		
Parametric information			
	Parameter	Qual.	Evidence
Min depth (km)	0	LD	various seismic profiles
Max depth (km)	18	EJ	hypocentres and aftershock distribution (various authors)
Strike (deg)	235 - 275	LD	bathymetry and various seismic profiles
Dip (deg)	65 - 90	LD	various focal mechanisms and seismic profiles
Rake (deg)	190 - 225	LD	various focal mechanisms
Slip rate (mm/a)	1.0 – 3.5	AR	calculated from geodetic strain rate field
Max magnitude (Mw)	7.5	EJ	fault geometry considerations and application of empirical relationships (Wells and Coppersmith, 1994)
Approximate location (Lat/Lon)	40.455 / 26.396	AR	map derived
Total length (km)	275.3	AR	map derived
Total width (km)	18.9	AR	derived from depth and dip
Typical fault length (km)	120.2	ER	derived from maximum magnitude
Typical fault width (km)	18.4	ER	derived from maximum magnitude
Typical fault slip (m)	3.37	AR	derived from moment and fault size

Appendix

General information			
Code:	GRCS290		
Name:	North NAT		
Associated ISSs:	Saros Gulf (GRIS290) and Samothraki SE (GRIS291)		
Parametric information			
	Parameter	Qual.	Evidence
Min depth (km)	0	LD	various seismic reflection profiles and sea-floor morphology
Max depth (km)	18	EJ	aftershock spatial distribution (Karabulut <i>et al.</i> , 2006)
Strike (deg)	60 - 110	LD	seismic reflection profiles, sea-floor morphology and foci (various authors)
Dip (deg)	60 - 90	EJ	foci, seismic profiles and aftershock distribution (various authors)
Rake (deg)	180 - 225	LD	various focal mechanisms
Slip rate (mm/a)	2.0 – 3.2	AR	calculated from geodetic strain rate field
Max magnitude (Mw)	7.1	EJ	fault geometry considerations and application of empirical relationships (Wells and Coppersmith, 1994)
Approximate location (Lat/Lon)	40.429 / 25.780	AR	map derived
Total length (km)	127.3	AR	map derived
Total width (km)	19.4	AR	derived from depth and dip
Typical fault length (km)	67.9	ER	derived from maximum magnitude
Typical fault width (km)	14.4	ER	derived from maximum magnitude
Typical fault slip (m)	1.92	AR	derived from moment and fault size

General information			
Code:	GRIS290		
Name:	Saros Gulf		
Associated CSS:	North NAT (GRCS290)		
Parametric information			
	Parameter	Qual.	Evidence
Location (Lat/Lon)	40.454 / 26.219	EJ	epicentral location, seismic profiles and bathymetry
Length (km)	26	ER	after the relationships of Wells and Coppersmith (1994)
Width (km)	15	AR	derives from other parameters (dip, minimum and maximum depth)
Min depth (km)	0	LD	various seismic reflection profiles and sea-floor morphology
Max depth (km)	13.6	EJ	aftershock distribution (Karabulut <i>et al.</i> , 2006) and focal depth
Strike (deg)	68	LD	seismic reflection profiles, sea-floor morphology and foci (various authors)
Dip (deg)	65	EJ	various focal mechanisms and seismic profiles
Rake (deg)	215	LD	various focal mechanisms
Slip per event (m)	0.78	AR	calculated from Mo (Aki, 1966)
Slip rate (mm/a)	0 – 0	UN	unknown
Recurrence (y)	0 – 0	UN	unknown
Max Magnitude (Mw)	6.6	ER	after the relationships of Wells and Coppersmith (1994) and Hanks and Kanamori (1979)
Associated earthquake			
Latest Eq	1975\03\27	Mw = 6.6 (EMMA catalogue)	
Penultimate Eq	N/A	see text for discussion	
Elapsed Time	25	as of year 2000 (assigned datum)	

Appendix

General information			
Code:	GRIS291		
Name:	Samothraki SE		
Associated CSS:	North NAT (GRCS290)		
Parametric information			
	Parameter	Qual.	Evidence
Location (Lat/Lon)	40.407 / 25.917	EJ	epicentral location, aftershock distribution and sea-floor morphology
Length (km)	24	EJ	aftershock spatial distribution (Karabulut <i>et al.</i> , 2006) and sea-floor morphology
Width (km)	15	AR	derives from other parameters (dip, minimum and maximum depth)
Min depth (km)	0	LD	various seismic reflection profiles and sea-floor morphology
Max depth (km)	14.5	EJ	aftershock distribution (Karabulut <i>et al.</i> , 2006) and focal depth
Strike (deg)	83	LD	foci, sea-floor morphology and seismic reflection profiles (various authors)
Dip (deg)	75	EJ	various focal mechanisms and seismic profiles
Rake (deg)	185	LD	various focal mechanisms
Slip per event (m)	0.75	AR	calculated from Mo (Aki, 1966)
Slip rate (mm/a)	0 – 0	UN	unknown
Recurrence (y)	0 – 0	UN	unknown
Max Magnitude (Mw)	6.6	ER	after the relationships of Wells and Coppersmith (1994) and Hanks and Kanamori (1979)
Associated earthquake			
Latest Eq	2003/07/06	Mw = 5.7 (Karabulut <i>et al.</i> , 2006)	
Penultimate Eq	N/A	see text for discussion	
Elapsed Time	-3	as of year 2000 (assigned datum)	

General information			
Code:	GRIS288		
Name:	North Samothraki Fault		
Associated CSS:	none		
Parametric information			
	Parameter	Qual.	Evidence
Location (Lat/Lon)	40.519 / 25.641	LD	geological/morphotectonic maps (Pavlidis <i>et al.</i> , 2005)
Length (km)	22	EJ	inferred from magnitude and sea-floor morphology
Width (km)	15	AR	derives from other parameters (dip, minimum and maximum depth)
Min depth (km)	0	LD	geomorphic records (Pavlidis <i>et al.</i> , 2005)
Max depth (km)	13	EJ	inferred from seismogenic layer thickness of nearby areas
Strike (deg)	286	LD	geological/morphotectonic maps (Pavlidis <i>et al.</i> , 2005)
Dip (deg)	60	EJ	inferred from geological considerations
Rake (deg)	250	LD	field observations (Pavlidis <i>et al.</i> , 2005)
Slip per event (m)	0.60	AR	calculated from Mo (Aki, 1966)
Slip rate (mm/a)	0 – 0	UN	unknown
Recurrence (y)	0 – 0	UN	unknown
Max Magnitude (Mw)	6.5	ER	after the relationships of Wells and Coppersmith (1994) and Hanks and Kanamori (1979)
Associated earthquake			
Latest Eq	1893/02/09	M = 6.8 (Papazachos & Papazachou, 1997; 2003)	
Penultimate Eq	N/A	unknown	
Elapsed Time	107	as of year 2000 (assigned datum)	

Appendix

General information			
Code:	GRCS825		
Name:	Lemnos		
Associated ISSs:	none		
Parametric information			
	Parameter	Qual.	Evidence
Min depth (km)	0	LD	geomorphic records (Koukouvelas and Aydin, 2002; Pavlides <i>et al.</i> , 2009)
Max depth (km)	16	EJ	inferred from seismogenic layer thickness of nearby areas
Strike (deg)	210 - 235	LD	geological/morphotectonic maps (Koukouvelas and Aydin, 2002; Pavlides <i>et al.</i> , 2009)
Dip (deg)	75 - 90	EJ	field observations (Koukouvelas and Aydin, 2002; Pavlides <i>et al.</i> , 2009)
Rake (deg)	180 - 215	EJ	various field observations and regional stress field pattern
Slip rate (mm/a)	0.8 – 2.7	AR	calculated from geodetic strain rate field
Max magnitude (Mw)	6.8	ER	calculated from the empirical relationships of Wells and Coppersmith (1994)
Approximate location (Lat/Lon)	39.931 / 25.273	AR	map derived
Total length (km)	39.2	AR	map derived
Total width (km)	16.3	AR	derived from depth and dip
Typical fault length (km)	44.3	ER	derived from maximum magnitude
Typical fault width (km)	11.9	ER	derived from maximum magnitude
Typical fault slip (m)	1.26	AR	derived from moment and fault size

General information			
Code:	GRIS831		
Name:	Aghios Efstratios Fault		
Associated CSS:	Aghios Efstratios (GRCS831)		
Parametric information			
	Parameter	Qual.	Evidence
Location (Lat/Lon)	39.516 / 25.003	LD	geological/morphotectonic maps (Pavlides <i>et al.</i> , 1990; Pavlides and Tranos, 1991)
Length (km)	75	LD	aftershock spatial distribution (Drakopoulos & Economides, 1972; North, 1977)
Width (km)	15	AR	derives from other parameters (dip, minimum and maximum depth)
Min depth (km)	0	LD	geomorphic records (Pavlides <i>et al.</i> , 1990; Pavlides and Tranos, 1991)
Max depth (km)	14.8	EJ	inferred from aftershock spatial distribution (North, 1977)
Strike (deg)	230	LD	geological/morphotectonic maps (Pavlides <i>et al.</i> , 2005)
Dip (deg)	80	LD	focal mechanisms (various authors)
Rake (deg)	180	LD	kinematic indicators and focal mechanisms (various authors)
Slip per event (m)	1.80	LD	calculated from Mo (North, 1977)
Slip rate (mm/a)	5.0 – 5.0	LD	estimated from seismological and GPS data (Papadimitriou and Sykes, 2001)
Recurrence (y)	0 – 0	UN	unknown
Max Magnitude (Mw)	7.1	ER	after the relationships of Wells and Coppersmith (1994) and Hanks and Kanamori (1979)
Associated earthquake			
Latest Eq	1968/02/19	Mw = 7.2 (EMMA catalogue)	
Penultimate Eq	N/A	unknown	
Elapsed Time	32	as of year 2000 (assigned datum)	



Il tuo indirizzo e-mail
smpsrs@unife.it

Oggetto:
Dichiarazione di conformità della tesi di Dottotato

Io sottoscritto Dott. (Cognome e Nome)
Smporas Sotirios

Nato a:
Salonicco

Provincia:
Grecia

Il giorno:
27/08/1977

Avendo frequentato il Dottorato di Ricerca in:
Scienze della Terra

Ciclo di Dottorato
24

Titolo della tesi (in lingua italiana):
The Greek Database of Seismogenic Sources: seismotectonic implications for North Greece

Titolo della tesi (in lingua inglese):
The Greek Database of Seismogenic Sources: seismotectonic implications for North Greece

Tutore: Prof. (Cognome e Nome)
Caputo Riccardo

Settore Scientifico Disciplinare (S.S.D.)
GEO/03

Parole chiave della tesi (max 10):
GreDaSS, seismogenic sources, North Greece, Aegean, database

Consapevole, dichiara

CONSAPEVOLE: (1) del fatto che in caso di dichiarazioni mendaci, oltre alle sanzioni previste dal codice penale e dalle Leggi speciali per l'ipotesi di falsità in atti ed uso di atti falsi, decade fin dall'inizio e senza necessità di alcuna formalità dai benefici conseguenti al provvedimento emanato sulla base di tali dichiarazioni; (2) dell'obbligo per l'Università di provvedere al deposito di legge delle tesi di dottorato al fine di assicurarne la conservazione e la consultabilità da parte di terzi; (3) della procedura adottata dall'Università di Ferrara ove si richiede che la tesi sia consegnata dal dottorando in 4 copie di cui una in formato cartaceo e tre in formato pdf, non modificabile su idonei supporti (CD-ROM, DVD) secondo le istruzioni pubblicate sul sito: <http://www.unife.it/studenti/dottorato> alla voce ESAME FINALE – disposizioni e modulistica; (4) del fatto che l'Università sulla base dei dati forniti, archiverà e renderà consultabile in rete il testo completo della tesi di dottorato di cui alla presente dichiarazione attraverso l'Archivio istituzionale ad accesso aperto "EPRINTS.unife.it" oltre che attraverso i Cataloghi delle Biblioteche Nazionali Centrali di

Commissari di esame finale e alla copia che produrrò in seduta d'esame finale. Di conseguenza va esclusa qualsiasi responsabilità dell'Ateneo stesso per quanto riguarda eventuali errori, imprecisioni o omissioni nei contenuti della tesi; (2) di prendere atto che la tesi in formato cartaceo è l'unica alla quale farà riferimento l'Università per rilasciare, a mia richiesta, la dichiarazione di conformità di eventuali copie; (3) che il contenuto e l'organizzazione della tesi è opera originale da me realizzata e non compromette in alcun modo i diritti di terzi, ivi compresi quelli relativi alla sicurezza dei dati personali; che pertanto l'Università è in ogni caso esente da responsabilità di qualsivoglia natura civile, amministrativa o penale e sarà da me tenuta indenne da qualsiasi richiesta o rivendicazione da parte di terzi; (4) che la tesi di dottorato non è il risultato di attività rientranti nella normativa sulla proprietà industriale, non è stata prodotta nell'ambito di progetti finanziati da soggetti pubblici o privati con vincoli alla divulgazione dei risultati, non è oggetto di eventuali registrazioni di tipo brevettale o di tutela. PER ACCETTAZIONE DI QUANTO SOPRA RIPORTATO

Firma del dottorando

Ferrara, li _____ (data) Firma del Dottorando

Firma del Tutore

Visto: Il Tutore Si approva Firma del Tutore
